THE PHYSICAL REVIEW

VOLUME 92 Second Series NUMBER 4

NOVEMBER 15, 1953

Published for the

AMERICAN PHYSICAL SOCIETY

by the

AMERICAN INSTITUTE OF PHYSICS

LANCASTER, PA., AND NEW YORK, N. Y.

THE
PHYSICAL REVIEW

A journal of experimental and theoretical physics established by E. L. Nichols in 1893

SECOND SERIES, VOL. 92, NO. 4 NOVEMBER 15, 1953

The Non-Maxwellian Distribution in a Shock Front and the Anomaly of the Chromospheric Temperature

HARI K. SEN
National Bureau of Standards, Washington, D. C.
(Received May 22, 1953)

An estimate is made of the departure from the Maxwellian distribution of the particle velocities in a shock front, as a function of the shock strength. Expressions are derived for the absorption and emission coefficients (for electronic free-free transitions in a completely ionized gas) in a shock front of given strength. The results obtained are applied to resolve the apparent conflict between the two electronic temperatures of the chromosphere, as indicated by optical (30 000°K from emission line widths) and radio (10 000°K from centimetric radiation intensity) observations of the sun.

1. INTRODUCTION

IT is well known that the solar chromosphere departs considerably from thermodynamic equilibrium: the radiation field traversing it corresponds to the photospheric temperature (≃6000°K), whereas its material constituents (electrons and ions) are in thermal equilibrium at a much higher (electron) temperature. Recent evidence, however, shows that the departure is much deeper in that the chromosphere seems to have more than one electron temperature.[1] The width of the chromospheric lines[2] and the low density gradient[3] in the chromosphere indicate a temperature ≃30 000°K, whereas the radio observations of the quiet sun in the centimetric range of wavelengths (1–5 cm) are consistent with a temperature of the order of the photospheric temperature throughout most of the chromosphere.[4] The flash spectrum of the Balmer continuum[5] also indicates a temperature of this order (10 000°K).

In order to explain the above temperature anomaly, some workers have suggested the coexistence of hot and cold regions in the chromosphere.[6] The view adopted in this paper is that the two electronic temperatures obtained from the optical and radio observations point to a non-Maxwellian distribution of the particles in the shock fronts traversing the chromosphere. The medium in a shock front acts as a bimodal atmosphere, partaking of the temperatures both before and behind the shock,[7] and the departure from the Maxwellian distribution increases with the strength of the shock.[8]

There are several possible mechanisms giving rise to the shock front, but the most promising one is the convective cells in the subphotospheric layers that are responsible for the photospheric granules.[9] Even assuming that there are shock fronts causing a non-Maxwellian velocity distribution of the particles in the medium traversed, we have yet to see how quickly the collisions of the particles of the medium will restore the steady state Maxwellian distribution. This is a difficult question, but we can make a rough estimate.[10] Qualitatively, we can see that the higher up we ascend from the solar photosphere, the more granules we encompass in the tangent cone of sight—the frequency of the shock waves increases, whereas the collision frequency of the particles goes down. It appears, therefore, that from some height onward, the non-Maxwellian distribution will persist as a quasi-steady state. The author has made a quantitative estimate of this height in the Appendix, and finds that the departure from the Maxwellian distribution will begin in the high, and possibly even in the low, chromosphere.

[1] Shotaro Miyamoto, Publs. Astron. Soc. Japan **3**(**2**), 67 (1951).
[2] R. O. Redman, Monthly Notices Roy. Astron Soc. **102**, 140 (1942).
[3] R. Wildt, Astrophys. J. **105**, 36 (1947).
[4] John P. Hagen, Astrophys. J. **113**, 547 (1951).
[5] D. H. Menzel and G. G. Cillié, Astrophys. J. **85**, 88 (1937).
[6] Attention to this possibility was first drawn by Giovanelli. See S. F. Smerd, Australian J. Sci. Research **A3**(**1**), 53 (1950).
[7] H. M. Mott-Smith, Phys. Rev. **82**, 885 (1951).
[8] J. F. Denisse and Y. Rocard, J. Phys. et radium **12**, 893 (1951).
[9] M. Schwarzschild, Astrophys. J. **107**, 1 (1948).
[10] The author is indebted to Dr. G. P. Kuiper for this suggestion.

2. THE NON-MAXWELLIAN DISTRIBUTION IN A SHOCK FRONT

For simplicity, we shall assume the gas to be completely ionized with equal numbers of positive ions and electrons. We shall also neglect the small polarization effect[8] and assume the electrons and ions to have a common mass velocity $\bar{u}$. Then, to a first approximation,[11] the velocity distribution function f of the electrons (or ions) in the shock front is given by Mott-Smith's interpolation formula,[7]

$$f=f_\alpha+f_\beta, \tag{1}$$

where

$$f_\alpha=n_\alpha(x)(m/2\pi kT_\alpha)^{\frac{1}{2}}\exp[-(m/2kT_\alpha)(\mathbf{c}-\mathbf{i}u_\alpha)^2], \tag{2}$$

and f_β has a corresponding expression. In the above, $\mathbf{i}$ is a unit vector in the X direction, $\mathbf{c}$ is the vector velocity of a particle with u as its x component, k is Boltzmann's constant, and m is the mass of the electron (or ion). u_α, T_α and u_β, T_β are the stream velocities and temperatures before and behind the shock, respectively. These quantities are connected by the following Rankine-Hugoniot conditions at a shock front:

$$u_\beta=\frac{M^2+a-2}{M^2(a-1)}u_\alpha, \tag{3}$$

and

$$T_\beta=\frac{(M^2+a-2)(aM^2-1)}{M^2(a-1)^2}T_\alpha, \tag{4}$$

where M is the Mach number of the stream before the shock:

$$M=u_\alpha\left(\frac{a-2}{a}\frac{m}{kT_\alpha}\right)^{\frac{1}{2}};\quad a=\frac{2\gamma}{\gamma-1}, \tag{5}$$

γ being the ratio of specific heats.

The functions $n_\alpha(x)$, $n_\beta(x)$ in (2) represent the concentrations of the particles in the shock front. As we neglect polarization effects, the concentration functions refer indifferently to the ion or the electron. The Mach number M, however, refers to the ions, as these mainly determine the shock wave.

If n_0 and n_0' represent the particle concentrations before and behind the shock, respectively, we must have the following equations of continuity:

$$n_\alpha u_\alpha+n_\beta u_\beta=n_0u_\alpha=n_0'u_\beta. \tag{6}$$

From (6) we see that the concentration n_α decreases from n_0 before the shock to zero behind it, whereas the corresponding concentration n_β increases from zero to $(u_\alpha/u_\beta)n_0$. For the center of the shock front, we choose the point where $n_\alpha=\frac{1}{2}n_0$, and, hence, from (6), $n_\beta=(n_0/2)(u_\alpha/u_\beta)$. The total particle concentration at this point is therefore, from (3):

$$n=\tfrac{1}{2}n_0(1+u_\alpha/u_\beta)=\tfrac{1}{2}n_0\frac{a(M^2+1)-2}{M^2+a-2}. \tag{7}$$

We shall regard the shock center as the representative point in the shock front. We refer the distribution function (2) to axes moving with the stream velocity $\bar{u}$, where

$$\bar{u}=\frac{n_0}{n}u_\alpha=\frac{2(M^2+a-2)}{a(M^2+1)-2}u_\alpha. \tag{8}$$

We set

$$U'=(m/2kT_\alpha)^{\frac{1}{2}}(u-\bar{u}), \tag{9}$$

integrate the function (2) with respect to v and w, and use the relations (3), (4), and (8) to obtain the following normalized form for the electron velocity distribution function $f(U')$ at the shock-center:

$$f(U')=\frac{1}{2\sqrt{\pi}}\frac{n_0}{n}\exp\left[-\left\{U'-\left(\frac{a(a-2)}{2}\right)^{\frac{1}{2}}\times\frac{M(M^2-1)}{a(M^2+1)-2}\right\}^2\right]+\frac{1}{2\sqrt{\pi}}\frac{n_0}{n}\frac{M^3(a-1)^2}{(M^2+a-2)^{\frac{1}{2}}(aM^2-1)^{\frac{1}{2}}}\times\exp\left[-\frac{M^2(a-1)^2}{(M^2+a-2)(aM^2-1)}\left\{U'+\left(\frac{a(a-2)}{2}\right)^{\frac{1}{2}}\times\frac{(M^2-1)(M^2+a-2)}{M(a-1)(aM^2+a-2)}\right\}^2\right]. \tag{10}$$

For the electronic gas we shall take $\gamma=5/3$ and $a=5$ from (5). The function $\pi^{\frac{1}{2}}f(U')$ in (10) is plotted against U' in Fig. 1 for various values of the Mach number M. The corresponding Maxwellian distribution $[\exp(-U'^2)$, the limit of $\pi^{\frac{1}{2}}f(U')$ as $M\to1]$, is also given in the same figure for comparison. Notice how the velocity distribution curve departs more and more from the Maxwellian form with increasing M, until it develops a secondary hump (for $M\simeq3$) that accentuates with the strength of the shock.

3. THE DOPPLER HALF-WIDTH

We shall now calculate the Doppler half-width for the velocity distribution $f(U')$ in (10). In order to take account of the slight asymmetry of the function for the higher values of M, we shall add (for $M=3$ onward) the Doppler displacements $\Delta\lambda_1$, and $\Delta\lambda_2$ on each side of the maximum where the intensity drops to half the maximum. In terms of the velocity U' in (9), this half-width, $\Delta(M)$, is given in Table I. Within the range of M shown, $\Delta(M)$ is approximately a linear function of M.

After correcting for instrumental and systematic errors, Redman[2] finds that his measured Doppler half-widths for lines which are fairly free of self-reversal

[11] The Mott-Smith analysis does not apply to weak shocks. We shall, however, be concerned with shocks of moderate strength in this paper.

can be fitted to a kinetic temperature of 30 000°K. If we compare this result with the formula for the Doppler half-width for a Maxwellian distribution,[12] we find that the shock strength M that will make the front simulate with respect to Doppler half-width a Maxwellian atmosphere of temperature 30 000°K is given by

$$T_a=\frac{(1.665)^2}{\Delta(M)}\times 30\,000°\mathrm{K}, \tag{11}$$

where $\Delta(M)$ is the half-width given in the second column of Table I. In the third column of the same table, we have given T_a (the temperature of the undisturbed atmosphere) rounded to the nearest thousand, as a function of M.

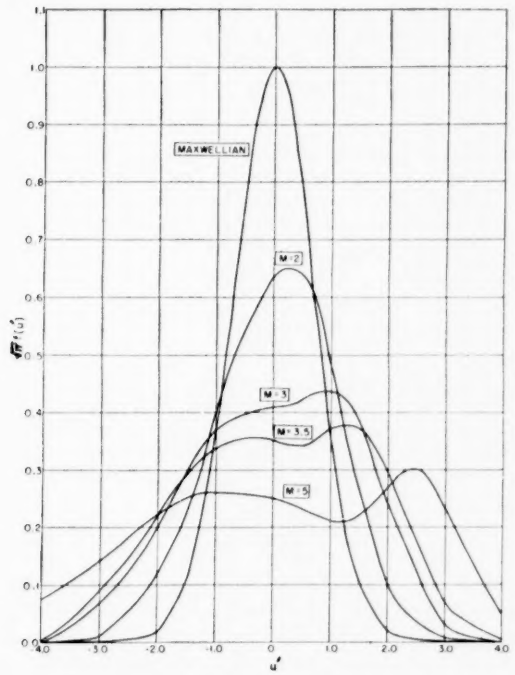

FIG. 1. Velocity distribution at center of shock front.

We see that for a moderate shock ($M\simeq 2.5-3$), an atmosphere of the photopheric temperature ($\simeq 6000$°K) can produce the Redman broadening.

4. CHROMOSPHERIC SUPPORT

The difficulties usually met with in a nonthermodynamic atmosphere are enhanced for a non-Maxwellian distribution such as (10), as we cannot here speak of *the* temperature of the atmosphere, even for the electrons.

The closest approach we can make to a thermodynamic temperature is to define an *average* temperature[13] T (in one dimension) by the relation

$$\tfrac{1}{2}m\int u^2 f(u)du=\tfrac{1}{2}kT, \tag{12}$$

where $f(u)$ is the *normalized* velocity distribution function. For a Maxwellian distribution, T reduces to the thermodynamic temperature.

We can attach a physical meaning to T if we consider that the (mean) hydrostatic pressure p is given by[13]

$$p=nkT, \tag{13}$$

where n is the particle concentration.

If we perform the averaging indicated by (12) over (10), and take account of the scale factor in (9), we obtain as in Table II the ratio T/T_a as a function of the shock strength M. The third column of the table gives the values of T corresponding to T_a in Table I.

We see from Table II that for support of the chromosphere, a shock front of moderate strength simulates a static atmosphere of kinetic temperature $\simeq 20\,000°$–$30\,000$°K. This serves to explain the observed low chromospheric density gradient.[3] If this picture is correct, we will have to abandon the current theory of hydrostatic support of the chromosphere and go back to McCrea's[14] suggestion of a chromosphere supported by turbulent pressure. We may note in this connection Piddington's[15] conclusion "that the radio observations indicate that conditions of hydrostatic equilibrium do not hold in the chromosphere."

TABLE I. The Doppler half-width and the temperature of the undisturbed atmosphere as functions of the shock strength.

M	$\Delta(M)$	T_a(°K)
1.2	1.80	257 000
2.0	2.55	13 000
2.5	3.37	7000
3.0	3.99	5000
3.5	4.65	4000
4.0	5.28	3000
5.0	6.32	2000

TABLE II. The average temperature as a function of the shock strength.

M	T/T_a	T(°K)
1.2	1.14	292 980
2.0	2.20	28 600
2.5	3.13	21 910
3.0	4.25	21 250
3.5	5.57	22 280
4.0	7.08	21 240
5.0	10.69	21 380

[12] A. Unsöld, *Physik der Stern Atmosphären* (Julius Springer, Berlin, 1938), p. 158, Eq. (43.11).

[13] S. Chapman and T. G. Cowling, *The Mathematical Theory of Non-uniform Gases* (Cambridge University Press, London, 1939), p. 37.

[14] W. H. McCrea, Monthly Notices Roy. Astron. Soc. **89**, 718 (1929); **95**, 80 (1934).

[15] J. H. Piddington, Proc. Roy. Soc. (London) **A203**, 431 (1950).

5. EMISSION AND ABSORPTION IN A NON-MAXWELLIAN ATMOSPHERE

In order to derive the expressions for the absorption and emission coefficients for electronic free-free transitions in a shock front, we shall follow Cillié's[16] procedure, and use our non-Maxwellian velocity distribution in place of the Maxwellian one used by Cillié. Corresponding to (10), our normalized velocity distribution function in the shock front in polar coordinates $[R=(U'^2+V'^2+W'^2)^{\frac{1}{2}}]$ is

$$f(R)dR=\frac{1}{\sqrt{\pi}}\frac{M^2+a-2}{a(M^2+1)-2}\times\left\{\frac{\exp[-(R-A)^2]-\exp[-(R+A)^2]}{A}+\frac{B}{CD}\{\exp[-C(R-D)^2]-\exp[-C(R+D)^2]\}\right\}RdR, \quad (14)$$

where A, B, C, and D are constants given by

$$A=\left\{\frac{a(a-2)}{2}\right\}^{\frac{1}{2}}\frac{M(M^2-1)}{a(M^2+1)-2},$$

$$B=\frac{M^5(a-1)^4}{(M^2+a-2)^{5/2}(aM^2-1)^{3/2}},$$

$$C=\frac{M^2(a-1)^2}{(M^2+a-2)(aM^2-1)},$$

$$D=\left\{\frac{a(a-2)}{2}\right\}^{\frac{1}{2}}\frac{(M^2-1)(M^2+a-2)}{M(a-1)(aM^2+a-2)}. \quad (15)$$

Note that the total particle concentration n is given by (7) and that V' and W' in (14) have the same scale factor $(m/2kT_a)^{\frac{1}{2}}$ as U' in (9).

In free-free absorption of a quantum $h\nu$ of radiation, an electron of mass m gains energy according to the relation

$$\tfrac{1}{2}m(v^2-v'^2)=h\nu, \quad (16)$$

where v' is the initial and v the final velocity of the electron. Equation (16) also governs the converse process of emission of a quantum, $h\nu$, in which a v electron goes over into a v' electron.

The rate of absorption by an ion of effective nuclear charge Ze per unit density of v' electrons and per unit intensity of ν radiation is[17]

$$\frac{16\pi^2}{3\sqrt{3}}\frac{Z^2e^6}{hcm^2}\frac{1}{v'\nu^3}. \quad (17)$$

The spontaneous emission/cm³ sec of v electrons is[16]

$$\frac{32\pi^2}{3\sqrt{3}}N_iN_e\frac{Z^2e^6}{c^3m^2}\frac{1}{v}y(v)dv, \quad (18)$$

where N_i is the concentration of ions and N_e that of free electrons of which $N_ey(v)dv$ are in the velocity range v to $v+dv$.

The stimulated emission/cm³ sec (to be reckoned as negative absorption) is

$$\frac{16\pi^2}{3\sqrt{3}}N_iN_e\frac{Z^2e^6}{hcm^2}\frac{1}{\nu^3v}y(v)dv. \quad (19)$$

Our departure from Cillié will be to average $1/v$ over our distribution function (14) instead of over the Maxwellian one. In our notation, and taking note of the scale factor $(m/2kT_a)^{\frac{1}{2}}$ in (9), the relation (16) becomes

$$R^2-R'^2=h\nu/kT_a, \quad (20)$$

where R' and R are the (nondimensional) speeds of the absorbing and emitting electrons. The limits of R' will be from 0 to ∞, and the corresponding limits for R from $(h\nu/kT_a)^{\frac{1}{2}}$ to ∞, when we do the averaging.

If we perform the averaging indicated above, we have the emissivity, j_ν', in the shock front given by

$$\frac{j_\nu'}{j_\nu(T_a)}=\frac{M^2+a-2}{a(M^2+1)-2}\left[\frac{B}{DC^{\frac{1}{2}}}\operatorname{erf}(D\sqrt{C})+\frac{1}{A}\operatorname{erf}(A)\right] \quad (21)$$

for radio-frequency radiation where $h\nu/kT\ll1$. In (21), $j_\nu(T_a)$ denotes the emissivity in a Maxwellian atmosphere of temperature T_a, and

$$\operatorname{erf}(A)=\int_0^A\exp(-x^2)dx. \quad (22)$$

TABLE III. The emission and absorption coefficients as functions of the shock strength.

M	$j_\nu'/j_\nu(T_a)$	$k_\nu'/k_\nu(T_a)$
1.2	0.95	0.85
2.0	0.73	0.40
2.5	0.61	0.23
3.0	0.54	0.14
3.5	0.47	0.09
4.0	0.41	0.06
5.0	0.34	0.03
7.0	0.24	0.01
10.0	0.17	0.004

[16] G. G. Cillié, Monthly Notices Roy. Astron. Soc. **92**, 820 (1932).

[17] J. A. Gaunt, Trans. Roy. Soc. (London) **A229**, 163 (1930). For simplicity we have omitted the slowly varying correction factor of order unity. Its effect presumably will tend to cancel out, as we have considered only the relative values of the emission and absorption coefficients.

The corresponding formula for the absorption coefficient k_ν' in the shock front is

$$\frac{k_\nu'}{k_\nu(T_a)}=\frac{M^2+a-2}{a(M^2+1)-2}[B\exp(-CD^2)+\exp(-A^2)], \quad (23)$$

where $k_\nu(T_a)$ denotes the absorption coefficient in a Maxwellian atmosphere of temperature T_a.

Table III gives the values of the ratios (21) and (23). Both absorption and emission decrease with increasing strength of shock. For shocks of moderate strength, the emission stays of the order of that of the undisturbed atmosphere, whereas the absorption goes down more rapidly.

6. THE RADIO-FREQUENCY INTENSITY IN THE SHOCK FRONT

We do not know precisely at what level in the chromosphere the shock conditions will begin to prevail. We shall assume that it is about the level of origin of 1-cm radiation. Van de Hulst[18] estimates this to be between 1000–3000 km (depending on the scale height of the chromosphere). Our analysis in the Appendix indicates that the shock conditions may begin to prevail at this level. Redman[2] estimates his emission lines to originate at 1500 km above the photosphere. In view of the uncertainty in this estimate, as well as in the estimate of the chromospheric scale height, we may well assume an approximate coincidence of the Redman, centimeter radiation, and shock levels.

Guided by the above consideration, we shall compare the emergent intensity of an optically thick atmosphere of temperature T_a to that when it is traversed by a shock front. We may consider the optical depth τ_ν defined by

$$\tau_\nu=\int_0^x k_\nu dx, \quad (24)$$

as "effectively infinite" when $\tau_\nu \geqslant 4.6[\exp(-\tau_\nu)\leqslant 0.01]$. From Table III we compute the "reduced" optical depth τ_ν' (corresponding to $\tau_\nu=4.6$), the ratio of the "ergiebigkeit" $J_\nu'(=j_\nu'/k_\nu')$ to the Planckian intensity $B_\nu(T_a)$, and the emergent intensity,

$$I_\nu'=J_\nu'[1-\exp(-\tau_\nu')]+B_\nu(T_a)\exp(-\tau_\nu'), \quad (25)$$

as a function of M. These quantities are tabulated in Table IV.

We see that for a fair range of shock strengths the emergent intensity in the front remains of the order of the Planckian intensity of the undisturbed atmosphere, e.g., for $T_a=4000°$, the equivalent Planckian temperature for I_ν' varies between 4400°K and 9600°K. The shock front can thus simulate at once a high temperature atmosphere that gives the Redman broadening and a low temperature one for radio emission.

[18] H. C. van de Hulst, *A Course in Radio Astronomy* (Sterrewacht, Leiden, 1951), p. 115.

TABLE IV. The radio-frequency intensity as a function of the shock strength.

M	τ_ν'	$J_\nu'/B_\nu(T_a)$	$I_\nu'/B_\nu(T_a)$
1.2	3.91	1.12	1.1
2.0	1.84	1.83	1.7
2.5	1.06	2.65	2.1
3.0	0.64	3.86	2.4
3.5	0.41	5.22	2.4
4.0	0.28	6.83	2.4
5.0	0.14	11.33	2.3
7.0	0.05	24.00	2.0
10.0	0.02	42.50	1.8

Presumably, similar considerations would apply to the intensity in the Balmer continuum, which involves averaging over the reciprocal speed.[16]

7. CONCLUDING REMARKS

A rigorous discussion should be based on an evaluation of the width of the shock zone and a detailed consideration of the transfer of radiation through the shock layers, across the solar disk. Such a discussion, however, will necessarily be complex and is beyond the scope of the present paper, which is confined to an estimate of the order of magnitude.

It may be objected that the shock strengths used are too high, as the turbulent velocities of the granules[19] do not exceed the value 3 km/sec and the sound velocity in the photospheric layers is ≃7 km/sec. No observational evidence is available of the strength of the shock caused by the granules. The closest estimate we can make is from the velocity of the chromospheric "spicules,"[20] which is ≃30 km/sec. These spicules closely resemble the solar granules and are quite as numerous. When we bear in mind that the shock front has a greater speed than the moving material and that prominences and corpuscles abound in the chromosphere moving with velocities of 50–500 km/sec, we may reasonably hope that the values used for the strength of the shock in our estimates are not too high. Indeed, it may be true, as Menzel[21] suggests, that "the difference between the chromosphere and the prominences is merely one of degree."

The author believes that the present method can be extended to explain some of the other anomalies in the solar chromosphere and the atmospheres of giant stars. What is needed is a development, for a non-Maxwellian distribution, of the expressions corresponding to the Boltzmann and Saha equations of thermal equilibrium. The interesting thing about these anomalies is that they have a tendency to increase with increasing height in the atmosphere. This is precisely what we should expect from our physical picture.[22]

[19] R. S. Richardson and M. Schwarzschild, Astrophys. J. **111**, 351 (1950).

[20] W. O. Roberts, Astrophys. J. **101**, 136 (1945).

[21] D. H. Menzel, Publ. Lick Observatory **17**, 287 (1931).

[22] The velocity distribution tends more to the non-Maxwellian form with increasing height. See p. 2 of paper.

TABLE V. The shock frequency as a function of height above photosphere.

Height above photosphere h(km)	Shock frequency f_s(sec^{-1})	Shock frequency f_s'(sec^{-1})	Collisional frequency ν(sec^{-1})
5×10^2	6.95×10^5	1.39×10	1.30×10^7
1×10^3	1.39×10^6	2.78×10	1.01×10^7
2×10^3	2.77×10^6	5.54×10	6.29×10^6
4×10^3	5.53×10^6	1.11×10^2	2.45×10^6
6×10^3	8.27×10^6	1.65×10^2	9.58×10^5
1×10^4	1.37×10^7	2.74×10^2	1.14×10^5
1.39×10^4	1.89×10^7	3.79×10^2	5.10×10^3
2×10^4	2.70×10^7	5.40×10^2	2.34×10^2

The author wishes to acknowledge his indebtedness to Dr. Joseph Feinstein and Dr. Chan-Mou Tchen for several helpful discussions during the course of the investigation, to Miss Loris B. Perry for preparing the tables and the figure, and to Mr. James W. Lowry for checking the algebra.

APPENDIX. THE SHOCK WAVE *VERSUS* COLLISIONAL FREQUENCY

It can be shown that the number of granules encompassed in the tangent cone to the photosphere from a point P in the solar atmosphere is

$$\frac{8R^2}{d^2}\frac{h}{R+h}, \tag{1}$$

where R is the solar radius, h the height of the point above the photosphere, and d the diameter of the granule.

If one supposes each granule to be the source of a shock wave, the frequency of the shock waves at P is

$$f_s=8\frac{R^2}{d^2}\frac{h}{R+h}\frac{1}{T}, \tag{2}$$

where T is the lifetime of a granule.

We take $R=6.95\times10^5$ km. We can only estimate the values of d and T, as the observational data are not precise enough.

Schwarzschild[9] considered the dissipation of energy by the solar granulation as a mechanism of heating the solar corona and adopted

$$d=1000 \text{ km}, \quad T=200 \text{ sec}. \tag{3}$$

In a later paper,[19] he suggested the possible existence of unresolved turbulent elements only 100–200 km in diameter. In the recent physical theory of turbulence,[23] it is difficult to fix a limit to the minimum size of the turbulent cells. If we adopt the estimate[24] that ninety percent of the energy is carried in cells up to the Kolmogoroff part of the spectrum (five-thirds power law), we may take the values obtained from the solar curve of growth[25]

$$d=20 \text{ km}, \quad v=1.7 \text{ km/sec}. \tag{4}$$

For the lifetime, we take

$$T\simeq d/v=10 \text{ sec}. \tag{5}$$

If we set (4) and (5) into (2), we have

$$f_s=\frac{1}{500}\frac{R^2h}{R+h} \text{ sec}^{-1}. \tag{6}$$

In Table V we give the shock frequency f_s at different heights h above the photosphere. For comparison, we quote the collisional frequency ν from Hagen's paper.[4] We see that f_s becomes comparable to ν even in the low chromosphere ($h=1500$ km) where the Redman lines are supposed to originate.

It may be contended that we have slanted the granule parameters d and T in our favor. Therefore, we give in the third column of Table V the shock frequency f_s' for the values d and T in (3). We see that even in this unfavorable case the shock frequency becomes comparable to the collisional frequency in the high chromosphere.

[23] S. Chandrasekhar, Astrophys. J. **110**, 329 (1949).

[24] Obtained from Fig. 26 of P. S. Klebanoff and Z. W. Diehl, Technical Note 2475, National Advisory Committee for Aeronautics, Washington, Oct. 1951 (unpublished).

[25] Right-hand point in Fig. 4 of reference 19.

A Condition on Uniform Field Breakdown in Electron-Attaching Gases*

RONALD GEBALLE AND MARVIN L. REEVES
Department of Physics, University of Washington, Seattle, Washington
(Received June 17, 1953)

The usual form of breakdown potential curves indicates that at large pd an asymptotic value of E/p seems to exist below which breakdown does not occur. A study of the equation for steady-state current in electron-attaching gases suggests that this $(E/p)_{\text{lim}}$ is nearly that for which the ionization and attachment coefficients are equal. Substantial agreement is found in CCl_4, CF_3SF_5, CCl_2F_2, SF_6, air, and O_2 between values of $(E/p)_{\text{lim}}$ so determined and those found experimentally. The order of $(E/p)_{\text{lim}}$ for these gases corresponds closely to that of their dielectric strengths.

THE general form of the curve that relates breakdown potential to the product of electrode separation and pressure (pd) in gases between plane-parallel electrodes is well-known.[1] A curve of this kind can be converted into one relating E/p for breakdown (where E is the electric field strength) and pd, assuming uniformity of field. As pd increases, the latter curve falls rapidly at first, but eventually more slowly and seems, where it has been carried sufficiently far, to approach an asymptotic value below which breakdown does not occur.[2,3] It is the main purpose of the present note to suggest an interpretation of this limiting E/p for breakdown in gases that form negative ions by electron attachment.

Since the existence of an asymptote seems common to all gases its explanation would appear to depend on the mechanism of breakdown. In particular it might be related to the failure of some secondary ionizing process at low E/p. However, the breakdown mechanism is incompletely understood at present, and it is difficult to make even a qualitative statement. In spite of this limitation the characteristics of attaching gases permit certain conclusions to be drawn.

An equation for steady-state pre-breakdown current in attaching gases has been presented previously.[4]† That equation is appropriate when secondary ionizing processes such as photoelectric effect or positive ion bombardment are unimportant. Discussions of breakdown, however, must include such processes. Assuming a secondary process at the cathode, one finds

$$i/i_0=\frac{[\alpha/(\alpha-\eta)]\exp[(\alpha-\eta)d]-\eta/(\alpha-\eta)}{1-\{\gamma\alpha/(\alpha-\eta)\}\{\exp[(\alpha-\eta)d]-1\}}, \quad (1)$$

where the symbols are to be interpreted as follows: i = total discharge current, i_0 = electron current produced at the cathode by an external source, α = number of ionizations/cm electron = the ionization coefficient, η = number of attachments/cm electron = the attachment coefficient, d = electrode separation, and γ = probability per positive ion or photon of liberating an electron from the cathode.

A threshold for a self-sustaining current is obtained by requiring the denominator of Eq. (1) to vanish, i.e.,

$$\{\gamma\alpha/(\alpha-\eta)\}\{\exp[(\alpha-\eta)d]-1\}=1. \quad (2)$$

It is well-known[5] that for non-attaching gases ($\eta=0$) Eq. (2) can be fitted to observed breakdown potentials within experimental error. In addition it has been shown recently[6] that a nearly equivalent procedure can be used to represent formative times of sparks at low overvoltages. If we suggest that Eq. (2) is equally valid for breakdown in attaching gases we note that when $\alpha/p \geq \eta/p$, breakdown is possible for sufficiently large pd regardless of the values of α/p, η/p, and γ. Under this condition the breakdown criterion always has a pd dependence. However for $\alpha/p<\eta/p$ Eq. (2) approaches, with increasing pd, an asymptotic form which is independent of pd, i.e.:

$$\alpha/p=(\eta/p)/(1+\gamma). \quad (3)$$

Equation (3) is a condition on E/p alone and fixes a limit for this parameter, $(E/p)_{\text{lim}}$, below which no sparking should be possible regardless of the magnitude of pd. In the following we shall compare, for several gases, values of $(E/p)_{\text{lim}}$ obtained from these considerations with asymptotic limits derived from experimental studies of breakdown potentials.

Values of α/p and η/p are now available in a number of attaching gases.[4] In all cases thus far α/p is the smaller at low E/p but grows more rapidly with increasing E/p and overtakes η/p. Values of E/p for equality vary widely from gas to gas, ranging from 30 to 300 volts/cm/mm. They are believed accurate within 5 percent.

Values of γ will vary with gas and electrode material.

* This work has been supported in part by the U. S. Office of Ordnance Research.

[1] L. B. Loeb, *Fundamental Processes of Electrical Discharge in Gases* (John Wiley and Sons, Inc., New York, 1939), Chap. X.

[2] M. J. Druyvesteyn and F. M. Penning, Revs. Modern Phys. **12**, 88 (1940).

[3] L. B. Loeb and J. M. Meek, *The Mechanism of the Electric Spark* (Stanford University Press, Stanford, 1941), p. 74.

† *Note added in proof:*—Dr. J. D. Craggs has kindly called our attention to an article by F. M. Penning, Ned. T. Natuurkde **5**, 33 (1938) in which this equation is derived.

[4] R. Geballe and M. A. Harrison, Phys. Rev. **85**, 372 (1952); M. A. Harrison and R. Geballe, Phys. Rev. **91**, 1 (1953); M. L. Reeves and R. Geballe (to be published).

[5] See references 1–3.

[6] G. A. Kachikas and L. H. Fisher, Phys. Rev. **88**, 878 (1952).

TABLE I. Comparison of predicted and observed $(E/p)_{\text{lim}}$.

Gas	$(E/p)_{\text{lim}}$ Pred.	Obs.	% dev.	Dielectric strength	Ref.
CCl_4	305	294	3	6	a
CF_3SF_5	186	160	15	3	b
CCl_2F_2	126	110	14	2.4	c
SF_6	117	103	13	2.2	d
Air	31.5	36.5	15	1	e
O_2	35.5	36.5	3	0.95	f

[a] B. M. Hochberg and E. J. Sandberg, J. Tech. Phys. (U.S.S.R.) **12**, 65 (1942).
[b] R. Geballe and F. S. Linn, J. Appl. Phys. **21**, 592 (1950).
[c] Trump, Safford, and Cloud, Trans. Am. Inst. Elec. Engrs. **60**, 132 (1941).
[d] Wilson, Simons, and Brice, J. Appl. Phys. **21**, 203 (1950).
[e] L. H. Fisher, Phys. Rev. **72**, 423 (1947).
[f] L. H. Fisher (private communication).

Its order of magnitude has been found in air[7] to be less than 10^{-3} near the asymptotic E/p for this gas. At high E/p, Hale,[8] using H_2 with electrodes of Pt and Na, found γ to lie below 0.05 for E/p below 600 except for a peak of no present concern. The magnitude of γ is expected, in general, to be sufficiently small that this quantity can be neglected in Eq. (3), a simplification further justified by uncertainties in the values of $(E/p)_{\text{lim}}$ available from experiment. Thus, we are led to adopt the relation

$$\alpha/p=\eta/p \tag{4}$$

as a working condition for the limiting E/p.

Comparison with experiment can be made through Eq. (2). The substitution of values of α/p and η/p yields, as for the non-attaching case, a relation between breakdown potential and pd with one parameter to be determined. In CCl_2F_2 and oxygen, for which the most extensive checks can be made at present, experimental curves are duplicated as closely as those of non-attaching gases. However, this is at best an insensitive test.

A direct test of Eq. (4) is illustrated in Table I. Here values of $(E/p)_{\text{lim}}$ predicted from this equation by the use of data from reference 4 are compared with those deduced from measurements of breakdown potentials. It is important to point out two principal causes of error in the latter. If measurements are not made under conditions of strict uniformity of electric field, breakdown will occur at abnormally low E/p. On the other hand, if measurements are not carried out to sufficiently large pd, the limiting E/p cannot be estimated accurately and will generally be given too high a value. Best conditions of uniformity seem to have been achieved in CCl_2F_2, oxygen and air. Only for the first two of these do measurements permit of reliable extrapolation to the asymptotic limit. It should be pointed out, in addition, that a failure of the kind described in the second paragraph might cause the observed $(E/p)_{\text{lim}}$ to lie above the predicted value. In view of these uncertainties, the agreement exhibited in Table I indicates the essential correctness of the proposed interpretation of Eq. (4). It can be seen from the table that an ordering according to $(E/p)_{\text{lim}}$ corresponds closely to relative dielectric strength as generally quoted.

The authors are grateful to Professor L. H. Fisher for supplying breakdown potential data in oxygen prior to publication.

[7] F. Llewellyn Jones and A. B. Parker, Proc. Roy. Soc. (London) **A213**, 185 (1952).
[8] D. H. Hale, Phys. Rev. **55**, 815 (1939).

Saturation Effects in Paramagnetic Resonance*†

A. H. ESCHENFELDER‡ AND R. T. WEIDNER
Department of Physics, Rutgers University, New Brunswick, New Jersey

(Received July 28, 1953)

Saturation effects have been observed in the paramagnetic resonance absorption of 3.2-cm microwaves by diluted samples of iron ammonium alum and chromium potassium alum at 2 to 4°K. For all samples the spin-lattice relaxation time T_1 was found to vary inversely with the temperature, in agreement with theoretical expectation that the direct rather than the "Raman" process for the spin-lattice quantum transfer predominates at helium temperatures. Diluted samples of iron ammonium alum with iron to aluminum atom ratios of 1:18, 1:59, and 1:80 showed T_1 to be essentially independent of dilution and yielded $TT_1=5\times10^{-4}$ sec °K for the $m=\frac{1}{2}\rightarrow-\frac{1}{2}$ transition. The low-field side peak in the iron alum spectrum for the (100) orientation, comprised of two unresolved transitions, yielded an effective value of $TT_1=1.4\times10^{-3}$ sec °K. The $m=\frac{1}{2}\rightarrow-\frac{1}{2}$ transition for diluted chromium alum with a chromium to aluminum atom ratio of 1:10 yielded $TT_1=3\times10^{-3}$ sec °K in agreement with the calculated value. In all samples the spin-spin relaxation time was found to be temperature independent and of the order of 10^{-9} sec. The results for T_1 are at variance with those obtained with low-frequency paramagnetic relaxation experiments, which show a faster temperature dependence than T^{-1} and an increase in T_1 with dilution.

I. INTRODUCTION

THE temperature dependence of the spin-lattice relaxation time, T_1, in paramagnetic salts depends upon which of two relaxation processes dominates in the transfer of energy between the lattice vibrations and the spin system. In the direct, or first-order, process a single quantum of lattice vibration is transferred between the spin and lattice systems; in the second-order, Raman-like process the lattice absorbs a quantum of one frequency and scatters a quantum of another frequency. It is theoretically expected that the first-order process will control the relaxation at low temperatures, leading to a T_1 temperature dependence of T^{-1} for chromium and iron alums in the liquid helium region.[1] For higher temperatures the Raman process should be effective, causing the relaxation time in these salts to exhibit a T^{-7} behavior. Experiments using the technique of paramagnetic relaxation at audio-frequencies with chromium and iron alum indicate,[2-5] however, a T_1 temperature dependence that is appreciably faster than T^{-1} in the liquid helium region. These experiments suggest then that the second-order process is at least partially effective in this temperature range.

The purpose of the experiment reported here was to measure the temperature dependence of T_1 at helium temperatures of chromium potassium sulfate and iron ammonium sulfate by an independent method, that of the saturation effect in paramagnetic resonance absorption at 3.2-cm wavelength. The saturation method, when used with salts for which the lines of the resonance spectrum are well resolved, permits the detailed study of transitions between separate pairs of energy levels and the evaluation of T_1 for a particular transition. On the other hand, the low-frequency relaxation measurements, in which T_1 is evaluated by examining the behavior of the bulk susceptibility of the sample, yield a value of T_1 which is an average for all possible transitions between magnetic levels.

II. THEORY

Spin-lattice relaxation effects are evidenced in paramagnetic resonance absorption when the power level is sufficiently high to disturb the Boltzmann distribution of the spins. Then the power absorbed in magnetic resonance is not proportional to the incident power at high power levels, but rather shows saturation.

If the separations of the magnetic energy levels of the paramagnetic salt is small compared with kT, the absorbed power at a resonance peak, P_a, is given by

$$P_a=\frac{N(h\nu)^2W_i}{(2S+1)kT(1+W_i/W_s)}, \tag{1}$$

where N is the number of spins in the paramagnetic salt, ν is the microwave frequency, S is the total spin quantum number, W_i is the transition probability for induced transitions, and W_s is the spontaneous transition probability characterizing the spin-lattice relaxation. The spin-lattice relaxation time T_1 is defined as $1/2W_s$.

If one assumes that only magnetic dipole transitions occur between unequally spaced Zeeman levels, $M\rightarrow M-1$,

$$W_i=\tfrac{1}{4}g(\nu)_m\gamma^2H_1^2(S+M)(S-M+1), \tag{2}$$

where γ is the gyromagnetic ratio $(2\pi\nu/H_0)$, H_1 is the amplitude of the circulating magnetic field effective in

* This work was supported by the U. S. Office of Naval Research, the Rutgers University Research Council, and the Radio Corporation of America.

† Based on the Ph.D. thesis submitted by A.H.E. to the Graduate School of Rutgers University.

‡ Now at International Business Machines Corporation, Poughkeepsie, New York.

[1] J. H. Van Vleck, Phys. Rev. **57**, 426 (1940).
[2] Kramers, Bijl, and Gorter, Physica **16**, 65 (1950).
[3] D. Bijl, Thesis, Leiden, 1950 (unpublished).
[4] R. J. Benzie and A. H. Cooke, Proc. Phys. Soc. (London) **A63**, 201 (1950).
[5] F. W. de Vrijer and C. J. Gorter, Physica **18**, 549 (1952).

resonance absorption, and $g(\nu)_m$ is the maximum value of the shape function of the absorption line. The spin-spin relaxation time T_2 is $\frac{1}{2}g(\nu)_m$ when the line is characterized by a Lorentz shape. Inasmuch as W_i is proportional to the microwave energy, Eq. (1) shows that saturation is significant at power levels for which W_i is comparable to W_s.

The common procedure for determining T_1 has been that of examining the saturation term, $W_i/W_s=\frac{1}{2}\gamma^2H_1^2 \times g(\nu)_m T_1(S+M)(S-M+1)$. When the saturation term $=1$, as indicated by the halving of the absorbed power per incident power or by the broadening of the line, T_1 can be evaluated providing H_1^2 and $g(\nu)$, or T_2, are known. In the procedure described below and used in our measurements it is possible to determine T_1 without recourse to a separate evaluation of H_1^2 and $g(\nu)$.

The paramagnetic salts were placed in a resonant cavity in order to increase the microwave magnetic energy density at the sample. The power absorbed in the salt, P_a, was measured as a function of the incident power by measuring the reflection coefficient looking into the cavity.

The cavity system can be considered equivalent to a series RLC circuit which is coupled to a line of characteristic impedance, Z_0, containing a matched generator of voltage E. When the cavity is tuned to resonance at the peak of an absorption line, the reactive components vanish and the magnetic absorption appears as an additional equivalent resistance $\omega L/Q_M$, where Q_M is the absorption Q of the paramagnetic salt. The loaded Q of the cavity in the absence of magnetic absorption, Q_L, is $\omega L/(R+Z_0)$. Therefore, the total impedance looking into the cavity, Z, is given by

$$Z=R+(R+Z_0)Q_L/Q_M. \tag{3}$$

The power P_c absorbed in the loaded cavity system (including the generator impedance Z_0) without magnetic absorption is then

$$P_c=E^2/(R+Z_0)=(4Z_0P_i)/(R+Z_0), \tag{4}$$

where P_i is the incident microwave power.

The ratio of the energies stored in the cavity with and without magnetic absorption is $(R+Z_0)^2/(Z+Z_0)^2$, and from the definition of the Q's,

$$\frac{Q_M}{Q_L}=\left(\frac{R+Z_0}{Z+Z_0}\right)^2\frac{P_c}{P_a}. \tag{5}$$

Using Eq. (4),

$$Q_M/Q_L=[4Z_0(R+Z_0)P_i]/[(Z+Z_0)^2P_a]. \tag{6}$$

The reflection coefficient $\Gamma=(Z-Z_0)/(Z+Z_0)$ refers to the cavity at resonance and with the dc magnetic field, H_0, adjusted for a magnetic resonance peak. At appreciably higher dc fields, the magnetic absorption vanishes, $Z=R$, and $\Gamma=\Gamma_0$.

Therefore, Eq. (6) may be written

$$Q_M/Q_L=[2(1-\Gamma)^2P_i]/[(1-\Gamma_0)P_a]. \tag{7}$$

Introducing Eqs. (1) and (2), Eq. (7) may be written

$$\frac{Q_M}{Q_L}=A\left(\frac{2T}{\gamma^2H_1^2g(\nu)_m(S+M)(S-M+1)}+TT_1\right) \times P_i(1-\Gamma)^2, \tag{8}$$

where $A=[4(2S+1)k]/[N(h\nu)^2(1-\Gamma_0)]$.

But $P_i(1-\Gamma)^2$ is a measure of the power that reaches the sample in the cavity without reflection at the cavity coupling hole, and is therefore proportional to H_1^2. Equation (8) can then be written

$$\frac{Q_M}{Q_L}=B\frac{T}{g(\nu)_m}+ATT_1P_i(1-\Gamma)^2, \tag{9}$$

where B is a constant. A plot of Q_M/Q_L against $P_i(1-\Gamma)^2$ yields a straight line whose slope is proportional to TT_1 and whose intercept is proportional to $T/g(\nu)_m$. The Q ratio is evaluated by using

$$Q_M/Q_L=(1-\Gamma)/(\Gamma-\Gamma_0), \tag{10}$$

which follows from Eq. (3) and the definitions of Γ and Γ_0.

It is seen then that T_1 can be determined without requiring the evaluation of H_1^2 and $g(\nu)_m$. An order-of-magnitude value of $g(\nu)_m$ can be arrived at by using the definition of Q_L,

$$Q_L=\frac{\nu H_1^2V_c}{2P_c}=\frac{\nu H_1^2V_c}{4(1-\Gamma_0)P_i}, \tag{11}$$

where V_c is the cavity volume and a uniform energy density throughout the cavity volume is assumed. This relation determines H_1^2 and, hence, B in Eq. (9).

III. EXPERIMENTAL ARRANGEMENT

In Fig. 1 is shown a cross section of the resonant cavity coupled to the waveguide. The cavity was of the cylindrical re-entrant type, coupled to the waveguide by a hole in the broad face of the waveguide. The waveguide was short-circuited one-quarter waveguide wavelength from the coupling hole. The samples, in the shapes of toroids of rectangular cross section,

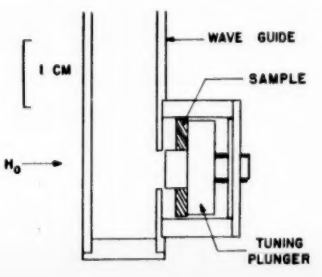

FIG. 1. The resonant cavity and sample.

were placed in the coaxial region of the cavity as shown. In this position the samples occupied a maximum part of the magnetic region of the cavity. The cavity was oriented with the dc field lines parallel to the cavity axis, thus assuring orthogonality of the dc and microwave magnetic fields.

For the re-entrant type resonant cavity the microwave magnetic field is not constant over the sample volume, and therefore H_1 must be averaged over the sample. The absorbed power is given by Eq. (1) when H_1^2 is constant over the sample volume and can be written in the form

$$P_a=\frac{KNW_i}{1+(W_i/W_s)}, \tag{12}$$

where K is a constant. In the coaxial region of the re-entrant cavity H_1 varies inversely with the radial distance r. Inasmuch as W_i is proportional to H_1^2 ,we may write $W_i=c/r^2$. But $dN/N=2rdr/(r_2^2-r_1^2)$ is the fraction of spins between r and $r+dr$, and Eq. (12) becomes

$$P_a=\frac{2NKc}{r_2^2-r_1^2}\int_{r_1}^{r_2}\frac{dr}{r(1+c/W_sr^2)}, \tag{13}$$

where r_1 and r_2 are the inner and outer radii in the coaxial region respectively. For the cavity used, $r_2/r_1=2.50$.

Expanding the logarithm which results from the integral in Eq. (13),

$$P_a=\frac{NKW_i(r_2)}{1+W_i(r_2)/W_s}\left[1+\frac{0.42}{1+W_i(r_2)/W_s}+\cdots\right]. \tag{14}$$

With strong saturation $W_i(r_2)\gg W_s$, and Eq. (14) approaches Eq. (12), where W_i, however, refers to r_2. Thus Eq. (9) may be used without correction in the evaluation of T_1 providing that severe saturation occurs. Tests with samples of varying thickness showed that axial variations in H_1^2 may be neglected for samples that are sufficiently thin.

The metal cavity section was thermally insulated from the Dewar cap by a glass waveguide section thinly plated with silver. Liquid helium was allowed to fill the resonant cavity and lower waveguide section to assure good thermal contact with the sample. A 2K39 Sperry klystron with a power output of 1 watt was used as the 3.2-cm oscillator. The reflection coefficients Γ and Γ_0 looking into the cavity arm were determined from the incident and reflected power as measured with a Magic-T bridge. The incident power P_i was measured with a barretter bridge circuit.

The samples were prepared by recrystallization from saturated aqueous solutions. Single crystals of diluted iron ammonium alum with iron to aluminum atom ratios of 1:18, 1:59, and 1:80 as determined by chemical analysis were used; diluted samples of chromium potassium alum with a chromium to aluminum atom ratio of 1:10 were used.

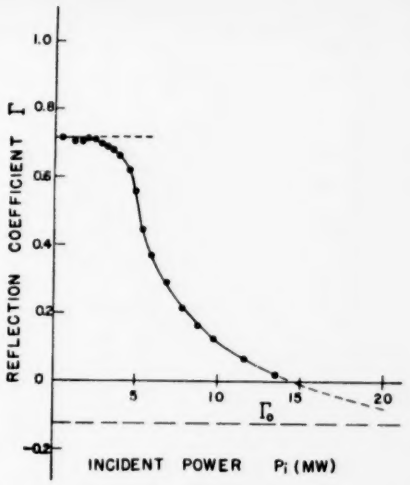

FIG. 2. Reflection coefficient looking into the sample-filled cavity as function of the incident microwave power

IV. RESULTS

The principal measurements on the iron alum samples were made with the dc field along the (100) axis. For this orientation the paramagnetic resonance spectrum is understood on the basis of the theory of Meijer.[6] The spectrum for diluted samples consists of a well-resolved, intense central peak ($M=\frac{1}{2}\rightarrow-\frac{1}{2}$), a low-field side peak containing two unresolved lines ($M=-3/2\rightarrow-5/2$ and $M=3/2\rightarrow1/2$), and a high-field side peak containing two unresolved lines ($M=5/2\rightarrow3/2$ and $M=-1/2\rightarrow-3/2$).

Saturation measurements were made at the peaks of the resolved line, $\frac{1}{2}\rightarrow-\frac{1}{2}$, and the unresolved lines, $-3/2\rightarrow-5/2$ and $3/2\rightarrow1/2$ for the (100) orientation; measurements with iron alum were also made using the $\frac{1}{2}\rightarrow-\frac{1}{2}$ line in the (111) orientation, where this principal line is less well-separated from neighboring lines. The measurements with diluted potassium chrome alum were made using the $\frac{1}{2}\rightarrow-\frac{1}{2}$ line in the (111) orientation, for which this transition is best resolved.

The results for a typical run are shown in Figs. 2 and 3. The sample in this case was 0.454 g of iron alum diluted 1:59, at 4.23°K. The measurements were made with the field adjusted to the central peak at about 3300 oersteds. Figure 2 shows the reflection coefficient plotted against the power incident on the cavity. At very low-power levels Γ is essentially constant; but as the power is increased and the saturation becomes appreciable, Γ approaches Γ_0, that is, the resistive losses overpower the magnetic losses. The sign of Γ is determined by observing whether magnetic absorption causes the power reflected from the cavity to increase or decrease, corresponding respectively to a positive or negative value of Γ. The Γ_0 value was determined at a

[6] P. H. E. Meijer, Physica **17**, 899 (1951).

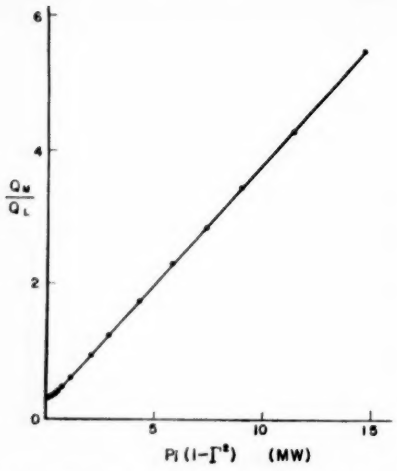

FIG. 3. Ratio of magnetic Q to loaded cavity Q as a function of the microwave power striking the sample.

dc field of about 6000 oersteds, far from the absorption lines.

In Fig. 3 Q_M/Q_L is plotted against $P_i(1-\Gamma)^2$ in accordance with Eqs. (9) and (10), using the data shown in Fig. 2. The points lie on a straight line as expected, except for points near the intercept, where the departure from linearity is to be attributed to the radial inhomogeneity of the microwave magnetic field in the cavity. The extreme plotted point in Fig. 3 corresponds to a saturation term (W_s/W_a) of 22; thus the approximation used in Eq. (12), assuming severe saturation, is justified. Only those data which showed a linear Q_M/Q_L *versus* $P_i(1-\Gamma)^2$ plot and which satisfied the severe saturation condition were considered acceptable; on this basis it was found that data for some samples and at some temperatures could not be used because unfavorable cavity coupling conditions precluded measurements at strong saturation conditions.

The loaded cavity Q, Q_L, which was measured by observing Γ_0 as a function of frequency and used in the approximate evaluation of $g(\nu)_m$, was found to be about 300; therefore, losses in the waveguide leading to the sample cavity could properly be neglected.

The results are shown in Fig. 4, where the logarithm of TT_1 is plotted against T. The data are identified according to the crystal used (iron ammonium or chromium potassium alum), the magnetic quantum numbers of the transition, the dilution in terms of magnetic ions to aluminum atoms, and the orientation of the crystal in the dc magnetic field. The observation that TT_1 is independent of temperature over the range 2 to 4°K for a given sample corresponds to an inverse-temperature dependence of the spin-lattice relaxation time.

The data shown for the $\frac{1}{2}\rightarrow-\frac{1}{2}$ transition in iron alum, diluted 1:59 and in the (100) orientation, arise from two samples of differing thicknesses, corresponding to masses of 0.171 and 0.458 gram. Inasmuch as no obvious difference in the TT_1 values for the two thicknesses appears, it can be assumed that the samples were thin enough so that no correction need be applied for the variation in microwave field along the cavity axis.

The results for the $\frac{1}{2}\rightarrow-\frac{1}{2}$ transition at 3300 oersteds in iron alum with samples of varying dilution show that TT_1 is close to 5×10^{-4} sec °K for dilutions from 1:18 to 1:80, the extremes differing by a factor of only 1.3. The combined transitions, $3/2\rightarrow1/2$ and $-3/2\rightarrow-5/2$ at 3000 oersteds for iron alum yield $TT_1=1.4\times10^{-3}$ sec °K, which is higher than the value for the $\frac{1}{2}\rightarrow-\frac{1}{2}$ line. The absolute value of T_1 is rendered uncertain for these transitions inasmuch as the data apply to the resultant peak of the two transitions, which are not exactly superimposed; the sizable difference in T_1 values for the central and side peaks suggests, however, that the spin-lattice relaxation time may differ from one transition to another, neglecting the field dependence of T_1. The central line at 3300 oersteds in the spectrum of diluted chromium potassium alum in the (111) orientation shows $TT_1=3.2\times10^{-3}$ sec °K from 2° to 4°K. The spin-lattice relaxation time was thus found to be longer in the chromium alum than in the iron alum for corresponding temperatures.

It was observed that the absorption line widths increased with saturation; no attempt was made, however, to evaluate T_1 from line widths because of the overlapping of adjacent lines and because of the un-

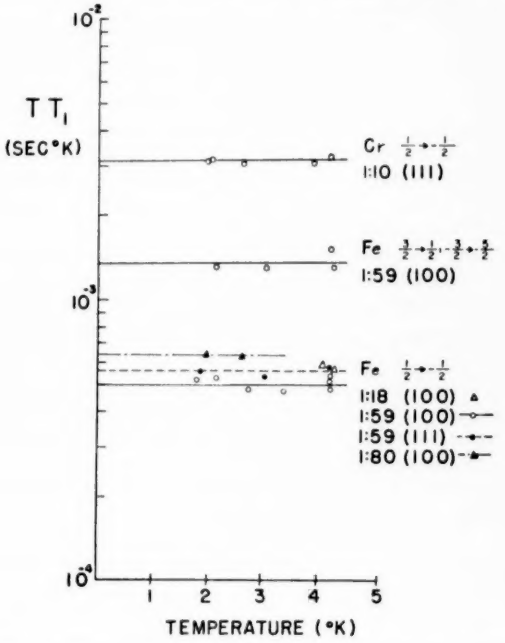

FIG. 4. TT_1 as a function of temperature. The data are identified according to the salt, transition, dilution, and crystal orientation on the right.

certainties involved in taking account of exchange narrowing.

For any sample it was found that the intercepts in the Q_M/Q_L *versus* $P_i(1-\Gamma)^2$ plot varied directly as the temperature; therefore, $g(\nu)_m$ was found to be temperature independent, as is theoretically expected. All samples gave $g(\nu)_m$ values of the order of 4×10^{-10} sec, corresponding to absorption line widths of about 300 oersteds, in agreement with the observed widths as to order of magnitude. The approximations involved in Eqs. (11) and (14) do not warrant more detailed evaluation of $g(\nu)_m$ values.

V. DISCUSSION

The inverse temperature dependence of T_1 found for iron and chromium alums at helium temperature is in accord with theory but at variance with the paramagnetic relaxation measurements at audio-frequencies, which show a faster temperature dependence than T^{-1} for T_1.

Kramer, Bijl, and Gorter,[2] using three undiluted samples of iron alum at 3370 oersteds find T_1 proportioned to T^{-n}, where n is between 4 and 5. The data are compatible with the assumption of a distribution of relaxation times rather than a single T_1. The values of T_1 at 2° and 4°K, respectively, are 1×10^{-3} sec and 7×10^{-3} sec. The measurements of Benzie and Cooke[4] on undiluted iron alum at lower fields of from 205 to 968 oersteds show an exponent in the temperature dependence of $n=2$ to 3; again a distribution of relaxation times was required to fit the data. Bijl[3] found T_1 increasing rapidly as the magnetic dilution of the sample was increased using iron alum samples diluted 1 to 16 (iron to aluminum atoms) and 1 to 80; the more dilute sample indicated that T_1 was greater than 0.02 sec at 4°K.

The results for chromium potassium alum are similar, showing a faster temperature dependence than T^{-1}, an increase in T_1 with dilution, and a distribution of relaxation times. Vrijer and Gorter[5] give the results for measurements with an undiluted sample of chromium potassium alum over the temperature range 2° to 90°K at a field of 4000 oersted. These data are in harmony with the choice of a single exponent, $n=2.6$, over this range. The values of T_1 at 2° and 4°K are 7.8×10^{-3} sec and 1.3×10^{-3} sec, respectively. The results of Kramers, Bijl, and Gorter[2] give a temperature exponent of 3 for 3370 oersteds with undilute chromium alum with T_1 values of 7.0×10^{-3} sec and 1.1×10^{-3} sec for 2° and 4°K. Bijl[7] found that a dilute sample of chromium potassium alum, with chromium to aluminum ratio of 1:13, followed a T^{-2} law with T_1 values which were approximately 10 times larger than for the undilute samples.

The relaxation measurements are characterized by a lack of agreement among the several investigators as to the temperature exponent of T_1. The marked increase in T_1 with dilution is surprising, as Eisenstein[8] remarks, because one expects T_1 to depend only on the interaction of the spins with lattice via the spin orbit and orbit-lattice couplings. These anomalies have been attributed to chemical and physical impurities in the samples.

Van Vleck[1] has derived a relation giving the spin-lattice relaxation time for chromium potassium alum as a function of (among other things) the external field, the root-mean-square internal field, and the zero-field Stark splitting of the ground state. For fields of the order of 3300 oersteds, the calculated T_1 values are relatively insensitive to a choice for the zero-field splitting, so that the two values found in paramagnetic resonance experiments with chromium potassium alum,[9] 0.15 cm^{-1} and 0.27 cm^{-1}, yield T_1 values which differ by only ten percent. The calculated value TT_1 is in agreement with measured value for chromium alum found here, $TT_1=3.2\times10^{-3}$ sec °K, if 340 oersteds is chosen as the root-mean-square internal field. Van Vleck remarks that iron alum, for which no detailed calculations were made, as well as chrome alum, should follow a T^{-1} low at helium temperatures but that the T_1 values for iron alum should be somewhat larger than those for chrome alum for any given temperature. The measurements here, however, show the reverse behavior, T_1 for chrome alum exceeding that for iron alum.

The principal result of this experiment is the T^{-1} behavior of T_1 for the diluted iron and chromium alums at liquid helium temperatures as determined by the saturation effect in paramagnetic resonance absorption at 3300 oersteds. This contrasts with the faster temperature dependence found with the paramagnetic relaxation method at audio-frequencies, but is in accord with theoretical predictions For iron alum T_1 is found to be essentially independent of dilution, whereas the relaxation measurements show a marked increase in T_1 with dilution. These differences between the saturation and relaxation results are as yet unexplained and require further experiments for their resolution.

[7] D. Bijl, Physica **8**, 497 (1941).

[8] J. Eisenstein, Revs. Modern Phys. **24**, 74 (1952).

[9] B. Bleaney, Proc. Roy. Soc. (London) **A204**, 203 (1950).

Transition Temperatures of Superconductors

B. T. MATTHIAS
Bell Telephone Laboratories, Murray Hill, New Jersey
(Received August 3, 1953)

Superconductivity has been found in a number of new compounds between the non-superconducting transition elements and nonmetals such as Si, Ge, and Te. These findings have suggested possible criteria for superconductivity in both elements and compounds.

INTRODUCTION

As has been pointed out before,[1] the superconducting elements lie in two distinct groups in the periodic system. Mo, W, and Bi border on these groups; although not superconducting themselves, they form many superconducting compounds.[2] Bismuth itself, when condensed below 20°K is a superconductor.[3]

Plotting the atomic volumes of the elements *versus* their atomic number, Clusius[4] found small atomic volumes for most superconductors. However, an equal number of non-superconductors fall in that same range of atomic volumes and the correlation is therefore not very satisfactory.

Fröhlich's and Bardeen's criteria are based on their now well-known theories of the lattice-electron interaction.[5,6] They contain the electrical conductivity, its temperature coefficient and the sound velocity and represent beyond any doubt the qualitative distinction between superconductors and non-superconductors. These theories offer also an interpretation of the isotope effect,[7] according to which for a series of superconducting isotopes the transition temperature varies inversely with the square root of the atomic mass:

$$T_c \propto 1/\sqrt{m}.$$

Although Bardeen does not mention compounds, Fröhlich suggests the investigation of the Au–Pd system. This is based on his calculation of an optimum number of free electrons in the superconducting phase. Magnetic measurements on Au–Pd alloys had shown that it was possible to vary this number by gradually filling the *d* shell of Pd. Neither Au nor Pd are superconducting, and as in former investigations all but one[8,9] superconducting compound of non-superconducting elements had contained either Mo, W, or Bi, the Au–Pd system was chosen as the starting point of our investigation of the superconducting compounds of non-superconducting elements.

NON-SUPERCONDUCTING COMPOUNDS

A range of binary alloy compositions with Au, Ag, or Cu as one element and Pd or Pt as the other were investigated. For those compositions in which a superlattice had been reported, the samples were annealed for three months. None of them gave any indication of superconductivity above 1°K.

Susceptibility measurements in the $MgCu_2$–$MgZn_2$ system had indicated a strong variation of the number of free electrons with change in relative composition.[10] This whole system was now investigated. No superconductivity above 1°K was detected in $MgCu_2$, $MgZn_2$ or any of eight intermediate alloys. Negative results were obtained as well for Au–Be and Pd–Be systems. These together with previous[1] negative results suggested that this approach was not likely to be fruitful.

SUPERCONDUCTING COMPOUNDS

Most of the previously investigated alloys and compounds had been truly metallic, distinguished by their rather small ratio of valence electrons/atom = R. In most cases $R<2$. (This is a good criterion for a pure metallic bond according to Schubert.)[11] It was noticed also that the elements, with the exception of Zn and Cd which are superconductors, all had more than two valence electrons/atom. Therefore a study was begun of compounds for which $R>2$. (Again according to Schubert[11] this implies that the predominant metallic bond has become partly replaced by an ionic or covalent bond.[12]) This approach proved more successful as we will indicate below.

The [CaF_2] crystal structure class, although usually

[1] B. T. Matthias and J. K. Hulm, Phys. Rev. **87**, 799 (1952).
[2] The superconducting Mo compounds observed heretofore contain a nonmetal such as B, C, N, Si, and Ge as the other partner. Relying on rules to be discussed, a more metallic compound Mo_3Sb_4 was prepared and found to become superconducting at 2.1°K.
[3] R. Hilsch, Oxford Conf. Low Temp. 119 (1952).
[4] K. Clusius, Z. Elektrochem. **38**, 312 (1932).
[5] H. Fröhlich, Phys. Rev. **79**, 845 (1950).
[6] J. Bardeen, Phys. Rev. **80**, 567 (1950).
[7] E. Maxwell, Phys. Rev. **78**, 417 (1950); C. A. Reynolds *et al.*, Phys. Rev. **78**, 487 (1950).
[8] The exception was CuS.
[9] W. Meissner, Z. Physik **58**, 570 (1929).
[10] Witte, Klee, and Lieser, Naturwiss. **38**, 185 (1951).
[11] K. Schubert, Z. Metallkunde **41**, 418 (1950).
[12] According to most theories the conduction electrons are the carrier of the supercurrents in the superconducting state. As their number is not always easily determined and, as will be shown later on, a connection between superconductivity and the number of *valence* electrons/atom can be more readily obtained, we will continue to consider the number of valence electrons/atom. The connection between valence electrons and conduction electrons is by no means obvious. For instance Nb and Bi both have 5 valence electrons/atom, but Nb is a good metal and a superconductor in contrast to Bi. The detailed band structure is of course a decisive factor. Bi condensed below 20°K becomes a superconductor, probably in a cubic modification (see reference 3).

considered typically ionic, contains a certain number of intermetallic compounds. In this class $CoSi_2$ has been found to become superconducting.[13] While it may be difficult to define the number of valence electrons for cobalt, it is safe to assume $R(\text{cobalt}) \geq 2$, therefore, $R(CoSi_2) \geq 3.3$. Other isomorphous intermetallic compounds have thus far not been found to become superconducting above 1°K. They are shown in Table I.

It is likely from a consideration of either electrons or holes in an incompleted d shell that the R's of the nonsuperconducting compounds are no larger in any case than $R(CoSi_2)$. For most of the remaining intermetallic compounds in this $[CaF_2]$ structure $R=8/3$ which, according to Mott and Jones, is the number of electrons required to fill a Brillouin zone.[14] It is therefore understandable why compounds like Mg_2Si which have values of R so close to those for a filled zone are not superconductors but semiconductors. One may therefore expect superconductivity in the $[CaF_2]$ structure for compounds whose $R>2$ but at the same time sufficiently different from 8/3.

The [NiAs] system of intermetallic compounds was the next one to be investigated[15] and the positive and negative results are compared in Table II.

Although NiSb very probably will become superconducting below 1°K, the rest of the negative group

TABLE I. Superconductivity in the fluorite lattice.

Superconducting	Non-superconducting
$CoSi_2$ (1.3°)	$NiSi_2$; $AuAl_2$; $PtAl_2$

becomes either ferromagnetic, antiferromagnetic, or highly paramagnetic a situation which from an empirical point of view excludes superconductivity. Again it is difficult to define a number of valence electrons/atom but it is evident that

$$R>2$$

in every case where superconductivity was observed.

The column neighboring on Ni, Pd, Pt of the transition elements contains Co, Rh, Ir. Following the above hypothesis concerning R, superconducting rhodium and iridium compounds were discovered. They are Rh_3Ge_2 (structure unknown) at 2.12°K and IrGe (MnP structure) at 4.7°K. The present picture of superconductivity among the transition elements and their compounds in the 8th column is given in Table III.

THE TERNARY SYSTEM OF (Co,Rh)Si_2

Any change in the lattice of a superconducting compound of nonsuperconducting elements should give information about the dependence of transition temperature on lattice parameters, as superconductivity is not due to a single dissolved superconducting element but solely to this special crystal lattice.

Our experiments show that if more than two atomic percent of Co in $CoSi_2$ are replaced by one of its neighboring elements such as Fe, Ni, or Rh, the transition temperature drops below 1°K where we were unable to observe. Larger percentages of Fe or Ni did not change this situation. Larger percentages of Rh however began to raise the transition temperature as shown in Fig. 1.

If we suppose that the electronic configuration of Co and Rh are about the same so that the change in mass is the only important factor, then one might have expected the opposite behavior for the transition temperature from Bardeen's and Fröhlich's theories, since Rh is about twice as heavy as Co. Strain could not account for this rise in transition temperature as this would have resulted in a monotonic function. It therefore became evident that the volume had to play a

TABLE II. Superconductivity in the nickel arsenide lattice.

Superconducting	Non-superconducting
PdSb (1.5°), PtSb (2.1°), PtBi (1.21°) PdTe (2.3°) (though superconducting PdBi is monoclinic, PtTe does not seem to exist)	NiSb,[a] CrSb,[a] MnSb[a] NiTe,[b] CoTe

[a] H. Nowotny, Z. Elektrochem. **49**, 254 (1953).
[b] W. Klemm and N. Fratini, Z. anorg. u. allgem. Chem. **251**, 222 (1943).

TABLE III. Superconducting elements and compounds from the 8th column of the periodic system. (The superconducting substances are printed in boldface type.)

Fe	Co **$CoSi_2$**	Ni **NiBi; $NiBi_2$**
Ru	Rh **Rh_3Ge_2**	Pd **PdSb; PdBi** **PdTe; $PdBi_2$**
Os	Ir **IrGe**	Pt **PtSb** **PtBi**

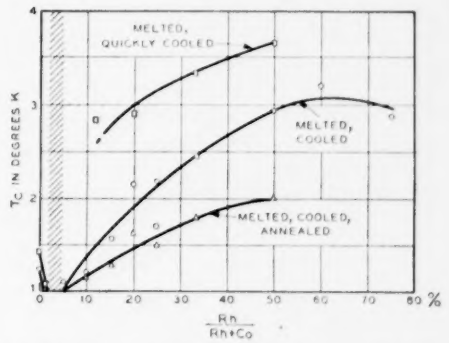

FIG. 1. Transition temperature vs percentage of Rh/(Rh+Co) in the melt. (The shaded area indicates no superconductivity above 1°K.)

[13] B. T. Matthias, Phys. Rev. **89**, 380 (1952).
[14] N. F. Mott and H. Jones, *Properties of Metals and Alloys* (Oxford University Press, London, 1936), pp. 169–170.
[15] B. T. Matthias, Phys. Rev. **90**, 487 (1953).

TABLE IV. Transiton temperature vs mass of corresponding elements in the 4th, respectively, 5th column.

Periodic system		M	T_c °K
4. column	Zr	91	0.70
	Hf	179	0.35
5. column	Nb	93	8.3
	Ta	181	4.3

major role, which was different from what Clusius had expected. X-ray investigation by Dr. E. A. Wood has now shown that with mounting Rh percentage there is an initial decrease in molecular volume and an increase thereafter. One can therefore show in this case that a rise in volume partly tends to increase the transition temperature.[16]

THE TERNARY SYSTEM OF Nb(C,N)

This consideration indicated that it might be possible to raise even the transition temperature of superconducting compounds such as NbN at 15.6°K.

The purpose here would be to enlarge the lattice without increasing the total mass nor reducing appreciably the total number of valence electrons/atom. Rögener, in his recent paper on NbN,[17] noticed a similar trend of the change of the transition temperature with the lattice constant. He got a variation of the lattice constant simply by different firing procedures. In our case now we enlarged the lattice by forming solid solutions between NbC−NbN.[18] We observed an increase of the transition temperature to 17.8°K for mixed crystals centering between 25 and 30 atomic percent NbC. This is the highest transition temperature known at this time.

SUPERCONDUCTING ELEMENTS

In the light of these results it may be worthwhile to look at some of the elements again.

With respect to electronic configuration and lattice parameter the pairs Zr−Hf and Nb−Ta are mutually nearly identical. However, their masses and their respective transition temperatures are both different by approximately a factor 2, as shown in Table IV.

The reciprocal linear dependence of the transition temperature upon the mass here is quite different from the isotope effect. Assuming nevertheless that the transition temperatures of the remaining isomorphous elements in the 4th and 5th column, i.e., Ti and V, are determined by this linear dependence of the mass as well as of a change in lattice parameter, one obtains approximately:

$$\frac{d\ln T_c}{d\ln a_0} \approx 13.$$

This exponent 13 is at least in the same order of magnitude as 30, the value deduced by Shoenberg for tin.[19] From Rögener's data on NbN, this value would be about 26. The data for the $(Co,Rh)Si_2$ system indicate that the lower limit of this exponent would be above 30, if the lattice change were the only decisive factor.

One may therefore conclude that while an increase in mass will lower the transition temperature, an increase in volume will raise it, with an exponent between 4 and 10 for the volume.

The existing superconductors with relatively high transition temperatures indicate that the ***optimum*** ratio of valence electrons/atom seems to be slightly below 5. (See Table V.) While this is at present purely empirical, the closeness of these values to 5 electrons/atom suggests a relation to the half-filled d shell.

TABLE V. Transition temperatures vs number of valence electrons/atom.

Element or compound	T_c °K	R = valence electrons/atom
Nb	8–8.3	5[a]
Pb−As	8.4	4.5–5[a]
Pb−Bi	7.3–8.8	≈5[a]
MoC	7.6–8.3	5[a]
ZrN	9.3–9.6	4.5[a]
2 Nb−1 Zr	10.8	4.67[b]
MoN	12–12.5	5.5[a]
V_2Si	17.0	4.75[c]
$Nb(C_{0.3}; N_{0.7})$	17.8	4.85[b]

[a] These data are taken from the references in Shoenberg's book (see reference 21).
[b] Indicate present results.
[c] G. F. Hardy and J. K. Hulm, Phys. Rev. **89**, 884 (1953).

My thanks to Professor W. H. Zachariasen, Dr. S. O. Morgan, Dr. J. K. Galt, Dr. H. W. Lewis, and Dr. P. W. Anderson for many helpful discussions and help. I would like to express my gratitude to Dr. E. A. Wood for determining the constants of the mixed crystals, Dr. S. Geller for the structure determination of RhSi, and to Mr. E. Corenzwit for his help with the cryogenics.

[16] A slight discontinuity at 25 percent was observed, which however was within the accuracy of the measurements.
[17] H. Rögener, Z. Physik **132**, 446 (1952).
[18] P. Duwez and F. Odell, J. Electrochem. Soc. **97**, 299 (1950).
[19] D. Shoenberg, *Superconductivity* (Cambridge University Press, London, 1952).

Irreversible Thermodynamics of Thermoelectric Effects in Inhomogeneous, Anisotropic Media*

CHARLES A. DOMENICALI
Franklin Institute Laboratories, Philadelphia, Pennsylvania
(Received July 30, 1953)

Beginning with the isotropic form of the thermoelectric equations of Onsager's irreversible thermodynamics as treated by Callen and deGroot, a direct transcription is made to the case of inhomogeneous and anisotropic media. The "emf" of Kelvin, Bridgman, Ehrenfest, and Rutgers is the gradient of the electrochemical potential and a general formula is given for this gradient in anisotropic media. Both the energy density vector and the electrochemical potential gradient are expressed in terms of a "transport entropy matrix" S_{ij}.* The theory leads in a natural and straightforward way to the postulated expression of Ehrenfest and Rutgers. The formulation is in a form easily adaptable to given experimental boundary conditions and, therefore, brings out the limited validity of the Kelvin symmetry relations, as first pointed out clearly by Kohler. Finally, the theory includes the irreversible effects of heat conduction and Joulean heating, as well as the reversible thermoelectric phenomena and is, therefore, more realistic and complete than the theory of Ehrenfest and Rutgers.

INTRODUCTION

THE Onsager theory of irreversible processes has recently been applied by Callen[1] to thermoelectric effects in isotropic media, and a more detailed discussion has been given by deGroot.[2] Ehrenfest and Rutgers[3] have given a brief treatment for anisotropic and inhomogeneous media, based on a postulated formulation which is simply a generalization of the basic equations found by Voigt.[4] Voigt, in turn, had attempted to generalize the theory of Kelvin,[5] but Voigt's theory has been shown to be incapable of predicting the "internal Peltier effect" discovered by Bridgman.[6] More recently other writers, notably Kohler and Meixner,[7] have treated thermoelectric anisotropy from the point of view of quantum kinetic theory. However, there has been no treatment of the problem of thermoelectric anisotropy on the basis of irreversible thermodynamics. Ehrenfest and Rutgers left out of account the irreversible thermal conduction and Joulean heat-generation effects. The treatment given here not only leads in a natural way to the postulated relations of Ehrenfest and Rutgers, but also includes these irreversible conduction and Joulean effects and thereby represents a more realistic and complete theory.

GENERAL EQUATIONS FOR INHOMOGENEOUS ISOTROPIC MEDIA

Let $\mathbf{J}^e$, $\mathbf{J}^s$, $\mathbf{W}$, and $\mathbf{Q}$ be, respectively, the particle current density, the entropy current density, the total energy current density, and the heat current density, and let $\bar{\mu}$ be the electrochemical potential (joules/particle) of an electron of charge $-e$ in the isotropic medium at a point which has absolute temperature T. It is known from the theory of irreversible thermodynamics[1,2] that these quantities are related as follows.

$$\mathbf{J}^e = -L_{ee}\nabla\bar{\mu} - L_{es}\nabla T, \tag{1}$$

$$\mathbf{J}^s = -L_{es}\nabla\bar{\mu} - L_{ss}\nabla T, \tag{2}$$

$$\mathbf{W} = \mathbf{Q} + \bar{\mu}\mathbf{J}^e, \quad \mathbf{Q} = T\mathbf{J}^s, \tag{3}$$

in which the so-called phenomenological coefficients L_{ee}, L_{es}, L_{ss} depend only on the temperature in the case of a homogeneous chemical phase and are related to physically measureable parameters by the expressions

$$L_{ee} = 1/(e^2\rho), \quad (T/L_{ee})(L_{ee}L_{ss} - L_{es}^2) = \kappa, \tag{4}$$

$$L_{es}/L_{ee} = S^* = -eS^{\text{abs}}.$$

Here ρ is the isothermal electrical resistivity, κ is the heat conductivity with no electrical current, and S^{abs} is the absolute thermoelectric power. S^* is the "transport entropy per particle" and plays a prominent role in the theory of irreversible thermodynamics. Throughout this paper we consider the charge carrier to be the electron, charge $-e$.

Substitution of Eqs. (4) into (1), (2), and (3) leads to the three fundamental relations:

$$\mathbf{J}^s = S^*\mathbf{J}^e - (\kappa/T)\nabla T, \tag{5}$$

$$\mathbf{W} = (TS^* + \bar{\mu})\mathbf{J}^e - \kappa\nabla T, \tag{6}$$

$$\nabla\bar{\mu} = -e^2\rho\mathbf{J}^e - S^*\nabla T. \tag{7}$$

Equation (6) states that at a point in an inhomogeneous

* This work supported by Squier Signal Laboratory, Fort Monmouth, New Jersey.

[1] H. B. Callen, Phys. Rev. **73**, 1349 (1948).

[2] S. R. deGroot, *Thermodynamics of Irreversible Processes* (Interscience Publishers, New York, (1951), Chap. 8.

[3] P. Ehrenfest and A. J. Rutgers, Proc. Acad. Sci. Amsterdam **32**, 698, 883 (1929).

[4] W. Voigt, *Kristallphysik* (Teubner, Leipzig, 1928).

[5] W. Thomson, Trans. Roy. Soc. (Edinburgh) **21**, 133 (1857).

[6] P. Bridgman, Proc. Am. Acad. Art. Sci. **61**, 101 (1926); and *Thermodynamics of Electrical Phenomena in Metals* (Macmillan and Company, Inc., New York, 1934), Chap. 6.

[7] M. Kohler, Ann. Physik **40**, 196 (1941); **27**, 201 (1936); W. Meissner, *Handbuch der Experimentalphysik* (Akademische Verlagsgesellschaft, Leipzig, 1935), Vol. 11, pt. 2. E. A. Uehling, Phys. Rev. **39**, 821 (1932); J. Meixner, Ann. Physik **35**, 701 (1939); **40**, 165 (1941).

isotropic medium at which there is electrical (particle) current flow as well as a temperature gradient, the total energy current density (watts per unit area) consists of three terms, *viz.*, an "entropy transport" term $TS^*\mathbf{J}^e$, an electrochemical potential term $\bar{\mu}\mathbf{J}^e$, and a thermal conduction term $-\kappa\nabla T$. Equation (7) may be called the "generalized Ohm's Law." The electrochemical potential $\bar{\mu}$ may be separated[1,2] into a chemical part and an electrical part, $\bar{\mu}=\mu-e\phi$. Thus, in an isothermal region of a chemically homogeneous phase with $\nabla T=0$, Eq. (7) gives the ordinary Ohm's Law, since the gradient $\nabla\mu$ of the chemical potential vanishes in this case. On the other hand, if no current flows, $\mathbf{J}^e=0$, Eq. (7) gives the "thermoelectric electrochemical potential gradient" $\nabla\bar{\mu}=-S^*\nabla T$.

GENERAL EQUATIONS FOR INHOMOGENEOUS ANISOTROPIC MEDIA

In setting up the general equations *we make the assumption that each component of the entropy current density J_i^s is a linear function of the components J_j^e of particle current density and of the components $\nabla_j T$ of the temperature gradient*, with $i, j=1, 2, 3$. The temperature T and the electrochemical potential $\bar{\mu}$ are considered as continuous and differentiable functions of position (x_1, x_2, x_3) within each separate phase. If an electrical current flows across a boundary between two media, there will be cases in which the electrochemical potential cannot be defined *within* the junction. In such cases, however, the finite *jump* in $\bar{\mu}$ across the junction can be defined, and one needs only to use the appropriate boundary conditions for $\bar{\mu}$; otherwise such cases introduce no particular difficulties. The relation (5) is thus replaced by the three equations:[8]

$$J_i^s=S_{ij}^*J_j^e-\frac{\kappa_{ij}}{T}\frac{\partial T}{\partial x_j}, \quad (i,j=1,2,3) \tag{8}$$

in which the quantities S_{ij}^* are the "transport entropy matrix" and the κ_{ij} are the "heat conductivity matrix." We emphasize the fact that relations (8) are postulates, reasonable extensions of the isotropic formula (5). It follows from (8), (5), and (3) that the component W_i of the total energy current density can be written

$$W_i=TS_{ij}^*J_j^e+\bar{\mu}J_i^e-\kappa_{ij}\partial T/\partial x_j. \tag{9}$$

Next we require the anisotropic formulation of the relation (7) between electrochemical potential gradient, particle current density and temperature gradient. Equation (7) derives from the same basic relations (1) and (2) as do (5) and (6), and it is therefore clear that the required anisotropic form of (7) must be consistent with (8) and (9). It is seen that the only uncertainty in the direct transcription of (7) into anisotropic form lies in the order of subscripts in the transport entropy matrix S_{ij}^*. The matrices of electrical resistivity ρ_{ij} and of thermal conductivity κ_{ij} are already known to be symmetric.[9] In order to deduce the correct form of the anisotropic transcription of Eq. (7), we make use of the conjugation of the "fluxes" J_i^s and J_i^e and "forces" $\partial\bar{\mu}/\partial x_i$ and $\partial T/\partial x_i$ as expressed by the invariance of the sum[1]:

$$T\zeta(s)=J_i^e(-\partial\bar{\mu}/\partial x_i)+J_i^s(-\partial T/\partial x_i). \tag{10}$$

According to the Onsager theory, the quantity $\zeta(s)$ is the time rate of *internal* entropy production per unit volume caused by irreversible processes, which in the present problem result from Joulean heat generation and heat conduction. Only the steady state need be considered for our purposes, so that the sum (10) is time independent as well as invariant with respect to transformations of the "fluxes" and "forces." If (8) is substituted into (10), one finds

$$\begin{aligned} T\zeta(s)&=-J_i^e\frac{\partial\bar{\mu}}{\partial x_i}-S_{ij}^*J_j^e\frac{\partial T}{\partial x_i}+\frac{\kappa_{ij}}{T}\frac{\partial T}{\partial x_j}\frac{\partial T}{\partial x_i}\\ &=-J_i^e\left(\frac{\partial\bar{\mu}}{\partial x_i}+S_{ji}^*\frac{\partial T}{\partial x_j}\right)+\frac{\kappa_{ij}}{T}\frac{\partial T}{\partial x_j}\frac{\partial T}{\partial x_i}. \end{aligned} \tag{11}$$

The terms in κ_{ij} are the contribution of the irreversible heat conduction to the entropy source strength, and the terms in J_i^e represent the contribution of the irreversible Joule heating. The quantity $\zeta(s)$ is required by the Onsager theory to be positive, though not every individual term in $\zeta(s)$ need be positive. Now the entropy of the material contained within a given volume ΔV is a constant in the steady state, since this entropy is a single-valued function of characteristic parameters of the material in ΔV such as the internal energy ΔU, number of particle ΔN, and the volume ΔV. The internal entropy production $\zeta(s)$ resulting from irreversible processes within ΔV is carried out by the vector J^s at a rate, div J^s, just sufficient (in the steady state) to balance out $\zeta(s)$ so as to maintain a constant entropy within ΔV.

The Joule contribution to $T\zeta(s)$ can also be written

$$\rho_{ij}J_iJ_j=e^2\rho_{ij}J_i^eJ_j^e, \tag{12}$$

where $J_i=-eJ_i^e$ and $\rho_{ij}=\rho_{ji}$ is the resistivity matrix of the crystal at temperature T. If we equate (12) to the Joule contribution in (11), we have

$$\begin{aligned} -J_i^e\left(\frac{\partial\bar{\mu}}{\partial x_i}+S_{ji}^*\frac{\partial T}{\partial x_j}\right)&\equiv e^2\rho_{ij}J_i^eJ_j^e\\ &=-J_i^e(-e^2\rho_{ij}J_j^e), \end{aligned} \tag{13}$$

and since the particle (electrical) current density com-

[8] The presence of two identical subscripts in a term indicates a summation.

[9] Reference 4, p. 345; reference 2, chap. 4. It has not yet been shown that for arbitrary crystal symmetry the matrix S_{ij}^* is symmetric. On the contrary, the work of Kohler[7] results in quantum-mechanical expressions for a matrix γ_{ij}, related to our S_{ij}^*, which are nonsymmetrical in the general case.

ponents are independently variable, (13) leads to

$$\partial\bar{\mu}/\partial x_i = -e^2\rho_{ij}J_j^e - S_{ji}^*\partial T/\partial x_j. \tag{14}$$

It is interesting to notice that the Joule heat is *not* correctly given in general by E_iJ_i, with $E_i=-\partial\phi/\partial x_i$. In fact, we can show that this is so even in an isotropic homogeneous phase, as follows. The correct Joule heat expression is, using (12) and (14),

$$\rho J\cdot J=\frac{1}{e}\left(\frac{\partial\bar{\mu}}{\partial x}+S^*\frac{\partial T}{\partial x}\right)\cdot J=\frac{1}{e}\left(\frac{\partial\mu}{\partial x}-e\frac{\partial\phi}{\partial x}+S^*\frac{\partial T}{\partial x}\right)J$$

$$=\frac{1}{e}\left(\frac{\partial\mu}{\partial T}+S^*\right)\frac{\partial T}{\partial x}\cdot J+E\cdot J, \tag{15}$$

where we have written $\partial\mu/\partial x=(\partial\mu/\partial T)(\partial T/\partial x)$ and $E=-\partial\phi/\partial x$ Thus, we have $\rho J^2=E\cdot J$ only for a phase at uniform temperature, when $\partial T/\partial x=0$

VOLUME AND SURFACE HEATING EFFECTS

The vector W_i in (9) gives the total energy current density at any point in the crystalline medium. In the steady state there can be no accumulation of energy within any infinitesimal volume element and the vector W_i must be divergenceless Thus,

$$\frac{\partial W_i}{\partial x_i}\equiv 0=T\frac{\partial(S_{ij}^*J_j^e)}{\partial x_i}+S_{ij}^*J_j^e\frac{\partial T}{\partial x_i}$$

$$+\bar{\mu}\frac{\partial J_i^e}{\partial x_i}+J_i^e\frac{\partial\bar{\mu}}{\partial x_i}-\frac{\partial}{\partial x_i}\left(\kappa_{ij}\frac{\partial T}{\partial x_j}\right). \tag{16}$$

This relation and the following are thus valid for non-homogeneous crystalline or crystalline-like media.[10] The third group of terms on the right-hand side of (16) vanish, since the particle current is divergenceless. Substitution of (14) into the fourth term on the right-hand side of (16) gives

$$J_i^e\partial\bar{\mu}/\partial x_i=-e^2J_i^e\rho_{ij}J_j^e-J_i^eS_{ji}^*\partial T/\partial x_j$$

$$=-e^2\rho_{ij}J_i^eJ_j^e-S_{ij}^*J_j^e\partial T/\partial x_i, \tag{17}$$

the last term here cancelling the second on the right-hand side of (16). If we solve for the derivative $\partial(\kappa_{ij}\partial T/\partial x_j)/\partial x_i$, we find from (16):

$$\frac{\partial}{\partial x_i}\left(\kappa_{ij}\frac{\partial T}{\partial x_j}\right)=-e^2\rho_{ij}J_i^eJ_j^e+T\cdot\frac{\partial(S_{ij}^*J_j^e)}{\partial x_i}, \tag{18}$$

or, set $J_i^e=-(1/e)J_i$, where J_i is the electrical current density,

$$\frac{\partial}{\partial x_i}\left(\kappa_{ij}\frac{\partial T}{\partial x_j}\right)=-\rho_{ij}J_iJ_j-\frac{1}{e}T\cdot\frac{\partial(S_{ij}^*J_j)}{\partial x_i}. \tag{19}$$

[10] An example of the latter kind of medium is a non-uniformly strained body in which the strains give rise to a crystalline-like anisotropy.

Equation (19) is a general expression for the production of heat in an inhomogeneous, anisotropic medium, crystalline or otherwise.

In general the components S_{ij}^* of the transport entropy matrix depend on temperature and on position in an inhomogeneous medium, so that the derivatives of S_{ij}^* in (19) must include spatial as well as temperature variations. Thus, since in general $S_{ij}^*=S_{ij}^*(x_i, T)$, we must write

$$\frac{\partial S_{ij}^*}{\partial x_i}=\left(\frac{\partial S_{ij}^*}{\partial x_i}\right)_T+\left(\frac{\partial S_{ij}^*}{\partial T}\right)_{x_i}\cdot\frac{\partial T}{\partial x_i}, \tag{20}$$

and the last group of terms in (19) breaks down into the three groups:

$$-\frac{T}{e}\frac{\partial(S_{ij}^*J_j)}{\partial x_i}=-\frac{T}{e}J_j\left(\frac{\partial S_{ij}^*}{\partial x_i}\right)_T$$

$$-\frac{T}{e}J_j\left(\frac{\partial S_{ij}^*}{\partial T}\right)_{x_i}\frac{\partial T}{\partial x_i}-\frac{T}{e}S_{ij}^*\frac{\partial J_j}{\partial x_i}. \tag{21}$$

Relation (21) is the starting point of the Ehrenfest-Rutgers theory. We shall use the following notation for the four separate groups of terms in (19) and (21):

$$\text{Joule:}\quad Q_J\equiv-\rho_{ij}J_iJ_j, \tag{22}$$

$$\text{Peltier:}\quad Q_P\equiv-\frac{1}{e}TJ_j\left(\frac{\partial S_{ij}^*}{\partial x_i}\right)_T, \tag{23}$$

$$\text{Thomson:}\quad Q_T\equiv-\frac{1}{e}TJ_j\left(\frac{\partial S_{ij}^*}{\partial T}\right)_{x_i}\frac{\partial T}{\partial x_i}, \tag{24}$$

$$\text{Bridgman:}\quad Q_B\equiv-\frac{1}{e}TS_{ij}^*\frac{\partial J_j}{\partial x_i}. \tag{25}$$

(Volume effects)

Each of the Q's represents a heat *absorbed* per unit volume per unit time. Our sign convention agrees with that of Bridgman, absorbed heat being taken as positive. Ehrenfest and Rutgers use the opposite convention. Equation (22) gives the Joule heat *evolved* and is therefore negative. If the medium is not homogeneous, there is a volume Peltier heating effect Q_P given by (23). Whether the medium is homogeneous or not, there is a Thomson heating effect given by (24). The last terms (25) describe an effect first predicted by Bridgman.[6]

We consider next the phenomena taking place when an electrical current crosses a boundary between two anisotropic media. The generalization to the anisotropic case follows directly from the formula (9) for total energy flow W_i. Consider a composite system consisting of two different anisotropic and inhomogeneous media X and R electrically and thermally jointed along some arbitrary surface AB, as shown in Fig. 1. The reference axes are x_1, x_2, x_3, and the principal crystallographic axes (or other characteristic axes) of each medium X and R may be oriented in any way whatever relative to these reference axes. As in the case of isotropic media,

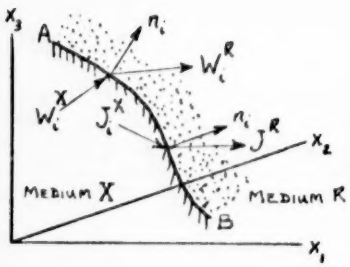

FIG. 1. The curve AB represents a junction between two anisotropic, inhomogeneous media X and R.

the joint or contact AB between X and R will, in general, be a very complex transition region of some finite thickness d. This thickness is, of course, somewhat indefinite, varying from place to place along the boundary and will depend upon the method used for joining the two media. Often the main bulk of the junction may consist primarily of some third material, for example, when two different crystals are cemented together with Wood's metal or with soft solder. In such cases the junction layer of solder may be several thousandths of an inch thick in many places. On the other hand, if the joining is done by electrical fusing of the two single crystals, the transition layer or sheath will probably be a physical mixture of polycrystals of X and R together with some alloy crystals, and so on. In almost all cases in which quantitative measurements are to be made on arbitrarily-oriented single crystals, the boundary AB will be a simple butt joint; in such cases some quantitative estimate can be made of the "contact resistance" or "sheath resistance" R_s, provided the resistance matrices $\rho_{ij}{}^X$ and $\rho_{ij}{}^R$ for the two crystals X and R are known. The procedure for determining R_s in the case of two crystals is essentially the same as that for isotropic phases, except for the added complications resulting from the crystalline nature of X and R. However, since these complications can be handled in a straightforward way having little to do with thermoelectricity, we shall not discuss the details.

If we return to formula (9) and the figure, we see that since in the steady state energy and charge cannot accumulate in the boundary region AB, the boundary conditions on total energy current density and electrical current density are

$$J_i{}^X n_i \equiv J_i{}^R n_i, \tag{26}$$

$$W_i{}^X n_i \equiv W_i{}^R n_i, \tag{27}$$

in which n_i are the three components of the unit normal vector which we agree always to point outward from medium X. The superscripts X and R refer to the medium in which the current flows. If we apply condition (27) to (9) and collect similar terms for the two media, we find

$$\begin{aligned} &e^{-1}T(S_{ij}{}^{*X}J_j{}^X n_i - S_{ij}{}^{*R}J_j{}^R n_i) \\ &\quad + e^{-1}(\bar{\mu}^X J_i{}^X n_i - \bar{\mu}^R J_i{}^R n_i) \\ &\quad + [\kappa_{ij}{}^X(\partial T/\partial x_j)^X n_i - \kappa_{ij}{}^R(\partial T/\partial x_j)^R n_i] \equiv 0. \end{aligned} \tag{28}$$

The bracketted groups of terms represent the energy flowing out of the boundary region (per unit area of the sheath) by ordinary heat conduction through media X and R. The middle group of terms give the Joule dissipation in the resistance R_s of the sheath; this can be seen as follows. If we write $J_i = -eJ_i{}^e$ in (14), we have

$$(\partial\bar{\mu}/\partial x_i)n_i = \iota\rho_{ij}J_j \cdot n_i - S_i{}^*(\partial T/\partial x_j)n_i.$$

Now we assume the resistive sheath to be isotropic, so that $\rho_{ij}=0$ for $i \neq j$, $\rho_{ii} \equiv \rho_s$; and if we further assume that the second term on the right-hand side of this last equation is negligible compared with the first, we find in crossing the boundary

$$\begin{aligned} \Delta\bar{\mu} \equiv \bar{\mu}^R - \bar{\mu}^X &= (\partial\bar{\mu}/\partial x_i)n_i d \\ &= (\partial\bar{\mu}/\partial s)d \cong e\rho_s(J_i n_i)d, \end{aligned} \tag{29}$$

where s is distance along the normal n and d is the thickness of the resistive sheath. Because of (26), it makes no difference which current components, $J_i{}^X$ or $J_i{}^R$, are used in the last parentheses in (29), and we choose $J_i{}^R$.

$$\begin{aligned} e^{-1}(\bar{\mu}^X J_i{}^X n_i - \bar{\mu}^R J_i{}^R n_i) &= e^{-1}(\bar{\mu}^X - \bar{\mu}^R)J_i{}^R n_i \\ &= e^{-1}(-e\rho_s J_i{}^R n_i d)J_i{}^R n_i = -\rho_s d(J_i{}^R n_i)^2. \end{aligned} \tag{30}$$

We can now rewrite (28):

$$\begin{aligned} &[\kappa_{ij}{}^X(\partial T/\partial x_j)^X n_i - \kappa_{ij}{}^R(\partial T/\partial x_j)^R n_i] - \rho_s d(J_i{}^R n_i)^2 \\ &\quad + e^{-1}T(S_{ij}{}^{*X}J_j{}^X n_i - S_{ij}{}^{*R}J_j{}^R n_i) = 0. \end{aligned} \tag{31}$$

Expression (31) describes the heat generation and transport at the boundary region between inhomogeneous, anisotropic media X and R and is the surface analog of the "volume" Eq. (19). We name the second and third sets of terms as follows:

$$\left.\begin{aligned} &\text{Joule: } q_J \equiv -\rho_s d(J_i n_i)^2, \qquad (32) \\ &\text{Peltier: } q_P \equiv e^{-1}(S_{ij}{}^{*X}J_j{}^X n_i - S_{ij}{}^{*R}J_j{}^R n_i). \qquad (33) \end{aligned}\right\} \text{(Surface effects)}$$

Each of the "q" represents a heat *absorbed* per unit area per unit time.

We next set down the definitions:

$$\Pi_{ij} \equiv +\frac{1}{e}TS_{ij}{}^* \equiv \Pi_{ij}(T; x_1, x_2, x_3), \tag{34}$$

$$\tau_{ij} \equiv -e^{-1}T(\partial S_{ij}{}^*/\partial T)_{x_i} \equiv \tau_{ij}(T; x_1, x_2, x_3); \tag{35}$$

we call Π_{ij} the *Peltier coefficient matrix* and τ_{ij} the *Thomson coefficient matrix* for a given inhomogeneous, anisotropic medium at temperature T and at point x_1, x_2, x_3 within the medium, when referred to rectangular coordinate axes x_1, x_2, x_3. Relations (22) through (25) for the volume heating effects become, with i, $j = 1, 2, 3$,

$$\left.\begin{aligned} &\text{Joule: } Q_J \equiv -\rho_{ij}J_i J_j, \qquad (36) \\ &\text{Peltier: } Q_P \equiv -(\partial\Pi_{ij}/\partial x_i)J_j, \qquad (37) \\ &\text{Thomson: } Q_T \equiv \tau_{ij}J_j\partial T/\partial x_i, \qquad (38) \\ &\text{Bridgman: } Q_B \equiv -\Pi_{ij}\partial J_j/\partial x_i; \qquad (39) \end{aligned}\right\} \text{(Volume effects)}$$

and (32) and (33) for the surface heating effects become

$$\text{Joule:}\quad q_J \equiv -\rho_s d(J_i n_i)^2, \qquad \left.\begin{matrix}\\ \\ \end{matrix}\right\}\ \text{(Surface effects)} \quad (40)$$

$$\text{Peltier:}\quad q_P \equiv -(\Pi_{ij}{}^R J_j{}^R - \Pi_{ij}{}^X J_j{}^X) n_i. \quad (41)$$

DISCUSSION

Starting with the isotropic theory of thermoelectricity we have postulated the fundamental relations (8) and from these have deduced without further assumptions the Ehrenfest-Rutgers equations (21). In addition, the irreversible effects of heat conduction and Joulean heat generation are included in the present theory in a natural way. Using our equations it is an easy matter to set down various boundary conditions appropriate to a given experimental arrangement, and thus one can easily derive the ordinary Kelvin symmetry relations which, as first shown clearly by Kohler,[7] are correct only for isothermal boundary conditions. If one applies adiabatic boundary conditions, he can derive more general relations which have been found by Kohler to give better agreement with experiment.

The author wishes to thank Mr. Erik Klokholm and Dr. D. P. Detwiler for several helpful discussions in connection with this work. Also, he wishes to express his appreciation for the encouragement as well as financial support he has received from the Squier Signal Laboratories. Finally, he thanks Dr. F. C. Nix for his continued interest and encouragement in the author's work.

PHYSICAL REVIEW VOLUME 92, NUMBER 4 NOVEMBER 15, 1953

Change of Electrical Conductivity of Sodium Chloride upon Bombardment with High-Energy Protons*

EDGAR A. PEARLSTEIN
Carnegie Institute of Technology, Pittsburgh, Pennsylvania
(Received July 15, 1953)

The conductivity of NaCl in the region 125°C to 400°C is considerably decreased by bombardment at room temperature with 10^{16} protons/cm² of energy 350 Mev. There are several temperatures where part of the effect anneals. A small decrease in conductivity still remains after heating to as high as 470°C. No satisfactory explanation for the results is evident.

A new method of measuring conductivity is described.

THE generally accepted picture of electrical conductivity of alkali halides is a motion of ions associated with the presence of lattice defects. Since nuclear radiation is known to produce lattice defects, it is of interest to study the conductivity of irradiated crystals and the annealing of the changes at various temperatures.

Single crystals of sodium chloride (obtained from the Harshaw Chemical Company) were bombarded with 350-Mev protons in the Carnegie Institute of Technology synchrocyclotron. Crystals of the order of a millimeter thick and a few square centimeters area were placed inside the cyclotron's vacuum chamber in the direct path of the circulating proton beam. Aluminum foil mounted alongside the crystals was used to measure the amount of irradiation by means of the reaction $Al^{27}(p,3pn)Na^{24}$.[1] It is estimated that the temperature of the crystals probably did not get higher than about 50°C during irradiation. Most crystals had been annealed in a helium atmosphere at 650°C after cleaving and before irradiation.

The conductivity measuring apparatus is shown in Fig. 1. This circuit compares the resistance of the crystal with the input resistance of the oscilloscope. This particular arrangement allows one to observe any polarization effects and to eliminate trouble with dc amplifier drift, or the capacitance of the crystals. The conductivity was measured over the temperature range from about 125° to 470°C, the lower limit being determined by the sensitivity of the apparatus, and the upper limit by failure of the electrodes on the crystal. The crystal holder holds two specimens at the same temperature so that a bombarded crystal can be directly compared with a "control" crystal (cut from the same large crystal as the bombarded one) which has not been bombarded. This gives one confidence about the reproducibility of the data. The maximum resistance detectable with the apparatus as shown is 2×10^{11} ohms. Electrodes were either graphite ("Dag") or silver conducting paint (Dupont 4817).

RESULTS

Figure 2 shows typical results, expressed as the ratio of the conductivity of a control crystal to that of an irradiated crystal. The arrows indicate time, the sequence starting from top left. The figure shows that there are several ranges of temperature where healing

* This work is supported by the U. S. Atomic Energy Commission. The results reported here were briefly described by the author at the meeting of the American Physical Society in Durham, North Carolina, March 28, 1953 [Phys. Rev. **91**, 244 (1953)].

[1] L. Marquez, Phys. Rev. **86**, 405 (1952).

takes place; it takes about one hour for healing at these temperatures. There are some ranges of temperature where there is no perceptible healing in several hours: 200° to 250° and 350° to 470°C. After all of this heat treatment, the conductivity at low temperatures is completely restored, but at higher temperatures it is still about 25 percent below that of an unirradiated crystal, as shown at the bottom of Fig. 2. This behavior is found in several specimens, having different amounts of bombardment in the vicinity of 10^{15} protons/cm^2. At present, nothing can be said about the dependence of the effects upon the amount of bombardment.

The bombarded crystals are strongly colored, and are kept in the dark after removal from the cyclotron. One specimen was partially bleached by exposure to skylight for several hours. Its conductivity was then measured. No differences were noted between it and a specimen which had not been bleached. Bombarded crystals are completely bleached, as far as the naked eye can tell, by heating to about 200°C.

DISCUSSION

It might seem that bombardment would increase the conductivity of an ionic crystal, since the conductivity

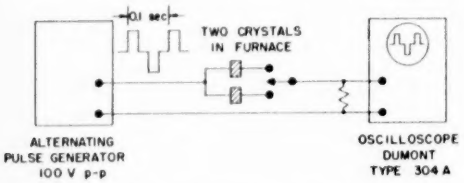

FIG. 1. Apparatus for measuring conductivity.

is ionic, and heavy particle bombardment should produce extra vacancies. Calculations based on the formulas of Seitz[2] indicate that each 350-Mev proton should produce about three sodium vacancies per centimeter of path. As Fig. 2 shows, the conductivity is appreciably decreased rather than increased by the bombardment.

These results are not in good agreement with the results of Nelson, Sproull, and Caswell[3] at Oak Ridge. They irradiated potassium chloride crystals with gamma rays from cobalt 60, and fast neutrons from a pile.

[2] F. Seitz, Discussions Faraday Soc. No. 5 (1949).
[3] Nelson, Sproull, and Caswell, Phys. Rev. **90**, 364 (1953). Also, private communication.

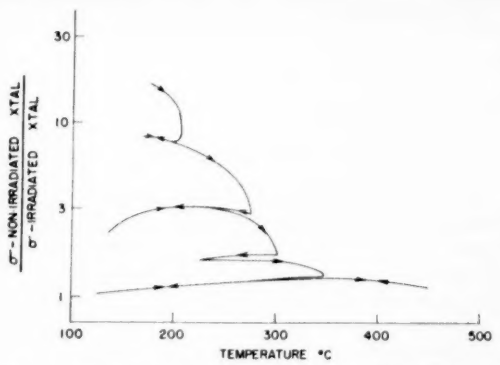

FIG. 2. Relative conductivity *vs* temperature for NaCl crystal irradiated with about 10^{15} protons/cm^2. The measurements started at the highest point on the curve and proceeded in time as indicated by the arrows.

They got both increases and decreases in conductivity, depending on conditions. But in all cases annealing of the change in conductivity was almost complete after a few hours at 200°C. Differences between their results and the results reported in this paper might be caused by differences in material, or type, energy, and amount of radiation. (The amount of irradiation received in our experiment is, of course, very small when compared to, say, pile irradiation.) Also interesting in this connection is the work of Mapother,[4] who found that self-diffusion of NaCl was decreased during x-ray irradiation.

It is hard to visualize a satisfactory mechanism to account for these results. Mechanisms involving only the electrical neutralization of vacancies by electrons or holes and non-equilibrium concentration of vacancies seem unlikely in view of the difficulty of completely annealing the specimens. Perhaps the motion of vacancies is impeded by mechanical distortions of the lattice in the vicinity of interstitial atoms or clusters of interstitials and/or vacancies; however it is possible that such distortions might have the net result of increasing, rather than decreasing the mobility of ions.[5]

It is intended to pursue this problem further with quantitative studies of annealing, dependence of the effects on the amount of bombardment, and correlation with optical effects.

The author is grateful to Professor R. Smoluchowski for advice and discussions.

[4] D. E. Mapother, Phys. Rev. **89**, 1231 (1953).
[5] A. W. Overhauser, Phys. Rev. **90**, 398 (1953).

Interaction of a Nonrelativistic Particle with a Scalar Field with Application to Slow Electrons in Polar Crystals*

TSUNG-DAO LEE† AND DAVID PINES
Department of Physics, University of Illinois, Urbana, Illinois
(Received August 10, 1953)

A general variational technique is developed to study the effect of recoil on the motion of a nonrelativistic particle in a scalar field. The ground-state energy is determined, and the results obtained are shown to be exact in the limit of both weak and strong field-particle coupling. This method is applied to investigate the low-lying energy levels of a conduction electron in a polar crystal. The ground-state energy and effective mass so obtained are shown to be in good agreement with the results of Lee, Low, and Pines for the intermediate coupling strengths occurring in real polar crystals.

I

THE motion of a nonrelativistic particle in a scalar field serves as a prototype for a wide variety of problems. Amongst these are the interaction between low-energy nucleons and scalar mesons, and the electron-lattice interaction in polar crystals, semiconductors, and metals. In these cases the field-particle interaction is frequently not weak so that the usual perturbation-theoretic methods are inapplicable. For such cases in which the coupling is not weak and in which the recoil of the source particle may be neglected, Tomonaga[1] has recently introduced a very useful method of approximation which has acquired the sobriquet, "intermediate coupling" approximation.

The Tomonaga approximation consists in a variational technique based on the physical assumption that successive virtual quanta (mesons or phonons) in the field around the source particle (nucleon or electron) are emitted independently, and hence that there is no correlation between different quanta. It is essentially a Hartree-Fock approximation, in that all identical quanta associated with the ground state of the system are assumed to be in the same physical state. The number of quanta in the field around the source is not limited. The probability amplitude for finding a given number of quanta and the particular functional form for their momentum distribution are found by a Rayleigh-Ritz variational calculation. This method for the case of the interaction of a charged meson with a fixed nucleon leads to the correct answer in the limit of both weak and strong coupling.

However, when the source particle is not fixed, it is easy to see that correlations will be introduced between successive field quanta since the recoil kinetic energy of the source will then come into play. Such correlations are indeed favored, especially when the field-particle coupling is strong, because they will act to reduce the momentum fluctuation of the source particle. Thus it is necessary to extend Tomonaga's formulation in such a way as to allow correlation between quanta to enter into the problem. This can be done by introducing additional degrees of freedom for the field quanta, such that a quantum can be emitted into any one of several states. Our generalization of Tomonaga's formulation is rendered easier by the introduction of certain formal techniques which are developed in Appendix I.

We shall show that for the case of zero total momentum of the system (source plus quanta) it is sufficient to introduce four possible states for the field quanta corresponding to one "s" and three "p" states. Indeed, the introduction of these extra degrees of freedom makes possible an *exact* solution in both the weak and strong coupling limits of the field-particle interaction. In the strong coupling limit the importance of correlations between successive quanta is reflected in the fact that the mean value of the source recoil kinetic energy turns out to be proportional to the square root of the total number of field quanta, in contrast to the linear dependence predicted by both weak coupling theory and the simple Tomonaga model neglecting such correlations.

Our variational technique is applied to the problem of a slow conduction electron (polaron) moving through a polar crystal, and both the ground-state energy and the polaron effective mass are calculated. For this latter case, in which the total system momentum is not zero, it is necessary to introduce somewhat more complicated trial functions than those required for zero system momentum. For the intermediate coupling strengths ($g^2 \lesssim 6$) encountered in real crystals, we find that the ground state energy differs very slightly from that calculated by Lee, Low, and Pines[2] using the simple Tomonaga approximation. The effective mass correction is somewhat larger and may be as appreciable as twenty percent for $g^2 \sim 5$.

II

The Hamiltonian for a nonrelativistic particle interacting with a scalar field may be written as

$$H = p^2/2m + g\Sigma_k (V_k a_k e^{i\mathbf{k}\cdot\mathbf{r}} + V_k^* a_k^* e^{-i\mathbf{k}\cdot\mathbf{r}}) + \Sigma_k \omega(k) a_k^* a_k, \quad (1)$$

* This work has been supported in part by the Office of Ordnance Research, U. S. Army.

† Now at Physics Department, Columbia University, New York, New York.

[1] S. Tomonaga, Prog. Theoret. Phys. **2**, 6 (1947).

[2] T. D. Lee and D. Pines, Phys. Rev. **88**, 960 (1952); Lee, Low, and Pines, Phys. Rev. **90**, 297 (1953), hereafter referred to as LLP. See also M. Gurari, Phil. Mag. **44**, 329 (1953).

where $(\mathbf{r}, \mathbf{p})$ are the position and momentum of the particle, α_k^* and α_k are the creation and annihilation operators for the scalar field, $\omega(k)$ is the frequency of the kth normal mode of this field, and g is the appropriate dimensionless coupling constant characterizing the strength of the field-particle interaction.[3] We find it convenient to take advantage of the fact that the total momentum of the system is a constant of the motion. The total momentum operator is $\Sigma_k \mathbf{k}\alpha_k^*\alpha_k + \mathbf{p}$ and commutes with the Hamiltonian, (1). It is therefore possible to transform to a representation in which the total momentum operator is diagonal and in which the Hamiltonian no longer contains the particle coordinates. The unitary transformation required is generated by

$$S = \exp i[(\mathbf{P} - \Sigma_k \alpha_k^* \alpha_k \mathbf{k}) \cdot \mathbf{r}],$$

which transforms

$$H \to S^{-1}HS = (\mathbf{P} - \Sigma_k \mathbf{k}\alpha_k^*\alpha_k)^2/2m + \Sigma_k \omega(k)\alpha_k^*\alpha_k + g\Sigma_k(V_k\alpha_k + V_k^*\alpha_k^*), \quad (2)$$

where $\mathbf{P}$ is a "c" number representing the total system momentum.

Let us first consider the case in which $P=0$. We shall use a variational technique and work in a representation in which the Schrödinger function Ψ of our system is described by a set of functions corresponding respectively to states of no quanta, one quantum, two quanta, etc. Let $\langle \mathbf{k}_1\mathbf{k}_2\cdots\mathbf{k}_N/\Psi\rangle$ be the probability amplitude of finding N quanta of momenta $\mathbf{k}_1\mathbf{k}_2\cdots\mathbf{k}_N$ respectively in the field around the source particle, assuming these quanta are distinguishable. A trial function which corresponds to allowing field quantum emission into one of four possible states is

$$\langle k_1\cdots k_N/\Psi\rangle = C_{n,m_1,m_2,m_3}(n!\prod_i m_i!/N!)^{\frac{1}{2}} \times S[\prod_{i=1}^{n} f(k_i) \prod_{j_1=n+1}^{n+m_1} g_x(k_{j_1}) \prod_{j_2=n+m_1+1}^{n+m_1+m_2} g_y(k_{j_2}) \times \prod_{j=n+m_1+m_2+1}^{N} g_z(k_{j_3})], \quad (3)$$

where $f(k)$ is a normalized "s" wave function for the field quanta, and the $g_x(k)$, etc., are the three normalized "p" wave functions. C_{n,m_1,m_2,m_3} is the probability amplitude for finding n "s" quanta, and m_1, m_2, and m_3 of the three kinds of "p" quanta, respectively. S is the symmetrization operator with respect to all quanta, and we also have

$$n + m_1 + m_2 + m_3 = N,$$

where N may vary from zero to infinity. The functional form of $f(k)$ and $g_i(\mathbf{k})$, together with the numerical value of the C_{n,m_1,m_2,m_3}, are to be determined in such a way as to minimize the system energy. It is clear that since no preferred direction exists (for $P=0$), our three "p" state wave functions must have the same radial dependence. Thus we have

$$g_i = (k_i\sqrt{3}/k)g(k), \quad (i = x, y, z), \quad (4)$$

where $g(k)$ is a normalized "s" wave function.

The calculation of this mean energy for a trial function of the form (3) is quite complicated. However, the manipulations in such mean value calculations may be simplified considerably by going over to a suitable reduced space for the operators α_k and α_k^*. In Appendix I, we show that if the Hamiltonian is ordered in such a way that *annihilation operators always appear on the right of creation operators*, then these operators may be formally replaced by

$$\alpha_k \to \alpha f(k) + \Sigma_i \beta_i k_i [\sqrt{3} g(k)/k], \quad (5)$$

with a corresponding expression for α_k^*. α and β_i are the annihilation operators for "s" and "p" wave quanta and are independent of k. The problem of finding the minimum energy for the Hamiltonian (2) then reduces to solving the equivalent minimum value problem in the reduced space,

$$\delta E = \delta \langle \Phi | \mathfrak{H} | \Phi \rangle = 0, \quad (6)$$

where Φ is a normalized reduced space wave vector, and $\mathfrak{H}$ is given by

$$\mathfrak{H} = \omega_1 \alpha^*\alpha + \omega_2 \sum_{i=x}^{z} \beta_i^*\beta_i + g(V\alpha + V^*\alpha^*) + M \sum_{i=x}^{z} [(\beta_i^*)^2\alpha^2 + (\alpha^*)^2\beta_i^2 + 2\alpha^*\beta_i^*\alpha\beta_i], \quad (7)$$

where[4]

$$\omega_1 = \Sigma_k(\omega + k^2/2m)|f(k)|^2, \quad (8a)$$

$$\omega_2 = \Sigma_k(\omega + k^2/2m)|g(k)|^2, \quad (8b)$$

$$V = \Sigma_k V(k) f(k), \quad (8c)$$

$$M = [\Sigma_k f^*(k) g(k) k]^2/6m. \quad (8d)$$

In carrying out the variation of E with respect to Φ, we shall restrict our trial function to the form

$$\Phi = [\exp(\alpha^* u)] F(\beta_i^*)|0\rangle, \quad (9)$$

where u is an arbitrary real numerical constant (to be determined variationally) and F is an arbitrary function of β_i^*. $|0\rangle$ is the state vector corresponding to no quanta in the field. This choice will be seen to be sufficiently general to enable us to obtain an exact solution in the limit of both strong and weak coupling. Using (9), we see that

$$\alpha\Phi = u\Phi,$$

and thus

$$\mathfrak{H}\Phi = [(\omega_1 - 3M)u^2 + 2guV + \omega_2\Sigma_i\beta_i^*\beta_i + Mu^2\Sigma_i(\beta_i + \beta_i^*)^2]\Phi. \quad (10)$$

The ground-state energy corresponding to (10) may

[3] Both $\hbar$ and the system volume will be taken $=1$ throughout this paper.

[4] It will be seen that V and M are both real.

readily be obtained, since the eigenvalue problem is just that of three simple harmonic oscillators. We find

$$E=(\omega_1-3M)u^2+2guV+\tfrac{3}{2}\omega_2[(1+4Mu^2/\omega_2)^{\frac{1}{2}}-1]. \quad (11)$$

Thus our minimum value problem becomes one of minimizing E with respect to the parameter u and the arbitrary functional form of $f(k)$ and $g(k)$.

We now wish to examine the solution of our minimum value problem in the limit of both weak and strong coupling. For both these limits, on differentiating (11) with respect to u it may easily be seen that u will be proportional to g. In the weak coupling case, ($g\ll 1$), we find on expanding in a power series in g,

$$E=\omega_1 u^2+2guV+O(g^3)+\cdots, \quad (12)$$

so that the minimum value of the energy with respect to u is

$$E=-g^2V^2/\omega_1. \quad (13)$$

In this limit, E depends only on $f(k)$. This follows from the fact that in our Hamiltonian the interaction term between the source particle and the field quanta directly excites only "s" waves, and hence just involves $f(k)$. The "p" waves are coupled to the source indirectly through their coupling with the "s" waves via the recoil term. Consequently in the limit of weak coupling these will only influence the energy for higher power of g.

Upon minimizing E with respect to an arbitrary functional variation of $f(k)$ we find the best form of $f(k)$ is

$$f(k)=\frac{N_1V^*(k)}{\omega+k^2/2m}, \quad (14)$$

where N_1 is a normalization constant. The corresponding minimum value for the energy is

$$E_0=-g^2\sum_k\frac{|V(k)|^2}{\omega+k^2/2m}. \quad (15)$$

This is precisely the familiar expression derivable from second-order perturbation theory.

For the strong coupling limit ($g\gg 1$), we find on expanding in a power series in $(1/g)$.

$$E=[(\omega_1-3M)u^2+2guV][1+O(1/g)], \quad (16)$$

so that minimum value of the energy with respect to u is

$$E=-g^2V^2/(\omega_1-3M). \quad (17)$$

Upon minimizing E with respect to an arbitrary functional variation of $f(k)$ and $g(k)$ we find these take the following optimum forms:

$$f(k)=N_1V(k)/\omega(k), \quad (18a)$$

$$g(k)=N_2f(k)k, \quad (18b)$$

where N_1 and N_2 are normalization constants. The corresponding minimum value for the energy is

$$E_0=-g^2\sum_k\frac{|V(k)|^2}{\omega(k)}. \quad (19)$$

To show that this is indeed the exact solution in the strong coupling limit, we return to our original Hamiltonian, (2). We note that if the recoil terms, $(\Sigma_k\mathbf{k}a_k^*a_k)^2/2m$, were absent, the minimum value of the energy would be just (19). The recoil term is, however, always positive, so that (19) constitutes a lower bound for the energy. On the other hand, E_0 is the result of a variational calculation and is hence an upper bound for the ground-state energy. Since the upper and lower bounds here coincide, E_0 must be the exact ground-state energy.

The magnitude of the recoil term can be obtained by carrying out the expansion of (16) in powers of $(1/g)$ to the next order, and one finds that it is of order g. Since the total number of quanta ($N=\alpha^*\alpha+\Sigma_i\beta_i^*\beta_i$) is on the average proportional to g^2, this result indicates that the mean square momentum fluctuation of the source particle, $\langle p^2\rangle_{Av}$, is proportional to $\langle N\rangle_{Av}^{\frac{1}{2}}$. If there were no correlation between the direction of emission of successive quanta by the source particle, $\langle p^2\rangle_{Av}$ would be proportional to $\langle N\rangle_{Av}$. Consequently in the strong coupling limit these correlations are seen to play a very important role by acting in such a way as to limit the recoil kinetic energy to order g.[5]

It is perhaps surprising that one can obtain an exact solution in the strong coupling case by using a simple trial function of the form (3) and (9). This may be understood in the following way. As we have remarked, in the general Hamiltonian (2), the source is directly coupled only to "s" waves. This coupling is linear in the amplitude of the "s" waves, and thus its main effect is to produce a simple displacement in the "s" wave amplitude, as reflected in our restricted trial wave function (9). The number of "s" quanta in the field is then proportional to g^2. On the other hand, the recoil term may be regarded as giving rise to a dipole-type coupling between the field quanta, i.e., "s" waves are coupled only with "p" waves, which in turn are coupled in addition just to "d" waves, etc. In virtue of this coupling, which according to (10) gives rise to a change in frequency for the "p" waves, the number of "p" wave quanta is proportional to the square root of the number of "s" wave quanta and hence to g. Since the "d" wave couples to the "p" wave in similar fashion, the total number of "d" wave quanta will be of still higher order in $1/g$, and their influence may be neglected, corresponding to our trial function (3).

For intermediate coupling strengths, the ground-

[5] A direct calculation of the strong coupling limit in this problem is also possible, provided one introduces creation and annihilation operators for spherical waves, rather than the plane waves used in (1). Similar results concerning the ground-state energy and the role of the source recoil can be obtained.

state energy depends on the specific form of $V(k)$, and we shall not enter on a general discussion of this here. In the following section we shall consider the detailed solution in this range of coupling for the polaron problem. It may be of interest to note here that the general form of $f(k)$ and $g(k)$ can be obtained by minimizing E with respect to arbitrary functional variations of $f(k)$ and $g(k)$, under the constraint that these functions are normalized. We find these may be written as

$$f(k)=\frac{N_1 V_k^*(k^2+2m\omega+\lambda)}{(k^2+2m\omega)^2+\mu(k^2+2m\omega)+\gamma+\eta k^2}, \tag{20}$$

$$g(k)=\frac{N_2 f k}{k^2+2m\omega+\lambda}, \tag{21}$$

where N_1 and N_2 are normalization constants, and λ, μ, γ, η are numerical constants to be determined by our variational calculation.

III

We now wish to apply the above considerations to a determination of the ground state energy of the polaron. In this case, we have from LLP,

$$V_k=-\frac{\omega i}{k}\left(\frac{8\pi^2}{m\omega}\right)^{\frac{1}{4}}, \tag{22}$$

$$g^2=\frac{e^2}{2c}\left(\frac{2mc^2}{\omega}\right)^{\frac{1}{2}}\left(\frac{1}{n^2}-\frac{1}{\epsilon}\right), \tag{23}$$

where n and ϵ are the optical index of refraction and the static dielectric constant, respectively, and ω is the constant frequency of the longitudinal optical mode of the lattice vibrations.[6] There exists a natural cutoff for our interaction in k space, k_0, due to the discrete nature of the crystal structure, and we shall understand that in this section k is always considered to be less than k_0. For the continuum theory of lattice vibrations, k_0 is the usual Debye limit.

For the case of the polaron, our weak coupling solution, (15), becomes, on substituting (22),

$$E_0=-g^2\omega, \tag{24}$$

a solution first obtained by Frohlich, Pelzer, and Zienau.[7] In the strong coupling limit, in contrast to weak coupling, the cutoff k_0, plays an important role, and we find from (19) and (22)

$$E_0=-\frac{2}{\pi}\left(\frac{k_0^2}{2m\omega}\right)^{\frac{1}{2}}g^2\omega. \tag{25}$$

It is of some interest to investigate the region of validity of our strong coupling solution, (25). This can be estimated by a consideration of the importance of the terms neglected in (16), and one finds that the strong coupling limit is valid when

$$g\gg\tfrac{3}{2}(M\omega_2/V^2)^{\frac{1}{2}}. \tag{26}$$

On substituting (8) and (18) into (26) we find

$$g^2\gg(3/40\pi)(k_0^2/2m\omega)^{\frac{1}{2}}. \tag{27}$$

For typical polar crystals $k_0^2/2m\omega\sim100$, and hence the criterion for the validity of the strong coupling solution is

$$g^2\gg25.$$

For real polar crystals, the coupling constant g^2 is generally of the order of 3 to 6, so that neither the weak nor strong coupling solutions are valid. Thus it is necessary to find the minimum value of E, (11), more precisely. The calculation is straightforward, albeit somewhat complicated, and the details are given in Appendix II. The results of a numerical calculation for three values of the coupling constant g^2 are given in Table I. We note that $-E_0/\omega$ is always greater than

TABLE I. Ground-state energy and polaron effective mass for three values of the coupling constant.

g^2	$-E_0/\omega$	m_{eff}/m	$1+g^2/6$
5.2	5.52	2.21	1.86
10	11.17	3.96	2.67
15	17.56	6.35	3.50

g^2, the result obtained by perturbation theory and also by the simple one-phenon state Tomonaga approximation of LLP. However, as anticipated by LLP, for the case of NaCl, where $g^2=5.2$, the correction is quite small, being of the order of five percent.

IV

In this section we consider the calculation of the effective mass of the source particle for the general Hamiltonian, (2). In order to do this, we must consider the case in which our Hamiltonian (2) describes a system for which $P\neq0$. We will however confine our attention to very small system momenta, such that $(P^2/2m\omega)\ll1$. For the effective mass is defined by the relation,

$$\frac{1}{2m_{\text{eff}}}=\left(\frac{\partial E}{\partial P^2}\right)_{P^2=0}, \tag{28}$$

and hence it is sufficient to calculate E to order P^2.

When $P\neq0$ it is necessary to adopt a somewhat more general trial function than that given in (3). This may be done by introducing in place of the spherically symmetric $f(k)$ an arbitrary function $F(k)$ which is normalized and orthogonal to the $g_1(k)$. The functional forms of $F(k)$ and $g_1(k)$ again are determined by the variational principle. Since we are only interested in

[6] Here g^2 denotes the coupling constant instead of α as used by LLP.

[7] Frohlich, Pelzer, and Zienau, Phil. Mag. 41, 221 (1950).

calculating E to order P^2, it will be sufficient to use a wave function which is accurate to order P. To this order, the $g_i(k)$ are found to be unchanged. However, $F(k)$ differs from the spherically symmetric $f(k)$ by the addition of a "p_z" wave, i.e.,

$$F(k)=f(k)+(dk_z\sqrt{3}/k)h(k)P+O(P^2),$$

where d is a constant, $h(k)$ is a spherically symmetric function, and we have taken $\mathbf{P}$ in the z direction. The presence of a "p_z" wave in $F(k)$ thus corresponds to a removal of the symmetry among the "p" waves and is to be expected since for $P\neq 0$ a preferred direction exists, namely that of $\mathbf{P}$.

The effective mass calculation is similar to that for the ground-state energy and is given in Appendix III, where we derive the following expression for the source particle effective mass,

$$m_{\text{eff}}/m=1+(4/3)\Sigma_k|f(k)|^2\{k^2/[k^2+2m\omega(k)]\}u^2, \quad (29)$$

where u and $f(k)$ are determined by the $P=0$ calculation. It may be seen directly that this expression reduces to the appropriate perturbation theory value in the limit of weak coupling. However, in contrast to the $P=0$ calculation, our expression (29) cannot be regarded as yielding the correct strong coupling limit, since the latter expression is not yet known.

For the polaron, we utilize the numerical results following from Appendix II, and the results of our calculation for three values of the coupling constant are given in Table I. There we have compared these new results with that obtained by LLP

$$m_{\text{eff}}/m=1+\tfrac{1}{6}g^2.$$

We remark that in general the change in effective mass due to our consideration of additional "p" wave phonon excitation is in the direction of increasing m_{eff}. Percentage-wise this correction is considerably large for m_{eff} than for the corresponding ground state energy calculation. For $g^2=5.2$, we find an increase of $\sim$twenty percent in m_{eff} over the LLP value, which is in good agreement with their estimate of the accuracy of their method. This leads us to believe that the present calculation is quite reliable for such intermediate coupling strengths.

We should like to thank Professors J. Bardeen, M. Gell-Mann, and F. Low for pleasant discussions on these and related matters.

APPENDIX I

In this appendix we should like to establish some elementary theorems concerning the use of Tomonaga-type wave functions. For simplicity we confine our attention to a trial function which corresponds to allowing field quantum emission into one of two possible states, which are described by any two orthonormal functions $f(k)$ and $g(k)$. Thus

$$\langle k_1\cdots k_n|\Psi\rangle=C_{n-m,m}\left(\frac{(n-m)!m!}{n!}\right)^{\frac{1}{2}}\times S[\prod_{i=1}^{n-m}f(k_i)\prod_{j=n-m+1}g(k_i)],$$

where S is the symmetrization operator with respect to all quanta. The system wave function Ψ may then be expressed in terms of the vacuum state as

$$\Psi=\sum_{n=0}^{\infty}\sum_{m=0}^{n}C_{n-m,m}\frac{1}{[(n-m)!m!]^{\frac{1}{2}}}\times(\sum_k f(k)\alpha_k^*)^{n-m}(\sum_k g(k)\alpha_k^*)^m|0\rangle,$$

where $|0\rangle$ denotes the vacuum state. Consider now a reduced space wave vector defined by

$$\Phi=\sum_{n=0}^{\infty}\sum_{m=0}^{n}D_{n-m,m}\frac{1}{[(n-m)!(m!)]^{\frac{1}{2}}}(\alpha^*)^{n-m}(\beta^*)^m|0\rangle,$$

where α^* and β^* are two independent creation operators which are not related to k. Φ and Ψ will be considered to describe equivalent physical situations if and only if $D_{n-m,m}=C_{n-m,m}$.

Theorem 1: If $\Psi\leftrightarrow\Phi$ and $\Psi'\leftrightarrow\Phi'$ then $\langle\Psi'|\Psi\rangle=\langle\Phi'|\Phi\rangle$.
Proof:

$$\langle\Psi'|\Psi\rangle=\sum_{n=0}^{\infty}\sum_{m=0}^{n}(C'_{n-m,m})^*(C_{n-m,m})$$

is by definition the same as $\langle\Phi'|\Phi\rangle$.

Theorem 2: If $\Psi\leftrightarrow\Phi$, then $\alpha_k\Psi\leftrightarrow[\alpha f(k)+\beta g(k)]\Phi$.
Proof: The coefficient of the term $(\Sigma_k f(k)\alpha_k^*)^{n-m}\times(\Sigma_k g(k)\alpha_k^*)^m|0\rangle$ in $\alpha_k\Psi$ is

$$[C_{n-m+1,m}(n-m+1)^{\frac{1}{2}}f(k)+C_{n-m,m+1}(m+1)^{\frac{1}{2}}g(k)]\times\frac{1}{[(n-m)!m!]^{\frac{1}{2}}},$$

which is the same as the corresponding coefficient of the term $(\alpha^*)^{n-m}(\beta^*)^m|0\rangle$ in $[\alpha f(k)+\beta g(k)]\Phi$. We remark that $\alpha_k^*\Psi$ is by no means equivalent to $[\alpha^* f(k)+\beta^* g(k)]\Phi$.

Theorem 3: If $\Psi\leftrightarrow\Phi$, and $\Psi'\leftrightarrow\Phi'$, then

$$\langle\Psi'|\prod_{i=1}^{N}\alpha_{k_i}^*\prod_{j=1}^{M}\alpha_{k_j}|\Psi\rangle=\langle\Phi'|\prod_{i=1}^{N}[\alpha^* f^*(k_i)+\beta^* g^*(k_i)]\prod_{j=1}^{M}[\alpha f(k_j)+\beta g(k_j)]|\Phi\rangle.$$

Proof: From Theorem 2, one has

$$\prod_{j=1}^{M}\alpha_{k_j}\Psi\leftrightarrow\prod_{j=1}^{M}[\alpha f(k_j)+\beta g(k_j)]\Phi.$$

and

$$\prod_{i=1}^{N}\alpha_{k_i}\Psi'\leftrightarrow\prod_{i=1}^{N}[\alpha f(k_i)+\beta g(k_i)]\Phi'.$$

Thus on using Theorem 1, one sees that Theorem 3 follows immediately.

These theorems can obviously be generalized to trial functions which allow quantum emission into one of any number of possible states.

APPENDIX II

For the case of the polaron for which ω is a constant, our general trial functions, (20) and (21), may be written as

$$f(k)=\frac{N_1 V_k^*(k^2+a^2)}{(k^2-b^2)^2+c^2k^2},$$

$$g(k)=\frac{N_2 k V_k^*}{(k^2-b^2)^2+c^2k^2},$$

where a, b, c are numerical constants to be determined. On substituting these expressions into (8a)–(8d), together with our expression (22) for V_k, we find, on changing the summation over k to an integral, and carrying out the indicated integrations,[8]

$$\omega_1=\omega\left\{1+\frac{c^2+(1+a^2/b^2)^2b^2}{(1+a^2/b^2)^2+a^4c^2/b^6}\right\},$$

$$\omega_2=\omega(1+b^2),$$

$$M=\frac{\omega}{3}\frac{b^2[1+(a^2/b^2)^2]}{(1+a^2/b^2)^2+a^4c^2/b^6},$$

$$V^2=6Mc\omega/b^2.$$

In obtaining these expressions, we have introduced dimensionless variables, in that all momenta (k, a, b, c) are measured in units of $(2m\omega)^{\frac{1}{2}}$. We then find that our general expression for E, (11) may be written as

$$\frac{E}{\omega}=\left[\frac{(1+a^2/b^2)^2+a^4c^2/b^6+c^2}{b^2(1+a^2/b^2)^2}\right][1+b^2]x^2+\frac{2g[(1+b^2)(2c)]^{\frac{1}{2}}x}{b}+\tfrac{3}{2}(1+b^2)\times\{[1+(4x^2/3)]^{\frac{1}{2}}-1\},\quad\text{(A1)}$$

where we have found it convenient to introduce

$$x^2=\frac{b^2(1+a^2/b^2)^2u^2}{(1+b^2)[(1+a^2/b^2)^2+a^4c^2/b^6]}$$

as a new independent variable in place of u^2. Thus our minimum value problem is reduced to minimizing (A1) with respect to the four parameters a, b, c, and x.

On varying (A1) with respect to a, one finds the simple result:

$$a^2=b^4.\quad\text{(A2)}$$

[8] The upper limit of integration may be taken as ∞ to a good degree of approximation as long as $g^2<15$.

On minimizing (A1) with respect to c, one finds

$$c=[g^2b^2(1+b^2)/2x^2]^{\frac{1}{3}}.\quad\text{(A3)}$$

Using these relationships, and minimizing with respect to x and b, one finds, after considerable simplification,

$$b^2=1+[1+(4/3)x^2]^{\frac{1}{2}},\quad\text{(A4)}$$

$$x^2=\frac{g^2b^2}{2(1+b^2)^{\frac{1}{2}}}\left(\frac{b^2-1}{2b^2-1}\right)^{\frac{1}{2}}.\quad\text{(A5)}$$

The corresponding value for the energy, (A1), is

$$\frac{E}{\omega}=-\frac{(1+b^2)(5b^2-2)x^2}{b^2(b^2-1)}+\tfrac{3}{2}(1-b^2)(b^2-2).\quad\text{(A6)}$$

Equations (A4) and (A5) may then be solved numerically to obtain the optimum values of b and x, which on substitution into (A6) yield the minimum value of the ground state energy E_0. The results for three values of the coupling constant are given in Table I.

APPENDIX III

As we have remarked, it is necessary to adopt a somewhat more general trial function than (3) for the case of $\mathbf{P}\neq 0$. This may be done by introducing an arbitrary function $F(\mathbf{k})$ in place of the "s" wave function $f(k)$. $F(\mathbf{k})$ is normalized and orthogonal to the $g_i(k)$. For small P, we may expand $F(\mathbf{k})$ as

$$F(\mathbf{k})=f(k)+d(k_z\sqrt{3}/k)h(k)P+O(P^2)+\cdots,$$

where $h(k)$ is symmetric. This form of $F(\mathbf{k})$ is just that adopted by LLP in the simple Tomonaga case. Thus we may regard our trial function in this case, just as was true for $P=0$, as a generalization of the LLP treatment in that we have simply added three "p" waves to take the correlation between quanta into account. One may then proceed to calculate the dependence of E on P^2 in a completely analogous manner to our $P=0$ calculation, with the difference that the energy should now be varied with regard to d and the functional form of $h(k)$ in addition to the other indicated variations. One finds that

$$E=(\omega_1-3M)u^2+2gVu+\tfrac{3}{2}\omega_2[(1+4Mu^2/\omega^2)^{\frac{1}{2}}-1]+\frac{P^2}{2m}-P^2\left\{\frac{[(M/m)^{\frac{1}{2}}u-\frac{1}{2}\omega_4 ud-2(2MN)^{\frac{1}{2}}u^3d]^2}{\frac{1}{2}\omega_2+2Mu^2}+(4Nu^2+\omega_3)u^2d^2-2(2N/m)^{\frac{1}{2}}u^2d\right\},\quad\text{(A7)}$$

where M, ω_1, ω_2, and V are defined in (8a)–(8d) and N, ω_3, ω_4 are

$$N=(\Sigma_k h^* gk)^2/6m,$$

$$\omega_3=\Sigma_k|h|^2(\omega+k^2/2m),$$

$$\omega_4=\Sigma_k h^* g(\omega+k^2/2m).$$

By inspection, we note that the optimum values for $f(k)$, $g(k)$, and u will differ from those obtained for $P=0$ only to order P^2. Consequently, this difference will contribute a change in the energy of order P^4 which may be neglected in our approximation of small P. Thus the determination of the effective mass reduces to finding that form of d and $h(k)$ which minimize (A7). This problem can, however, be simplified further by introducing an equivalent variational problem. This equivalent problem is obtained by regarding the operator β_z as a numerical constant. It may be readily verified that although this replacement yields a different value for E_0, the P^2 coefficient in the energy is unchanged, and it is this latter value which we seek to determine. Thus we write for our equivalent problem

$$\alpha_k \rightarrow \alpha[f(k)+\eta P\varphi(k)(k_z/k)\sqrt{3}] + (\beta_z k_z+\beta_y k_y)\sqrt{3}g(k)/k, \quad \text{(A8)}$$

instead of

$$\alpha_k \rightarrow \alpha F(k)+\sum_{i=x}^{z}\beta_i k_i\sqrt{3}g(k)/k.$$

In (A8), η is an arbitrary parameter and $\varphi(k)$ is a symmetric function which may be regarded as a linear combination of $g(k)$ and $h(k)$. Using (A8), we find that the P^2 terms in the energy may be written as

$$E_1(P)=P^2\left(\frac{1}{2m}+\eta^2u^2\omega'-4\eta u^2\left(\frac{M'}{2m}\right)^{\frac{1}{2}}+4M'u^4\eta^2\right), \quad \text{(A9)}$$

where

$$M'=[\Sigma_k\varphi^*(k)f(k)k]^2/6m,$$
$$\omega'=\Sigma_k(\omega+k^2/2m)|\varphi(k)|^2.$$

Upon minimizing (A9) with respect to η, we find

$$E_1=\frac{P^2}{2m}\frac{1}{1+4M'u^2/\omega'}. \quad \text{(A10)}$$

The variation with respect to $\varphi(k)$ is elementary and gives

$$\varphi(k)=N_3\frac{f(k)k}{k^2+2m\omega(k)}, \quad \text{(A11)}$$

where N_3 is a normalization constant. It is of interest to note that the corresponding best form of $h(k)$ is

$$h(k)=N_4\{\varphi(k)-[\Sigma_k\varphi(k)g^*(k)]g(k)\}.$$

On substituting (A11) into (A10), we obtain the effective mass,

$$\frac{m_{\text{eff}}}{m}=1+u^2(4/3)\sum_k\frac{|f(k)|^2k^2}{(k^2+2m\omega(k))}.$$

Electronic Polarizabilities of Ions in Crystals*

JACK R. TESSMAN† AND A. H. KAHN, *Department of Physics, University of California, Berkeley, California*

AND

WILLIAM SHOCKLEY, *Bell Telephone Laboratories, Murray Hill, New Jersey*

(Received August 10, 1953)

A set of electronic polarizabilities has been obtained from a least-squares fit of experimental refraction data using simple additivity and a Lorentz factor of $4\pi/3$. Except for the fluorides, the electronic polarizability values of the alkali-halide crystals calculated from this set agree with the experimental data within 3 percent. Similar least-squares fits were attempted with various values of the Lorentz factor, the best fit being obtained for $4\pi/3$. On the basis of $4\pi/3$, the additivity assumption and the alkali-halide set, polarizabilities have been obtained for other ions. The best values for the sodium D line in A^3 are Li^+ 0.03, Na^+ 0.41, K^+ 1.33, Rb^+ 1.98, Cs^+ 3.34, F^- 0.64, Cl^- 2.96, Br^- 4.16, I^- 6.43, Ca^{++} 1.1, Sr^{++} 1.6, Ba^{++} 2.5, O^{--} 0.5–3.2, S^{--} 4.8–5.9, Se^{--} 6.0–7.5, Te^{--} 8.3–10.2, Ag^+ 2.4, Cu^+ 1.6, Cu^{++} 0.2, Zn^{++} 0.8, Cd^{++} 1.8, Ge^{++} 1, Sn^{++} 3.4, Pb^{++} 4.9. Values represented by a spread indicate ions that cannot be treated additively.

I. INTRODUCTION

THE problem of electronic polarizability of individual ions has been the subject of numerous investigations. Among these, determinations of the polarizabilities of gaseous ions have been performed by Pauling[1] from the theory of the quadratic Stark effect, by Born and Heisenberg[2] from the Rydberg-Ritz correction for spectral series, by Fajans and Joos[3] from an examination of the indices of refraction of salts in aqueous solution, and by Mayer and Mayer[4] from spectral data.

A list of polarizabilities of ions in ionic crystals obtained from recent data, and an examination of the validity of employing the Lorentz factor, may be of use in the study of ferroelectricity. In the present paper we obtain values for the electronic polarizability of the alkali ions and halide ions from an examination of the indices of refraction of the alkali-halide crystals. Using these values as a starting point, we shall then obtain values for the electronic polarizability of a second group of ions that combine with the halide ions and form crystals for which optical data are available. In turn, the polarizabilities of these ions will be used to determine the polarizabilities of other ions which do not form halide crystals.

Throughout, the calculations will be based on the assumptions that the crystals considered are purely ionic, that the electronic polarizability of a crystal is simply the sum of the electronic polarizabilities of the individual ions, and that the Lorentz factor has a normal value of $4\pi/3$. The consistency of the results can be considered as a measure of the validity of these assumptions. It has been suggested[5] that the normal Lorentz factor may not be correct for some crystals because of the extended nature of the electronic charge distribution and the consequent overlapping of neighboring ions. However, we shall see that for the alkali-halides, the best fit of the empirical data is achieved with the normal Lorentz factor.

An empirical examination of the additivity of the total polarizability, ionic plus electronic, of individual ions has been made by Roberts.[6]

II. THE LORENTZ FACTOR

At optical frequencies, let the field acting on any ion of a crystal be expressed as

$$E_{\text{eff}}=E+LP, \tag{1}$$

where E is the applied field, P is the electronic polarization or electric dipole moment per unit volume, and L is a constant called the Lorentz factor. E and P are assumed to be in the same direction, and L is the same for all ions. The optical dielectric constant K is defined by

$$KE=E+4\pi P. \tag{2}$$

The optical dielectric constant and the index of refraction n are related, $K=n^2$.

If the electronic dipole moment p_i induced at each ion is proportional to E_{eff}, the factor of proportionality defines the electronic polarizability, α_i,

$$p_i=\alpha_i E_{\text{eff}}. \tag{3}$$

For a crystal of diatomic molecules, the dipole moment of each molecule is

$$p_m=p_i+p_j=(\alpha_i+\alpha_j)E_{\text{eff}}=\alpha_m E_{\text{eff}}. \tag{4}$$

Then

$$P=\alpha_m E_{\text{eff}}/V_m, \tag{5}$$

* Part of this work was reported to the American Physical Society at its meeting in Chicago of June 20–22, 1946. See W. Shockley, Phys. Rev. **70**, 105 (1946).

† Now at Department of Physics, Pennsylvania State College, State College, Pennsylvania.

[1] L. Pauling, Proc. Roy. Soc. (London) **A114**, 191 (1927).

[2] M. Born and W. Heisenberg, Z. Physik **23**, 388 (1924).

[3] K. Fajans and G. Joos, Z. Physik **23**, 1 (1924).

[4] J. E. Mayer and M. G. Mayer, Phys. Rev. **43**, 605 (1933).

[5] N. F. Mott and R. W. Gurney, *Electronic Processes in Ionic Crystals* (Oxford University Press, London, 1948), second edition, p. 16.

[6] S. Roberts, Phys. Rev. **76**, 1215 (1949).

TABLE I. Molecular volume V_m, indices of refraction at various wavelengths n_C, n_D, n_F, n_∞, and molecular electronic polarizability α_m of the alkali-halides. $C=6563$A, $D=5893$A, $F=4861$A.

Compound	V_m(A³)	n_C	n_D	n_F	n_∞	$\alpha_m(\lambda=D)$	$\alpha_m(\lambda=\infty)$
LiF	16.21		1.3915		1.386[b]	0.920A³	0.909A³
LiCl	33.74		1.662		1.658[b]	2.980	2.903
LiBr	41.37		1.784		1.778[b]	4.159	4.138
LiI	54.00		1.955		1.949[b]	6.248	6.226
NaF	24.65	1.3246	1.3258	1.3285	1.3188	1.186	1.163
NaCl	44.58	1.5407	1.5443	1.5534	1.5252	3.360	3.263
NaBr	52.95	1.6355	1.6412	1.6555	1.6111	4.560	4.388
NaI	67.46		1.7745		1.706[b]	6.721	6.264
KF	38.07		1.352		1.360[b]	1.966	2.008
KCl	61.86	1.4872	1.4904	1.4984	1.4770	4.272	4.173
KBr	71.42	1.5547	1.5594	1.5716	1.5332	5.508	5.293
KI	87.68	1.6589	1.6670	1.6876	1.6238	7.790	7.388
RbF	44.85	1.394	1.396	1.399	1.388	2.572	2.572
RbCl	69.93	1.4903	1.4936	1.5016	1.4765	4.856	4.712
RbBr	80.50	1.5483	1.5528	1.5646	1.5283	6.147	5.920
RbI	98.30	1.6397	1.6474	1.6672	1.6061	8.532	8.093
NaCl CsF	54.22	1.476	1.478	1.482	1.469	3.664	3.604
Structure CsCl	86.49	1.531	1.534	1.543	1.516	6.419	6.235
(α) CsBr	94.12[a]	1.577	1.582	1.594	1.566	7.497	7.329
CsI	112.80[a]	1.653	1.661	1.681	1.618	9.952	9.435
CsCl CsF	47.18	1.575	1.578	1.583	1.566	3.738	3.674
Structure CsCl	69.43	1.6377	1.6418	1.6523	1.6209	5.984	5.829
(β) CsBr	78.95	1.6924	1.6984	1.7126	1.6676	7.271	7.020
CsI	94.94	1.7784	1.7876	1.8115	1.7378	9.577	9.119

[a] Values obtained from density measurements.

[b] Values taken from Højendahl.

where V_m is the volume of the crystal divided by the number of molecules in the crystal.

From the above equations, it follows simply that

$$\alpha_m = V_m \frac{n^2-1}{Ln^2-L+4\pi}. \tag{6}$$

If L has the normal Lorentz value of $4\pi/3$, then Eq. (6) becomes the familiar Lorentz expression

$$\alpha_m = \frac{3V_m}{4\pi}\frac{n^2-1}{n^2+2}. \tag{7}$$

For an assembly of parallel point dipoles, located at the lattice points of a diagonal cubic lattice, such as the NaCl, CsCl, CaF_2, and ZnS type lattices, with equal dipoles at like-ion lattice points, the local field at any lattice point, E_{eff}, is correctly given by Eq. (1) with $L=4\pi/3$. For other lattices, the Lorentz factor L may have different values, but the sum of the three Lorentz factors for three mutually perpendicular arrangements of the parallel point dipoles is always 4π.

III. THE ALKALI-HALIDES AND THE EMPIRICAL DETERMINATION OF THE LORENTZ FACTOR

We shall first consider the alkali-halide crystals. These have either the NaCl-type structure in which the Na ions and Cl ions are each arranged on a f.c.c. lattice and together form a s.c. lattice, or the CsCl type structure in which the Cs ions and Cl ions are each arranged on a s.c. lattice and together form a b.c.c. lattice.

In Table I are listed the molecular volume V_m, the indices of refraction n at several wavelengths, and the electronic polarizability α_m for the alkali-halide molecules. The molecular volumes are obtained from x-ray data.[7] The refraction data are obtained from the compilation by Winchell.[8] The value of n for $\lambda=\infty$ is obtained by extrapolating to $\lambda=\infty$ the straight line which is fitted, by the method of least squares, to the Cauchy relation $n=A+B/\lambda^2$. In those cases where the only refraction data available are for the D line, the values of n for $\lambda=\infty$ are taken from a calculation by Højendahl.[9] The molecular electronic polarizability α_m is computed from Eq. (7).

On the basis of the values of the molecular electronic polarizability α_m, contained in Table I, a set of electronic polarizabilities α_A and α_H, was computed for all the alkali and halide ions by minimizing the sum of the squares of the differences in electronic polarizability as

TABLE II. Electronic polarizability of alkali ions and halides ions for $\lambda=D$ and $\lambda=\infty$.

	$(\lambda=D)$ α_A(A³)	$(\lambda=\infty)$ α_A(A³)		$(\lambda=D)$ α_H(A³)	$(\lambda=\infty)$ α_H(A³)
Li^+	0.029	0.029	F^-	0.644	0.759
Na^+	0.408	0.255			
K^+	1.334	1.201	Cl^-	2.960	2.974
Rb^+	1.979	1.797	Br^-	4.158	4.130
Cs^+	3.335	3.137	I^-	6.431	6.199

[7] R. W. G. Wyckoff, *Crystal Structure* (Interscience Publishers, New York, 1951).

[8] A. Winchell, *Microscopic Characters of Artificial Inorganic Substances or Artificial Minerals* (John Wiley and Sons, Inc., New York, 1931) second edition.

[9] K. Højendahl, Kgl. Danske Videnskab. Selskab, Mat.-fys. Medd. **16**, No. 2, 90 (1938).

TABLE III. Comparison of electronic polarizabilities, α_m of the alkali-halides, taken from Table I, with $\alpha_A+\alpha_H$, taken from Table II, (a) for $\lambda=D$; (b) for $\lambda=\infty$. First line α_m. Second line $\alpha_A+\alpha_H$. All values are in A³.

	F	Cl	Br	I
		(a) $\lambda=D$		
Li	0.920	2.980	4.159	6.248
	0.673	2.989	4.187	6.459
Na	1.186	3.360	4.560	6.721
	1.053	3.368	4.566	6.839
K	1.966	4.272	5.508	7.790
	1.981	4.297	5.495	7.767
Rb	2.572	4.856	6.147	8.532
	2.623	4.939	6.137	8.409
Cs	3.664	6.419	7.497	9.952
	3.979	6.295	7.493	9.765
		(b) $\lambda=\infty$		
Li	0.909	2.903	4.137	6.225
	0.788	3.003	4.159	6.228
Na	1.162	3.263	4.387	6.263
	1.014	3.227	4.385	6.452
K	2.007	4.172	5.294	7.388
	1.960	4.175	5.330	7.397
Rb	2.528	4.712	5.920	8.092
	2.556	4.772	5.929	7.996
Cs	3.604	6.235	7.328	9.436
	3.896	6.108	7.266	9.333

given by Table I and as given by α_A+A_H. Thus,

$$\sum_i(\alpha_{m_i}-\alpha_{A_i}-\alpha_{H_i})^2 \tag{8}$$

was made a minimum. The summation is over the 20 alkali-halide compounds of Table I. Cs compounds of the NaCl structure only are included in order to deal with crystals all having the same structure.

Table II gives the resulting computed values of electronic polarizability of the alkali and halide ions for $\lambda=5893$A and $\lambda=\infty$. The electronic polarizability of one of the ions must be selected arbitrarily in order to form such a table, since the minimizing of (8) still permits the polarizability of each of the alkali ions to be raised by a constant amount if the polarizability of each of the halide ions is reduced by the same amount. The electronic polarizability of Li^+ was taken as 0.029A³ from Pauling's calculation. Since Li^+ has the smallest electronic polarizability, large percentage errors in its value produce only small percentage changes in the polarizability of the other ions, and of course, no change in the value of $\alpha_A+\alpha_H$.

In Tables III(a) and III(b), the electronic polarizability values α_m are compared with $\alpha_A+\alpha_H$ obtained from Table II for $\lambda=D$ and $\lambda=\infty$. Deviations are no greater than 3 percent except for the fluorides where they are as high as 22 percent for $\lambda=D$ and 13 percent for $\lambda=\infty$.

In order to determine the best empirical value to use for the Lorentz factor, L in Eq. (6), the electronic polarizabilities α_m of Table I were recomputed for $\lambda=\infty$, using Eq. (6) with various values of L. For each value of L, a new set of electronic polarizabilities was computed for the 9 ions of Table II, by minimizing expression (8). A comparison is made in Fig. 1 between values of the sum of the squares of the deviations $\sum_i(\alpha_{m_i}-\alpha_{A_i}-\alpha_{H_i})^2$ for different values of L, and also between values of the mean square deviation divided by the mean polarizability,

$$\sum_i(\alpha_{m_i}{}^2-\alpha_{A_i}-\alpha_{H_i})^2/\sum_i\alpha_{m_i},$$

for different values of L. The second expression is the more significant measure of the effect of varying L, because as L increases, the calculated values of α_{m_i}, α_{A_i}, and α_{H_i} all decrease toward zero, causing $\sum(\alpha_{m_i}-\alpha_{A_i}-\alpha_{H_i})^2$ to approach zero.

It can be seen that these expressions have their minima in the neighborhood of $L=4\pi/3$ and are definitely larger for values of L less than $4\pi/3$. Hence, it may be concluded that the normal Lorentz factor of $4\pi/3$ appears to be highly satisfactory for computing a set of electronic polarizabilities for the individual alkali and halide ions such that the appropriate sums give the electronic polarizabilities of the alkali-halide molecules.

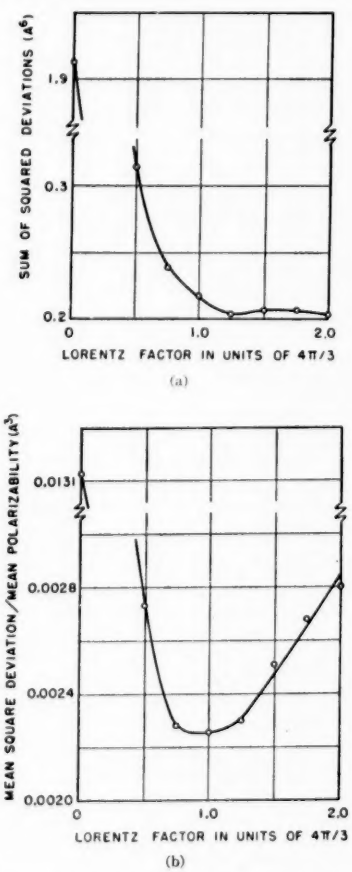

FIG. 1. Plots of the sum of the squared deviations, $\Sigma_i(\alpha_{m_i}-\alpha_{A_i}-\alpha_{H_i})^2$ *vs* Lorentz factor; and the mean square deviation/mean polarizability, $\Sigma_i(\alpha_{m_i}-\alpha_{A_i}-\alpha_{H_i})^2/\Sigma_i\alpha_{m_i}$, *vs* Lorentz factor.

TABLE IV (a). Molecular volumes, indices of refraction, molecular electronic polarizabilities, and electronic polarizabilities for ions which form diagonal cubic halide crystals.

Compound	V_m(A³)	n_D	α_m(A³)	Ion	α(A³) Electronic polarizability	$\alpha_{ Av}$(A³)
AgCl	42.67	2.071	5.327	Ag^+	2.37	
AgBr	47.98	2.252	6.593	Ag^+	2.44	2.4
TlCl	56.36	2.247	7.727	Tl^+	4.8	
TlBr	62.57	2.418	9.225	Tl^+	5.1	5.2
TlI	73.98	2.78	12.238	Tl^+	5.8	
CuCl	39.49	1.973	4.628	Cu^+	1.67	
CuBr	45.83	2.116	5.872	Cu^+	1.71	1.6
CuI	55.16	2.345	7.899	Cu^+	1.47	
CdF_2	39.37	1.56	3.038	Cd^{++}	1.75	
SrF_2	48.38	1.440	3.043	Sr^{++}	1.76	1.7
$SrCl_2$	87.75	1.6499	7.465	Sr^{++}	1.55	
CaF_2	40.49	1.43385	2.516	Ca^{++}	1.23	See Table IV(b)
BaF_2	59.21	1.475	3.976	Ba^{++}	2.69	See Table IV(b)
NH_4Cl	57.78	1.6426	4.984	NH_4^+	2.024	
NH_4Br	66.28	1.7108	6.187	NH_4^+	2.029	See Table IV(b)
NH_4I	95.03	1.7031	8.796	NH_4^+	2.365	

IV. OTHER IONS

In Table IV (a), the list of electronic polarizabilities for $\lambda = D$ is extended to other ions that form compounds with the halide ions and for which data are available. It is again assumed that polarizabilities are additive. The crystals of IV (a) are all of the diagonal cubic type. The normal Lorentz factor $L = 4\pi/3$ is used.

In Table IV (b), noncubic crystals are listed. For these the Lorentz factor is not strictly $4\pi/3$. However, only crystals having small optical anisotropy are listed. Therefore, in the absence of more accurate Lorentz factors for many of the noncubic crystals which we shall examine, we shall continue to use $L = 4\pi/3$ together with the average value of the index of refraction.

In Table V, additional compounds are listed and values calculated for the electronic polarizability of various ions, again assuming additivity, and using the polarizability values already obtained above. Experimental data not available in Winchell[9] were obtained from the International Critical Tables.[10]

As we get further away from the alkali-halides, homopolar binding may be expected to play an increased

TABLE IV (b). Data for ions which form halide crystals which are not diagonal cubic.

Compound	V_m(A³)	n_D	α_m	Ion	α(A³) Electronic polarizability	α_{Av}(A³)
$BaCl_2$	85.88	$n_\alpha = 1.73024$ $n_\beta = 1.73611$ $n_\gamma = 1.74196$	8.235	Ba^{++}	2.32	2.5
$CaCl_2$	84.26	1.600 1.605 1.613	6.937	Ca^{++}	1.02	1.1
MgF_2	34.45[a]	$n_0 = 1.378$ $n_e = 1.390$	1.914	Mg^{++}	0.63	
$MgCl_2$	64.34	1.675 1.59	5.581	Mg^{++}	−0.34	
$ZnCl_2$	73.01	1.687 1.713	6.705	Zn^{++}	0.79	
$FeCl_2$	63.44	$n_0 = 1.567$ $n_0 - n_e$ weak	4.948	Fe^{++}	−0.97	
$PbCl_2$	78.96	2.199 2.217 2.260	10.713	Pb^{++}	4.79	
SnI_4	220.97[a]	2.106	28.157	Sn^{4+}	2.43	
$GeBr_4$	207.79[a]	1.6269	17.578	Ge^{4+}	0.95	
$SiCl_4$ (liquid)	189.94[a]	1.412	11.281	Si^{4+}	−0.56	
NH_4F	46.74[a]	1.328	2.263	NH_4^+	1.62	2.0 See Table IV (a)

[a] Values obtained from density measurements.

[10] *International Critical Tables* (McGraw-Hill Book Company, Inc., New York, 1926), first edition.

TABLE V. Polarizabilities of additional ions.

Compound	V_m(A³)	n_{Ag}	α_m(A³)	Ion	α(A³)
$LiKSO_4$	98.00	1.4721	6.552	SO_4^{--}	5.19
Na_2SO_4	87.62	1.477	5.910	SO_4^{--}	5.09
K_2SO_4	107.22	1.4952	7.467	SO_4^{--}	4.80
Rb_2SO_4	120.23	1.5136	8.634	SO_4^{--}	4.68
Cs_2SO_4	138.70	1.5635	10.761	SO_4^{--}	4.09
$CaSO_4$	75.10	1.587	6.025	SO_4^{--}	4.9
$SrSO_4$	76.93[a]	1.626	6.500	SO_4^{--}	4.8
$BaSO_4$	86.08	1.639	7.393	SO_4^{--}	4.9
$ZnSO_4$	68.71	1.666	6.099	SO_4^{--}	5.3
Tl_2SO_4	125.53	1.8708	13.620	SO_4^{--}	3.2
$PbSO_4$	81.12	1.884	8.896	SO_4^{--}	4.1
$(NH_4)_2SO_4$	122.46	1.5256	8.966	SO_4^{--}	5.0
NaOH	31.15	1.3576	1.630	OH^-	1.22
Li_2CO_3	58.34[a]	1.522	4.246	CO_3^{--}	4.2
Na_2CO_3	70.05[a]	1.498	4.901	CO_3^{--}	4.1
$CaCO_3$	76.47[a]	1.6073	6.306	CO_3^{--}	5.2
$SrCO_3$	66.17	1.615	5.512	CO_3^{--}	3.8
$BaCO_3$	73.88	1.627	6.252	CO_3^{--}	3.8
$ZnCO_3$	46.83	1.751	4.559	CO_3^{--}	3.8
$PbCO_3$	67.22	1.897	7.447	CO_3^{--}	2.7
KNO_3	80.29	1.4489	5.139	NO_3^-	3.81
$RbNO_3$	78.65[a]	1.518	5.688	NO_3^-	3.71
$CsNO_3$	87.58[a]	1.553	6.691	NO_3^-	3.36
$AgNO_3$	64.85	1.753	6.326	NO_3^-	3.93
$Sr(NO_3)_2$	117.55[a]	1.567	9.166	NO_3^-	3.7
$Ba(NO_3)_2$	133.78[a]	1.572	10.508	NO_3^-	4.0
$PbNO_3$	121.26	1.782	12.167	NO_3^-	3.69
NaCN	49.54	1.452	3.191	CN^-	2.78
KCN	68.97	1.410	4.079	CN^-	2.75
Li_2O	24.64	1.644	2.129	O^{--}	2.07
Cu_2O	39.72[a]	2.705	6.428	O^{--}	3.2
CaO	27.60	1.837	2.910	O^{--}	1.8
SrO	34.03	1.870	3.690	O^{--}	2.0
BaO	42.12	1.980	4.959	O^{--}	2.5
ZnO	24.18[a]	2.009	2.903	O^{--}	2.1
CdO	25.77	2.49	3.900	O^{--}	2.2
PbO	39.35	2.622	6.218	O^{--}	1.4
SiO_2	37.58[a]	1.5472	2.845	O^{--}	1.7
SnO_2	35.20	2.0288	4.280	O^{--}	0.9
CaS	45.81	2.137	5.940	S^{--}	4.8
SrS	50.57	2.107	6.447	S^{--}	4.7
BaS	64.01	2.155	8.380	S^{--}	5.9
ZnS	39.63	2.368	5.729	S^{--}	4.9
CdS	49.70[a]	2.514	7.586	S^{--}	5.8
CaSe	51.61	2.274	7.165	Se^{--}	6.1
SrSe	60.45	2.220	8.181	Se^{--}	6.5
BaSe	72.53	2.268	10.042	Se^{--}	7.5
CaTe	63.86	2.51	10.039	Te^{--}	8.9
SrTe	67.71	2.408	9.945	Te^{--}	8.2
BaTe	85.24	2.440	12.672	Te^{--}	10.2
ZnTe	55.91	3.56	10.618	Te^{--}	9.8
Na_2SiO_3	84.34	1.523	6.149	SiO_3^{--}	5.3
$CaSiO_3$	66.30	1.628	5.617	SiO_3^{--}	4.5
$BaSiO_3$	80.45	1.675	7.216	SiO_3^{--}	4.7
$CuSO_4$	73.46[a]	1.732	7.013	Cu^{++}	2.3

[a] Values obtained from density measurements.

role. The simple additivity assumption of the pure ionic crystal would tend to lose validity. This perhaps may explain the negative polarizability values in Table IV (b) and the spread in polarizability values exhibited in Table V. It would also greatly decrease the usefulness of polarizability values deduced from data involving the presence of the ion in question is only one compound.

Table VI lists the polarizabilities as determined by Fajans and Joos, Born and Heisenberg, Pauling, and the present method.

V. CONCLUSION

As may have been expected, the assumption of simple additivity in crystals leads in some cases to an appreciable spread of the values of the electronic polarizability of an ion as calculated from different compounds. This would result from a departure from the ideal ionic crystal state and an overlapping and distortion of the ionic wave functions. The values obtained, however, do give an approximate measure of the electronic polarizabilities of various ions in crystals, rather than as "free" ions.

In the case of the alkali-halides, we have seen that departure from additivity is not to be attributed to the departure of the Lorentz factor from its normal value

TABLE VI. Electronic polarizabilities of ions (in A³).

Ion	Fajans and Joos	Born and Heisenberg	Pauling	Present paper ($\lambda = D$)
Li^+	0.08	0.075	0.029	0.03
Na^+	0.196	0.21	0.179	0.41
K^+	0.88	0.87	0.83	1.33
Rb^+	1.56	1.81	1.40	1.98
Cs^+	2.56	2.79	2.42	3.34
Cu^+	...	...	...	1.6
Ag^+	...	...	...	2.4
Be^{++}	0.04	...	0.008	...
Mg^{++}	0.12	0.012	0.094	...
Ca^{++}	0.51	...	0.47	1.1
Sr^{++}	0.86	1.42	0.86	1.6
Ba^{++}	1.68	...	1.55	2.5
Zn^{++}	...	...	...	0.8
Cd^{++}	...	...	...	1.8
B^{3+}	0.02	...	0.003	...
Al^{3+}	0.067	0.065	0.052	...
Sc^{3+}	0.35	...	0.286	...
Y^{3+}	...	...	0.55	...
La^{3+}	1.3	...	1.04	...
C^{4+}	0.012	...	0.0013	...
Si^{4+}	0.04	0.043	0.0165	...
Ti^{4+}	0.236	...	0.185	...
Ge^{4+}	...	...	...	1.
Zr^{4+}	...	...	0.37	...
Sn^{4+}	...	...	...	3.4
Ce^{4+}	...	...	0.73	...
O^{--}	2.75	...	3.88	0.5–3.2
S^{--}	8.6	...	10.2	4.8–5.9
Se^{--}	11.2	...	10.5	6.0–7.5
Te^{--}	15.7	...	14.0	8.3–10.2
F^-	0.98	0.99	1.04	0.64
Cl^-	3.53	3.05	3.66	2.96
Br^-	4.97	4.17	4.77	4.16
I^-	7.55	6.28	7.10	6.43
NH_4^+	...	...	...	2.0
Tl^+	...	...	...	5.2
Fe^{++}	...	...	...	−1.
Cu^{++}	...	...	...	0.2
Pb^{++}	...	...	...	4.9
CN^-	...	...	...	2.8
NO_3^-	...	...	...	3.4–4.0
CO_3^{--}	...	...	...	2.7–5.2
SiO_3^{--}	...	...	...	4.5–5.3
SO_4^{--}	...	...	...	3.0–5.3

TABLE VII. Molecular volumes, cation volumes, volume per O^{--} ion, molecular polarizabilities, cation polarizabilities, and polarizability of O^{--} in the presence of various ions. All values in A^3.

Compound	V_m	V_{cation}	$V_{O^{--}}$	$(4\pi/3)\alpha_m$	$(4\pi/3)\alpha_{cation}$	$(4\pi/3)\alpha_{O^{--}}$
BeO	13.8	0.1	13.7	5.4	0.03	5.4
MgO	18.6	1.15	17.4	7.3	0.4	6.9
CaO	27.5	4.05	23.4	11.9	2.0	9.9
SrO	33.2	6.0	27.2	14.4	3.6	10.8
BaO	41.6	10.3	31.3	19.1	6.5	12.6
ZnO	24.0	1.7	22.3	11.3	1.2	10.1
CdO	26.1	3.8	23.3	16.6	4.5	12.1
HgO	32.0	5.5	26.5	20.4	5.2	15.2
Al_2O_3	42.3	0.6	13.6	17.2	0.2	5.6
Li_2O	24.7	0.9	22.8	8.9	0.1	8.7
TiO_2	30.9	1.3	14.7	19.5	0.8	9.3

of $4\pi/3$. On the contrary, the best fit of a set of electronic polarizabilities to the empirical data is obtained for a Lorentz factor of $4\pi/3$.

We should like to thank Elizabeth Wood for having collected some of the data, and C. Kittel and P. W. Anderson for discussions of the work. The research was assisted in part by U. S. Office of Naval Research. One of the authors (A. H. K.) is indebted to the National Science Foundation with whom he had a fellowship during the tenure of this work.

APPENDIX I

It has been reported by one of the authors[11] that some regularity can be observed in the spread of polarizabilities obtained for oxygen. Figure 2 shows a plot of the polarizability of the O^{--} ion as a function of the volume per O^{--} ion. The molecular volumes were determined from density measurements and the cation volumes are those given by empirical ionic radii.[7] (See Table VII.)

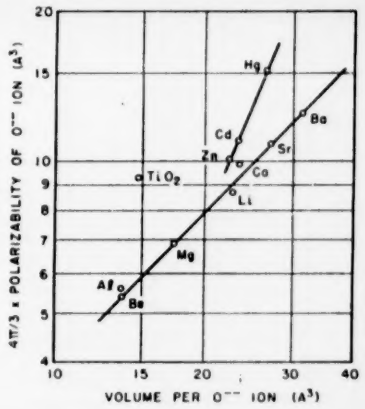

FIG. 2. Polarizability of the O^{--} ion as a function of volume per O^{--} ion for several compounds.

Polarizabilities for O^{--} were obtained from refractive index data, using a Lorentz factor of $4\pi/3$ for all compounds, regardless of high refractive anisotropy. The cation polarizabilities for determining the O^{--} polarizabilities were taken from Pauling's work. The graph of Fig. 2 shows that values of the O^{--} polarizability of Al, Be, Mg, Li, Ca, Sr, and Ba oxides fall near one line; Zn, Cd, and Hg about 20 percent higher and TiO_2 about 80 percent higher.

[11] W. Shockley, Phys. Rev. **73**, 1273 (1948).

Influence of Irradiation on the Characteristic of a Glow Discharge in Pure Rare Gases

K. W. MEISSNER AND W. F. MILLER
Purdue University, Lafayette, Indiana

(Received August 14, 1953)

Irradiation of the positive column of a glow discharge in pure rare gases by the radiation from a second discharge tube filled with the same gas influences the $V-I$ characteristic of the irradiated glow discharge, shifting it to a higher voltage for the same current. The effect arises from the reduction of the concentration of metastable atoms by absorption. In the case of helium the effect could be studied separately for the two mainly absorbed lines 10 830A and 20 581A. Practically the whole effect is caused by the latter. This result can be understood by considering the possible transitions involved.

INTRODUCTION

IT is well known that in a gaseous discharge metastable atoms play an important role as a source of secondary ionization. Thus, decreasing the lifetime and concentration of metastable atoms should have an effect on the characteristic quantities of the discharge. Such a decrease in lifetime and concentration may be effected by irradiation with light from an auxiliary discharge tube filled with the same gas. The explanation for this process may be given as follows.

Without irradiation the concentration of metastable atoms can be reduced by collisions which transfer the atoms to the ground state or which raise them to some nonmetastable state from which they may undergo transitions to the ground state either directly or by steps. With irradiation an additional process is involved, namely the absorption of radiation of the proper wavelength which raises the metastable atoms to nonmetastable states.

That the irradiation decreases the lifetime and concentration of metastable atoms, was first shown experimentally by Meissner and Graffunder[1] for neon and argon. More recently, much improved measurements have been carried out by Phelps and Molnar[2] who also have contributed new theoretical ideas. Further, Penning[3] found in experiments on starting potentials of neon and argon that the starting potentials are changed by addition of impurities to the main gas, the cause for which was attributed to a change in the role played by the metastable atoms. It was found that addition of a gas whose ionization potential is less than the excitation potential of the metastable atoms of the main gas causes a decrease in the starting potential. For example, a small amount of mercury added to argon resulted in the lowering of the starting potential of the mixture below that of pure argon. The following explanation was offered by Penning. Since the ionization potential of mercury (10.38 volt) is lower than the excitation potential of metastable argon atoms (11.49 volt), the mercury atoms may be ionized by collisions of the second kind, leaving the argon atoms in the ground state. In this manner metastable argon atoms cause the formation of secondary ions and herewith a decrease in the starting potential of the mixture. If the decrease of the starting potential is attributed to the action of the metastable atoms, then diminishing the number of metastable atoms present should again raise the starting potential. The reduction of metastable argon atoms may be achieved by either addition of a third gas or irradiation with argon light. Indeed, Penning found that irradiating the argon-mercury mixture with argon light raised the starting potential.

Similar experiments in mixtures of mercury and rare gases were carried out by Kenty,[4] who found that for a given value of current the tube voltage was raised appreciably by irradiating the discharge with light from another source of mercury vapor.

Penning[5] in two patent papers describes a similar effect on the $V-I$ characteristic curve for pure rare gases. The effect was found experimentally by Meissner and Pierson[6] for pure neon and rather pure helium.

In the present investigation the latter experiments were repeated for neon and pure helium and new experiments were conducted in pure argon, krypton, and xenon.

TECHNICAL DETAILS

A conventional vacuum system was employed to permit pressure control and purification of the rare gases. The design of the system varied slightly from gas to gas. In the case of helium, circulation through a charcoal trap at liquid nitrogen temperature was used. The other gases were cleaned by circulation through a large discharge tube, in which intense sputtering of the magnesium electrodes was maintained. After the tubes were sealed off from the vacuum system, the sputtered deposit from the molybdenum electrodes of the tubes themselves served as a getter. The dimensions and construction of the discharge tubes can be seen from Fig. 1.

The measurements of the $V-I$ characteristics of the discharge tubes were made by means of the electrical circuit shown in Fig. 2. The electric source was a dc

[1] K. W. Meissner and W. Graffunder, Ann. Physik **84**, 1009 (1927).
[2] A. V. Phelps and J. P. Molnar, Phys. Rev. **89**, 1202 (1953).
[3] F. M. Penning, Phil. Mag. **11**, 961 (1931).
[4] Carl Kenty, Phys. Rev. **80**, 95 (1950).
[5] F. M. Penning, U. S. Patent No. 1,958,066 May 8, 1934; U. S. Patent No. 2,080,926 May 18, 1937.
[6] K. W. Meissner and R. M. Pierson, Proc. Indiana Acad. Sci. **59**, 269 (1950).

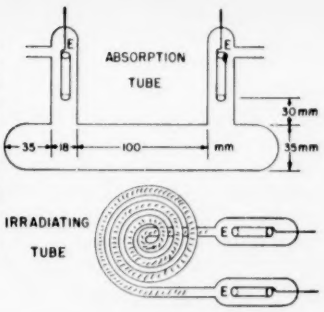

FIG. 1. Dimensions and construction of absorption tube and spiral shaped irradiating tube. *E* are hollow cylindrical molybdenum electrodes. The axes of the endparts of the irradiating tube containing the electrodes are in reality perpendicular to the plane of the spiral as indicated in Fig. 2.

choke input power supply employing full wave rectification with input controlled by a variac rated at 110 volt and 5 ampere. A 7500 volt transformer, a 4400 volt high current transformer, and a 0–15 000 volt dc Radar Power Unit served as sources for operating the irradiating tubes.

After cleaning the gases, the spiral shaped irradiating tubes were sealed off from the vacuum system. Before sealing off the absorption tubes, preliminary measurements were made to determine the pressure at which

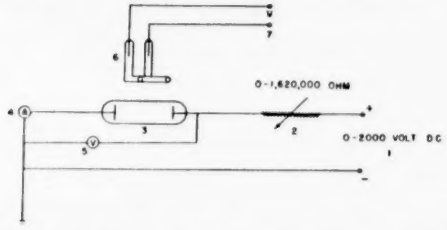

FIG. 2. Electrical Circuit. (1) dc power supply, (2) variable resistance, (3) absorption tube, (4) ammeter, (5) voltmeter, (6) irradiating tube, (7) power supply for 6.

the greatest irradiation effect is observed. The final measurements were made with the absorption tubes sealed off at optimum pressure. The irradiating tube was placed about 4 cm away from the absorption tube, and a grounded wire screen was interposed between irradiating tube and absorption tube. The position of the irradiating tube relative to the absorption tube was such that mainly the positive column was irradiated.

In all experiments the points on the $V-I$ characteristic curves were obtained by adjusting the tube current

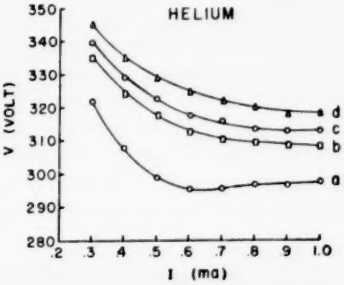

FIG. 3. Characteristics of helium (pressure 5.3-mm Hg) with different irradiating intensities. (a) without irradiation, (b) irradiation with source No. 1, (c) irradiation with source No. 2, (d) irradiation with sources No. 1 and No. 2.

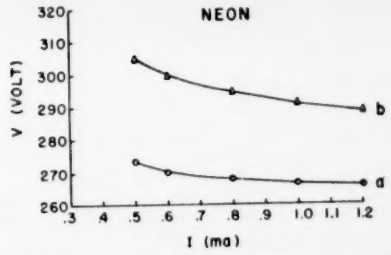

FIG. 4. Characteristics of neon (pressure 2.8-mm Hg). (a) without irradiation, (b) with irradiation.

to a desired value by emf control, reading the tube voltage, turning on the irradiating tube, adjusting the tube current back to the original value, and reading the new tube voltage. This procedure was repeated throughout the range of the measurements.

Two experiments were made to show that the changes in the $V-I$ characteristics were due only to incident irradiation. In the first experiment, instead of turning

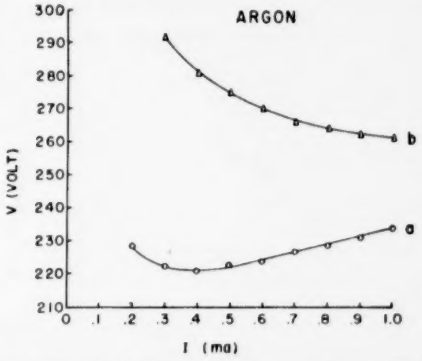

FIG. 5. Characteristics of argon (pressure 1.5-mm Hg). (a) without irradiation, (b) with irradiation.

off the irradiating tube to measure the $V-I$ curve without irradiation, the irradiating tube was left in operation, but a sheet of black paper was interposed between the two tubes. The results were the same as those obtained in the usual manner. In the second experiment the irradiating tube was placed about one meter from the absorption tube and the irradiation tube was focused on the positive column of the absorption

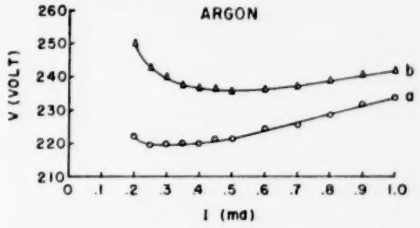

FIG. 6. Characteristics of argon (pressure 1.5-mm Hg), (a) without irradiation, (b) with irradiation produced by imaging the removed irradiating tube on the positive column of the absorption tube.

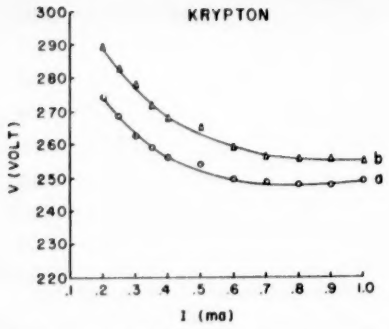

FIG. 7. Characteristics of krypton (pressure 1.1 mm Hg). (a) without irradiation, (b) with irradiation.

tube by a large concave mirror. The shift in the $V-I$ curve was about one-third of that observed for direct irradiation (compare Figs. 5 and 6), the difference being accounted for by the reduction of intensity with the mirror arrangement (diminished aperture and reflection losses).

EXPERIMENTAL RESULTS

Typical results of the experiments with helium are given in Fig. 3 for three different irradiation intensities. The greater the intensity, the greater is the shift of the $V-I$ characteristic to higher voltages for the same current value. The irradiation sources 1 and 2 were operated under different conditions such that source 2 was more intense than source 1.

Typical results for neon are shown in Fig. 4, for argon in Figs. 5 and 6, for krypton in Fig. 7, and for xenon in Fig. 8.

The outstanding irradiation effect found for argon at optimum pressure is of particular interest; however, thus far it has not been possible to find a satisfactory explanation for it. Most likely this outstanding effect is connected with the relative long mean life of argon metastables. Measurements of the lifetimes of metastable atoms under experimental conditions comparable to those of the present investigations have shown that for helium, neon, and argon the maximum values are 8×10^{-4} sec, 6×10^{-4} sec, and 35×10^{-4} sec, respectively.[1]

In the experiments already discussed the whole spectrum of emitted light from the irradiating tube was directed on the absorption tube. It would be of interest to separate the effects of the different strongly absorbed wavelengths. By use of filters it was possible for the case of helium to study separately the effects of the two strongly absorbed lines 10 830A and 20 581A. One of the filters employed was a glass cell containing a 1 mm thickness of water which absorbed the 20 581A line and transmitted the 10 830A line. The transmission of the water filter was checked by photography. The other filter employed was a 90 micron thick Biotite Mica[7] sheet which had 60 percent transmittance for 20 582A and 1 percent transmittance for 10 830A. The transmittance of the Biotite Mica was checked by means of a recording Perkin-Elmer infrared spectrometer.

Figure 9 shows the results of the filtering experiments. When the absorption tube was irradiated through the water filter, no detectable effect was produced, whereas irradiation through the Biotite Mica filter gave an effect corresponding to the high transmittance for the 20 581A line. These experiments show that practically the entire irradiation effect is due to absorption of the 20 581 line.

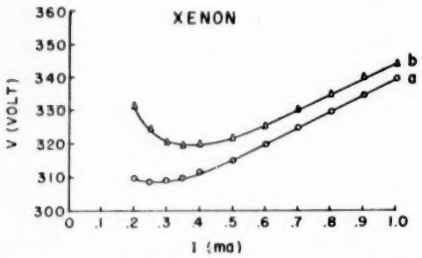

FIG. 8. Characteristics of xenon (pressure 3.5 mm Hg). (a) without irradiation, (b) with irradiation.

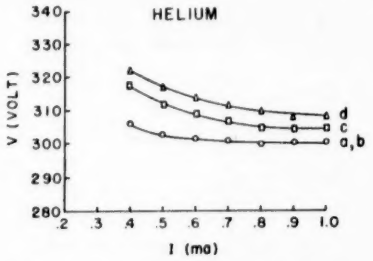

FIG. 9. Effect of filtered irradiation on the characteristics of helium (pressure 5.3 mm Hg). (a) without irradiation, (b) water filter transmitting 10 830A line, absorbing 20 582A line, (c) Biotite Mica filter transmitting 20 581A line, absorbing 10 830A line, (d) without filter.

This result can be explained as follows. The two strongly absorbed lines 20 581A and 10 830A start from the metastable states 2^1S_0 and 2^3S_1, respectively. Absorption of the 20 581A line raises the atoms from the 2^1S_0 state to the 2^1P_1 state from which most of them go to the ground state, emitting the strong 584A line. It is interesting to note that Paschen[8] had remarked in an early paper that no resonance radiation of the 20 581A line could be observed. Thus, absorption of the 20 581A line is quite effective in reducing the concentration of the 2^1S_0 metastables. However, absorption of the 10 830A line raises the metastable atoms from the 2^3S_1 state to the 2^3P state, from which the only permitted transition leads back to the metastable 2^3S_1 state. Hence, absorption of the 10 830A line has no detectable effect on the concentration of the 2^3S_1 metastables.

[7] A. Ignatieff, Ann. Physik **43**, 1123 (1914).
[8] F. Paschen, Ann. Physik **45**, 625 (1914).

Note on the Interchange of Rotational and Vibrational Energy in Collisions of Diatomic Molecules*

EDWARD H. KERNER†
Department of Physics, Iowa State College, Ames, Iowa
(Received July 27, 1953)

The results of a previous report are extended to molecule-molecule scattering with interchange of rotational or vibrational energy. Differential and total cross sections for O_2-N_2 scattering are given.

IN a previous report[1] we discussed the excitation of molecular rotations and vibrations in various inelastic scattering processes, giving detailed results for excitation by impinging single charged particles. In the present note we extend the results to include the case of a molecule A-A in a specified state of rotation or of vibration colliding with a molecule B-B initially in the ground state, with de-excitation of A-A to the ground state and excitation of B-B to A-A's former state. In addition, we investigate the process in which A-A is initially in a vibrationally excited state and excites B-B to a rotational state from its ground state, itself going finally to the ground state.

The general process for collisions of this type is discussed in reference 1 under "molecule-molecule collisions," so we just recapitulate briefly and state a few results. We use the Born approximation for the calculation of the scattering amplitude (since the internal velocities of rotation and vibration are small), Fues's model of the diatomic molecule to describe the vibration, and a simple repulsive potential of the form $v_{AB}=c\exp(-\alpha R_{AB})$ to describe the interaction of an A atom with a B atom. The latter merely assigns an effective range and strength to the interaction and has no quantitative significance beyond this.

For the transition A(state a), B(state b)$\rightarrow A$(state s), B(state t) we have the scattering amplitude (center-of-mass system), Eq. (13) of reference 1,

$$f(A(a),B(b);A(s),B(t))=\frac{-1}{4\pi}\frac{2\mu}{\hbar^2}4\int\exp(i\mathbf{K}\cdot\mathbf{s})v_{AB}(s)d\mathbf{s}\int f_s^*\times\cos(\tfrac{1}{2}\mathbf{K}\cdot\mathbf{r})f_a d\mathbf{r}\int\varphi_t^*\cos(\tfrac{1}{2}\mathbf{K}\cdot\boldsymbol{\varrho})\varphi_b d\boldsymbol{\varrho},$$

where μ is the reduced mass of A-A and B-B, $\mathbf{r}$ and $\boldsymbol{\varrho}$ the internal coordinates of A-A and B-B, and K the momentum change ($K^2=k_{ab}^2+k_{st}^2-2k_{ab}k_{st}\cos\theta$, θ being the angle of scattering in the center-of-mass system, and $k_{ij}^2=(2\mu/\hbar^2)(E-E_i-E_j)$, $E=\frac{1}{2}\mu v^2+E_a+E_b$, v = initial relative velocity of A-A and B-B). Using now Eqs. (7), (8), and (12) of reference 1, we construct at once the differential cross sections:

(a) for the interchange of rotational energy,

$$I(A(l),B(0);A(0),B(l))\equiv\frac{d\sigma}{d\omega}\frac{1}{c^2(\mu/m)^2}=\frac{k_{ab}}{k_{st}}\frac{256}{\pi}\frac{\alpha^2}{(\alpha^2+K^2)^4}(2l+1)^2 j_l^2(Ka)j_l^2(Kb);$$

(b) for the interchange of vibrational energy,

$$I(A(n),B(0);A(0),B(n))=\frac{k_{ab}}{k_{st}}\frac{256}{\pi}\frac{\alpha^2}{(\alpha^2+K^2)^4}J_{n0}^2(A)J_{n0}^2(B);$$

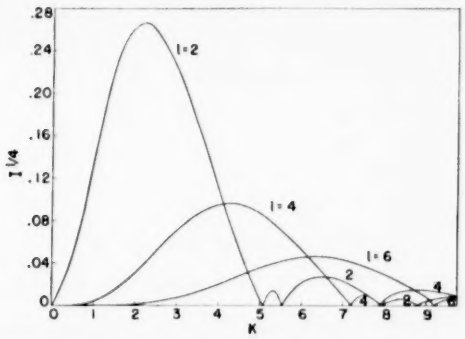

FIG. 1. Differential cross section for scattering of O_2 by N_2 with interchange of 2, 4, and 6 rotational quanta.

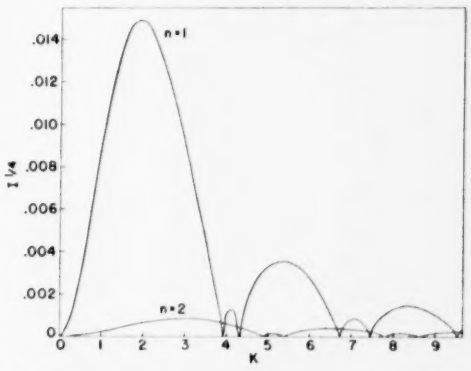

FIG. 2. Differential cross section for scattering of O_2 by N_2 with interchange of 1 and 2 vibrational quanta.

* The research reported in this paper has been sponsored by the Geophysics Research Directorate of the Air Force Cambridge Research Center, Air Research and Development Command.

† Present address: Physics Department, University of Buffalo, Buffalo, New York.

[1] E. H. Kerner, Phys. Rev. **91**, 1174 (1953).

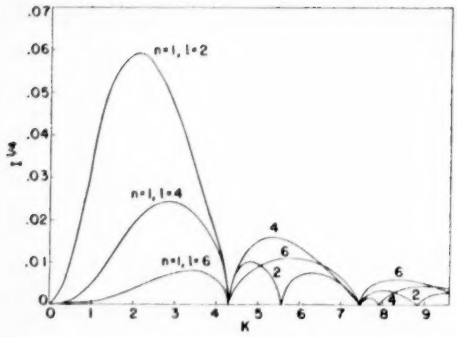

FIG. 3. Differential cross section for scattering of O_2 by N_2 with the interchange: 1 vibrational quantum→2, 4, and 6 rotational quanta.

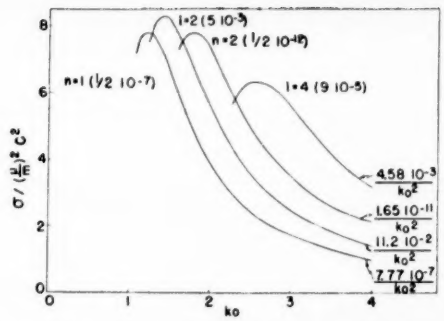

FIG. 4. Total cross sections corresponding to Figs. 1 and 2. The numbers in parentheses are factors by which the ordinate must be multiplied.

(c) for the interchange, vibrational energy in A-A→ rotational energy in B-B,

$$I(A(n), B(0); A(l), B(0)) = \frac{k_{ab}}{k_{st}} \frac{256}{\pi} \frac{\alpha^2}{(\alpha^2+K^2)^4} J_{n0}^2(A)(2l+1) j_l^2(Kb).$$

Here $2a$ and $2b$ are the equilibrium nuclear separations of A-A and B-B, and $J_{n0}^2(A)$ is the function specified in Eq. (12) of reference 1 for A-A. The cross section is given in units πa_0^2 when atomic units are used for all quantities. j_l is the spherical Bessel function.

In Figs. 1–3 we illustrate these results for the collision of O_2 with N_2, plotting $I^{\frac{1}{4}}$ *versus* K for various l, n, and taking $\alpha=2$ atomic units. In Fig. 4 we give total cross sections for cases (a) and (b). We expect, and find, complicated interference effects in the angular distribution of scattered molecules. The interchange of rotational energy is generally much easier than that of vibrational energy, but note that already the ease of transfer of $l=6$ rotational energy is comparable with that of $n=1$ vibrational energy. The first maximum of I dominates the scattering for a rotational or vibrational interchange but not necessarily for a vibrational→ rotational interchange ($n=1$, $l=6$ curve of Fig. 3); that is, in the rotational or vibrational interchange the angular distribution of scattered molecules has a first large lobe followed by much smaller lobes as one goes to larger scattering angles, but in a vibrational→rotational interchange it may be the second or higher lobe that is the largest.

Thanks are due Miss Elaine Kratosky for assistance with the numerical computations.

Microwave Spectra of CsF, CsCl, and CsBr†

A. HONIG, M. L. STITCH,* AND M. MANDEL
Columbia University, New York, New York

(Received July 7, 1953)

Molecular constants for CsF, CsCl, and CsBr have been determined from measurements of their pure rotational spectra in the microwave region. These and other data allow a test of the constancy of ionic bonding radii. Measurements of isotopic species of these molecules give the mass ratios of the stable Cl and Br isotopes.

THE pure rotational spectra of CsF and CsBr have been observed using a high-temperature microwave spectrometer.[1]

The absorption lines corresponding to the $J=1\rightarrow2$ transition for CsF were seen at a temperature of about 700°C. From the measured lines, the following molecular parameters[2] have been obtained: $B_e=5527.27\pm0.04$ Mc/sec, $\alpha_e=35.13\pm0.05$ Mc/sec, $\omega_e=227\pm60$ cm^{-1}, $\mu_{v=0}=7.85\pm0.25$ debye, and $r_e=2.3453\pm0.0001$A.

The ω_e was determined from relative intensity measurements of the excited vibrational state transitions, and the magnitude of the error is due to unusually large standing waves in the wave guide during the measurement of this molecule. The dipole moment was measured by splitting the $v=0$ line in an electric field. Its value agrees within the experimental error with the value $\mu_{v=0}=7.874\pm0.025$ deduced from the μ^2A quantity measured in a molecular beam experiment.[3] The value $r_e=2.34\pm0.05$A obtained in that experiment also agrees with our value.

CsBr lines were observed at a temperature of about 680°C. The measured lines for the $J=9\rightarrow10$, $10\rightarrow11$, and $11\rightarrow12$ rotational transitions yield the following molecular parameters:

$CsBr^{79}$	$CsBr^{81}$
$B_e=1081.3392\pm0.02$ Mc/sec	$B_e=1064.5853\pm0.02$ Mc/sec
$\alpha_e=3.7175\pm0.0029$ Mc/sec	$\alpha_e=3.6313\pm0.0024$ Mc/sec
$\gamma_e=3.1\pm0.4$ kc/sec	$\gamma_e=3.1\pm0.5$ kc/sec
$D_e=-0.27\pm0.08$ kc/sec	
$\omega_e=143\pm22$ cm^{-1}	

$$r_e=3.0720\pm0.0001\text{A}.$$

The ω_e in the foregoing list was calculated from the experimental values of D_e and B_e. Relative intensity measurements yielded a value $\omega_e=155\pm40$ cm^{-1}.

The calculated mass ratio of the Br isotopes is:

$$Br^{79}/Br^{81}=0.9753068\pm0.0000045.$$

This agrees well within the experimental error with a value obtained in a molecular beam experiment with KBr.[4]

The mass ratio, which is derived from the values of B_e for the two isotopes, is quite insensitive to the principle contribution to the error in B_e, namely the uncertainty of the D_e values. Hence, the error attributed to the mass ratio is considerably smaller than the error in the B_e values.

The lines of CsCl reported in a previous note[1] were found to be 30 Mc/sec too high in frequency. Table I lists the corrected lines as well as some new measured lines. The corrected molecular parameters are as follows:

$CsCl^{35}$	$CsCl^{37}$
$B_e=2161.195\pm0.015$ Mc/sec	$B_e=2068.761\pm0.015$ Mc/sec
$\alpha_e=10.085\pm0.004$ Mc/sec	$\alpha_e=9.46\pm0.03$ Mc/sec
$\gamma_e=7.1\pm0.7$ kc/sec	

$$r_e=2.9062\pm0.0001\text{A}.$$

TABLE I. Observed lines for $J=5\rightarrow6$ transition of CsCl.

	$CsCl^{35}$		$CsCl^{37}$
v	Frequency	v	Frequency
0	25 873.11±0.10	0	24 767.86±0.10
1	25 752.16±0.20	1	24 654.26±0.30
2	25 631.58±0.20	*2	*24 541.4 ±0.5
3	25 511.25±0.20		
4	25 390.36±0.40		
*5	*25 270.0 ±0.5		
*6	*25 150.1 ±0.5		
*7	*25 031.0 ±0.5		
*8	*24 911.2 ±0.5		

* Signifies corrected measurements of a previous run. Other lines are additional or remeasured lines.

The calculated mass ratio of the Cl isotopes is

$$Cl^{35}/Cl^{37}=0.9459781\pm0.0000030.$$

This agrees within the experimental error with the value obtained from other microwave measurements[5,6] as well as with mass spectroscopic results.[7]

It is of interest to establish the extent to which alkali and halogen ionic bonding radii are constant, and for this purpose, we can now examine the group of molecules KCl, KBr, CsCl, and CsBr. If the ionic bonding

† Research sponsored jointly by the Signal Corps and The U. S. Office of Naval Research.

* Present address—Varian Associates, Palo Alto, California.

[1] Stitch, Honig, and Townes, Phys. Rev. **86**, 813 (1952).

[2] The molecular parameters reported in this paper are based upon the usual Bohr theory expansion for the molecular energy levels, and have not been corrected for the Dunham expansion. The only quantity appreciably altered is B_e, which may differ from the given value by about 1 part in 100 000.

[3] J. W. Trishka, Phys. Rev. **76**, 1365 (1949).

[4] Fabricand, Carlson, Lee, and Rabi, Phys. Rev. **91**, 1403 (1953).

[5] C. H. Townes, Physica **17**, 354 (1951).

[6] Lee, Fabricand, Carlson, and Rabi, Phys. Rev. **91**, 1395 (1953).

[7] Collins, Nier, and Johnson, Phys. Rev. **84**, 717 (1951).

radii are constant, then $(r_e^{KBr}-r_e^{KCl})^{4.6}$ should be equal to $(r_e^{CsBr}-r_e^{CsCl})$, and each quantity should represent the difference between the Br and the Cl ionic bonding radii. From the measured values, $(r_e^{KBr}-r_e^{KCl})=0.1541$A, and $(r_e^{CsBr}-r_e^{CsCl})=0.1658$A. Hence the ionic bonding radii vary by about ½ percent in the group of molecules we have considered here.

Work on the microwave spectra of the alkali halides is continuing, and a more detailed article summarizing the results for most of the alkali halides is planned.

PHYSICAL REVIEW VOLUME 92, NUMBER 4 NOVEMBER 15, 1953

Decay of Rh^{106}†

BERND KAHN AND W. S. LYON
Health Physics and Analytical Chemistry Divisions, Oak Ridge National Laboratory, Oak Ridge, Tennessee
(Received June 1, 1953)

The gamma radiations from 30-sec Rh^{106} have been examined using a NaI(Tl) gamma-ray spectrometer. These consist of: 0.516 Mev (20.5 percent), 0.619 Mev (10.4 percent), 0.88 Mev (0.3 percent), 1.04 Mev (1.7 percent), 1.14 Mev (0.4 percent), 1.54 Mev (0.2 percent), and several gamma rays of higher energies with intensities of less than 0.1 percent.

THE gamma radiations from 30-sec Rh^{106}, in equilibrium with 1-year Ru^{106}, have been examined with a NaI(Tl) spectrometer (Fig. 1). Ru^{106} decays to Rh^{106} by emitting a 39-kev beta group.[1] The Rh^{106} decay has been reported to be complex, and energy levels for excited states of Pd^{106} have been suggested by Hayward[2] and Alburger.[3]

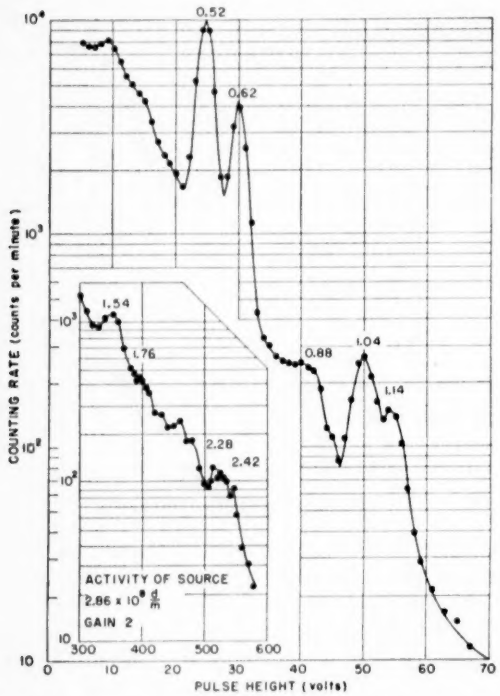

FIG. 1. Pulse-height spectrum of Rh^{106} between 50 kev and 2.50 Mev on NaI(Tl) scintillation spectrometer. Distance from crystal 2.45 cm; activity 1.11×10^7 disintegrations/min; gain 4.

The Ru, in the form of $RuCl_3$, was separated from 4 year old fission products by the Operations Division, Oak Ridge National Laboratory. The activity of the Rh^{106} was determined by 4π counting and by 4π-coincidence counting, the sample being evaporated on an aluminum foil 4 mg/cm² thick and covered with another foil of the same thickness in order to absorb the Ru^{106} beta particles. The activity determined by the two methods was identical, and was in agreement with the activity determined by absolute beta counting with G-M counters and by coincidence counting of an external source. The external source was placed between a NaI gamma counter (shielded with sufficient aluminum to absorb all beta particles) and a proportional beta counter. A large amount of weak continuous radiation was detected by the NaI counter, hence the counter was biased to detect only radiation in excess of 0.30 Mev.

TABLE I. γ radiation from Rh^{106}.

Energy (Mev)	Percent of beta activity
0.516	20.5%
0.619	10.4
0.88	0.3
1.04	1.7
1.14	0.4
1.54	0.2
1.76 2.28 2.42	<0.1 each

The energies and intensities of the gamma rays observed on the NaI spectrometer are given in Table I.

The counting rate was taken to be the area under the

† Based on work performed under contract to the U. S. Atomic Energy Commission.

[1] H. M. Agnew, Phys. Rev. **77**, 655 (1950).

[2] R. H. Hayward, Phys. Rev. **85**, 760 (1952).

[3] D. E. Alburger, Phys. Rev. **88**, 339 (1952).

photoelectric peak in Fig. 1. The spectrometer—having a cylindrical crystal 1 in. in length and $1\frac{1}{2}$ in. in diameter—was calibrated for gamma counting efficiency by using gamma-emitting radioisotopes of known activities. The average deviation of the values in repeated determinations is less than 5 percent. The ratios of the 1.55-, 1.04-, 0.88-, and 0.619-Mev gamma rays to the 0.516-Mev gamma ray are in agreement with the values given by Kraushaar and Goldhaber.[4] The efficiency of a high-pressure ion chamber for measuring Rh^{106} was calculated with the data of Table I using the method of Jones and Overman.[5] The efficiency determined experimentally was within 1 percent of this calculated value.

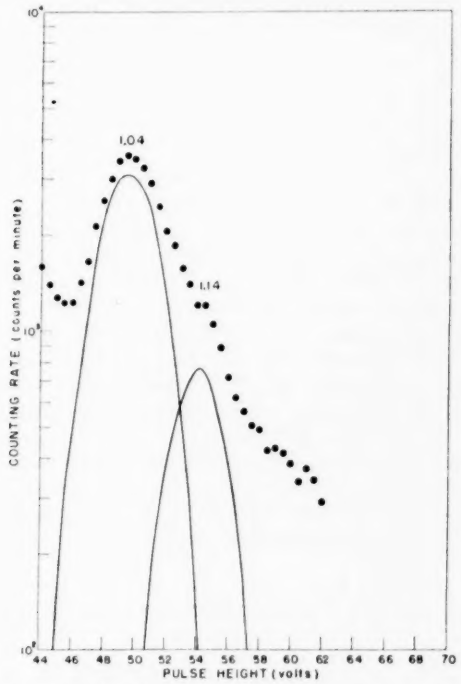

FIG. 2. Pulse-height spectrum of Rh^{106} between 0.90 and 1.30 Mev on NaI(Tl) scintillation spectrometer. Distance from crystal 27.5 cm; activity 1.13×10^{10} disintegrations/min; gain 4.

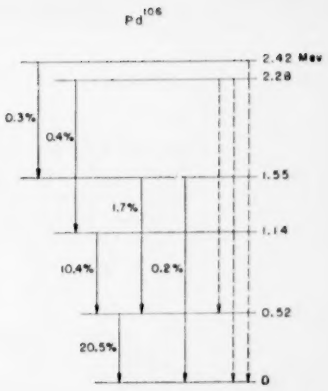

FIG. 3. Gamma rays in the decay of Rh^{106}.

The existence of the 1.14-Mev gamma ray was checked by counting sources of increasing intensity at source-to-crystal distances between 2.45 cm (Fig. 1) and 27.5 cm (Fig. 2). A 1.14-Mev peak resulting from a gamma ray of that energy would decrease approximately as the square of this distance, while a peak resulting from 0.516–0.619-Mev coincidences would decrease as the fourth power of the distance. The ratio of the 1.14–1.04-Mev peaks indicates that the amount of the 1.14-Mev γ listed in Table I cannot be ascribed to γ-γ coincidences. The occurrence of small peaks at 2.28 Mev and 1.76 Mev suggests that a 2.28-Mev level exists, and that the 1.14-Mev γ originates at this level. (See Fig. 3.)

[4] J. J. Kraushaar and M. Goldhaber, Phys. Rev. **89**, 1081 (1953).

[5] J. W. Jones and R. T. Overman, U. S. Atomic Energy Commission Report AECD 2367, March 20, 1948 (unpublished).

Angular Correlation of the Gamma Rays from Mn^{56}†

F. R. METZGER AND W. B. TODD
Bartol Research Foundation, Franklin Institute, Swarthmore, Pennsylvania

(Received August 4, 1953)

The angular correlations of the gamma rays of Fe^{56} emitted in the decay of Mn^{56} have been studied using sodium iodide scintillation counters. All three excited states of Fe^{56} involved in the decay of Mn^{56} were found to have spin 2, even parity. The spin of the ground state of Mn^{56} is probably 2, the parity even.

The admixture of electric quadrupole radiation to the magnetic dipole 2–2 transitions is 2 percent for the 1.8-Mev gamma ray and 8 percent for the 2.1-Mev transition, i.e., small compared to the admixtures in other 2–2–0 cascades.

INTRODUCTION

OUR knowledge of the properties of the excited states of even-even nuclei has recently been summarized.[1] The first excited states emerge from this survey as a very uniform group, 95 percent of all spins being 2+, the rest 0+. All first excited states discussed in the summary[1] have even parity. As one proceeds to higher excited states, the amount of information available decreases rapidly and so does the uniformity. The second excited states fall into three equal groups: 2+, 4+ and "others." Here, too, the preference for even parity is still large; at least $\frac{2}{3}$ of all second excited states have even parity. Odd-parity states seem to appear as the excitation exceeds ~2 Mev, e.g., at 2.75 Mev in Sr^{88} (reference 2) and at 2.3 and 2.6 Mev in Te^{124} (reference 3).

In a search for more of these odd-parity states, we decided to investigate the 2.65- and 2.95-Mev excited levels in Fe^{56} which are involved in the decay of Mn^{56} (Fig. 1). The decay scheme of Fig. 1 is essentially the one proposed by Elliott and Deutsch.[4] The two crossover transitions were reported by Bishop *et al.*,[5] who observed the photoprotons produced by the Fe^{56} gamma rays in a deuterium filled ion chamber.

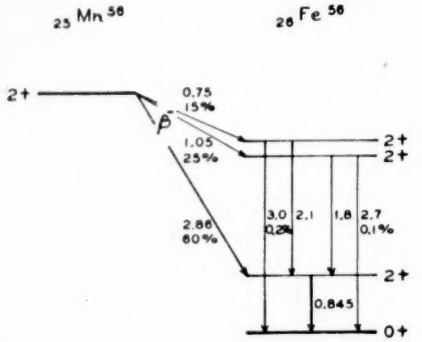

FIG. 1. Disintegration scheme of Mn^{56}. The spins and parities assigned are the result of the present paper. Energies are given in Mev.

A measurement of the internal pair formation coefficients[6] indicates that the 1.8-Mev gamma ray is probably $E1$, the 2.1-Mev transition $E2$. However, the logft values of 5.3 and 5.6 for the β-ray transitions to the two levels in question seem to indicate the same parity for both levels.

Lifetime measurements[7] restrict the spin of the 0.845-Mev level to 1 or 2, spin 2+ being the more likely assignment. No information concerning the internal conversion of the Fe^{56} gamma rays is available. At these low Z values, conversion measurements are very difficult and, in the case of Fe^{56}, impossible with the means we had at our disposal. On the other hand, the simple decay scheme encouraged an investigation of the angular correlations of the gamma rays of Fe^{56}, the only handicap being the relatively short half life of Mn^{56}.

MEASUREMENTS

Sodium iodide scintillation counters with conventional electronics equipment were used for all the measurements. The resolving time of the coincidence circuit was $\sim 1.5 \times 10^{-7}$ second; the solid angle subtended by the crystals at the source was ~0.1 steradian.

Sources of metallic manganese and manganese chloride sources were prepared from manganese metal which had been irradiated for a few hours in the Brookhaven National Laboratory pile.

Figure 2 represents the pulse-height distribution, due to the Fe^{56} gamma rays, obtained with a sodium iodide crystal 35 mm in diameter and 40 mm long. No indication of gamma rays different from the reported ones was found below 2.1 Mev. All the small peaks in the Compton distributions can be satisfactorily assigned to the pairs produced by the 1.8- and 2.1-Mev gamma rays.

In a first set of correlation experiments both channels accepted all pulses corresponding to more than 580-kev energy. The correlation thus obtained is presented in Fig. 3; it is a mixture of the two individual correla-

† Assisted by the joint program of the U. S. Office of Naval Research and the U. S. Atomic Energy Commission.

[1] G. Scharff-Goldhaber, Phys. Rev. **90**, 587 (1953).
[2] F. R. Metzger and H. C. Amacher, Phys. Rev. **88**, 147 (1952).
[3] F. R. Metzger, Phys. Rev. **90**, 328 (1953).
[4] L. G. Elliott and M. Deutsch, Phys. Rev. **64**, 321 (1943).
[5] Bishop, Wilson, and Halban, Phys. Rev. **77**, 416 (1950).
[6] H. Slätis and K. Siegbahn, *Manne Siegbahn Commemorative Volume* (Uppsala, Sweden, 1951), p. 153.
[7] T. C. Engelder, Phys. Rev. **90**, 259 (1953).

tions in a ratio dependent on the discriminator settings. Analyzing the pulse-height distribution of Fig. 2 into the contributions of the individual gamma rays one finds that, for the discriminator settings used, the 1.8–0.85 Mev cascade contributed 1.60 ± 0.25 times as many counts as the 2.1–0.85 Mev cascade.

To arrive at the two individual correlations, one has to take a second set of measurements with a very different mixing ratio. The most drastic change is obtained if one moves the discriminator in one channel above the photopeak of the 1.8-Mev gamma ray, accepting the 2.1-Mev photopeak only, i.e., if one measures the pure 2.1–0.85 Mev correlation. By subtracting this correlation with the proper weight from the bulk correlation, one obtains the pure 1.8–0.85 Mev correlation.

The counting rate in the 2.1-Mev photopeak is rather small and limits the accuracy with which the pure 2.1–0.85 Mev correlation can be measured. Figure 4 gives the experimental points with their statistical uncertainties. Fitting these points with a distribution of the form $1+a\cos^2\theta$, one obtains $1+(0.07\pm0.04)\cos^2\theta$ as the best fit. However, if one admits $\cos^4$ terms also, a large variety of combinations will fit within the experimental error, the best fit being obtained with $1+0.14\cos^2\theta-0.08\cos^4\theta$.

Using for the ratio of the two cascade contributions the value 1.60 ± 0.25 and for the pure 2.1–0.85 Mev correlation the form $1+0.07\cos^2\theta$, one calculates for the pure 1.8–0.85 Mev correlation, after correcting for finite resolution, $1+0.51\cos^2\theta+0.13\cos^4\theta$. In view of the uncertainity in the coefficients of the 2.1–0.85 Mev correlation, the relative magnitude of the $\cos^2$ and $\cos^4$ terms is subject to considerable error. However, the uncertainty in the value of $W(180°)$ is less than six percent, i.e., $W(180°)/W(90°)=1.64\pm0.10$.

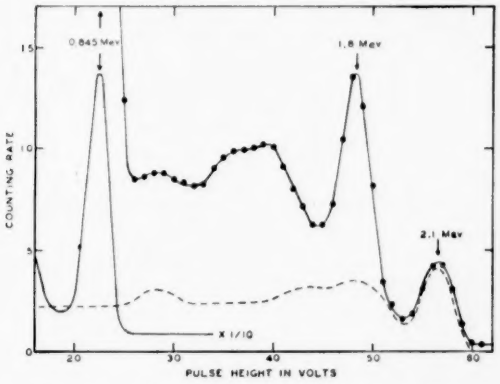

FIG. 2. Pulse-height distribution due to the gamma rays accompanying the decay of Mn^{56}. The dashed line indicates the contribution of the 2.1-Mev gamma ray. The residual counting rate above 2.25 Mev is due to the cross-over gamma rays.

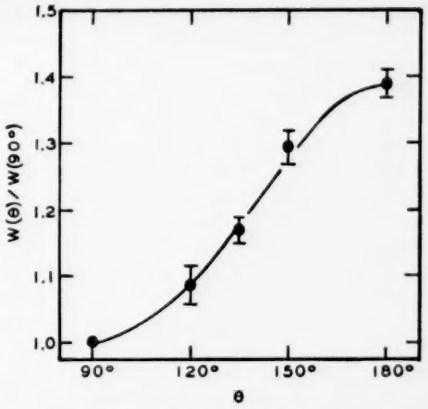

FIG. 3. Angular correlation of the Fe^{56} gamma rays (bulk correlation). All pulses corresponding to energies greater than 580 kev were accepted in both channels. The solid line represents the least square fit to the experimental points:

$$W(\theta)=1+0.32\cos^2\theta+0.066\cos^4\theta.$$

DISCUSSION

Summarizing the results of the preceding section, we write down the two angular correlations:

1.8–0.85 Mev cascade: $1+0.51\cos^2\theta+0.13\cos^4\theta$, $W(180°)/W(90°)=1.64\pm0.10$;

2.1–0.85 Mev cascade: $1+0.07\cos^2\theta$.

For the following it is assumed that the spin of the first (0.85 Mev) excited state of Fe^{56} is 2+. The spin assignment 2–2–0 is then the only one agreeing with the experimental evidence for the 1.8–0.85 Mev cascade.

The combination 3–2–0 cannot exceed a value of 1.43 for the ratio $W(180°)/W(90°)$ and, moreover, cannot have a positive $\cos^4$ term for any mixture.

For 0–2–0 and 4–2–0 no mixtures are expected and the pure correlations are very different from the ex-

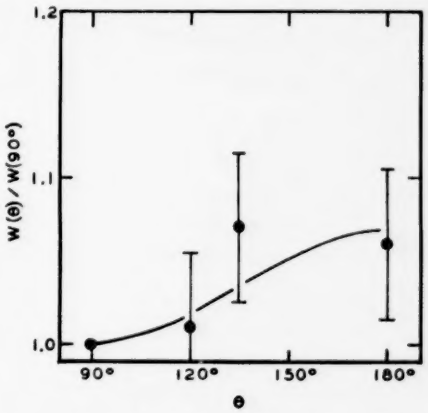

FIG. 4. Angular correlations of the 2.1–0.85 Mev cascade. The solid line represents the distribution $1+0.07\cos^2\theta$ used in correcting the bulk correlation.

perimental one. For 1–2–0 one can find a mixture which gives the correct value at 180°, however, the distribution would have the form $1+2\cos^2\theta-1.38\cos^4\theta$ which certainly does not match the experimental correlation. In addition, one would have difficulties understanding the very low cross-over intensity.

The spin combination 2–2–0 gives the correct value for $W(180°)/W(90°)$ if the admixture of quadrupole radiation to the dipole radiation is 2.2 percent and if the phase is 180°. The uncertainity of the $W(180°)/W(90°)$ ratio allows mixtures ranging from 0.5 percent quadrupole to 4 percent quadrupole. For 2.2 percent quadrupole admixture the correlation has the form[8] $1+0.60\cos^2\theta+0.04\cos^4\theta$ which agrees satisfactorily with the experimental correlation.

The 2 percent quadrupole admixture makes it rather certain that the 1.8-Mev transition involves no change in parity; i.e., that it is magnetic dipole with a small electric quadrupole admixture. The angular correlation measurements in the cases of Sr^{88} [9] and Te^{124} [3] indicate that admixture of $M2$ to $E1$, though present, is smaller than one part in a thousand.

The $E2$ admixture in the 1.8-Mev transition of Fe^{56} is about 5 times larger than expected on the basis of Weisskopf's lifetime formulas;[10] compared with other 2–2–0 transitions,[11] however, it is unusually small.

The intensity of the 2.65-Mev cross-over transition is of the order of magnitude expected for the competition of an $E2$ of 2.65 with a $M1$ of 1.8 Mev.

Based on all this evidence, spin 2+ is assigned to the 2.65-Mev excited state of Fe^{56}.

In view of the large uncertainity involved in the measurements of the internal pair coefficients, we do not consider the $M1$ assignment to be in disagreement with the pair coefficient experiment.[6] It would be worthwhile to measure the internal pair coefficient with improved accuracy.

The angular correlation measured for the 2.1–0.85 Mev cascade excludes the spin assignments 0 and 4 for the 2.95-Mev excited state. These spins were, however, already ruled out by the observation of the cross-over transitions.[5] Both 2–2–0 and 3–2–0 easily fit the observed points, while 1–2–0 could only be accommodated with difficulty.

It is felt that 2–2–0 is the correct assignment for the 2.1–0.85 Mev cascade. However, the arguments leading to this conclusion are less stringent than those used for the 1.8–0.85 Mev cascade.

The logft values of the two beta transitions leading to the 2.65- and 2.95-Mev excited states of Fe^{56} are 5.6 and 5.3 respectively. Both transitions seem, therefore, to be allowed; hence the two levels have the same parity. Under these circumstances the cross-over transitions will only be of comparable intensity, as observed, if the spins of the two levels are the same. Therefore, we have to assign spin 2, even parity to the 2.95-Mev level.

With this assignment, the 2.1-Mev transition becomes a mixture of 92 ± 3 percent $M1$ and 8 ± 3 percent $E2$ with zero phase. Thus, the disintegration of Mn^{56} leads to three excited states of Fe^{56} which all have spin 2, even parity. The most probable spin assignment for the ground state of Mn^{56} is 2+. The logft value of 6.6 for the transition to the 0.85-Mev excited state is somewhat large for an allowed transition, but does not constitute a serious objection to the spin assignment. It should be mentioned that a β-γ angular correlation experiment[12] on Mn^{56} revealed isotropy, indicating that the β transition to the 0.85 level does not have a forbidden shape and might well be allowed.

The reason for choosing 2+ instead of 3+ for the spin of the Mn^{56} ground state lies in the Co^{56} decay. Already Elliott and Deutsch[4] concluded that Co^{56} has a large spin.[13] The Co^{56} decay does not lead directly to any of the 2+ levels or to the ground state of Fe^{56}, but reaches some of these levels through cascades from levels with presumably high spins. Among others, the Co^{56} decay leads directly to a level 2.1 Mev above the Fe^{56} ground state. From this level, a 1.26-Mev gamma ray leads to the 0.85-Mev, 2+ level in Fe^{56}. It seems quite reasonable to assign spin 4+ to this 2.1-Mev level in Fe^{56}. The fact that this 2.1-Mev, 4+ level in Fe^{56} is not reached in the Mn^{56} beta decay favors strongly spin 2+ over 3+ for the ground state of Mn^{56}.

We are thus led to conclude that Mn^{56} decays from a 2+ ground state to three excited states in Fe^{56} which all have spin 2+. The γ-ray transitions between the 2+ levels are magnetic dipoles with small admixtures of electric quadrupoles. The apparent preponderance of 2+ states in Fe^{56} is due to the low spin of Mn^{56} which favors transitions to low spin states in Fe^{56}.

[8] D. S. Ling and D. L. Falkoff, Phys. Rev. **76**, 1639 (1949).
[9] R. M. Steffen, Phys. Rev. **90**, 321 (1953).
[10] V. Weisskopf, Phys. Rev. **83**, 1073 (1951).
[11] J. J. Kraushaar and M. Goldhaber, Phys. Rev. **89**, 1081 (1953).
[12] Walter, Huber, and Zünti, Helv. Phys. Acta **23**, 697 (1950).
[13] Presumably 5+ from a combination of a $f_{7/2}$ proton with a $p_{3/2}$ neutron.

Spontaneous Fission Yields from Uranium and Thorium*

GEORGE W. WETHERILL†
Department of Physics, University of Chicago, Chicago, Illinois
(Received August 13, 1953)

Relative spontaneous fission yields from uranium and thorium have been determined by extracting xenon krypton from geologically old uranium and thorium minerals and measuring the isotopic abundances of these gases in a mass spectrometer. Arguments are presented for believing that the anomalous isotopic abundances observed are caused by spontaneous fission rather than by some other fission process. The spontaneous fission yield curve peaks were found to be much sharper than those associated with other fission processes. Evidence was found for fine structure in the fission yield curve at mass 132, possibly connected with preferential formation of spontaneous fission fragments containing 50 protons and 82 neutrons. Evidence for neutron induced fission in pitchblende was found.

I. INTRODUCTION

THE first attempt to find spontaneous fission was made by Libby[1] who set a lower limit of 10^{+14} years for this process. Spontaneous fission was first observed in uranium by Flerov and Petrzhak in 1940.[2] More recently the partial half-life for spontaneous fission of U^{238} has been determined by Segrè to be 8.0×10^{15} years and that of Th^{232} to be 1.4×10^{18} years.[3] Segrè also measured the U^{235} spontaneous fission half-life and found it to be 1.7×10^{17} years. Since this is longer than the U^{238} half-life and the normal ratio of U^{238} to U^{235} is about 138, the contribution of U^{235} to spontaneous fission in natural uranium is very small.

These long half-lives make it very difficult to isolate and observe spontaneous fission products from uranium and thorium by conventional radiochemical techniques, and as yet no results have been obtained by this method. An alternative technique is to extract from uranium and thorium minerals the stable fission product isotopes which have been accumulating in the mineral throughout geological time. An observable change in the total quantity and in the isotopic abundances of fission product elements will be produced if the uranium or thorium concentration is sufficiently high, the mineral sufficiently old, and the concentration of the normal isotopes sufficiently low. The change in isotopic abundance may then be used to calculate relative spontaneous fission yields.

Because of their low terrestrial abundances[4,5] the inert gases are particularly suitable for an investigation of this kind. The spontaneous fission from one gram of uranium produces about 10^{-7} cc at S.T.P. of Xe^{136} in 300 million years. In a six-percent uranium mineral having this age the ratio of fission product Xe^{136} to normal Xe^{136} should be about sixty. Thus in radioactive minerals the total amount of xenon and krypton as well as the isotopic distribution should be very different from that which is found in ordinary minerals. In 1947 Khlopin, Gerling, and Baronovskaya[6] found that pitchblende contained much more xenon than is usually found in minerals and that the quantity of xenon found was in rough agreement with the assumption that the xenon was produced by spontaneous fission. In 1950 MacNamara and Thode[7] reported measurements of the isotopic abundances of xenon and kypton extracted from pitchblende. These writers stated that the abnormal isotopic abundance which they found were the result of spontaneous fission of uranium and in this way calculated spontaneous fission yields of krypton and xenon. Their hypothesis is not altogether tenable however since the discovery of about 10^{-11} gram of plutonium per gram of uranium in pitchblende[8,9] indicates that the neutron flux in this mineral is sufficiently high to cause appreciable neutron fission of uranium, thus partially masking the effects of spontaneous fission.

As yet no theoretical calculations of the shape of the spontaneous fission yield curve have appeared in the literature. Fong[10] has calculated the shape of the slow neutron fission yield curve for U^{235} and states that the same theory is applicable to spontaneous fission. According to Frankel,[11] fission asymmetry is understandable on the basis of barrier penetration. Since the reduced mass of asymmetrical fragments is smaller, they should penetrate the barrier more readily. Hill and Wheeler[12] state that their collective model of the

* This work was supported in part by a grant from the National Science Foundation. Some of the work was done at the Argonne National Laboratory.
† U. S. Atomic Energy Commission predoctoral fellow.
[1] W. F. Libby, Phys. Rev. **55**, 1269 (1939).
[2] K. A. Petrzhak and G. N. Flerov, J. Exptl. Theoret. Phys. (U.S.S.R.) **10**, 1013 (1940); Chem. Abs. **35**, 4677 (1941).
[3] E. Segrè, Phys. Rev. **86**, 21 (1952).
[4] K. Rankama and T. G. Sahama, *Geochemistry* (University of Chicago Press, Chicago, 1950), p. 771.
[5] The abundance of normal krypton and xenon in minerals has not been previously reported. In the investigation reported in this paper about 10^{-10} cc at S.T.P./g of mineral were found. The normal krypton was about four times as abundant as the normal xenon.
[6] Khlopin, Gerling, and Baronovskaya, Bull. acad. sci. U.R.S.S. Classe sci. chim. **599** (1947); Chem. Abs. **42**, 3664 (1948).
[7] MacNamara and H. G. Thode, Phys. Rev. **80**, 471 (1950).
[8] C. A. Levine and G. T. Seaborg, J. Am. Chem. Soc. **73**, 3278 (1951).
[9] Peppard, Studier, Gergel, Mason, Sullivan, and Mech, J. Am. Chem. Soc. **73**, 2529 (1951).
[10] Peter Fong, Phys. Rev. **89**, 332 (1953).
[11] S. Frenkel, J. Phys. (U.S.S.R.) **10**, 553 (1946).
[12] D. L. Hill and J. A. Wheeler, Phys. Rev. **89**, 1102 (1953).

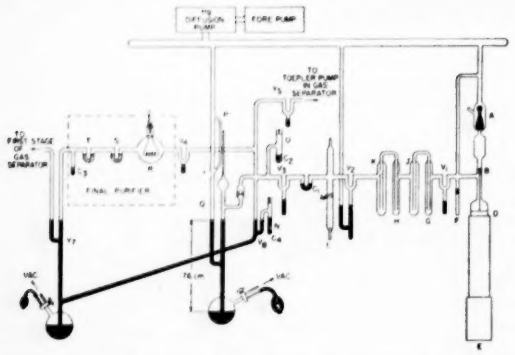

FIG. 1. Apparatus for the extraction of inert gases from minerals. A. Magnetic valve; B. Stirring rod; C_1. Tubes containing 5 g of activated charcoal; C_2. Tubes containing 5 g of activated charcoal; C_3. Tube containing 5 g of activated charcoal; C_4. Tube containing 10 g of activated charcoal; D. Nickel furnace; E. Electric heater winding; F. Xe^{128} tracer; G. Magnesium perchlorate trap; H. Potassium hydroxide trap; J. Cupric oxide trap; K. Magnesium perchlorate trap; L. Calcium vapor furnace; M. Quartz-pyrex graded seal; N. Neon sample tube; O. Argon, krypton, xenon sample tube; P. McCleod gauge; Q. McCleod exhust; R. Tungsten bulb; S. Copper oxide trap; T. Magnesium perchlorate trap.

nucleus is not inconsistent with fission asymmetry, but no quantitative statements regarding this are made in their paper.

In this investigation spontaneous fission yields are obtained for uranium and thorium by extracting xenon and krypton from euxenite $[(Y, Er, Ce)_2O_3UO_2Nb_2O_5TiO_2H_2]$ and monazite $[(Ce, La, Nd, Pr)PO_4]$, respectively, and analyzing these gases in a mass spectrometer. Reasons are given for believing that the yields obtained actually represent spontaneous fission rather than some competing fission process.

II. EXPERIMENTAL METHODS

In order to measure the isotopic abundances of the inert gas contained in a mineral, it is necessary to prepare the gas samples in a form suitable for analysis in a mass spectrometer. To accomplish this it is necessary that the gases be removed from the mineral being investigated, that they be purified of chemically reactive gases such as oxygen, nitrogen, hydrogen, and hydrocarbons. It is also necessary to remove the large quantity of helium which is always found in radioactive minerals in order that the sample be sufficiently small for analysis. These requirements were met by use of the greaseless high vacuum apparatus shown in Fig. 1.

After all parts of this apparatus were thoroughly degassed by heating, the system was isolated from the pumps and the finely divided mineral sample was dropped into the nickel electric furnace (D) by raising the magnetic valve (A) with an alnico magnet. In this furnace the mineral was fused with NaOH, releasing the gases occluded in the mineral. As the gases were being released, a known quantity of Xe^{128} (F) was added in order to measure the quantity of xenon released. The first magnesium perchlorate trap (G) removed the water which was evolved from the mineral. The CuO trap (J), operated at 400°C, reacted with H_2 and CO oxidizing these gases to H_2O and CO_2, respectively. The KOH trap (H) reacted with CO_2 to form K_2CO_3 and water. This reaction is greatly facilitated by the presence of water vapor, but it was not necessary to add water since a small amount always comes through the first trap. The water produced by these reactions was taken up by the second magnesium perchlorate trap (K). Most of the remaining chemically reactive gases were removed by volatilizing calcium in the calcium furnace (L), where such compounds as CaO, Ca_3N_2 and CaC_2 were formed. After this treatment the charcoals (C_1, C_2, C_3) were brought to -195°C with liquid nitrogen and the helium and neon pumped off with a Toepler pump through V_5 into the "gas separator" and retained for further studies. When no further decrease in pressure could be effected by the use of the calcium furnace, the residual gases were transferred by use of the charcoals into the final purifier. Here the remaining hydrocarbons were cracked on the hot tungsten filament of the tungsten bulb (R). The hydrogen produced was oxidized by the CuO trap (S) and the water formed was absorbed by the magnesium perchlorate (T). After the total quantity of gas had been reduced to between 10^{-2} and 10^{-3} cc at S.T.P. the gas was transferred to C_2 and the samples sealed off. This sample contained the argon, krypton, and xenon extracted from the mineral.

The gas samples were analyzed in a 60°, 12-in. radius of curvature mass spectrometer especially designed for work with small gas samples. High sensitivity was obtained by the use of an electron multiplier in the ion collector, and a resolving power of two thousand was achieved by the use of 0.002-in. defining slits in the ion source and an adjustable defining slit in the collector, together with differential pumping between the source region and the analyzer. This differential pumping permitted the high pressure necessary in the source for an intense ion beam without introducing pressure scattering in the analyzer region. Background impurities were kept low by eliminating the usual greased joints and stopcocks both in the high-vacuum part of the mass spectrometer and in the sample system supplying the gas to be analyzed to the machine. Both the analyzer and source vacuum system employed two liquid nitrogen traps in series. The main mercury diffusion pump was backed by an ejector stage mercury diffusion pump which in turn was backed by a mechanical pump. Another liquid nitrogen trap was located between the mechanical pump and this diffusion pump in order to prevent oil from the mechanical pump diffusing into the high vacuum. The entire high-vacuum portion of the instrument was frequently baked at over 300°C for several days by the use of nichrome heaters wound directly onto the glass

and metal tubing. This precaution was necessary in order to reduce the background to the level required by the investigation.

The sample tubes containing the gases adsorbed on charcoal were sealed onto the sample system of the mass spectrometer, and the gas introduced by the use of conventional glass breakeffs. The krypton and xenon were desorbed successively by changing the temperature of the charcoal. The quantities of xenon and krypton analyzed were of the order of 10^{-7} cc S.T.P. With the resolving power of two thousand which was obtainable with this instrument it was possible to resolve the hydrocarbon impurities from the inert gas which was being studied. This was especially important at masses 82 and 130 where small peaks had to be measured in order to correct for normal krypton and xenon in the samples.

The data were recorded on a Brown chart recorder. Because the peak heights decay as the gas supply is depleted, it was necessary to correct for this decrement. An exponential correction was used. In some cases it was necessary to correct for the change in isotopic composition with time, since the lighter isotopes flow through the leak more rapidly than the heavy ones, causing the gas remaining in the reservoir behind the leak to become enriched in the heavier isotopes. Molecular flow was maintained at all times, so it was not necessary to correct for fractionation of the isotopes in flowing through the apparatus. Since the sensitivity of the electron multiplier varies slightly with mass it was necessary to correct for this discrimination. The discrimination was determined by running samples of normal gas and comparing the results with the accepted values of the isotope ratios as given by Bainbridge and Nier.[13]

III. EXPERIMENTAL RESULTS

A. Spontaneous Fission Yields from Uranium

Spontaneous fission yields in the region of krypton and xenon were obtained by processing the mineral euxenite as described in Sec. II. The results of the isotopic analysis, after making corrections for normal krypton and xenon, are shown in Table I. The normal corrections were made by assuming the Kr^{82} and Xe^{130} peaks to represent normal krypton and xenon respectively. By analogy to neutron fission the independent yields at masses 82 and 130 should be less than 10^{-4} percent and may be neglected. The ratio of fission xenon to normal xenon was 23.4; the ratio of fission krypton to normal krypton was 0.58. The errors shown in Table I represent the mean deviations of the peak heights. Xenon measurements on two samples of euxenite are reported; the large sample is believed to give the most accurate data because in this case the peaks were sufficiently large to effectively eliminate background errors. Krypton results are reported for the large sample only. Data were obtained from a number of other samples all of which showed the same yields within their larger experimental errors; the yields presented in Table I represent the most accurate results which were obtained. The results are normalized by assigning a six percent yield to mass 136, thus allowing the results to be compared with U^{235} slow neutron fission yield curve. This comparison is shown in Figs. 2 and 3.

TABLE I. Yields of xenon and krypton isotopes from the spontaneous fission of U^{238}.

Xenon Yield[a] (percent)			Krypton Yield[b] (percent)	
Mass	109.6 g sample	33.8 g sample	Mass	109.6 g sample
136	6.00	6.00	86	0.75 ±0.11
134	4.99 ±0.07	4.91 ±0.06	84	0.119±0.040
132	3.57 ±0.06	3.51 ±0.07	83	0.036±0.015
131	0.455±0.02	0.474±0.02		
129	<0.012	<0.02		

[a] Xe^{136} yield taken as 6.00 percent.
[b] Xe/Kr ratio determined by calibration of mass spectrometer with stable isotope tracers.

TABLE II. Neutron sources in Madagascar euxenite.

Neutron source	Yield (Neutrons/g sec)
Cosmic rays[a]	10^{-4}
Spontaneous fission[b]	8.8×10^{-4}
(α,n) reactions[c]	10^{-3}

[a] See footnote 15.
[b] See footnote 16.
[c] See footnote 17.

The limit at mass 129 represents the accuracy of the normal correction to the peak at mass 129. The large errors at masses 83 and 84 are caused by the error in the normal correction at these masses; the error at mass 86 represents the accuracy of the Xe/Kr ratio which in turn depends on the accuracy of calibration of the stable isotope tracers which were used to calibrate the mass spectrometer.

In order to make sure that the yields presented in Table I actually represent spontaneous fission, it is necessary to evaluate the relative importance of other possible causes of fission in the mineral, and compare the rate of these other fission processes with the spontaneous fission rate in the mineral. Since the sample of euxenite studied contains six percent uranium the spontaneous fission rate is about 4×10^{-4} fission /g sec. Fission by alpha particles may be excluded because the penetration coefficient of the uranium coulomb barrier for alpha particles is less than 10^{-10}. Similarly, the effect of cosmic-ray mesons may be neglected since according to the measurement of George and Evans[14] the number of μ mesons stopped per gram of absorber at a depth of 20 meters of water

[13] K. T. Bainbridge and A. O. Nier, *Relative Isotopic Abundances of the Elements*, Preliminary Report No. 9, Nuclear Science Series, National Research Council, 1950 (unpublished).

[14] E. P. George and J. Evans, Proc. Phys. Soc. (London) **A64**, 193 (1951).

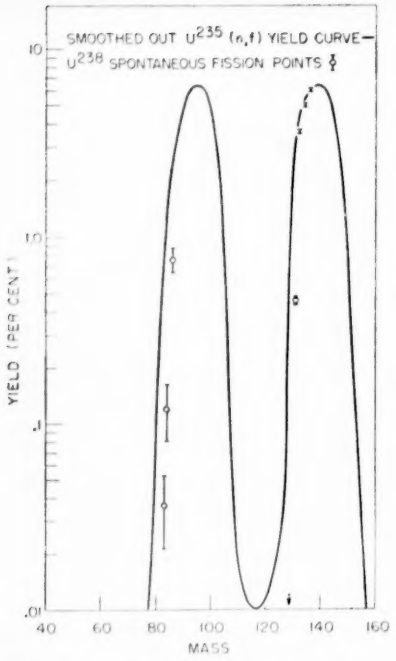

FIG. 2. Comparison of U^{238} spontaneous fission and U^{235} slow neutron fission yields.

equivalent underground is less than 10^{-6} per second. The π-meson intensity is much less. The importance of neutron fission can be estimated by considering the yields of various possible sources of neutrons in the mineral as shown in Table II.[15–17]

The neutron production rate is therefore about 2×10^{-8} neutron/g sec. The mineral sample studied was analyzed chemically and found to contain about one percent gadolinium and one percent dysprosium. Because of the large thermal neutron cross sections of these elements about one in three thousand of the neutrons captured in the mineral will be captured in U^{235}. Since many of the neutrons will escape from the mineral without being thermalized, the rate of neutron fission of U^{235} is less than 7×10^{-7}/g sec. Because U^{238} will not fission by capture of slow neutrons, only fast neutron fission of this isotope need be considered. Since the euxenite occurs as small lumps of less than one cc volume embedded in large masses of rock, most of the fast neutrons produced in the mineral will escape into the surrounding rock. Using a fast neutron cross section of 2.9×10^{-25} cm^2, the number of fast neutron fissions induced in U^{238} per gram per second is less than 10^{-6}. Thus the effect of fast neutron fission can also be neglected. The only gamma rays of sufficient energy to cause fission are the neutron capture gammas; the number of these is approximately equal to the number of neutrons. Since the photofission cross sections are smaller than the fast neutron fission cross sections, and the total cross section for absorption of the gammas is comparable to that for the fast neutrons, the effect of photofission must also be negligible. For these reasons one may have some confidence that the fission yields obtained truly represent spontaneous fission of U^{238}.

From the quantity of lead and uranium in this mineral the age is calculated to be about 600 million years. However the quantity of helium and spontaneous fission xenon which was found in the mineral indicates an age of only about 50 million years. This low gas age might lead one to suspect that the mass-129 yield obtained is too low, the Xe^{129} yield being held up by the 1.7×10^7-year I^{129}. This is probably not the case however, because as long as the I^{129} remains in equilibrium with the uranium the measured Xe^{129} yield will be correct, even though the inert gases may leak from the mineral either slowly over the entire lifetime of the mineral or all at once 50 million years ago. Since the I^{129} is produced as a "hot atom," it will react quickly with one of the common elements in the mineral and should not be removed by leakage along with the inert gases. In the unlikely event that the I^{129} was separated from the mineral by a sudden outgassing process 50 million years ago, the upper limit for the Xe^{129} yield in Table I should be raised to 0.02 percent. This does not affect the general features of the spontaneous fission yield curve.

It may be noted that the spontaneous fission yields, shown in Figs. 2 and 3, are even more asymmetric than

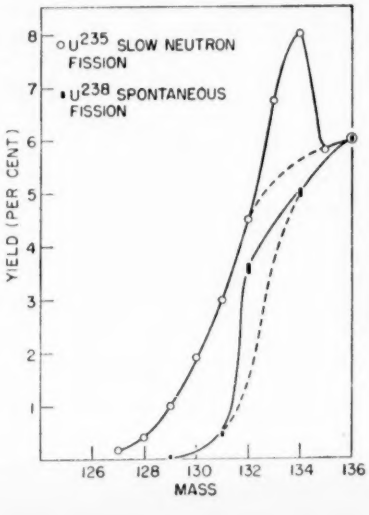

FIG. 3. Comparison of U^{238} spontaneous fission and U^{235} slow neutron fission showing the differences in the fine structure in the region of xenon.

[15] Korff and Hamermesh showed that the cosmic ray neutron intensity is about 10^{-4} neutrons/g sec at a depth of six meters of water equivalent from the top of the atmosphere. It should be much less underground. S. A. Korff and B. Hamermesh, Phys. Rev. **69**, 155 (1946).

[16] The value $\nu = 2.2$ was used. See footnote 3.

[17] The yield of neutrons from the (α,n) reactions was estimated using the results of measurements of the amount of excess Ne^{21} and Ne^{22} produced in these minerals by the (α,n) reaction on O^{18} and F^{19} respectively. These results and this calculation will be described in a separate paper.

neutron fission yields, the most striking effect being at mass 129 where the yields differ by a factor of about one hundred. Furthermore, the yield at mass 131 is about 50 percent lower that that reported by MacNamara and Thode,[7] and the yield at mass 129 is lower than that reported by these investigators by a factor of at least seven. The krypton results are also significantly different. This is the effect which might be expected if MacNamara and Thode had observed a mixture of neutron-induced and spontaneous fission. The sharpness of the spontaneous fission yield peaks is in agreement with Glendenin's and Steinberg's[18] work on curium. In experiments on high-energy fission it is found that the fission becomes a more symmetric when the excitation energy of the nucleus is increased.[19] In spontaneous fission where there is no excitation, it might be expected that the fission would tend to be even less symmetric than in thermal neutron fission, as was found in this investigation.

It should also be noted that it is difficult to place the mass-132 point on a smooth curve containing the other points. This is an indication of fine structure similar to that found in neutron fission by MacNamara, Collins, and Thode,[20] and by Glendenin, Steinberg, Inghram, and Hess.[21] This "spike" at mass 132 may indicate preferential formation of spontaneous fission fragments containing 50 protons and 82 neutrons. It may be pointed out that the barrier penetration theory of Frenkel[22] predicts a peak to trough ratio of only about ten, whereas the experimental value as reported in this paper is greater than 500.

B. Spontaneous Fission of Thorium

Spontaneous fission of thorium is much more difficult to detect because the half-life for the process is 168 times as long as for the spontaneous fission of uranium.[3] For this reason it is necessary to obtain a mineral sample with a high ratio of thorium to uranium and which has other desirable characteristics, the most important of which are great age, small leakage, and high concentration of thorium. The best mineral which could be obtained for this investigation was monazite [(Ce, La, Nd, Pr)PO_4]. This mineral usually contains about six percent thorium and a few tenths percent uranium. Although a higher thorium to uranium ratio would be very desirable, some information concerning thorium spontaneous fission yields can be obtained from a mineral of this kind.

TABLE III. Comparison of spontaneous fission xenon from monazite with U^{235} spontaneous fission yields.

Mass	Monazite yield[a] (percent)	U^{235} yield (percent)
136	6.00	6.00
134	5.12 ±0.10	4.99 ±0.07
132	3.63 ±0.08	3.57 ±0.06
131	0.509±0.02	0.455±0.02
129	0	<0.012

[a] Xe^{136} yield taken as 6.00 percent. Xe^{129} taken to be 100 percent normal xenon.

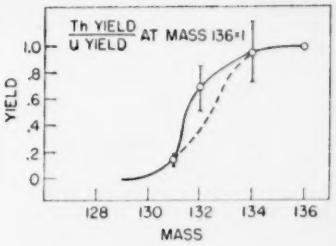

FIG. 4. Spontaneous fission yields from Th^{232} in the region of xenon.

The most accurate data for xenon was obtained from a sample of Ceylon monazite sand, containing 7.79 percent thorium and 0.301 percent uranium and having an age of 530 million years. The xenon isotopic abundances found in this mineral are shown in Table III. If one assumes a ratio of the thorium to uranium yield at mass 136 together with the thorium and uranium concentrations given above and the known spontaneous fission half-lives, it is possible to determine within rather wide limits the thorium spontaneous fission yields at other mass numbers. The results of this calculation are shown in Fig. 4. It may be noted that again there is evidence for fine structure at mass 132. Thus, while these results for thorium are not very precise, they show that thorium spontaneous fission yields are similar to those from uranium.

A calculation of the mass-136 fission yield based on the age of the mineral, the quantity of gas obtained as measured with Xe^{128} tracer, and the known spontaneous fission rates of uranium and thorium, gives a result of 3.3 percent. Thus the quantity of gas obtained agrees in order of magnitude with the assumption that the anomalous abundances are caused by spontaneous fission. A more exact measurement of the absolute spontaneous fission yield could not be made because of uncertain effects cause by leakage of gas from the mineral, difficulty in equilibrating the evolved gas with the tracer, and possible errors in the calibration of the tracer.

Krypton results were obtained from another sample of monazite of Brazilian origin. These are shown in Table IV, and it may be seen that again there is no great difference from the euxenite results.

An estimation of the importance of other causes of fission in monazite can be made as was done earlier in the case of euxenite. In this connection it should be pointed out that for the greatest part of their life the monazite sand grains were a minor constituent of a

[18] E. P. Steinberg and L. E. Glendenin, U. S. Atomic Energy Commission Declassified Document, A.E.C.D. 3520, 1953 (unpublished).
[19] R. W. Spence, U. S. Atomic Energy Commission Unclassified Document BNL-C-9, 1949, Brookhaven Chemistry Conference No. 3 (unpublished).
[20] MacNamara, Collins, and Thode, Phys. Rev. **78**, 129 (1950).
[21] Glendenin, Steinberg, Inghram, and Hess, Phys. Rev. **84**, 860 (1951).
[22] S. Frenkel, J. Phys. (U.S.S.R.) **10**, 553 (1946).

TABLE IV. Comparison of spontaneous fission krypton from monazite with U^{238} spontaneous fission yields.

Mass	Monazite yield[a] (percent)	U^{238} yield[a] (percent)
86	0.87 ±0.12	0.75 ±0.11
84	0.180±0.040	0.119±0.040
83	0.036±0.025	0.036±0.015

[a] Normalized to $Xe^{136}=6.00$ percent. Xe/Kr ratio determined by calibration of mass spectrometer with stable isotope tracers.

granite and fast neutrons produced in the monazite would have been lost in the surrounding rock. Furthermore it should be noted that this mineral contains large quantities of the rare earth elements which will be effective in absorbing slow neutrons. Again the conclusion is that other causes of fission are negligible compared to spontaneous fission.

C. Neutron Fission in Pitchblende

Xenon and krypton extracted from a twenty-gram sample of Belgian Congo pitchblende containing 44 percent uranium indicated the presence of neutron fission as well as spontaneous fission. The yields of fission xenon and krypton from the sample are shown in Table V.

It may be noted that the fission yields in the pitchblende fall off much more slowly on the sides of the fission yield peaks than is the case in euxenite and monazite. By using the U^{238} spontaneous fission yields as determined from the euxenite sample and the U^{235} slow-neutron fission yields of Thode and Graham[23] it is possible to claculate the relative contributions of neutron-induced and spontaneous fission in this mineral. The result of this calculation is that about 35 percent of the fission is neutron-induced. If an estimate of the neutron production rate is then made in the same way as was done in the case of euxenite, it is found that about ten percent of the neutrons produced in the pitchblende induce a neutron fission. The pitchblende sample used was 650 million years old; since the half-life of U^{235} is only 700 million years, considerably more neutron fission may have occurred in a pitchblende of similar constitution but with an age of 2100 million years, since at the time of formation of this mineral the U^{235} abundance was about six percent. This may be related to the fact that the oldest pitchblende or uraninite deposits which have been found have an age of about 2100 million years, whereas the earth itself is considerably older.

[23] H. G. Thode and R. L. Graham, Can. J. Research **A25**, 1 (1947).

TABLE V. Comparison of fission yields of xenon and krypton from pitchblende with U^{238} spontaneous fission yields.

Mass	Belgian Congo pitchblende yield (percent)	U^{238} spontaneous fission yield (percent)
136	6.00	6.00
134	5.62 ±0.05	4.99 ±0.07
132	3.69 ±0.04	3.57 ±0.06
131	1.18 ±0.02	0.455±0.02
129	0.190±0.004	<0.012
86	1.26 ±0.18	0.75 ±0.11
84	0.401±0.06	0.119±0.040
83	0.166±0.03	0.036±0.015

IV. ACKNOWLEDGMENT

The writer wishes to express appreciation to C. Patterson for instruction in the chemical techniques used in lead analyses which were made to determine mineral ages, and for the use of some purified reagents, to G. Tilton for several uranium analyses, to O. Joensuu for emission spectrometric lead analyses, to D. F. Peppard and J. P. Marble who supplied mineral samples, and to R. J. Hayden who constructed the mass spectrometer which was used in this investigation and who prepared the xenon and krypton tracers which were used.

Special thanks must be given to M. G. Inghram whose counsel and encouragement guided this work from its inception to its completion.

Alpha-Gamma Angular Correlation in Ionium (Th^{230})†

G. M. TEMMER* AND J. M. WYCKOFF
National Bureau of Standards, Washington, D. C.
(Received August 13, 1953)

The angular correlation between the alpha particle leading to the first excited state of Ra^{226} at 67.8 kev and the subsequent gamma ray to the ground state leads to a definite assignment of $I=2^+$ for this state. The correlation is weakened by what is believed to be an interaction of the nuclear electric quadrupole moment with crystalline electric field gradients in the source. The lifetime of the excited state is about 1×10^{-8} second.

1. INTRODUCTION

THE study of the fine structure in the alpha radiation of ionium has revealed two major lines at 4.682 Mev (~75 percent) and 4.612 Mev (~25 percent), respectively, separated by about 70 kev.[1] The gamma-ray spectrum following the alpha decay was studied by means of the conversion electrons by several investigators.[2–5] The latest work on the gamma spectrum with a NaI crystal spectrometer and gamma-gamma coincidences[6] leads to the decay scheme shown in Fig. 1. The numbers in parentheses give the intensities in quanta per disintegration. Rosenblum and Valadares,[7] from a comparison of their observed ratios of conversion coefficients in the (unresolved) L_I+L_{II} and L_{III} shells with some theoretical values obtained by Gellman *et al.*[8] conclude that the 67.8-kev gamma radiation is of the $E2$ type. Our observations on the alpha-gamma angular correlation establish the sequence $0^+-2^+-0^+$ and thus add another $I=2^+$ case to the growing number of first excited states of even-even nuclei of this type.[9,10]

While these measurements were in progress an explanation was put forward by Abragam and Pound[11] to account for the pronounced departure of the much investigated alpha-gamma angular correlation in radiothorium[12–14] from the predicted shape. Our results in ionium show features very similar to the RdTh case and are believed to be due to similar causes.

2. EXPERIMENTAL DETAILS

An over-all schematic diagram of our experimental arrangement is shown in Fig. 2. An electromagnetically separated source of 90-percent pure Th^{230} (in the form of $ThCl_4$) deposited on a thin rubber hydrochloride film, furnished by the Argonne National Laboratory, was located at the center of a small hemispherical vacuum chamber made of 0.033-in. aluminum. This chamber was mounted directly on the front face of an RCA 5819 photomultiplier tube and was continuously evacuated. The source diameter was 4.7 mm. A thin, single crystal of terphenyl was prepared from a supersaturated solution of terphenyl in xylene and was about 0.001 in. thick, i.e., about equal to the alpha-particle range. The crystal turned out to be completely insensitive to all but alpha radiation. It was mounted in the center of the multiplier face and subtended a half-angle of five degrees at the source. The gamma detector consisted of a 1.40 cm×1.56 cm×0.50 cm NaI(Tl) crystal mounted on another 5819 tube and also subtended a half-angle of about 5 degrees at the source. The small thickness of this crystal reduced the background and response to higher energy gamma rays without affecting the near 100 percent efficiency

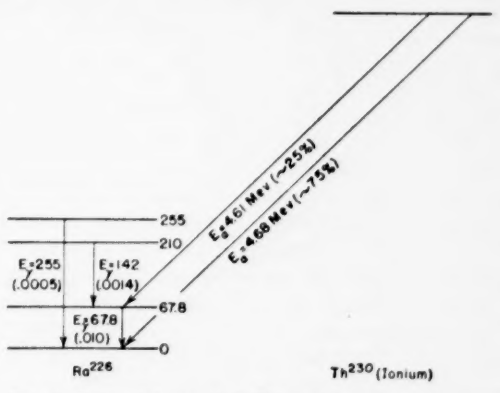

FIG. 1. Decay scheme of Ra^{226} as proposed in reference 6. Gamma-ray energies are given in kev. Numbers in parentheses give intensities in quanta/disintegration.

† A preliminary account of this work was presented at the Rochester meeting of the American Physical Society, Bull. Am. Phys. Soc. **28**, No. 4, 13 (1953).

* Now at the Department of Terrestrial Magnetism, Carnegie Institution of Washington, Washington, D. C.

[1] Rosenblum, Valadares, and Vial, Compt. rend. **227**, 1088 (1948).

[2] J. Teillac, Compt. rend. **227**, 1227 (1948); Albouy, Faraggi, Riou, and Teillac, Compt. rend. **229**, 435 (1949).

[3] S. Rosenblum and M. Valadares, Compt. rend. **232**, 501 (1951).

[4] C. J. D. Jarvis and M. A. S. Ross, Proc. Phys. Soc. (London) **A64**, 535 (1951).

[5] P. Falk-Vairant and J. Teillac, J. phys. radium **12**, 659 (1951).

[6] F. Rasetti and E. C. Booth, Phys. Rev. **91**, 315 (1953).

[7] S. Rosenblum and M. Valadares, Compt. rend. **234**, 2359 (1952).

[8] Gellman, Griffith, and Stanley, Phys. Rev. **85**, 944 (1952).

[9] M. Goldhaber and A. W. Sunyar, Phys. Rev. **83**, 906 (1951).

[10] G. Scharff-Goldhaber, Phys. Rev. **90**, 587 (1953).

[11] A. Abragam and R. V. Pound, Phys. Rev. **89**, 1306 (1953).

[12] Kulchitski, Latyshev, and Bulyginski, Doklady Akad. Nauk. (S.S.S.R.) **64**, 57 (1949).

[13] Beling, Feld, and Halpern, Phys. Rev. **84**, 155 (1951).

[14] Battey, Madansky, and Rasetti, Phys. Rev. **89**, 182 (1953).

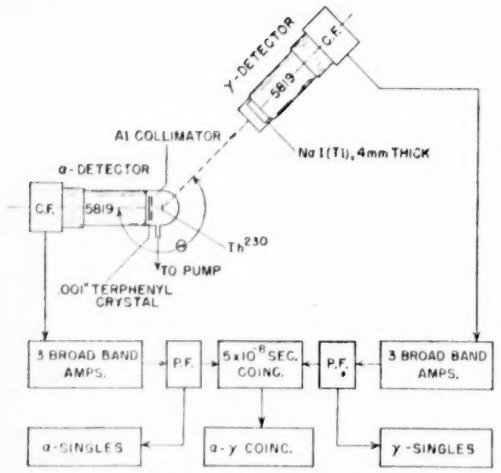

FIG. 2. Schematic diagram of experimental arrangement. Θ is the angle referred to throughout this paper. The entire apparatus is surrounded by a 2-in. lead shield.

for the radiation of interest (67.8 kev). The gamma detector could be set at angles between 84° and 276° with respect to the alpha counter direction. We were thus able to investigate angles on either side, thus having a check on possible systematic left-right differences. The correlation was measured over the hemisphere $\Theta=90°$ to $\Theta=180°$, which is necessarily identical to the hemisphere $\Theta=0°$ to $\Theta=90°$ because all correlation functions involve only even powers of $\cos\Theta$.

The cathode follower outputs from the two multipliers were amplified by three broad band amplifiers (Hewlett-Packard and SKL) in cascade and fed into two pulse-forming stages using Philips EFP-60 secondary emission pentodes. A diode limiter network in the gamma channel prevented overloading of the amplifier chain by large pulses. The standard height outputs of the shaping stages entered a fast coincidence circuit similar to one described by DeBenedetti and Richings.[15] An inherent delay in the gamma channel of about 7×10^{-8} second, probably due to the slower pulse coming from the NaI crystal, was compensated by an appropriate length of cable. The output in turn was stretched, amplified, and recorded by both a scaler and a pen recorder. Both single channels were continuously monitored. The pen recorder made it possible to check the arrival in time of the very small number of coincidences (<8 counts/hour) in this experiment and to distinguish any spurious counts. The resolving time of the circuit was measured to be about 5×10^{-8} second, both by the double-source method and from delay cable measurements (see below). The accidental coincidence rate never exceeded five percent of the total rate at any angle.

[15] S. DeBenedetti and H. J. Richings, Rev. Sci. Instr. **23**, 37 (1952).

The gamma-ray pulse-height distribution as obtained with a conventional linear amplifier and single-channel analyzer is shown in Fig. 3. During our coincidence experiments the gamma-ray pulse height was selected by integral bias just below the 68 kev peak. The effect of the higher energy gamma rays at 142 kev and 255 kev will be discussed below. The small peak at about 35 kev is due to the escape of some of the iodine K x-radiation (~30 kev) following the photoelectric conversion of the gamma rays. We showed this to be so by means of a critical absorber check with tin.

The alpha-ray pulses received from the source presented a rather broad range of pulse heights due to source thickness, although the system itself was capable of good resolution, as may be seen from Fig. 4. It was nevertheless possible to keep the noise contribution to less than 10 percent of the total counting rate in the alpha channel. The entire apparatus was surrounded by two inches of lead to reduce the rather high gamma-ray background from our building.

Our results were obtained during a more or less continuous run of about 1000 hours and consist of six coincidence counting rates at the crucial points of the angular correlation. The angle was changed at least every 24 hours to minimize systematic errors. The photomultiplier voltages were monitored by a precision potentiometer and were kept constant to within 4 volts.

3. RESULTS

The final values of the coincidence rates at six angles together with the various major corrections which were

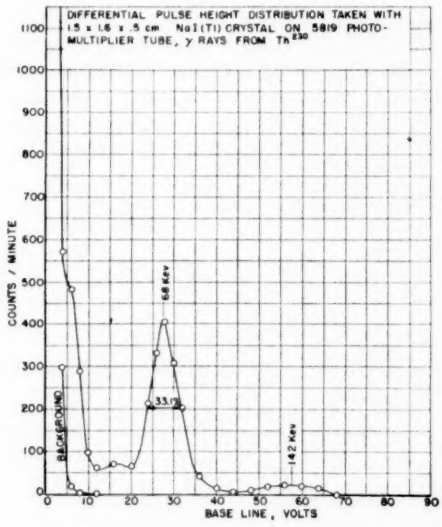
DIFFERENTIAL PULSE HEIGHT DISTRIBUTION TAKEN WITH 1.5 x 1.5 x .5 cm NaI(Tl) CRYSTAL ON 5819 PHOTO-MULTIPLIER TUBE, γ RAYS FROM Th230
COUNTS / MINUTE
BASE LINE, VOLTS
68 Kev
33 Kev
142 Kev
BACKGROUND

FIG. 3. Pulse-height distribution in the gamma channel. The 255-kev gamma ray is not shown. Bias during experiment set between 68-kev peak and small peak at about 35 kev. The latter is an iodine escape peak (see text).

applied are shown in Table I. All rates were normalized according to the singles rates in both the alpha channel and the gamma channel, the latter by means of a strong ionium source counted before and after each run. This was necessitated by the low gamma rate (~130 counts/minute) and its consequent sensitivity to changes in the background rate (~30 counts/minute). The values at 84° and 276° (not 90° and 270° because of an obstruction) as well as at 135° and 225° are seen to be in fairly good agreement. Those two pairs of points were combined for the final computations. The point at 120° was taken merely to rule out a possible $0^+-3^--0^+$ sequence. We refer to papers by Arnold[16] and Falkoff and Uhlenbeck[17] for the basic theoretical expressions for alpha-gamma angular correlations. Figure 5 shows a plot of the experimental results. Our results agree best with the $\sin^2 2\Theta$ function expected for the transition $0^+-2^+-0^+$ except for considerable deviations believed to be due to extranuclear effects which we shall discuss presently.

4. CORRECTIONS

All corrections applied to the raw results were quite small and can be seen in Table I.

(1) Contribution of Higher Energy Gamma Rays

Because of the integral pulse-height selection in the gamma channel we made a crude check on the angular correlation for energies greater than 68 kev at the low rate points (84° and 180°). This check indicated approximate isotropy, which is reasonable in view of the undoubtedly more complicated (and hence more nearly isotropic) nature of the main higher energy component at 142 kev ending on an $I=2^+$ level. We have therefore subtracted an appropriate constant amount (0.43 count/hour) from all observed points. This agrees with our experimentally observed ratio of gamma-ray intensities, which in turn is in good agreement with the work of Rasetti and Booth.[6]

(2) Effects of Finite Source and Detector Size

The observed angular correlation was approximated by an expression of the form $W(\Theta)=a+b\sin^2\Theta$ and integrated over both the extent of the source and the solid angles subtended by the two crystals. This correction turned out to be quite small (~5 percent in the worst case) and is also shown in Table I.

TABLE I. Summary of experimental results. All numbers in coincidence counts per hour. (1) are original data (normalized according to single rates); (2) corrected for accidentals; (3) corrected for other gamma rays; (4) corrected for finite detectors and source; (5) standard deviations (statistical only).

Θ	(1)	(2)	(3)	(4)	(5)
84°	3.62	3.51	3.08	2.97	±0.17
120°	8.61	8.50	8.07	8.12	±0.56
135°	9.05	8.94	8.51	8.63	±0.43
180°	3.52	3.41	2.98	2.75	±0.15
225°	8.82	8.71	8.28	8.40	±0.36
276°	4.12	4.00	3.57	3.46	±0.27

[16] W. R. Arnold, Phys. Rev. **80**, 34 (1950).
[17] D. L. Falkoff and G. E. Uhlenbeck, Phys. Rev. **79**, 323 (1950).

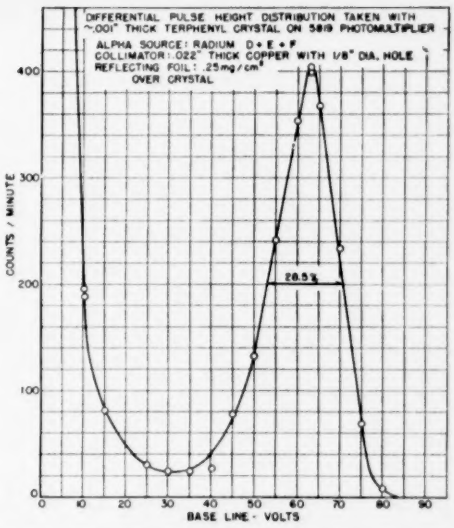
DIFFERENTIAL PULSE HEIGHT DISTRIBUTION TAKEN WITH
~.001" THICK TERPHENYL CRYSTAL ON 5819 PHOTOMULTIPLIER
ALPHA SOURCE: RADIUM D+E+F
COLLIMATOR: .022" THICK COPPER WITH 1/8" DIA. HOLE
REFLECTING FOIL: .25mg/cm²
OVER CRYSTAL
COUNTS / MINUTE
BASE LINE - VOLTS
28.5%

FIG. 4. Pulse-height distribution in the alpha channel, as obtained with a thin RaD+E+F (polonium) alpha source.

(3) Minor Corrections

The correction due to accidental coincidences was already mentioned. Several long runs with incoherent sources at the usual counting rates confirmed the value (5×10^{-8} sec) of the resolving time obtained regularly with a stronger gamma source. The scattering of gamma rays in the thin spherical shell was found to be negligible.

5. INTERPRETATION

(1) Spin and Parity Assignment

A comparison of the experimental angular correlation with various possible sequences $I_A-I_B-I_C$ leaves $0^+-2^+-0^+$ as the most likely choice even before considering coupling effects: a *less* pronounced anisotropy than the observed one obtains for nonzero values of I_A and I_C (ground states of Th^{230} and Ra^{226}) because of the distribution of nuclei over magnetic substates. Furthermore these two nuclei undoubtedly have $I=0^+$ in their ground states because of their even-even character. This leaves the various $0^+-I_B-0^+$ possibilities. $I_B=1^-$ requires a maximum at 90° and minima at 0° and 180°; $I_B=3^-$ leads to minima at 0°, 60°, 120°, and 180° with maxima at 30°, 90°, and 150°. Furthermore, the lifetime of an $E3$ transition would be too long to have yielded coincidences with our resolving time; this is true *a fortiori* for all $I_B>3$. Hence we are left with $0^+-2^+-0^+$ as the only satisfactory choice. The even parity of the inter-

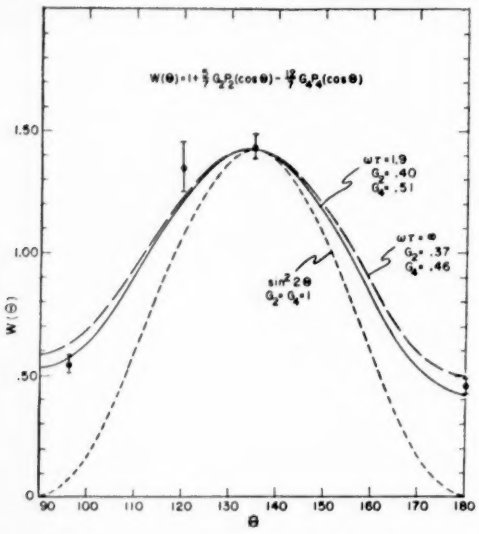

FIG. 5. Plot of experimental results of alpha-gamma angular correlation. Left and right points have been combined to appear in one quadrant. Standard deviations shown are statistical only. Short-dashed curve shows $\sin^2 2\Theta$ correlation for $0^+-2^+-0^+$ case and bare nucleus. Solid curve shows theoretical electric quadrupole attenuation for parameters shown in figure. Long-dashed curve shows maximum theoretical attenuation ($\omega\tau=\infty$). General expression used is given on top of figure [see reference (11)].

mediate state follows from the plausible assumption of even ground states for even-even nuclei.

(2) Extra-nuclear Effects

Even though a $\sin^2 2\Theta$ angular correlation comes closest to the observed results, we note a very definite attenuation of the angular pattern (see Fig. 5) that cannot be due to experimental causes, as we have seen above. In Fig. 6 we have plotted the effect on the $0^+-2^+-0^+$ sequence of both nuclear magnetic dipole coupling with electronic magnetic fields[18] and nuclear electric quadrupole coupling with crystalline electric field gradients.[11] Both effects depend on the product $\omega\tau$; ω is the Larmor precession frequency in the magnetic case and the characteristic splitting frequency between the $m_B=0$ and $m_B=\pm 1$ substates in the electric case, τ is the mean lifetime of the intermediate state. The quantities $G_2(\omega\tau)$ and $G_4(\omega\tau)$ are the "attenuation" coefficients of the second and fourth Legendre polynomials occurring in the angular correlation function. All curves refer to the case of a crystalline powder, i.e., no preferential orientation. The magnetic dipole interaction curves apply to the special but representative case $J=\frac{1}{2}$ for the electronic configuration. Figure 7 illustrates the dependence of the electric quadrupole attenuation coefficients G_2 and G_4 on $\omega\tau$. We see that the coefficients are relatively insensitive to the value of $\omega\tau$ above $\omega\tau\sim 1$. The corresponding plot for the magnetic case can be found in a paper by Heer.[19] Although our data certainly do not permit a definite choice of $\omega\tau$, we can see from Fig. 5 that $\omega\tau$ must be larger than about 1.9. Magnetic interaction to any large extent is ruled out from the relative magnitudes of the 90° and 180° points. We see in Fig. 6 that the 90° point in the magnetic case *always* lies *below* the 0°—180° point. Alghough equality is certainly not excluded by our results, the *strength* of our anisotropy would require values for G_2 and G_4 (magnetic) that would produce a 180°/90° ratio greater than 2, which is certainly ruled out. Our upper limits for G_2 and G_4 are 0.40 and 0.51 respectively, while the lower limits are given by the $\omega\tau=\infty$ (irreducible minimum) values $G_2(\infty)=0.37$ and $G_4(\infty)=0.46$, so that $0.37\leqslant G_2\leqslant 0.40$; $0.46\leqslant G_4\leqslant 0.51$. These rather narrow limits on the coefficients actually correspond to an infinite upper limit on $\omega\tau$.

(3) Lifetime Considerations

Rasetti and Booth[6] estimate that the lifetime of the 67.8-kev state is less than 0.3 microsecond from gamma-gamma coincidence measurements. From the dependence of alpha-gamma coincidence counting rate on delay inserted in either channel we believe that we can set an upper limit of $\sim 1\times 10^{-8}$ second on the mean lifetime of the 67.8-kev state in Ra^{226}. A slight asymmetry in the delay curve seems to indicate that the

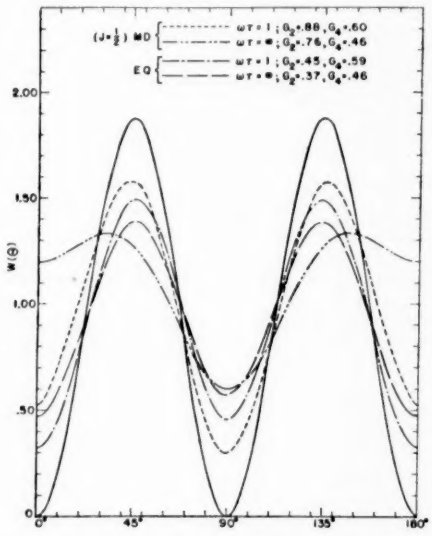

FIG. 6. Electric and magnetic coupling effects on alpha-gamma angular correlation. All curves are for $0^+-2^+-0^+$ sequence, and for isotropic distribution of the extranuclear fields (powder). For an explanation of symbols, refer to text. Magnetic curves are calculated for special case $J=\frac{1}{2}$ according to reference (18); electric curves according to reference (11). Solid curve is undistorted $\sin^2 2\Theta$ distribution. Note characteristic difference between electric and magnetic 180°/90° ratios.

[18] K. Alder, Helv. Phys. Acta **25**, 234 (1952).

[19] E. Heer, Physica **18**, 1215 (1952).

lifetime may actually be of that order of magnitude. A further argument in favor of a lifetime considerably shorter than our resolving time is the fact that our experimentally observed coincidence rate agrees almost exactly with the rate to be expected from the known alpha branching ratio,[1] total internal conversion coefficient[5] and our solid angles.

The lifetime calculated on the basis of Weisskopf's single particle expression[20] for an electric quadrupole transition of this energy yields a value

$$\tau = 2.4 \times 10^{-6} \text{ second.}$$

The experimental value for the total internal conversion coefficient of the 67.8-kev transition[5] is about 22, so that the corrected lifetime is about 1×10^{-7} second. This is at least ten times the experimental value. Although Weisskopf's formula gives a lower limit on the independent particle picture, it is not too surprising to find a matrix element $\gg 1$ for the transition between low-lying states of an even-even nucleus where cooperative effects are presumably very important.[21,22]

6. CONCLUSIONS

Our measurements seem to establish an $I = 2^+$ assignment for the first excited state of Ra^{226}. The deviation of the observed angular correlation from the pure $\sin^2 2\Theta$ distribution predicted for a bare nucleus and a $0^+ - 2^+ - 0^+$ transition receive a satisfactory interpretation on the basis of the coupling of the nuclear electric quadrupole moment to a crystalline electric field gradient in the source material.[11] Although the deviation is thus explained, the large recoil energy imparted to the residual nucleus by the first alpha emission ($\sim$100 kev) frustrates attempts to extract the actual value of the quadrupole moment because of the impossibility of knowing the appropriate electric field gradient at the site of the nucleus. Gamma-gamma angular correlation studies seem to offer considerably greater promise in this respect.[23] It is interesting to note that the only other known case of alpha-gamma angular correlation showing these interaction effects is that of radiothorium (Th^{228}), leading to Ra^{224}.[12–14] This nucleus and the one studied by us differ by just two neutrons and could be examined in the same chemical environment. Hence one could in principle obtain a ratio of quadrupole moments of Ra^{224} and Ra^{226} in their first excited states as soon as the lifetimes are pinned down more accurately. This whole argument is of course weakened in practice by the inherent insensitivity of the correlation to the value of $\omega\tau$.

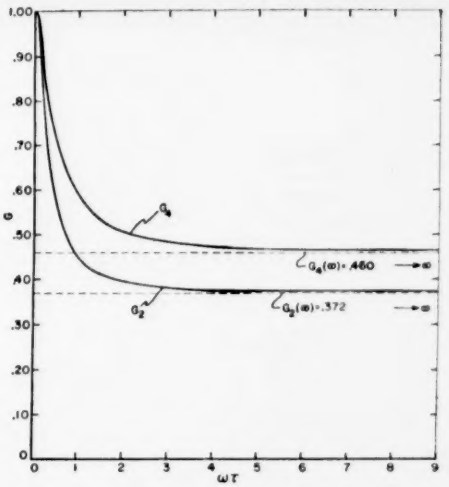

FIG. 7. Theoretical attenuation coefficients for $I = 2$ nucleus with electric quadrupole coupling. Case of crystalline powder source (isotropic distribution of extranuclear field gradient). For explanation of symbols refer to text. Note insensitivity of coefficients to value of $\omega\tau > 1$. Limiting values are shown by dashed horizontal lines.

We express our thanks to Dr. Paul Fields of the Argonne National Laboratory for supplying us with the electromagnetically separated source of ionium and to Professor Franco Rasetti for sending us his manuscript in advance of publication.

Note added in proof:—The angular correlation between the alpha particles of ionium and *conversion electrons* (92.3-percent *L* shell, 7.7-percent *M* shell) corresponding to the same 70-kev transition in Ra^{226} as the gamma ray in our work has recently been determined [R. R. Roy and M. L. Goes, *Nature* **172**, 360 (1953)].

[20] J. M. Blatt and V. F. Weisskopf, *Theoretical Nuclear Physics* (John Wiley & Sons, Inc., New York, 1952), p. 627.
[21] A. Bohr and B. Mottelson, Phys. Rev. **89**, 316 (1953).
[22] K. W. Ford, Phys. Rev. **90**, 29 (1953).
[23] Albers-Schönberg, Hänni, Heer, Novey, and Scherrer, Phys. Rev. **90**, 322 (1953).

Neutron-Deficient Isotopes of Thallium*

I. BERGSTRÖM,† R. D. HILL, AND G. DE PASQUALI
Physics Department, University of Illinois, Urbana, Illinois
(Received August 11, 1953)

The activities of the K-capturing isotopes of $Tl^{198-202}$ have been investigated. Using 180° beta-ray spectrographs, more than 150 conversion lines have been observed. A new isomer of 1.9-hr half-life has been found and assigned to mass number 198. There are three gamma rays of 282.4, 260.7 (isomeric), and 48.7 kev associated with this activity. No thallium isomers, other than Tl^{198m}, or mercury isomers, other than the already known Hg^{199m}, were found. The first excited states in Hg^{200} and Hg^{202} were found to be 2+ states. The level schemes of Hg^{198} and Hg^{200} are complex.

INTRODUCTION

THE present work is concerned mainly with an investigation of thallium activities in an attempt to understand why isomers which might be expected to exist in thallium and mercury have not been observed. (Thallium has 81 protons and for this reason isomerism might be expected, as in gold where isomers exist in all odd-A isotopes. For the odd-odd isotopes, the odd neutron is also close to the magic number 126. Thus for these isotopes there exist several possibilities of coupling between the odd neutron and the odd proton which could give rise to high spins and which could therefore result in isomerism.)

Thus far thallium activities have been investigated mainly by two groups of workers. The Berkeley[1] group has produced a number of thallium activities by bombarding gold with alpha particles, and has identified three activities of 1.8-hr, 7-hr, and 27-hr half-lives which they attribute to Tl^{198}, Tl^{199}, and Tl^{200}, respectively. The Indiana group[2,3] has been concerned mainly with spectrometer investigations of the complex spectra of Tl^{199} and Tl^{200}. Other workers[4] from different laboratories have investigated the 3-day activity of Tl^{201} and the 12-day activity of Tl^{202}, but beta-ray spectrometer data are lacking. Very recently Sugarman[4] has produced all the thallium activities mentioned above by bombarding mercury with negative pions.

We have used 11.5-Mev deuterons to produce the neutron-deficient isotopes of thallium. As a result of either or both (d,n) and $(d,2n)$ reactions from Hg^{198} (10 percent), Hg^{200} (23 percent), Hg^{201} (13 percent), and Hg^{202} (30 percent) present in ordinary mercury, we obtained good yields of all thallium activities from $A=198$ to $A=202$. The mercury was usually in the form of powdered $HgCl_2$, and the active thallium was separated using ether extractions of $TlBr_3$. The thallium activities were analyzed using 180° beta-ray spectrographs of approximately 0.2 percent resolution and with an energy range up to energies of about 850 kev.

THALLIUM 198. ISOMERIC STATE

K, L, M, and N conversion lines corresponding to gamma-ray energies of 282.4 and 260.7 kev, and decaying with a half-life of about 1.9 hr, were found. The exceptionally low value of 0.61 for the K/L ratio of the 260.7-kev transition indicates that it is associated with an isomeric transition. Another gamma ray with an energy of 48.7 kev, decaying with a half-life of approximately 2 hr, was also found. Since no other short-lived activities appear to be present, we believe that all three gamma rays belong to the same activity.

Careful energy measurements of the conversion lines of the 282- and 261-kev gamma rays showed that they were definitely converted in thallium.

Orth *et al.*[1] also observed a 1.8-hr activity when gold was bombarded with alpha particles. Their excitation curves showed that the 1.8-hr activity should be attributed to mass number 198. In order to assign this activity to a definite mass number, we have also made activation experiments as a function of the incident deuteron energy. To summarize these experiments briefly, we found that the ratio of the intensity of the 1.8-hr lines to the 6.5-hr lines of Tl^{199} changes from a value of 1.0 (arbitrary units) at 11.5 Mev to 0.76 at 10.0 Mev. The falling off in intensity of the 1.8-hr lines is attributed to a more rapid falling off of the $(d,2n)$ cross section with decreasing deuteron energy than that of the (d,n) cross section. Since Tl^{198} is the only activity produced by a $(d,2n)$ reaction alone, this would mean that the 1.8-hr activity belongs to mass number 198 in agreement with the Berkeley experiments.[1] This conclusion is also supported by the fact that Wilkinson[3] did not observe the 1.8-hr activity when gold was bombarded with 20-Mev alpha particles. Since the threshold for the $(\alpha,3n)$ reaction is higher than 20 Mev, one would not expect Tl^{198} to be produced in those experiments from Au^{197}.

* Assisted by the joint program of the U. S. Office of Naval Research and the U. S. Atomic Energy Commission.
† On leave of absence from the Nobel Institute of Physics, Stockholm, Sweden. Assistance in part from Svenska Atomkommittén is gratefully acknowledged.
[1] Orth, Marquez, Heiman, and Templeton, Phys. Rev. **75**, 1100 (1949); H. M. Neuman and I. Perlman, Phys. Rev. **78**, 191 (1950).
[2] H. I. Israel and R. G. Wilkinson, Phys. Rev. **83**, 1051 (1951).
[3] R. G. Wilkinson (private communication, 1953).
[4] R. S. Krishnan and E. A. Nahum, Proc. Cambridge Phil. Soc. **36**, 490 (1940); K. Fajans and A. F. Voigt, Phys. Rev. **58**, 177 (1940); **60**, 619 (1941); W. Maurer and W. Ramm, Z. Physik **119**, 602 (1942); H. C. Martin and B. C. Diven, Phys. Rev. **86**, 565 (1952); N. Sugarman and A. Haber, Phys. Rev. **92**, 730 (1953).

It is difficult on the basis of the experimental evidence to make a definite statement regarding the multipole nature of the isomeric transition. Some tentative suggestions can be made by comparing theoretical and experimental values of the mean-life, K/L and L_I/L_{III} ratios shown in Table I.

On the basis of K/L and L_I/L_{III} ratios alone, there seems little doubt that the isomeric transition is largely either $M3$ or $M4$. Unfortunately there is considerable uncertainty in the theoretical values of these ratios for the higher electric multipoles.

On the basis of lifetimes alone, the transition is in accord with purely $M4$ radiation. However, since the isomeric transition occurs in an odd-odd nucleus there is some basis for believing that the theoretical $M4$ lifetime may be even longer than is given in Table I. There is also a considerable spread in the theoretical lifetimes of the electric multipole radiations.

Assuming that the 261- and 282-kev gamma rays are in cascade, and provided that the multipolarity of two gamma rays are known, it is possible to calculate

TABLE I. Data pertinent to the assignment of multipolarity of the isomeric transition of 260.7 kev in Tl^{198m}.

Multipole	K/L	L_I/L_{III}	T_γ theory[a] (sec)	T_γ exptl. (sec)
	0.6 (obs)	1.33 (obs)		1×10^4 (obs)
$M3$	3.1[b]	1.25[c]	7×10^{-1}	1.6×10^5
$M4$	1.2[d]	0.7[c]	9×10^5 [b]	5.0×10^5
$M5$	0.6[b]	0.4[c]	1×10^{12}	1.4×10^6
$E3$	0.8[b]	0.1?	4×10^{-3}	1.7×10^4
$E4$	0.2[b]	?	5×10^3	3.2×10^4
$E5$	0.1?	?	6×10^9	6.2×10^4

[a] V. F. Weisskopf, Phys. Rev. **83**, 1073 (1951).
[b] M. Goldhaber and A. W. Sunyar, Phys. Rev. **83**, 90 (1951).
[c] N. Tralli and I. S. Lowen, Phys. Rev. **76**, 1541 (1949).
[d] W. L. Bendel, thesis, University of Illinois, 1953 (unpublished); I. Bergström *et al.*, Arkiv. Fysik (to be published).

the intensity ratio of the corresponding K-conversion lines. The predicted cascade intensities are in this case most sensitive to a change in the multipolarity of the 282-kev gamma ray. As can be seen from Table II it is to be concluded that the 282-kev transition is unlikely to be either a pure $E2$, $E1$, or $M1$ transition, but is more probably a mixture of $M1$ and $E2$ multipole transitions.

Tl^{198} consists of 81 protons and 117 neutrons. Thus both the odd proton and the odd neutron are close to filled shells. According to the shell model the odd proton would be expected to be either $s_{1/2}$, $d_{3/2}$, $(d_{5/2})$, or $h_{11/2}$. The corresponding possible assignments for the odd neutron are expected to be either $p_{1/2}$, $f_{5/2}$, or $i_{13/2}$. It is therefore evident that an isomer in Tl^{198} might be associated with quite an abnormally high spin state.

THALLIUM 198. GROUND STATE

There is a large number of gamma rays in the thallium activities with half-lives of about 5 or 6.5 hr. Only the strongest gamma rays could be definitely assigned to either one of these half-lives. Associated with the 5-hr half-life are gamma rays of the following energies: 195, 284, 402, 411.1, and 675 kev. The latter two gamma rays are almost certainly identical with those found in the decay of Au^{198}. The K/L and $(L_I+L_{II})/L_{III}$ ratios of the 411-kev gamma ray are in good agreement with those found for the 411-kev gamma ray in the beta decay of Au^{198}. We therefore assign the 5-hr activity to the ground state of Tl^{198}.

TABLE II. Expected ratios of the K-conversion lines of the 261- to 282-kev transitions of Tl^{198m} for different multipole assignments.

Multipolarity of 282-kev transition / Multipolarity of 261-kev transition	$E1$	$E2$	$M1$
$M3$	12.0	4.8	1.07
$M4$	12.4	4.9	1.10
$M5$	12.5	5.0	1.12
$E3$	5.5	2.2	0.49
$E4$	8.5	3.4	0.77
$E5$	10.8	4.3	0.97

(Experimental ratio $K_{261}/K_{282} = 1.45$)

In the activation experiments mentioned previously, when the deuteron bombarding energy was decreased from 11.5 to 10.0 Mev, it was found that the intensity of the isomeric lines decreased relatively to those of the ground state activity. However, the intensity ratio of the 5-hr lines (Tl^{198} ground state) to the 6.5-hr lines (Tl^{199} ground state) remained approximately constant. This might be understood if, of the total reduced activations at the lower energy, the fraction reaching the isomeric state were to decrease in comparison with those reaching the ground state of Tl^{198}. This explanation might be possible in view of the fact that the isomeric state probably has a spin considerably higher than that of the ground state.

Because the spin of the Tl^{204} ground state is very probably 2−,[5] and also because the K-capture decays of Tl^{202} and Tl^{200} are consistent with 2− assignments, it would seem plausible that the ground state of Tl^{198} would also be 2−. Assuming shell structure and Nordheim's rule, such a state could arise consistently in several ways for Tl^{198}.

Since the 411- and 1086-kev levels of Hg^{198} are both known to be 2+, a 2− assignment to the 5-hr Tl^{198} ground state would determine the K capture to the Hg^{198} levels as first forbidden. If we use the theoretical curves for $\log f_k$,[6] the maximum K-capture energy release would then be ~2 Mev, and the branching to the 411- and 1086-kev levels would be approximately 1:0.8.

Experimentally it was found that the intensity ratio of the gamma rays from the 411- and 1086-kev levels was of the order 10:1. This might indicate that the

[5] Lidofsky, Macklin, and Wu, Phys. Rev. **87**, 204, 391 (1952); E. der Mateosian and A. Smith, Phys. Rev. **88**, 1186 (1952).
[6] King, Dismuke, and Way, Oak Ridge National Laboratory Report ORNL-1450 (unpublished).

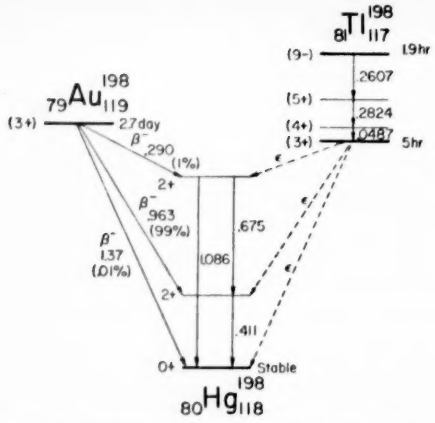

FIG. 1. Proposed decay scheme of Tl^{198} and Tl^{198m}.

411-kev level is fed from several other levels in addition to the 1086-kev level, and the presence of other observed gamma rays lends some support to this viewpoint. It seems more probable, however, that the K-capture transitions are not first forbidden and that the Tl^{198} ground state is not $2-$.

It has recently been shown that the 2.7-day Au^{198} decays to the ground state of Hg^{198} with a beta ray of a high $\log(ft)$-value equal to 11.35.[7] A $3+$ assignment for Au^{198} is therefore probable, and a similar assignment for the Tl^{198} ground state could arise from a coupling of an $h_{11/2}$ proton and an $f_{5/2}$ neutron. The 5-hr K-capture transitions would then be allowed, and for a $\log ft$-value of 5.5 the energy release to the 411-kev state would be approximately 900 kev. For an energy release of about 225 kev to the 1086-kev state, a similar $\log ft$-value would be associated with an approximately 10 percent branch. This is in excellent agreement with our experimental intensities of the 411- and 675-kev gamma rays.

A possible decay scheme of the isomeric and ground state of Tl^{198} activities is shown in Fig. 1. Very tentative level assignments are given.

THALLIUM 199. GROUND STATE

In the radioactive thallium there is a large number of conversion lines with a half-life of about 6.5 hr. The strongest lines correspond to gamma rays of 50.0, 158.4, 208.1, 247.2, 333.6, 454.6, and 491.3 kev. From the fact that the three lowest energy gamma rays are also found in the decay of Au^{199}, we conclude that the 6.5-hr activity belongs to mass number 199. These gamma-ray identifications are in excellent agreement with those of Wilkinson.[3]

The energy accuracy is estimated to be about 0.1 percent. Intercombinations of the gamma rays fit within this accuracy into the decay scheme presented in Fig. 2. This scheme is also consistent with that suggested by Wilkinson[3] and based on coincidence measurements. He showed that both the 247- and 334-kev gamma rays coincide with the 158-kev gamma ray.

From earlier work[8] on the beta decay of Au^{199} it has been suggested that the 158- and 208-kev levels are $f_{5/2}$ and $p_{3/2}$, respectively. Tentative assignments of the 455- and 491-kev levels can also be given, by considering the multipolarity of the gamma rays emitted.

No L_{III} conversion has been observed for the 247-, 455-, and 491-kev gamma rays. In all three gamma rays the L_I and L_{II} lines are observed and in the case of the 247-kev gamma ray, $L_I:L_{II}$ is about 10. This indicates that the 247-, 455-, and 491-kev gamma rays are due to magnetic dipole transitions. Unfortunately the L line of the 334-kev gamma rays was obscured by a 5-hr K line. Wilkinson,[3] however, did not have this disturbing activity in his experiments and his value of $K/L = 1.8$ for the 334-kev transition indicates an $E2$ transition. It is therefore suggested that the 491-kev level is $\frac{1}{2}-$ and that the 455-kev level is a $\frac{1}{2}-$ or $\frac{3}{2}-$level.

It is interesting to speculate on the possibility that the 455- and 491-kev levels arise from a coupling of the 158- and 208-kev one-particle levels with the 411-kev $2+$ excitation of the even-even core of Hg^{198}. The separation of the 455- and 491-kev levels is much the same as that of the 158- and 208-kev levels and the proposed spins of the 455- and 491-kev levels could arise from combinations of the $2+$ and $p_{3/2}$ levels and of the $2+$ and $f_{5/2}$ levels, respectively.

The most probable shell structure assignment for the ground state of Tl^{199} is $s_{1/2}$. As in the case of the ground state of Tl^{198}, K capture could then take place to a number of Hg^{199} levels with comparable intensity. For a maximum energy release to the Hg^{199} ground state of about 1 Mev, the $\log ft$-values of the four partial K-capture transitions of Fig. 2 would be of the order of 6.2, consistent with the first forbidden transition required by the decay scheme.

The suggested decay scheme also agrees with other experimental data. It is consistent, for example in our experiments, with the nonappearance of the isomeric transition in Hg^{199}. A K-capture transition from the

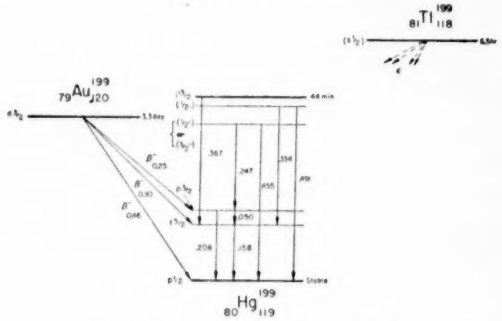

FIG. 2. Proposed decay scheme of Tl^{199}.

[7] L. G. Elliott and J. L. Wolfson, Phys. Rev. **82**, 333 (1951).

[8] P. M. Sherk and R. D. Hill, Phys. Rev. **83**, 1097 (1951).

ground state of Tl^{199} to the isomeric state of Hg^{199} is energetically possible but is strongly forbidden by the large spin change to the $i_{13/2}$ level. For the same reason it is evident that the most probable transition from the isomeric state is that to the $f_{5/2}$ level, the other transitions being more forbidden. Hole[9] also observed only the 158-kev gamma ray in addition to the isomeric gamma ray. If the 455- and 247-kev gamma rays are both emitted from the same level and are both $M1$ transitions their intensity ratio should be $(455/247)^2 = 6.2$. This should be compared with the experimental value 3.4. (This value has been obtained by using the experimental ratio of the K-conversion lines and the theoretical K-conversion coefficients of Rose *et al.*) In the same way the $M1$ transition from the 491-kev level to the ground state would be about 250 times stronger than an $M1$ transition to the 455-kev level. Undoubtedly for this reason, the corresponding 36-kev gamma ray between these levels has not been observed.

THALLIUM 200. GROUND STATE

The conversion spectrum decaying with 27-hr half-life is very complex. This activity has been assigned to mass number 200.[1] We have found conversion lines corresponding to gamma rays of 252, 289, 367.8, 579, 629, and 829 kev. Gamma rays of energies 116, 660, and 786 kev probably also belong to this activity. There are certainly still weaker gamma rays associated with the 27-hr activity. Many of these gamma rays have been observed by Wilkinson[2,3] who further lists gamma rays of 1210 kev, 1360 kev, and probably also 1520 kev. Butement and Shillito[10] using a scintillation spectrometer have reported gamma rays of energies 390 and 1130 kev in the beta decay of Au^{200}.

The energy of the most intense 367.8-kev gamma ray is considered to be absolutely known with an accuracy of better than 1:1000 since its L_I line was measured as a close doublet with the L_I line of the 364.18-kev gamma ray of I^{131}. Active iodine was added to the thallium source so that both L_I lines appeared on the same film.

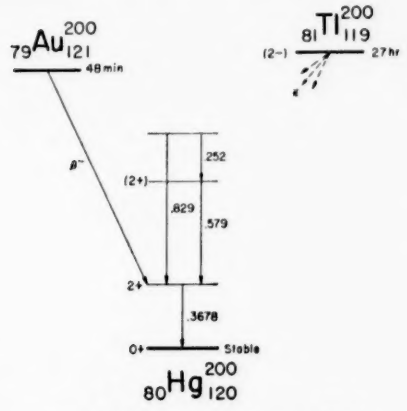

FIG. 3. Proposed decay scheme of Tl^{200}.

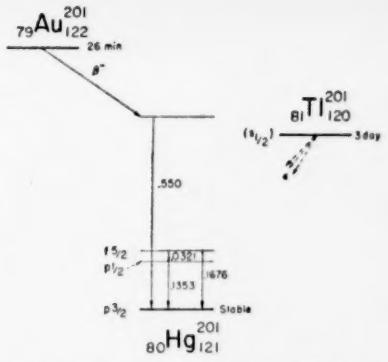

FIG. 4. Proposed decay scheme of Tl^{201}.

Wilkinson[3] showed that all the strong gamma rays are in coincidence with the 368-kev gamma ray. Thus the 368-kev excited state is very probably the first excited state. Our values of $K/L = 2.0$ and $(L_I + L_{II})/L_{III} = 3.0$ indicate that the 368-kev gamma ray corresponds to an $E2$ transition. Thus, in agreement with the extensive investigations of even-even nuclei,[11] the first excited state in the even-even nucleus Hg^{200} is a 2+ state. The decay scheme in Fig. 3 is very incomplete and indicates only some of the more obvious features. For example, the energy sum of the 252- and 579-kev transitions agrees within our experimental error with the 829-kev transition, and the 579-kev transition from K/L ratio and L_I intensity is predominantly an $M1$ radiation.

THALLIUM 201. GROUND STATE

Neuman and Perlman[1] have reported a gamma ray of 210 kev associated with the decay of the 3-day activity of Tl^{201}. We were not able to observe this gamma ray but found conversion lines corresponding to gamma rays of 30.5, 32.1, 135.3, and 167.6 kev which decayed with a half-life of approximately 3 days.

For the two low-energy gamma rays we observed only L_I component lines. This indicates that these two transitions probably are of the $M1$ type. In the case of the 135- and 168-kev gamma rays the L_I and L_{II} lines could be well resolved and in both cases their $L_I : L_{II}$ intensity ratios were about 10. For $M1$ transitions of these energies Gellman *et al.*[12] give a theoretical $L_I : L_{II}$ value of about 11.

Since the 32.1-kev transition is probably a link between the 135.3 and 167.6-kev transitions, a possible decay scheme is as shown in Fig. 4. The level from which the 30.5-kev gamma ray is emitted is uncertain,

[9] N. Hole, Arkiv Mat. Astron. Fysik **36**, (No. 2) (1948).
[10] F. D. S. Butement and R. Shillito, Proc. Phys. Soc. (London) **A65**, 945 (1952).
[11] G. Scharff-Goldhaber, Phys. Rev. **90**, 487 (1953); P. Preiswerk and P. Stahelin, Helv. Phys. Acta **24**, 623 (1952); A. H. Wapstra, Physica **18**, 799 (1952); F. Asaro and I. Perlman, Phys. Rev. **87**, 799 (1952).
[12] Gellman, Griffith, and Stanley, Phys. Rev. **85**, 944 (1952).

TABLE III. Energies (in kev) and spin assignments of the first excited states in even-Hg isotopes.

	Hg^{198}	Hg^{198}	Hg^{200}	Hg^{202}
1st excited level	426(2+)	411(2+)	368(2+)	439(2+)
2nd excited level		1086(2+)	947(2+)	

and there is no *a priori* reason that the order of the 32.1- and 135.3-kev γ rays should not be reversed. The decay of the 26-min Au^{201} measured by Butement and Shillito[10] is also included in the figure. Since we did not observe the 550-kev gamma ray, it is possible that the ground state of Tl^{201} lies below the 550-kev excited level in Hg^{201}.

We have also looked for an $i_{13/2}$ isomeric state in Hg^{201} (and Hg^{203}). The energy separations of the $f_{5/2}$ and $p_{1/2}$ levels from the $i_{13/2}$ levels in the odd-A isomers of Hg are smooth curves when plotted as a function of the odd neutron number.[13] Extrapolating these curves to higher neutron numbers, one might expect to find $M4$ isomers in Hg^{201} and Hg^{203} associated with the half-lives of approximately 10 and 1 min arising from transitions of energies of approximately 600 and 850 kev, respectively. In order to check this, enriched isotope samples of Hg^{200}, Hg^{202}, and Hg^{204} were irradiated with gamma rays from the 20-Mev betatron. By measuring the activity of Hg^{199m} produced in a (γ,n) reaction, we were able to calculate the activities of the expected $M4$ transitions in Hg^{201} and Hg^{203}. No such activity, even 100–1000 times weaker than the expected, was observed. One possible explanation of the absence of isomerism of the expected type is that the $i_{13/2}$ level has moved energetically so high that another underlying level of intermediate spin has destroyed the metastability of the $i_{13/2}$ level. It would, however, still seem worthwhile searching for shorter-lived isomers in Hg^{201}, Hg^{203}, and Hg^{205}.

THALLIUM 202. GROUND STATE

In agreement with earlier observations,[4] only one gamma ray has been observed in the decay of the 12-day Tl^{202}. Since the K line was measured as a close doublet with the L_I line of the 364.18-kev gamma ray in I^{131}, the energy of 439.1 kev for this gamma ray should be absolutely known with an accuracy of better than 1:1000. The K/L ratio = 2.6 and the $(L_I+L_{II})/L_{III}$ ratio = 3.5, strongly suggesting an $E2$ transition. Since no other gamma ray was observed, we believe that the 439-kev gamma ray is emitted from the lowest level in Hg^{202}. That this level should be a 2+ level is in agreement with the systematics of even-even nuclei.[11] The proposed decay scheme is shown in Fig. 5.

TABLE IV. Energies (in kev) and level assignments of low-lying states in the odd-A Hg isotopes. (g.s. = ground state.)

Nucleus / Level	Hg^{193} [a]	Hg^{195} [b,c]	Hg^{197}	Hg^{199}	Hg^{201}
$p_{1/2}$			g.s.	g.s.	135
$p_{3/2}$	g.s.	g.s.		208	g.s.
$f_{5/2}$	37	36	134	158	168
$i_{13/2}$	138	158	299	525	very high

[a] J. W. Mihelich *et al.*, Phys. Rev. **91**, 498 (1953).
[b] Gopalakrishnan, de Shalit, and Mihelich, Phys. Rev. **89**, 908 (1953).
[c] Huber, Joly, Scherrer, and Verster, Helv. Phys. Acta **25**, 621 (1952).

[13] M. Goldhaber and R. D. Hill, Revs. Modern Phys. **24**, 179 (1952).

SYSTEMATICS OF NUCLEAR LEVELS IN MERCURY

Even A

As pointed out by Goldhaber and Sunyar (reference b, Table I), G. Scharff-Goldhaber,[11] and others,[11] the first excited states in even-even nuclei are predominantly 2+ levels. The energies of these levels also show a regular energy dependence with A.[11] A summary of data pertaining to mercury is shown in Table III. The energies are given in kev and are followed by the spin assignments in parentheses.

ODD A

Energy level trends in odd-A nuclei have been pointed out in connection with the study of isomers.[13] The energy levels, assignments and separations of the odd-A isotopes, many of them tentative, are collected in Table IV.

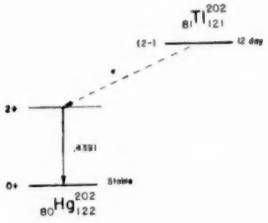

FIG. 5. Proposed decay scheme of Tl^{202}.

It is apparent from Table IV that the $i_{13/2}$ and $f_{5/2}$ levels vary energetically in a systematic manner. However, the behavior of the $p_{1/2}$ and $p_{3/2}$ levels is rather capricious. It would seem somewhat anomalous that the $\frac{3}{2}$ state at one stage ($A=193$, 195) should be lowest, should later ($A=197$, 199) concede to the $\frac{1}{2}$ state as lowest state, and then return again to be the ground state at $A=201$. It is possible also that the unexpected interchange of the $p_{3/2}-p_{1/2}$ spin-orbit doublet for $A=199$ is associated with this irregular behavior of the spin-$\frac{3}{2}$ ground state.

The present work on the thallium activities remains somewhat incomplete. There are for example many weak conversion lines which we have been unable to classify. These lines are listed below, arranged in order of increasing energy (in kev): (No Auger lines are listed. Abbreviations: ew = extremely weak, vw = very weak, w = weak.) 36.9, 37.6 ew 5–27 hr; 81.4, 82.9, 83.8, 99.7 w 27 hr?; 132.6 ew <27 hr, 137.1 vw 27 hr?; 165.1, 188.7 ew ?; 195.9 w ?; 201.5 ew ?; 226.0 w 27 hr?,

271.7 ew 27 hr; 293.5, 299.6, 303.8 w 27 hr?; 332.6, 333.6 ew ?; 392.4 w ?; 414 ew ?; 458 vw 6 hr; 465, 473, 480 ew 6 hr?; 503, 508, 513 w 6 hr?; 582, 604, 618, 640 ew ?; 667, 687 w ?.

ACKNOWLEDGMENTS

We are indebted to the University of Illinois cyclotron and betatron laboratories for furnishing irradiations required for these experiments. We are also deeply grateful to Dr. R. G. Wilkinson for allowing us to use unpublished data of his researches on the thallium activities.

Note added in proof:—M. C. Michel (thesis, University of California, 1953) has recently made a time-of-flight analysis of the thallium isotopes. Independently he assigns the 1.8-hr activity to $A=198$ and also observes the 5.3-hr activity of Tl^{198} which is reported in our work.

PHYSICAL REVIEW VOLUME 92, NUMBER 4 NOVEMBER 15, 1953

Large-Angle Scattering of Co^{60} Gamma Rays*†

THOMAS D. STRICKLER
Sloane Physics Laboratory, Yale University, New Haven, Connecticut
(Received May 19, 1953)

Measurements of the scattering of Co^{60} gamma rays from lead, tin, copper, and aluminum have been made at a mean angle of 135°. In addition to Compton scattering and annihilation radiation, some higher energy components are present. Elastic scattering was observed in each of these scatterers and the cross section for this process has been measured. Results are shown to be consistant with recent theoretical calculations on Rayleigh and Thomson scattering.

INTRODUCTION

INVESTIGATION of the large-angle scattering of gamma rays permits the measurement of scattering events other than Compton scattering. This is of low energy and can be discriminated against. Investigations of this type were made by Chao[1] and Gray and Tarrant[2] in a study of the scattering of ThC″ gamma-rays from lead and other scatterers, and first showed the presence of annihilation radiation from positrons produced in the scatterer.

Pollard and Alburger[3] employed this method in 1948 in an attempt to measure nuclear resonance scattering of Na^{24} gamma rays in magnesium. Their results showed no marked excess in intensity of gamma rays scattered from magnesium over those scattered from aluminum. However, measurements on scattering from magnesium, aluminum, lead, and mercury showed, in each case, an unidentified component of hard radiation having an absorption coefficient characteristic of the unmodified incident beam.

Moon[4] and Storruste[5] have made similar measurements on scattering from lead, copper, and aluminum. Moon has attempted to explain the results of Pollard and Alburger on the basis of interference between coherent scattering by bound electrons (Rayleigh scattering) and Thomson scattering from the nucleus. In addition, he has confirmed the calculations of Franz[6] on Rayleigh scattering at a mean angle of 115° and at an energy of 0.41 Mev, and Storruste has extended his measurements to other angles in the region from 60° to 150°.

More recently, Wilson[7] has measured this elastic scattering from lead at various angles in the energy regions near 1.3 Mev and 2.6 Mev in an attempt to find evidence of Delbrück scattering (potential scattering by virtual pair formation in the field of the nucleus). With this background in mind, an investigation was undertaken of large-angle scattering of Co^{60} gamma rays, with particular attention paid to the elastic scattering. Knowledge of the cross sections for this process, and their dependence on the atomic number of the scatterer, would be useful in the interpretation of existing calculations on Rayleigh scattering and might provide additional evidence for the existence of Delbrück scattering or resonance scattering.

THEORY

In addition to Compton scattering and annihilation radiation, other scattering events are possible in the energy region of 1.3 Mev by the processes of bremsstrahlung, Thomson scattering, Rayleigh scattering,

* This work has been supported by the joint program of the U. S. Office of Naval Research and the U. S. Atomic Energy Commission.
† Part of a dissertation presented to the Faculty of the Graduate School of Yale University, in partial fulfillment of the requirements for the degree of Doctor of Philosophy.
[1] C. Y. Chao, Phys. Rev. **36**, 1519 (1930).
[2] L. H. Gray and G. T. P. Tarrant, Proc. Roy. Soc. (London) **136**, 662 (1932).
[3] E. C. Pollard and D. E. Alburger, Phys. Rev. **74**, 926 (1948).
[4] P. B. Moon, Proc. Phys. Soc. (London) **A63**, 1189 (1950).
[5] A. Storruste, Proc. Phys. Soc. (London) **A63**, 1197 (1950).
[6] W. Franz, Z. Physik **98**, 314 (1935).
[7] R. R. Wilson, Phys. Rev. **90**, 720 (1953).

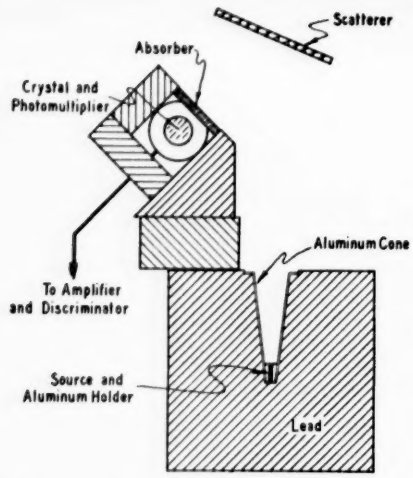

FIG. 1. Arrangement of apparatus for measurement of gamma-ray scattering at a mean angle of 135°.

resonance scattering, and Delbrück scattering. The last four can contribute to elastic scattering.

The classical scattering calculation of Thomson[8] is applicable to scattering from the nucleus in this energy region (by replacing the electronic charge e by Ze and the mass by the nuclear mass) since the rest energy of the heavy nucleus is large in comparison with the incident gamma-ray energy and relativistic effects can be neglected. The differential cross section is approximately proportional to Z^2 and is independent of the incident gamma-ray energy.

Franz[6] has calculated the cross section to be expected from Rayleigh scattering in the gamma-ray region for small scattering angles, and Moon[4] has given an extension of his results for the case of large angles. This calculation, computed on the basis of a Thomas-Fermi electronic charge distribution, predicts a Z^3 dependence for the scattering cross section and shows that the scattering is mainly in the forward direction. Levinger[9] discusses Bethe's interpretation of these form-factor calculations, showing that for values of the photon change in momentum greater than the characteristic momentum of a K electron, a better approximation would be obtained by using Dirac wave functions for K electrons. His calculations predict a somewhat lower cross section than Franz' and show that the scattering may be proportional to Z^8 or Z^{10} in the energy region of 1.3 Mev. It would thus be negligible in comparison to the Thomson scattering in the case of the lower atomic number scatterers. Levinger has described the approximations involved in these calculations and the relativistic corrections to be expected in this energy region, and Brown and Woodward[10] have discussed the effects of binding in the intermediate state.

The probability for the occurrence of resonance scattering by nuclear excitation depends on how near the incident gamma-ray energy is to that of an excited state. Levinger[11] has calculated the cross section to be expected when the incident energy is far enough from the nearest energy level so that the contribution to the scattering from it is small compared to the scattering from all other levels. (Twenty electron volts seems to be far enough.) In that case, he has concluded that, at 1.3 Mev, the scattering to be expected from resonance absorption is negligible compared to the Thomson scattering intensity.

Very little theoretical work has been done on potential scattering. Rohrlich and Gluckstern[12] have made an exact calculation of this scattering of 1.33-Mev gamma rays from lead at 0° and predict a differential cross section of 0.15 mb/sterad. Since the angular dependence is rather high, and the scattering is proportional to Z^4, it is doubtful if there is any substantial scattering at 135° in comparison with other processes such as those mentioned above.

APPARATUS

The scintillation spectrometer used in the energy measurements consisted of a large NaI(Tl) crystal mounted on an RCA type 5819 photomultiplier tube used in conjunction with a single-channel pulse-height analyzer. The instrument has been fully described in a previous paper.[13]

The Co^{60} source, with a strength of about five curies, was obtained in the form of a wire $\frac{1}{8}$ inch in diameter by $\frac{5}{8}$ inch long and was mounted in the center of a large lead cylinder 12 inches in diameter by 12 inches long, with a conical opening to define the beam dimensions. A diagram of this and the geometry used in the scattering measurements is shown in Fig. 1. Measurements were made at a mean angle of 135°.

Scatterers were cut from lead, tin, copper, and aluminum in the form of ellipses of such a thickness as to have, in each scatterer, the same number of electrons. These were supported on a thin aluminum stand whose effect on the scattering was negligible in comparison with the scatterers, but which was left in place during background measurements. All background measurements were made with the source in place but with scatterers removed.

RESULTS

Figure 2 shows the spectra of radiation scattered from $\frac{3}{8}$ inch of lead, and equivalent thicknesses of tin

[8] J. J. Thomson, *Conduction of Electricity Through Gases* (Cambridge University Press, London, 1906).
[9] J. S. Levinger, Phys. Rev. **87**, 656 (1952).
[10] G. E. Brown and J. B. Woodward, Proc. Phys. Soc. (London) **A65**, 977 (1952).
[11] J. S. Levinger, Phys. Rev. **84**, 523 (1951).
[12] F. Rohrlich and R. L. Gluckstern, Phys. Rev. **86**, 1 (1952).
[13] T. D. Strickler and W. G. Wadey, Rev. Sci. Instr. **24**, 13 (1953).

and copper, using $\frac{3}{16}$ inch of lead absorber between scatterer and counter. Calibration curves are shown at pulse heights corresponding to energies of 0.51 Mev, 1.17 Mev, and 1.33 Mev. The Compton scattering peaks at 0.24 Mev, and the annihilation peaks are easily distinguishable. Pulses were observed with pulse heights up to 83 volts, corresponding to energies up to 1.33 Mev although the intensities were very low and cannot be seen in these curves.

Figure 3 shows an expanded portion of the curves in the energy region of 1.33 Mev of scattering from lead, tin, copper, and aluminum. These were run with $\frac{3}{8}$ inch of lead absorber between scatterer and counter to further discriminate against the Compton scattering. Vertical bars on the measured points indicate the statistical accuracies (standard deviations). The set of runs shown required about one week of running time on the spectrometer and the pulse height during this time was stable within a few percent. Calibration curves over the 1.33-Mev peak of Co^{60} were taken repeatedly during these runs as a check on the stability.

To eliminate the possibility that any substantial part of these curves was due to pileup of lower energy photons in the crystal, a spectrum of the direct radiation from a source of Cs^{137} was measured at a distance such as to give an over-all counting rate greater than that scattered from the scatterers. This spectrum, with a peak at 0.661 Mev, was found to fall off much more rapidly at higher energies than the scattered spectra.

To measure the cross sections for this apparant elastic scattering, a weak Co^{60} source of known intensity was placed in the center of the position of the scatterer and the spectrum measured again in the region of the 1.33-Mev peak. From the known strengths of the two Co^{60} sources, the ratio of the counting rates at the 1.33-Mev peaks, and the geometry of the system, the corresponding cross sections were calculated. The effect of absorption of the incident and scattered beam

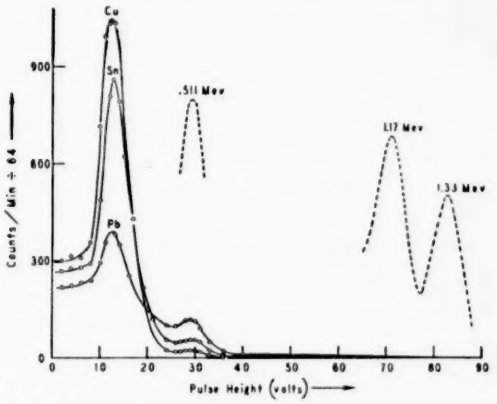

FIG. 2. Spectra of Co^{60} gamma rays scattered at 135° from lead, tin, and copper. Dotted curves show calibration lines from Co^{60} and Na^{22} at 0.51 Mev, 1.17 Mev, and 1.33 Mev.

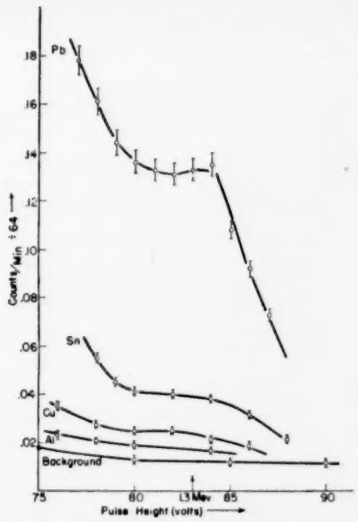

FIG. 3. Spectra in the energy region of 1.3 Mev of scattering from lead, tin, copper, and aluminum. Vertical lines on measured points indicate statistical accuracies.

in the scatterer was accounted for using values for the absorption coefficients calculated from cross sections for Compton effect and photoelectric effect given by Heitler,[14] and for pair production given by Hirschfelder and Adams.[15]

Several checks were made to confirm the validity of these cross section measurements. A spectrum was measured of a weak gamma-ray source of I^{131} extended over the dimensions of the scatterer, and this compared with that of the same source concentrated near the center. The effective decrease in counting rate due to the extended source was less than five percent. A sheet of photographic paper placed at the position of the scatterer and exposed to the gamma radiation of the strong source, showed an even irradiation over the entire face of the scatterer. Also, the strengths of the two sources were compared with a third source of intermediate strength using a Lauritsen electroscope and a number of pencil type ionization chambers, and the relative intensities (though not the absolute intensity) were thus determined within about fifteen percent.

These differential cross sections are listed in Table I along with the theoretical values for the coherent combination of Rayleigh scattering (using Bethe's form-factor calculation), and Thomson scattering. The experimental errors given in these measurements represent those introduced by inaccuracies in measurements of source strengths, effect of the extended source, pulse height instability, etc., as well as statistics

[14] W. Heitler, *The Quantum Theory of Radiation* (Oxford Univeristy Press, London, 1935).

[15] J. O. Hirschfelder and E. N. Adams, Phys. Rev. **73**, 863 (1948).

TABLE I. Differential elastic-scattering cross sections in millibarns/steradian.

	Pb	Sn	Cu	Al
Thomson	0.019	0.0080	0.0031	0.0007
Rayleigh	0.06	4.5×10^{-4}	3.2×10^{-6}	2×10^{-9}
Rayleigh plus Thomson	0.15	0.012	0.003	0.0007
Measured	0.12±0.04	0.015±0.006	0.004±0.002	0.0008±0.0004

in the counting rates. The largest of these in the case of lead was in the estimate of source strength.

DISCUSSION

Although for pure elastic scattering one would expect to measure a peak in the scattered spectrum at 1.33 Mev, it can be seen from the lead spectrum that no peak was observed. A definite change in slope, however, was recorded at this point which would seem to indicate that the elastic scattering was superimposed on a monotonically decreasing scattered component such as one might attribute to bremsstrahlung (from photoelectrons produced in the scatterer). Comparing the shape of the curve with the direct spectrum of Co^{60} gamma rays through $\frac{1}{2}$ inch of lead absorber, however, indicates that at 1.33 Mev the contribution of this component to the total scattering is probably small. The measured cross sections given in Table I, of course, include the effect of this component. This continuously decreasing component will be proportionally smaller than the elastic scattering in the case of the lighter elements because of the high Z dependence of the scattering at lower energy as pointed out below. This is confirmed by the measurements of Pollard and Alburger[3] which show considerable high-energy scattering (with a more continuous energy distribution) from lead, and much less from aluminum and magnesium—but all of it with an absorption coefficient equivalent to that of the incident beam. It is thus unnecessary to distinguish a peak in the scattered spectrum, since a measurement of the counting rate at the pulse height corresponding to the incident energy is sufficient to calculate a cross section with the accuracy shown above. Results are also in agreement with recent measurements made by Wilson[7] on elastic scattering from lead.

The continuous energy spectrum observed between 0.51 Mev and about 1.2 Mev (not shown in detail in the accompanying figures) appeared to be of some interest. Taking into consideration the thickness of the scatterers and the absorption coefficients at these energies, the measurements indicate that the Z dependence is very high in this region—proportional to Z^5 or more. If this radiation were due to bremsstrahlung from Compton electrons produced in the scatterer, one would expect the intensity to be dependent on Z^3. Consideration of the radiation from photoelectrons would partially explain this discrepancy. It is possible that other processes such as one-quantum annihilation of positrons would explain this high Z dependence but the explanation would require a more careful study than that attempted here.

The agreement between the measured cross sections and those calculated for Rayleigh and Thomson scattering may not be too significant, particularly in the case of the Rayleigh scattering. Considerations of the binding in the intermediate state and relativistic effects may be serious and the contributions of the potential scattering to the total elastic-scattering component is yet to be determined.

It is a pleasure to acknowledge the encouragement and support of Professor H. L. Schultz and Professor W. G. Wadey during the progress of this work. Thanks are also due J. S. Levinger and to R. L. Gluckstern who furnished the author with considerable information and advice concerning the recent theoretical developments.

Half-Life of Zr^{88}†

EARL K. HYDE
Radiation Laboratory, University of California, Berkeley, California
(Received July 29, 1953)

The half-life of Zr^{88} has been determined to be 85 days by following the growth and decay of its 105-day Y^{88} daughter.

IN an earlier report[1] concerning some neutron deficient isotopes of zirconium, brief mention was made of Zr^{88}. This was reported to be a long-lived activity emitting only x-radiation, 406-kev gamma radiation and conversion electrons. The determination of the half-life posed some difficulty, as it could not be determined directly by following the decay of the x- and gamma radiation because of the interference of of similar radiation from the 105-day daughter Y^{88}. The method selected as most suitable was the determination of the growth and decay of the 1.85-Mev gamma radiation of Y^{88} counted through sufficient absorber to eliminate the 406-kev gamma radiation of Zr^{88}. Because of the length of the parent and daughter half-lives, this method requires that the sample be followed for over two years. At the time of the above report, an estimate based on the determination of only the initial portion of the growth and decay curve gave 150 days as an approximate value of the Zr^{88} half-life. Sufficient time has now elapsed to permit completion of the growth and decay curve (see Fig. 1), and an accurate value of 85 days has been determined.

The zirconium sample used to obtain the experimental data of Fig. 1 was isolated from a niobium target which had been bombarded with 100-Mev protons in the 184-inch cyclotron on August 4, 1950. The zirconium was isolated 95 days after the bombardment, at which time the Zr^{86}, Zr^{87}, and Zr^{89} had decayed completely, by the chemical methods outlined before.[1] No zirconium activity other than that of Zr^{88} was present. The sample, mounted on platinum foil, was counted through 16.1 grams/cm² lead absorber placed immediately below a chlorine filled Geiger tube (Amperex). This tube was chosen because of its long-term stability. Each time the sample was counted, a UX_2 standard was counted immediately afterward. The 16.1 g/cm² of absorber reduced the gamma radiation of Zr^{88} to 3 percent or less of its original amount. The decay of Y^{88} is almost 100 percent by electron capture, and each electron capture event is followed by a 908-kev gamma ray and a 1.85-Mev gamma ray. The 16.1 g/cm² of lead is one half-thickness for this latter gamma. Hence the observed activity can be considered as due almost solely to Y^{88}.

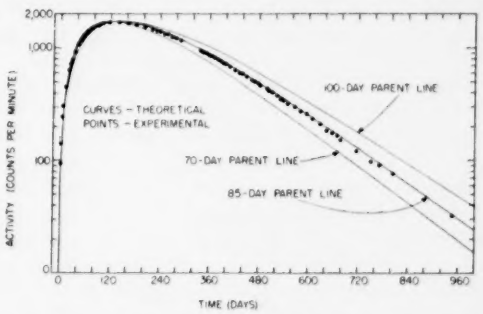

FIG. 1. Half-life determination of Zr^{88}. Experimental points represent growth and decay of energetic gamma radiation of 105-day Y^{88}. Sample was pure Zr^{88} initially. Curves are theoretical curves calculated for 3 values of parent half-life.

The experimental points are plotted against the time from the final purification of the zirconium fraction. Theoretical growth and decay curves were calculated for a 105-day daughter produced by a parent of various half-lives. Three of these curves normalized to the maximum of the experimental points are shown, including that for a parent half-life of 85 days which seems to fit the data best.

† This work was carried out under the auspices of the U. S. Atomic Energy Commission.
[1] E. K. Hyde and G. D. O'Kelley, Phys. Rev. **82**, 944 (1951).

The Angular Correlation of the Cascade Gamma Rays from the Decay of Au^{198}†

CARLTON D. SCHRADER*
State University of Iowa, Iowa City, Iowa
(Received June 18, 1953)

The angular correlation of the 0.411-Mev and 0.64-Mev cascade gamma rays resulting from the beta decay of Au^{198} to Hg^{198} has been measured with scintillation counters. If only pure multipole radiations are assumed, the experimental data do not agree with theoretical calculations for any reasonable values of the spins of the relevant states in Hg^{198}. They do agree well, however, with spins of 0, 2, and 2 for the ground state, 0.411-Mev state, and 1.09-Mev state of Hg^{198}, respectively, if the first transition (0.68-Mev gamma) is assumed to be a mixture of 60 percent dipole and 40 percent quadrupole radiation and the second transition (0.41-Mev gamma) is assumed to be pure quadrupole radiation. The parities of all three states are the same, presumably even. These results are in general agreement with the internal conversion measurements of other investigators.

I. INTRODUCTION

IT has recently been discovered[1–3] that about two percent of the decay of Au^{198} occurs through the emission of a 0.295-Mev beta to a 1.09-Mev level in Hg^{198}. This level decays both by a direct 1.09-Mev gamma to the ground state and by cascade emission of gammas of energies 0.68 and 0.411 Mev. Cavanagh[4] measured the intensities of the 0.68 and 1.09-Mev gammas relative to the 0.411-Mev gamma and found values of 1.4 percent and 0.4 percent, respectively. Elliott and Wolfson[5] have measured the internal conversion coefficients of all three gammas and in addition have reported a very low-intensity 1.38-Mev beta to the ground state. A determination of the angular correlation of the two cascade gamma rays should serve to verify the spin and parity assignments made on the basis of the internal conversion measurements, and if sufficiently precise should permit the determination of the multipole mixing ratio of the radiations.

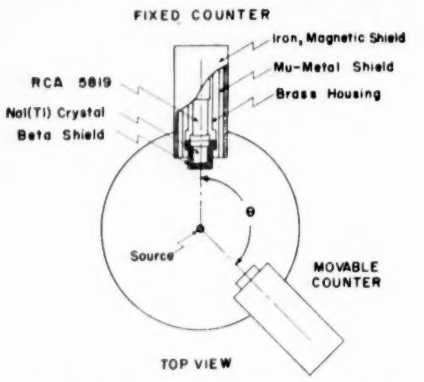

FIG. 1. Top view of scintillation spectrometer table. The details of the magnetic shielding of the photomultiplier tube and the β shields of the crystals are shown.

II. APPARATUS, PROCEDURE, AND EXPERIMENTAL RESULTS

The Au^{198} source used for the angular correlation was in the form of a metallic colloidal suspension. The source holder was made of aluminum and was constructed in the form of a hollow needle with a wall thickness of 0.020". The scattering of the gamma rays in the walls of the source holder was estimated to have a negligible effect on the angular correlation. The scintillation counters were NaI(Tl) crystals on RCA 5819 photomultiplier tubes. The crystal and phototube were sealed in a light tight housing as shown in Fig. 1. The Au^{198} differential pulse-height curve measured in one of the counters is shown in Fig. 2. The shoulder on the curve at 0.82 Mev is due to the coincidence of random 0.411-Mev gammas within the single counter. The peak near 0.20 Mev is the Compton peak of the 0.411-Mev gammas. The peak near 0.069 Mev is thought to be due to the K x-ray of gold.[3]

The electronic components of the two counting channels and coincidence circuit are shown schematically in Fig. 3. The discriminator of the amplifier for counter No. 1 was set at a point which corresponded approximately to point A of Fig. 2. This point was high enough to avoid pile-up from low-energy pulses and noise, low enough for the counter to have very good efficiency for the 0.411-Mev gamma, and at this setting the effect of amplifier drift was also minimized. The discriminator of the amplifier for counter No. 2 was set at a point corresponding to B of Fig. 2. This setting again minimized the effect of amplifier drift while permitting good efficiency for the counting of 0.68-Mev gammas without allowing a tremendously high accidental coincidence rate from the intense 0.411-Mev gammas.

The discriminator settings were calculated to be high enough so that it was energetically improbable

† This work was supported in part by the U. S. Atomic Energy Commission.
* Now at the University of California Radiation Laboratory, Berkeley, California.
[1] R. W. Pringle and S. Standil, Phys. Rev. **80**, 762 (1950).
[2] Brosi, Ketelle, Zeldes, and Fairstein, Phys. Rev. **84**, 586 (1951).
[3] Cavanagh, Turner, Booker, and Dunster, Proc. Phys. Soc. (London) **A64**, 13 (1951).
[4] P. E. Cavanagh, Phys. Rev. **82**, 791 (1951).
[5] L. G. Elliott and J. L. Wolfson, Phys. Rev. **82**, 333 (1951).

for any gammas from the decay of Au^{198} to be counted in one counter, scatter, and be counted in the other counter. The same settings obviated any contribution from coincidences between possible 0.97-Mev beta bremsstrahlung and a subsequent 0.411-Mev gamma (see Fig. 4).

The problem of accidental coincidences was particularly acute in this experiment since the gammas following the direct beta transition to the 0.411-Mev level are approximately seventy times more intense than the cascade gammas. The accidental coincidence rate was determined by delaying the pulses in channel two by 1.3 microseconds, approximately three times the resolving time of the coincidence circuit. This

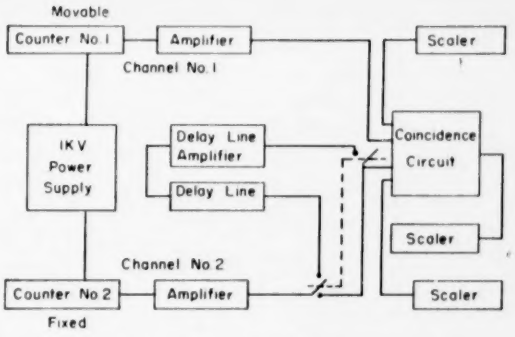

FIG. 3. Block diagram of electronic equipment.

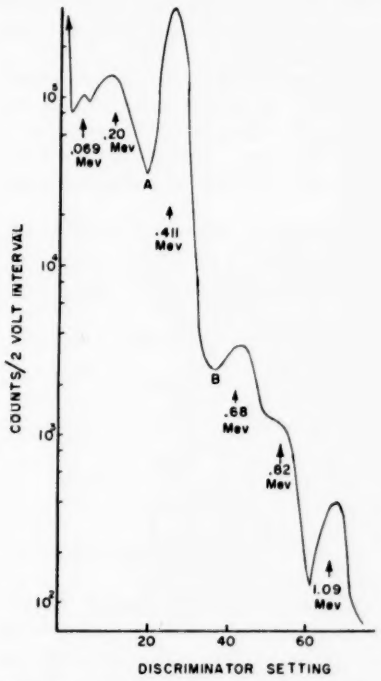

FIG. 2. Differential pulse-height distribution of pulses produced in NaI crystal by Au^{198} γ rays.

eliminated all true coincidences but left the accidental coincidence rate unchanged. The accidental coincidence rate was approximately 20 percent of the total coincidence rate. Also, because the true cascade gamma coincidence rate from Au^{198} was so small, the cosmic-ray background coincidence rate became an important correction to the observed coincidence rate. This background rate was approximately 10 percent of the total coincidence rate.

The final experimental quantity actually obtained was $W_{exp}(\theta)$. This is the ratio of the true coincidence rate (observed rate corrected for background and accidental rate) to the true rate in counter No. 1. The division by the true rate in counter No. 1 automatically corrected for decay of the source and any slight decentering of the source.

Since theory shows that angular correlation functions are expressible in terms of Legendre polynomials, $W_{exp}(\theta)$ was fitted to such an expansion by the method of weighted least squares. The normalized result was

$$W_{exp}(\theta)=1+A_2P_2(\cos\theta)+A_4P_4(\cos\theta),$$

where

$$A_2=-0.261\pm0.023, \quad A_4=0.137\pm0.012.$$

Although the interpretation of the data will be made in terms of the coefficients A_2 and A_4 of the Legendre polynomials, a conventional plot of $W_{exp}(\theta)$ against θ is shown in Fig. 5. The vertical bars through the experimental points represent the standard deviations based on counting statistics only.

III. DISCUSSION AND INTERPRETATION OF RESULTS

Since the lifetime of the intermediate (0.411-Mev) level has been measured[6,7] and is known to be about 10^{-11} second, the observed correlation should not have been perturbed by extra-nuclear fields. Thus a direct comparison with theoretical calculations can be made. It will be shown that such a comparison leads to a unique assignment of the spin for the second excited state of Hg^{198} and that this result agrees with all other information concerning the decay of Au^{198}.

Since $_{80}Hg^{198}$ is an even-even nucleus, its ground

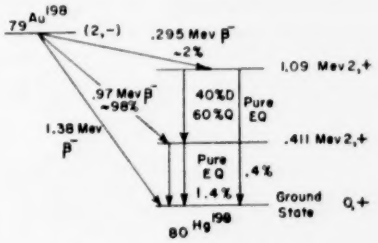

FIG. 4. Decay scheme of Au^{198}.

[6] P. B. Moon, Proc. Phys. Soc. (London) **A64**, 76 (1951).
[7] Bell, Graham, and Petch, Can. J. Phys. **30**, 35 (1952).

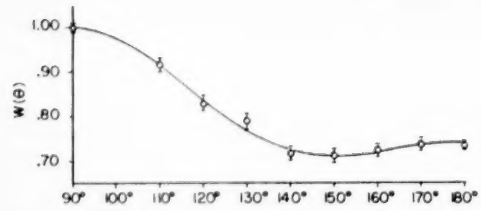

FIG. 5. Coincidence rate as function of angle between the counters. The vertical bars through the experimental points indicate the standard deviation due to counting statistics. The theoretical curve shown is calculated for a 2(60 percent D, 40 percent Q)2(Q)0 cascade.

state is assumed to have 0 spin and + parity (see also Burger and Van Cittert[8]). Moon[9] and Simons[10] are among the latest of several workers to measure the internal conversion coefficient for the 0.411-Mev gamma. All results show that this gamma is pure electric quadrupole radiation. This leads to the assignment of spin 2 and + parity for the 0.411-Mev level.

The spin of the 1.09-Mev level in Hg^{198} could be either 1, 2, or 3; a spin greater than 3 would mean a spin change of more than 3 in the crossover gamma-ray transition which is very highly improbable since the crossover gamma competes favorably with the first cascade gamma. Table I shows the theoretical Legendre polynomial coefficients for possible pure multipole transitions, and also shows the same coefficients corrected for the finite resolution of the counters used in this experiment. (The correction was made according to the method of Church and Kraushaar.)[11] Since there is no theoretical set of pure 1, 2, or 3 (D or Q) 2(Q)0 angular correlation coefficients which agree with the experimental coefficients, it becomes necessary to calculate the possible multipole mixtures which might occur in the first transition.

Theoretical expressions for angular correlations involving mixed radiations have been calculated by several authors, including Coester and Jauch.[12] The particular equations used were taken from Sec. III of Rose and Biedenharn.[13] The general angular correlation function for the cascade emission of a mixed dipole-quadrupole radiation and a pure quadrupole radiation may be written as

$$W(\theta)=\alpha^2W_1(\theta)+\beta^2W_2(\theta)+2\alpha\beta W_3(\theta),$$

where W_1 is the correlation function for a pure D-Q cascade, W_2 is the function for a pure Q Q cascade, and W_3 is the interference term, and where the α's and the β's are the reduced matrix elements of the respective transitions. The W's involve sums of products of Clebsch-Gordon coefficients, which may be calculated from equations given in Condon and Shortley,[14] and Racah coefficients, which can be found in tables prepared under the direction of Biedenharn.[15] The relative intensity of the quadrupole component to the dipole component of the mixed radiation is given by β^2/α^2. Lloyd[16] (see also Coester[17]) has pointed out that α and β are real with their signs undetermined. Thus the sign and the magnitude of the ratio β/α are arbitrary and can be adjusted to the data.

TABLE I. Coefficients in the expansion $1+A_2P_2(\cos\theta)+A_4P_4(\cos\theta)$.

Transition	Theoretical coefficients for pure multipole transitions A_2	A_4	Coefficients corrected for counter resolution A_2	A_4
1(D)2(Q)0	−0.200	0	−0.192	0
1(Q)2(Q)0	1.895	−0.0764	1.821	−0.0666
2(D)2(Q)0	0.250	0	0.240	0
2(Q)2(Q)0	−0.0775	0.327	−0.0745	0.285
3(D)2(Q)0	−0.0714	0	−0.0686	0
3(Q)2(Q)0	−0.204	−0.0817	−0.196	−0.0713
(Experimental)	...	...	−0.261	0.137

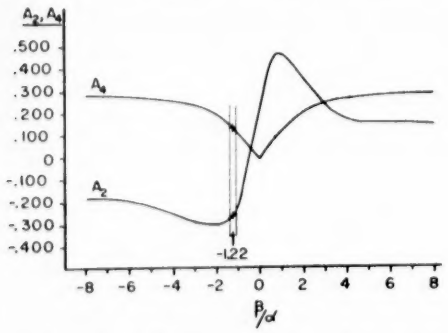

FIG. 6. Legendre coefficients as a function of the quadrupole-dipole amplitude ratio, β/α. The mean value of β/α which is compatible with the experimentally possible values of A_2 and A_4 (enclosed by the vertical lines) is −1.22.

In the present case a consideration of the possible dipole-quadrupole mixtures for a spin of either 1 or 3 shows that for all values of β/α the coefficient of the $P_4(\cos\theta)$ term is either zero or negative. Such mixtures are thus ruled out because of the observed positive coefficient of the $P_4(\cos\theta)$ term. Therefore, it is most probable that a theoretical mixture of spin 2-D, Q will agree with the experimental data.

Figure 6 shows the values of the angular correlation coefficients possible for a dipole-quadrupole, spin-2 mixture as a function of β/α. A mixing ratio of 60Q/40D with $\beta/\alpha=-1.225$ gives theoretical values of $A_2=-0.261$ and $A_4=0.136$ which most nearly coincide

[8] H. C. Burger and P. H. Van Cittert, Physica **5**, 177 (1938).
[9] M. Moon, Thesis, State University of Iowa, 1951 (unpublished).
[10] L. Simons, Phys. Rev. **86**, 570 (1952).
[11] E. L. Church and J. Kraushaar, Phys. Rev. **88**, 419 (1952).
[12] F. Coester and J. M. Jauch, Helv. Phys. Acta **26**, No. 1 (1953).
[13] M. E. Rose and L. C. Biedenharn, Revs. Modern Phys. (to be published).
[14] E. U. Condon and G. H. Shortley, *Theory of Atomic Spectra* (The Macmillan Company, Inc., New York, 1952), pp. 76–77.
[15] L. C. Biedenharn, "Table of Racah Coefficients," Oak Ridge National Laboratory Report ORNL-1098, 1952 (unpublished).
[16] S. P. Lloyd, Phys. Rev. **81**, 161 (1951).
[17] F. Coester, Phys. Rev. **89**, 619 (1953).

with the observed coefficients, although any values of β^2/α^2 between about 55/45 and 65/35 (β/α between -1.11 and -1.30) would be within the statistical accuracy of the experiment. The theoretical coefficients have been corrected for finite resolution of the counters.

Because of the excellent agreement of the observed correlation with the theoretical 2(40 percent D, 60 percent Q)2(Q)0 correlation, it is concluded that the spin of the 1.09-Mev level in Hg^{198} is 2 and that the 0.68-Mev radiation consists of a mixture of about 40 percent dipole and 60 percent quadrupole radiation.

Recently Elliott and Wolfson[5,18] have measured the internal converson of all three gamma rays and have found the coefficients to be consistent with the theoretical values of pure $E2$ for the 1.09- and 0.411-Mev gammas and 60 percent $M1$ plus 40 percent $E2$ for the 0.68-Mev gamma. They also measured the intensities of the 0.68- and 1.09-Mev gammas relative to the 0.411-Mev gamma, finding values of 0.48 percent and 0.13 percent, respectively. The pure $E2$ coefficient for the crossover transition allows immediate assignment of 2+ to the 1.09-Mev level. This agrees with the present experiment in the assignment of spin. Also, since the first announcement[19] of the present work, Schiff and Metzger[20] have published an independent account of essentially the same work with essentially the same results.

[18] Dr. L. G. Elliott (private communication, December, 1952).

IV. ACKNOWLEDGMENTS

The author wishes to express his sincere appreciation to Professor James A. Jacobs, Director of Nuclear Research, to Professor E. B. Nelson who suggested the problem, and to Professors J. M. Jauch and F. Coester, with whom several discussions concerning the theory were held. Thanks are also due Mr. J. G. Sentinella and the members of the instrument shop who constructed part of the apparatus, and to Dr. H. B. Elkins of the Radiology Department who supplied the radioactive gold.

[19] Schrader, Nelson, and Jacobs, Phys. Rev. **90**, 159 (1953).
[20] D. Schiff and F. R. Metzger, Phys. Rev. **90**, 849 (1953).

PHYSICAL REVIEW VOLUME 92, NUMBER 4 NOVEMBER 15, 1953

Method for the Determination of the End-Point Energy of Beta Emitters*

M. Forro
Barat College, Lake Forest, Illinois
(Received June 5, 1953)

It was found that the absorption of beta spectra in materials of high atomic number is exponential. The absorption coefficients in gold are inversely proportional to the $\frac{3}{2}$ power of the end-point energy of the spectrum. This experimental law holds with 2 percent accuracy in the energy interval from 0.3 Mev to 2.2 Mev and in the intensity domain from $\frac{1}{2}$ to 1/100 of the original intensity, if a detector with less than 2 percent relative opening is used. The end-point energy of beta emitters can, therefore, be determined by measuring only two points on a gold absorption curve and is expressed by the equation: $E=9\mu^{-1}+0.015$ with 2 percent accuracy from 0.17 Mev to 2.2 Mev; where E is the end-point energy in Mev and μ the absorption coefficient in cm^2/g.

THE most characteristic feature of a beta spectrum is its end-point energy. Spectroscopic and absorption methods so far used require strong sources and tedious measurements.[1] They cannot be used in cases when the source is weak, has a short lifetime, or when for other reasons a quick determination is required.

The method presented here is based on two experimental observations made by the author.

(1) It was found that the absorption curve of beta emitters in materials of high atomic number, e.g., gold, is a fairly straight line in a semi-logarithmic plotting, if the detector used has a relative opening of less than 2 percent and the absorbers are placed close to the source (see Fig. 1). Consequently the slope of such an absorption curve is determined by measuring only two points on the curve.

(2) It was found that the slope of the absorption curve in gold, i.e., the absorption coefficient, and the maximum energy of the beta spectrum are connected by the equation:

$$E=9\mu^{-1}+0.017, \tag{1}$$

where

$$\mu=\frac{\ln(J_1/J_2)}{a_2-a_1},$$

E denoting the end-point energy in Mev; a_1 and a_2 the thicknesses of the gold absorbers in g/cm^2; J_1 and J_2 the measured intensities at the two absorber thicknesses.

All in all, seven substances have so far been investi-

* This research has been supported by Frederick Gardner Cottrell grant of Research Corporation.
[1] See the comprehensive paper discussing absorption methods by L. Katz and A. S. Penfold, Revs. Modern Phys. **24**, 31 (1952).

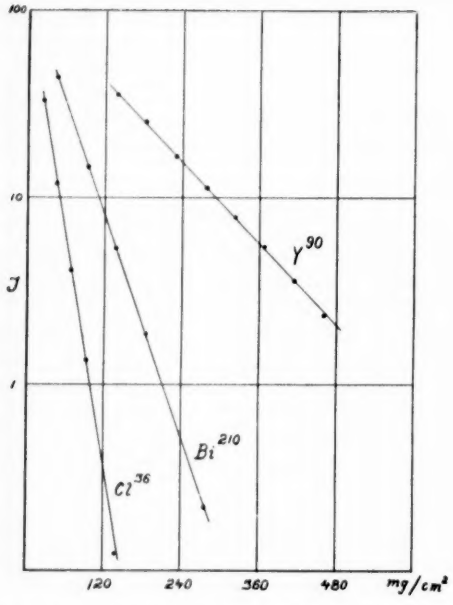

FIG. 1. Absorption curves of Cl^{36}, Bi^{210}(RaE), and Y^{90} in gold, measured with a detector of less than 2 percent relative opening. The error in each point is less than 1 percent with the exception of the lowest point on the Cl^{36} and Bi^{210} curves in which it is 2.5 percent.

gated. The results are given in Table I. With each material and each absorber thickness about 20 000 coincidences were recorded, and the two absorber thicknesses were interchanged in 20-min. intervals. The indicated errors are standard errors.

Of the seven substances, S^{35}, Pm^{147}, W^{185}, and P^{32} have allowed shape, Bi^{210}(RaE) and Y^{90} first forbidden shape, and Cl^{36} second forbidden shape. Bi^{210} and Y^{90} were in secular equilibrium with their mother substances (RaD with end-point energy 0.029 Mev and Sr^{90} with end-point energy 0.537 Mev). None of the substances investigated had a gamma radiation with the exception of W^{185} (0.134 Mev). The investigation of a larger number of isotopes will disclose to what extent the factors of Eq. (1) are influenced by the shape of the spectrum and whether the method could be used to determine the spectrum type.

The accuracy of the method is much better than indicated in the table, when a comparison source is used which has an end-point energy close to the end-point energy of the substance under investigation. If the two spectra are of identical shape, the accuracy is limited in practice by the statistical errors of the counting rates alone.

The factors of Eq. (1) depend, of course, to some extent upon the geometry used. The actual measurements were made with an equipment which is suggested as standard. It is a double-coincidence equipment with brass flow-counters of 1-in. outer diameter, 0.065-in. wall thickness, and 1-in. effective wire length. The counters have circular windows of 6.5-mg/cm² thickness and $\frac{3}{4}$-in. diameter on the sides facing each other and $\frac{3}{8}$-in. diameter on the source side, allowing thus the use of sources up to $\frac{1}{4}$-in. diameter. The counters were spaced $\frac{1}{8}$ in. apart, and above 0.7 Mev 24 mg of aluminum was placed between the counters to reduce coincidences due to the bremsstrahlung. The source was placed $\frac{1}{16}$ in. before the first counter, with the gold absorbers put between source and first counter. For end-point energies below 0.20 Mev (S^{35}), instead of double coincidences the counting rate of the first counter was measured; in this case the source was placed at such a distance that the relative solid angle remained the same (2 percent). At such low energies the counting rate due to internal or external bremsstrahlung is already negligible.

The first absorber thickness (a_1) should preferably be chosen in such a way that it decreases the original intensity by a factor of 2 to 3 $a_1 \sim 0.03\ E^{\frac{1}{2}}$ g/cm². In the case of a complex beta spectrum, or a substance with a beta-radiating mother substance, the thickness of the first absorber ought to be greater than the maximum range of all the other beta components with the exception of the one with the highest energy. For instance, in the case of Y^{90}, a_1 was taken to be 184 mg/cm² in order to absorb the beta rays of Sr^{90}.

TABLE I. Comparison of end-point energies with values calculated from Eq. (1). The indicated errors are standard errors.

Emitter	End point energy in Mev		Difference in percent
	Spectroscopic[a]	Equation (1)	
S^{35}	0.167	0.167	0.0±0.3
Pm^{147}	0.226	0.223	−1.3±0.5
W^{185}	0.428	0.431	+0.7±0.7
Cl^{36}	0.714	0.714	0.0±0.8
Bi^{210}	1.17	1.148	−1.9±0.7
P^{32}	1.701	1.726	+1.5±1.1
Y^{90}	2.23	2.207	+1.0±0.6

[a] See Hollander, Perlman, and Seaborg, Revs. Modern Phys. **25**, 469, 1953.

If, in addition to the beta spectrum, a source also has gamma rays, the total absorber between the counters should be sufficient to absorb the photoelectrons created by the gamma radiation in the gold absorber. For instance, in the case of W^{185}, 30 mg/cm² total absorber between the counters was sufficient.

The method is extremely sensitive with respect to the thickness of the additional absorber ($a_2 - a_1$); therefore the additional absorber should either be measured with great accuracy, or its effective thickness be determined with the help of a source of well known end-point energy.

The relative error of the determination of the end-point energy is:

$$\frac{\Delta E}{E} = \frac{2}{3}\left(\frac{1}{N_1}+\frac{1}{N_2}\right)^{\frac{1}{2}} \Big/ \ln\left(\frac{J_1}{J_2}\right), \qquad (2)$$

where N_1 and N_2 denote the total number of counts with the two gold layers respectively. The measuring time necessary to reach a given accuracy is:

$$T=t_1+t_2=\frac{4}{9}\frac{1}{J_1}\left(\frac{\Delta E}{E}\ln\frac{J_1}{J_2}\right)^{-2}\left(1+\frac{J_1t_1}{J_2t_2}\right)\left(1+\frac{t_2}{t_1}\right), \quad (3)$$

where t_1 and t_2 stand for the measuring times with the first and second absorbers, respectively. T will be a minimum if

$$t_2/t_1=(J_1/J_2)^{\frac{1}{2}} \quad \text{and} \quad J_1/J_2=13, \quad (4)$$

in which case $T=(\Delta E/E)^{-2}$ hours for one micromicrocurie source strength. (In this calculation it is assumed that the first absorber decreases the original intensity by a factor of two.) For instance if the end-point energy of a source of 1 millimicrocurie should be determined with a statistical error of 2 percent, the total measuring time will be 2.5 hours. The length of the total measuring time is, however, very insensitive with respect to the chosen intensity ratio (J_1/J_2); it increases by less than a factor of two when the intensity ratio is reduced to 3. Accordingly, whenever the source strength is low and the coincidence rates become comparable to the background rate, a lower ratio for J_1/J_2 should be chosen than the optimum ratio of 13.

The coincidence equipment described had a background rate of about 100 coincidences per hour, limiting the method to sources of not less than 100-micromicrocurie strength. A triple-coincidence equipment with counters similar to those described has, by a relative opening of 0.6 percent, a background rate of about 10 coincidences per hour, thus providing an extension of the method to source strengths of 30 micromicrocuries possible. The background rate can be reduced by a further factor of two if the absorbers between the counters are considerably increased.

In the case of strong sources, great care should be taken to correct for counting losses due to the dead-time of the first counter and to the resolving time of the coincidence circuit and the register. By careful design of the circuit, and using electronic scalers before the mechanical register, only the losses due to the dead-time of the counter remain to be considered. A method for determining all losses is the following:

A source with high-energy beta rays is placed before the counters, not less than 2 in. from the first counter, giving a coincidence rate comparable with the rate to be measured and the coincidence rate noted. Thereafter, a second source with very soft beta rays is placed sidewise before the window of the first counter, in such a position that its rays are not capable of reaching the second counter. Hence the coincidence rate is not increased, but only the counting rate of the first counter. From the difference in the coincidence rates and the difference in the counting rates with the first source and the two sources together, the coincidence loss due to the dead-time can be evaluated in the usual manner. Since the dead-time of G.M. counters depends upon the counting-rate and upon other factors, it is not advisable to allow more than 1 to 2 percent loss; this is equivalent to a maximum counting rate of 100–200 counts per sec in the first counter, if special methods are not used to decrease the dead-time. The counting rate of the first counter can be reduced either by increasing the thickness of the first absorber or by placing the source in greater distance from the first counter. The latter procedure has the advantage that it decreases the counting rate of the first counter considerably and the coincidence rate only slightly.

In its present form the method is restricted: (a) to single beta emitters, (b) to the determination of the end-point energy of the highest-energy component of a complex beta spectrum, and (c) to beta-gamma emitters in which the gamma energy is much lower than the end-point energy of the beta spectrum.

It is intended to investigate

(1) The theoretical explanation of the constant slope of the absorption curve and the $\frac{2}{3}$ power in Eq. (1).

(2) The factors influencing and limiting the accuracy of the method.

(3) The influence of the shape of the spectrum.

(4) The possibilities and limitations of the method in case of beta-gamma emitters.

(5) The limitation of the method toward low energies.

(6) Whether the method, or a modification of it, could be used for the determination of gamma-ray energies, by means of their secondary electrons.

(7) The applicability of scintillation counters.

(8) Whether the method could be developed into an end-point energy monitor, which would enable the instantaneous identification of radioactive substances, with special attention to its usefulness in case of contamination of objects, food, etc., due to an atomic blast.

Technetium of Mass Number 98

JOHN K. LEROHL,* M. L. POOL, D. N. KUNDU, AND R. A. HOUSE†
Ohio State University, Columbus, Ohio

(Received July 1, 1953)

By (p,n) reactions on enriched molybdenum isotopes, it has been found that Tc^{98} does not have a half-life in the neighborhood of either 42 minutes or 2.8 days as had been variously claimed.

IN 1948 an activity with a half-life of 2.8 days[1] and characterized by negatively charged particles was assigned to Tc^{98}. This proposal was supported[2] in 1950. Also, in 1948, an activity of positively charged particles with a half-life of 40 ± 5 minutes, which could reasonably be attributed to Tc^{98}, was reported.[3] However, this 40-minute activity was not observed by other investigators at that time.[4] In 1952, evidence for a 42-minute positron activity was presented but the activity of 2.8-day half-life, assigned to Tc^{98}, was not confirmed.[5]

Since enriched isotopes of Mo^{95}, Mo^{98}, and Mo^{100} were avilable, it was thought advisable to reinvestigate the activities attributed to Tc^{98}.

Two samples of enriched molybdenum isotopes, one of mass number 98 and the other of mass number 100, were bombarded under similar conditions with 7.4-Mev protons. The resulting activities were compared. Both target samples were in the oxide form and the F^{18} activity produced by a (p,n) reaction on the oxygen present served as a monitor of the relative total bombardment afforded each sample. A positron activity of 53 ± 2 minute half-life was observed from both samples. The ratio of the intensity of 53-minute activity from the target enriched in Mo^{98} to that enriched in Mo^{100} was 1.0/1.2. The ratio of abundance of Mo^{94} in the above two samples was 0.33 percent/0.40 percent or 1.0/1.2. The abundance of Mo^{98} in the enriched Mo^{98} sample was 95 percent and that in the Mo^{100} sample, 0.6 percent. The total intensity of the 53-minute activity in each of the enriched samples can therefore be accounted for by Tc^{94} from the $Mo^{94}(p,n)$ reaction.[6] Thus, there is no activity of measurable intensity in the range of 40 to 55 minutes that can be assigned to Tc^{98}.

Attempts were made to produce an activity that could be attributed to Tc^{98} by bombarding with 20-Mev alpha particles a sample of molybdenum, enriched in isotope of mass number 95 (80.75 percent). All of the resulting activities that were observed could be attributed to well established alpha-particle reactions with molybdenum and with the traces of Cu, Si, and Ca present in the target sample. It was noted that the relative intensities of the 1.1-hour and 9.45-hour half-life activities produced by an (α,n) reaction on the copper impurity (0.02 percent) were as expected. After subtracting the 1.1-hour activity, there was no measurable activity of approximately 42 or 50 minutes half-life remaining which could be attributed to Tc^{98} by the $Mo^{95}(\alpha,n)$ reaction.

Tc^{98} thus appears not to possess an activity with a half-life in the neighborhood of either 42 minutes or 2.8 days. The half-life of Tc^{98} may, however, be very long in accordance with the expectations from the shell theory.[7]

* Captain, United States Air Force. Research under auspices of U. S. Air Force Institute of Technology, Wright-Patterson Air Force Base, Ohio.
† Lt. Col., United States Air Force. Research under auspices of U. S. Air Force Institute of Technology, Wright-Patterson Air Force Base, Ohio.

[1] E. E. Motta and G. E. Boyd, Phys. Rev. **74**, 220 (1948).
[2] L. E. Glendenin, *Radiochemical Studies: The Fission Products* (McGraw-Hill Book Company, Inc., New York, 1950), Paper No. 329, National Nuclear Energy Series, Plutonium Project Record, Vol. 9, Div. IV.
[3] E. E. Motta and G. E. Boyd, Phys. Rev. **73**, 1470 (1948).
[4] D. N. Kundu and M. L. Pool, Phys. Rev. **74**, 1775 (1948).
[5] House, Colligan, Kundu, and Pool, Phys. Rev. **86**, 654 (1952).
[6] Medicus, Preiswerk, and Scherrer, Helv. Phys. Acta **23**, 299 (1950).
[7] E. Segrè, Nuovo cimento **9**, 1008 (1952).

Gamma Rays from Proton Bombardment of B^{10}†

R. W. KRONE AND L. W. SEAGONDOLLAR
University of Kansas, Lawrence, Kansas

(Received July 3, 1953)

The γ-ray spectrum resulting from the radiative decay of C^{11}, produced by the proton bombardment of B^{10}, has been investigated using thick and thin targets. Observations were made for proton energies ranging from 500 kev to 1.7 Mev. A broad resonance with a maximum at 780 kev appears well established. The compound nucleus decays in a one-step transition to the ground state of C^{11} with the emission of a γ ray of energy approximately equal to 9 Mev. The existence of two other resonances, observed for proton energies of 0.95 and 1.33 Mev, is less certain.

INTRODUCTION

IN a recent publication Walker[1] has reported that a high-energy γ ray is observed when thick B^{10} targets are bombarded with protons of 1.2 Mev. This γ ray has been attributed to the radiative decay from a highly excited compound state in C^{11}. The low intensity of this radiation, and the large background from the 12- and 16-Mev γ rays from $B^{11}(p,\gamma)$ make it awkward to observe this process by the technique commonly utilized for (p,γ) experiments. This undoubtedly accounts for the failure to detect this γ ray in earlier experiments. Inasmuch as the results of Walker were obtained with a proton beam of just a single energy, it appeared of interest to make a more detailed study of this reaction.

EXPERIMENTAL PROCEDURE

A beam of monoenergetic protons is available from the University of Kansas electrostatic generator.[2] The analyzed beam enters the target chamber shown in Fig. 1 which has been designed so that either thin or thick targets may be used. An RCA 5819 photomultiplier tube, on which is mounted a $1\frac{1}{2}$ in. long NaI(Tl) crystal, serves as the detector of the γ rays. With the arrangement used, the scintillation detector can be placed to within $\frac{3}{8}$-inch of the target. Because of the small cross section of the reaction it is essential to bring the detector as close as possible to the target to have a counting rate significantly larger than the background.

Measurements were made with both thick and thin targets. The thick targets were prepared by pressing enriched B^{10} into a molybdenum cup. A background run taken with the empty cup in place revealed no significant background of γ radiation having energy greater than 5 Mev. Two thin B^{10} targets, evaporated on a 1-inch diameter tantalum disk, were available. The thickness of these targets was approximately 40 $\mu g/cm^2$. Both of these targets exhibited contamination of fluorine and sodium. The sharp resonance peaks of both contaminants were readily detectable but could always be distinguished from the B^{10} γ rays by a careful analysis of γ-ray energies.

The observation of the capture radiation resulting from B^{10} is awkward for the following reason. Even with enriched targets, the background from the $B^{11}(p,\gamma)$ reaction is sufficiently large to mask the much lower intensity γ rays resulting from B^{10}. Recent experiments[3,4] have shown the existence of two broad resonance states in C^{12}. These states correspond to maxima in the γ-ray yield for bombarding energies 680 kev and 1.38 Mev. Two high-energy γ rays having energy of 12 Mev and 16 Mev are observed in the resultant decay. These two γ rays produce in the scintillation detector not only the usual peak, corresponding to the production of an electron-positron pair, but also a continuous distribution of pulses which tends to mask those pulses arising from a 9-Mev γ ray expected from the B^{10} reaction. Since this distribution depends on the dimensions of the crystal and the material surrounding it, it may not readily be computed. The usual technique of counting all the pulses produced, as a function of bombarding energy, leads therefore to no significant results, as long as there are no rapid fluctuations in the yield corresponding to well-defined resonances in the compound nucleus.

A more promising, though more qualitative, procedure consists of photographing the pulse-height distribution appearing on an oscilloscope for various bombarding energies. This method is equivalent to pulse-height analysis with a single-channel discriminator. The latter method has the advantage of allowing quantitative comparison of the peaks at various energies. Because of the extremely low counting rates available, this advantage is offset by the statistical uncertainties of the data so obtained. Experience has shown that with the proton currents available (2 microamperes or less) no significant results could be obtained with thin targets for runs lasting less than one hour. Because of the danger of carbon deposits on the target and possible drifting of the electronic circuits, no pulse-height analysis with discriminating circuits was at-

† This work was supported in part by the U. S. Office of Naval Research.

[1] W. D. Walker, Phys. Rev. **79**, 172 (1950).

[2] A detailed description of the Van de Graaff generator, its method of control, and energy stability will be published elsewhere.

[3] Cochran, Ryan, Givin, Kern, and Hahn, Phys. Rev. **87**, 672 (1952).

[4] T. Huus and R. B. Day, Phys. Rev. **85**, 761 (1952).

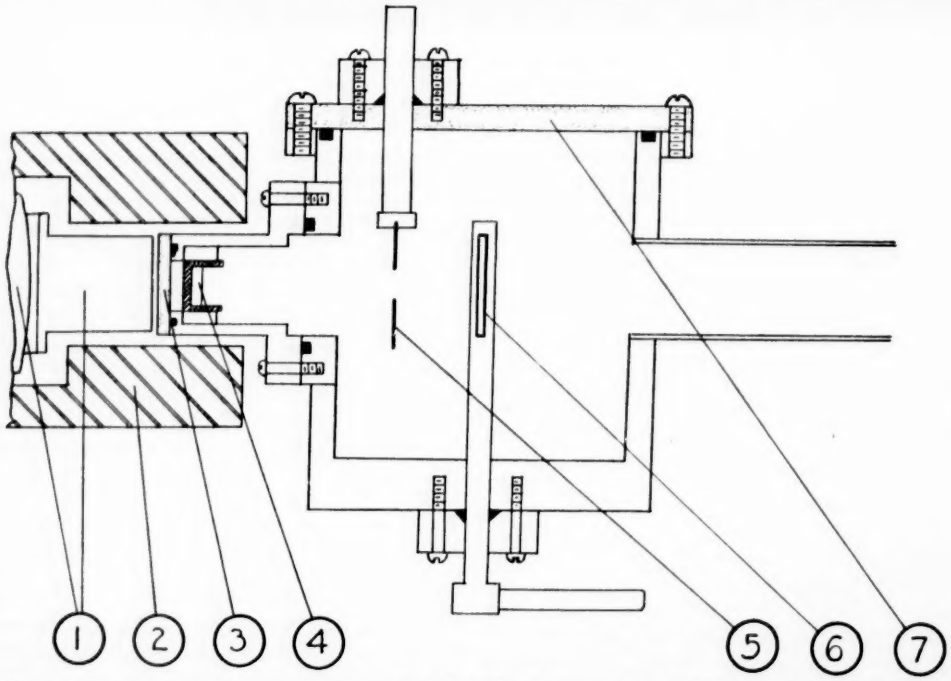

FIG. 1. Target chamber used for (p,γ) experiments. 1. NaI(Tl) crystal mounted on a RCA 5819 photomultiplier tube; 2. lead shield; 3. lucite window; 4. thick target assembly consisting of a molybdenum cup which is held in place by brass ring. For thin target observations the cup is removed and the thin target inserted between the brass ring and the end wall of the chamber; 5. tantalum disk with $\frac{1}{4}$-inch hole serving as an aperture. The disk is electrically insulated from the remainder of the target chamber; 6. rotating quartz window; 7. lucite cover.

tempted, except with thick targets for which the counting rate was very much larger.

RESULTS

Data have been taken using bombarding energies ranging between 520 kev and 1.7 Mev. As a general rule this energy region was scanned in steps of 40 kev.

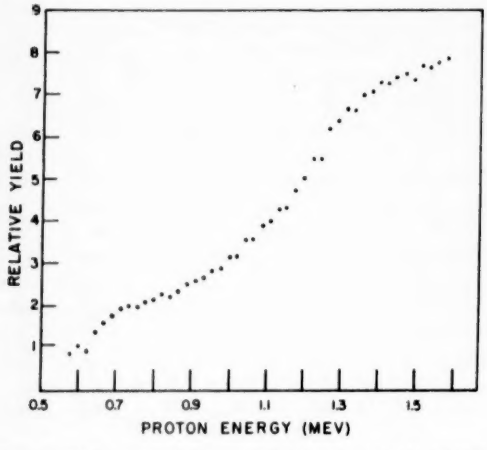

FIG. 2. Thick target yield as a function of proton bombarding energy obtained with enriched B^{10}. This curve was obtained by counting all γ rays greater than 6 Mev.

Much more detailed data were obtained with a thin target between 0.9 and 1.3 Mev to ascertain the possible existence of a well-defined resonance state in the neighborhood of 1.16 Mev in conformity with the results of Walker. A sharp resonance was observed at 1.162 Mev and others at 1.210, 1.254, and 1.281 Mev. A careful check showed, however, that all these peaks were due to sodium contamination of the target.

The results of a typical thick target run, with the discriminator bias adjusted to accept only pulses corresponding to γ rays of energy greater than 6 Mev, are shown in Fig. 2. The shape of this curve may be understood by assuming the existence of two very broad resonances, the maximum of one corresponding to a proton bombarding energy of approximately 700 kev, that of the other to an energy of approximately 1.35 Mev. This is precisely what would be expected from the $B^{11}(p,\gamma)$ process. Any resonances arising from the $B^{10}(p,\gamma)$ reaction must, therefore, be very much weaker in intensity, unless they occur at approximately the same bombarding energies as those of the competing process.

Pulse-height distributions were obtained with thick targets over the entire energy range. The system was calibrated by recording the pair peaks resulting from the γ rays of $Li^7(p,\gamma)$ and $F^{19}(p,\gamma)$. The results indicate the existence of a γ ray of approximately 9 Mev which

must be ascribed to the $B^{10}(p,\gamma)$ reaction. These data also show the 4.4- and 12-Mev γ rays from the $B^{11}(p,\gamma)$ process, and at higher energies the 16-Mev γ ray from that same reaction. A comparison run taken with a thick target of elemental boron confirms this conclusion by the absence of the 9-Mev radiation. Figure 3 shows two photographs comparing a typical pulse-height distribution of B^{10} and elemental boron. The bombarding energies for both of these runs was 1.07 Mev. Figure 4 shows the identical pulse-height distribution of B^{10} as obtained with a single-channel pulse-height discriminator. A careful examination of a series of such pulse-height distributions indicates the gradual appearance of the 9-Mev radiation beginning at a bombarding energy of approximately 650 kev. An attempt has been made to obtain from these data the usual thick target yield curve by plotting the number of counts above the continuous distribution as a function of bombarding energy. The results of this analysis, plotted in Fig. 5, show the yield rapidly increasing above bombarding energies of 670 kev and leveling off above 900 kev, as would be expected from a broad resonance level. This indicates that the low-energy resonance apparent in Fig. 2 is really the result of two processes; the 680-kev resonance due to the $B^{11}(p,\gamma)$ reaction, as well as another due to $B^{10}(p,\gamma)$ at somewhat higher energy.

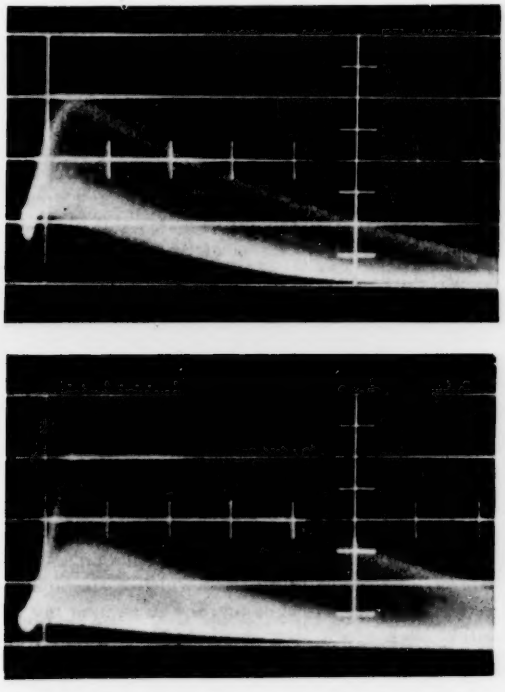

FIG. 3. Thick target pulse-height distributions resulting at proton bombarding energy of 1.07 Mev. The photograph on top was obtained with an enriched B^{10} target. The photograph below was obtained under identical conditions with an elemental boron target.

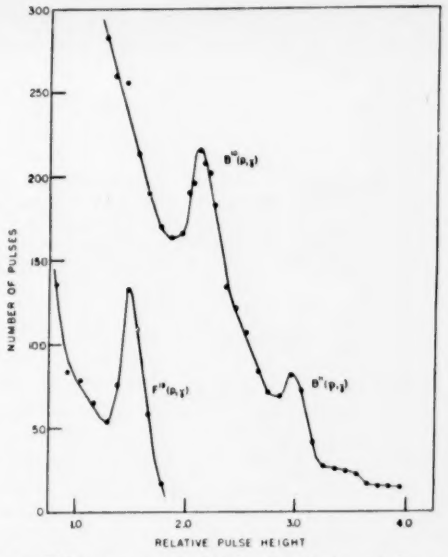

FIG. 4. Thick target pulse-height distribution of the γ rays resulting from $B^{10}(p,\gamma)$ at proton bombarding energy of 1.07 Mev. The curve at the lower left shows the peak from the $F^{19}(p,\gamma)$ reaction which has been used as a calibration for the single channel pulse-height analyzer.

Pulse-height distributions obtained by photographic means with thin targets confirm the existence of a broad resonance with a maximum at approximately 780 kev. At higher energies the 9-Mev radiation decreases in intensity but remains detectable to 1.5 Mev.

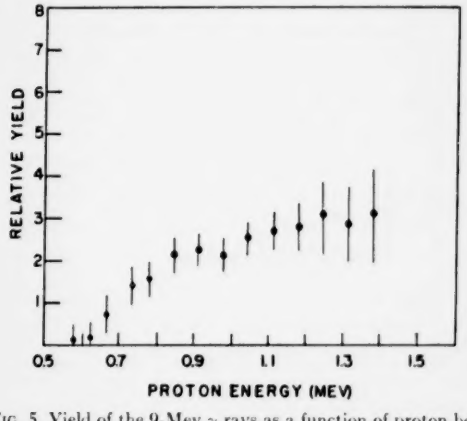

FIG. 5. Yield of the 9-Mev γ rays as a function of proton bombarding energy obtained with a thick target of B^{10}. The data for this graph were obtained by taking pulse-height distributions for a series of bombarding energies, and calculating the number of counts above the continuous distribution.

The photographic records of the distributions indicate two peaks in this range of energies having their respective maxima at 0.95 and 1.33 Mev. Of these, the first is the better established. These variations in the yield are too small to be detectable with thick targets. They should therefore be considered as questionable.

Scintillation Spectrometer Determination of L-Capture to K-Capture Ratio in Cd^{109} and I^{125}†

E. DER MATEOSIAN
Brookhaven National Laboratory, Upton, New York
(Received July 28, 1953)

A useful technique of scintillation spectrometry developed in this laboratory—that of growing crystals containing radioactive nuclei—was employed to measure the L-capture to K-capture ratio in the orbital electron capture occurring in Cd^{109} and I^{125}. Marshak's formulas were used to calculate the energy of the transition. The L-capture to K-capture ratio and the energy of the transition are reported as 0.28 ± 0.03 and 73_{-6}^{+12} kev for Cd^{109}, and 0.23 ± 0.03 and 108_{-10}^{+20} kev for I^{125}, respectively.

INTRODUCTION

WHEN a nucleus decays by means of orbital electron capture, a knowledge of the L-capture to K-capture ratio is significant because this ratio is a function of the order of and the energy available for the transition.[1] If the total disintegration energy is known (as would be the case if positron emission competed with orbital electron capture) as well as the spin and parity change, the experimentally determined L-capture to K-capture ratios can be compared with calculated values as a check of β theory.[2] On the other hand, as belief in β theory strengthens, the L-capture to K-capture ratio becomes a useful and important tool in the study of the systematics of energy levels, for it offers a way to determine the energy differences between states connected by orbital electron capture alone.

Not many experimental data exist on L-capture to K-capture ratios, the reason being that the detection and absolute measurement of soft x-radiations has been experimentally difficult.[3] A technique developed in this laboratory,[4] whereby radioactivity is introduced into a NaI scintillating crystal, lends itself readily to the study of L-capture to K-capture ratios by providing one with a detector which has no window corrections for soft radiations and, at the same time, has an efficiency of approximately 100 percent.

EXPERIMENTAL DETAILS

The method consists of growing a thallium-activated sodium iodide single crystal from a mass of sodium iodide to which has been added a trace of the radioactive material under investigation. The single crystal of sodium iodide which is obtained in this manner contains evenly dispersed throughout its volume a source of radiations which is for practical purposes of zero thickness. If the ratio of the weight of radioactive matter to thallium activator is kept small (<10 percent) the crystal exhibits in most cases scintillation properties equal to those of an ordinary sodium iodide scintillator. Observations are made with the crystal mounted on a photomultiplier tube connected through an Atomic Instrument Company type 204B linear amplifier to either a Dumont type 301 oscilloscope (for photographic recording) or an Atomic Instrument Company single channel pulse-height analyzer.

The chief source of error in this method for determining this ratio is the escape of photons from the crystal. If large crystals (1 cm^3) are used, the escape of x-rays for atoms of low or intermediate Z will be small and approximate corrections can be made.

Cd^{109}

The radioactive isotope Cd^{109} decays by orbital electron capture to the first excited state of Ag^{109}, which in turn decays through the emission of a highly converted 87-kev gamma ray to the ground state.[5] The half-life of Cd^{109} is reported to be 330 days or greater. The first excited state of Ag^{109} is metastable and has a half-life of 39.2 sec. Orbital electron capture leading to the ground state of Ag^{109} has not been reported, and the probability for such a transition is small for any spin assignment made to the Cd^{109} in view of the spins assigned to the first excited state and to the ground state of Ag^{109} (7/2 and 1/2, respectively). Positron emission has been looked for and not seen.[6] Thus each orbital electron capture has associated with it an 87-kev gamma ray, which is internally converted over 90 percent of the time.

When a source of Cd^{109} is dispersed throughout a crystal by the above described method and the pulses resulting in the crystal are observed with a pulse-height analyzer, one sees a pulse peak which corresponds to the conversion electrons of the 87-kev gamma ray and another peak which corresponds to the K x-ray which accompanies the K-electron capture (Fig. 1). Although both these pulses originate in the detector and the

† Work carried out under the auspices of the U. S. Atomic Energy Commission.
[1] R. E. Marshak, Phys. Rev. **61**, 431 (1942).
[2] P. Radvanyi, Compt. rend. **235**, 428 (1952).
[3] See for example, Pontecorvo, Kirkwood, and Hanna, Phys. Rev. **75**, 982 (1949); G. Friedlander and W. L. Orr, Phys. Rev. **84**, 484 (1951).
[4] Scharff-Goldhaber, der Mateosian, Goldhaber, Johnson, and McKeown, Phys. Rev. **83**, 480 (1951).
[5] References are given in Hollander, Perlman, and Seaborg, Revs. Modern Phys. **25**, 469 (1953); M. Goldhaber and R. D. Hill, Revs. Modern Phys. **24**, 179 (1952).
[6] Dreyfus, Major, and Radvanyi, Compt. rend. **232**, 617 (1951).

detector has a 4π solid angle geometry, the x-rays and the 87-kev gamma rays are not added together in the crystal since the two pulses are usually separated in time by an interval greater than the resolving time of the circuit. Because of the high degree of conversion of the Ag^{109m} internal transition and low loss of 87-kev gamma rays from the crystal, the area under the 87-kev gamma-ray peak may be taken as a measure of the total number of orbital electron captures in a given unit of time, regardless of whether capture takes place in the K, L, or a higher shell. The area under the K x-ray peak is a measure of the K-capture rate and by difference one may obtain the L-capture rate, assuming M and N capture to be negligible. The experimentally obtained L-capture to K-capture ratio is 0.28 ± 0.03.

I^{125}

The decay of 60-day I^{125} is very similar to that of Cd^{109}, proceeding by orbital electron capture[5] to the

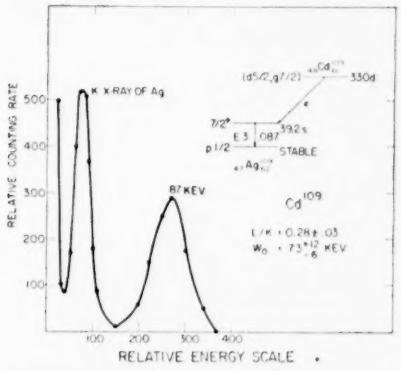

FIG. 1. Soft photons of Cd^{109} observed with a scintillation spectrometer. The output of a single channel pulse-height analyzer is plotted as a function of energy. Two peaks are observed, one corresponding to the K x-rays of Ag resulting from the orbital electron capture in Cd^{109} and the other corresponding to the 87-kev transition in Ag^{109} following the orbital electron capture.

first excited state of Te^{125}. Unlike Ag^{109m} however, the first excited state of Te^{125} is not metastable so that the internal transition to the ground state (35 kev) and the x-radiations accompanying orbital electron capture are not resolved and one sees, in a pulse-height analysis of the pulses resulting from a crystal containing I^{125}, peaks corresponding to the addition of conversion electrons and x-rays. This is a fortunate state of affairs, because both the L x-ray peaks and K x-ray peaks are shifted by 35 kev to higher positions on the energy axis, rendering both peaks resolvable above instrument noise (see Fig. 2). The ratio of the areas under the L x-ray peaks and K x-ray peaks is a direct measure of the L-capture to K-capture ratio, which in this case is 0.23 ± 0.03.

TRANSITION ENERGIES

The calculation of transition energies from L-capture to K-capture ratios was based upon formulas developed

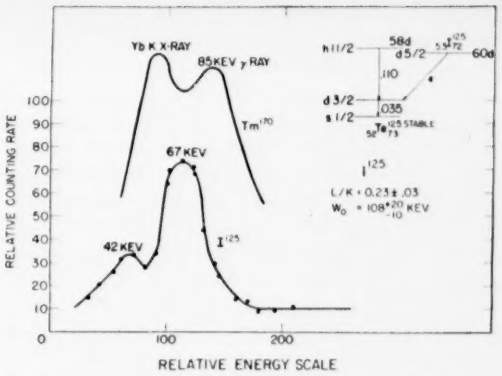

FIG. 2. Soft photons of I^{125} observed with a scintillation spectrometer. The output of a single channel pulse-height analyzer is plotted as a function of energy. Two peaks are observed, one corresponding to the addition of 35-kev pulses and L x-rays of Te and the other corresponding to the addition of 35-kev pulses and K x-rays of Te. The upper curve shows the radiations of Tm^{170} which were used to calibrate the instrument.

by Marshak[1] for the lifetime for orbital electron capture. In an allowed transition the relationship between the L-capture to K-capture ratio and the transition energy may be written as

$$R_{L/K}=\left[\frac{\Psi_{L1}}{\Psi_K}\right]^2\left[\frac{W_0+W_L}{W_0+W_K}\right]^2,$$

where $R_{L/K}$ is the L-capture/K-capture ratio, Ψ_{L1}/Ψ_K is the ratio of L- and K-shell electron densities at the nuclear radius and W_0, W_L, and W_K are the transition energy, the L-shell energy, and the K-shell energy, respectively.[7] Values for the quantity $[\Psi_{L1}/\Psi_K]^2$ as a function of Z have been published by Rose and Jackson.[8] Table I gives a summary of our data and results. It is of interest to note that in the region where $(W_0+W_L)/(W_0+W_K)$ is appreciably different from 1, W_0 is a slowly varying function of $R_{L/K}$, hence sizeable experimental errors can be tolerated in the L-capture to K-capture ratio.

TABLE I. Measured L-capture to K-capture ratios and calculated transition energies for orbital electron capture in Cd^{109} and I^{125}.

Isotope	L-capture to K-capture ratio	Transition energy (kev)[a]	Log(ft)
Cd^{109}	0.28 ± 0.03	73_{-6}^{+12}	5.1
I^{125}	0.23 ± 0.03	108_{-10}^{+20}	4.8[b]

[a] Values for W_K and W_L in these calculations were computed from the expressions given by Marshak (reference 1): $W_K=1-\frac{1}{2}\alpha^2Z_{eff}^2$ and $W_L=1-\frac{1}{8}\alpha^2Z_{eff}^2$ where $Z_{eff}=Z-0.3$.

[b] A slightly higher value for log(ft) was reported for I^{125} by G. Friedlander and W. L. Orr, who extrapolated S. A. Moszkowski's nomograph [Phys. Rev. **82**, 35 (1951)] to make their calculation.

[7] Marshak defines W_K as $1-\frac{1}{2}\alpha^2Z_{eff}^2$ and W_L as $1-\frac{1}{8}\alpha^2Z_{eff}^2$, where $Z_{eff}=Z-0.3$ and $\alpha=1/137$.

[8] M. E. Rose and J. L. Jackson, Phys. Rev. **76**, 1540 (1949).

DISCUSSION OF RESULTS

Friedlander and Orr[3] determined the L-capture to K-capture ratio in I^{125} by using a windowless proportional counter to compare the ratio of 35-kev gamma rays to K x-rays in an I^{125} source with the same ratio in a Te^{125} source. They reported a transition energy of 80_{-18}^{+160} kev, which is confirmed by our measurement. As an additional point of reassurance, these authors calculated $\log(ft)$ values for the K capture and showed that the energy was consistent with an allowed transition. The $\log(ft)$ for Cd^{109} calculated by means of a formula appearing in Feenberg and Trigg's[9] article, appears in Table I. It also is compatible with an allowed transition. In both cases the classification of the transition as allowed agrees with spin assignments for the initial and final states of the nuclei involved.[10]

The author wishes to express his appreciation to Dr. M. Goldhaber for his interest in this problem and for many helpful suggestions generously offered.

[9] E. Feenberg and G. Trigg, Revs. Modern Phys. **22**, 399 (1950).
[10] M. Goldhaber and R. D. Hill, Revs. Modern Phys. **24**, 179 (1952).

PHYSICAL REVIEW VOLUME 92, NUMBER 4 NOVEMBER 15, 1953

Excitation Function for the Photodisintegration of Beryllium*

R. NATHANS AND J. HALPERN
University of Pennsylvania, Philadelphia, Pennsylvania
(Received August 7, 1953)

Using filtered betatron bremsstrahlung, the $Be^9(\gamma,n)$ excitation function has been determined from threshold to 24 Mev. The results show two peaks, one due to excitation of the odd neutron and the second to the excitation of the Be^8 core.

THE photoneutron disintegration cross section of beryllium in the vicinity of the threshold (1.6 Mev) has been measured by several investigators,[1] and the results are in substantial agreement with the calculations of Guth and Mullin[2] for $P\rightarrow S$ and $P\rightarrow D$ transitions of a neutron moving in the field of a Be^8 core. The photoproton excitation function,[3] as determined by successive subtractions of yields produced by betatron bremsstrahlung, shows the characteristic dipole resonance found in other elements. Determination of the (γ,n) excitation function from threshold to 24 Mev by this method is of particular interest but is difficult because of the low threshold and the preponderance of low-energy photons in the bremsstrahlung, spectrum when the betatron is run at high energies.

We have measured the neutron yield as a function of betatron energy by the method of direct neutron detection[4] for betatron bremsstrahlung filtered by 30 cm of carbon absorber to flatten the bremsstrahlung distribution. Figure 1 shows the calculated bremsstrahlung curves at 10 and 20 Mev, normalized to 100r, with and without the carbon filter. As a test of the method, the bismuth (γ,n) yield curve[5] was repeated using filtered radiation, and the excitation functions computed therefrom are shown in Fig. 2. The data of reference 5 are drawn for comparison. Aside from a 20 percent discrepency in the absolute values of the cross sections, the data taken with the hardened beam are in good agreement with the previous work.

Figure 3 shows the excitation function for beryllium computed from yield data using the filtered beam. Also shown are the $Be^9(\gamma,p)$ data of reference 3, and

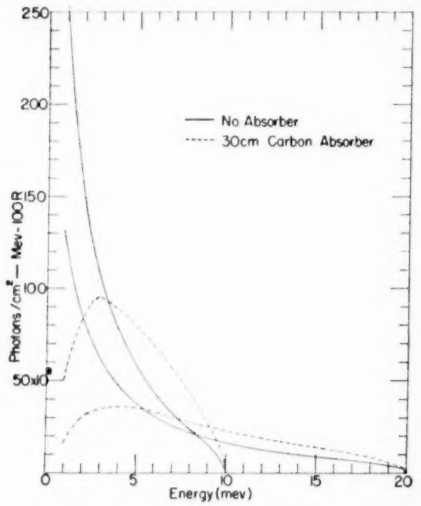

FIG. 1. Theoretical bremsstrahlung distributions for betatron energies of 10 and 20 Mev with and without 30-cm carbon absorber.

* Supported in part by the U. S. Air Research and Development Command and by the joint program of the U. S. Office of Naval Research and the U. S. Atomic Energy Commission.
[1] Russell, Sachs, Wattenberg, and Fields, Phys. Rev. **73**, 545 (1948), B. Hamermesh and C. Kimball, Phys. Rev. **90**, 1063 (1953).
[2] E. Guth and C. J. Mullin, Phys. Rev. **76**, 234 (1949).
[3] R. N. H. Haslam *et al.*, Can. J. Phys. **31**, 210 (1953).
[4] Halpern, Mann, and Nathans, Rev. Sci. Instr. **23**, 678 (1952).
[5] Halpern, Nathans, and Mann, Phys. Rev. **88**, 679 (1952).

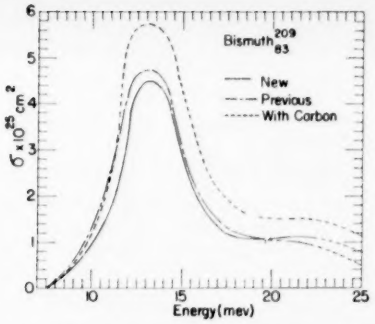

FIG. 2. Bismuth (γ,n) excitation functions constructed from yield curves taken with and without carbon absorber.

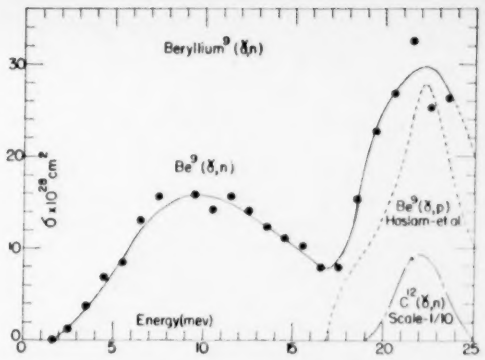

FIG. 3. Beryllium (γ,n) excitation function.

the (γ,n) excitation function of carbon. The method of constructing cross section from yield curves does not permit detailed check with Guth and Mullin near threshold, but the general behavior of the first portion of the beryllium excitation function is in agreement with their model for the $P\rightarrow D$ transitions. In fact, our measured maximum value of 15.8×10^{28} cm^2 for the cross section is in remarkable agreement with the calculations. The coincidence of the second peak with the (γ,p) curve and the (γ,n) excitation in carbon suggests the excitation of the Be^8 core as the photon energy increases and indicates the onset of the large dipole resonance for the core.

The integrated (γ,n) cross section in beryllium up to 25 Mev. is measured to be 0.037 Mev-barns. The (γ,p) integrated cross section of 0.013 Mev-barns[3] is not sufficient to bring the total to 0.187 Mev-barns as calculated[6] from the dipole sum rules. Thus, in beryllium as in other light elements, other modes of disintegration are important or there are large contributions to these reactions at energies above 25 Mev.[7]

[6] J. S. Levinger and H. A. Bethe, Phys. Rev. **85**, 577 (1952).
[7] Jones and Terwilliger [Phys. Rev. **91**, 699 (1953)] report a large high-energy tail on the $Be^9(\gamma,n)$ excitation function above 25 Mev.

PHYSICAL REVIEW VOLUME 92, NUMBER 4 NOVEMBER 15, 1953

Resonant Effects and Spin Dependence in Potential Scattering of Slow Neutrons*

W. SELOVE
Harvard University, Cambridge, Massachusetts
(Received July 24, 1953)

The potential scattering of a nucleus can be considerably different from $4\pi R^2$, where R is the size of the nucleus, if the potential well parameters happen to give an appreciable resonance effect. Strong resonance effects are expected to be accompanied by strong spin dependence. The potential scattering of beryllium shows an appreciable resonant effect but very small spin dependence in the scattering cross section. From an examination of the numerical parameters involved it is concluded that the small spin dependence in the cross section does not preclude a moderate amount of spin dependence in the potential wells for the two spin states—the close equality of the two scattering lengths involved may be the result of a coincidental combination of well depths and ranges.

THE "potential" scattering cross section of most nuclei for slow neutrons, especially of heavier nuclei, is of the order of $4\pi R^2$, where the nominal nuclear radius R is given by $r_0A^{\frac{1}{3}}$ with $r_0\sim1.5\times10^{-13}$ cm. Some nuclei, however, show "potential" cross sections considerably different from this value.

These differences can be accounted for by "potential-well resonances." These are purely scattering resonances, associated with resonant values of the scattering phase shift on the potential-well model, and are to be distinguished from resonances of the compound nucleus. These potential-well resonances will have a "width" given roughly by $ka\sim1$, where k is the neutron wave number and a is the magnitude of the scattering amplitude $(\sigma_{scat}/4\pi)^{\frac{1}{2}}$ for $k\rightarrow0$.

In the case of nuclei with nonzero spin, strong potential-well resonant effects are likely to be accompanied

* Supported by the U. S. Atomic Energy Commission, and written while the author was at the Brookhaven National Laboratory, summer 1953.

by relatively strong spin dependence of potential scattering, because near a resonance the cross section is especially sensitive to the strength of the interaction and so a relatively small change in the potential well can produce a relatively large effect on the cross section. Na is an example of such effects and has been discussed previously.[1] Resonant effects and spin dependence may be detectable by measurement of the total scattering and coherent scattering cross sections, although care must be exercised in the analysis of such data, to separate the potential scattering from compound-nucleus effects.[2]

For a rectangular well of depth V_0, in which a neutron wave number is K_0, and of radius R, the scattering cross section at $k\to 0$ is $4\pi[\tan(K_0R)/K_0-R]^2$. Potential-well resonances thus occur for $K_0R=(2n+1)\pi/2$, $n=0, 1, 2, \cdots$. Taking $V_0\sim 20$ Mev,[3] resonances occur for $R\approx 1.6, 4.8, 8.0, \cdots\times 10^{-13}$ cm. If we take $R=1.5\times 10^{-13}A^{\frac{1}{3}}$ cm, this gives $A\approx 1, 33, 152$. The resonance at $A=1$ corresponds to the large cross section for $n-p$ scattering (especially in the singlet state). A number of the light elements ($A<16$) also show resonant effects in the potential scattering. These are probably to be accounted for by variations in the effective values of V_0 and the nuclear radius, from the simple values given above. As R becomes larger, i.e., for heavier nuclei, resonant effects are less likely to be observed, since K_0R must be closer to a resonant value in order to make the cross section appreciably different from $4\pi R^2$.

It is one purpose of this note to discuss the scattering of slow neutrons by Be^9. The thermal scattering cross section of Be^9 is 6.04 barns, as compared to a value of $4\pi(1.5A^{\frac{1}{3}}\times 10^{-13})^2=1.3$ barns. This indicates a near-resonance in the potential scattering. Such a near-resonance would be expected to be accompanied by an appreciable spin dependence and, consequently, appreciable incoherent scattering. Yet the incoherent scattering of Be is less than 0.01 barn,[4] which means the scattering lengths for the two spin states are within 6 percent of each other, the scattering cross sections within 12 percent. The average scattering length is 6.9×10^{-13} cm.

If we take a potential well of range equal to the nominal radius $R=1.5\times 10^{-13}A^{\frac{1}{3}}=3.24\times 10^{-13}$, the depth of the well is found to be 8.7 Mev. This is rather smaller than the average value of ~ 20 Mev mentioned above[3] but may be reasonable in view of the alpha-particle nature of the "core" of Be; in fact, a similar calculation shows that the effective potential for interaction of a slow neutron with C^{12} appears to be similarly weak.

If both spin states have this same range of 3.24×10^{-13}, then the difference in depths of the potential wells is restricted to be <0.35 Mev, from the smallness of the incoherent scattering. This would represent a rather rigid requirement as to accidental equality of the potential wells for the two spin states. However, the scattering amplitude is determined essentially by V_0 times the square of the range, and so much more leeway can be allowed in the well depths for the two spin states if the two states have different ranges. For example, for a range of 3×10^{-13} cm, the proper scattering length would be obtained with a well of depth 9.7 Mev. A rough attempt has been made to see if the effective ranges for the two spin states could be determined from the cross section of Be as a function of energy.[5] Matching was attempted up to 0.35 Mev. (The calculations become considerably more involved, and more shape-dependent, at higher energies. Moreover, there is some uncertainty as to the width of the energy region over which the effect of possible negative-energy compound-nucleus resonances can safely be neglected.) Within this energy range the experimental uncertainties in the data make it impossible to detect a difference in effective ranges for the two spin states. For a rectangular-well model the data are fitted by a range of $(3\pm 0.5)\times 10^{-13}$ cm.[6]

One can thus conclude that the small incoherent scattering of Be does not preclude a moderate amount of spin dependence in the scattering. It may be that the close equality of the scattering lengths for the two spin states is at least partially due to a coincidental combination of well depths and ranges.

[1] W. Selove, Phys. Rev. **80**, 290 (1950).

[2] K. W. Ford and D. Bohm, Phys. Rev. **79**, 745 (1950), have made an analysis of resonant effects but did not make a proper separation of potential-well and compound-nucleus effects.

[3] This value seems to give good agreement over a large region; see Feshbach, Porter, and Weisskopf, Phys. Rev. **90**, 166 (1953).

[4] D. J. Hughes (private communication).

[5] C. K. Bockelman, Phys. Rev. **80**, 1011 (1950).

[6] It should be noted that this analysis has been carried out in the spirit of a potential-well effective range approach, with the energy region so restricted as to make the estimated effects of compound-nucleus resonances negligible. For a discussion of the comparison between this formulation and a resonance level formulation, see T. Teichmann, Phys. Rev. **83**, 141 (1951), and R. G. Thomas, Phys. Rev. **88**, 1109 (1952), especially p. 1115 and p. 1125.

Influence of Electric and Magnetic Fields on Angular Correlations

A. ABRAGAM* AND R. V. POUND
Lyman Laboratory of Physics, Harvard University, Cambridge, Massachusetts
(Received June 26, 1953)

The theory of the influence on angular correlations of perturbing interactions in the intermediate state is reformulated to allow the description of the effects of time-dependent as well as of static perturbations. For static interactions of the nuclear electric quadrupole moment with crystalline fields of axial symmetry in polycrystalline sources, attenuation factors are calculated for the coefficients of the various terms in the expansion of the correlation function in Legendre polynomials. No matter how strong the quadrupole interaction, some anisotropy must remain for polycrystalline sources but, for the same interaction in simple single crystals, the anisotropy can be either undisturbed or completely destroyed, depending on the orientation of the crystal. Fields of lower symmetry are shown also to leave, for polycrystalline sources, some anisotropy. Expressions for the influence of randomly fluctuating interactions, such as must exist in liquid sources, are calculated and these predict arbitrarily complete destruction of the correlation under certain conditions, but explain the more nearly unperturbed results usually found with such sources. For electronic shells having magnetic moments, the influences of electronic paramagnetic relaxation and of anisotropy of the hyperfine structure interaction are examined. An applied static magnetic field in the presence of static quadrupole interactions in polycrystalline sources is shown to have differing effects depending on the relative strengths of the two interactions. Application of a magnetic field directed toward a counter cannot reduce the disturbance of the intermediate state in liquid sources, except under special circumstances. The influences of an applied field in the presence of time dependent anisotropic hyperfine structure interactions are discussed. Finally, the feasibility of resonance experiments, for the precise determination of nuclear moments in the intermediate state, is explored.

I. INTRODUCTION

THE theory of the correlation of the directions of emission of a sequence of two particles by radioactive nuclei has been treated extensively in the literature. For references to the literature of that field the review articles by Deutsch[1] and by Frauenfelder[2] are recommended. The conclusions of those treatments are only applicable, as was clearly recognized from the beginning by D. R. Hamilton, if the intermediate state of the nucleus, between the first and second emissions, is completely unperturbed. Many angular correlations observed experimentally are found to depend on the physical and chemical nature of the source. In other examples of angular correlation the experimental results also do not agree with the theoretical predictions based on that simplifying assumption.

The effects of perturbation of the intermediate nucleus by interaction through its magnetic moment with its electronic shell, the interaction responsible for the well-known hyperfine structure in atomic spectra, and also with applied magnetic fields have been analyzed by Goertzel.[3] He showed, for a hyperfine-structure interaction, that only for an extremely short nuclear lifetime τ_N would the correlation be unaffected, and he gave formulas for the calculation of the resulting correlations for longer lifetimes. Alder[4] reformulated and extended that treatment in a way which very clearly displays the influence of the perturbation on the correlation.

The present paper treats the effect of several magnetic and electric perturbing interactions not previously discussed. Particular emphasis is given to the effect of the nuclear electric quadrupole moment of the nucleus in solid and liquid sources. This cause of disturbance has not been given much attention previously. In the course of this study a few brief reports of work along these lines by others have appeared,[2,5,6] including some most conclusive experiments at Zürich on the effect of the quadrupole interaction in a single crystal of indium.[7]

The basic theory of the effect of disturbances in the intermediate state is reformulated in the present paper in a manner that allows its application to both static and time-dependent perturbations. A particular application of the latter type is to the effect of electric quadrupole interactions in liquids. A short section is included describing the possibilities of observing resonant transitions, in the intermediate state, induced by suitable radio-frequency fields.

The possibility is discussed of applying the results of this work to the measuremnt of nuclear magnetic and electric moments. Some of these measurements would be analogs of the experiment of the Zürich group[8] on the magnetic moment of 8×10^{-8}-sec Cd^{111}.

II. GENERAL

The problem of the perturbation of angular correlations by atomic hyperfine structure, treated by Goertzel,[3] is complicated by the fact that the nuclear spin is coupled to the electron shell which must be considered quantum mechanically. In order to simplify the discussion, we shall first assume that the fields acting on the nuclear spin in the intermediate state

* Present address: Centre d'Études Nucléaires de Saclay, France. (On leave during 1952–1953.)

[1] M. Deutsch, Repts. Progr. Phys. **14**, 196 (1951).

[2] H. Frauenfelder, *Annual Review of Nuclear Science* (Annual Reviews, Inc., Stanford, 1953), Vol. 2.

[3] G. Goertzel, Phys. Rev. **70**, 897 (1946).

[4] Kurt Alder, Helv. Phys. Acta **25**, 235 (1952).

[5] Ernst Heer, Physica **18**, 1215 (1952).

[6] F. Coester, Bull. Am. Phys. Soc. **28**, No. 3, 28 (1953).

[7] Albers-Schönberg, Hänni, Heer, Novey, and Scherrer, Phys. Rev. **90**, 322 (1953).

[8] Aeppli, Alberg-Schönberg, Frauenfelder, and Scherrer, Helv. Phys. Acta **25**, 339 (1952).

(but not the nuclear spin itself) can be described classically. This is true, for instance, of applied magnetic fields or, to a very good approximation, of crystalline electric fields which will be our main concern. The coupling of the nuclear spin to the field can be described by a certain Hamiltonian $\mathbf{K}$, represented by a $(2I+1)$ by $(2I+1)$ matrix, where I is the spin of the intermediate state. The field partially or completely lifts the $(2I+1)$-fold degeneracy of the intermediate state B.

Goertzel shows the angular correlation to be given by

$$W=S_1S_2\sum_{a,b,b',c}\frac{(a|H_1|b)(b|H_2|c)(c|H_2|b')(b'|H_1|a)}{1-i\tau_N(E_b-E_{b'})/\hbar}. \tag{1}$$

In this formula, a and c are quantum numbers specifying the different substates of the initial state A and the final state C; $|b)$ and $|b')$ are the eigenstates of the Hamiltonian $\mathbf{K}$ in the intermediate nuclear state B and E_b and $E_{b'}$ are the corresponding eigenvalues of $\mathbf{K}$. The eigenstates $|b)$ can be expressed as linear combinations of the states $|m)$ which are eigenstates of the projection I_z of the nuclear spin along a certain axis $0z$;

$$|b)=\textstyle\sum_m c_{bm}|m). \tag{2}$$

In Eq. (1), H_1 and H_2 are the Hamiltonians for the emission of the first and second radiation. The symbols S_1 and S_2 indicate summations over the unobserved features of these radiations, such as their polarizations, and τ_N is the exponential lifetime of the intermediate nuclear state.

Goertzel's proof is based essentially on an extension of the Weisskopf-Wigner theory of natural line width. It is a self-consistent theory in the sense that the existence of a nuclear lifetime τ_N is a consequence of the Schrödinger equations describing the evolution of the nucleus as a radiating system. Although straightforward in principle, Goertzel's proof, even simplified by the introduction of the Laplace transform as suggested by Bičdenharn and Rose,[9] remains somewhat involved. Also, the domain of applicability of Eq. (1) is somewhat restricted. First, it applies only if the perturbing fields are static. This requires that the nuclear spin in the external field, or, more generally, the quantum-mechanical system formed by the nuclear spin and its surroundings, such as the electronic shell, have stationary energy states. Goertzel's formula makes no provision for the perturbation of the correlation by time-dependent fields such as electric fields that fluctuate due to thermal vibrations or to Brownian motion, in crystals or liquids respectively, or applied rf fields. Second, Eq. (1) cannot be applied directly to the measurement of delayed coincidence rates with finite resolving time.

An expression applying in the above situations and reducing to Goertzel's formula, Eq. (1), in the same domain of validity can be derived simply in the following manner. Let us first assume that no perturbation acts on the nucleus in the intermediate state. The correlation can then be written:

$$W=S_1S_2\sum_{a,c,\beta,\beta'}(a|H_1|\beta)(\beta|H_2|c)(c|H_2|\beta')(\beta'|H_2|a). \tag{3}$$

Apart from the absence of denominators, Eq. (3) differs from Eq. (1) by the fact that the state vectors $|\beta)$ form an arbitrary complete set in the intermediate state B, whereas in Eq. (1) the $|b)$ represented eigenstates of $\mathbf{K}$. Suppose, now, that the second emission takes place at time t exactly (the first emission being taken as the time origin) and that the perturbing Hamiltonian $\mathbf{K}$, which may be time-dependent, acts on the nuclear spin during this time t. This can be taken into account by replacing in Eq. (3), the quantities $(\beta|H_2|c)(c|H_2|\beta')$ by $(\beta|\mathbf{U}^+H_2|c)(c|H_2\mathbf{U}|\beta')$, where $\mathbf{U}(t)$ is a unitary operator describing the evolution of a state vector $|\beta')$ during the time t and $\mathbf{U}^+$ is its Hermitian conjugate. The corresponding hypothetical correlation $w(t)$ can be written

$$w(t)=S_1S_2\sum_{a,c,\beta,\beta'}(a|H_1|\beta)(\beta|\mathbf{U}^+H_2|c)\times(c|H_2\mathbf{U}|\beta')(\beta'|H_1|a). \tag{3'}$$

If the perturbing Hamiltonian $\mathbf{K}$ is time-independent, $\mathbf{U}$ is simply $\exp(-i\mathbf{K}t/\hbar)$. If $\mathbf{K}$ depends on t, we can still write symbolically $\mathbf{U}=\exp[-(i/\hbar)\int_0^{t'}\mathbf{K}(t')dt']$, where the integral has to be evaluated according to Feynman's prescriptions on ordered operators.[10]

The second radiation, however, is not emitted t seconds after the first but rather has a probability $\exp(-t/\tau_N)(dt/\tau_N)$ to be emitted between times t and $t+dt$. If all coincidences taking place between t_1 and t_2 are registered, the correlation becomes

$$\begin{aligned}W&=(1/\tau_N)\int_{t_1}^{t_2}e^{-t/\tau_N}w(t)dt\\&=S_1S_2\sum_{a,\beta,\beta',c}(1/\tau_N)\int_{t_1}^{t_2}e^{-t/\tau_N}(a|H_1|\beta)\\&\quad\times(\beta|\mathbf{U}^+(t)H_2|c)(c|H_2\mathbf{U}(t)|\beta')(\beta'|H_1|a)dt.\end{aligned} \tag{4}$$

If the Hamiltonian $\mathbf{K}$ is static, the eigenstates $|b)$ of $\mathbf{K}$ may be chosen as the state vectors $|\beta)$. Equation (4) can then be written

$$W=S_1S_2\sum_{a,b,b',c}(1/\tau_N)\int_{t_1}^{t_2}e^{-t/\tau_N}\exp[i(E_b-E_{b'})t/\hbar]\times(a|H_1|b)(b|H_2|c)(c|H_2|b')(b'|H_1|a)dt. \tag{5}$$

For $t_1=0$ and $t_2=\infty$, Eq. (5) reduces to Eq. (1).

[9] L. C. Biedenharn and M. E. Rose, Revs. Modern Phys. **25**, 729 (1953).

[10] R. P. Feynman, Phys. Rev. **84**, 108 (1951).

The generalization to a nuclear spin coupled to another quantum mechanical system S surrounding it, such as the electronic shell in an atom or molecule, is straightforward. There the Hamiltonian $\mathbf{K}$ contains variables characterizing the surroundings S as well as the nuclear spin. The hyperfine coupling $a\mathbf{I}\cdot\mathbf{J}$, between nuclear and electronic moments in free atoms provides an example of this situation. Each of the quantum numbers a, b, c, β, and β' in Eqs. (1), (3), (4), and (5) must now be thought of as a set of quantum numbers describing a state of the entire system, atom or molecule, rather than of the nuclear spin alone. An eigenstate $|b)$ of the Hamiltonian $\mathbf{K}$ can be represented by a formula of the type

$$|b)=\sum_{m,n} C_{mn}{}^{b}|m)|n), \tag{6}$$

where m and n are the magnetic quantum numbers specifying nuclear and electronic states, respectively. The coefficients $C_{mn}{}^{b}$ are elements of a unitary matrix that depends on the nature of the problem. In the hyperfine structure interaction of free atoms they are the Clebsch-Gordan coefficients.

From now on, to simplify notations, we shall usually omit summation and average signs and sum over repeated indices.

In order to apply Eq. (1), one must know the energies E_b and the eigenstates $|b)$ of the static Hamiltonian $\mathbf{K}$ defined by Eq. (2) or Eq. (6). This may require the solving of a secular equation in the more complicated cases. The solving of the secular equation can always be avoided if the perturbation introduced by the Hamiltonian $\mathbf{K}$ is small, which, according to Eq. (1), requires that $(E_b-E_{b'})\tau_N/h$ be small compared to unity. If this is true, we can expand the operator $\mathbf{U}=\exp[-(i/h)\mathbf{K}t]$ as

$$\begin{aligned}\mathbf{U}&=\boldsymbol{\varepsilon}-(i\mathbf{K}t)/h-\mathbf{K}^2t^2/2h^2+\cdots,\\ \mathbf{U}^{+}&=\boldsymbol{\varepsilon}+(i\mathbf{K}t)/h-\mathbf{K}^2t^2/2h^2+\cdots,\end{aligned} \tag{7}$$

where $\boldsymbol{\varepsilon}$ is the unit operator. Using only the first-order terms from the expansion, Eq. (4) becomes

$$\begin{aligned}W=W_0-(1/\tau_N)\int_{t_1}^{t_2} te^{-t/\tau_N}dt[&(i/h)(a|H_1|\beta)\\ &\times(\beta|H_2|c)(c|H_2|\beta'')(\beta''|\mathbf{K}|\beta')(\beta'|H_1|a)\\ &+\text{complex conjugate}],\end{aligned}$$

and for $t_1=0$ and $t_2=\infty$,

$$\begin{aligned}W=W_0-(\tau_N/h)[&i(\beta''|\mathbf{K}|\beta')(a|H_1|\beta)\\ &\times(\beta|\mathrm{H}_2|c)(c|H_2|\beta'')(\beta'|H_1|a)\\ &+\text{complex conjugate}],\end{aligned} \tag{8'}$$

where W_0 is the unperturbed correlation. It often happens, and it will be shown to be true for perturbation of the correlation by an electric quadrupole interaction, that the first-order term in τ_N vanishes. Higher order terms in the expansion of Eq. (7) must then be used.

Equation (8') shows that, when the perturbation is small, it is sufficient to know the matrix elements of the perturbing Hamiltonian in an arbitrary representation and, thus, it is not necessary to diagonalize $\mathbf{K}$.

Alder[4] has given an important reformulation of Eq. (1). He has shown that Eq. (1) can be rewritten as follows:

$$W=\sum_{k_1k_2\mu}\mathrm{I}(k_1)\mathrm{II}(k_2)\mathrm{III}(k_1k_2,\mu)Y_{k_1}{}^{\mu}(\boldsymbol{\Omega}_1)Y^{*}{}_{k_2}{}^{\mu}(\boldsymbol{\Omega}_2). \tag{9}$$

In this formula the $Y_k{}^{\mu}$ are ordinary spherical harmonics, and $\boldsymbol{\Omega}_1$ and $\boldsymbol{\Omega}_2$ specify the directions of emission of the first and second radiation. The indices k_1 and k_2 are even integers which obey the inequalities:

$$\begin{aligned}&0\leqslant k_1\leqslant 2I, \quad 0\leqslant k_2\leqslant 2I,\\ &0\leqslant k_1\leqslant 2L_1, \quad 0\leqslant k_2\leqslant 2L_2,\end{aligned}$$

where L_1 and L_2 are the highest orders in the multipole expansions of the first and second radiation, respectively. We need not concern ourselves with the exact expressions for the coefficients $\mathrm{I}(k_1)$ and $\mathrm{II}(k_2)$. All we need to know is that they are independent of $\mathbf{K}$. The influence of $\mathbf{K}$ on the correlation is entirely contained in the third coefficient $\mathrm{III}(k_1k_2,\mu)$, for which Alder gives the formula:

$$\begin{aligned}\mathrm{III}(k_1k_2,\mu)=\sum_{m,m'}&(Ik_1m'\mu|Ik_1Im)(Ik_2m'\mu|Ik_2Im)\\ &\times[1-(i/h)(E_m-E_{m'})\tau_N]^{-1},\end{aligned} \tag{10}$$

where the factors (1) are the Clebsch-Gordon coefficients. If in Eq. (10), $(i/h)(E_m-E_{m'})\tau_N$ can be neglected in comparison with 1, it follows from the properties of the Clebsch-Gordan coefficients that

$$\mathrm{III}(k_1k_2,\mu)=\frac{2I+1}{2k+1}\delta(k_1,k_2).$$

(A slightly different normalization of the coefficients I, II, III which would lead to $\mathrm{III}(k_1k_2,\mu)=\delta(k_1,k_2)$ in the absence of perturbation would have been preferable. However, to avoid any confusion we shall retain Alder's definitions.)

Alder's formulas, Eq. (9) and Eq. (10), are only valid if there exists an axis $0z$ such that the projection I_z of the nuclear spin on this axis is a good quantum number; that is to say, if the operator I_z commutes with the perturbing Hamiltonian $\mathbf{K}$. These formulas are valid, in particular, if $\mathbf{K}$ represents the coupling of the nuclear magnetic moment to an applied magnetic field or of the nuclear quadrupole moment to an electric field gradient of axial symmetry. The well-known result, that the correlation is unperturbed by such a coupling if either one of the two radiations is emitted along $0z$, follows immediately from Eq. (9) and Eq. (10).

We want to extend Alder's formulation to more general perturbations. We first consider the case in which the perturbing field can be described classically. The formula (3') in which we replace β by m, the value

of I_z along an arbitrary axis 0z, can be rewritten:

$$w(t)=(a|H_1|m)(m|\mathbf{U}^+|m'')(m''|H_2|c)\times(c|H_2|m''')(m'''|\mathbf{U}|m')(m'|H_1|a). \quad (11)$$

From Eq. (11) it is easy to show, retracing the steps which led Alder from Eq. (1) to Eq. (9) and Eq. (10), that $w(t)$ can be expressed as:

$$w(t)=\mathbf{I}(k_1)\mathrm{II}(k_2)\mathrm{III}(k_1k_2,\mu_1\mu_2,t)Y_{k_1}^{\mu_1}(\mathbf{\Omega}_1)Y_{k_2}^{\mu_2*}(\mathbf{\Omega}_2), \quad (12)$$

where $\mathbf{I}(k_1)$ and $\mathrm{II}(k_2)$ are the same as Alder's and $\mathrm{III}(k_1k_2,\mu_1\mu_2,t)$ is given by:

$$\mathrm{III}(k_1k_2,\mu_1\mu_2,t)=(Ik_1m'\mu_1|Ik_1Im)\times(Ik_2m'''\mu_2|Ik_2Im'')(m|\mathbf{U}^+|m'')(m'''|U|m'). \quad (13)$$

If the Hamiltonian $\mathbf{K}$ is static and has eigenstates $|b)$ and eigenvalues E_b, the unitary evolution operator $\mathbf{U}$ can be written

$$\mathbf{U}=\textstyle\sum_b|b)(b|\ \exp(-iE_bt/\hbar),$$

and Eq. (12) becomes:

$$\mathrm{III}(k_1k_2,\mu_1\mu_2,t)=(Ik_1m'\mu_1|Ik_1Im)(Ik_2m'''\mu_2|Ik_2Im'')\times(m|b)(b|m'')(m'''|b')(b'|m')\times\exp[i(E_b-E_{b'})t/\hbar]. \quad (14)$$

If all coincidences are registered, the observed correlation W is equal to $\int_0^\infty w(t)e^{-t/\tau_N}dt/\tau_N$ and can be written

$$W=\mathbf{I}(k_1)\mathrm{II}(k_2)\mathrm{III}(k_1k_2,\mu_1\mu_2)Y_{k_1}^{\mu_1}(\mathbf{\Omega}_1)Y_{k_2}^{\mu_2*}(\mathbf{\Omega}_2), \quad (15)$$

where

$$\mathrm{III}(k_1k_2,\mu_1\mu_2)=(Ik_1m'\mu_1|Ik_1Im)\times(Ik_2m'''\mu_2|Ik_2Im'')(m|b)(b|m'')(m'''|b')\times(b'|m')[1-i(\tau_N/\hbar)(E_b-E_{b'})]^{-1}. \quad (16)$$

Among other things, Alder's formula, Eq. (9), differs from the more general formula, Eq. (15), by the fact that in the latter the indices μ_1 and μ_2 of $Y_{k_1}^{\mu_1}(\mathbf{\Omega}_1)$ and $Y_{k_2}^{\mu_2*}(\mathbf{\Omega}_2)$ are independent. This is to be expected. If in Eq. (15) we choose the direction to the counter detecting, say, particle one as the 0z axis, only terms with $\mu_1=0$ remain. If μ_2 were equal to μ_1, and thus also zero, as in Eq. (9), only correlations independent of rotations about the z axis could be described by the formulation. This would represent a restriction on the generality of the Hamiltonian $\mathbf{K}$.

When the electronic shell must be described quantum mechanically, the problem is handled by the same methods. The formulas, Eq. (12) and Eq. (15), are still valid but Eq. (13) and Eq. (14) have to be modified as follows:

$$\mathrm{III}(k_1k_2,\mu_1\mu_2,t)=(Ik_1m'\mu_1|Ik_1Im)(Ik_2m'''\mu_2|Ik_2Im'').\times(mn|\mathbf{U}^+|m''p)(m'''p|\mathbf{U}|m'n), \quad (13')$$

where n and p are electronic magnetic quantum numbers. In the derivation of Eq. (13′) the assumption has been made that the nuclear transitions leave the electronic shell unaffected, which is equivalent to say that the Hamiltonians H_1 and H_2 responsible for these transitions commute with the electronic variables. If the Hamiltonian $\mathbf{K}$ is static, Eq. (14) must be replaced by

$$\mathrm{III}(k_1k_2,\mu_1\mu_2,t)=(Ik_1m'\mu_1|Ik_1Im)(Ik_2m'''\mu_2|Ik_2Im'')\times(mn|b)(b|m''p)(m'''p|b')(b'|m'n)\times\exp[(i/\hbar)(E_b-E_{b'})t], \quad (14')$$

where the state vectors $|b)$ are eigenstates of $\mathbf{K}$, and coefficients like $(mn|b)$ are the $C_{mn}{}^b$ in Eq. (6).

Equation (16) must be replaced by Eq. (16′):

$$\mathrm{III}(k_1k_2,\mu_1\mu_2)=\frac{1}{\tau_N}\int_0^\infty e^{-t/\tau_N}\mathrm{III}(k_1k_2,\mu_1\mu_2,t)dt$$

$$=(Ik_1m'\mu_1|Ik_1Im)(Ik_2m'''\mu_2|Ik_2Im'')\times(mn|b)(b|m''p)(m'''p|b')(b'|m'n)\times[1-(i/\hbar)\tau_N(E_b-E_{b'})]^{-1}. \quad (16')$$

It has already been pointed out that when $\mathbf{K}$ is the magnetic hyperfine structure, $a\mathbf{I}\cdot\mathbf{J}$, the coefficients $(mn|b)$ are the Clebsch-Gordan coefficients. Racah's summation rules can then be used to bring Eq. (16′) to a closed form leading to Alder's formula, Eq. (33) of reference 4, for a correlation perturbed by isotropic magnetic hyperfine structure. In that case, it follows from the properties of Clebsch-Gordan coefficients that that $\mu_1=\mu_2$ in Eq. (16′). This is natural since there is no privileged direction in space.

III. CRYSTALLINE POWDERS

The description of angular correlations perturbed by a static Hamiltonian $\mathbf{K}$ is greatly simplified if the radioactive source has the behavior of a crystalline powder which is an ensemble of microcrystals oriented at random. Each microcrystal gives a certain correlation W described by Eq. (15) where the directions of emission $\mathbf{\Omega}_1$ and $\mathbf{\Omega}_2$ are referred to a frame of reference attached to the microcrystal. The observed correlation W is obtained by averaging Eq. (15) over all orientations of the frame of reference. This is obviously equivalent to keeping the frame of reference fixed and averaging over the directions of emissions $\mathbf{\Omega}_1$ and $\mathbf{\Omega}_2$, keeping constant the angle $\psi=(\mathbf{\Omega}_1,\mathbf{\Omega}_2)$ between the two counters registering the coincidences. From the orthogonality properties of spherical harmonics, it is easily seen that this procedure leads to the disappearance from Eq. (15) of all terms except those for which

$\mu_1=\mu_2=\mu$ and $k_1=k_2=k$. The correlation $\bar{W}$ can then be written:

$$\bar{W}=\sum_k G_k A_k P_k(\cos\psi), \tag{17}$$

where the A_k are the coefficients of the expansion in Legendre polynomials of the unperturbed correlation W_0 and the G_k are attenuation coefficients given by

$$G_k=\frac{1}{(2I+1)}\sum_{\mu} \mathrm{III}(kk,\mu\mu). \tag{18}$$

If instead of the integrated correlation $\bar{W}$ we consider the time dependent expression $w(t)$, defined in Eq. (3'), we can similarly write:

$$w(t)=\sum_k G_k(t) A_k P_k(\cos\psi),$$

where

$$G_k(t)=\frac{1}{2I+1}\sum_{\mu} \mathrm{III}(kk,\mu\mu,t). \tag{19}$$

The attenuation coefficients G_k, which contain all the information on the perturbation of the angular correlation, depend only on the intermediate nuclear state but not on the radiative transitions to and from it.

We rewrite below the explicit expressions for the attenuation coefficients G_k, both integrated and time dependent, in the following cases.

(a) The perturbing static field is described classically and has axial symmetry.

$$G_k=\left(\frac{1}{2I+1}\right)\sum_{m,m',\mu}(Ikm'\mu|IkIm)^2 \times\left[1-\frac{i\tau_N}{\hbar}(E_m-E_{m'})\right]^{-1}, \tag{20}$$

$$G_k(t)=\left(\frac{1}{2I+1}\right)\sum_{m,m',\mu}(Ikm'\mu|IkIm)^2 \times\exp[i(E_m-E_{m'})t/\hbar]. \tag{20'}$$

(b) The perturbing static field is described classically but with no restrictions on its symmetry.

$$G_k=\frac{1}{2I+1}(Ikm'\mu|ikIm)(Ikm'''\mu|IkIm'') \times(m|b)(b|m'')(m'''|b')(b'|m') \times\left[1-\frac{i\tau_N}{\hbar}(E_b-E_{b'})\right]^{-1}, \tag{21}$$

$$G_k(t)=\frac{1}{2I+1}(Ikm'\mu|IkIm)(Ikm'''\mu|IkIm'') \times(m|b)(bm'')(m'''|b')(b'|m') \times\exp[i(E_b-E_{b'})t/\hbar]. \tag{21'}$$

(c) There is a quantum-mechanical coupling between the nucleus and the electronic shell.

$$G_k=\frac{1}{(2I+1)r}(Ikm'\mu|IkIm)(Ikm'''\mu|IkIm'') \times(mn|b)(b|m''p)(m'''p|b')(b'|m'n) \times\left[1-\frac{i\tau_N}{\hbar}(E_b-E_{b'})\right]^{-1}, \tag{22}$$

$$G_k(t)=\frac{1}{(2I+1)r}(Ikm'\mu|IkIm)(Ikm'''\mu|IkIm'') \times(mn|b)(b|m''p)(m'''p|b')(b'|m'n) \times\exp[(i/\hbar)(E_b-E_{b'})t]. \tag{22'}$$

In Eqs. (22) and (22') r is a normalizing factor equal to the number of degrees of freedom of the electronic shell. If the shell has a moment J, $r=2J+1$. From the expressions (20), (21), and (22) it is easy to see that $G_0=1$ and that $G_k\to 1$ when all the differences $E_m-E_{m'}$ or $E_b-E_{b'}$ tend toward zero.

One interesting feature of the formulas (20), (21), and (22) is that, even when the perturbing Hamiltonian becomes so large or the lifetime τ_N so long that $\tau_N(E_b-E_{b'})/\hbar$ is much larger than unity, the attenuation coefficients G_k with $k>1$ have finite limits or "hard cores" given by the contribution of the terms for which $m=m'$ in Eq. (20) or $b=b'$ in (21) and (22).

The anisotropy of the correlation is never completely wiped out. For instance, for axial symmetry we obtain from Eq. (20) with no degeneracies:

$$G_k(\lim)=\frac{1}{2I+1}\sum_m (Ikm_0|IkIm)^2=\frac{1}{2k+1}. \tag{23}$$

This is obviously only a lower limit. If there are degeneracies such that, for some levels, one has $E_m=E_{m'}$ for $m\neq m'$, $G_k(\lim)$ can be larger than $1/(2k+1)$. The existence of such hard cores has already been pointed out by Alder[4] for the case of isotropic magnetic hfs.

It is important to emphasize that the existence of a hard core is subordinated to the following assumptions:

(a) The perturbing interactions are static;
(b) No privileged direction exists in the radioactive source considered as a whole.

If either one of these assumptions is violated, the correlation can be wiped out completely.

IV. STATIC ELECTRIC QUADRUPOLE INTERACTIONS

A. Crystalline Powders

An important example of the effect on the angular correlation of a perturbation describable by Eqs. (20) and (20') is that of the interaction of the nuclear electric quadrupole moment[11] with an electric field

[11] H. B. G. Casimir, *On the Interaction Between Atomic Nuclei and Electrons* (De Erven F. Bohn N.V., Haarlem, 1936).

having an axis of threefold or higher symmetry in a sample composed of a large number or randomly oriented microcrystals. Such interactions in solids are well known in nuclear magnetic resonance and in pure quadrupole resonance.[12–14] Separations of adjacent levels as high as about 900 Mc/sec have been observed. For example, the levels $m=\pm 5/2$ and $m=\pm 3/2$ of I^{127} in the solid ICN are separated by about 750 Mc/sec. Thus, such a perturbation could be significant even with intermediate nuclear lifetimes as short as 10^{-10} sec. Axially symmetric fields are not the most general kind nor is the method of treatment limited to them, but the calculations are simplest and results can most easily be displayed for such fields. Some features of the results with fields of lower symmetry are discussed in Sec. IV(C). The results discussed here should be directly applicable, for example, for a nucleus in its normal lattice site in a metal of hexagonal crystal structure.

The energy levels specified in terms of the component m of the spin along the axis of symmetry[12] are given by

$$E_m=[eQ(\partial^2V/\partial z^2)/4I(2I-1)][3m^2-I(I+1)]. \quad (24)$$

Using these values in Eq. (20′), the attenuation coefficients $G_k(t)$, for the detection of delayed coincidences, for $1\leqslant I\leqslant 3$ are:

$$I=1:\quad G_2(t)=\tfrac{1}{5}(3+2\cos\omega_0 t), \quad (25)$$

$$I=\tfrac{3}{2}:\quad G_2(t)=\tfrac{1}{5}(1+4\cos\omega_0 t), \quad (26)$$

$$I=2:\begin{cases} G_2(t)=\frac{1}{5}\left[\frac{13}{7}+\frac{2}{7}\cos\omega_0 t+\frac{12}{7}\cos 3\omega_0 t+\frac{8}{7}\cos 4\omega_0 t\right], & (27)\\ G_4(t)=\frac{1}{9}\left[\frac{29}{7}+\frac{12}{7}\cos\omega_0 t+\frac{16}{7}\cos 3\omega_0 t+\frac{6}{7}\cos 4\omega_0 t\right]. & (28)\end{cases}$$

$$I=\tfrac{5}{2}:\begin{cases} G_2(t)=\frac{1}{5}\left[1+\frac{13}{7}\cos\omega_0+\frac{10}{7}\cos 2\omega_0 t+\frac{5}{7}\cos 3\omega_0 t\right], & (29)\\ G_4(t)=\frac{1}{9}\left[1+\frac{15}{7}\cos\omega_0 t+\frac{18}{7}\cos 2\omega_0 t+\frac{23}{7}\cos 3\omega_0 t\right], & (30)\end{cases}$$

$$I=3:\begin{cases} G_2(t)=\frac{1}{5}\left[\frac{11}{7}+\frac{2}{21}\cos\omega_0 t+\frac{5}{7}\cos 3\omega_0 t+\frac{20}{21}\cos 4\omega_0 t+\frac{25}{21}\cos 5\omega_0 t+\frac{10}{21}\cos 8\omega_0 t\right], & (31)\\ G_4(t)=\frac{1}{9}\left[\frac{17}{7}+\frac{30}{77}\cos\omega_0 t+\frac{92}{77}\cos 3\omega_0 t+\frac{6}{77}\cos 4\omega_0 t+\frac{60}{77}\cos 5\omega_0 t+\frac{192}{77}\cos 8\omega_0 t+\frac{126}{77}\cos 9\omega_0 t\right], & (32)\\ G_6(t)=\frac{1}{13}\left[5+\frac{50}{33}\cos\omega_0 t+\frac{23}{11}\cos 3\omega_0 t+\frac{32}{33}\cos 4\omega_0 t+\frac{67}{33}\cos 5\omega_0 t+\frac{34}{33}\cos 8\omega_0 t+\frac{4}{11}\cos 9\omega_0 t\right]. & (33)\end{cases}$$

In these formulas, ω_0 is the angular frequency equivalent to the smallest nonvanishing energy difference or, thus, 2π times the lowest frequency of resonance that could be observed were pure quadrupole resonance practicable. For integer I, or for half-odd integer I, respectively,

$$\omega_0(\text{even})=[\tfrac{3}{4}I(2I-1)][eQ(\partial^2V/\partial z^2)/\hbar], \quad (34)$$

or

$$\omega_0(\text{odd})=[\tfrac{3}{2}I(2I-1)][eQ(\partial^2V/\partial z^2)/\hbar]. \quad (35)$$

The quantity $eQ(\partial^2V/\partial z^2)/h$ is 2π times the frequency $\Delta\nu_Q$ frequently used to describe the electric quadrupole interaction.

As an application of these formulas, an example that would allow the determination of an electric quadrupole interaction may be considered. The $\gamma-\gamma$ cascade of Cd^{111}, following K capture in In^{111}, studied by the Zürich group and others[2] has an angular correlation described by $W(\theta)=1+A_2P_2(\cos\theta)+A_4P_4(\cos\theta)$ with $|A_4|\ll|A_2|$. The intermediate state has I equal to 5/2 and a half-life of 8×10^{-8} sec or $\tau_N=1.2\times10^{-7}$ sec. The ratio of delayed coincidences at 180° to those of same delay at 54°, where P_2 vanishes, should, as a function of the delay time t behave just as $1+A_2G_2(t)$, where $G_2(t)$ is given by Eq. (29), provided that a number of conditions are satisfied. First, all Cd^{111} nuclei must be in closely similar electric fields of axial symmetry. Because a nuclear recoil plus a chemical change accom-

[12] R. V. Pound, Phys. Rev. **79**, 685 (1950).
[13] R. V. Pound, Progr. Nuclear Phys. **2**, 21 (1952).
[14] Gordy, Smith, and Trambarulo, *Microwave Spectroscopy* (John Wiley & Sons, Inc., New York, 1953), Chap. 5.

panies the K capture, it is not safe simply to assume that the symmetry and uniformity pertaining to the indium of the source would apply for the Cd^{111} daughter. However, the beautiful experiment of Albers-Schönberg, Hänni, Heer, Novey, and Scherrer[7] with a single crystal of indium show that, for that lattice, the daughter element does remain in the indium lattice site and, thus, a polycrystalline metallic indium source would satisfy this condition.

The second condition is that ω_0 must not be much smaller than $1/\tau_N$ in order that coincidences be still observable with a delay time as large as $2\pi/\omega_0$. This condition is also satisfied by the indium metal source, as evidenced by the Zürich experiments and those of Steffen,[15] in that the time-integrated correlation is severely perturbed by the crystalline field.

Finally, the resolving time of the coincidence circuits must be much shorter than $2\pi/\omega_0$, or, thus, ω_0 cannot be determined if it is too large. With a resolving time not negligible compared to $2\pi/\omega_0$, some smearing out of the function $G_2(t)$ would result. The function $G_2(t)$, Eq. (29), is plotted in Fig. 1. The time of the first maximum is $2\pi/\omega_0$ or $40\pi/3\Delta\nu_Q$.

From such a measurement the magnitude of the electric quadrupole moment (but not the sign) could be determined if the difficult problem of determining the value of $(\partial^2V/\partial z^2)$ could be solved. In this respect the problem is less easy for the In^{111} source than for some others because, in spite of remaining at an indium lattice site, the Cd^{111} is both an impurity and in an unknown electronic state. These additional complexities could be avoided by the use of 48-min Cd^{111} in metallic cadmium as a source instead, which has the same intermediate state. Even in the pure metal, however, reliable values for $\partial^2V/\partial z^2$ are not available.

A more informative example would be an element that has a stable isotope of spin higher than $\frac{1}{2}$. For it, by rf resonance methods, the electric quadrupole interaction of the stable isotope in the same chemical form as used in the source could be determined and, thus,

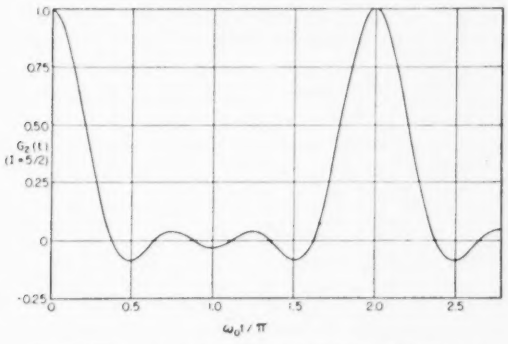

FIG. 1. The attenuation coefficient $G_2(t)$ for $I=5/2$ as a function of $\omega_0 t/\pi$.

[15] Rolf M. Steffen, Phys. Rev. **89**, 903 (1953); Phys. Rev. **90**, 1119 (1953).

TABLE I. Observed frequencies, $\Delta\nu_Q$, of electric quadrupole interactions of stable nuclei in representative compounds.

Nucleus	Compound	$\Delta\nu_Q$, Mc/sec	Reference
D^2	$Li_2SO_4\cdot D_2O$	0.30	a
Li^6	$LiAl(SiO_3)_2$	0.0015	b
Li^7	$LiAl(SiO_3)_2$	0.066	b
B^{11}	$B(CH_3)_3$	4.87	c
N^{14}	ICN	3.39	c
Na^{23}	Na_2NO_3	0.33	d
Al^{27}	Al_2O_3	2.39	d
Cu^{63}	Cu_2O	52	c
As^{75}	As_4O_6	232	c
Br^{79}	Br_2	765	c
Sb^{123}	$SbCl_3$	489	c
I^{127}	ICl	3037	c
Bi^{209}	$Bi(C_6H_5)_3$	669	c

[a] R. V. Pound (unpublished).
[b] N. A. Schuster and G. E. Pake, Phys. Rev. **81**, 157 (1951).
[c] See Gordy, Smith, and Trambarulo, *Microwave Spectroscopy* (John Wiley & Sons, Inc., New York, 1953), Appendix, Table A.6.
[d] See reference 12.

the magnitude of the ratio of the electric quadrupole moments established.

The effect of the static quadrupole interaction, in powdered sources, on angular correlations of the usual type in which the resolving time is longer than τ_N and delays are not used, is given by attenuation factors G_k. These are found from the functions $G_k(t)$ of Eqs. (25)–(33) by replacing all quantities of the form $\cos n\omega_0 t$ by $[1+(n\omega_0\tau_N)^2]^{-1}$. In the limit $\omega_0\tau_N \ll 1$, the attenuation factors approach unity, or the correlation is undisturbed. For $\tau_N = 10^{-7}$ sec, $\Delta\nu_Q$ must, for this, be small compared to 1 Mc/sec. As examples of what might be expected, Table I lists electric quadrupole interactions in solids determined by rf resonance. It is reasonable to assume that the quadrupole moments, and, so, the quadrupole interactions of low-lying excited nuclear levels would be of similar magnitudes. Thus an effect from this interaction must be expected to be present in a large fraction of cases of observation of angular correlations from solid sources.

The situation obtaining in the source for many angular correlation measurements is complicated by recoil of the nucleus in emissions preceding the formation of the intermediate state. For example, in the $\alpha-\gamma$ correlation of radio thorium observed by Battey *et al.*[16] and by Beling *et al.*[17] one cannot ascribe any properties of the symmetry or the chemical bonding of the primary compound to the surroundings of the intermediate nucleus because the recoil energy of approximately 100 kev from the α decay is certainly sufficient to move the nucleus many atomic radii through the lattice. One would, then, expect some dispersion in the values of ω_0 from nucleus to nucleus and, thus, to be able only to observe some average effect. Nevertheless, as reported earlier,[18] application of the appropriate formulas, G_2 and G_4 for $I=2$, to the results

[16] Battey, Madansky, and Rasetti, Phys. Rev. **89**, 182 (1953).
[17] Beling, Feld, and Halpern, Phys. Rev. **84**, 155 (1951).
[18] A. Abragam and R. V. Pound, Phys. Rev. **89**, 1306 (1953).

shows that a value of $\omega_0\tau_N$ a little larger than unity brings the results into agreement with the 0–2–0 scheme predicted on other grounds for that cascade. Indeed, convincing evidence of the validity of this explanation of the original discrepancy is the consistency of the experimentally determined values $G_2=0.42$ and $G_4=0.50$ with $G_2=0.40$ and $G_4=0.52$ obtained for $\omega_0\tau_N$ taken as 1.8. This test differentiates much more clearly from magnetic perturbations for $I=2$ than it does for half-odd integral spins because, for $I=2$, $G_4>G_2$ for all values of $\omega_0\tau_N$. For other spins the contrasts between the relative attenuations from the two effects are less marked. A value for $\Delta\nu_Q$ of 160 Mc/sec, by no means unreasonably large, is required if τ_N is taken as 1.5×10^{-8} sec.

Extensive studies of the dependence of the correlation on the nature of the source have been made by Aeppli *et al.*[19] and by Steffen[15] for the γ-γ cascade of the Cd^{111} daughter of In^{111}. It seems likely that the ability to obtain a correlation near to the unperturbed one (the anisotropy observed later by the Zürich group with one counter along the hexagonal axis of the single crystal of indium[7] must be considered more completely unperturbed) from a source of In^{111} embedded in metallic silver[19] is a result of the indium, and its cadmium daughter, being situated and remaining in a vacancy of the cubic silver lattice, even though some recoil energy is imparted in the K capture. Consistent with this is the observation that thin films did not give as large anisotropies as thick, which may be the result of the existence of considerable lattice strain in thin films, with consequent departures from cubic symmetry. The retention of the Cd^{111}, with a recoil energy probably smaller than 1.5 volts at a lattice site, or else its capture in a neighboring one, in both a silver and an indium lattice must be considered demonstrated by these experiments.

It is not entirely safe to assume that the quadrupole effect is absent even if the nucleus is known to lie in a cubic lattice at a good lattice site. Studies of nuclear paramagnetic resonance of iodine and bromine in crystals of KI and KBr have revealed that these ions are extremely sensitive to the symmetry of their surroundings.[20] Even in the most perfect single crystals obtainable, lattice strains probably resulting from a certain density of dislocations, cause a mean squared electric quadrupole interaction of many kilocycles. Much larger interactions, perhaps of the order of a megacycle/sec, are found in powders. Metallic ions seem less sensitive to this source of interaction.

The nuclei most likely to be observable in predictable environments would be reasonably long lived isomers from which a γ-γ correlation can be studied. With such nuclei, the chemistry of preparing a source can be performed with the isomer itself, and, unless it is very energetic, the recoil from the first γ emission would be insufficient to break a chemical bond or to displace the nucleus from its lattice site. Furthermore, the electronic shell should remain unexcited for such nuclei for which the γ ray is not internally converted. An n-γ reaction, in a metal, that produces such an isomer could be used directly, although the recoil energy in the (n-γ) reaction could certainly be sufficient to displace the nuclei. Annealing or melting and refreezing the metal should restore the normal metallic lattice. Such a simple remedy may not work for compounds, especially for molecular crystals.

It has already been noted that, even for $\omega_0\tau_N\gg1$, no term in the correlation is completely destroyed by the axially symmetric quadrupole interaction in the polycrystalline source. This means that the mechanism described, if the compounds are truly randomly oriented powders, cannot explain the results of the Zürich group and of Steffen for several solid compounds where the correlation was found to be much smaller than the hard core for G_2.

The attenuations measured for coincidences with resolving times longer than τ_N can, of course, be used to determine $(\omega_0\tau_N)^2$ and, thus, if τ_N is known, $\Delta\nu_Q$. For $\omega_0\tau_N>1$, the functions G_k are nearly reduced to the hard cores and the accuracy of determination of $(\omega_0\tau_N)^2$ is correspondingly poor. For large $\omega_0\tau_N$ the delayed coincidence technique would be much superior if sufficiently short resolving time can be obtained.

The failure of magnetic fields, directed toward a counter, to restore the correlations perturbed by quadrupole interactions can be understood in terms of the discussion in Sec. VI(B).

B. Single Crystals

In discussing the influence of the quadrupole interaction in single crystals, we restrict ourselves for simplicity to cases where all the radioactive nuclei experience fields of threefold or higher symmetry, identical in direction as well as in magnitude. It is evident from Eq. (10) and it has been demonstrated experimentally[7] that, if the axis of symmetry of such a crystal is parallel to the direction of emission of one of the radiations, the correlation is the same as if no quadrupole interaction were present. If the axis of the crystal is perpendicular to the plane of the counters, the correlation can be written

$$W=\sum_\mu B_\mu e^{i\mu\psi}, \tag{36}$$

where

$$B_\mu=\mathrm{I}(k_1)\mathrm{II}(k_2)a(k_1,\mu)a^*(k_2,\mu)(Ik_1m'\mu\,|\,Ik_1Im)\times(Ik_2m'\mu\,|\,Ik_2Im)[1-i\omega_q\tau_N(m^2-m'^2)]^{-1}, \tag{37}$$

and, of course, no summation is made over the index μ. In Eq. (37), the quantities $a(k,\mu)$ are defined by

$$V_k{}^\mu(0,\psi)=a(k,\mu)e^{i\mu\psi}.$$

[19] Aeppli, Bishop, Frauenfelder, Walter, and Zünti, Phys. Rev. **82**, 550 (1951).

[20] G. D. Watkins, thesis, Harvard University, 1952 (unpublished); G. D. Watkins and R. V. Pound, Phys. Rev. **89**, 658 (1953).

The quantity ω_q is ω_0, defined by Eq. (34) for integral I and is $(\omega_0/2)$ of Eq. (35) for half-odd integral I.

Interference terms with $k_1 \neq k_2$ exist in Eq. (36). No simple relationship can be established between B_μ and the analogous coefficient b_μ of the unperturbed correlation, given by

$$b_\mu = \mathrm{I}(k)\mathrm{II}(k)|\sigma(k,\mu)|^2(2I+1)/(2k+1). \quad (38)$$

The situation is more complicated than when the perturbation is entirely caused by a magnetic field since then the terms with $k_1 \neq k_2$ vanish. To interpret the results of an experiment which intends to determine ω_q or $\Delta\nu_Q$ by comparing the experimental values of b_μ and B_μ, the coefficients I_{k1} and II_{k2} must be known separately, rather than only through their diagonal product $I_k II_k$ given by a measurement of the unperturbed correlation. In general, this requires an accurate knowledge of the multipole expansion of both the first and the second radiation. The requirement may prove difficult to meet when one of them or both are mixtures of different multipoles. The interference terms disappear, and

$$\frac{B_\mu}{b_\mu} = \frac{2k+1}{2I+1}(Ikm'\mu|IkIm)^2[1-i\omega_q\tau_N(m^2-m'^2)]^{-1}, \quad (39)$$

only when $\mathrm{I}(k_1)$ and $\mathrm{II}(k_2)$ vanish for k_1 and k_2 larger than two. This condition is more restrictive than the requirement that the expansion of the unperturbed correlation contain no harmonics higher than the second. The present condition is satisfied only when the spin I is smaller than two or when both radiations are dipolar. The difficulty of interferences can, of course, always be met by taking averages of correlations measured with different crystalline orientations.

C. Rhombic Fields

We now briefly consider the effects of quadrupole interactions of lower than axial symmetry, limiting ourselves to sources in the form of crystalline powders. The attenuation coefficients G_k are given by Eq. (21). In order to apply that equation we must know the eigenstates and eigenvalues of the general quadrupole interaction, as it is given, for instance, by Eq. (15) of reference 12.

Symmetry considerations somewhat reduce the order of the secular equations to be solved. The maximum order of these equations is $I+\frac{1}{2}$, if I is a half-odd integer, $(I/2)+1$ if I is an even integer, and $(I/2)+(1/2)$ if I is an odd integer.[21] If I is an integer, the $\pm m$ degeneracy of the axial case is lifted but if I is half-odd, an essential so-called Kramers' degeneracy remains. The two degenerate states $|b)$ and $|\bar{b})$ are sometimes called Kramers' conjugate and satisfy the condition

$$(b|m) = (-m|\bar{b}). \quad (40)$$

For any spin, the only nonvanishing matrix elements of the quadrupole interaction $\mathbf{K}$ are $(m|\mathbf{K}|m)$ and $(m|\mathbf{K}|m\pm 2)$ if one of the principal axes of the electric field is chosen as the z axis.[12,22] As a consequence, if an eigenstate $|b)$ has components along two states $|m)$ and $|m')$, $m-m'$ is even; if two Kramers' conjugate states have components along two states m and m', respectively, $m-m'$ is odd.

Our main interest in considering fields of lower than axial symmetry is to find out whether such interactions could lead to very small values of the hard cores and thereby explain the very small attenuation coefficients G_k observed in some crystalline compounds such as indium chloride.[15,19] The hard core, having been defined as the limit of G_k when the strength of the interaction tends toward infinity, is given, for integral spin where there is no remaining degeneracy, by Eq. (21) taking $b=b'$;

$$G_k(\mathrm{lim}) = \left(\frac{1}{2I+1}\right)(Ikm'\mu|IkIm)(Ikm'''\mu|IkIm'') \times (m|b)(b|m'')(m'''|b)(b|m'). \quad (41)$$

For half-odd integral spins, terms of the form

$$(Ikm'\mu|IkIm)(Ikm'''\mu|IkIm'') \times (m|b)(b|m'')(m'''|\bar{b})(\bar{b}|m') \quad (42)$$

would seem to contribute to $G_k(\mathrm{lim})$. However, to each term of the sum (42) corresponds another term obtained by replacing m by $-m'$, and m' by $-m$. This latter term is equal and opposite to the former because of the properties of the Clebsch-Gordan coefficients. Equation (41) is therefore valid for all I, integral or half-odd integral.

The values of $G_k(\mathrm{lim})$ for a few values of I are given below:

$I=1$; $G_2(\mathrm{lim})=\frac{2}{5}$. It will be remembered that the value of the hard core for an axially symmetric field was $\frac{3}{5}$. Although the degeneracy is completely lifted $G_k(\mathrm{lim})$ does not reach the value $1/(2k+1)$, equal to $\frac{1}{5}$.

$I=\frac{3}{2}$; $G_2(\mathrm{lim})=\frac{1}{5}$. This is the same as for a field of axial symmetry.

$I=2$; $G_2(\mathrm{lim})=G_4(\mathrm{lim})=2/7$. This can also be written 10/35 or 18/63. For axial symmetry $G_2(\mathrm{lim})$ and $G_4(\mathrm{lim})$ were, respectively, 13/35 and 29/63.

$I=5/2$. Here the hard core depends on the amount of the asymmetry which can be characterized by the coefficient η defined in reference 12 or 22. A cubic equation must be solved to find the eigenstates $|b)$ of the quadrupole interaction. For small η, perturbation formulas can be used to determine the states $|b)$ and G_2 is found to be

$$G_2(\mathrm{lim}) = \frac{1}{5} + \frac{1373}{210\times 27}\eta^2 + 0(\eta^4) \simeq \frac{1}{5} + 0.24\eta^2.$$

[21] King, Hainer, and Cross, J. Chem. Phys. **11**, 27 (1943).

[22] R. Bersohn, J. Chem. Phys. **20**, 1505 (1952).

For maximum anisotropy $|\eta|=1$, the cubic secular equation reduces to a quadratic and a linear equation.[22] Thus, for $|\eta|=1$,

$$G_2(\text{lim})=443/1715\simeq 0.258.$$

It is seen that $G_2(\text{lim})$ is larger than the value $\frac{1}{5}$ of axial symmetry. An asymmetric field therefore cannot explain the very low values of anisotropy observed in the solid indium compounds.

The following sum rule can be deduced from Eq. (41):

$$\sum_k (2k+1)G_k(\text{lim})=2I+1. \tag{43}$$

In this formula both odd and even k should be counted. However, if I is integral, it follows from the properties of the Clebsch-Gordan coefficients that the quantities $G_k(\text{lim})$ vanish for odd k. For that case the summation in Eq. (43) can be limited to even k.

D. Free Molecules and Atoms

We now briefly consider the problem when the system producing the inhomogeneous electric in the quadrupole interaction must itself be treated quantum mechanically. This is true for free atoms or molecules and would apply to gaseous radioactive sources. The reason why, in solids or liquids, the pure quadrupole interaction can be treated classically as far as the electronic shell is concerned, is that, there, the orbital degeneracy of the shell is lifted. The shell can still have degrees of freedom connected with spin degeneracy in a solid but the electric field does not depend on these. Classical treatment is not valid in the presence of magnetic hyperfine structure.

The interaction between the nuclear spin I and the gradient of the electric field can be represented by the usual operator,

$$\mathbf{K}=a\frac{3(\mathbf{I}\cdot\mathbf{J})^2+\frac{3}{2}(\mathbf{I}\cdot\mathbf{J})-I(I+1)J(J+1)}{2J(2J-1)2I(2I-1)},$$

where $\mathbf{J}$ is the angular momentum of the electronic shell of the atom, if the gas is monatomic, or that of the electronic shell plus the rotational moment in a gaseous molecule.

For atoms, where the total angular momentum F is a good quantum number, Goertzel's treatment of the correlation and Alder's formulas (33) and (34) of reference 4 remain valid. There is only a trivial change in the energy differences $E_F-E_{F'}$.

The same statement applies to molecules if $\mathbf{F}=\mathbf{I}+\mathbf{J}$ remains a good quantum number; that is to say, if no other nuclear spins in the molecule are coupled to the moment J. (The magnetic couplings between the different nuclear spins themselves are always much smaller than the quadrupole interaction and can be disregarded.) If this is not the case, the treatment is more complicated. The general formulas, Eqs. (15) and (16′), have to be used.

It is important to point out that these considerations are valid only if the collision time in the gas is so much longer than the nuclear lifetime τ_N that the gas molecules can really be considered as isolated during the decay process. Incidentally, this also applies to Goertzel's treatment of the atomic hyperfine structure.

We have seen that observations of correlations perturbed only by quadrupole interactions do not give the sign of the quadrupole interaction. The sign of the nuclear quadrupole moment is even more important than its magnitude for an understanding of nuclear structure. If a measurement of perturbed correlation in a free atom, where magnetic and quadrupole interaction are both present, could ever be so precise as to detect the departure from the Landé interval rule due to the presence of a quadrupole interaction, the relative sign of the magnetic and quadrupole moments (or the absolute sign of the quadrupole moment if the sign of the magnetic moment is known) could be obtained. Such an experiment seems hardly feasible in the present stage of experimental techniques. A possible suggestion of such an experiment is made in Sec. VII.

V. TIME DEPENDENT ELECTRIC QUADRUPOLE INTERACTIONS

Several experimenters have found that liquid sources, usually aqueous solutions, give much more nearly the expected theoretical correlations than do solid sources of the same chemicals. Steffen has found that molten metallic indium, for the γ-γ scheme following K capture in In^{111}, gives nearly five times the anisotropy of the solid metal.[15] The improved performance of liquid sources has been attributed to rapid disappearance of magnetic electronic states previously invoked to explain the disturbance in solids, or to the smallness of electric fields in liquids. In terms of the effect of the nuclear electric quadrupole moment an explanation that can reveal the limitations as well as the utility of liquid sources can be constructed.

Liquids possess, instantaneously, certain local configurations characteristic of their particular composition not very dissimilar to local configurations in solids. The work of Bernal and Fowler on x-ray diffraction of water,[23] for example, demonstrates that a pseudo-crystalline structure exists in the liquid state. On the other hand, it is clear that no given configuration, and so no preferred direction, can exist for very long at the position of any particular constituent of the liquid. The local configuration of a given nucleus, and so any electric quadrupole interaction resulting from it, is in a state of continual change, in a random manner. Particularly significant is the resultant continual reorientation of the direction of the normal axes of the interaction relative to external coordinates. If many uncorrelated directions of the axes occur in the nuclear lifetime τ_N, we can say that the nature of the source

[23] J. D. Bernal and R. H. Fowler, J. Chem. Phys. **1**, 515 (1933).

imposes no preferred direction at any particular nucleus and the direction of the first particle in the cascade decay can, then, be taken as an axis of quantization of the nuclear spin.

Under this condition, detection of the first decay establishes the probabilities of occupancy of the various intermediate substates relative to the axis to the counter at the instant of the first decay. Then, as usual, the angular correlation function is just the angular distribution of the second decay from such a distribution over the intermediate substates, if they are not disturbed before the second decay. However, because of the Brownian motion and its accompanying fluctuating electric quadrupole interaction, transitions between these substates can result. Eventually, the nucleus must become likely to be found in any one substate with equal probability. Thus, if τ_N were sufficiently long, the second emission would become isotropic and the correlation would be completely destroyed. The mechanism described is the direct analog of that giving rise to thermal equilibrium between spins and the liquid in nuclear paramagnetism. (The corresponding effect is usually far less rapid in solid sources and, in them, it would usually be negligible in any of the lifetimes τ_N we are considering.) Although the effect of the random fluctuations in direction of the axes of the interaction would be to reduce its influence as compared to a static one of the same magnitude, unlike the static effect, no recovery after a time delay and no hard core should exist.

A. Formal Treatment

The time dependent angular correlation $w(t)$ in liquids can be obtained from the general formulas, Eqs. (12) and (13). Choosing as the z axis the direction to the first counter makes μ_1 equal to zero and, accordingly, μ_2 is also zero because there is no other privileged direction associated with the source. Equations (12) and (13) become

$$w(t)=\mathbf{I}(k_1)\mathbf{II}(k_2)\mathbf{III}(k_1k_2,00,t)Y_{k_1}{}^0(0)Y_{k_2}{}^0(\boldsymbol{\Omega}_2), \quad (44)$$

and

$$\mathbf{III}(k_1k_2,00,t)=(Ik_1m0|Ik_1Im)\times(Ik_2m'0|Ik_2Im')|(m'|\mathbf{U}(t)|m)|^2, \quad (45)$$

where $|(m'|\mathbf{U}(t)|m)|^2$ is the probability $W_{mm'}(t)$ that if the nucleus were in the state m at $t=0$, it would be in the state m' at the time t. Equations (44) and (45) may also be used to describe the behavior of a crystalline powder. However, in that case it is more convenient to use Eq. (21) where the z axis of quantization is referred to the axes of each microcrystal.

The Hamiltonian $\mathbf{K}$ describing the quadrupole interaction of the nuclear spin with its surroundings can be most generally written

$$\mathbf{K}=\sum_\mu T_{2\mu}(X)T_2{}^{\mu*}(I_x,I_y,I_z), \quad (46)$$

where the functions $T_2{}^\mu$ are tensor operators defined by Racah[24] and the quantities X are parameters describing the local electric field at the nucleus. In accordance with the above model for a liquid, they are randomly fluctuating functions of time.

The ensemble average, taken over all the nuclear sites at a given time, given by

$$G=\langle f(t)f^*(t-\tau)\rangle_{\text{Av}}, \quad (47)$$

we call the correlation function of the random function f.[25] If the ensemble is stationary, this quantity is independent of t and can be written $G(\tau)$. The function $G(\tau)$ can be shown to be a real, positive, even function of τ decreasing to zero with increasing $|\tau|$. For $\tau=0$, $G(0)=\langle|f|^2\rangle_{\text{Av}}$. The Fourier transform of $G(\tau)$,

$$J(\omega)=\int_{-\infty}^{\infty}e^{-i\omega\tau}G(\tau)d\tau, \quad (48)$$

may be termed the spectral density of the random function f. We define somewhat loosely the correlation time τ_c as the time τ such that for $\tau=\tau_c$, $G(\tau)$ is appreciably smaller than $G(0)$. One often assumes

$$G(\tau)=G(0)e^{-|\tau|/\tau_c}. \quad (49)$$

As a consequence of the above assumption of random rotation of the axes of the electric field,

$$\langle T_2{}^\mu(X)T_2{}^{\mu*}\rangle_{\text{Av}}=d^2\delta(\mu,\mu'),$$

where the constant d^2 is independent of μ. It then follows from the properties of the tensor operators that

$$\langle(m|\mathbf{K}|m')(m|\mathbf{K}|m'')^*\rangle_{\text{Av}}=b^2\delta(m',m'')(I2m'\mu|I2Im)^2. \quad (50)$$

With the usual notations, the constant b^2 is given as

$$b^2=\frac{1}{80}\frac{(I+1)(2I+3)}{I(2I-1)}(eQ)^2\left\langle\left(\frac{\partial^2V}{\partial z'^2}\right)^2\right\rangle_{\text{Av}}, \quad (51)$$

where z' is the direction of largest field gradient in coordinates moving with the fluctuation. The Hamiltonian $\mathbf{K}$ induces transitions between different magnetic substates of the nucleus. According to first-order perturbation theory the probability of transition in a time t from a state m to a state m', for a single spin, is given by

$$W_{mm'}(t)=(1/\hbar^2)\left|\int_0^t K_{mm'}(t')e^{-i\omega_{mm'}t'}dt'\right|^2, \quad (52)$$

where $\omega_{mm'}$ is the angular frequency corresponding to the energy difference between the two states m and m' in the absence of the perturbing random field.

In order to display the properties of the random

[24] G. Racah, Phys. Rev. **62**, 438 (1942).
[25] See, for example, Ming Chen Wang and G. E. Uhlenbeck, Revs. Modern Phys. **17**, 323 (1945).

functions $K_{mm'}(t')$ we rewrite Eq. (52) as

$$W_{mm'}(t)=(1/\hbar^2)\int_0^t dt'\int_0^t dt''K_{mm'}(t')\times K_{mm'}{}^*(t'')e^{-i\omega_{mm'}(t'-t'')}. \quad (53)$$

Introducing $t'-t''=\tau$, this can be rewritten as

$$W_{mm'}(t)=(1/\hbar^2)\left[\int_0^t d\tau e^{-i\omega_{mm'}\tau}\times\int_\tau^t K_{mm'}(t')K_{mm'}{}^*(t'-\tau)dt'+\int_{-t}^0 d\tau e^{-i\omega_{mm'}\tau}\times\int_0^{t+\tau}K_{mm'}(t')K_{mm'}{}^*(t'-\tau)dt'\right]. \quad (54)$$

If we take the ensemble average of Eq. (54), we get

$$\langle W_{mm'}(t)\rangle_{Av}=(1/\hbar^2)\left[\int_0^t d\tau e^{-i\omega_{mm'}\tau}(t-\tau)G_{mm'}(\tau)+\int_{-t}^0 d\tau e^{-i\omega_{mm'}\tau}(t+\tau)G_{mm'}(\tau)\right], \quad (55)$$

where

$$G_{mm'}(\tau)=\langle K_{mm'}(t')K_{mm'}(t'-\tau)\rangle_{Av}.$$

Equation (55) is equivalent to

$$\langle W_{mm'}(t)\rangle_{Av}=(1/\hbar^2)\left[t\int_{-t}^t e^{-i\omega_{mm'}\tau}G_{mm'}(\tau)d\tau-2\int_0^t\cos(\omega_{mm'}\tau)\tau G_{mm'}(\tau)d\tau\right]. \quad (56)$$

If t is large compared with the correlation time τ_c, the ratio of the two integrals is approximately t/τ_c, and the second can be neglected compared with the first. In the first integral, the integration limits can be replaced by $+$ and $-\infty$. The result is

$$\langle W_{mm'}(t)\rangle_{Av}=(t/\hbar^2)J(\omega_{mm'}). \quad (57)$$

A transition probability per unit time can be defined as

$$Q_{mm'}=\langle W_{mm'}(t)\rangle_{Av}/t=(1/\hbar^2)J_{mm'}(\omega_{mm'}). \quad (58)$$

Taking $G(\tau)$ as $G(0)\exp(-|\tau|/\tau_c)$, the result becomes

$$Q_{mm'}=\frac{2\tau_c}{\hbar^2}\frac{G_{mm'}(0)}{1+(\omega_{mm'}\tau_c)^2}=\frac{2\tau_c}{\hbar^2}\frac{\langle|K_{mm'}|^2\rangle_{Av}}{1+(\omega_{mm'}\tau_c)^2}. \quad (59)$$

Frequently for nonviscous liquids $\omega_{mm'}\tau_c\ll 1$ and

$$Q_{mm'}=(2\tau_c/\hbar^2)\langle|K_{mm'}|^2\rangle_{Av}. \quad (60)$$

In Eq. (56), for $t\ll\tau_c$, on the other hand, the quantity (τ) in both integrals can be replaced by $G(0)=\langle|K_{mm'}|^2\rangle_{Av}$. For $\omega_{mm'}=0$, this is precisely the case of the crystalline powder ($\omega_{mm'}$ is the distance between levels m and m' *in the absence* of the quadrupole interaction) which should obviously correspond to an infinitely viscous liquid (long τ_c). Equation (56) gives then

$$\langle W_{mm'}(t)\rangle_{Av}=(1/\hbar^2)t^2\langle|K_{mm'}|^2\rangle_{Av}. \quad (61)$$

As a consequence, for times much larger than τ_c but still so small that $\langle|K_{mm'}|^2\rangle t\tau_c/\hbar^2\ll 1$, the time dependent correlation $w(t)$ for a liquid can be obtained by expanding the suitable formulas of Eqs. (25)–(33) as a power series in t and replacing in the first term, which is the square, t^2 by $2t\tau_c$. This is equivalent to replacing $\tau_N{}^2$ by $\tau_N\tau_c$ in the series expansion of the time independent correlation

$$W=\int_0^\infty\exp(-t/\tau_N)w(t)dt/\tau_N,$$

and explains why in many cases liquid sources give better correlations than solids.

For the intermediate situation between Eq. (60) and Eq. (61), when t is neither large nor small compared with τ_c but $\langle|K_{mm'}|^2\rangle_{Av}t\tau_c/\hbar^2$ is still small, the transition probability is given by the general formula, Eq. (56).

If $\langle W_{mm'}\rangle_{Av}$, given by $Q_{mm'}$ of Eq. (60) multiplied by t, is not small compared with unity, it is not correct to use that expression for $\langle|(m|\mathbf{U}|m')|^2\rangle_{Av}$ in Eq. (46). $\langle W_{mm'}\rangle_{Av}$ must then be calculated as follows. If the probabilities of occupancy of the different states $|m)$ are called $P_m(t)$, these quantities obey the usual differential equations for a relaxation process,

$$\frac{dP_m}{dt}=\sum_{m'=-I}^{I}Q_{mm'}(P_{m'}-P_m), \quad (62)$$

where $Q_{mm'}$ are the transition probabilities per unit time defined in Eqs. (59) and (60). In order for the system of equations described by Eq. (62) to be valid, the condition that $Q_{m'm}\tau_c\ll 1$ must be satisfied. If it is, the passage from the ordinary quantum-mechanical equation for the probability amplitudes C_m,

$$\frac{\hbar}{i}\frac{dC_m}{dt}=\sum_{m'}K_{mm'}e^{-i\omega_{mm'}t}C_{m'}, \quad (63)$$

to Eqs. (62) can be jusified, formally, using arguments analogous to the derivation of Eq. (57) from Eq. (52).

The function $W_{mm'}(t)$ is now defined as the solution $P_{m'}(t)$ of the system, Eqs. (62), corresponding to the initial conditions $P_{m'}(0)=\delta_{mm'}$. From Eqs. (50), (51), and (60) it is found that

$$Q_{mm'}=a(I2m'\mu|I2Im)^2, \quad (64)$$

where

$$a=\frac{\tau_c}{40}\frac{(I+1)(2I+3)}{I(2I-1)}\left(\frac{eQ}{\hbar}\right)^2\left\langle\left(\frac{\partial^2 V}{\partial z'^2}\right)^2\right\rangle_{\text{Av}}. \quad (65)$$

Remembering that $\sum_{m'}(I2m'\mu|I2Im)^2=1$, (62) can be written:

$$\frac{1}{a}\frac{dP_m}{dt}+1=\sum_{m'}(I2m'\mu|I2Im)^2P_{m'}. \quad (66)$$

If the substitution $P_m(t)=P_me^{-\lambda/t}$ is made,

$$(1-\lambda/a)P_m=\sum_{m'}(I2m'\mu|I2Im)^2P_{m'}. \quad (67)$$

Equation (67) is an eigenvalue linear system of the type

$$\mathbf{AX}=\mu\mathbf{X},$$

where $\mathbf{X}$ is a vector with $(2I+1)$ components. The matrix element $A_{mm'}$ is $(I2m'\mu|I2Im)^2$, and the eigenvalue is $\mu=(1-\lambda/a)$.

Using Racah's formula for the reduction of a product of three Clebsch-Gordan coefficients, it can be shown that the $(2I+1)$ eigenvectors $\mathbf{V}^{(k)}$ of Eq. (67) are given by

$$V_m{}^{(k)}=(Ikm0|IkIm),$$

and the eigenvalues μ_k are

$$\mu_k=(2I+1)W(I2kI/II), \quad (68)$$

where W is the Racah function.

The function $\langle W_{mm'}(t)\rangle_{\text{Av}}$ is then easily seen to become

$$\langle W_{mm'}(t)\rangle_{\text{Av}}=\frac{1}{2I+1}\sum_k(Ikm0|IkIm)(Ikm'0|IkIm')\times(2k+1)e^{-a(\mu_k-1)t}. \quad (69)$$

Equation (69), introduced in Eq. (45), shows that $\text{III}(k_1k_2,00)$ vanishes unless $k_1=k_2$ and

$$\text{III}(kk,0)=\frac{2I+1}{2k+1}e^{-\lambda_k t}, \quad (70)$$

where[26]

$$\lambda_k=a(1-\mu_k)=\frac{3}{80}\left(\frac{eQ}{\hbar}\right)^2\left\langle\left(\frac{\partial^2 V}{\partial_{z'}{}^2}\right)^2\right\rangle_{\text{Av}}\times\tau_c\frac{k(k+1)[4I(I+1)-k(k+1)-1]}{I^2(2I-1)^2}. \quad (71)$$

The time-dependent attenuation coefficients are

$$G_k(t)=e^{-\lambda_k t}, \quad (72)$$

and the integrated coefficients are

$$G_k=\int_0^\infty e^{-t/\tau_N}G_k(t)dt/\tau_N=\frac{1}{1+\lambda_k\tau_N}. \quad (73)$$

B. Applications of the Results for Liquids

The foregoing results appear capable of explaining for at least some cases the discrepancies remaining between the angular correlations expected and those observed from liquid sources. As an example, reported briefly previously,[27] the γ-γ correlation of Pd^{106}, following the 2.44-Mev β emission of Rh^{106} shows, from the results of Kraushaar and Goldhaber,[28] relative to a $0-E2\to2-E2\to0$ decay scheme, a G_2 of 0.779 and a G_4 of 0.864. The values of the quantity

$$[(eQ)^2\langle(\partial^2V/\partial z'^2)^2\rangle_{\text{Av}}/h^2]\tau_N\tau_c$$

required to give these values of G_2 and G_4 are, respectively, 2.66 and 2.53. The consistency of these two independent determinations of the same quantity seems to be strong evidence for attributing the discrepancy to this cause.

Neither τ_N nor τ_c are known for this example. From nuclear paramagnetism and from Debye's studies of polar liquids, it seems reasonable to take a value of about 10^{-11} sec for the τ_c of water molecules themselves in dilute aqueous solutions at room temperatures. Sufficient information to allow estimates of values for τ_c appropriate to the ions in the solution is not available but it might be supposed that the same 10^{-11} sec applies for the Pd^{106} ion or atom. If the lifetime τ_N is taken as less than 5×10^{-9} sec, then $\Delta\nu_Q'=eQ\langle(\partial^2V/\partial z'^2)^2\rangle_{\text{Av}}^{\frac{1}{2}}/h$ must be larger than 1160 Mc/sec. Any interaction of that scale would, in the solid state, cause attenuation nearly to the "hard core," thus explaining Steffen's failure to observe differences among various solid sources of differing composition.[29] If the nuclear lifetime were only 5×10^{-10} sec, a three times larger $\Delta\nu_Q'$ would be required to explain the liquid results and the remark about solid sources still holds. It should be kept in mind that the Zürich group's ability to obtain an essentially unperturbed correlation from Cd^{111} in thick silver films probably results from the fitting of the parent In^{111} into and retention of the daughter Cd^{111} at a

[26] The procedure used to calculate the inverse time constants λ_k is a generalization of a procedure that can be used to calculate in liquids the inverses of the well-known relaxation times T_1 and T_2 of nuclear paramagnetism. One, then, is normally concerned with the rate of approach to a Boltzmann distribution over the substates $|m\rangle$ from a distribution initially uniform, because an applied field splits the substates. The procedure used here relates to the inverse process of the disappearance of nonuniform distributions. If ω_L is 2π times the Larmor frequency $g_NH/\hbar$ and if $\omega_L\tau_c\ll1$, $T_1=T_2$ and the value obtained from Eq. (71) by putting $k=1$ is just $(T_1)^{-1}$ or $(T_2)^{-1}$ for nuclei of spin I in a liquid when the relaxation results from fluctuating electric quadrupole interactions. An analogous calculation for relaxation by local, continuously reorienting, magnetic interactions, such as an $\mathbf{I}\cdot\mathbf{J}$ interaction in a tumbling molecule, can easily be made by using 1 for 2 in Eq. (46), Eq. (64), and following, and using $k=1$ for relaxation of magnetic moments or $k=2$, 4, $\cdots$ for effects on angular correlations. The expression for the paramagnetic relaxation $\lambda_1=(T_1)^{-1}$ derived from Eq. (71) for quadrupole relaxation is identical to that found by R. K. Wangsness and F. Bloch, Phys. Rev. **89**, 728 (1953), using a different approach.

[27] R. V. Pound and A. Abragam, Phys. Rev. **90**, 903 (1953).

[28] J. J. Kraushaar and M. Goldhaber, Phys. Rev. **89**, 1081 (1953).

[29] R. M. Steffen, Phys. Rev. **86**, 632 (1952).

normal lattice site of the cubic silver lattice. That evidence is not sufficient to allow the inference that other "double stream" metal sources would have similar qualities in general, independently of the nature and energy of the decay from parent to daughter and of the chemistry of the three metal atoms involved. Relevant to the difference is the fact that the Cd^{111} nucleus has much smaller recoil energy than that of Pd^{106}.

As to the magnitude of $\Delta\nu_Q'$, probably greater than 1160 Mc/sec, the value of 2500 Mc/sec for $\Delta\nu_Q$ for I^{127} with a single pure p bond may be compared.[30] The electronic state of the Pd^{106} is not known but it is unlikely that $\langle(\partial^2V/\partial z'^2)^2\rangle_{Av}^{\frac{1}{2}}$ is as large as that of the p electron in iodine. Thus it seems likely that the magnitude of Q is at least as large as 0.2×10^{-24} cm^2.

If the magnitude of the electric quadrupole interaction is such that $2\pi\Delta\nu_Q'\tau_c\gg1$, in spite of limitations on the realm of validity of the quantitative formulas, the behavior of the factors G_k as functions of τ_c can be seen qualitatively on physical grounds. They start from unity and decrease toward zero as τ_c increases from zero since λ_k is proportional to τ_c. For τ_c of the order of magnitude of τ_N, the values of the G_k begin to rise again and approach the "hard core" values of the static quadrupole interaction as τ_c becomes large compared to τ_N because the liquid is then indistinguishable from a crystalline solid except, perhaps, with respect to the uniformity of the magnitudes of the interactions.

Measurement of the attenuation factors G_k for liquid sources can be seen to allow determination of $\Delta\nu_Q'(\tau_N\tau_c)^{\frac{1}{2}}$. If τ_N is known, a determination of τ_c would result in evaluation of $\Delta\nu_Q'$. Some information on τ_c can be found from studies of nuclear paramagnetic resonance of stable isotopes in similar solutions or liquids because of the analogy between the mechanism causing the attenuation G_k and that producing the line width and the thermal equilibrium in paramagnetic resonance. This comparison could be safely made only for γ-γ cascades not immediately preceded by a chemical change like that accompanying K capture or α or β emission, because the chemical behavior must be known to be identical for the isotopes compared in the two experiments. If a stable isotope of known quadrupole moment is available for the comparison, a direct elimination of τ_c and $\langle(\partial^2V/\partial z'^2)^2\rangle_{Av}^{\frac{1}{2}}$ can be made to obtain the ratio of the magnitudes of the quadrupole moments of the short-lived intermediate isomer and of the stable nucleus. Unfortunately the scale of effects that make the attenuation coefficients G_k appreciably less than unity is such as to make the paramagnetic resonance very difficult to detect unless either τ_N is quite large or the quadrupole moment of the isomer is much larger than that of the stable isotope.

The result to be expected from the application of a static magnetic field to liquid sources that show some attenuation because of the rapidly fluctuating electric quadrupole interaction can now easily be seen. The description of the behavior of an ensemble of spins in the presence of a static applied field is frequently much simplified if it is considered relative to a system of coordinates that rotates about its z axis, taken parallel to the direction of the applied field, with the angular velocity of Larmor precession $\omega_L=g_NH_0/\hbar$, where g_N is the nuclear gyromagnetic ratio. With respect to the rotating coordinates the field H_0 can be ignored and any other interactions present must be suitably transformed. The rapidly fluctuating electric fields that act on the nucleus through its quadrupole moment, with respect to the rotating coordinates, appear essentially unchanged provided that the frequencies characteristic of them, measured by $1/\tau_c$, are large compared to ω_L, or, thus, $\omega_L\tau_c\ll1$. This restriction is analogous to the earlier one $\omega_{mm'}\tau_c\ll1$. For ordinary nuclear magnetic moments and fields up to 20 kilogauss this condition is satisfied for $\tau_c<10^{-9}$ sec. This approach shows in a simple way that a field applied along the direction to a counter can have no influence on the attenuations of the correlations, so long $\omega_L\tau_c\ll1$, because the correlation is independent of rotation about that direction. For a magnetic field applied normal to the plane of the counters, the correlation function becomes

$$w(\theta,t)=1+\textstyle\sum_k G_k(t)A_kP_k[\cos(\theta-\omega_Lt)], \qquad (74)$$

where $G_k(t)$ is given in Eq. (72).

If the coincidence rate at, say, 180° is observed as a function of a variable time delay with a small resolving time compared to $1/\omega_L$, and multiplied by $\exp(t/\tau_N)$, the result $w(180,t)$ is an oscillating function of time with the fundamental frequency $2\omega_L$, just as in the absence of a quadrupole interaction, but the various harmonics of the fundamental frequency are damped. The damping factor of each harmonic k is a linear combination of terms $\exp(-\lambda_{k'}t)$ with $k'\geqslant k$. On the other hand, for observation of the coincidence rates without time delay and with resolving times greater than τ_N, as in the usual experiments, the interpretation is more complicated.

If, however, only A_2 is significant a rather simple result obtains. In that case $w(\theta,t)$ can be written

$$w(\theta,t)=1+\tfrac{1}{4}A_2e^{-\lambda_2t}+\tfrac{3}{4}A_2e^{-\lambda_2t}\cos[2(\theta-\omega_Lt)]. \qquad (75)$$

The correlation integrated over all nuclear lifetimes is obtained as before as

$$W(\theta)=\int_0^\infty w(\theta,t)e^{-t/\tau_N}dt/\tau_N,$$

which gives

$$W(\theta)=1+\frac{A_2}{2(1+\lambda_2\tau_N)}+\frac{3A_2}{4(1+\lambda_2\tau_N)}\times\frac{\cos(2\theta)+[2\omega_L\tau_N/(1+\lambda_2\tau_N)]\sin(2\theta)}{1+[2\omega_L\tau_N/(1+\lambda_2\tau_N)]^2} \qquad (76)$$

[30] C. H. Townes and B. P. Dailey, J. Chem. Phys. **17**, 782 (1949).

if the two counters distinguish between the first and second radiations. It is interesting to note that, without independent knowledge of A_2 or of λ_2, the correlation might be considered unperturbed and the quantity $A_2'=A_2/(1+\lambda_2\tau_N)$ would be mistaken for A_2. In that event the effect of the field, measured by the quantity $[2\omega_L\tau_N/(1+\lambda_2\tau_N)]$ would be mistaken for the quantity $2\omega_L\tau_N$. Thus the Larmor frequency would be mistaken for $\omega_L A_2'/A_2$. For this example, then, an error identical to that in the coefficient A_2 itself would be made in the nuclear magnetic moment so measured. The argument also holds if the counters do not distinguish between the two decays.

VI. ANGULAR CORRELATIONS PERTURBED BY MAGNETIC FIELDS

The influence of an applied magnetic field on angular correlations has been considered by Goertzel[3] and by Alder.[4] Alder's treatment assumed that the coupling of the nuclear spin to the applied field is the only perturbation present. Because of the frequent presence of quadrupole interactions, often much larger than the magnetic coupling, this assumption is fulfilled only under special circumstances. For moderately large nuclear quadrupole moments the quadrupole coupling could be ignored only when it is greatly reduced by either cubic symmetry of the crystal structure in solids or by Brownian motion in liquids. The influence of applied fields in liquid sources has been considered in Sec. V(B).

A. The Quadrupole Coupling Small Compared to the Magnetic

In solids, when the quadrupole interaction is much smaller than the coupling of the nuclear magnetic moment to the applied field, it can be treated using first order perturbation theory, i.e., taking into account the small changes, due to the quadrupole coupling, in the eigenvalues of the magnetic coupling but neglecting the changes in the eigenvectors.

If the direction of the applied field is chosen as the axis of quantization, the correlation can be written

$$W=\mathrm{I}(k_1)\mathrm{II}(k_2)Y_{k_1}^{\mu}(\mathbf{\Omega}_1)Y_{k_2}^{\mu*}(\mathbf{\Omega}_2)\times(Ik_1m'\mu\,|\,Ik_1Im)(Ik_2m'\mu\,|\,Ik_2Im)\times\frac{1}{1-i\mu\omega_L\tau_N-i(m^2-m'^2)\omega_q\tau_N\cos^2\delta},\quad(77)$$

where ω_q is ω_0 of Eq. (34) for integral spins and $\omega_0/2$ of Eq. (35) for half-odd integral spins. In Eq. (77), δ is the angle of the axis of symmetry of the crystalline field with respect to the direction of the magnetic field and ω_L is 2π times the Larmor frequency of the nuclear magnetic moment in the applied field. We can rewrite the denominator of Eq. (77) as

$$[1-i\mu\omega_L\tau_N]\left[1-\frac{i(m^2-m'^2)\omega_q\tau_N\cos^2\delta}{1-i\mu\omega_L\tau_N}\right],\quad(78)$$

and expand W as a power series of $\omega_q\tau_N$. In this series the interpretation of terms in $(\omega_q\tau_N)^p$ with $p>0$ is complicated because they contain interference terms with $k_1\neq k_2$, which do not exist either in the unperturbed theoretical correlation or, if the substance is a powder, in the zero field correlation perturbed by the quadrupole interaction only.

When $\mu\omega_L\tau_N$ becomes significantly larger than unity, we take the second bracket equal to 1, remembering that $\omega_q\ll\omega_L$, and the correlation perturbed by both the magnetic field and the quadrupole interaction is the same as if the latter did not exist. As a consequence, if the field is perpendicular to the plane of the counters and the correlation is expanded as

$$W=\textstyle\sum_k B_k e^{ik\phi},\quad(79)$$

the coefficients B_k are given by

$$B_k=b_k/(1-ik\omega_L\tau_N).\quad(80)$$

Here b_k is the corresponding coefficient in the completely unperturbed correlation, rather than the one which is observed in zero magnetic field where an effect by the quadrupole interaction is present. The simplified view that it is the coefficients b_k' in the expansion analogous to Eq. (79) for the correlation in zero field, rather than the completely unperturbed coefficients b_k, which are reduced by the factors $[1-ik\omega_L\omega_N]^{-1}$ leads to a nuclear magnetic moment in error by a factor b_k'/b_k for $(b_k-b_k')/b_k\ll 1$. This error is reduced to $(b_k'/b_k)^{\frac{1}{2}}$ if the counters do not distinguish between the two radiations. In Cd^{111}, if we regard the anisotropy of, say, 0.23, as observed by the Zurich group,[7] in experiments on a single crystal of indium metal, as completely unperturbed, a value for the magnetic moment obtained by assuming that the unperturbed anisotropy is 0.20,[8] should be increased by about 7 percent. This last statement applies only if the value of the magnetic moment has been extracted from the measurement of magnetic fields so strong that $(2\omega_L\tau_N)^2$ is much larger than unity.

B. The Quadrupole Coupling Large Compared to the Magnetic

When the quadrupole interaction is much larger than the applied field, we consider the latter as a perturbation and choose the axis of the crystal as axis of quantization. The correlation can be written with the same notation as Eq. (77).

$$W=\mathrm{I}(k_1)\mathrm{II}(k_2)Y_{k_1}^{\mu}(\mathbf{\Omega}_1)Y_{k_2}^{\mu*}(\mathbf{\Omega}_2)\times(Ik_1m'\mu\,|\,Ik_1Im)(Ik_2m'\mu\,|\,Ik_2Im)\times\frac{1}{1-i\omega_q(m^2-m'^2)\tau_N-i\omega_L\mu\cos\delta}.\quad(81)$$

In writing Eq. (81) we have again assumed that the small perturbation, in this case the magnetic field, changes only the eigenvalues but not the eigenvectors of the principal Hamiltonian which is now the quadrupole interaction, and that I_z quantized along the axis of the crystal, remains a good quantum number. This assumption may be questioned since, in the quadrupole interaction, the states $\pm m$ are degenerate and may not be the right zero-order states in a perturbation by a magnetic field making an angle with the quadrupole axis. Since the magnetic coupling $g_N\mathbf{H}\cdot\mathbf{I}$ has only matrix elements $\Delta m=0, \pm 1$, the question only arises for the states $m=\pm\frac{1}{2}$ of half-odd integral spins. It is well known that there the right zero-order states are two linear combinations, $|b\rangle$ and $|b'\rangle$, of the $\pm\frac{1}{2}$ states with coefficients depending on the angle δ. The more general formula, Eq. (16), must be used to calculate the contribution of these states but it is easy to show that, because of the properties of the Clebsch-Gordan coefficients, the contribution of the states $|b\rangle$ and $|b'\rangle$ to W in Eq. (16) is the same as if the magnetic field did not exist. Equation (81) can therefore be used quite generally. We can rewrite the denominator of Eq. (81) as

$$[1-i\omega_q(m^2-m'^2)\tau_N]\left[1-\frac{i\omega_L\tau_N\mu\cos\delta}{1-i\omega_q(m^2-m'^2)\tau_N}\right],$$

and expand W as a power series of $\omega_L\tau_N$. If the source is a powder and if the quadrupole interaction is so strong, or the lifetime so long, that $\omega_q\tau_N\gg 1$ and the correlation in zero magnetic field is reduced to its minimum value or "hard core," Eq. (81) shows that the effect of the magnetic field is greatly reduced except for the terms $m^2=m'^2$, $\mu\neq 0$, i.e., for $m=-m'$. The situation is different depending on whether the nuclear spin I is integral or not. If it is not integral the Clebsch-Gordan coefficients $(Ik;-m, 2m|IkIm)$ vanish and the hard core is practically unaffected by the applied field. On the other hand, for integral spins, these coefficients do not vanish and the magnetic field may change the angular correlation appreciably. If the magnetic field is so strong that $\omega_L\tau_N$, although still much smaller than $\omega_q\tau_N$, is much larger than unity, the only terms which give an appreciable contribution to Eq. (81) are those for which $m=m'$, except if $\cos\delta$ is so small that $\omega_L\tau_N\cos\delta$ is not much larger than one. If $\omega_L\tau_N$ is sufficiently large, the proportion of microcrystals in a powder for which this is true is small and their contribution to the average correlation $\overline{W}$ may be neglected. Then $\overline{W}$ becomes

$$\overline{W}=\sum\frac{1}{2k+1}A_kP_k(\cos\psi),$$

where the A_k are the coefficients of the completely unperturbed correlation. This result is independent of the direction of the magnetic field with respect to the counters.

C. The Quadrupole and the Magnetic Couplings of Comparable Strength

Finally, when the coupling to the applied magnetic field and the quadrupole interaction are of comparable magnitude, the treatment becomes complicated and the general formulas, Eqs. (15) and (16), have to be used. These are used after the secular equation, giving the eigenvectors and the eigenvalues of the Hamiltonian $\mathbf{K}$, the sum of the magnetic and electric couplings, has been solved. This must be done numerically except in special cases.[22] As already mentioned in Sec. II, there is no need to solve the secular equation if the correlation is only little perturbed because of short nuclear lifetime or because both the quadrupole and the magnetic couplings are small.

If the source is a crystalline powder, the simplified treatment of Sec. III cannot be applied since the perturbing Hamiltonian is different for two microcrystals differently oriented with respect to the applied magnetic field. The correlation has to be calculated by the general formulas, Eqs. (15) and (16) and averaged over the orientations of the microcrystals, taking into account the angular dependence of the energy levels E_b themselves. Until the results of a specific experiment can be discussed there seems little to be gained by going beyond these general considerations in this complicated case.

D. Static, Anisotropic Magnetic Hyperfine Structure

The perturbation by an atomic magnetic hyperfine structure has been discussed by Goertzel[3] and Alder[4]. Goertzel showed that an applied magnetic field directed toward one of the counters, and sufficiently strong to decouple the nuclear and electronic spins could restore the full correlation otherwise perturbed by the hyperfine structure. Both Goertzel and Alder have considered only the isotropic hyperfine structure described by the coupling $a\mathbf{I}\cdot\mathbf{J}$ which exists in free atoms. In solids, however, this description is inadequate in general. In the iron group of paramagnetic elements, where the hyperfine structure has been most extensively studied experimentally[31] and theoretically,[32] this coupling can be represented by the expression

$$\mathbf{K}=\mathbf{I}\cdot\mathbf{T}\cdot\mathbf{S}, \tag{82}$$

where $\mathbf{T}$ is a symmetrical tensor and $\mathbf{S}$ the spin of the electronic shell. Reduced to its principal axes, Eq. (82) can be written

$$\mathbf{K}=AI_xS_z+BI_xS_x+CI_yS_y. \tag{83}$$

A correlation perturbed by such a Hamiltonian can be described by the general formulas, Eqs. (15) and (16′), after determination of the eigenstates and eigenvalues

[31] B. Bleaney, Physica **17**, 175 (1951).
[32] A. Abragam and M. H. L. Pryce, Proc. Roy. Soc. (London) **A205**, 135 (1951).

of $\mathbf{K}$. If no external field is applied and if the substance is a powder, the somewhat simpler formulas, Eqs. (17) and (22) can be used.

We consider in some detail the simple example of a crystalline powder where one of the coefficients A, B, and C in Eq. (83), say A, is so much larger than the other two that $\mathbf{K}$ can be approximately taken as AI_zS_z. This case is physically significant. It occurs both in copper and cobalt Tutton salts where A is several times larger than B and C, and is the basis of Bleaney's method for aligning nuclear spins at low temperatures.[33]

Formula (22) is then simplified, since both I_z and S_z are good quantum numbers, and leads, for $S=\frac{1}{2}$, to the following expression for the attenuation coefficients.

$$G_k=\frac{1}{2k+1}\sum_{\mu=-k}^{k}[1-i\mu A\tau_N/2\hbar]^{-1}. \tag{84}$$

If $A\tau_N/\hbar$ is large compared with 1,

$$G_k(\lim)=1/(2k+1). \tag{85}$$

The magnetic hyperfine structure is usually several times larger than the quadrupole interaction, and we can, as a first approximation, disregard the latter. An interesting feature of this example is that, even in the absence of quadrupole interaction, an external magnetic field, however strong, applied toward one of the counters cannot restore the correlation perturbed by $\mathbf{K}$. This can be shown as follows.

Let us consider one microcrystal. We call $0z$ the direction of the magnetic field, which is also the direction toward the counter, and $0z'$ the axis of the microcrystal, making with $0z$ the angle θ. The total Hamiltonian $\mathbf{K}$ can be written

$$\mathbf{K}=g\beta_0HS_z+AI_{z'}S_{z'},$$

or

$$\mathbf{K}=g\beta_0HS_z+AI_{z'}(S_z\cos\theta+S_x\sin\theta). \tag{86}$$

Here g and β_0 are, respectively, the gyromagnetic ratio of the paramagnetic ion and the Bohr magneton. (We neglect the direct coupling of the applied field with the nuclear moment.) If the Zeeman interaction $g\beta_0HS_z$ is much larger than the hyperfine coupling $AI_{z'}S_{z'}$, which is the condition required for the decoupling, we can in Eq. (86) treat the second part of $\mathbf{K}$ as a perturbation and replace there S_z and S_x by their expectation values. The expectation value of S_x in an eigenstate of S_z is zero. For this particular microcrystal there is an effective Hamiltonian which is

$$\mathbf{K}_{\text{eff}}=AI_{z'}S_z\cos\theta. \tag{87}$$

If $A\tau_N/\hbar$ is so much larger than unity that the coefficients G_k given by Eq. (84) are practically reduced to their limiting values $1/(2k+1)$, the Hamiltonian $AS_zI_{z'}\cos\theta$ of Eq. (87) will have practically the same effect as $AI_{z'}S_z$ except for the small proportion of microcrystals for which $\cos\theta\ll1$.

[33] B. Bleaney, Phil. Mag. **42**, 441 (1951).

Because the energy levels of $\mathbf{K}_{\text{eff}}$ depend on the orientation of the microcrystal, Eq. (22) cannot be used as it was in the absence of the applied field. However, because of the linear dependence of these energy levels on the magnetic numbers $I_z=m$, and because of the orthogonality properties of the Clebsch-Gordan coefficients, the correlation $\bar{W}$ averaged over all microcrystals can still be represented by Eq. (17), where the attenuation coefficients G_k are defined by

$$G_k=\frac{1}{2k+1}\sum_{\mu=-k}^{k}\int\frac{|Y_k^{\mu}(\theta,\psi)|^2d\Omega}{1-(i\mu A\tau_N\cos\theta)/2\hbar}. \tag{88}$$

The attenuation coefficients G_k in Eq. (88) are larger than those given by Eq. (84), but still smaller than unity and, when A becomes very large, they decrease toward $1/(2k+1)$, although more slowly than in Eq. (84).

If we introduce $\beta=\hbar/A\tau_N$, we find

$$G_2=\frac{1}{5}+\frac{27}{4}\beta^2+\frac{189}{4}\beta^4-24\beta^3(4\beta^2+1)\arctan(1/2\beta)+\frac{3\beta}{4}(1+\beta^2)\arctan(1/\beta). \tag{89}$$

This can be compared to

$$G_2=\frac{1}{5}\left\{1+\frac{8\beta^2}{1+4\beta^2}+\frac{32\beta^2}{1+16\beta^2}\right\} \tag{90}$$

in the absence of the decoupling field.

As an order of magnitude, in copper Tutton salts $A\sim0.01$ cm^{-1}. If $\tau_N=10^{-7}$, $\beta\sim1/200$ and G_2 is practically $\frac{1}{5}$ even in the presence of the applied field.

E. The Influence of Electronic Paramagnetic Relaxation

The discussion of the attenuations caused by magnetic hyperfine structure interactions in Sec. VI(D) supposed that entirely stationary electronic states, at least over times comparable to τ_N, exist. There must always be present some coupling of those states to the thermal vibrations of the lattice which, for most ions that show spin-only paramagnetism, is a result of spin-orbit coupling. A relaxation time for the electron moment can be defined and this can, in some cases, be so short as to require a different approach to be taken to the treatment of the effect on angular correlations. In electronic paramagnetic resonance it is necessary to work at temperatures as low as 4°K, in some cases, in order to obtain lifetimes of the electronic states sufficiently long to allow detection of the resonance lines.

The methods applied to the discussion of the electric quadrupole effect in liquid sources, Sec. V, can be used in some circumstances to analyze this effect. The effect of the spin-lattice coupling would mainly be to cause

continual random changes in the orientation of the electronic spin angular momentum **S**. The result of this would be equivalent to a continuously reorienting classical magnetic field at the nucleus and the resulting time dependent behavior of the nuclear spin can be calculated in a manner analogous to the calculations of Sec. V. If the interaction energy is $h\omega_S \mathbf{I}\cdot\mathbf{S}$ and $\omega_S\tau_S \ll 1$, where τ_S is the relaxation time of the electron spin, the effect on the angular correlation is expressible by attenuation coefficients

$$G_k=(1+\lambda_k'\tau_N)^{-1},$$

where, here, the λ_k' are calculated as in Sec. V, but in Eq. (46) T_1^{μ} is used and corresponding changes are made in the expressions leading to Eq. (71). Expressions for the λ_k' are then

$$\lambda_k'=a'[1-(2I+1)W(I1kI/II)] \tag{91}$$

and

$$a'=\tfrac{2}{3}\tau_S\omega_S^2 I(I+1)S(S+1). \tag{92}$$

It is apparent that the attenuation considered here can be arbitrarily complete for sufficiently large values of the quantities $\lambda_k'\tau_N$.

Because τ_S, in general, shortens as the temperature increases, the correlation largely destroyed by such an effect would improve as the temperature is raised. The quantitative formula is not valid for $\tau_S \sim \tau_N$ or for $\omega_S\tau_S$ not much smaller than unity but, nevertheless, if τ_S becomes greater than τ_N, as it must at sufficiently low temperatures, the effect goes into that of the isotropic static hyperfine structure interaction for which a "hard core" remains no matter how strong the interaction. There is, thus, for a large ω_S, a maximum disturbance somewhere between a very small τ_S and one longer than τ_N.

A sufficiently strong magnetic field applied along the direction to the first counter can completely restore the correlation. The condition for that is for $g\beta_0 H/h$, the angular Larmor frequency of the electron in the field H, to be made sufficiently large compared to the larger of ω_S and $1/\tau_S$. In effect, the spectral density of the fluctuating component of local magnetic field in the plane normal to the direction to the counter must be reduced and this results only if the above condition is satisfied. The g factor of the electron is such that a field of 10 kilogauss would be sufficient to partially restore the correlation unless τ_S were shorter than 5×10^{-12} sec. At room temperatures shorter relaxation times than this do occur for some ions.

VII. RESONANCE METHODS

If angular correlations are to be used to measure nuclear moments of the intermediate state the improvement over the observation of the effect of static fields obtained by inducing resonant transitions by an rf field, analogous to that gained by Rabi in molecular beams, might be considered. Several difficulties present themselves as discussed for a couple of examples below.

A. Nuclear Magnetic Resonance

It has already been stated that in a double decay cascade the first radiation can be considered as creating in the intermediate state of the nucleus unequally populated magnetic states quantized along the direction of emission of this radiation. The existence of an angular correlation between the two radiations, i.e., of an anisotropy in the direction of emission of the second radiation with respect to the first, is precisely due to these inequalities of population.

If resonant transitions between the magnetic substates can be induced by an applied rf field, their effect will be to decrease these inequalities of population and therefore to decrease the anisotropy of the angular correlation, thus providing a means of detecting the resonance. If there is no static quadrupole interaction or magnetic hyperfine structure, a uniform magnetic field H applied along the direction to the first counter splits the magnetic substates without affecting the correlation and the resonance frequency for an rf field in the plane normal to H is the Larmor frequency $\omega_L/2\pi$ of the intermediate nucleus in the static field.

In order for a resonance experiment to provide an accurate measurement of the nuclear magnetic moment, the following conditions must be realized.

(a) The natural width of the magnetic levels due to the finite lifetime of the intermediate state of the nucleus must be much smaller than the spacings between these levels. The ratio of the spacing between two adjacent levels to the line width is $\omega_L\tau_N$ which, thus, should be much larger than unity. This is equivalent to saying that the uniform field, if applied perpendicular to the plane of the counters, should destroy the correlation completely. As an example, for Cd^{111} where $\tau_N \sim 10^{-7}$ and $g_n \sim 0.3$ nuclear magneton, $\omega_L\tau_N \simeq 2$ in a field of 15 000 gauss, which makes this type of experiment for this particular nucleus relatively unrewarding.

(b) The amplitude of the rf field should be sufficiently large for the resonant transitions to have an appreciable probability during the nuclear lifetime. This requires that $\omega_1\tau_N \simeq 1$ where ω_1 is 2π times the Larmor frequency of the nucleus in a constant field equal to the amplitude of the rf field. It is equivalent to say that such a constant field, if applied perpendicular to the plane of the counters, should have a detectable effect on the correlation. This rules out this experiment for Cd^{111}, since rf fields so large would be extremely difficult to produce. More conventional resonance experiments seldom utilize rf fields larger than about 10 gauss.

(c) The lifetime of the nucleus should be shorter than the relaxation time of the nuclear spin in the source. Since, in order for the resonant experiment to be feasible, rather long nuclear lifetimes are required, this may be a limitation in liquid sources. with strong quadrupole relaxation, but probably is not a limitation in solid sources. In the latter a crystal structure of cubic sym-

metry is required in order to avoid perturbation by the static quadrupole interaction.

To sum up, it can be said that a resonance experiment is probably feasible for a nucleus for which the product $g_n\tau_N$ is as large as for a free proton with a lifetime of one microsecond. No such nucleus is known at present.

The time-dependent correlation $w(t)$ in the presence of the rf field is given by the general formulas of Eq. (12) and Eq. (13). If the z axis is parallel to the direction of the applied magnetic field $\mu_1=\mu_2=0$. In Eq. (13), $(m|\mathbf{U}^+|m'')(m'''|\mathbf{U}|m')$ becomes $|(m''|\mathbf{U}|m)|^2$, which is the well-known Majorana function $P(I, m'', m, t)$,[34] expressing the probability of finding the spin in the state m'' at time t if it was in the state m at $t=0$. The integrals

$$\int_0^\infty e^{-t/\tau_N}P(t)dt/\tau_N$$

have been calculated and tabulated by Bitter and Brossel for several values of the spin.[35]

In principle, the resonance method could also apply to the quadrupole interaction in a single crystal with its axis parallel to the applied field, or to a crystalline powder.

B. Resonance in Magnetic Atoms

If the atom containing the radioactive nucleus has a magnetic moment and therefore a hyperfine structure, $A\mathbf{I}\cdot\mathbf{J}$, a somewhat different resonance experiment might be attempted.

If a strong magnetic field parallel to one of the counters restores the correlation perturbed by the hyperfine structure interaction as already discussed, the correlation could again be disturbed by an rf field. The energy levels of the system are given by $K=g\beta_0HJ_z+AJ_zI_z$, and transitions $\Delta J_z=0$, $\Delta I_z=\pm1$ can be induced between the levels $J_z=M$, $I_z=m$ and $J_z=M$, $I_z=m\pm1$, whose separation is AM. The point of these remarks is that AM, which measures the hyperfine structure of the atom, can be orders of magnitude larger than the Zeeman splittings of the nuclear moment in an applied field, thus relaxing the limitation (a) of the resonance method. The limitation (b), however, remains unchanged and especially difficult to meet because the frequency is high.

Perhaps a better method is to induce transitions between different eigenstates of the total atomic moment F, where $\mathbf{F}=\mathbf{I}+\mathbf{J}$, in zero applied field. Alder has shown that, even if $(E_F-E_{F'})\tau_N/h$ is very large, which is precisely the condition (a), the correlation does not disappear completely but leaves a "hard core." A resonant rf field could produce a detectable change in this hard core. The important point here is that in these transitions the rf field flips the electronic moment but since the electronic moment is coupled to the nuclear spin both flip and the angular correlation is altered. Since the coupling of the rf field to the electronic spin is thousands of times larger than its coupling to the nuclear spin, the probability of a transition during the time τ_N is considerably increased and condition (b) can be met.

The measurement of the hyperfine structure in a stable isotope of known nuclear moment by conventional methods would, by comparison, give the magnetic moment of the radioactive nucleus.

As remarked in Sec. IV(D), by measuring the departures from Landé's interval rule in the energy differences $E_F-E_{F'}$, the sign and magnitude of the quadrupole interaction could be measured if $J>\frac{1}{2}$.

These considerations apply most directly to free atoms such as those in a gaseous source. It is clear that a condition that should be met by the source is that collisions between atoms or against the walls, which result in changes in $\mathbf{F}$, must not occur, on the average, in times shorter than, or of the order of, τ_N.

VIII. CONCLUSION

It has been shown that static electric quadrupole interations in polycrystalline sources can reduce the angular correlation. For both axially symmetric and rhombic fields, no matter how strong the interaction, there remains some anisotropy.

In liquid sources, the electric quadrupole moment interacts with a randomly fluctuating field and the resulting attenuations are expressed as $G_k=(1+\lambda_k\tau_N)^{-1}$, where the λ_k are given in Eq. (71). Here the correlation, although usually less disturbed than in solid sources, can be completely destroyed for sufficiently long τ_N. A similar effect is possible if the electronic shell is magnetic with a short lifetime of a given magnetic substate. The application of magnetic fields in the first of these cases should have little effect if directed toward either counter. In the second, unless the relaxation time τ_S is very short, it should be possible to reduce the disturbance by application of such a field.

The explanation of the observation by the Zürich group and by Stefen of correlations from the γ-γ cascade from the Cd^{111} daughter of In^{111} in solid compounds of indium remains unclear. It would appear that a purely static interaction in the intermediate state could not be the sole effect unless the crystallites of the source were preferentially oriented, which seems unlikely. Instead, the existence of a magnetic shell, following the K capture, in compounds is a possibility. In that event, the most likely mechanism for the disturbance would be that associated with relaxation of the electron spin. Even more speculative would be the suggestion that the recoil energy accompanying K capture excites vibrations of a complex or molecule in

[34] I. I. Rabi, Phys. Rev. **51**, 652 (1937); F. Bloch and I. I. Rabi, Revs. Modern Phys. **17**, 237 (1945).

[35] F. Bitter and J. Brossel, Technical Report No. 176, Research Laboratory of Electronics, Massachusetts Institute of Technology, 1950 (unpublished).

which the Cd^{111} is contained. The vibrations might, in turn, cause reorientations of the spin in times shorter than τ_N. Such vibrations, on the other hand, should be very short lived and this, too, seems an unlikely mechanism.

It should be emphasized that for γ-γ cascades following almost instantaneously after K capture, the electronic configuration during the lifetime of the intermediate state of the nucleus is less clearly defined than it would be for a γ-γ cascade from a long-lived isomer, such as 48-min Cd^{111}. In such a case, the radiation from the isomer could be observed in a normal chemical environment. For all other correlations than pure γ-γ and γ-conversion electron, the surroundings of the nucleus in its intermediate state are not well known and it is difficult to draw quantitative conclusions from observed perturbations of the correlation.

IX. ACKNOWLEDGMENTS

Our interest in this subject was aroused through discussion of a related subject with Professor N. Bloembergen. We wish to thank him and also Professor H. Brooks, Professor M. Deutsch, Dr. M. Goldhaber, and Professor E. M. Purcell for helpful discussions. One of us (A.A.) wishes to thank the Shell Oil Company for support through a research grant.

PHYSICAL REVIEW VOLUME 92, NUMBER 4 NOVEMBER 15, 1953

Nuclear Spin Relaxation by Translational Diffusion*

H. C. TORREY
Department of Physics, Rutgers University, New Brunswick, New Jersey
(Received July 21, 1953)

The general theory of Bloembergen, Purcell, and Pound of nuclear spin relaxation has been extended to a more quantitative study of relaxation by translational diffusion. It has been found necessary to treat the problem by the theory of random walk. In the case of isotropic diffusion two cases have been studied: one in which the flight distance has a probability distribution, and the other in which it is constant. The problem of random walk to nearest neighbor sites in a lattice is also treated and quantitative results are obtained for a face-centered cubic lattice.

I. INTRODUCTION

BLOEMBERGEN, Purcell, and Pound have given a general solution to the problem of nuclear spin relaxation.[1,2] An important and prevalent mechanism has been shown to be the coupling of spin orientation with nuclear thermal motion via the dipolar magnetic interaction of the nuclear moments. This influence and the corresponding relaxation are particularly strong whenever the nuclei perform random diffusive motions such as occur in liquids of appropriate viscosity. Such diffusive motions may occur also in the solid phase particularly in the case of solid solutions; for example, hydrogen in palladium, but also in the case of self-diffusion. Bloembergen[2] has applied his theory to diffusive motions. His treatment of translational diffusion is, however, admittedly crude and must be regarded as only semiquantitative. It is the purpose of this paper to present a more quantitative theory and in particular to emphasize the possibility of examining certain microscopic details of the diffusion process which cannot be ascertained from a study of gross diffusion phenomena alone. In Bloembergen's treatment only the diffusion constant D enters as a parameter. Thus his theory gives no basis for a closer study of the diffusion mechanism than can be obtained by conventional measurements of macroscopic diffusion. Nuclear spin relaxation is however essentially microscopic in character. The magnetic field of one nucleus at the position of another depends on the inverse cube of the distance and the influence of nearest neighbors is thus relatively strong. It is apparent from this that one needs to consider the individual motions of neighboring spins, that is to say, the process of random flights of which, as is well known, the phenomenon of diffusion is only the limiting macroscopic approximation. Thus it may be expected that certain details of random flights such as $\langle r^2 \rangle$, the mean squared flight distance, and τ, the mean time between flights, will enter into the description of relaxation in other ways than merely in the familiar combination:

$$D = \langle r^2 \rangle / 6\tau. \tag{1}$$

This is indeed the case and leads at least in principle to the possibility of independent measurement of these parameters in certain cases.

II. APPLICATION OF THE THEORY OF RANDOM FLIGHTS

We start from the general formula derived by Bloembergen[1,2] for the relaxation time T_1:

$$T_1^{-1} = \tfrac{3}{4}\gamma^4\hbar^2 I(I+1)[S_2(2\omega_0) + 2S_1(\omega_0)]. \tag{2}$$

* Supported by the joint program of the U. S. Office of Naval Research and U. S. Atomic Energy Commission, by the Radio Corporation of America, and by the Rutgers Research Council.
[1] Bloembergen, Purcell, and Pound, Phys. Rev. **73**, 679 (1948).
[2] N. Bloembergen, thesis, Leiden, 1948 (Martinus Nijhoff, The Hague).

Here S_1 and S_2 are the spectral densities of the random time functions:

$$F_1=\sum_j F_{ij}^{(1)}(t), \tag{3a}$$

$$F_2=\sum_j F_{ij}^{(2)}(t), \tag{3b}$$

where

$$F_{ij}^{(1)}(t)=\sin\theta_{ij}\cos\theta_{ij}e^{i\varphi_{ij}}/r_{ij}^3, \tag{4a}$$

$$F_{ij}^{(2)}(t)=\sin^2\theta_{ij}e^{2i\varphi_{ij}}/r_{ij}^3, \tag{4b}$$

and $(r_{ij}, \theta_{ij}, \varphi_{ij})$ are the spherical coordinates of spin j relative to spin i and are to be regarded as random functions of the time.

The functions S_1 and S_2 may be more specifically defined as follows. Let $k_1(t)$ and $k_2(t)$ be correlation functions given by

$$k_1(t)=\sum_j\langle F_{ij}^{(1)}(t')F_{ij}^{(1)*}(t'+t)\rangle_{\mathrm{Av}(t')}, \tag{5a}$$

$$k_2(t)=\sum_j\langle F_{ij}^{(2)}(t')F_{ij}^{(2)*}(t'+t)\rangle_{\mathrm{Av}(t')}, \tag{5b}$$

where an asterisk denotes the complex conjugate.

Then

$$S_{1,2}(\omega)=\int_{-\infty}^{+\infty}e^{i\omega t}k_{1,2}(t)dt. \tag{6}$$

In evaluating the spectral density functions, we replace the time averages in (5) by ensemble averages. To do this we first introduce probability functions as follows:

(*a*) Let $P(\mathbf{r}, \mathbf{r}_0, t)d\mathbf{r}$ be the probability that, if spin j is located at zero time at $\mathbf{r}_0$ relative to spin i, at time t spin j will lie within the volume element $d\mathbf{r}$ located at $\mathbf{r}$ relative to the new position of spin i.

(*b*) Let $N^{-1}f(\mathbf{r}_0)d\mathbf{r}_0$ be the probability that at zero time, spin j is located in $d\mathbf{r}_0$ at $\mathbf{r}_0$ relative to spin i. N designates the number of spins in the system; thus $f(\mathbf{r}_0)$ is the initial spin density.

We may now write for the correlation functions the ensemble averages,

$$k_1(t)=\int\int P(\mathbf{r}, \mathbf{r}_0, t)F_{ij}^{(1)}(\mathbf{r}_0)F_{ij}^{(1)*}(\mathbf{r})f(\mathbf{r}_0)d\mathbf{r}_0d\mathbf{r}, \tag{7}$$

with a similar expression for $k_2(t)$. The sum over j in (5) has been replaced by multiplication by N.

The solution of the problem thus depends on the construction of the probability functions. Of these $f(\mathbf{r}_0)$ is an initial datum depending on the circumstances of the particular problem. Thus for a uniform spin density $f(\mathbf{r}_0)$ is a constant, while for lattice diffusion $f(\mathbf{r}_0)$ may be expressed as a sum over delta functions centered at the lattice points. The function $P(\mathbf{r}, \mathbf{r}_0, t)$ can be found from the theory of random flights as follows.

We shall assume that every position of a spin is statistically equivalent in the sense that at each position the same probability exists that after one flight from this position, the new spin position will be at $\mathbf{r}$ in $d\mathbf{r}$ relative to the previous position. We designate this probability by $P_1(\mathbf{r})d\mathbf{r}$ and the corresponding probability after n flights by $P_n(\mathbf{r})d\mathbf{r}$. The theory of random flights then gives[3]

$$P_n(\mathbf{r})=(1/8\pi^3)\int A^n(\boldsymbol{\varrho})\exp(-i\mathbf{r}\cdot\boldsymbol{\varrho})d\boldsymbol{\varrho}, \tag{8}$$

where the integration is over the whole of $\boldsymbol{\varrho}$ space.

The function $A(\boldsymbol{\varrho})$ occurring in (8) is defined by inverting the three-dimensional Fourier transform (8) in the case $n=1$:

$$A(\boldsymbol{\varrho})=\int P_1(\mathbf{r})\exp(i\boldsymbol{\varrho}\cdot\mathbf{r})d\mathbf{r}. \tag{9}$$

The probability $P(\mathbf{r}, t)d\mathbf{r}$ that a spin initially at the origin will at time t be located in $d\mathbf{r}$ at $\mathbf{r}$ is

$$P(\mathbf{r}, t)=\sum_n P_n(\mathbf{r})w_n(t), \tag{10}$$

where $w_n(t)$ is the probability that n flights take place in time t. For $w_n(t)$ we assume the Poisson distribution

$$w_n(t)=(1/n!)(t/\tau)^ne^{-t/\tau}, \tag{11}$$

where τ is the mean time between flights.

The sum in (10) includes of course $n=0$ where evidently

$$P_0(\mathbf{r})=\delta(\mathbf{r}), \tag{12}$$

$\delta(\mathbf{r})$ being the three-dimensional delta function.

Substituting (8) and (11) in (10) we get

$$P(\mathbf{r}, t)=(1/8\pi^3)\int\exp\{-i\mathbf{r}\cdot\boldsymbol{\varrho}-(t/\tau)[1-A(\boldsymbol{\varrho})]\}d\boldsymbol{\varrho}. \tag{13}$$

Finally $P(\mathbf{r}, \mathbf{r}_0, t)$ is found by

(*a*) forming the product

$$P(\mathbf{r}_i, t)P(\mathbf{r}_j-\mathbf{r}_0, t)d\mathbf{r}_id\mathbf{r}_j, \tag{14}$$

where $\mathbf{r}_i$ and $\mathbf{r}_j$ are the position vectors of spins i and j relative to a common origin;

(*b*) transforming to relative-centroidal coordinates,

$$\mathbf{r}=\mathbf{r}_j-\mathbf{r}_i, \quad \mathbf{R}=\tfrac{1}{2}(\mathbf{r}_j+\mathbf{r}_i);$$

and (*c*) integrating (14) over all centroidal positions $\mathbf{R}$. If, as is usually the case, $A(\boldsymbol{\varrho})=A(-\boldsymbol{\varrho})$ the result is easily found to be

$$P(\mathbf{r}, \mathbf{r}_0, t)=(1/8\pi^3)\int\exp\{-i\boldsymbol{\varrho}\cdot(\mathbf{r}-\mathbf{r}_0)-(2t/\tau)\times[1-A(\boldsymbol{\varrho})]\}d\boldsymbol{\varrho}, \tag{15}$$

or

$$P(\mathbf{r}, \mathbf{r}_0, t)=P(\mathbf{r}-\mathbf{r}_0, 2t). \tag{16}$$

If the condition $A(\boldsymbol{\varrho})=A(-\boldsymbol{\varrho})$ does not hold, one must replace $A(\boldsymbol{\varrho})$ in (15) by $\frac{1}{2}[A(\boldsymbol{\varrho})+A(-\boldsymbol{\varrho})]$ and (16) no longer holds.

[3] See, for example, S. Chandrasekhar, Revs. Modern Phys. **15**, 1 (1943).

Substitution in Eq. (7) of $P(\mathbf{r}, \mathbf{r}_0, t)$ as given by (15), together with an appropriate $f(\mathbf{r}_0)$, completes the formal solution of the problem. In the following sections we shall investigate the results of particular assumptions as to the forms of $P_1(\mathbf{r})$ and $A(\boldsymbol{\varrho})$.

It might be thought that a useful approximation could be obtained by taking $P(\mathbf{r}, t)$ as that solution of the diffusion equation,

$$\partial P/\partial t = D\nabla^2 P, \tag{17}$$

with the initial form $P(\mathbf{r}, 0) = \delta(\mathbf{r})$. This solution is, as is well known,

$$P(\mathbf{r}, t) = (4\pi Dt)^{-\frac{3}{2}} \exp(-r^2/4Dt). \tag{18}$$

However, the conditions under which this approximation is justified are so stringent that it is unlikely to correspond, except under exceptional circumstances, to any physical reality. Equation (18) is of course the limiting case of the random flight theory in which the mean squared flight path $\langle r^2 \rangle$ is small and the mean time τ between flights is short. It can in fact be obtained from the above theory under these assumptions, as will now be shown. In the case of isotropic diffusion we may expand (9) in powers of ρ:

$$A(\boldsymbol{\varrho}) = \sum_{n=0}^{\infty} \frac{(i\rho)^n}{n!} \int\int\int P_1(\mathbf{r}) r^{n+2} dr \cos^n\theta \sin\theta d\theta d\varphi,$$

or

$$A(\boldsymbol{\varrho}) = \sum_{n=0}^{\infty} (-1)^n \langle r^{2n} \rangle \rho^{2n}/(2n+1)! \tag{19}$$

$$= 1 - \tfrac{1}{6}\langle r^2 \rangle \rho^2 + O(\rho^4), \tag{20}$$

where

$$\langle r^n \rangle = 4\pi \int_0^{\infty} P_1(\mathbf{r}) r^{n+2} dr \tag{21}$$

is the nth moment of the distribution $P_1(\mathbf{r})$.

If the series (19) is substituted in (13), it is clear that if $\langle r^2 \rangle$ is sufficiently small and t/τ sufficiently large, the integral will be cut off by the term in ρ^2 in (19) before higher powers of ρ become effective. We then obtain precisely (18) with $D = \langle r^2 \rangle / 6\tau$. In the following section it will appear that the physical conditions thus imposed on $\langle r^2 \rangle$ and τ are so severe that this approximation has little physical interest. Thus it is necessary to assume specific forms for $P_1(\mathbf{r})$ and examine their consequences. In Sec. III we treat the case of isotropic diffusion and in Sec. IV the case of random flights to nearest neighbor positions in a lattice.

III. ISOTROPIC DIFFUSION

The case of isotropic diffusion is defined by the conditions: (1) $A(\boldsymbol{\varrho})$ depends on the magnitude of $\boldsymbol{\varrho}$ only and (2) $f(\mathbf{r}_0) = n$ (uniform spin density). If these conditions hold, we may perform all integrations in the calculation of the correlation functions and their spectral densities save that over ρ which must await a specific choice for the form of $A(\boldsymbol{\varrho})$. As an illustration we shall carry out these calculations for $k_1(t)$ and $S_1(\omega)$. Substituting (4a) and (15) in (7) we obtain

$$k_1(t) = \frac{n}{4\pi} \int\int\int \frac{\sin\theta_0 \cos\theta_0 \cdot \sin\theta \cos\theta}{r_0^3 r^3} e^{i(\varphi_0 - \varphi)} \times \exp\left\{ -i\boldsymbol{\varrho} \cdot (\mathbf{r} - \mathbf{r}_0) - \frac{2t}{\tau}[1 - A(\boldsymbol{\varrho})] \right\} d\mathbf{r} d\mathbf{r}_0 d\boldsymbol{\varrho}. \tag{22}$$

We now introduce expansions of $\exp(-i\boldsymbol{\varrho}\cdot\mathbf{r})$ and $\exp(i\boldsymbol{\varrho}\cdot\mathbf{r}_0)$ by means of the formula:

$$\exp(i\rho r \cos\Phi) = (\pi/2\rho r)^{\frac{1}{2}} \sum_{n=0}^{\infty} (2n+1) i^n J_{n+\frac{1}{2}}(\rho r) P_n(\cos\Phi), \tag{23}$$

where J_m and P_n are the usual Bessel and Legendre functions. For $P_n(\cos\Phi)$ in (23) we use the addition formula for the Legendre polynomials:

$$P_n(\cos\Phi) = P_n(\cos\theta) P_n(\cos\alpha) + \sum_{m=1}^{n} \frac{(n-m)!}{(n+m)!} \times P_n^m(\cos\theta) P_n^m(\cos\alpha) \cos m(\varphi - \beta), \tag{24}$$

where (θ, φ) and (α, β) are the polar-azimuthal angular coordinates of two directions separated by the angle Φ. The integrals over r and r_0 have the limits a and ∞ where a may be physically interpreted as approximately the closest possible distance of approach of two nuclei. Making use of the orthonormal properties of the Legendre functions, we obtain after some reduction

$$k_1(t) = \frac{8\pi n}{15a^3} \int_0^{\infty} \exp\left\{ -\frac{2t}{\tau}[1 - A(\rho)] \right\} J_{\frac{5}{2}}^2(a\rho) \frac{d\rho}{\rho}. \tag{25}$$

A similar calculation for $k_2(t)$ gives

$$k_2(t) = 4k_1(t). \tag{26}$$

The spectral density function by Eq. (6) is, e.g.,

$$S_1(\omega) = 2\int_0^{\infty} \cos\omega t \; k_1(t) dt. \tag{27}$$

Substituting (25) in (27) and integrating first with respect to t, we get

$$S_1(\omega) = \frac{8\pi n\tau}{15a^3} \int_0^{\infty} J_{\frac{5}{2}}^2(a\rho) \frac{1 - A(\rho)}{[1 - A(\rho)]^2 + (\omega\tau/2)^2} \frac{d\rho}{\rho} \tag{28}$$

and

$$S_2(\omega) = 4S_1(\omega). \tag{29}$$

Before proceeding to discuss the consequences of possible assumptions as to the form of $A(\boldsymbol{\varrho})$, we first consider three limiting cases to which all possible choices of $A(\boldsymbol{\varrho})$ must conform.

We shall first consider the limiting cases (*a*) $\omega\tau \gg 1$ and (*b*) $\omega\tau \ll 1$. Since in practice we may assume that τ

varies with temperature according to

$$\tau = \tau_0 e^{E/kT}, \tag{30}$$

where E is an activation energy, these limiting cases give respectively the low-temperature and high-temperature asymptotes for T_1 in between which T_1 will have a minimum.

(*a*) ($\omega\tau \gg 1$). By Eq. (9)

$$|A(\boldsymbol{\rho})| \leq \int |\exp i\boldsymbol{\rho}\cdot\mathbf{r}|\, P_1(\mathbf{r})d\mathbf{r} = 1.$$

Thus $1-A(\boldsymbol{\rho})$ never becomes larger than the order of unity, and we may neglect the factor $[1-A(\boldsymbol{\rho})]^2$ in the denominator of (28), obtaining

$$S_1(\omega) = \frac{32\pi n}{15a^3\omega^2\tau}\int_0^\infty J_{\frac{1}{2}}^2(a\rho)[1-A(\rho)]\frac{d\rho}{\rho}. \tag{31}$$

Thus,

$$T_1 \propto \omega^2\tau = \omega^2\tau_0 e^{E/kT}. \tag{32}$$

(*b*) ($\omega\tau \ll 1$). Here we simply put $\omega\tau = 0$ in the denominator of the integrand in (28) and obtain

$$S_1(\omega) = \frac{8\pi n\tau}{15a^3}\int_0^\infty \frac{J_{\frac{1}{2}}^2(a\rho)d\rho}{[1-A(\rho)]\rho}. \tag{33}$$

By Eq. (20) the integral in (33) always converges and so

$$T_1 \propto 1/\tau = (1/\tau_0)e^{-E/kT}. \tag{34}$$

(*c*) We now consider the special case for which the mean flight path is long: $\langle r^2\rangle \gg a^2$. The function $1-A(\rho)$ which enters in the integrand of (28) in two places has the following general behavior. By Eq. (20) it vanishes at $\rho = 0$; at large ρ it approaches unity by Eq. (9). It may increase monotonously or may oscillate about its asymptotic value. In any case, the rapidity with which it approaches unity is essentially determined by the magnitude of the mean squared flight path $\langle r^2\rangle$. Thus, if $\langle r^2\rangle \gg a^2$, the value of $P_1(\mathbf{r})$ is everywhere small and by Eq. (9) $1-A(\rho)$ approaches unity quickly for small values of $a\rho$. Thus it may be replaced by unity in the integrand of (28).

We then obtain

$$S_1(\omega) = \frac{8\pi n}{45a^3}\cdot\frac{\tau}{1+(\omega\tau/2)^2}, \tag{35}$$

and, for the relaxation time,

$$\frac{1}{T_1} = \frac{8\pi}{15}\gamma^4\hbar^2 I(I+1)\frac{n}{a^3}\left[\frac{\tau/2}{1+(\omega\tau/2)^2} + \frac{\tau}{1+\omega^2\tau^2}\right]. \tag{36}$$

It will be recognized that (35) and (36) have the well-known forms appropriate to an exponentially decaying correlation function with a "correlation time" $\tau_c = \tau/2$.

The minimum T_1 obtained from (36) when $\omega\tau = \sqrt{2}$ is given by

$$T_{1m}^{-1} = (16\sqrt{2}\pi/45)\gamma^4\hbar^2 I(I+1)n/a^3\omega. \tag{37}$$

It may be shown that the approximation made here by putting $A(\rho) = 0$ is equivalent to the neglect of all but the first term in the series of Eq. (19).

(*d*) We now consider the consequences of assuming special forms for $P_1(\mathbf{r})$ and $A(\boldsymbol{\rho})$. We first take

$$P_1(\mathbf{r}) = (4\pi D\tau r)^{-1}\exp[-r/(D\tau)^{\frac{1}{2}}], \tag{38}$$

which corresponds to

$$A(\boldsymbol{\rho}) = [1+D\tau\rho^2]^{-1}. \tag{39}$$

Equation (39) is the mathematically simplest form for A which satisfies all the conditions that can be imposed for an acceptable form. It leads to a closed form solution for T_1 expressible in terms of elementary functions. We first show that the following physical conditions lead to (39). Let us suppose that a spin can exist in one of two states: (*a*) bound in a potential well, or (*b*) a thermally excited state in which the nucleus may move rapidly about in a random diffusive type of motion. We suppose that the motion in the excited state is so rapid that its details contribute only to very high frequencies in the Fourier spectrum $S(\omega)$ and have no effect on the relaxation. It is possible that this type of motion may approximate the motion of protons in highly rifted metallic lattices such as in hydrogenated palladium or other metallic hydrides. It will not be necessary to specify the excited state precisely, but we shall assume that the motion in this state can be described by the solution of the diffusion equation (17) given by Eq. (18). That is, we shall suppose that after a spin has vacated a trapping site and before capture by another, the probability after time t that it will be at $\mathbf{r}$ in $d\mathbf{r}$ relative to the site it has vacated is

$$(4\pi D't)^{-1}\exp(-r^2/4D't)d\mathbf{r}, \tag{40}$$

where D' is a diffusion coefficient appropriate to the excited state. We shall later see how D' is related to the overall diffusion constant D. We now multiply (40) by $e^{-t/\tau'}\cdot dt/\tau'$, which we take to be the probability that the nucleus will become trapped again after a time t in dt. Thus τ' is the mean life time in the excited state and will be small compared with $\tau-\tau'$, the mean life of the trapped state. Integrating the resulting expression over t we obtain the probability $P_1(\mathbf{r})d\mathbf{r}$ that a single jump (i.e., a single life in the excited state) will find the nucleus a distance $\mathbf{r}$ in $d\mathbf{r}$ from its starting place. Hence:

$$P_1(\mathbf{r}) = \int_0^\infty (4\pi D't)^{-\frac{3}{2}}\exp(-r^2/4D't - t/\tau')dt/\tau'. \tag{41}$$

This integral is easily evaluated[4] and we get Eq. (38)

[4] See, for example, W. Magnus and F. Oberhettinger, *Formulas and Theorems for the Special Functions of Mathematical Physics* (Chelsea Publishing Company, New York, 1949), p. 128.

TABLE I. Tables of the functions $f(\alpha, x)$ [Eq. (55)] and $\varphi(\alpha, x)$ [Eq. (56)].

x	$f(1/12, x)$	$\varphi(1/12, x)$	$f(\frac{1}{2}, x)$	$\varphi(\frac{1}{2}, x)$
0.2			0.0130	0.0455
0.4	0.0266	0.0770	0.0688	0.1996
0.6	0.0552	0.1531	0.1451	0.3915
0.8	0.0890	0.2425	0.2286	0.5445
1.0	0.1265	0.3336	0.2920	0.6090
1.071				0.6128(max)
1.1			0.3112	0.6122
1.2	0.1685	0.4160	0.3215	0.5983
1.3			0.3231	0.5756
1.4	0.2046	0.4784	0.3182	0.5489
1.6	0.2353	0.5240	0.2942	0.4849
1.8	0.2596	0.5490	0.2582	0.4135
2.0	0.2753	0.5566	0.2290	0.3585
2.041		0.5568(max)		
2.2	0.2866	0.5534	0.1989	0.3075
2.4	0.2902	0.5392	0.1728	0.2649
2.6	0.2884	0.5185	0.1493	0.2281
2.8	0.2823	0.4931	0.1318	0.1998
3.0	0.2730	0.4655	0.1161	0.1757
3.6	0.2354	0.3813	0.0821	0.1269
4.2	0.1954	0.3070	0.0608	0.0936
4.8	0.1604	0.2475		
5.4	0.1323	0.2022		
6.0	0.1097	0.1667		
6.6	0.0918	0.1391		
7.2	0.0782	0.1180		
7.8	0.0669	0.0909		

with $D'\tau'$ in place of $D\tau$. Now clearly $D'\tau'=\langle r^2\rangle/6=D\tau$, and so we get Eq. (39).

We shall now adopt Eq. (39) and examine its consequences. Substituting (39) in (28) we get

$$S_1(\omega)=(16\pi n/15a^3)\,\mathrm{Re}(J), \tag{42}$$

where

$$J=\int_0^\infty \frac{1+D\tau\rho^2}{2D\rho^2-i\omega(1+D\tau\rho^2)}\cdot J_{\frac{1}{2}}^2(a\rho)\frac{d\rho}{\rho}. \tag{43}$$

If now we define

$$\beta^2=i\omega/D(2-i\omega\tau), \tag{44}$$

we can put (43) in the form:

$$J=\frac{\tau}{2-i\omega\tau}\int_0^\infty\left[\left(1+\frac{1}{D\tau\beta^2}\right)\frac{\rho^2}{\rho^2-\beta^2}-\frac{1}{D\tau\beta^2}\right]J_{\frac{1}{2}}^2(a\rho)\frac{d\rho}{\rho}. \tag{45}$$

Making use of the integral formula,[5]

$$\int_0^\infty J_{\frac{1}{2}}^2(a\rho)(\rho^2-\beta^2)^{-1}\rho d\rho=(i\pi/2)J_{\frac{1}{2}}(a\beta)H_{\frac{1}{2}}^{(1)}(a\beta), \tag{46}$$

we obtain

$$J=i/3\omega+\{\pi/[\omega(2-i\omega\tau)]\}J_{\frac{1}{2}}(a\beta)H_{\frac{1}{2}}^{(1)}(a\beta), \tag{47}$$

where β is the root of (44) with positive imaginary part. Substituting (47) in (42), we get

$$S_1(\omega)=\frac{16\pi^2 n}{15a^3\omega}\,\mathrm{Re}\left\{\frac{J_{\frac{1}{2}}(a\beta)H_{\frac{1}{2}}^{(1)}(a\beta)}{2-i\omega\tau}\right\}. \tag{48}$$

If we put

$$a\beta=u+iv, \tag{49}$$

where u and v are real, we obtain from Eq. (44):

$$\binom{u}{v}=\frac{(\omega a^2/2D)^{\frac{1}{2}}}{(4+\omega^2\tau^2)^{\frac{1}{4}}}\left\{1\mp\frac{\omega\tau}{(4+\omega^2\tau^2)^{\frac{1}{2}}}\right\}^{\frac{1}{2}}. \tag{50}$$

If we define parameters x, q, and α by

$$\alpha=\langle r^2\rangle/12a^2,\quad x=(\omega a^2/D)^{\frac{1}{2}}, \tag{51}$$

$$q=\frac{\omega\tau/2}{[1+(\omega\tau/2)^2]^{\frac{1}{2}}}=\frac{\alpha x^2}{(1+\alpha^2x^4)^{\frac{1}{2}}}, \tag{52}$$

we can write Eq. (50) as

$$\binom{u}{v}=\frac{1}{2}\left[\frac{q(1\mp q)}{\alpha}\right]^{\frac{1}{2}}. \tag{53}$$

If now we substitute (49) in (48), and use the expressions of the half-integral Bessel and Hankel functions in terms of elementary functions,

$$J_{\frac{1}{2}}(z)H_{\frac{1}{2}}^{(1)}(z)=(1/\pi z)[1+1/z^2+(1+i/z)^2e^{2iz}]$$

we get

$$S_1(\omega)=(8\pi n/15a^3\omega)f(\alpha, x), \tag{54}$$

where

$$f(\alpha, x)=(2/x^2)\{v[1-1/(u^2+v^2)]+[v(1+1/(u^2+v^2))+2]e^{-2v}\cos 2u+u[1-1/(u^2+v^2)]e^{-2v}\sin 2u\}. \tag{55}$$

The function $f(\alpha, x)$ is tabulated in Table I as a function of x for $\alpha=\frac{1}{12}$, ($\langle r^2\rangle=a^2$) and $\alpha=\frac{1}{2}$, ($\langle r^2\rangle=6a^2$).

From (58), (29), and (2) we get for T_1:

$$T_1^{-1}=\tfrac{4}{5}\pi\gamma^4\hbar^2I(I+1)(n/a^3\omega)\varphi(\alpha, x), \tag{56}$$

where $\varphi(\alpha, x)=f(\alpha, x)+f(\alpha, \sqrt{2}x)$.

The function $\varphi(\alpha, x)$ is tabulated as a function of x for $\alpha=\frac{1}{2}, \frac{1}{12}$ in Table I. In this table are also given the maximum values of $\varphi(\alpha, x)$ from which the minimum values of T_1 may be obtained.

The asymptotic forms of $\varphi(\alpha, x)$ for large and small x are of interest. First, if $\alpha x^2=\omega\tau/2\gg 1$ (limiting case of low temperature or high frequency), u and v reduce approximately to $u=0$, $v=1/(2\alpha)^{\frac{1}{2}}$, and

$$f(\alpha, x)=(4/3\omega\tau)F(v), \tag{57}$$

where

$$F(v)=(3/2v^3)[v^2-1+(v+1)^2e^{-2v}]. \tag{58}$$

For the relaxation time, we obtain in this case:

$$(\omega\tau\gg 1):\quad T_1^{-1}=(8\pi/5)\gamma^4\hbar^2I(I+1)(n/a^3\omega^2\tau)\times F[(6a^2/\langle r^2\rangle)^{\frac{1}{2}}]. \tag{59}$$

[5] G. N. Watson, *Treatise on the Theory of Bessel Functions* (Cambridge University Press, Cambridge, 1944), second edition, p. 428, Eq. (4).

$F(v)$ as given by (58) descends monotonously from unity at $v=0$. For small v,

$$F(v)\simeq 1-\tfrac{2}{3}v^2+\tfrac{1}{3}v^3-(6/35)v^4+\cdots. \quad (60)$$

In order to obtain the limiting case for $\omega\tau\ll 1$, one may expand the Bessel and Hankel functions in (48) in powers of $a\beta$ and then proceed to the limit $\omega\tau\to 0$. In this way it is found that

$$(\omega\tau\ll 1): \quad T_1^{-1}=(4\pi/5)\gamma^4\hbar^2 I(I+1) \times(n\tau/a^3)(1+12a^2/5\langle r^2\rangle). \quad (61)$$

If in Eq. (50) one neglects $\omega\tau$ in comparison with unity, one obtains $u=v=x/2$ and, substituting these values in (55), one gets

$$f(\alpha, x)\simeq\frac{1}{x}-\frac{2}{x^3}+\frac{e^{-x}}{x}\left[\left(1-\frac{2}{x^2}\right)\sin x + \left[1+\frac{4}{x}+\frac{2}{x^2}\right]\cos x\right], \quad (62)$$

which no longer depends explicitly on α. If (62) is substituted in (56) one obtains precisely the same result that follows on taking for $P(\mathbf{r}, t)$ the expression (18). A detailed analysis shows that (62) is valid only if in addition to $\omega\tau\ll 1$ one assumes $\langle r^2\rangle\ll 6a^2$. Thus (62) and inferentially (18) have only a very limited range of validity. Equation (62) has a maximum giving a minimum T_1, but of course does not behave correctly at the low temperature limit.

(*e*) As a final example we mention the case in which a nucleus walks randomly in direction, but makes jumps of equal magnitude l in distance. In this case we may take for $P_1(\mathbf{r})$:

$$P_1(\mathbf{r})=\delta(r-l)/4\pi l^2. \quad (63)$$

The corresponding $A(\boldsymbol{\varrho})$ is given by

$$A(\boldsymbol{\varrho})=(\sin l\rho)/l\rho, \quad (64)$$

and by Eq. (28)

$$S_1(\omega)=(8\pi n\tau/15k^3l^3)G(k, \tfrac{1}{2}\omega\tau), \quad (65)$$

where $k=a/l$ and

$$G(k, y)=\int_0^\infty J_{\frac{5}{2}}^2(kx)\frac{1-\sin x/x}{(1-\sin x/x)^2+y^2}\cdot\frac{dx}{x}. \quad (66)$$

We shall defer a detailed study of this case to the following section, in which it will be shown it has particular relevance in the case of lattice diffusion.

IV. LATTICE DIFFUSION

We now attempt to apply Eq. (7) with $P(\mathbf{r}, \mathbf{r}_0, t)$ given by (15) to the case of random walk in a space lattice. We consider specifically the case in which a spin-bearing nucleus jumps between nearest-neighbor lattice sites. For $f(\mathbf{r}_0)$ we may take

$$f(\mathbf{r}_0)=c\sum_k\delta(\mathbf{r}_0-\mathbf{r}_k), \quad (67)$$

where c is the ratio of the number of nuclei to the number of lattice sites. The sum is over all lattice sites. Also,

$$P_1(\mathbf{r})=(1/z)\sum_{i=1}^{z}\delta(\mathbf{r}-\mathbf{r}_i), \quad (68)$$

where the sum is over the z nearest neighbors of a lattice site. From (9) we find

$$A(\boldsymbol{\varrho})=(1/z)\sum_{i=1}^{z}\exp(i\boldsymbol{\varrho}\cdot\mathbf{r}_i). \quad (69)$$

It is not possible to carry out explicitly all the integrations to find $k(t)$ or $S(\omega)$ in the general case. We can, however, find $k(0)$ which normalizes the spectral density function according to the transform of (6):

$$k(t)=(1/2\pi)\int_{-\infty}^{+\infty}e^{-i\omega t}S(\omega)d\omega, \quad (70)$$

so that

$$k(0)=(1/2\pi)\int_{-\infty}^{+\infty}S(\omega)d\omega. \quad (71)$$

Putting $t=0$ in (15) and substituting in (7), we get

$$\begin{aligned}k(0)&=(c/8\pi^3)\int\int\int F(\mathbf{r}_0)F^*(\mathbf{r})\sum_k\delta(\mathbf{r}_0-\mathbf{r}_k) \times\exp[-i\boldsymbol{\varrho}\cdot(\mathbf{r}-\mathbf{r}_0)]d\mathbf{r}d\mathbf{r}_0d\boldsymbol{\varrho},\\ &=(c/8\pi^3)\sum_k\int\int F(\mathbf{r}_k)F^*(\mathbf{r}) \times\exp[-i\boldsymbol{\varrho}\cdot(\mathbf{r}-\mathbf{r}_k)]d\mathbf{r}d\boldsymbol{\varrho},\\ &=c\sum_k|F(\mathbf{r}_k)|^2. \end{aligned} \quad (72)$$

Making use of (4a) and (4b) we find, after averaging over all crystal orientations,

$$k_1(0)=(2c/15)\sum_k r_k^{-6}; \quad k_2(0)=4k_1(0). \quad (73)$$

There is one extreme case in which an explicit result for $S(\omega)$ may be obtained, namely the case $\omega\tau\gg 1$, i.e., the low-temperature asymptote.

For $S(\omega)$ we have, in general,

$$S(\omega)=c\tau\sum_k\frac{1}{8\pi^3}\int\int F(\mathbf{r}_k)F^*(\mathbf{r})\exp[+i\boldsymbol{\varrho}\cdot(\mathbf{r}_k-\mathbf{r})] \times\frac{1-A(\boldsymbol{\varrho})}{[1-A(\boldsymbol{\varrho})]^2+(\omega\tau/2)^2}\cdot d\mathbf{r}d\boldsymbol{\varrho}. \quad (74)$$

If $[1-A(\boldsymbol{\varrho})]^2$ in the denominator is negligible com-

pared with $(\omega\tau/2)^2$, we get

$$S(\omega)=\frac{4c}{\omega^2\tau}\sum_k\frac{1}{8\pi^3}\int\int F(\mathbf{r}_k)F^*(\mathbf{r})\exp[+i\boldsymbol{\varrho}\cdot(\mathbf{r}_k-\mathbf{r})]\times\left[1-\frac{1}{z}\sum_{i=1}^{z}\exp i\boldsymbol{\varrho}\cdot\mathbf{r}_i\right]d\mathbf{r}d\boldsymbol{\varrho}$$

$$=\frac{4c}{\omega^2\tau}\sum_k\left[|F(\mathbf{r}_k)|^2-\frac{1}{z}F(\mathbf{r}_k)\sum_{i=1}^{z}F^*(\mathbf{r}_k+\mathbf{r}_i)\right]. \quad (75)$$

As an example we compute $S_1(\omega)$. Substituting from Eq. (4a) we get

$$S_1(\omega)=\frac{4c}{\omega^2\tau}\sum_k\left\{\frac{\sin^2\theta_k\cos^2\theta_k}{r_k^6}-\frac{1}{z}\sum_j\frac{\sin\theta_k\cdot\cos\theta_k}{r_k^3}\cdot\frac{\sin\theta_j\cos\theta_j}{r_j^3}e^{i(\varphi_k-\varphi_j)}\right\}. \quad (76)$$

In this expression $\mathbf{r}_j=\mathbf{r}_k+\mathbf{r}_i$; θ_j, φ_j are the polar and azimuthal angles of $\mathbf{r}_j$, and the sum over j is over all nearest neighbors of the lattice site at $\mathbf{r}_k$. In this sum all terms for which $\mathbf{r}_j=0$ have to be excluded of course. This expression must now be averaged over all lattice orientations. We average each term in the sum over k, independently. For each term we transform to Eulerian angular coordinates θ, β, ψ where $\theta=\theta_k$, $\beta=\varphi_k+\pi/2$ and ψ is the azimuthal angle of $\mathbf{r}_j$ about $\mathbf{r}_k$. Averaging over the angle ψ we find

$$\langle\sin\theta_j\cos\theta_j e^{-i\varphi_j}\rangle_{Av}=\left[1-\tfrac{3}{2}(l^2/r_j^2)\sin^2\alpha_j\right]\sin\theta_k\cos\theta_k e^{-i\varphi_k}, \quad (77)$$

where α_j is the angle between $\mathbf{r}_j$ and $\mathbf{r}_k$.

Thus we obtain, after the average over ψ,

$$S_1(\omega)=\frac{4c}{\omega^2\tau}\sum_k\frac{\sin^2\theta_k\cos^2\theta_k}{r_k^6}\left\{1-\frac{1}{z}\sum_j\left(\frac{r_k}{r_j}\right)^3\times\left(1-\frac{3l^2}{2r_j^2}\sin^2\alpha_j\right)\right\}. \quad (78)$$

Finally averaging over θ_k, since $\langle\sin^2\theta_k\cos^2\theta_k\rangle_{Av}=2/15$, we get

$$S_1(\omega)=\frac{8c}{15\omega^2\tau}\sum_k\frac{1}{r_k^6}\left\{1-\frac{1}{z}\sum_j\left(\frac{r_k}{r_j}\right)^3\times\left(1-\frac{3l^2}{2r_j^2}\sin^2\alpha_j\right)\right\}. \quad (79)$$

This sum which converges fairly rapidly can be applied to find $S_1(\omega)$ for various lattice structures. For a face-centered cubic lattice we obtain

$$S_1(\omega)=98.245b^{-6}(8c/15\omega^2\tau), \quad (80)$$

where b is the edge of a unit cell. A similar calculation gives $S_2(\omega)=4S_1(\omega)$.

Since it is not possible to integrate (74) in the general case, we have sought to obtain an approximate formula which will give $S(\omega)$ with sufficient accuracy over the whole range of $\omega\tau$.

To this end we turn to the case, considered in Sec. III(e), of isotropic diffusion for which the single jump distance has always the value l. There are good reasons for believing that Eq. (65) properly normalized will meet these requirements. For the case of random walk in a lattice the jumps are to nearest neighbors which in many cases (e.g., f. c.c. lattice) are symmetrically disposed on a sphere. The use of Sec. III(e) approximates this situation by allowing a jump to any point on the sphere. Furthermore, the fact that in the lattice case we eventually would average the result over all lattice orientations, lends support to the isotropic approximation in which this averaging may be considered to have already been performed in a different, if less precise, way.

Normalization of (65) involves a proper choice of the parameter k, which amounts to a proper choice of the lower limits of integration for r and r_0 in Eq. (22). Fortunately, the proper normalization to apply to the lattice case can be obtained from Eqs. (71) and (73). From Eqs. (65) and (66) we obtain

$$(2\pi)^{-1}\int_{-\infty}^{+\infty}S_1(\omega)d\omega=8\pi n/45k^3l^3. \quad (81)$$

Substituting for n, $n=cn_0b^{-3}$, where n_0 is the number of lattice sites in a unit cell, and by Eq. (71) equating the right member of (81) to $k_1(0)$ as given by (73a), we obtain

$$k^3=(4/3)\pi n_0b^{-3}l^{-3}/\textstyle\sum_k r_k^{-6}. \quad (82)$$

For a face-centered cubic lattice $\sum_k r_k^{-6}=115.375b^{-6}$, $n_0=4$, and $b=\sqrt{2}l$, and inserting these values in (82) we find

$$k=0.74335. \quad (83)$$

The assumption that Eq. (65) gives a good approximation to the lattice diffusion problem may be tested by comparing its low temperature ($\omega\tau\gg1$) asymptote with the exact result of Eq. (80) for a f. c.c. lattice. For large y we may neglect the term in $1-\sin x/x$ in the denominator of the integrand of Eq. (66), and find

$$G(k,y)=(4/\omega^2\tau^2)\int_0^\infty J_{\frac{1}{2}}^2(kx)(1-\sin x/x)dx/x.$$

This integration can be performed exactly, with the result

$$G(k,y)=(1/\omega^2\tau^2)(1-1/12k^2)\quad(k>\tfrac{1}{2}). \quad (84)$$

Substituting (84) in (65), using k as given by (83), and putting $n=4c b^{-3}$, $l=b/\sqrt{2}$, we obtain from (65)

$$S_1(\omega)=98.85b^{-6}(8c/15\omega^2\tau), \tag{85}$$

which agrees with (80) to 0.6 percent. We may therefore have some confidence in the use of (65) as an adequate approximation to the lattice diffusion problem. The function $G(k, y)$ as given by Eq. (66) has been calculated by numerical methods with k as given by (83) and is tabulated as a function of y in Table II.

Substituting (65) and $S_2(\omega)=4S_1(\omega)$ in Eq. (2), we get (with $y=\frac{1}{2}\omega\tau$)

$$T_1^{-1}=(8\pi/5)\gamma^4\hbar^2I(I+1)(n/k^3l^3\omega)\psi(k, y), \tag{86}$$

where

$$\psi(k, y)=yG(k, y)+2yG(k, 2y). \tag{87}$$

In Table II we have also tabulated $\psi(k, y)$ as a function of y for k given by (83).

Finally we state the limiting form of (86) for $\omega\tau\ll 1$ (high temperature asymptote). For small y, $\psi(k, y)\simeq 3yG(k, 0)$. By numerical integration $G(k, 0)=0.6151$ (f. c.c. lattice) so that Eq. (86) reduces to

$$(\omega\tau\ll 1):\quad T_1^{-1}=11.292\gamma^4\hbar^2I(I+1)n\tau/l^3. \tag{88}$$

V. APPLICATION

In applying the results obtained above to nuclear spin relaxation times as determined from nuclear resonance data, one must be sure that the relaxation is entirely the result of the diffusion process. It is rarely possible to be perfectly sure of this, but one can be more confident about it in the neighborhood of the minimum in $T_1(T_{1m})$ than well up on the asymptotes of the T_1-temperature curve. One needs therefore a way of analyzing data in terms of the above theory in the neighborhood of the minimum T_1. It is convenient for this purpose to express the above results in terms of universal curves. One way of doing this is to express T_{1m}/T_1 as a function of τ/τ_m, where τ_m is the value of τ at $T_1=T_{1m}$. From experimental values of T_{1m}/T_1 one can then obtain from these curves the corresponding values of τ/τ_m. Plots of $\log(\tau/\tau_m)$ thus obtained against the reciprocal of the absolute temperature should result in straight lines whose slopes give the activation energy, provided a relationship of the type of Eq. (30) holds.

TABLE II. Tables of the functions $G(k, y)$ [Eq. (66)] and $\psi(k, y)$ [Eq. (87)] ($k=0.74335$).

y	$G(k, y)$	$\psi(k, y)$
0	0.61505	0
0.025	0.53804	0.03887
0.05	0.50844	0.07181
0.10	0.46388	0.12632
0.15	0.42913	0.16936
0.20	0.39965	0.20325
0.25	0.37357	0.22959
0.30	0.34997	0.24966
0.35	0.32832	0.26458
0.40	0.30831	0.27535
0.45	0.28971	0.28262
0.50	0.27239	0.28732
0.55	0.25621	0.28981
0.60	0.24111	0.29060
0.6024		0.29060(max)
0.65	0.22700	0.29003
0.70	0.21381	0.28840
0.80	0.19004	0.28287
0.90	0.16916	0.27528
1.00	0.15113	0.26662
1.20	0.12161	0.24802
1.40	0.09909	0.22958
1.60	0.08178	0.21242
1.80	0.06835	0.19687
2.00	0.05775	0.18282
2.25	0.04749	0.16742
2.5	0.03963	0.15406
3.0	0.02867	0.13236
3.5	0.02161	0.11570
4.0	0.01683	0.10249
5.0	0.01100	0.08327
6.0	0.00772	0.06999
7.0	0.00571	0.06030
10.0	0.00283	0.04253
20.0	0.000712	0.02138
30.0	0.000317	0.01427
40.0	0.000178	0.01070

Graphs of T_{1m}/T_1 *versus* τ/τ_m can easily be constructed with the aid of the above tables.

VI. CONCLUSION

It is hoped that the results derived here will be of some aid in analyzing data on nuclear spin relaxation when the dominant mechanism is of the translational diffusion type. We have not attempted to treat certain special diffusive processes such as ring-type diffusion involving the correlated motion of several nuclei. For rotational diffusion, the Bloembergen treatment is satisfactory.

The author wishes to acknowledge the help of Mr. J. Olds, Mr. S. Hussieni, and Mr. E. Apgar in computational work.

Compton Scattering of 2.62-Mev Gamma Rays by Polarized Electrons*,†

S. B. GUNST‡ AND L. A. PAGE
University of Pittsburgh, Pittsburgh, Pennsylvania
(Received July 20, 1953)

The differential cross section for Compton scattering of a circularly polarized photon by an electron with given initial spin orientation can be written as a sum of the common Klein-Nishina formula for no polarization and a term sensitive to polarization. The total cross section is $\sigma=\sigma_0\pm\sigma_1$. A measurement of the transmission of 2.62-Mev gamma rays through iron magnetized along the transmission direction relative to that through unmagnetized iron gives the absolute value of σ_1 for this energy, if the number ν_a of polarized electrons per iron atom at saturation is known. For $\nu_a=2.06$, $\sigma_1/\pi r_0^2=0.089\pm0.007$. This agrees with the theoretical value 0.093. Alternatively, the theoretical σ_1 and the measurements would yield $\nu_a=1.97\pm0.15$.

The application of the method of this experiment to measurement of gyromagnetic ratios for ferromagnets is suggested, as is its application to the analysis of circularly polarized radiation.

I. INTRODUCTION

THE analysis of circularly polarized photons by Compton scattering from polarized electrons has been mentioned a number of times.[1] The differential cross section for the process (see Appendix A) may be written as the sum of two terms. One term is the common Klein-Nishina formula for unpolarized incident quanta and unpolarized electrons and the other term takes account of polarization. The total cross section is $\sigma=\sigma_0\pm\sigma_1$, where σ_0 is independent of polarization and σ_1 depends on polarization.

The term σ_1 is measured in this experiment by the Compton scattering of gamma rays by polarized electrons. An apparatus that measures σ_1 must act, so to speak, like a "quarter-wave plate for gamma rays."[2]

II. EXPERIMENTAL METHOD

Let gamma rays from a radioactive source pass through a ferromagnet magnetized along the axis defined by the incident gamma rays in one case and unmagnetized in the other. It can be shown (see Appendix B) that the ratio of the difference between the transmissions through the magnetized and unmagnetized ferromagnet to the transmission through the unmagnetized ferromagnet is given by

$$[T(\nu)-T(0)]/T(0)=\tfrac{1}{2}(NL\nu\sigma_1)^2. \qquad (1)$$

Here N is the number of atoms per unit volume, L is the axial length of the ferromagnet, ν is the number of axially polarized electrons per atom, and σ_1 is the part of the total Compton cross section dependent on polarization. The experimental determination of the ratio expressed by (1) leads to the evaluation of σ_1 and a test of the theory. The 2.62-Mev gamma ray of ThC″ (see Fig. 3) is used in this experiment.

III. DESCRIPTION OF APPARATUS

A. Magnet Design

An electromagnet 12 inches long (approximately 8 mean free paths at 2.62 Mev) was designed. Tapered ends of the Armco-iron core (1½-in. diameter) fit snugly in mild-steel end plates which are secured to a length of cold-rolled seamless steel tubing (5-in. o.d. by 4-in. i.d.) by screws at each end. The end plates and tubing, which complete the magnetic circuit, have a reluctance only a few percent of that of the core.

A water-cooled, copper coil form was fabricated to fill the annulus. Primary and secondary windings of copper wire fill the coil form. Current through the series-connected primary windings magnetizes the core; or, by switching connections to "anti-series" (alternate windings bucking), the same coil current induces negligible magnetization in the core. The secondary was wound so as to permit a survey of the state of magnetization of the core in ten steps along the axis.

B. Arrangement of Equipment

Equipment is arranged as shown in Fig. 1. The thorium source is contained in a lead housing, opened adjacent to the core of the magnet. The magnet is enclosed in a loosely fitting magnetic shield. A lead shield with a 1-inch collimation hole at the exit end of the core surrounds a 1½-inch diameter by 1-inch thick NaI(Tl) crystal. Mineral oil couples the crystal to a light pipe of lucite 46-in. long; the other end of the lucite is similarly coupled to a type 5819 photomultiplier tube. Cylindrical magnetic shields of mumetal and steel surround the photomultiplier tube. Signals from the

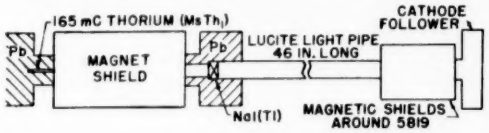

FIG. 1. Arrangement of equipment for final experiments. The cathode follower feeds a linear amplifier and then two discriminator scalers.

* Work done in the Sarah Mellon Scaife Radiation Laboratory and assisted by the U. S. Office of Ordnance Research.
† Based on Ph.D. thesis by SBG.
‡ Now at Westinghouse Atomic Power Division, Pittsburgh, Pa.
[1] Biedenharn, Rose, and Arfken, Phys. Rev. **83**, 683 (1951); O. Halpern, Phys. Rev. **82**, 753 (1951); F. P. Clay and F. L. Hereford, Phys. Rev. **85**, 675 (1952).
[2] S. P. Lloyd, Phys. Rev. **88**, 906 (1952).

photomultiplier tube go through a cathode follower and linear amplifier before being fed to two discriminator scalers.

IV. PRELIMINARY EXPERIMENTS

Extensive preliminary experiments were made in order to obviate certain possible difficulties in the interpretation of final results. These experiments were concerned with the stability of electronic equipment, the linearity of the pulse-height energy response for the NaI(Tl) crystal and its associated electronic equipment, the spectrum of the thorium source used and the portion of the spectrum admitted to the discriminator scalers for any discriminator settings, the distribution of magnetization in the iron core, the coil current required to saturate the core, and the demonstration that the magnet does not perturb the operation of the detector prohibitively. In addition, it was established that the "saturation current" induces negligible magnetization in the core when the primary windings are connected in anti-series.

The investigation of the spectrum of the thorium source employed the Hofstadter and McIntyre method[3] for Compton scattering of collimated gamma rays from a trans-stilbene crystal into a second *trans*-stilbene crystal at approximately 90°. Results show that the thorium source emits gamma rays of the same energies and in approximately the same intensities as found by other investigators[4] for typical thorium sources.

V. FINAL EXPERIMENTS

A. Fraction of Counts Caused by Transmission through Magnet Core

For equipment and source arranged as in Fig. 1, not all the counts obtained in the scalers are caused by gamma rays which pass through the core of the magnet. Some of the counts arise from scattering around the core as well as cosmic-ray and other background activities. To minimize cosmic-ray effects, one of the discriminators was operated at a setting just above the 2.62-Mev photoline. Counts observed on this discriminator scaler were subtracted from those on the other discriminator scaler to give "net counts."

To determine what fraction of the net counts is caused by gamma rays passing through the magnet core, a substitute core was used. This core has the same over-all dimensions as the iron core but consists of a two inch length of iron joined to a ten inch length of lead. Substitution of this composite core for the iron core, with the iron portion adjacent to the source, permits determination of the fraction f of the net counts caused by gamma rays passing through the iron core, as a function of discriminator setting. This fraction is thus a function of net counting rate.

[3] R. Hofstadter and J. A. McIntyre, Phys. Rev. **78**, 619 (1950).
[4] I. E. Dayton (private communication); G. D. Latyshev, Revs. Modern Phys. **19**, 132 (1947).

Expressed in terms of net counting rate, Eq. (1) can now be written

$$(1/f)(\Delta C/C)=\tfrac{1}{2}(NL\nu\sigma_1)^2. \quad (2)$$

Here C is the net counting rate for the core unmagnetized, and ΔC is the difference in net counting rates for the magnetized and unmagnetized core.

B. Experimental Procedure

Since the primary windings can be connected in series or anti-series and can carry current in either of two directions, there are four possible ways in which the "saturation current" may flow through the primary windings. These are designated anti-series left AL, series left SL, anti-series right AR, and series right SR. Net counts/500 sec were obtained for magnet coils switched to AL, SL, AR, and SR in succession. Before the AL and AR "runs" the magnet was carefully degaussed so that AL and AR give an unmagnetized core, SL and SR a magnetized core.

The same current flowed in the magnet primary windings during counting runs for both the magnetized and unmagnetized conditions. This was done in order to minimize thermal expansion effects which might arise if the magnet-core temperature differed between the magnetized and unmagnetized runs. Instruments showed the magnet-core temperature changed negligibly.

The AL, SL, AR, and SR runs were repeated in that order many times and the net counts per 10 runs for each comprises a "sequence."

C. Experimental Result

Two experiments were done as follows.

Twenty-eight sequences (280 runs for each magnet condition) were made with the discriminator set to give a net counting rate of approximately 7 counts/sec; and twenty-two sequences were made with the discriminator set to give a net counting rate of approximately 10 counts/sec. The uncertainties in the total net counts for the AL and AR runs consistently overlapped, as did the uncertainties for the SL and SR runs. The net counts obtained for the core magnetized minus net counts for the core unmagnetized are tabulated in Table I for each sequence of the two experiments. The totals in the table give values of ΔC, and the values of $(1/f)(\Delta C/C)$ for the two experiments are 0.0047 ± 0.00135 and 0.0069 ± 0.00121. (The value of f is in the neighborhood of 0.8 for these runs.) Each uncertainty is based on the observed rms deviation per run and exceeds the standard deviation associated with counting by less than 10 percent. For the two experiments the mean of $(1/f)(\Delta C/C)$ is 0.0059 ± 0.00090.

This gives σ_1 from (2) if N, L, and ν are known. The number N of atoms/unit volume is obtained from atomic constants and the measured density of the iron core. The effective length L of the core is determined

TABLE I. Net counts with iron magnetized minus net counts with iron unmagnetized for each sequence (20-ksec running time). The net counting rates during the experiments were approximately those shown in the column headings. Totals give values of ΔC.

7 counts/sec		10 counts/sec	
283	53	555	−413
228	324	−134	278
396	−151	443	−23
638	−126	428	734
229	52	1078	1333
134	411	415	1213
267	1227	44	1002
457	222	113	−78
26	83	591	622
204	612	695	1310
−386	567	517	1487
674	−211		
827	256		12 210
229	105		
	7630		

from the preliminary experiment (with uncertainty ~one percent).

The number ν of polarized electrons/atom is determined as follows. Fluxmeter measurements on the secondary windings of the magnet give 2.20 Bohr magnetons/atom at the "saturation current." If the figure for saturated iron is taken as 2.22 Bohr magnetons/atom,[5] ν is the product of 2.20/2.22 and the number ν_s of polarized electrons/atom at saturation. Argyres and Kittel[6] give 2.06 for ν_s.

The result for σ_1 is $(2.22\pm0.18)\times10^{-26}$ cm^2.

D. Comparison with Theory

The theoretical value of $\sigma_1/\pi r_0^2$ at 2.62 Mev is 0.093, while the experimental result is 0.089 ± 0.007.

The experimental σ_1 is actually the effective value for that portion of the thorium spectrum transmitted and counted. For 100 gamma rays at 2.62 Mev, we estimate three at ~2.2 and one at ~1.8 Mev are counted. From the theoretical behavior of σ_1 over these energies (see Fig. 3), the influence of the lower-energy components on the experimental σ_1 should be ~0.2 percent and is neglected.

VI. CONCLUSIONS

The total Compton cross section for scattering of a circularly polarized photon by a polarized electron has been investigated at 2.62 Mev and the polarization sensitive part σ_1 is found to agree with theory to 8 percent standard deviation.

The experiment demonstrates the use of a ferromagnetic absorber as a polarizer or analyzer for circularly-polarized radiation.

If the theoretical value for σ_1 is accepted, the method of this experiment could be applied to the determination of gyromagnetic ratios for ferromagnets. This would serve as an independent check of the results obtained by microwave resonance techniques.

In particular, this experiment would give the number ν_s of polarized electrons per iron atom at saturation as 1.97 ± 0.15. Increased precision might be obtained by using a very strong source of gamma rays. Energies higher than 2.6 Mev are preferable as curve σ_1/σ_0 in Fig. 3 indicates. The source need not be monochromatic; any spectrum from 2 to 7 Mev should be usable since σ_1 is fairly flat over these energies.

VII. ACKNOWLEDGMENT

The authors are indebted to Professor A. J. Allen whose encouragement and support made the investigation possible; to Professor P. Stehle for theoretical results, and for stimulating discussions throughout the experiment; to Professor Frederic Keffer for information concerning recent work in ferromagnetism; to Mr. Milton Heinberg, Mr. R. H. Bassel, and Mr. B. J. Mathewson for assisting with experimental operations; to Mr. Eugene Perkins for supervising the construction of equipment; and to the other members of the Laboratory who gave valuable aid. The loan of a thorium source from the Cornell University Laboratory of Nuclear Studies is gratefully acknowledged. Materials kindly furnished by the Gulf Research and Development Company expedited the investigation.

APPENDIX A: UNDERLYING THEORY

Let a circularly polarized photon $\mathbf{k}_0$, incident along the 3 axis, be Compton scattered into the 2,3 plane (outgoing photon $\mathbf{k}$ at an angle θ with the 3 axis) by a free electron at rest whose spin direction is given by polar angle ψ (with the 3 axis) and azimuthal angle ϕ (with the 1,3 plane). The cross section[7] is

$$\frac{d\sigma}{d\omega}=\frac{1}{2}r_0^2\frac{k^2}{k_0^2}\left\{\left[\frac{k_0}{k}+\frac{k}{k_0}-\sin^2\theta\right]\mp\left[\left(\frac{k_0}{k}-\frac{k}{k_0}\right)\cos\theta\cos\psi+\left(1-\frac{k}{k_0}\right)\sin\theta\sin\phi\sin\psi\right]\right\}, \quad (A.1)$$

where $r_0=e^2/mc^2$, and $d\omega=d\phi d(\cos\theta)$. The upper sign refers to an incident l.c.p. (left circularly polarized) photon.

For $\psi=0$, integration over ϕ gives

$$d\sigma/d\Omega=d\sigma_0/d\Omega\pm d\sigma_1/d\Omega, \quad (A.2)$$

where σ_0 is the common Klein-Nishina expression for unpolarized photons and electrons, σ_1 is the part of the

[5] L. F. Bates, *Modern Magnetism* (Cambridge University Press, Cambridge, 1951), third edition, p. 317; R. M. Bozorth, *Ferromagnetism* (D. Van Nostrand Company, Inc., New York, 1951), p. 867.

[6] P. Argyres and C. Kittel, Acta Metallurgica **1**, 241 (1953).

[7] The expression (A.1) was calculated by *P.* Stehle. The simple case, $\sin\psi=0$, follows from W. Heitler, *Quantum Theory of Radiation* (Oxford University Press, Cambridge, 1944), second edition, Eq. (18) f.f., p. 149. It has been pointed out to us by Professor O. Halpern that the above cross section is contained in a paper by W. Franz, Ann. Physik **33**, 698 (1938).

Compton cross section sensitive to circular polarization and spin, and the upper sign refers to an l.c.p. photon as before. The ratio $(d\sigma_1/d\Omega)/(d\sigma_0/d\Omega)$ is sketched in Fig. 2 for several values of k_0/mc^2.

Integration over the sphere yields the total Compton cross section,

$$\sigma=\sigma_0\pm\sigma_1. \tag{A.3}$$

Here,

$$\frac{\sigma_1}{2\pi r_0^2}=\frac{1+4\gamma+5\gamma^2}{\gamma(1+2\gamma)^2}-\frac{1+\gamma}{2\gamma^2}\ln(1+2\gamma),$$

where $\gamma=k_0/mc^2$. Figure 3 shows σ_1 and σ_1/σ_0. For k_0 greater than $1.25mc^2$, the *forward* "lobe" in $d\sigma_1/d\Omega$ predominates in the total cross section.

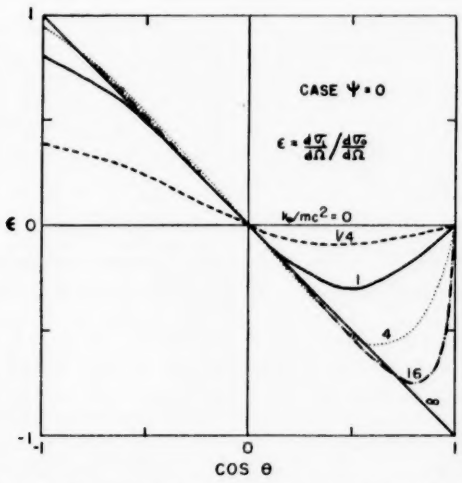

FIG. 2. The fractional change in the differential Compton cross section which obtains because electrons are polarized along the axis of the incident circularly polarized photon plotted as a function of the angle through which the photon is scattered.

APPENDIX B: TRANSMISSION THROUGH A FERROMAGNET

Let a ferromagnetic absorber of N atoms per unit volume and uniform magnetization along the 3 axis have ν polarized electrons per average atom. Circularly polarized photons of a certain sense, propagating along the 3 axis, can undergo Compton scattering with the

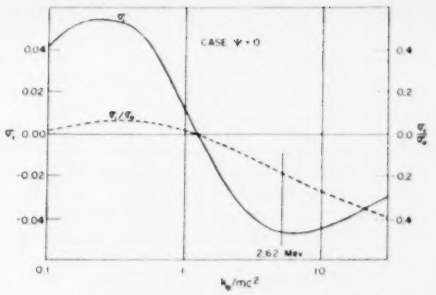

FIG. 3. The polarization-sensitive part σ_1 of the total Compton cross section is in units of $2\pi r_0^2$. The part independent of polarization is σ_0.

$\frac{1}{2}(Z+\nu)Ndx_3$ electrons according to one sign in (A.3) and with the $\frac{1}{2}(Z-\nu)Ndx_3$ electrons according to the opposite sign.

The probability that a photon having no circular polarization will survive (in good geometry) a length L of the ferromagnet is

$$\begin{aligned}T(\nu)&=\tfrac{1}{2}\exp\{-NL[(\sigma_0+\sigma_1)\tfrac{1}{2}(Z+\nu)\\&\quad+(\sigma_0-\sigma_1)\tfrac{1}{2}(Z-\nu)+\sigma_2]\}\\&\quad+\tfrac{1}{2}\exp\{-NL[(\sigma_0-\sigma_1)\tfrac{1}{2}(Z+\nu)\\&\quad+(\sigma_0+\sigma_1)\tfrac{1}{2}(Z-\nu)+\sigma_2]\}\\&=\cosh(NL\nu\sigma_1)\exp[-NL(Z\sigma_0+\sigma_2)],\end{aligned} \tag{B.1}$$

where σ_0 and σ_1 are the terms defined in (A.3) and σ_2 represents all processes in addition to Compton scattering. Spin-polarization effects in σ_2 are taken to be nil; for example, photoeffect involving the polarized electrons has a very small cross section compared to σ_1 at energies of interest in this experiment.

The ratio of magnetized transmission to unmagnetized transmission is

$$T(\nu)/T(0)=\cosh(NL\nu\sigma_1). \tag{B.2}$$

Ideally, $(NL\nu\sigma_1)$ may be measured in the shortest time if $NL(Z\sigma_0+\sigma_2)=4$.

The transmission ratio R of l.c.p. relative to r.c.p. photons is, by (B.1),

$$R=\exp(2NL\nu\sigma_1), \tag{B.3}$$

where the magnetization is in the direction of transmission.

Positive Pi-Meson Interactions in Beryllium*

F. H. TENNEY† AND J. TINLOT
University of Rochester, Rochester, New York
(Received August 14, 1953)

A 10-in. diameter magnet cloud chamber containing a $\frac{1}{4}$-in. Be plate has been operated in both the 40-Mev and 50-Mev π^+-meson beams of the Rochester 130-in. cyclotron. Meson interactions in Be were obtained for three bands of energy: 15 to 30 Mev, 25 to 40 Mev, and 35 to 50 Mev. The events recorded as nuclear interactions were: stars, stops, and scatterings of greater than 30 degrees. From a survey of some 22 700 g/cm² of Be traversed, a total of 159 such events were found. Analysis of the data from each energy band indicates the absorption cross section to be energy dependent. The ratio of corrected stars to corrected scatterings was found to be roughly 2:1.

INTRODUCTION

A CLOUD-CHAMBER study of π^+-meson interactions in the element beryllium has been made. A 10-in. diameter diaphragm type cloud chamber, with an illuminated depth of about 2 in. and containing a beryllium plate 1.24 g/cm² thick, was exposed to the 40-Mev and 50-Mev π^+-meson beams of the University of Rochester's 130-in. cyclotron in a series of three runs. Each run sampled a different range of incident meson energies: 15 to 30 Mev for run *A*, 25 to 40 Mev for run *B*, and 35 to 50 Mev for run *C*. The incident meson energy distributions are shown in Fig. 1. The low mean energy of run *A* was obtained by degrading the energy of the 40-Mev meson beam with a $\frac{3}{4}$-in. thick piece of polyethylene placed in front of the chamber. The chamber was operated in a pulsed magnetic field of from 12 to 15 kilogauss for runs *B* and *C* and in a steady field of about 8 kilogauss for run *A*. The pulsed field was provided by two air core coils. The steady field was provided by these coils in conjunction with an iron yoke. It is estimated that the magnetic field was known to within 5 percent. To reduce background radiation to a tolerable level, the cyclotron beam was pulsed in conjunction with the fast expansion of the chamber. The chamber was expanded and stereoptically photographed at regular intervals of time.

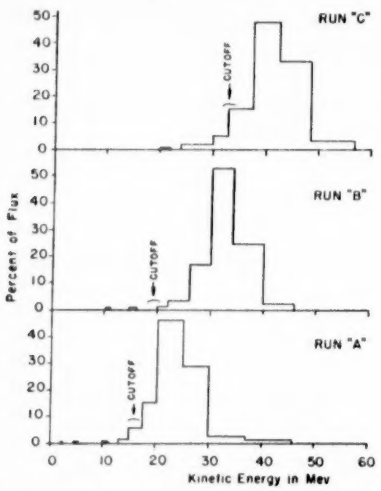

FIG. 1. Incident meson kinetic energy distribution.

EXPERIMENTAL PROCEDURE

About 2000 useful photographs were obtained during run *A*, and approximately 1000 useful photographs were taken in each of runs *B* and *C*. These photographs were reprojected and scanned for the flux of mesons and for meson stars, stops, and scatterings of greater than 20 degrees projected angle. Pi-mu decays were generally noted and used to check geometrical measurements and momentum estimates. These checks were always satisfactory. In run *B* a systematic survey was made for π-μ decays for purposes of estimating flux contamination.

Mesons and electrons were readily distinguished from protons on the basis of curvature and relative ionization. These criteria did not serve to distinguish π^+ mesons from μ^+ mesons or high-energy positrons. The flux contamination of μ^+ and e^+ was taken to be 10 percent. This estimate was based on considerations of: (a) the number of pi-mu decays observed in run *B*, (b) the energy loss of flux particles in passing through the beryllium plate for the low-energy run *A*, (c) a rough calculation of the expected number of μ^+ mesons from pi-mu decays in the incident beam outside the chamber, and (d) scintillation counter data.[1]

Radii of curvature and projected angles were measured by means of arcs of different radii scribed on transparent sheets of cellulose acetate. The energy resolution obtained by this method is indicated by the width of the histogram blocks in Fig. 1. True angles were computed from knowledge of projected angles and the dip of the tracks involved. An angular error of $\pm 2.5°$ is placed on all true angles, except in cases of steeply dipping tracks the angular error is estimated to be as high as $\pm 10°$.

* This work was performed under the auspices of the U. S. Atomic Energy Commission.
† At present at Princeton University, Princeton, New Jersey.

[1] C. Angell and J. Perry (private communication).

TABLE I. Summary of data. The energy interval is defined for the $1/e$ points of energy distribution at the center of the Be plate. Uncorrected data are in parentheses.

Energy range Mev	g/cm² traversed	Total No. of events	Stops	Stars $1p$	Stars $2p$	Stars $3p$	Scatts $\theta \geq 30°$	Total stars	Total scatts	σ_{abs} mb	σ_{scatt} mb
26.5–16											
Run *A*	12 170	75 (111)	18 (48)	22	12 (39)	0	23 (24)	46	29	56±9	35±7
35.5–26											
Run *B*	6399	45 (54)	9 (15)	16	9 (29)	2	9 (10)	32	13	74±13	30±8
46–34											
Run *C*	4195	39 (52)	12 (21)	13	6 (23)	0	8 (8)	27	12	96±20	42±12

From samples of the incident flux, the energy and depth distributions of the incident flux were determined. Subsequently a low-energy cutoff was assigned for each run (see Fig. 1) and events caused by mesons of energy below the appropriate cutoff were rejected. Some events were also rejected on the basis of their depth in the chamber. The need for depth correction of events is most clearly illustrated by consideration of the stop events. A meson passing through the beryllium plate near the edge of the illumination may easily be confused with a meson that stops in the plate. Consequently, only those stops falling within a specified central portion of the flux depth distribution were considered valid. This fraction of the valid stops was then corrected with the help of the flux depth distribution, to obtain the total number of valid stops.

RESULTS AND DISCUSSION

The results of this experiment are presented in Table I.

In view of the small cross section expected for charge exchange scattering in light elements,[2] the stop events have been considered to be stars or scattering events hidden by the beryllium plate. Approximately one third of the stops were assigned to the scattering events on the basis of a determination of the average solid angle available to detectable elastic scattering events.

Absorption Data

The absorption cross sections measured are presented in Fig. 2. The energy dependence of the absorption cross section is consistent with similar data at somewhat higher energies for carbon,[3,4] nuclear emulsions,[5,6] and for aluminum.[7]

Brueckner, Serber, and Watson[8] relate the π^+-meson absorption cross section in complex nuclei to the meson absorption cross section in deuterium by the following relation:

$$\frac{1}{(A-Z)}\sigma[\pi^+ + \text{nucleus} \rightarrow \text{star}] = \Gamma \cdot \sigma[\pi^+ + d \rightarrow 2p].$$

This experiment yields a value of Γ between $3.2_{-0.8}{}^{+1.1}$ at 39 Mev and $5.6_{-1.1}{}^{+2.1}$ at 20 Mev. In this calculation the experimental values for $\sigma[\pi^+ + d \rightarrow 2p]$ found by Durbin, Loar, and Steinberger[9] have been used. The significance of the energy dependence of Γ, if it is real, is not clear. One possible qualitative explanation is that mesic absorption may also proceed via nuclear substructures more complex than the deuteron substructure and that the probability of absorption by the more complex substructures does not fall off as rapidly with decreasing meson energy as does the probability of absorption by the deuteron structure. In fact, for the absorption of slow π^- mesons in nuclear emulsions, the weight of evidence favors absorption via a multinucleon substructure.[10–12] More will be said concerning the absorption mechanisms in the following section on the analysis of star fragments.

The absolute value of Γ found in this work may be

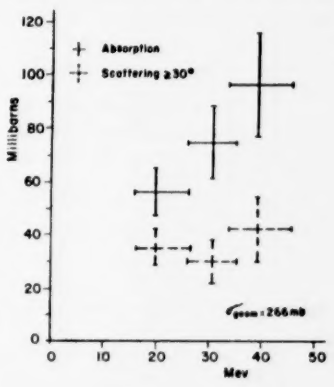

FIG. 2. Absorption and scattering cross sections, π^+ on Be *vs* π^+ kinetic energy.

[2] A. Roberts and J. Tinlot, Phys. Rev. **90**, 951 (1953).
[3] L. Lederman (private communication).
[4] Isaacs, Sachs, and Steinberger, Phys. Rev. **85**, 803 (1952).
[5] Bernardini, Booth, and Lederman, Phys. Rev. **83**, 1075 (1951).
[6] G. Bernardini and F. Levy, Phys. Rev. **84**, 610 (1951).
[7] James F. Tracy, Phys. Rev. **91**, 960 (1953).
[8] Brueckner, Serber, and Watson, Phys. Rev. **84**, 258 (1951).
[9] Durbin, Loar, and Steinberger, Phys. Rev. **84**, 581 (1951).
[10] D. Perkins, Phil. Mag. **40**, 601 (1949).
[11] W. Cheston and L. Goldfarb, Phys. Rev. **78**, 683 (1950).
[12] F. L. Adelman, Phys. Rev. **85**, 249 (1952).

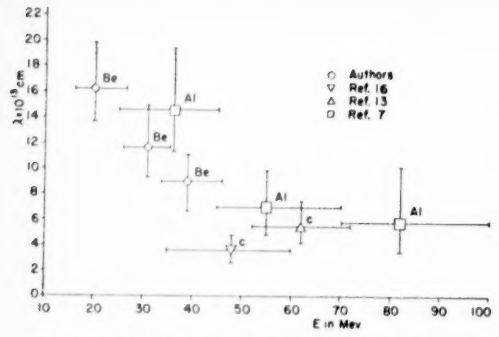

FIG. 3. Mean free path for absorption in nuclear matter *vs* meson kinetic energy.

compared to the value of $\Gamma \sim 3.3$ found by Byfield *et al.*[13] in carbon at 62 Mev and to the value of $\Gamma \sim 10$ found by Bernardini *et al.*[6] in nuclear emulsions at 50 Mev.

Finally, following the optical model,[14] the absorption data is presented in Fig. 3 in terms of the mean free path for π^+ absorption in nuclear matter.[15] For comparison the π^+ absorption data of other workers[7,13,16] are also presented.

Scattering Data

All observed scattering events were elastic. This result is consistent with the results from plate data[5] and cloud-chamber data for carbon[3] which indicate that the inelastic scattering of pi mesons has a threshold energy between 50 and 70 Mev. The scattering cross section found (Fig. 2) is about half the absorption cross section. The total number of scattering events was too low to warrant more than the rough angular distribution presented in Fig. 4. In this plot the stops assigned to the scattering events have been equally divided between the angular intervals 60°–90° and 90°–120°. A study of the meson scattering between 5° and 15° projected angle was also made. The results were entirely consistent with multiple scattering in the beryllium plate.

Analysis of Star Fragments

The analysis of the star fragments can throw light on the important mechanisms for mesic absorption in beryllium. The two absorption mechanisms considered are:[8,10,17] (a) absorption by a pair of nucleons ($\pi^+ + "d" \rightarrow 2p$ or $\pi^+ + 2n \rightarrow n + p$) and (b) absorption by a nuclear substructure of several nucleons, e.g., $\pi^+ + He^4 \rightarrow He^3 + p$. If a 30-Mev π^+ meson is absorbed by a deuteron structure, the resulting star fragments will have energies of 85 Mev or less. In contrast mesic absorption by a multinucleon structure may lead to the emission of a single proton having a kinetic energy of 140 Mev or more.

All of the ionizing star fragments were assumed to be protons with one exception. In this case the single visible star fragment appeared to be doubly charged. Eighty-six percent of the visible star fragments had energies exceeding 30 Mev and 21 percent probably had energies of more than 100 Mev. We consider that the appreciable number of star fragments of energy greater than 100 Mev constitute clear evidence for a multinucleon absorption mechanism.

Of the 2-prong stars, about 65 percent exhibited a correlation angle between prongs of 140° or greater. About 10 percent (2 or 3 stars) of the 2-prong stars exhibited an angle of 170°–180° between their prongs. This prong correlation may be considered evidence for the absorption of the π^+ meson by a deuteron structure in the beryllium nucleus. It is estimated[18] that about 30 percent of the time the two protons arising from such a "deuteron" absorption should escape from the beryllium nucleus without undergoing any nuclear interactions en route. If one accepts 140° between prongs as "good" correlation, then at most about two thirds of the visible stars can be accounted for on the basis of a deuteron absorption.

In 19 cases of 2-prong stars it was possible to measure the energy of both prongs. In Fig. 5 the sum of the kinetic energy of the two prongs is plotted against the true angle between the prongs. For comparison the energy-angle correlation has been computed for a 30-Mev π^+ meson absorbed by a deuteron structure. This relation is shown by the dotted curve in Fig. 5 where it has been further assumed that: (a) the nucleons are at rest in the nucleus, (b) collisions between the initial fast protons and other nucleons can be treated as if the nucleons were free, and (c) only one of the ejected protons undergoes a nuclear collision within the nucleus. At most 9 of the 19 stars exhibit this energy-angle correlation. This corresponds to 47 percent of the 2-prong stars plotted or 16 percent of all visible stars. On this basis, not more than 54 percent of the visible stars are results of a "deuteron" absorption. These estimates may be compared with the estimate of Byfield, Kessler, and Lederman[13] that about 60 percent

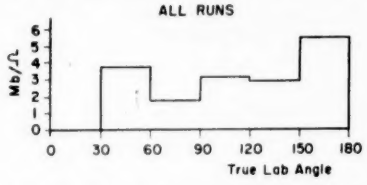

FIG. 4. Scattering angular distribution, π^+ on Be. Combined data from all runs.

[13] Byfield, Kessler, and Lederman, Phys. Rev. **86**, 17 (1952).
[14] Fernbach, Serber, and Taylor, Phys. Rev. **75**, 1352 (1949).
[15] Admittedly the applicability of the optical model is questionable since λ for mesons of such low energy is of the same order of magnitude as the diameter of the Be nucleus.
[16] A. M. Shapiro, Phys. Rev. **84**, 1063 (1951).
[17] S. Tamor, Phys. Rev. **77**, 412 (1950).
[18] This estimate is based on the assumption that the meson is absorbed at random in the nucleus and that the subsequent protons have a mean free path in nuclear matter of 3.3×10^{-13} cm (see reference 14).

of the stars produced in carbon by 62-Mev π^+ mesons may be attributed to a deuteron absorption. Mesic absorption by a "dineutron" substructure cannot easily be distinguished in these experiments. On an *a priori* basis, however, this process is less probable than absorption by a deuteron substructure and cannot account for the remainder of the stars.

The three 2-prong stars (Fig. 5) for which the correlation angle is about 90° are thought to be the result of multinucleon absorption. These three stars may be thought to result from the collision of the single fast proton emitted by the multinucleon substructure with another proton in the nucleus, both protons then appearing as star fragments.

Finally, one can examine the angular distribution of the star prongs for a clue as to the validity of the two absorption models. The angular distribution of protons from the reaction $\pi^+ + d \rightarrow 2p$ has been measured by Durbin, Loar, and Steinberger[19] who find the differential cross sections at 0° and 90° in the center-of-mass system to be in the ratio of about 3:1. On this basis one expects some forward and backward peaking of the star prong angular distribution. It is not clear what angular distribution to expect on the basis of the multinucleon absorption model.

The angular distribution of star prongs having energies greater than 50 Mev was analyzed on the basis of two ratios, namely: $R = f/(1-f)$, where f is the fraction of star prongs found in the interval 0°–45° and 135°–180°, and F/B equal to the ratio of prongs in the angular interval 0°–60° to those in the interval 120°–180°. In determining these ratios, star prongs of unknown energy were considered to have a kinetic energy of more than 50 Mev, and two-thirds of the stops were added into the figure $(1-f)$. The experimental ratios may be compared (Table II) with those expected for the following center-of-mass angular distributions:

$$P_1(\theta) = 1/2, \quad P_2(\theta) = (6/10)\cos^2(\theta) + 3/10.$$

The greatest asymmetry in the laboratory system would be predicted for the smallest number of interacting particles, e.g., two nucleons. The corresponding ratios R and F/B are computed on this basis, for the case of a 30-Mev meson energy (Table II). $P_2(\theta)$ simulates the angular distribution[19] of protons for the reaction $\pi^+ + d \rightarrow 2p$. The computed and average experimental ratios are presented in Table II.

TABLE II. Computed and average experimental ratios.

	Computed		Experimental
	P_1	P_2	
R	0.42	0.77	0.52±0.19
F/B	1.44	1.29	2.7 ±1.0

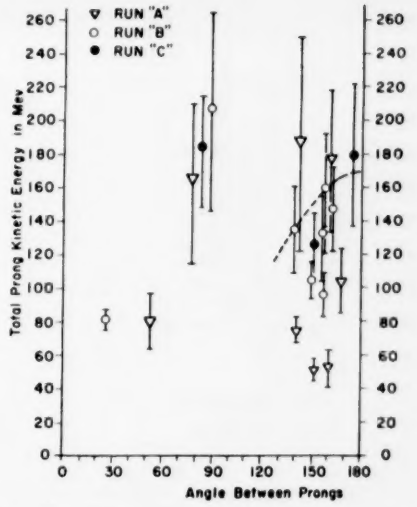

FIG. 5. Two-prong star energy vs angle between prongs, π^+ on Be.

The angular distribution of the star prongs appears to have some forward peaking but cannot be said to be inconsistent with isotropy. The disagreement between the experimental and calculated values of the ratio F/B for the P_2 distribution is more severe, however, and constitutes further evidence that the deuteron absorption cannot be the only absorption mechanism

CONCLUSIONS

The principle conclusions drawn from this work are: (a) the absorption cross section, σ_{abs}, decreases with decreasing meson kinetic energy to 59±9 millibarns at 20 Mev; (b) $\sigma_{abs}/\sigma_{scatt} \sim 2:1$; (c) at most 60 percent of the absorptions may occur via a deuteron structure, but the fraction of absorptions attributable to a nucleon pair absorption mechanism is somewhat higher; and (d) definite evidence exists for mesic absorption by a multinucleon structure in beryllium.

ACKNOWLEDGMENTS

We are indebted to Messrs. Coombs and H. Logeman for efficient operation of the cyclotron, and to Messrs. R. Mortenson and J. Dungan for invaluable assistance in design of the cloud chamber and magnet. I. Goldberg, M. Halbert, R. Harding, and J. Wyckoff assisted in the preparation and operation of the apparatus.

[19] Durbin, Loar, and Steinberger, Phys. Rev. **83**, 646 (1951).

High-Energy Electron Scattering and Nuclear Structure Determinations*,†,‡

R. HOFSTADTER, H. R. FECHTER, AND J. A. MCINTYRE
Department of Physics and W. W. Hansen Laboratories, Stanford University, Stanford, California

(Received June 26, 1953)

Electrons of energies 125 and 150 Mev are deflected from the Stanford linear accelerator and brought to a focused spot of dimensions 3 mm×15 mm at a distance of 9 feet from a double magnet deflecting system. The focus is placed at the center of a brass-scattering chamber of diameter 20 inches. Thin foils are inserted in the chamber and elastically-scattered electrons from these foils pass through thin aluminum windows into the vacuum chamber of a double focusing analyzing magnet of the inhomogeneous field type. The energy resolution of the magnet has been about 1.5 percent in these experiments. This resolution is enough to separate clearly hydrogen or deuterium elastic peaks from carbon peaks in the same scattering target. The energy loss in the foils is readily measurable. In the case of light nuclei, e.g., H, D, Be, C, the shift of the peak of the elastic curve as a function of scattering angle indicates the recoil of the struck nucleus. Relative angular distributions are measured for Be, Ta, Au, and Pb. It is possible to interpret these data in terms of a variable charge density within the nucleus.

I. INTRODUCTION

IN a recent publication[1] it was suggested that the gold nucleus does not have a sharp boundary. In this paper it is proposed to amplify this statement and to present data on other nuclei which tend to bear out this conclusion.

Guth[2] first pointed out that the finite size of the nucleus should produce large deviations from the expected scattering resulting from a point charge whenever the electron wavelength is of the order of nuclear dimensions. In principle, such deviations might be wholly or partially ascribed to departures from the Coulomb law of electric interaction at very small distances. In the following discussions it will be assumed that the Coulombian interaction holds at small distances and that the departures, if any, from point charge scattering are assignable to the finite dimensions of the nuclear charge distribution.

Other authors have subsequently considered the problem of the finite size of nuclei in relation to scattering experiments.[3–8] Parzen, Smith, and Schiff have dealt with energies of the order of 100 Mev and higher, while the other authors have been concerned mainly with lower energies. Parzen has made an exact calculation at a high energy (100 Mev). Unfortunately, a numerical error crept into Parzen's work and his published scattering curve cannot be considered reliable.[9] For nuclei having a uniform or spherical shell distribution of charge all Born approximation calculations predict maxima and minima in the angular distribution. These features are essentially diffraction phenomena and are similar to the observations in electron diffraction studies of atoms. The first Born approximation[2,4,7] for these models produces the first of a set of zeros in the angular intensity pattern at those angles where

$$qa \cong 3.5, \tag{1}$$

$$q = (4\pi/\lambda)\sin(\theta/2), \tag{2}$$

in which λ is the wavelength of the incident electrons and "a" is the rms value of the nuclear radius, calculated with the charge as the weighting factor. Yennie *et al.*[10] have shown that for a uniform model the exact calculation provides a result in which the first diffraction minimum is practically washed out and the second and third less pronounced than in the Born approximation but approximately in the same angular positions. Experimental indications of a deviation from point charge scattering have been found by Lyman, Hanson, and Scott[11] at an electron energy of 15.7 Mev. $\lambda = \lambda/2\pi$ is, in this case, of the order of 1.25×10^{-12} cm and, if one uses a conventional radius for gold ($R = 8.1\times10^{-13}$ cm, $a = 6.3\times10^{-13}$ cm), qa is found to be close to or less than unity. Thus, no maxima or minima are to be expected in the experiment of Lyman *et al.*, although marked deviations in the angular distribution were expected and, in fact, found. The experimental data proved to be consistent with a uniformly charged model of the nucleus in which

$$R = r_0 A^{\frac{1}{3}}, \tag{3}$$

where r_0 was 1.45×10^{-13} cm. In gold a twenty percent smaller radius gave a very slightly improved fit of the

* This work was initiated and aided at all stages by a grant from the Research Corporation. It was supported by the joint program of the U. S. Office of Naval Research and the U. S. Atomic Energy Commission. In the latter stages of the work, support has been received from the Office of Scientific Research, Air Research, and Development Command.

† This material was presented in part at the April 29, 30–May 1, 1953 Meeting of the American Physical Society in Washington, D. C.

‡ Portions of the theoretical interpretation were revised in proof.

[1] Hofstadter, Fechter, and McIntyre, Phys. Rev. **91**, 422 (1953).

[2] E. Guth, Wiener Anzeiger Akad. Wissenschaften No. 24, 299 (1934).

[3] G. Parzen, Phys. Rev. **80**, 261 (1950); **80**, 355 (1950).

[4] L. R. B. Elton, Proc. Phys. Soc. (London) **A63**, 1115 (1950); **65**, 481 (1952); Phys. Rev. **79**, 412 (1950).

[5] H. Feshbach, Phys. Rev. **84**, 1206 (1951); **88**, 295 (1952).

[6] L. K. Acheson, Phys. Rev. **82**, 488 (1951).

[7] J. H. Smith, Ph.D. thesis, Cornell University, 1951 (unpublished).

[8] L. I. Schiff, following paper, Phys. Rev. **93**, 988 (1953).

[9] G. Parzen (private communication). The error was first found by Elizabeth Baranger (private communication).

[10] Yennie, Wilson, and Ravenhall have recently recalculated the exact scattering at high energies (private communication).

[11] Lyman, Hanson, and Scott, Phys. Rev. **84**, 626 (1951).

data. Lyman *et al.* have noted that the smaller radius in gold might indicate a more dense packing of protons in the interior of the nucleus. A suggestion of this type had been made previously by Born and Yang.[12]

The experiments to be described below were intended to search for possible clear-cut signs of nuclear finite dimensions and by this means to find nuclear radii and charge distributions.

II. APPARATUS

Only the main features of the experimental equipment will be described at this time. Figure 1 shows the principal experimental arrangement. A monoenergetic group of electrons is deflected by a system of two magnets from the main beam of the Stanford linear accelerator.[13] The first magnet bends and disperses the beam and the second magnet bends in a reverse direction and refocuses the spread-out beam. A slit at position S determines the width of the accepted energy band, in this case about 3 percent. The initial width of the beam entering the first magnet is determined by the collimator C, in this case a $\frac{1}{4}$-inch cylindrical hole in a uranium block 1.0-inch long. A well focused beam emerges from the second magnet and closes to a small spot 9 feet from the second magnet. The position of the spot is accurately given by simple first-order calculation of trajectories. The size of the spot is approximately 1-mm high and 3-mm wide for a $\frac{1}{16}$-inch collimator and 3 mm$\times$15 mm for a $\frac{1}{4}$-inch collimator. The beam has extremely little divergence because of the 9.0-foot focal distance and small slit S used (0.75). As many as 2×10^8 electrons per pulse have been measured in the focused beam, sixty pulses occurring per second, each lasting about 0.5 microsecond. The beam is quite free of any gamma rays produced at the collimator and slit because of the double deflection. The beam stopper B prevents gamma rays produced at C from traveling down the accelerator tube and producing unwanted background in the experimental area.

The focused beam is directed towards a scattering target, usually a thin foil of any one of various materials. The scattering target is placed at the center of a brass scattering chamber of diameter twenty inches and twelve inches high. The scattering chamber is built in the form of a large bell-jar which can be detached readily from the main base plate. The whole deflection system and scattering chamber are evacuated to high vacuum. The base of the scattering chamber contains electrical lead-in connections and provisions for mounting and internally moving one or more scintillation counters on a large ring gear whose position is controllable remotely. A thin aluminum window (0.006 in.) stretches around the chamber from about $-150°$ to $150°$ over a vertical distance of three inches. Scattered electrons from the target emerge from the chamber

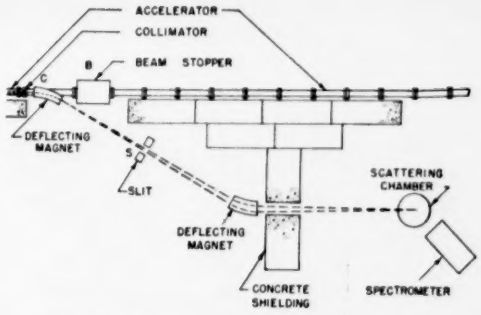

FIG. 1. The experimental arrangement of the electron-scattering system.

through the aluminum window and pass through about one inch of air before reaching the entrance port of the vacuum chamber of the analyzing magnet M. The C-shaped vacuum chamber lies between the shaped pole pieces of the inhomogeneous field magnet. The entrance and exit ports of the vacuum chamber are fitted with 3-mil aluminum windows. The magnet M is similar to the design of Snyder *et al.*,[14] weighs about two and a half tons and has a mean radius of curvature of 16 inches. It is located on the movable platform of a modified twin 40-mm anti-aircraft gun mount kindly lent us by the U. S. Navy, with the cooperation of the U. S. Office of Naval Research.[15] The magnet is of the double focusing variety and employs an inhomogeneous field of index $n=\frac{1}{2}$. Fields up to 12 or 13 kilogauss have been obtained and maintained over long periods of time without excessive heating. The field is usually maintained constant by manual regulation of the current.

A rotatable foil-holder that can be remotely controlled is now being installed in the scattering chamber. The experiments to be described were carried out with a substitute foil-holder which could be rotated and raised or lowered. The raising or lowering operation was remote, but the rotation was not. The holder could accommodate two foils at a time.

After the scattered electrons are analyzed in the magnet they leave the vacuum chamber and are collimated by a $\frac{1}{2}$-in. cylindrical hole in a lead block $2\frac{1}{2}$ inches long. Behind this collimator a conical Čerenkov counter, four inches long, detects the electrons admitted by the collimator. The Čerenkov counter is made of highly polished lucite and is one inch at the narrow input end and 1.5 in. at the output end where the lucite is coupled via heavy silicone oil to a 6292 Dumont

[12] M. Born and L. M. Yang, Nature **166**, 399 (1950).

[13] Among those mainly responsible for this system are Dr. J. A. McIntyre and Dr. W. K. H. Panofsky.

[14] Snyder, Rubin, Fowler, and Lauritsen, Rev. Sci. Instr. **21**, 852 (1950); C. W. Li, Ph.D. thesis, California Institute of Technology, 1951 (unpublished).

[15] The gun mount was modified and machined most capably by the machine shop of the Mare Island Shipyard of the U. S. Navy. We are very grateful to the officers and civilians of the yard for the excellent job done. The U. S. Office of Naval Research very kindly helped us make the necessary arrangements with the shipyard.

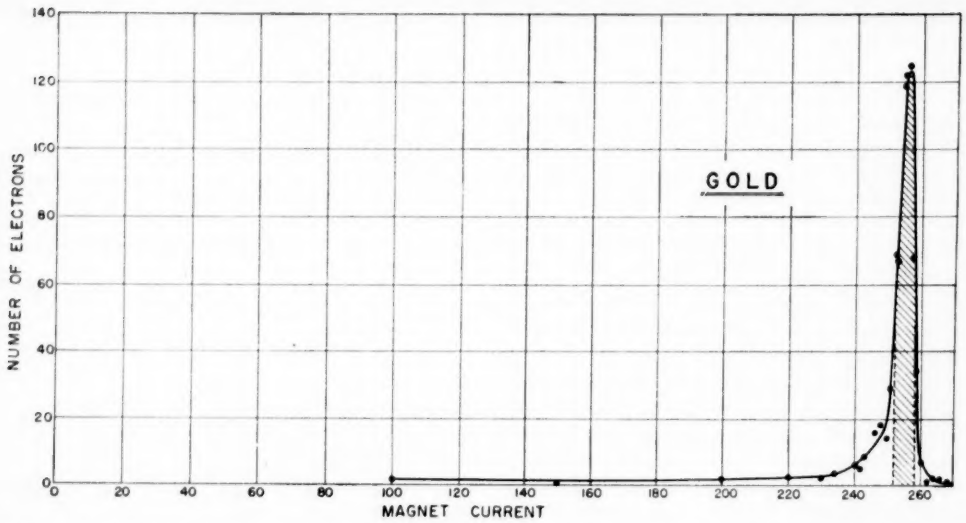

FIG. 2. An elastic-scattering curve in gold taken at 125 Mev, at a scattering angle of 35°, and with a 2-mil foil set at 45° with respect to the beam. The shaded portion of the peak shows the fraction of electrons counted in an individual peak setting. The abscissa is proportional to electron energy.

Photomultiplier. The pulses from the photomultiplier are amplified in an Elmore model 501 amplifier and fed to a gated scaler (gate 12 microseconds long) and also to an oscilloscope viewed by a monitor photomultiplier which has been made to act as a counter.[16] Both counters are gated by the main trigger signal of the linear accelerator. The biases against which both counters operate are adjusted so that the two agree on number of counts. Good plateaus in counting rates are thus obtained. An effort is made to count not more than one count a second so that pileup and loss of counts may be avoided. A large lead shield surrounds the Čerenkov counter and photomultiplier and has greatly helped in avoiding background troubles.

The main beam passing through the scattering target is monitored by a helium-filled ionization chamber designed by W. C. Barber of this laboratory. Dr. Barber has kindly calibrated and tested the chamber with 25-Mev electrons and has verified that it does not saturate under beam intensities up to 2×10^8 electrons per pulse, where a pulse lasts about 0.3 microsecond, and where the beam is about 2 cm² or larger on entering the chamber. Under the conditions of the experiments here reported the ion chamber does not saturate. The output of the chamber is brought to a charge integrator of a conventional type.

The deflecting magnets are presently stabilized by an electronic regulator to better than one part in a thousand. The analyzing magnet is manually controlled by an operator who reads the voltage across a shunt in series with the current. A Rubicon potentiometer is used to read the shunt voltage. With careful control the analyzing magnet current may be maintained constant between limits of ±0.1 percent during a run of 10 minutes duration.

The magnet has been calibrated by using the known energy of the Am^{241} α particles and by measurement of the magnetic field at the center of the magnet.

The angular position of the magnet on the gun mount stand is controlled remotely and measured by a combination of high and low speed selsyn indicators. The error in determining position is less than 0.1°.

III. EXPERIMENTAL PROCEDURE

Because of the temporary nature of the target holder the scattering foils were not rotated during the angular runs. This procedure has the advantage that one always uses the same region of the scattering foil provided that the beam spot does not shift during a run. When setting the analyzing magnet from one side of zero to the other, it is of course necessary to rotate the target foil and this was done. Also when points beyond 90° were examined, the foil was rotated to a new fixed position. A typical setting of the foil for a run between 35° and 90° was with foil plane at 45° with respect to the beam. The lineup of the beam was carefully carried out at the beginning of each run by a photographic method.

At a given angular position of the analyzing magnet an "elastic curve" can be obtained by measuring the total number of counts per unit integrated beam for various settings of the magnetic field. The magnetic field settings are assumed to be proportional to the magnet currents and the former are also proportional to the electronic momenta. For these high energies, the currents are therefore also proportional to the electronic energies. Typical elastic curves so obtained are shown in

[16] R. Hofstadter and J. A. McIntyre, Rev. Sci. Instr. **21**, 52 (1950).

Figs. 2, 3, 4, and 5. The abscissa on these curves is proportional to the magnet current, and in all cases except Fig. 2 the zero of abscissa is far off to the left of the ordinate axis. The curve of magnetic field against magnet current shows little saturation in the region here investigated[14] (about 100 amperes).

The elastic curves show typical bremsstrahlung tails on the low-energy side and sharper cutoffs on the high-energy side, as expected. Figure 2 shows the appearance of an elastic curve for gold and indicates also the fraction of electrons collected in individual peak settings. Figure 3 shows a typical displacement between the peak of the main beam and that of the transmitted beam at zero degrees, the difference being the result of the energy loss in the gold foil (2-mils thick). Figures 3 and 4 show that the elastic curves have the same appearance at angular settings of 0°, 35°, and 70° and presumably, therefore, at other angles. Figure 5 and Figs. 1 and 2 of our earlier communication[1] show that the elastic curves of hydrogen and deuterium in polyethylene as well as beryllium shift with the angular position. This shift has been explained[1] by the recoil of the struck nucleus (H, D, Be, C). With improved resolution this recoil shift will permit scattering measurements to be made on unseparated isotopes in the same foil and also with the elements of compounds. In the case of Ta, Au, and Pb the recoil shift is too small to be observed at the present time. In those cases in which the elastic curves have the same appearance at all angles, it is sufficient to measure the total elastic yield at a given angle by an average of two measurements taken at positions on either side of the peak, for example, at abscissas 326 and 330 in Fig. 4 for tantalum. All angular distributions have been measured in this way. Measurements in light elements, for example, Be or C, must be taken at the positions of the shifted peaks. Figure 6 shows how the Be elastic curves shift with angular position. In fact, in Be the elastic curve changes in appearance as well as shifts with change in angular position. The peculiar curve in Be at 90° requires further investigation. It is possible that inelastic scattering may be observed in such light elements at large angles.

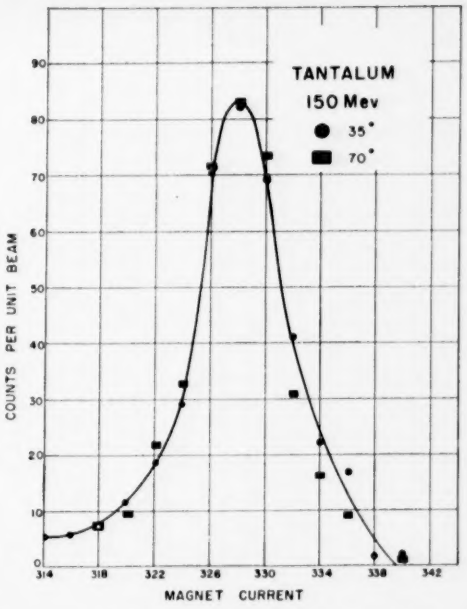

FIG. 4. Elastic-scattering curves in tantalum at 150 Mev. The data at 35° and 70° are essentially identical when normalized to the same peak value. The foil was 2.6 mils thick and was placed at 30° with respect to the direction of the beam.

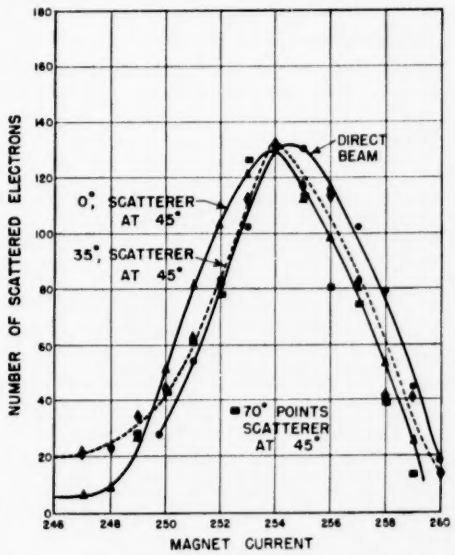

FIG. 3. Elastic-scattering curves for a 2-mil gold foil at 125 Mev. The foil was placed at 45° with respect to the beam. The abscissa is proportional to electron energy. Some of the curves were observed with a CsBr(Tl) detector by a dc method and have higher residual backgrounds (directly and indirectly the result of neutrons) than the normal Čerenkov detector curves.

The shift of the peak in Be is the result not only of the recoil energy but also of the energy loss of the incoming and outgoing electrons in the target foil. At a scattering angle of 45°, and a target setting of 45° with respect to the beam, the average energy loss in the 50-mil beryllium target is 0.49 Mev, and the recoil shift is 0.46 Mev. At 70° the corresponding figures are 0.51 Mev and 1.04 Mev, and at 90° they are 0.58 Mev and 1.58 Mev. The expected shifts relative to 35° are therefore 0.60 Mev for 70° and 1.21 Mev for 90°. The observed relative shifts are 0.60 ± 0.20 Mev and 1.20 ± 0.20 Mev and are in good agreement with the calculations. Similarly, good agreement has been obtained for the hydrogen and deuterium shifts. In fact the H, D shifts relative to carbon or some other standard may be used to measure the energy of the incident beam. With the present resolution and the accompanying experimental error in measuring the shifts, the calculated beam energy is of the order of 140 ± 20 Mev while the

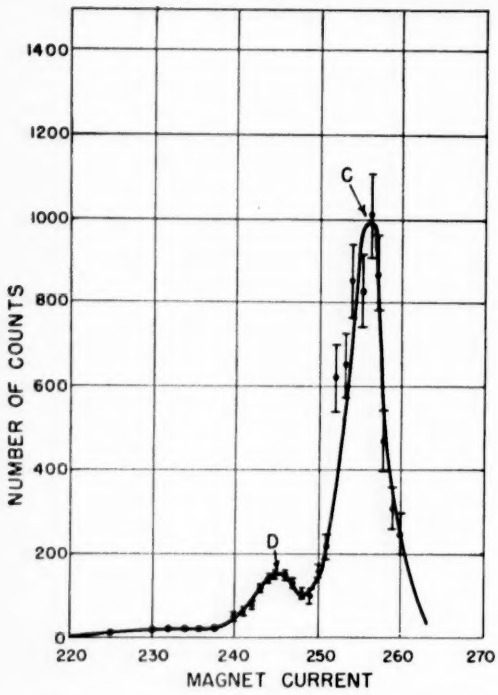

FIG. 5. An elastic curve at 125 Mev, showing the deuterium and carbon peaks observed in deuterated polyethylene at a scattering angle of 65°.

value obtained by calibration with alpha particles gives a value of 125±5 Mev. Obviously, the method can be refined.

A further check on the internal consistency of the scattering data is obtained by comparison of the ratio of the areas under the carbon and hydrogen or deuterium peaks in Fig. 1 of this paper and also in Fig. 2 of reference 1. The ratio in Fig. 5 is $\sigma_C/\sigma_D = 14\pm5$ and for Fig. 2 of reference 1 the ratio $\sigma_C/\sigma_H = 20\pm5$, where σ_C, σ_H, σ_D, are the respective cross sections. The accuracy of these measurements is not high because of the carbon bremsstrahlung background which must be subtracted from the H or D peaks. An average of the two results gives 17 which is close to the ratio, $Z_C^2/2(Z_{H,D})^2 = 18$, of the scattering from carbon and hydrogen or deuterium in polyethylene. Again, with better resolution this measurement of relative areas can be greatly improved, and, in fact, this method suggests itself for measuring the hydrogen and deuterium scattering cross sections relative to carbon as a standard.

To check the over-all behavior of the scattering measurements, two tests have been made: (1) the scattering

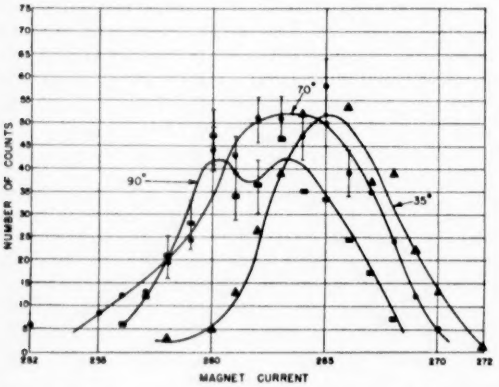

FIG. 6. Elastic curves in Be at 125 Mev at 35°, 70°, and 90°, observed with a 50-mil scattering target. The elastic peak shifts to lower energies at larger angles of scattering and also broadens as it shifts.

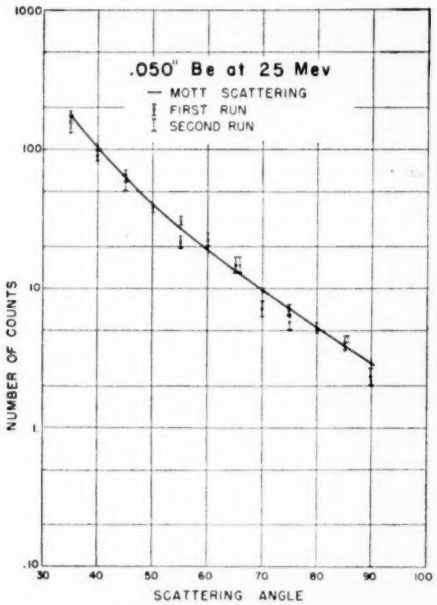

FIG. 7. The angular distribution of electrons scattered from a Be target, 50 mils thick, at 25 Mev. The target plane was at 45° with respect to the beam. The Mott curve for a point charge is shown. Arbitrary normalization is made at 35°.

of Be has been examined in the angular range 35°–90° at 25±2 Mev, and (2) the scattering from a gold foil of ¼-mil thickness has been studied in the same angular range at 25 Mev. In case (1), because of the relatively low energy, the Be nucleus may be approximated by a point charge and the exact calculations of Feshbach[5] and Parzen[3] for a point charge may be compared with the experimental data. In case (2) the observed angular distribution may be compared with the data of Lyman *et al.* at 15.7 Mev.

Figure 7 shows the Be data at 25 Mev using a 50-mil foil. The data are in excellent agreement with the accurate calculations and also with the Mott formula, which for low Z's is very close to the accurate formulas.

Figure 8 shows the data for gold found at 25 Mev

with a $\frac{1}{4}$-mil foil. The observed curve is seen to lie above the Mott curve, just as in the work of Lyman *et al.*[11] Our data show slightly less rise relative to the Mott curve as compared with the data of Lyman *et al.*, but this is to be expected, to some extent, because of the higher energy and therefore the shorter wavelength relative to nuclear size. On the whole, the agreement is better than might have been anticipated, since our windows were not designed for energies as low as 25 Mev. It is gratifying that the results for Be and Au at 25 Mev are so well in accord with expectation.

To check whether some systematic error might be prejudicing results on one side of zero preferentially the data for tantalum at 150 Mev have been observed on both sides of zero. Figure 9 shows the data and shows there is nothing special on either side. The data agree very well, and, in fact, the only point seriously off is at 80° on the left side where there was a steel supporting post blocking out part of the solid angle seen by the magnet chamber.

It is also pleasing that the background counting rate has been virtually absent. Without the target in place we have never observed a background count at angles between 35° and 120°. If some of the concrete shields and lead around the Čerenkov counter are removed it is easily possible however to obtain background counts. These are usually small pulses in the photomultiplier and it is anticipated that with further study even these can be removed by applying a higher bias.

IV. CORRECTIONS TO DATA

The corrections usually applied to the raw scattering data have been excellently summarized by Lyman *et al.*[11] Many of these corrections are not needed in the present work, because the data to be presented are entirely of a relative kind. A precise absolute calibration of the scattering data has not been attempted up to the present time, although work is now under way to obtain absolute cross sections in gold.

Since we shall be concerned only with relative data, there is probably no need to take into account such small corrections as the radiative type of Schwinger[17] which were calculated with Born approximation and depend very little on angle.

In order to avoid a variable loss of counts due to pileup, we have made an attempt to count approximately at the same rate at all angles so that a dead-time correction, if present, will be the same for all positions. Actually the dead time correction is negligible.

The largest corrections for multiple scattering are encountered in the case of the gold foils. For most measurements a foil 2 mils thick was used. In one run, to get more intensity at angles larger than 120° a four-mil foil was used. For the 2-mil foil the multiple scattering correction amounts to −0.3 percent at 35°, to −0.1 percent at 90°, and to −0.1 percent at 140°.

[17] J. Schwinger, Phys. Rev. **75**, 898 (1949).

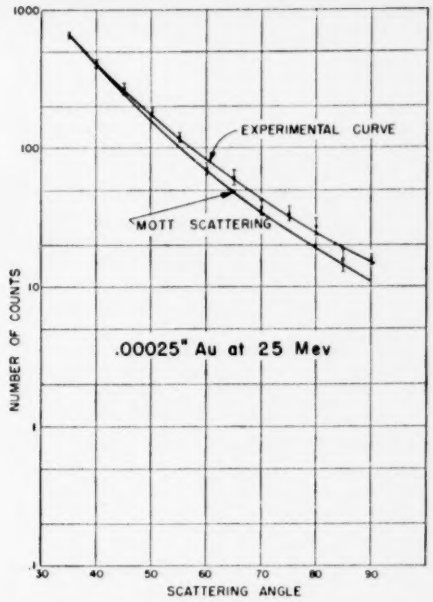

FIG. 8. The angular distribution of scattered electrons from a gold foil, $\frac{1}{4}$-mil thick, at 25 Mev. The foil plane was at 45° with respect to the beam. The Mott curve for a point charge is shown. Arbitrary normalization is made at 35°.

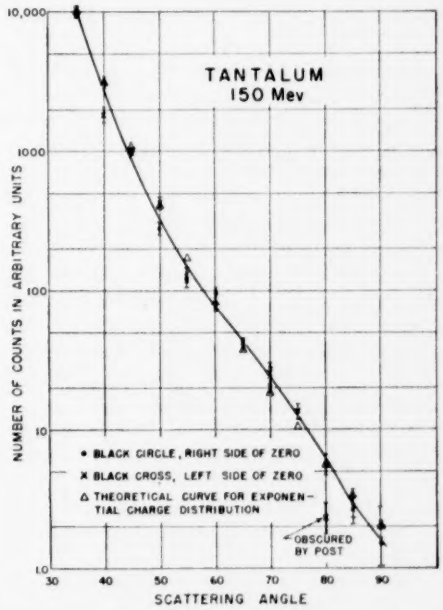
TANTALUM
150 Mev
• BLACK CIRCLE, RIGHT SIDE OF ZERO
× BLACK CROSS, LEFT SIDE OF ZERO
△ THEORETICAL CURVE FOR EXPONENTIAL CHARGE DISTRIBUTION
OBSCURED BY POST
NUMBER OF COUNTS IN ARBITRARY UNITS
SCATTERING ANGLE

FIG. 9. The angular distribution of scattered electrons from a tantalum foil, 2.6-mil thick, at 150 Mev. The foil plane was at 30° relative to the beam direction. Curves on the left and right of zero are shown. A theoretical curve based on an exponential charge distribution is shown as well as the Feshbach point charge curve. All curves are normalized arbitrarily at 35°.

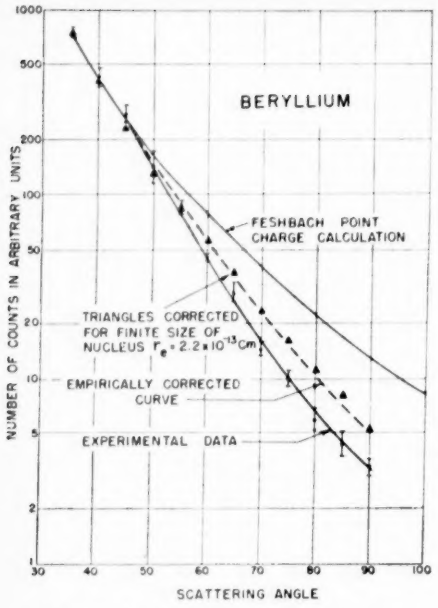
BERYLLIUM
FESHBACH POINT CHARGE CALCULATION
TRIANGLES CORRECTED FOR FINITE SIZE OF NUCLEUS $r_e = 2.2 \times 10^{-13}$ cm
EMPIRICALLY CORRECTED CURVE
EXPERIMENTAL DATA
NUMBER OF COUNTS IN ARBITRARY UNITS
SCATTERING ANGLE

FIG. 10. The angular distribution of scattered electrons from a beryllium foil, 50-mils thick, at 125 Mev. The experimental curve has been corrected empirically for the broadening observed in the elastic curves at larger scattering angles. (See Fig. 6.) The dashed curve is the corrected curve. A theoretical curve based on the first Born approximation for an exponential charge distribution is shown. Also shown is the point charge calculation of Feshbach. Arbitrary normalization of all curves is made at 35°.

Thus, multiple scattering corrections in the target foil are unnecessary for the accuracy involved in this work. The multiple scattering in the aluminum windows is of the order of 0.4° and can be neglected since it is 4 times as small as the rms scattering angle in the gold foil. The beryllium 50-mil foil has an rms scattering angle of 0.6° which is negligible also.

The errors resulting from double (large-angle) scattering are estimated to be 0.15 percent at 90° for two mils of gold at 125 Mev and 0.01 percent at 150° under the same conditions. For 50 mils of Be at 125 Mev the errors are 1.5 percent at 150° and 0.04 percent at 90°. Hence, all double scattering corrections are ignored since they are very small effects.

The geometrical corrections for the aperture can be estimated from the effective aperture which is approximately 0.8 square inch at twelve inches. A calculation similar to that of Lyman *et al.* leads to corrections of a few tenths of a percent, which are thus negligible for our purposes.

The angular resolution of our scattering results depends on the size of the beam spot on the target foil and on the effective aperture of the entrance port of the analyzing magnet. Each of these contributions is about the same at the present time and each contributes about 2°, fairly independently of angles between 35° and 140°, for a target foil setting of 45°. Hence, our angular acceptance width is about ±4°, or a total of 8°. Structure in the scattering curves within such small angular ranges would not be resolved in our experiments. On the other hand, such fine structure is not expected.

Radiative straggling and electron-electron straggling affect the shape of the elastic-scattering peaks. Since in all the cases we have studied, with the exception of Be, the elastic profile is the same at all angles, no relative corrections for these effects need to be made. As a matter of fact, the same argument applies to the Schwinger correction.

With the exception of Be, all corrections are extremely small and will be ignored. In the case of Be (Fig. 6) the elastic profile changes as a function of angle, because of the combination of the recoil effect and the energy loss straggling in the target. Both effects are appreciable for Be. The correction has been taken into account empirically by measuring the areas under the elastic curves taken at various angles. At 90° the area is approximately 1.5 times the area at 35° when both curves are normalized to the same peak values. Hence, a correction of 50 percent is applied to the counting rate at 90°. At 35° the correction is zero, and a smooth curve has been drawn in Fig. 10 (the dashed line) to represent the corrected data at intermediate angles. Since the cross section varies rather violently with angle, the largest correction of 50 percent produces only a mild effect.

V. RESULTS

The relative angular distributions have been measured in Be, Au, and Pb at 125 Mev and in Ta at 150 Mev. In addition, as mentioned previously, check runs

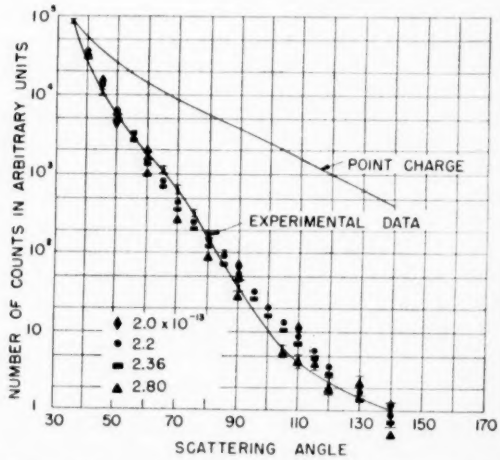

FIG. 11. The angular distribution of electrons scattered from a 2-mil gold foil at 125 Mev. The point charge calculation of Feshbach is indicated. Theoretical points based on the first Born approximation for exponential charge distributions are shown. Values of $\alpha = 2.0$, 2.2, 2.36, 2.8×10^{-13} cm are chosen to demonstrate the sensitivity of the angular distribution to change of radius. All curves are normalized arbitrarily at 35°.

were made on Be and Au at 25 Mev. The experimental curves are shown in Figs. 9, 10, 11, 12. The limits of errors indicated in the figures are entirely of statistical origin. In all cases except gold, the background counting rates were zero so that the present data represent the actual numbers taken in a run. In only one case, namely Au beyond 120°, was a small background observed in one of the counters. The other counter showed no background. The small background makes the data beyond 120° slightly less reliable than the other data.

Near 100° on the right side of zero it has not been possible to obtain data because of the presence of a steel post which is used as a support for the upper half of the scattering chamber. There is a similar post near 80° on the left-hand side of zero. In future experiments it will be possible to move the posts to other positions while taking data near these two angles.

In occasional runs we have noticed that after long periods of time the data do not check exactly. For example, after a couple of hours of running a point at 70° may change by 30 percent or so. Invariably the neighboring points will be down by the same factor. Thus, a slow drift in some part of the counting system or magnetic field appears at irregular times. The explanation of this effect is being sought. However, we do not feel that this effect is significant because the relative counting rates agree with those first obtained to better than 30 percent.

VI. ANALYSIS OF THE DATA

The experimental distributions lie far below the point charge calculations of Feshbach[5] which are shown typically in Fig. 11. Within the resolution of the experimental data (points were taken every 5 degrees apart) there is no pronounced evidence of diffraction minima or maxima. These curves are in striking contrast to the beautiful curves of Cohen and Neidigh[18] which show diffraction peaks in the scattering of 22-Mev protons.

The absence of pronounced diffraction peaks suggests that, from the viewpoint of the Born approximation, heavy nuclei do not have sharp boundaries. The accurate calculations of Yennie *et al.*[10] confirm this suggestion in a qualitative way but not quantitatively. We shall sketch briefly some qualitative considerations provided by the Born approximation, merely in order to obtain a feeling for the meaning of the experimental results. In the discussion below we have used the exact calculations of Feshbach for the point charge and have multiplied the point charge curve by the appropriate form factors obtained from the first Born approximation[2,4] for various assumed charge-density distributions.

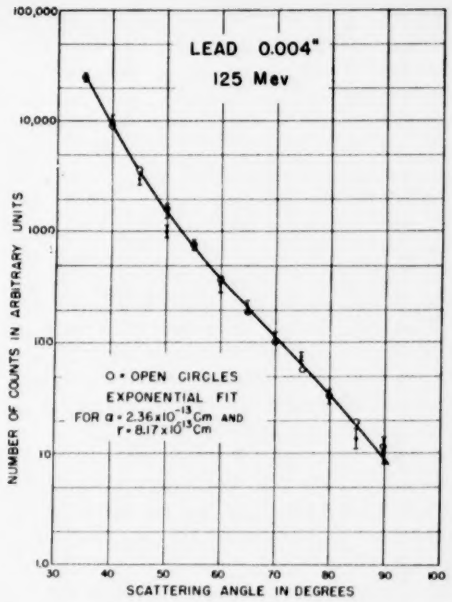

FIG. 12. The angular distribution of electrons scattered from a 4-mil lead foil at 125 Mev. A theoretical curve based on the first Born approximation for an exponential charge distribution is shown. Arbitrary normalization is made at 35°.

Among the types of charge-density (ρ) distributions tried[19] were the following:

(A) exponential

$$\rho=\rho_0 e^{-r/a}; \tag{4}$$

(B) "half-uniform and half-Gaussian"

$$\rho=\rho_1, \quad 0\leqslant r\leqslant c; \quad \rho=\rho_1 \exp[-\tfrac{1}{2}(r-c)^2/d^2], \quad r\geqslant c; \tag{5}$$

(C) gaussian

$$\rho=\rho_2 \exp(-\tfrac{1}{2}r^2/r_0^2); \tag{6}$$

(D) uniform

$$\rho=\rho_3, \quad 0\leqslant r\leqslant c; \quad \rho=0, \quad r\geqslant c. \tag{7}$$

The ρ_0, ρ_1, ρ_2, and ρ_3 are all constants with the dimensions of charge density. For these charge distributions the root-mean-square radii, calculated with the charge as the weighting factor are, respectively:

$$\text{(A)} \quad r_a=3.46a, \tag{8}$$

$$\text{(B)} \quad r_{ug}=2.31c \quad \text{for} \quad d=c, \tag{9}$$

$$\text{(C)} \quad r_g=1.732r_0, \tag{10}$$

$$\text{(D)} \quad r_u=0.775c. \tag{11}$$

In the following, we discuss the data obtained for the various elements.

[18] B. L. Cohen and R. V. Neidigh, Phys. Rev. (to be published). We wish to thank Dr. A. M. Weinberg and Dr. B. L. Cohen for informing us of these results. See also J. W. Burkig and B. T. Wright, Phys. Rev. **82**, 451 (1951).

[19] See also L. I. Schiff (reference 8) for other charge distributions and relevant remarks. A slightly different approach from ours has been used in Schiff's paper.

Gold

The "best fit" with the experimental data was obtained for the exponential charge distribution with $\alpha=2.3\pm0.3\times10^{-13}$ cm and $r_e=7.95\times10^{-13}$ cm. The experimental data and the exponential fit are shown in Fig. 11. The half-uniform and half-Gaussian model provides a "best fit" which is somewhat inferior to the exponential fit and requires $c=2.46\times10^{-13}$ cm and $r_{ug}=5.7\times10^{-13}$ cm. This angular distribution is a poor fit at angles greater than 110° where it drops off too rapidly. The pure Gaussian model (C) is also not as good as the exponential but gives a best fit for $r_0=2.48\times10^{-13}$ cm with $r_g=4.3\times10^{-13}$ cm. As in the last case the pure Gaussian drops off too rapidly beyond 115°. These rms radii are to be compared with the usual rms value of about 6.3×10^{-13} cm for gold and are of the correct order of magnitude.

The Born approximation is clearly quite poor for a uniform distribution of charge because of its true zeros. Therefore, no attempt will be made to use the Born approximation for this model. On the other hand, the exact calculations of Yennie *et al.*,[10] carried out both for a uniform charge distribution and an exponential charge distribution, show that the exponential fits better because of the absence of diffraction structure, which does occur for the uniform distribution. In either event, the most important conclusion is that the exact theoretical curves reflect the very steep falloff of cross section with angle shown by the experiments. The large departures from a point charge are, therefore, satisfactorily demonstrated in theory, as well as experiment. The rather extreme exponential model, when treated exactly, appears to fit the experimental data (35°–120°) quite well, but it is by no means ruled out that other less violent models with, e.g. Gaussian tails, might not do equally well. To see the qualitative effect of a small rounding off of the edge of a uniform charge distribution, a uniform model and Gaussian tail with parameter $d=0.2c$ in Eq. (5) has been tried in Born approximation but does not remove the zeros. This model simply moves the zeros out a little towards larger angles. A uniform model with a small exponential tail has a similar behavior, as shown by Smith.[7]

Lead

The lead foil used in the experiments was an isotopic mixture in the natural proportions and was 4-mils thick. The experimental curve for 125 Mev is given in Fig. 12. It may be seen that the points are fitted quite well by a theoretical Born curve based on an exponential model. The theoretical curve is hardly distinguishable from the experimental curve. The radius obtained from the best exponential fit is $r_e=8.17\times10^{-13}$ cm or $\alpha=2.36\times10^{-13}$ cm. This value is slightly larger than the radius for gold in the ratio 1.03.

Tantalum

The experimental curve for 2.6 mils of tantalum at 150 Mev is given in Fig. 9. By fitting with an exponential charge distribution corresponding to $\alpha=2.80\pm0.3\times10^{-13}$ cm or $r_e=9.7\times10^{-13}$ cm, an excellent reproduction of the data is obtained. Again, as in lead, the theoretical Born points are scarcely distinguishable from the experimental ones. While the tantalum should have a radius slightly smaller than lead or gold according to the rule expressed by Eq. (3), the scattering data indicate a larger radius. Relative to lead the rms radius is 1.18 times as large. This result may possibly have some connection with the extremely large quadrupole moment of Ta.

Beryllium

Beryllium has been studied at 125 Mev. The results obtained with a 50-mil scattering target are shown in Fig. 10. The curve which has been empirically corrected for the change in elastic profile as a function of angle is shown as a dashed line in the figure. The point charge curve of Feshbach is shown in open circles. In the case of beryllium the Born approximation should be quite valid. The triangles represent the point charge curve as modified by the "best fit" form factor corresponding to an exponential charge distribution with $r_e=2.2\times10^{-13}$ cm or $\alpha=6.36\times10^{-14}$ cm. This radius is quite a bit smaller than the radii measured for heavy nuclei and is in good agreement with what might be expected from Eq. (3). In the case of such a small nucleus as Be, the form factor can be chosen quite arbitrarily to correspond either to the exponential, Gaussian, or uniform model, since all give essentially the same behavior. For example, the best fit for a uniformly charged model gives $r_u=1.90\times10^{-13}$ cm and for a Gaussian model $r_g=1.96\times10^{-13}$ cm.

VII. CONCLUSIONS

With the angular resolution attained in these experiments, the absence of diffraction maxima and minima in the observed scattering of 125- and 150-Mev electrons from Ta, Au, and Pb suggests tentatively the concept that these nuclei have charge distributions tapering off gradually from near the center to the outside. This conclusion is not definite at this time because both theory and experiment are in preliminary stages.

The differences between the nuclear diffraction patterns observed in the scattering of 22-Mev protons[18] and the electron scattering results reported here may perhaps reflect the facts that nuclei interact with protons through short-range forces (also to a lesser extent through Coulomb forces) and are not transparent to protons of 22-Mev energy, while nuclei interact with electrons through long-range Coulomb forces and are transparent to electrons. Hence, the elastically-scattered protons interact effectively only with the outer edges of the

nucleus giving the impression of a sharp boundary. Electrons interact with the entire nuclear volume.

It might be wondered whether the peaked charge distribution suggested here could influence arguments concerning saturation of nuclear forces. A simple electrostatic calculation was carried out for the exponential charge distribution with $\alpha = 2.3 \times 10^{-13}$ cm for gold. The result obtained indicates that the Coulomb energy is changed by not more than a factor of two relative to that of the uniform distribution. Hence, on this score there will be no serious change regarding nuclear saturation.

It is recognized that the charge distribution in heavy nuclei tentatively suggested by this work differs rather seriously from the uniform model generally proposed. For this reason we are attempting to improve the accuracy of the experiments by increasing the angular resolution, energy resolution and stability of all parts of the apparatus.

ACKNOWLEDGMENTS

We wish to thank Mrs. P. Hanson, Mr. G. Masek, and assistant crew members for their kind and efficient help in running the accelerator. Miss E. Wiener and Mr. J. Fregeau have kindly assisted in taking some of the data. V. Prosper, E. Wright, B. Chambers, B. Stuart, F. Renga, and P. Abreu deserve our special thanks for the skill they have shown in building and designing various parts of our scattering apparatus. Mr. R. H. Helm was of great assistance in designing the magnet support and in constructing the spectrometer. We appreciate the help of Drs. W. A. Fowler and W. Whaling of California Institute of Technology, who provided us with the drawings and advice needed in constructing the analyzing magnet, and Dr. I. Perlman of the University of California Radiation Laboratory, for lending us an alpha-particle calibration source. We are grateful to the Office of Naval Research which gave us early support in this project and particularly to Dr. Urner Liddel, Mr. F. Niemann, and Lt. M. S. Jones who helped us obtain the gun mount for this work. We wish to thank Dr. L. I. Schiff and Dr. W. E. Lamb, Jr., who have given us valuable advice in theoretical matters. Dr. E. Guth has read our work critically and has our special thanks for his comments. Drs. D. R. Yennie and D. G. Ravenhall and Mr. R. N. Wilson are to be thanked most cordially for their kindness in permitting us to use their results before publication. We acknowledge with thanks the recent support of the Office of Scientific Research of the Air Research and Development Command. Finally we are grateful for a grant received from the Research Corporation which enabled this project to obtain its start.

Interpretation of Electron Scattering Experiments*†

L. I. SCHIFF
Stanford University, Stanford, California
(Received June 26, 1953)

Experiments on the elastic scattering of fast electrons by several elements, reported by Hofstadter, Fechter, and McIntyre in the preceding paper, are interpreted with the help of the first Born approximation. This interpretation of the experiments implies nuclear charge distributions that are peaked at the center and taper off smoothly. The root-mean-square radii of the charge distributions, and the nuclear Coulomb energies, are, however, in approximate agreement with those computed from the usual uniform charge distribution. The effects of radiation loss and nuclear excitation are discussed qualitatively, and the effect of a nuclear electric quadrupole moment is considered more quantitatively. It is concluded that these effects probably cannot account for the discrepancy between the observed scattering cross section which decreases monotonically with increasing angle and the diffraction minima and maxima expected on the basis of the Born approximation from a uniform charge distribution with a sharp or moderately rounded edge. Exact calculations of the elastic scattering from various charge distributions are now under way.

1. INTRODUCTION

THE preceding paper by Hofstadter, Fechter, and McIntyre[1] reports experimental results on the elastic scattering of fast electrons by several elements. The energy resolution of the incident and scattered electrons is such that the measured differential cross sections include both elastic events and inelastic events in which the energy loss to radiation or nuclear excitation is less than about 1 Mev, after allowance is made for the recoil energy of the struck nucleus. The observed monotonic decrease of the scattering cross section with increasing angle is in striking contrast with the diffraction minima and maxima calculated by means of the Born approximation[2] when the nuclear charge is assumed to be roughly uniformly distributed over a sphere of approximate radius $1.4\times10^{-13}A^{\frac{1}{3}}$ cm. While the first Born approximation is not reliable for heavy elements such as tantalum, gold, and lead, it should give a qualitative indication of the general character of the scattering for various assumed forms of the nuclear charge distribution. This view is confirmed by exact scattering calculations now in progress,[3a] which show that the principal effect of the improvements on the Born approximation in the case of a uniformly charged nucleus is the filling in of the zeros in the cross section to convert the minima and maxima into wiggles. This effect was noted earlier by M. Goldhaber and A. W. Sunyar [Phys. Rev. **83**, 906 (1951)].

All of the calculations in this paper are based on the first Born approximation. This enables us to make a rapid survey of the qualitative effect of the form of the nuclear charge distribution on the elastic scattering, and also to estimate the relative importance of inelastic processes and of the nuclear distortion implied by the existence of electric quadrupole moments. The results obtained cannot be taken literally for the heavy elements, but are expected to be more reliable for lighter elements and quite good for beryllium and deuterium.

2. USE OF THE FIRST BORN APPROXIMATION

For an electron of energy E that is scattered by a nucleus that is represented by wave functions Ψ_i, the differential scattering cross section per unit solid angle is[2]

$$\sigma(\theta)=[(4e^4E^2\cos^2\tfrac{1}{2}\theta)/(hcq)^4]\times\left|\int\Psi_f^*\sum_{k=1}^{Z}e^{i\mathbf{q}\cdot\mathbf{R}_k}\Psi_i d\tau\right|^2, \quad (1)$$

where $\hbar\mathbf{q}$ is the momentum transfer from the electron to the nucleus that makes a transition from state i to state f, and $\mathbf{R}_k$ is the coordinate of a proton in the nucleus; it is assumed that E is large in comparison with the rest energy of the electron, and that the scattering angle θ is not close to π. For elastic scattering, $q=(2E/\hbar c)\sin\frac{1}{2}\theta$, and Eq. (1) can be written in one of the forms

$$(e^4\cos^2\tfrac{1}{2}\theta/4E^2\sin^4\tfrac{1}{2}\theta)\left|\int\sum_{k=1}^{Z}|\Psi_i|^2e^{i\mathbf{q}\cdot\mathbf{R}_k}d\tau\right|^2$$
$$=(Z^2e^4\cos^2\tfrac{1}{2}\theta/4E^2\sin^4\tfrac{1}{2}\theta)\left|\int\rho(\mathbf{R})e^{i\mathbf{q}\cdot\mathbf{R}}d\tau_R\right|^2, \quad (2)$$

where $\rho(\mathbf{R})$ is the nuclear charge distribution, normalized to unit volume integral.

In the case of inelastic scattering with small energy loss, Eq. (1) must be summed over all final states f that have excitation energies less than about 1 Mev.[2]

* Supported in part by the Office of Scientific Research, Air Research and Development Command.

† Sections 1, 2, and 7 revised in proof.

[1] Hofstadter, Fechter, and McIntyre, preceding paper [Phys. Rev. **92**, 978 (1953)]. See also Phys. Rev. **91**, 422 (1953).

[2] E. Guth, Anz. Akad. Wiss. Wien. Math.-naturw. Kl. **24**, 299–307 (1934); M. E. Rose, Phys. Rev. **73**, 279 (1948); J. H. Smith, Ph.D. Thesis, Cornell University, February, 1951 (unpublished); Thie, Mullin, and Guth, Phys. Rev. **87**, 962 (1952). Magnetic interactions may be ignored for the low nucleon energies involved here.

[3a] Yennie, Ravenhall, and Wilson, private communication. Earlier calculations by G. Parzen, Phys. Rev. **80**, 355 (1950) have been found to contain an error (private communications from E. Baranger and G. Parzen).

If we use the independent-particle model to estimate the ratio of inelastic to elastic scattering cross sections, only one term in the summation of Eq. (1) can enter for a particular final state (this assumes unsymmetrized nuclear wave functions, but the result is not greatly different if they are symmetrized). Also, su[illegible] matrix element will be somewhat smaller in the inelastic than in the elastic case, due to the partial interference between initial and final proton wave functions. Finally, not all of the protons in the nucleus can be excited if the final state must lie within 1 Mev of the ground state. If one considers all of these factors, one arrives at an estimate of between 0.01 and 0.1 for the ratio of inelastic to elastic scattering at a particular angle, in a heavy nucleus. On the other hand, recent experimental[3b] and theoretical[3c] work shows that quadrupole transition probabilities are ten to a hundred times larger than estimated above on the basis of the independent-particle model, for low-lying excited (collective rotational) states of heavy nuclei. This makes the inelastic cross section for favorable excited states comparable with the elastic cross section, and tends to smooth out oscillations in the computed form factor (see Sec. 3). Doubly magic Pb^{208}, which constitutes more than half of normal lead, is exceptional in that its first excited state lies more than 2.5 Mev above its ground state. Such an energy loss can be resolved by the experiments, so that it is unlikely that inelastic processes can account for the observed smoothness of the lead-scattering curve.

It is very difficult to estimate the effect of radiation on the observed scattering. The existing theory[4] is only useful for light elements and breaks down completely for large angle scattering from an element as heavy as gold. It does, however, indicate that the radiative correction does not depend strongly on energy loss and scattering angle. Experiments to date[1] show that most scattering events are only slightly inelastic, and it seems likely that this represents radiation loss rather than nuclear excitation.

The effect of the nuclear quadrupole is discussed more quantitatively in Sec. 6.

3. ELASTIC SCATTERING FROM HEAVY ELEMENTS USING BORN APPROXIMATION

We define the nuclear charge form factor as the integral which appears in the right side of Eq. (2):

$$F(\mathbf{q})=\int\rho(\mathbf{R})e^{i\mathbf{q}\cdot\mathbf{R}}d\tau_R. \tag{3}$$

If $\rho(\mathbf{R})$ is real and spherically symmetric, $F(\mathbf{q})$ is also real and spherically symmetric. In this case, Eq. (3) can be written

$$F(q)=(4\pi/q)\int_0^\infty\rho(R)\sin(qR)RdR, \tag{4}$$

and conversely

$$\rho(R)=(2\pi^2R)^{-1}\int_0^\infty F(q)\sin(qR)qdq. \tag{5}$$

According to Eq. (2), $F(q)$ can be determined from the experimental observations:

$$F(q)=\pm[4E^2\sin^4\tfrac{1}{2}\theta\sigma(\theta)/Z^2e^4\cos^2\tfrac{1}{2}\theta]^{\frac{1}{2}},$$
$$q=(2E/\hbar c)\sin\tfrac{1}{2}\theta; \tag{6}$$

here only the sign is indeterminate, and it can be inferred from the sign of $\rho(R)$ and the behavior of $F(q)$ near its zeros, if any. Thus, if accurate experiments were available over the entire range of q (0 to ∞), $\rho(R)$ could be determined uniquely from Eqs. (5) and (6), within of course the limits of the first Born approximation.

In practice, somewhat inaccurate experiments are available over a finite range of q. Also, no absolute values of $\sigma(\theta)$ have been measured as yet. The procedure followed in this paper consists in assuming a variety of forms for the charge density $\rho(R)$ and the corresponding form factor $F(q)$, and plotting the experimental values of $G(q)\equiv(\sin^2\frac{1}{2}\theta/\cos\frac{1}{2}\theta)\sigma^{\frac{1}{2}}(\theta)$ against q in such a way that an easily recognizable curve will result if $F(q)$ has the assumed form. This procedure makes consistent use of the first Born approximation. An alternative method, used by Hofstadter, Fechter, and McIntyre,[1] consists in defining the experimental form factor $G(q)$ as the square root of the ratio of the observed scattering to the exactly computed point-charge scattering rather than to the first Born approximation point-charge scattering. The optimum procedure probably lies somewhere between these two, since the first Born approximation is somewhat better for a finite nucleus than for a point nucleus, where the electrostatic potential is stronger. It is gratifying that the numerical results obtained here and in reference 1 are in such good agreement.

Suppose, for example, that it is desired to see how well the observations can be fitted with the assumption that the charge density is uniform over a sphere of radius R_0. In this case,

$$\rho(R)=\rho_0,\ R<R_0;\quad \rho(R)=0,\ R>R_0;$$
$$F(q)=4\pi\rho_0R_0^3[(\sin qR_0-qR_0\cos qR_0)/(qR_0)^3]. \tag{7}$$

If then $F(q)$ is plotted against q on one sheet of log-log graph paper, and $G(q)$ is plotted against q on another sheet of log-log paper, superposition of the two will at once show the measure of agreement between Eq. (7) and the experimental observations. Vertical translation of the two sheets with respect to each other changes the absolute magnitude of the scattering, and horizontal translation changes the nuclear radius R_0.

[3b] T. Huus and Č. Zupančič, Kgl. Danske Videnskab. Selsk., Mat.-fys. Medd. **28**, 1 (1953); C. L. McClelland and C. Goodman, Phys. Rev. **91**, 760 (1953).
[3c] A. Bohr and B. Mottelson, Kgl. Danske Videnskab. Selsk., Mat.-fys. Medd. **27**, 16 (1953).
[4] J. Schwinger, Phys. Rev. **75**, 898 (1949).

A trial shows that the observations on gold do not fit unless it is assumed that the first minimum in the cross section expected theoretically is filled in by experimental inaccuracy, inelastic processes (Sec. 2), quadrupole moment effect (Sec. 6), or by higher order corrections to the Born approximation (Sec. 1). Even assuming that such a fill-in occurs, the rest of the experimental curve can only be fitted with a radius of about 4.7×10^{-13} cm, which is substantially smaller than that given by the usual expression $1.4\times10^{-13}A^{\frac{1}{3}}$ cm. Similar poor fits are obtained with the other elements.

The same technique was used to attempt a fit of the experiments with charge distributions that are uniform over most of the radius of the nucleus and rounded at the edge. If the usual radius is assumed, these predict diffraction minima and maxima that are not observed, as in the case of the sharp-edged uniform distribution. On the other hand, if the radius is assumed small enough to push the first diffraction minimum out to larger angles than are covered by the observations, the theoretically predicted small angle portion of the curve is too flat to agree with experiment. With sufficient rounding, the latter difficulty disappears; for example, the observations on gold can be fitted well with a charge distribution proportional to $[1+(R/a)^4]^{-1}$, where $a=3.3\times10^{-13}$ cm, but not with a charge distribution proportional to $[1+(R/a)^6]^{-1}$.

With charge distributions for which $F(q)$ has a simpler analytic form, a comparison with experiment can sometimes be achieved by plotting suitable functions of G and q against each other so that a straight line results when the experiments agree with the assumed form for $F(q)$. Four such forms are as follows:

$$\rho(R)=\rho_0\exp[-(R/a)^2];\quad F(q)=\pi^{\frac{3}{2}}\rho_0a^3\exp[-(qa/2)^2]. \tag{8}$$

$$\rho(R)=\rho_0e^{-R/a};\quad F(q)=8\pi\rho_0a^3/(1+q^2a^2)^2. \tag{9}$$

$$\rho(R)=\rho_0[1+(R/a)]e^{-R/a};\quad F(q)=32\pi\rho_0a^3/(1+q^2a^2)^3. \tag{10}$$

$$\rho(R)=\rho_0a^4/(a^2+R^2)^2;\quad F(q)=\pi^2\rho_0a^3e^{-qa}. \tag{11}$$

To fit Eq. (8), we plot G against q^2 on semilog graph paper; to fit Eq. (9), we plot $G^{-\frac{1}{2}}$ against q^2 on ordinary paper; to fit Eq. (10), we plot $G^{-\frac{1}{3}}$ against q^2 on ordinary paper; and to fit Eq. (11), we plot G against q on semilog paper. In each case, a straight line results if the fit is perfect, and the corresponding value of a is easily obtained.

A preliminary plot of G against q or q^2 on semilog paper shows that the experimental data for tantalum at 150 Mev and for gold and lead at 125 Mev can be superposed within the experimental errors for the separate elements by vertical translation (adjustment of the absolute magnitude of the scattering at some angle, which has not been measured). This is not surprising, since the values of $A^{\frac{1}{3}}$ for these three elements spread over a range of less than 5 percent. When all three elements are plotted together, it is found that a Gaussian charge distribution, Eq. (8), does not give a very good straight line. If a straight line is fitted to the whole curve, the value of a can lie between 3.1 and 3.6 (all lengths are expressed in units of 10^{-13} cm). The small-angle data are best fitted by $a=3.7$, and the large-angle data by $a=2.9$. If a Gaussian charge distribution is peaked enough (small enough a) at small R to fit the large-angle data, it falls off too rapidly at large R to give enough small-angle scattering; conversely, if it is spread out enough (large enough a) at large R to fit the small-angle data, it is too flat at small R to give enough large-angle scattering. The root-mean-square radius of the charge distribution for the Gaussian form is $R_s=(\frac{3}{2})^{\frac{1}{2}}a=1.224a$, so that R_s lies between 3.6 and 4.5 in this case.

The exponential charge distribution, Eq. (9), yields a fairly good straight line with $a=2.0$ (see Fig. 1), It is difficult to gauge the extreme values of a that are consistent with the experiments, because of the compression of the data that occurs in going from $\sigma(\theta)$ to $G^{-\frac{1}{2}}$. However, it is probably safe to say that a must lie between 1.6 and 2.9 on the basis of the present data. In this case, $R_s=(12)^{\frac{1}{2}}a=3.46a$, so that R_s lies between 5.5 and 10.0, with the best fit occurring at 6.9. The modified exponential charge distribution, Eq. (10), which has zero slope at the origin, also yields a straight line with $a=1.3$, and extreme values of 1.1 and 1.6. Here, $R_s=(18)^{\frac{1}{2}}a=4.24a$, so that R_s lies between 4.7 and 6.8, with the best fit occurring at 5.5. Finally, the

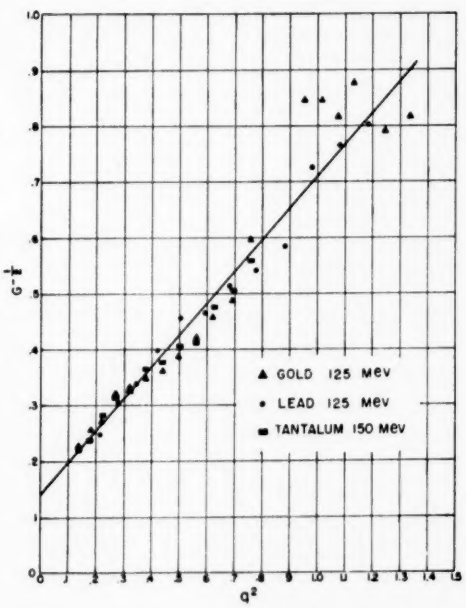

FIG. 1. Plot of $G^{-\frac{1}{2}}$ against q^2 (q in units of 10^{13} cm^{-1}), where G is the experimental form factor and $\hbar q$ is the momentum transfer. A straight line implies that the nuclear charge density has the form $\rho(R)=\rho_0e^{-R/a}$. The line corresponds to $a=2.0\times10^{-13}$ cm.

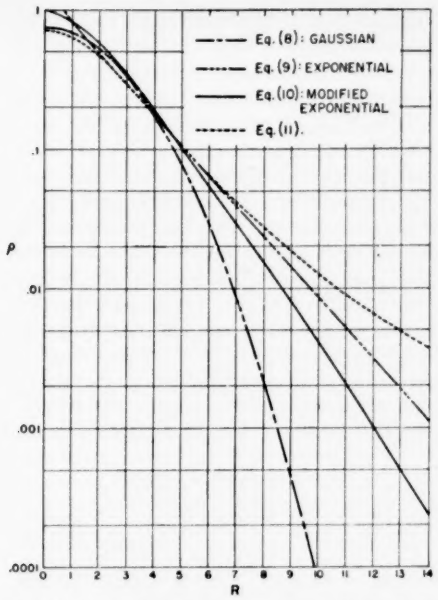

FIG. 2. Nuclear charge densities ρ computed from Eqs. (8), (9), (10), and (11) with optimum values of a. The last three are in good agreement between $R=2$ and $R=6$ (in units of 10^{-13} cm), but the first only agrees between $R=2$ and $R=4$.

charge distribution, Eq. (11), can be fitted well with $a=3.9\pm0.5$; because of its long tail, this distribution is rather unrealistic, and indeed R_s is infinite in this case.

The variety of shapes of charge distributions that fit the experiments about equally well suggests that only certain features of $\rho(R)$ are significant in this respect. This is confirmed when the above four charge densities are plotted against R on semilog graph paper, each with the optimum value of a. If the curves are translated vertically with respect to each other, it is found that Eqs. (9), (10), and (11) can be made to superpose within 15 percent over the region from $R=2$ to $R=6$ (see Fig. 2). The Gaussian distribution, Eq. (8), with $a=3.3$ can, however, only be fitted with the other three between $R=2$ and $R=4$. This suggests that the range of q covered in the experiments, from $q=0.37$ to $q=1.1$ (in units of 10^{13} cm^{-1}) is only sufficient to determine the shape of the nuclear charge distribution between $R=2$ and $R=6$. Very roughly and qualitatively, we can say that experiments with momentum transfers between $\hbar q_1$ and $\hbar q_2$ explore the shape of the charge distribution at distances between $R_2=2.2/q_2$ and $R_1=2.2/q_1$ from the center of the nucleus, provided that there is no anomalous behavior of $\rho(R)$ elsewhere.

4. ELASTIC SCATTERING FROM BERYLLIUM

The more limited experimental data on beryllium[1] at 125 Mev can be fitted well with any of the four charge distributions, Eqs. (8) through (11). The results are as follows:

$$\begin{aligned}
&\text{Eq. (8):} \quad a=1.8\ \pm0.1, \quad R_s=2.2\pm0.1;\\
&\text{Eq. (9):} \quad a=0.74\pm0.03, \quad R_s=2.7\pm0.1;\\
&\text{Eq. (10):} \quad a=0.55\pm0.01, \quad R_s=2.3\pm0.04;\\
&\text{Eq. (11):} \quad a=0.91\pm0.04, \quad R_s=\infty.
\end{aligned}$$

As with the heavier elements, Eqs. (10), (9), and (11) yield increasing values of a, and Eq. (9) gives a larger R_s than Eq. (10).

5. ELASTIC SCATTERING FROM DEUTERIUM

When Eq. (2) is applied to deuterium, it must be remembered that the ground state wave function is a mixture of $^3S_1$ and $^3D_1$ and is threefold degenerate. We write it[5]

$$\psi_m=(4\pi)^{-\frac{1}{2}}r^{-1}(u+8^{-\frac{1}{2}}wS_{12})\chi_m, \quad m=0,\pm1,$$
$$S_{12}=3r^{-2}(\boldsymbol{\sigma}_1\cdot\mathbf{r})(\boldsymbol{\sigma}_2\cdot\mathbf{r})-(\boldsymbol{\sigma}_1\cdot\boldsymbol{\sigma}_2), \tag{12}$$

where χ_m is a triplet spin function. The normalization is such that

$$\int_0^\infty (u^2+w^2)dr=1. \tag{13}$$

Because of the degeneracy, the squared matrix element on the left side of Eq. (2) must be replaced by

$$\tfrac{1}{3}\sum_m\sum_{m'}\left|\int\psi_{m'}{}^*e^{\frac{1}{2}i\mathbf{q}\cdot\mathbf{r}}\psi_m d\tau\right|^2. \tag{14}$$

The factor $\frac{1}{2}$ in the exponent arises because the proton coordinate is half the relative coordinate that appears in Eq. (12). Equation (14) may be reduced to

$$\left[\int_0^\infty (u^2+w^2)j_0(\tfrac{1}{2}qr)dr\right]^2 + \left[\int_0^\infty (2uw-2^{-\frac{1}{2}}w^2)j_2(\tfrac{1}{2}qr)dr\right]^2, \tag{15}$$

where

$$j_0(z)=z^{-1}\sin z, \quad j_2(z)=(3z^{-3}-z^{-1})\sin z-3z^{-2}\cos z$$

are spherical Bessel functions.

For use in connection with the next section, the expression for the quadrupole moment of the deuteron is quoted here[5]

$$Q=(200)^{-\frac{1}{2}}\int_0^\infty (2uw-2^{-\frac{1}{2}}w^2)r^2dr. \tag{16}$$

6. EFFECT OF NUCLEAR ELECTRIC QUADRUPOLE MOMENT

A nucleus that possesses an electric quadrupole moment is somewhat distorted from spherical shape, and we might expect that even if the charge distribution

[5] W. Rarita and J. Schwinger, Phys. Rev. **59**, 436 (1941).

had a sharp edge, this edge would be effectively fuzzed out because the observations average the scattering produced by nuclei with all possible orientations.

In dealing with elastic scattering from a heavy nucleus, it is sufficient for a discussion of quadrupole moment effects to assume a charge distribution

$$\rho(\mathbf{R})=\rho_0(R)+\rho_2(R)P_2(\cos\theta), \tag{17}$$

where θ is the angle between the vector $\mathbf{R}$ and the nuclear axis, and $P_2(\mu)=\frac{1}{2}(3\mu^2-1)$ is a Legendre polynomial. The electric quadrupole moment measured with respect to an axis fixed in space that makes an angle θ' with the nuclear axis is

$$Q(\theta')=Z(8\pi/5)P_2(\cos\theta')\int_0^\infty \rho_2(R)R^4dR. \tag{18}$$

Equation (18) is classical, and from it we want to obtain an expression for the quadrupole moment Q, which can be related to the quantum analog of Eq. (18)[6]

$$Q(m)=\frac{3m^2-I(I+1)}{I(2I-1)}Q, \tag{19}$$

where I is the total angular momentum of the nucleus, and m is its component along the axis fixed in space. We could simply equate the maximum value $Q(0)$ of Eq. (18) to the maximum value $Q(I)$ of Eq. (19). However, a better comparison in the case of the deuteron (see below) is obtained if we equate the mean square computed from Eq. (18) by integrating over θ', to the mean square computed from Eq. (19) by summing over m. The result is

$$Q=A_IZ(8\pi/5)\int_0^\infty P_2(R)R^4dR, \tag{20}$$

where $A_1=(1/10)^{\frac{1}{2}}$, $A_{3/2}=(1/5)^{\frac{1}{2}}$, $A_2=(2/7)^{\frac{1}{2}}$, $A_{5/2}=(5/14)^{\frac{1}{2}}$, $A_3=(5/12)^{\frac{1}{2}}$, $A_{7/2}=(7/15)^{\frac{1}{2}}$, $\cdots A_\infty=1$.

In calculating the scattering, we make use of the fact that the period of rotation of the nucleus is large in comparison with the transit time of a fast electron across the nucleus. Thus, the form factor calculated from Eq. (3) refers to a particular orientation of the nucleus with respect to $\mathbf{q}$. The scattering, which is proportional to F^2, must then be averaged over all orientations of the nucleus. It is easily shown that

$$\langle F^2(q)\rangle_{\text{Av}}=16\pi^2\left[\int_0^\infty \rho_0(R)j_0(qR)R^2dR\right]^2 + (16\pi^2/5)\left[\int_0^\infty \rho_2(R)j_2(qR)R^2dR\right]^2, \tag{21}$$

which agrees with Eq. (4) if $\rho_2=0$.

[6] J. M. Blatt and V. F. Weisskopf, *Theoretical Nuclear Physics* (John Wiley and Sons, Inc., New York, 1952), p. 28.

It is interesting to compare Eqs. (17), (20), and (21) with the corresponding Eqs. (13), (16), and (15) for the deuteron (Sec. 5), when it is remembered that $\rho(R)$ is normalized to unit volume integral. We note that $\mathbf{R}=\frac{1}{2}\mathbf{r}$; then if $4\pi\rho_0R^2dR$ is identified with $(u^2+w^2)d\mathbf{r}$, and $(16\pi^2/5)^{\frac{1}{2}}\rho_2R^2dR$ is identified with $(2uw-2^{-\frac{1}{2}}w^2)d\mathbf{r}$, the normalization of $\rho(\mathbf{R})$ in Eq. (17) agrees with Eq. (13), (21) agrees with (15), and (20) agrees with (16).

We can now see under what circumstances the second term on the right side of Eq. (21) can fill in the first diffraction minimum of the first term, that is predicted by a sharp-edged uniform charge distribution. We assume that $\rho_0(R)=\rho_0$, a constant, out to $R=R_0$, and is zero for larger values of R. We also assume, as is justified if the quadrupole moment or the eccentricity is not too large, that $\rho_2(R)=B\delta(R-R_0)$. Then B can be expressed in terms of Q from Eq. (20):

$$Q=A_IZ(8\pi/5)BR_0^4.$$

It is convenient to define the nuclear eccentricity[7] $\eta\equiv 5Q/4R_0^2Z$, in which case Eq. (21) can be written

$$\langle F^2(q)\rangle_{\text{Av}}=9(\sin qR_0-qR_0\cos qR_0)^2/(qR_0)^6 + 4\eta^2j_2^2(qR_0)/5A_I^2, \tag{22}$$

when it is remembered that $4\pi\rho_0R_0^3/3=1$.

The first term on the right side of Eq. (22) vanishes when $qR_0\cong 4.5$, and has its second maximum at $qR_0\cong 6$, where it is equal to 7.0×10^{-3}. At the zero point of the first term, the second term is equal to $0.038(\eta/A_I)^2$. We can say that the zero predicted when the quadrupole moment is neglected would be difficult to observe as a minimum if the second term had there a value comparable with the value of the first term at its second maximum, that is, if $0.038(\eta/A_I)^2\cong 7.0\times10^{-3}$, or if $(\eta/A_I)\cong 0.43$. For Ta^{181}, $\eta=0.14$ (one of the largest values known) and $I=7/2$, so that $(\eta/A_I)=0.205$. For Au^{197}, $I=3/2$, and the quadrupole moment has not been measured; however, it would have to be extremely large to be effective in the present connection, and this seems unlikely from other considerations. Three-quarters of normal lead consists of the isotopes Pb^{208} ($I=0$) and Pb^{207} ($I=\frac{1}{2}$), neither of which can have a quadrupole moment. It seems probable, therefore, that a nuclear electric quadrupole moment cannot account for the smoothness of the observed scattering curves.

7. CONCLUDING REMARKS

The picture of the nuclear charge distribution arrived at on the basis of the Born approximation is radically different from that which has been commonly accepted until now.[8] However, such centrally peaked, smoothly tapering charge distributions are not necessarily inconsistent with information obtained from other types of

[7] Reference 6, p. 26.

[8] A slight indication of a central charge concentration was obtained from the scattering of 15.7-Mev electrons, by Lyman, Hanson, and Scott [Phys. Rev. **84**, 626 (1951)].

experiments. As an example, any experiment that measures the average value of the difference between the actual electrostatic potential and that of an equal point charge, measures in effect the root-mean-square radius R_s of the charge distribution. For a uniform charge distribution of radius R_0, $R_s=(3/5)^{\frac{1}{2}}R_0=0.775R_0$. This gives R_s values ranging from 6.14 for tantalum to 6.42 for lead, if the usual expression $R_0=1.4A^{\frac{1}{3}}$ is used; for beryllium, $R_s=2.25$. It is apparent from Sec. 3 that the heavy elements are consistent with this if either Eq. (9) or Eq. (10) is used. In the case of beryllium (Sec. 4), the values found from Eqs. (8) and (10) are consistent with that obtained from the $A^{\frac{1}{3}}$ rule, and Eq. (9) yields a somewhat larger value; for such a light nucleus, the $A^{\frac{1}{3}}$ rule probably underestimates the radius.

The nuclear Coulomb energy may be calculated for each of the charge distributions considered here. It is characterized by a length, which is equal to the ratio of the square of the total charge to the Coulomb energy. This length is $(5/3)R_0$ for a uniform charge distribution of radius R_0, $(2\pi)^{\frac{1}{2}}a$ for the Gaussian distribution (8), $(32/5)a$ for the exponential distribution (9), $(512/63)a$ for the distribution (10), and $(\pi/2)a$ for the distribution (11). With the optimum values for a, the distributions (9) and (10) are 5 and 14 percent, respectively, higher than the Coulomb energy calculated with $R_0=1.4A^{\frac{1}{3}}$, while the other two distributions give about twice as large a Coulomb energy. Thus, as with the root-mean-square radius, the more likely charge distributions (9) and (10) are in satisfactory agreement with earlier results.

It is important also to realize that electron scattering and nucleon scattering measure quite different properties of a nucleus. We have assumed here that electron scattering is determined by the electric charge density, which is equivalent to assuming that there is no appreciable non-electric interaction of electrons and nuclear matter. Since lower energy scattering experiments are in good agreement with this assumption,[9] any anomalous interaction would have to be strongly momentum-dependent in order to be significant in the present situation, and we suppose that such an interaction does not exist. According to present ideas, the electric charge density is proportional to the density of protons, since meson charges are expected to average to zero. Nucleon scattering, on the other hand, is determined by the nucleonic potential, which is believed to depend on the nucleon density but need not be proportional to it. Indeed, it is quite possible that this potential is proportional to the density only for quite low densities, and that for higher densities the potential increases less rapidly than linearly.[10] In this case, the potential that is effective in nucleon scattering will be more nearly uniform and have a sharper boundary than the electric charge density, and hence make the nucleus appear more like a uniform sphere. This might explain the agreement between the usual R_0 and the nuclear radius measured from fast neutron scattering and alpha-particle decay, and also the very striking diffraction patterns recently observed in the scattering of 22-Mev protons by various elements.[11]

It is, of course, possible that exact calculations will fit the experimental observations on electron scattering with charge distributions that are less peaked at the center and fall off more sharply at the edge of the nucleus. Such calculations are now under way here, and will be reported in the near future by D. R. Yennie, D. G. Ravenhall, and R. N. Wilson.

It is a pleasure to acknowledge numerous discussions with Professor R. Hofstadter on the experimental information and his treatment of it. The writer is also indebted to Professors R. F. Christy, E. Guth, W. E. Lamb, E. Teller, and C. H. Townes for helpful conversations, and to Mr. K. G. Dedrick for aid with one aspect of the calculations.

[9] See reference 8, and Buechner, Van de Graaff, Sperduto, Burrill, and Feshbach, Phys. Rev. **72**, 678 (1947).

[10] L. I. Schiff, Phys. Rev. **84**, 1 (1951); B. J. Malenka, Phys. Rev. **86**, 68 (1952); W. E. Thirring, Z. Naturforsch. **7a**, 63, 279 (1952).

[11] B. L. Cohen and R. V. Neidigh, Phys. Rev. (to be published). The author is indebted to Dr. A. M. Weinberg for informing him of these results prior to publication.

Magnetic Moments of Neutron and Proton

F. J. BELINFANTE
Purdue University, Lafayette, Indiana
(Received May 18, 1953)

After a discussion of the importance of results recently found by Sachs, some weaknesses of his theory are pointed out, and a contribution to the nucleon magnetic moment from the state with two-pion cloud in an S-state is calculated. A proposal of Sugawara to include admixtures of states with a one-pion cloud around a spin-$\frac{3}{2}$ ("baryon") core is criticized, and the contribution of such states to the nucleon magnetic moments is calculated. It is discussed what value might be taken for the magnetic moment of such "baryon" core.

1. INTRODUCTION

IN a recent paper, Sachs[1] has shown the importance of the two-pion admixture in the nucleon wave function for the explanation of the magnetic moments of the neutron and the proton. As a special example he considered a model consisting of 91.0 percent bare nucleon core (called "nucleore" by him) and 9.0 percent this nucleore accompanied by two pions each in a p state forming together a P state with "square" radial distribution.[2] In this case, the contributions to the neutron magnetic moment were[3] -0.020 from nucleore moment in the 9 percent two-pion state, -0.133 from pion orbits in the 9 percent two-pion state, and -1.792 from cross terms between two-pion and no-pion states; total -1.945 for the neutron.

Applying the mirror property to this model, we find for the corresponding proton state: $+0.910$ from nucleore moment in the 91 percent no-pion state, -0.010 from nucleore moment in the 9 percent two-pion state, $+0.133$ from pion orbits in the 9 percent two-pion state, and $+1.792$ from cross terms between two-pion and no-pion states; total $+2.825$ for the proton. These figures show the importance of the cross terms between two-pion and no-pion states arising from the pion-pair creation and annihilation terms in the expression for the magnetic moment of a pion field.[1]

Sachs' calculations neglect any separation of the nucleore from a fixed point chosen as the origin, and they neglect relativistic effects. This means that the large components of the Dirac wave-function of the nucleore are assumed to be s states. The p state small components are then neglected. Sachs makes it plausible that only pions in p states should be expected. His argument is clearly based on assumption of an interaction between nucleores and pions linear in the latter and coupling among each other nucleore states with s-state large components but not necessarily with the same spin. An example of such interaction is a single pseudo-vector coupling without further interactions. The interaction between pions and nucleores proposed by Foldy and collaborators[4] is of course of a different type: It can be formulated as a single linear coupling between nucleores and pions; but this pseudoscalar coupling connects states with s-state large components just as well (with comparable matrix element) with states with p-state large components, under emission of pions in s states.[5] On the other hand, after Foldy's transformation to pseudo-vector coupling there are all kinds of non-linear terms,[4,6] and there is no clear reason for restriction to p-state pions either. Therefore it may be that Sachs' nucleon model is a too simple one, even if the special assumptions leading him to the numerical values mentioned above are dropped. Nevertheless Sachs' results are interesting as they show that only a moderate admixture of a two-pion state (about 30 percent of the wave function) suffices for explanation of the magnetic moments of proton and neutron.

Sachs himself points out that the agreement[7] of his[3] value (-1.945) with the experimental magnetic moment (-1.910) of the neutron is fortuitous, as his assumptions (29)–(30) on the absence of pion clouds in S states, of one-pion states, and of two-pion P states antisymmetric in the two-pion radial function, as well as his assumption of a square form of the two-pion P-state symmetric radial function, are just one out of many ways in which the experimental facts could be explained in terms of the parameters of his theory.

In this connection it should be pointed out that in Sachs' general expression for the neutron magnetic moment (Eqs. (27)–(28)) a term

$$P_0^-(2)=P_0^-(2,\,\alpha)=\tfrac{2}{3}P_0(2,\,\alpha)$$

is missing. This is due to the fact that Sachs overlooked

[1] R. G. Sachs, Phys. Rev. **87**, 1100 (1952).

[2] By "square" radial distribution Sachs understands a sharp cutoff of the radial function at some fixed maximum value for the distance of the two pions from the nucleore frozen in the origin.

[3] In Sachs' formulas we substitute $\mathfrak{M}/\mu=6.64_2$ and $I_1(8)=1$. We obtain $\mathfrak{M}_n=-1.94_5$, as contrasted to the figure -1.93 given by Sachs himself. The 91 percent to 9 percent mixture was adjusted by Sachs to the value 0.880 of $\mathfrak{M}_n+\mathfrak{M}_p$. All magnetic moments were measured in nuclear magnetons assumed to be practically identical with nucleore magnetons.

[4] L. L. Foldy, Phys. Rev. **84**, 168 (1951); Berger, Foldy, and Osborn, Phys. Rev. **87**, 1061 (1952).

[5] In this case the $\psi^\dagger\beta\gamma_0\psi$-interaction is purely relativistic, and Sachs' nonrelativistic approximation cannot be maintained. This necessitates explicit introduction of the space function for the nucleore, and thus Sachs' selection rule (3) is broken; thence also his Eq. (11).

[6] G. Wentzel, Phys. Rev. **86**, 802 (1952).

[7] In view of the effects neglected, such as states with more than two pions, recoil of nucleore, difference in mass between charged and neutron pions in applying charge-independence, etc., accuracy cannot be expected, so that $1.945\approx1.910$.

the contribution $\langle N=2, L=0|\mathfrak{M}_n|N=2, L=0\rangle$ to the neutron magnetic moment arising from the magnetic moment of the proton-nucleore in states with pion charge $C=-1$ in an S-state two-pion cloud. In this case, the proton-nucleore spin has always the direction of the total neutron spin, so that it contributes $P_0^-(2)$ nucleore magnetons, where $P_0^-(2)$ according to Sachs' notation is the probability of the state with a two-pion single-negative S-state pion cloud. In his special numerical example discussed above, this forgotten term drops out anyhow on account of the assumption expressed by Sachs' Eq. (29).

2. POSSIBLE NECESSITY OF EXTENDING SACHS' THEORY

In a complete theory one cannot just postulate values for the probabilities of the various nucleore-pion cloud states building up the nucleon wave function, or for the various overlap integrals and other radial integrals entering the theory; but one should take values for such quantities derived from some kind of meson theory, and then it should be hoped that these, on substitution in Sachs' formulas,[8] will yield the experimental values for the nucleon magnetic moments. Therefore it is worthwhile to consider what other terms beside those discussed by Sachs might possibly have to be taken into account in order to obtain such agreement.

It was already mentioned previously that it may be necessary to consider s-state pions, which means taking into account the "recoil" (the coordinate function) of the nucleore. Even if this recoil is neglected, s-state pions may be emitted in pairs by the interaction terms appearing in the Hamiltonian after Foldy's transformation.[4] Also there is no reason why states with more than two pions should not be important.

Further, there may be some reason to suspect the possibility of admixture of states in which the pion cloud surrounds a nuclear particle of a mass slightly more than the nucleon mass (maybe between 2350 and 2400 m_e), of ordinary spin $\frac{3}{2}$, and of isobaric spin $\frac{3}{2}$. For the sake of brevity in discussion, we have called such particule a *baryon*.[9] The possibility of its existence has been suggested by the results of scattering experiments and explanations proposed for these results by several authors.[10] It was recently proposed by Sugawara[11] that such baryon-pion states be incorporated in the calculation of the magnetic moment of the nucleon.

While it is possible that this suggestion makes some sense, Sachs has shown the incorrectness of Sugawara's further statement that the nucleon magnetic moments observed could not be explained simply by second-order pion interaction without consideration of baryon states.[11]

For the rest, we do not agree with Sugawara's way of calculating these magnetic moments, simply adding the magnetic moments of the constituent particles in each state as in the calculation of a Paschen-Back effect, without considering the fact that (like in the anomalous Zeeman effect) the interactions between these constituent particles (between the nucleore spin and pion orbital moments) are much stronger than the individual interactions of those particles with the external magnetic field. Also, Sugawara's method never takes into account the cross terms between zero and two pions, which Sachs has shown to be so important. We should therefore use Sachs' method to calculate the contribution of an admixture of a (baryon+one pion)-state to the magnetic moments of a neutron and of a proton. This is done in the next chapter.

3. BARYON-PION CONTRIBUTION TO NUCLEON MAGNETIC MOMENTS

We shall follows Sachs in assuming the pion to be in a p state. We use a notation explained earlier,[9,12] according to which states of "spin" (orbital angular momentum, spin, or isobaric spin) J with z-component J_z are indicated by $[J, J_z]$. Subscript 1 will indicate the nucleore or baryon core; subscript 2 will here indicate the pion. In our case, $[\frac{1}{2}, \pm\frac{1}{2}]_1$, $[\frac{3}{2}, \pm\frac{1}{2}]_1$, and $[\frac{3}{2}, \pm\frac{3}{2}]_1$ may be considered as ordinary spin functions, and $[1, 0]_2$ and $[1, \pm 1]_2$ to be normalized spherical harmonics $Y_1^m(\theta, \varphi)$ for the pion orbit, with the sign convention used by Rojansky.[13] The isobaric spin functions we shall here distinguish from these space and spin functions by enclosing them between boldface braces $\{\ \}$.

For a baryon-pion state of total angular momentum $\frac{1}{2}$ along the positive z axis, and with isobaric spin $\frac{1}{2}$ in the $-\zeta$ direction as for a neutron, the wave function is found from the tables **(1) × (3/2)** in the Appendix of reference 9:

$$\begin{aligned}\Psi_n^{+\frac{1}{2}} &= f_{12}[\tfrac{1}{2}, \tfrac{1}{2}]_{12}\{[\tfrac{1}{2}, -\tfrac{1}{2}]_{12}\} = \\ &f_{12}[[\tfrac{3}{2}, -\tfrac{1}{2}]_1[1, 1]_2\sqrt{\tfrac{1}{6}} - [\tfrac{3}{2}, \tfrac{1}{2}]_1[1, 0]_2\sqrt{\tfrac{1}{3}} + \\ &[\tfrac{3}{2}, \tfrac{3}{2}]_1[1, -1]_2\sqrt{\tfrac{1}{2}}] \times \{[\tfrac{3}{2}, -\tfrac{3}{2}]_1[1, 1]_2\sqrt{\tfrac{1}{2}} - \\ &[\tfrac{3}{2}, -\tfrac{1}{2}]_1[1, 0]_2\sqrt{\tfrac{1}{3}} + [\tfrac{3}{2}, \tfrac{1}{2}]_1[1, -1]_2\sqrt{\tfrac{1}{6}}\}. \quad (1)\end{aligned}$$

Here, f_{12} is a radial wave function of the baryon-pion system.

Since we don't consider two-pion states with the baryon,[14] we need not consider here the pion-pair terms in the pion magnetic moment. We shall further assume that the baryon magnetic moment is proportional to $\mathbf{S}$=its spin angular momentum in units $\hbar$,

[8] Corrected by the addition of $P_0^-(2)=\frac{3}{4}P_0(2, \mathfrak{C})$. See the introduction.

[9] F. J. Belinfante, Phys. Rev. **92**, 145 (1953).

[10] K. A. Brueckner, Phys. Rev. **86**, 106 (1952); G. S. Janes and W. L. Kraushaar, Phys. Rev. **90**, 341 (1953); B. T. Feld, Phys. Rev. **90**, 342 (1953); G. Wentzel, Phys. Rev. **86**, 437 (1952).

[11] M. Sugawara, Progr. Theoret. Phys. (Japan) **8**, 549 (1952).

[12] While in reference 9 this notation was used for isobaric spin functions only, we shall use it here for angular momenta as well.

[13] V. Rojansky, *Introductory Quantum Mechanics* (Prentice-Hall, Inc., New York, 1938), p. 414. Compare Eq. (A.1) of the Appendix of reference 9.

[14] This approximation made by Sugawara is feasible insofar as cross terms to no-pion states are here impossible, since conservation of isobaric spin forbids (baryon+no pion)-states.

as well as to $(t_\xi+\frac{1}{2})$ = its charge (q) in units e:

$$\mathfrak{M}_b(\text{in nuclear magnetons})=k(t_\xi+\tfrac{1}{2})\mathbf{S}. \quad (2)$$

The contribution to the z component of the magnetic moment of the neutron by the admixture $\Psi_n^{+\frac{1}{2}}$ in the neutron wave function is then given by the matrix element of the operator,

$$k(t_\xi+\tfrac{1}{2})S_z+(\mathfrak{M}/\mu)L_zC, \quad (3)$$

between $\Psi_n^{+\frac{1}{2}}$ and $\Psi_n^{+\frac{1}{2}}$, where $\mathfrak{M}/\mu$ is the ratio of proton mass to pion mass, where $\mathbf{L}$ is the orbital angular momentum of the pion, and C is its charge in units e. By $S_z[s, m_s]_1=m_s[s, m_s]_1$, $L_z[l, m]_2=m[l, m]_2$, $t_\xi\{[l, m_t]_1\}=m_t\{[l, m_t]_1\}$, $C\{[T, m_T]_2\}=m_T\{[T, m_T]_2\}$, this matrix element is easily found to be

$$\delta\mathfrak{M}_n=-P(b, 1)[(5/2)k+\mathfrak{M}/\mu]/9, \quad (4)$$

where

$$P(b, 1)=\int|f_{12}|^2r^2dr \quad (5)$$

is the probability of the (baryon+one pion)-state. While (4) is to be added to Sachs' expression (27) or (28) increased by $\frac{2}{3}P_0(2, \alpha)$, (see footnote 8), at the same time $P(b, 1)$ is to be included in P_1 in the expression $(1-P_0-P_1)$ occurring in Sachs' Eqs. (27)–(28).

Similarly, the corresponding admixture,

$$\begin{aligned}\Psi_p^{+\frac{1}{2}} \;=\; & f_{12}[\tfrac{1}{2}, \tfrac{1}{2}]_{12}\{[\tfrac{1}{2}, \tfrac{1}{2}]_{12}\} \;= \\ & f_{12}[[\tfrac{3}{2}, -\tfrac{1}{2}]_1[1, 1]_2\sqrt{\tfrac{1}{6}} \;- \\ & [\tfrac{3}{2}, \tfrac{1}{2}]_1[1, 0]_2\sqrt{\tfrac{1}{3}} \;+ \\ & [\tfrac{3}{2}, \tfrac{3}{2}]_1[1, -1]_2\sqrt{\tfrac{1}{2}}] \;\times \\ & \{[\tfrac{3}{2}, -\tfrac{1}{2}]_1[1, 1]_2\sqrt{\tfrac{1}{6}} \;- \\ & [\tfrac{3}{2}, \tfrac{1}{2}]_1[1, 0]_2\sqrt{\tfrac{1}{3}} \;+ \\ & [\tfrac{3}{2}, \tfrac{3}{2}]_1[1, -1]_2\sqrt{\tfrac{1}{2}}\}, \end{aligned} \quad (6)$$

to the proton state with spin in positive z direction contributes to the z component of the magnetic moment of the proton an amount given by the matrix element of the same operator (3) between $\Psi_p^{+\frac{1}{2}}$ and $\Psi_p^{+\frac{1}{2}}$. The amount of this contribution is

$$\delta\mathfrak{M}_p=+P(b, 1)[10k+\mathfrak{M}/\mu]/9. \quad (7)$$

The effect of all this on Sachs' Eq. (22) for $\mathfrak{M}_n+\mathfrak{M}_p$ is the following. In the derivation of (22), we must include $P(b, 1)$ in P_1 (= probability of P-state pion cloud) where we write $(1-P_0-P_1)$ for the probability of the no-pion state just above Sachs' Eq. (22); but we must *not* include $P(b, 1)$ in the contribution $-\frac{1}{3}P_1$ from the (nucleore+P-state pion cloud)-state. Instead, our two expressions (4) and (7) contribute to $\mathfrak{M}_n+\mathfrak{M}_p$. Thus, Sachs' Eq. (22) is replaced by

$$\begin{aligned}\mathfrak{M}_n+\mathfrak{M}_p=&\,1-(4/3)\{P_1(1)+P_1(2)\} \\ &-[1-(5k/6)]P(b, 1), \end{aligned} \quad (8)$$

where $P_1(N)$ = probability for a P-state N-pion cloud around a regular (spin-$\frac{1}{2}$) nucleore, and $P(b, 1)$ = probability for a P-state one-pion cloud around a baryon (other pion clouds around a baryon not considered).

4. THE MAGNETIC MOMENT OF THE BARYON CORE

In Eqs. (2), (4), and (7), the value of k would have to be taken from some theory of the properties of a baryon. Here, two different points of view are possible.

One is to consider the baryon itself to be a nucleoid,[9] that is, a compound particle consisting of an ordinary nucleore and a pion cloud, like the excited states of the nucleore-pion system discussed by Pauli and Dancoff.[15] (Since Pauli and Dancoff did not succeed in explaining by their model the observed magnetic moments of nucleons, the question arises whether a value of k for a baryon calculated on the basis of such model could be trusted.)

Use of such compound baryon as the core in a certain admixture to a nucleon state makes sense only if the pion cloud inside the compound baryon is bound to the nucleore much stronger than the pion we assumed to surround the baryon. Thus our admixture would be a nucleoid state with "pions in layers" (some pions close to the core and one pion loosely bound at the outskirts of the nucleoid), and the internal pion shells in such state might be said to be "incomplete."[16] It does not seem probable that the ground state of a nucleoid would contain important admixtures of such kind.

Therefore Sugawara's suggestion of considering (baryon+pion)-admixtures to the nucleon ground state would seem rather meaningless, unless one decides to take a second point of view, according to which the baryon core is to be treated as a new elementary particle of spin $\frac{3}{2}$, different from a nucleore, even though reactions baryon+pion$\rightleftarrows$nucleon and baryon$\rightleftarrows$nucleon +pion may be allowed. This point of view seems to have been taken by Sugawara himself in so far as he postulated an *a priori* value for k in Eq. (2). Neglecting the difference in mass between nucleon and baryon, he chose $k=2$, by an unjustifiable analogy to the Thomas factor of spin-$\frac{1}{2}$ particles.

This value 2 postulated by Sugawara seems unreasonably high. For vector mesons of mass $\mathfrak{m}$ and charge q one finds a magnetic moment[17] $(qh/2\mathfrak{m}c)\mathbf{S}$, where $\mathbf{S}$ is the meson spin. Apart from the mass ratio, this corresponds to $k=1$ for vector mesons. As in the same sense we have $k=2$ for electrons, this seems to suggest $k=1/S$ in general for particles of spin $S\neq 0$.

[15] W. Pauli and S. M. Dancoff, Phys. Rev. **62**, 85 (1942).

[16] The word "incomplete" is used here loosely. Of course, as pions satisfy Einstein-Bose statistics, there is no such thing as a "complete" pion shell. We mean to say only that the internal shells have a total orbital angular momentum different from zero, which combines with the nucleore spin to a total angular momentum $\frac{3}{2}$, different from the nucleore spin. The same is true for the isobaric spin.

[17] Yukawa, Sakata, and Taketani, Proc. Phys.-Math. Soc. Japan **30**, 319 (1938); F. J. Belinfante, Physica **6**, 870 (1939).

Indeed it can be shown that, if the baryon core would satisfy Fierz-Pauli's theory of spin-$\frac{3}{2}$ particles,[18] one finds $k=\frac{2}{3}$ for such particles.[19]

In conclusion we may say that, until there is some further experimental evidence that spin-$\frac{3}{2}$ particles really exist, there may be little reason for accepting Sugawara's suggestion at all. If the need of consideration of (baryon+pion)-states would arise, contributions from such states to the nucleon magnetic moment should be calculated by the methods outlined above, and more likely with the value $k=\frac{2}{3}$ than with $k=2$.

[18] M. Fierz and W. Pauli, Proc. Roy. Soc. (London) **A173**, 211 (1939).
[19] F. J. Belinfante, Phys. Rev. **92**, 994 (1953).

PHYSICAL REVIEW VOLUME 92, NUMBER 4 NOVEMBER 15, 1953

Intrinsic Magnetic Moment of Elementary Particles of Spin $\frac{3}{2}$

F. J. BELINFANTE
Purdue University, Lafayette, Indiana
(Received May 21, 1953)

Fierz-Pauli's theory of spin-$\frac{3}{2}$ particles has been reformulated in a manner somewhat resembling the usual formulation of Dirac's equation for the electron. The discussion is simplified by complete reduction of the representation of the spatial rotation and reflection group by the field. The dependent variables can then be expressed in terms of the spin-$\frac{3}{2}$ field. The magnetic moment and the gyromagnetic ratio of "bare" spin-$\frac{3}{2}$ particles of charge q and mass m are found to be $(qh/2mc)$ and $(q/3mc)$, respectively.

1. INTRODUCTION

IN a theory of the anomalous magnetic moments of nucleons, Sugawara[1] has recently tacitly assumed that the intrinsic magnetic moment of a spin-$\frac{3}{2}$, isobaric-spin-$\frac{3}{2}$ particle of slightly more than nucleon mass (a so-called *baryon*[2,3]) should be about six nuclear magnetons in its state of charge $2e$. Pauli and Dancoff's strong-coupling theory[4] of the excited states of the nucleoid[2] (=nucleore-pion system[5]) predicts a magnetic moment proportional to $(q-\frac{1}{2}e)/(j+1)$, which would make the total magnetic moment of a baryon of charge $2e$ (and with $j=\frac{3}{2}$) equal to $1.8\times$ the magnetic moment of a proton ($j=\frac{1}{2}$). However, the Pauli-Dancoff theory of the magnetic moments of nucleoids is not only not trustworthy, as shown by its prediction that the neutron magnetic moment would be opposite and equal to the proton magnetic moment, but probably it is not even applicable in a theory like Sugawara's, in which the nucleon is assumed to be part of its time a nucleore, part of its time a nucleore with a pion cloud, and part of its time a baryon core and pion(s). Such an assumption becomes rather improbable, if one does not at the same time assume the baryon (core particle) to be an elementary particle itself,[3] like the proton-nucleore, neutron-nucleore, and pions figuring in Sugawara's theory. That is, we would have to assume that there is such a thing as a "bare elementary particle" of spin $\frac{3}{2}$, into which a nucleore could be transformed under emission or absorption of a pion.

The "bare baryon" would then have an intrinsic magnetic moment of its own—like the proton and neutron as "nucleores" are supposed to have magnetic moments of 1 and 0 nucleore magnetons respectively. The question then arises whether the magnetic moment to be expected for such bare baryon would have so large a value as assumed by Sugawara. We have reasoned that this is unlikely, and that it seems more plausible to guess that the gyromagnetic ratio of a spin-$\frac{3}{2}$ particle of charge q and mass m will be $q/3mc$, and its intrinsic magnetic moment $qh/2mc$. (See reference 3.) It is the purpose of this paper to show[6] that this conjecture is correct, if for a "bare" particle of spin $\frac{3}{2}$ in interaction with an external electromagnetic field one assumes Fierz-Pauli's theory of such particles to be valid.[7]

2. FIELD COMPONENTS FOR ELEMENTARY PARTICLES OF SPIN $\frac{3}{2}$

For their Lorentz-covariant theory of particles of spin $\frac{3}{2}$ in interaction with a Maxwell field, Fierz and Pauli[7] formulated the field equations in a manifestly covariant form using spinor notation. The field has 16 complex components (not counting their conjugates). Between these 16 field components there are 8 relations ("subsidiary equations") not involving differentiation with respect to time, so that at some fixed initial time only eight field components can be chosen independently.

[1] M. Sugawara, Progr. Theoret. Phys. Japan **8**, 549 (1952). For a criticism of this theory see reference 3.
[2] F. J. Belinfante, Phys. Rev. **92**, 145 (1953).
[3] F. J. Belinfante, this issue Phys. Rev. **92**, 994 (1953).
[4] W. Pauli and S. M. Dancoff, Phys. Rev. **62**, 85 (1942).
[5] Nucleore=bare nucleon core; see R. G. Sachs, Phys. Rev. **87**, 1100 (1952).
[6] Without committing ourselves as to the value of Sugawara's suggestion. See also reference 3.
[7] M. Fierz and W. Pauli, Proc. Roy. Soc. (London) **A173**, 211 (1939).

Once the relativistic covariance of a theory has been established, it often has certain advantages[8] to drop covariant notation.[9] One reason for this is the special part taken by the time in solving problems using an ordinary Schrödinger equation with a Hamilton operator. Also, in canonical quantization one likes to distinguish "derived variables" from "canonical variables,"[10] and this requires selection of a time axis (or of a time-like unit vector n^μ, in Schwinger's terminology[11]).

A further most important advantage of dropping manifest covariance is the following. The transformation of the spinor components of the field form a (two-valued) representation of the complete Lorentz group (including spatial reflections); therefore, also of its subgroup of spatial rotations and reflections. While the representation of the Lorentz group by the pair of symmetrical 3-index spinors used by Fierz and Pauli is irreducible,[12] the representation of the subgroup of spatial rotations and reflections is not. Therefore, it is natural to group the sixteen components of the field together in the following fashion: (1) An *undor*,[13] ($\gamma_5\chi$ in Eq. (1)), that is, a pair of a Kramers spinor and spin-conjugate spinor,[14] together transforming like a Dirac electron wave function in Kramers representation,[13–14] in particular transforming into each other under spatial reflection;[15] this undor corresponds to Fierz-Pauli's spinors c^α and $d_{\dot\alpha}$; (2) another such pair of Kramers spinor and spin-conjugate spinor, (the undor $\gamma_5\eta$ below); and (3) an 8-component quantity, consisting of a pair of what one might call a "four-spinor" and a "spin-conjugate four-spinor" (forming the representation $\mathfrak{D}^{(\frac{1}{2})}$ of the spatial rotation group;[12] compare $Z_1\cdots Z_8$ in Eq. (1) below). Such complete reduction of the representation of the spatial group by the field separates the dynamical field components Z forming the spin-$\frac{3}{2}$ field, from the dependent field components χ and η transforming as fields of spin-$\frac{1}{2}$ particles, and thus reduces the equations of motion and the subsidiary equations to a form in which they are most easily handled.

For the details of Fierz-Pauli's theory we refer to their original publication.[7] If under spatial reflection $x, y, z, ct \rightarrow -x, -y, -z, +ct$ (thence $\mathbf{p}\rightarrow-\mathbf{p}$, $p_0\rightarrow+p_0$ for the momentum in vector notation, or $p_{\dot\beta}{}^\alpha\rightarrow-p_{\dot\alpha}{}^\beta$ in spinor notation) we assume Fierz-Pauli's spinor $d_{\dot\alpha}$ to transform into ϵc^α (with $\epsilon^4=1$, see reference 15), the invariance of their Lagrangian requires transformation of their c^α into $\epsilon d_{\dot\alpha}$, of their $a_{\dot\alpha}{}^{\beta\nu}$ into $-\epsilon b^\alpha{}_{\dot\beta\dot\nu}$, and of their $b^\alpha{}_{\dot\beta\dot\nu}$ into $-\epsilon a_{\dot\alpha}{}^{\beta\nu}$. After reduction of the six-component representation of the spatial rotation group by $a_{\dot\alpha}{}^{\beta\nu}(\equiv a_{\dot\alpha}{}^{\nu\beta})$, into a representation by quartet and doublet states (by a "four-spinor" and an ordinary (two-)spinor respectively), and similarly for $b^\alpha{}_{\dot\beta\dot\nu}$, we shall find it convenient to introduce linear combinations of the two-spinor $d_{\dot\beta}$ with the two-spinor representing the doublet part in $a_{\dot\alpha}{}^{\beta\nu}$. [Compare η_1 and η_2 in Eq. (1).] Then, for ensuring complete reduction with respect to spatial reflections, we should similarly combine c^β with the corresponding two-spinor part in $-b^\alpha{}_{\dot\beta\dot\nu}$. [See $-\eta_3$ and $-\eta_4$ in Eq. (1).] Following Van der Waerden's interpretation of the dotted and undotted spinor indices,[16] and using Kramers' representation[17] of Dirac wave functions or undors,[13] we can identify $d_{\frac{1}{2}}$, $d_{\frac{1}{2}}$ with the first two components of such undor, and c^1, c^2 with the third and fourth component of such undor. To be consequent, we should then alter Fierz and Pauli's definition of $\sigma^4=iI$ into $\sigma^4=-iI$. (This also affects the definition of the momentum spinor in terms of the momentum four-vector.) With our conventions, Fierz-Pauli's "rest-mass" terms $-\delta\kappa c^{*\dot\alpha}d_{\dot\alpha}+\kappa(-b^*)^{\dot\alpha}{}_{\dot\beta\nu}a_{\dot\alpha}{}^{\beta\nu}$ +conj. (with minus signs due to our lowering and raising of spinor indices in order to obtain a notation fitting our conventions) show a minus sign in front of the rest-mass term depending on the doublet wave function, but a plus sign in front of the terms $\kappa(-b)^*a$ depending on the quartet wave function. As the quartet terms are physically most important (containing the independent canonical variables), we want the latter to appear with a negative coefficient in the Lagrangian, as the mass term in the Dirac theory of electrons. Therefore, we now have to change the sign of the entire Lagrangian.

We shall now define the eight-component four-spinor pair Z and the two four-component undors (two-spinor pairs), by which we want to describe the field. The latter two undors we shall denote by $\gamma_5\chi$ and $\gamma_5\eta$,[18] where γ_5 is the Dirac matrix $i\gamma_1\gamma_2\gamma_3\gamma_0$, so that in the notation of footnote 17 in general $\boldsymbol{\alpha}=\gamma_5\boldsymbol{\sigma}$, and in

[8] Besides possible disadvantages.

[9] To some extent this has been done by Fierz and Pauli, reference 7, where they treat s^α as equivalent to s_α in the discussion of the "subsidiary conditions."

[10] F. J. Belinfante, Physica **7**, 765 (1940).

[11] J. Schwinger, Phys. Rev. **74**, 1439 (1948).

[12] For a discussion of the theory of representations, see for instance E. Wigner, *Gruppentheorie* (F. Vieweg, Braunschweig, 1931). Watch, however, the completely different notation used by Wigner. About the representations of the Lorentz group, see B. L. Van der Waerden, *Die Gruppentheoretische Methode in der Quantenmechanik* (J. Springer, Berlin, 1932), in particular Sec. 20, pp. 78–86.

[13] F. J. Belinfante, Physica **6**, 849 (1939).

[14] H. A. Kramers, *Grundlagen der Quantentheorie, Quantentheorie des Elektrons und der Strahlung* (Akademische Verlagsgesellschaft, Leipzig, 1938), pp. 259–269; (compare also pp. 272–280).

[15] But for a factor ϵ such that $\epsilon^4=1$. See W. Pauli, Annales Institut H. Poincaré **6**, 130 (1936); E. Majorana, Nuovo cimento **14**, 171 (1937); G. Racah, Nuovo cimento **14**, 322 (1937). See also reference 13.

[16] B. L. Van der Waerden, Nachr. Akad. Wiss. Göttingen Math.-physik. Kl. IIa **1929**, 100 (1929); or O. Laporte and G. E. Uhlenbeck, Phys. Rev. **37**, 1380 (1931).

[17] H. A. Kramers, reference 14, pp. 280–294; or F. J. Belinfante, reference 13, pp. 850–851. In this representation of a Dirac wave function, the electron energy $mc^2\beta-ih\mathbf{c}\boldsymbol{\alpha}\cdot\boldsymbol{\nabla}$ is represented with $(\mathbf{v}/c=)\boldsymbol{\alpha}=\rho_3\boldsymbol{\sigma}$, and with $(mc^2/\mathcal{E}=)\beta=\rho_1$.

[18] The quantities $(\gamma_5\chi)$ and $(\gamma_5\eta)$ are meant to be undors under *spatial* rotations and reflections. Under Lorentz transformations, only $(\gamma_5\chi)$ transforms like an undor, but not $(\gamma_5\eta)$. The reason why we call these (spatial) undors here $(\gamma_5\chi)$ and $(\gamma_5\eta)$ instead of using a single letter, lies in the fact that most formulas contain γ_5 times these undors, and thus are simplified by our notation. The difference in transformation between $(\gamma_5\chi)$ and the "pseudo-undor" χ itself is only a minus sign in the spatial reflection.

Kramers representation[17] $\gamma_5=\rho_3$. Thus the components of $\gamma_5\chi$ are $\{\chi_1, \chi_2, -\chi_3, -\chi_4\}$ as listed in Eq. (1). In this Kramers representation, we define our field components in terms of the components of the Fierz-Pauli field by:

$$\left.\begin{aligned}
+\chi_1&=\sqrt{(8/3)}\cdot d_{\dot 1},\\
+\chi_2&=\sqrt{(8/3)}\cdot d_{\dot 2},\\
-\chi_3&=\sqrt{(8/3)}\cdot c^1,\\
-\chi_4&=\sqrt{(8/3)}\cdot c^2;\\
+\eta_1&=\sqrt{(2/27)}\cdot(a_{\dot 1}{}^{12}-a_{\dot 2}{}^{11})-(\sqrt{\tfrac{2}{3}})d_{\dot 1},\\
+\eta_2&=\sqrt{(2/27)}\cdot(a_{\dot 1}{}^{22}-a_{\dot 2}{}^{12})-(\sqrt{\tfrac{2}{3}})d_{\dot 2},\\
-\eta_3&=\sqrt{(2/27)}\cdot(b^2{}_{\dot 1\dot 1}-b^1{}_{\dot 1\dot 2})-(\sqrt{\tfrac{2}{3}})c^1,\\
-\eta_4&=\sqrt{(2/27)}\cdot(b^2{}_{\dot 1\dot 2}-b^1{}_{\dot 2\dot 2})-(\sqrt{\tfrac{2}{3}})c^2;\\
Z_1&=a_{\dot 1}{}^{11},\\
Z_2&=(\sqrt{\tfrac{1}{3}})(2a_{\dot 1}{}^{12}+a_{\dot 2}{}^{11}),\\
Z_3&=(\sqrt{\tfrac{1}{3}})(a_{\dot 1}{}^{22}+2a_{\dot 2}{}^{12}),\\
Z_4&=a_{\dot 2}{}^{22},\\
Z_5&=-b^1{}_{\dot 1\dot 1},\\
Z_6&=(-\sqrt{\tfrac{1}{3}})(2b^1{}_{\dot 1\dot 2}+b^2{}_{\dot 1\dot 1}),\\
Z_7&=(-\sqrt{\tfrac{1}{3}})(b^1{}_{\dot 2\dot 2}+2b^2{}_{\dot 1\dot 2}),\\
Z_8&=-b^2{}_{\dot 2\dot 2}.
\end{aligned}\right\}\quad(1)$$

Explanation: We may consider a^{11}, $a^{12}\sqrt{2}$, a^{22} as a "three-spinor" for triplet states (spin 1), and $a_{\dot 1}$, $a_{\dot 2}$ as a spinor for doublet states (spin $\frac{1}{2}$). The formulas for Z_1-Z_4 are then easily[19] seen to take the form of the linear combinations of wave functions of spin $\frac{3}{2}$ obtained by vector addition of spins 1 and $\frac{1}{2}$.—We defined η_1 and η_2 as a linear combination of the spinor $\{\chi_1, \chi_2\}$ and of the doublet states obtained by this same vector addition.[19] The reason for using this particular combination lies in the simple-to-solve form (20), (27) thus found for the subsidiary conditions. (Compare footnote 20.) The components $-\chi_3$, $-\chi_4$, $-\eta_3$, $-\eta_4$, Z_5, Z_6, Z_7, Z_8 are obtained from χ_1, χ_2, η_1, η_2, Z_1, Z_2, Z_3, Z_4 by spatial reflection and omission of the factors $\epsilon=(1)^{\frac{1}{2}}$ mentioned above. Normalization factors in χ, η, and Z have been chosen arbitrarily in such way as to give the coefficients in the Lagrangian (2) relatively simple values.

The labels 1 and 3 on χ and η correspond to "spin up" ($m=+\frac{1}{2}$), and the labels 2 and 4 on χ and η to "spin down" ($m=-\frac{1}{2}$), as in the Dirac electron theory. For Z, the labels 1 and 5 mean $m=\frac{3}{2}$, 2 and 6 mean $m=\frac{1}{2}$, 3 and 7 mean $m=-\frac{1}{2}$, and 4 and 8 mean $m=-\frac{3}{2}$. We do not use the values of m itself as indices because fractions used as indices are hard on the eyes.

3. LAGRANGIAN FOR ELEMENTARY PARTICLES OF SPIN $\frac{3}{2}$ IN AN ELECTROMAGNETIC FIELD

With the notation just explained, and with the discussed alteration of the sign of σ_4 (and of derived quantities such as the momentum spinor) as well as of the sign of Fierz-Pauli's entire Lagrangian, we can find their (=minus our) Lagrangian by writing it out in components, substituting (1), and collecting the resulting terms. Thus we obtain

$$\left.\begin{aligned}
-L=Z^\dagger\{\kappa\beta+\pi_0-\tfrac{2}{3}\gamma_5\mathbf{S}\cdot\boldsymbol{\pi}\}Z+Z^\dagger\mathbf{K}\cdot\boldsymbol{\pi}\chi\\
+Z^\dagger\mathbf{K}\cdot\boldsymbol{\pi}\eta+\chi^\dagger\mathbf{K}^\dagger\cdot\boldsymbol{\pi}Z+\chi^\dagger\{3\boldsymbol{\alpha}\cdot\boldsymbol{\pi}-(9/2)\kappa\beta\}\eta\\
+\eta^\dagger\mathbf{K}^\dagger\cdot\boldsymbol{\pi}Z+\eta^\dagger\{3\boldsymbol{\alpha}\cdot\boldsymbol{\pi}-(9/2)\kappa\beta\}\chi\\
+\eta^\dagger\{(15/2)\boldsymbol{\alpha}\cdot\boldsymbol{\pi}-(9/2)\pi_0-9\kappa\beta\}\eta.
\end{aligned}\right\}(2)$$

Here, manifest covariance has been lost, but complete reduction with respect to the spatial rotation and reflection group has been gained. We have given the Lagrangian in units hc, and $\kappa=mc/h$. Further, $\beta=\rho_1$ and $\gamma_5=\rho_3$ in our representation (1), in which ρ_1 and ρ_3 transform the vertical (one-column) matrix

$$(\chi_1\chi_2,\ \chi_3\chi_4;\ \eta_1\eta_2,\ \eta_3\eta_4;\ Z_1Z_2Z_3Z_4,\ Z_5Z_6Z_7Z_8)$$

into the vertical (one-column) matrices

$$(\chi_3\chi_4,\ \chi_1\chi_2;\ \eta_3\eta_4,\ \eta_1\eta_2;\ Z_5Z_6Z_7Z_8,\ Z_1Z_2Z_3Z_4)$$

and

$$(\chi_1\chi_2,\ -\chi_3\ \ -\chi_4;\ \eta_1\eta_2,\ -\eta_3\ \ -\eta_4;\ Z_1Z_2Z_3Z_4,\ -Z_5\ \ -Z_6\ \ -Z_7\ \ -Z_8),$$

respectively. The operators π_λ (kinetic momenta in units h) are given by

$$\left.\begin{aligned}
\pi_0&=p_0-\mathfrak{e}A_0=-i\partial/c\partial t+\mathfrak{e}\Phi=-\mathcal{E}_{\text{kin}}/hc,\\
\boldsymbol{\pi}&=\mathbf{p}-\mathfrak{e}\mathbf{A}=-i\boldsymbol{\nabla}-\mathfrak{e}\mathbf{A}=\text{kinetic momentum}/h,\\
\mathfrak{e}&=q/hc,
\end{aligned}\right\}(3)$$

where q is the charge of the particle. (For instance, $q=2e$, e, 0, $-e$ for a baryon.) The Pauli matrices $\boldsymbol{\sigma}$ operate on each of the four two-spinors $\chi_{1,2}$, $\chi_{3,4}$, $\eta_{1,2}$, and $\eta_{3,4}$. The Dirac matrices

$$\boldsymbol{\alpha}=\gamma_5\boldsymbol{\sigma}\text{ and }\beta\ \text{ (with }\gamma_5\beta+\beta\gamma_5=0,\ \beta^2=1,\text{ etc.)}\quad(4)$$

operating on undors like $\gamma_5\chi$ and $\gamma_5\eta$ or on 4-component quantities like χ or η are then represented as described in footnote 17. The 4×2-matrices $\mathbf{K}$ and their 2×4 hermitian conjugates $\mathbf{K}^\dagger$ are defined by

$$K_x=\begin{pmatrix}-\sqrt{\frac{3}{2}} & 0\\ 0 & -\sqrt{\frac{1}{2}}\\ +\sqrt{\frac{1}{2}} & 0\\ 0 & +\sqrt{\frac{3}{2}}\end{pmatrix},\quad K_y=\begin{pmatrix}i\sqrt{\frac{3}{2}} & 0\\ 0 & i\sqrt{\frac{1}{2}}\\ i\sqrt{\frac{1}{2}} & 0\\ 0 & i\sqrt{\frac{3}{2}}\end{pmatrix},$$

$$K_z=\begin{pmatrix}0 & 0\\ \sqrt{2} & 0\\ 0 & \sqrt{2}\\ 0 & 0\end{pmatrix};\qquad(5a)$$

thence

$$K_y^\dagger=\begin{pmatrix}-i\sqrt{\frac{3}{2}} & 0 & -i\sqrt{\frac{1}{2}} & 0\\ 0 & -i\sqrt{\frac{1}{2}} & 0 & -i\sqrt{\frac{3}{2}}\end{pmatrix},\text{ etc.}\quad(5b)$$

[19] Compare for instance the table **(1/2)×(1)** in the Appendix to reference 2.

The hermitian 4×4-matrices $\mathbf{S}$ are defined by

$$S_x=\begin{pmatrix}0 & \frac{1}{2}\sqrt{3} & 0 & 0\\ \frac{1}{2}\sqrt{3} & 0 & 1 & 0\\ 0 & 1 & 0 & \frac{1}{2}\sqrt{3}\\ 0 & 0 & \frac{1}{2}\sqrt{3} & 0\end{pmatrix},$$

$$S_y=\begin{pmatrix}0 & -\frac{1}{2}i\sqrt{3} & 0 & 0\\ \frac{1}{2}i\sqrt{3} & 0 & -i & 0\\ 0 & i & 0 & -\frac{1}{2}i\sqrt{3}\\ 0 & 0 & \frac{1}{2}i\sqrt{3} & 0\end{pmatrix}, \tag{6}$$

$$S_z=\begin{pmatrix}\frac{3}{2} & 0 & 0 & 0\\ 0 & \frac{1}{2} & 0 & 0\\ 0 & 0 & -\frac{1}{2} & 0\\ 0 & 0 & 0 & -\frac{3}{2}\end{pmatrix};$$

they obviously are the components of the spin-$\frac{3}{2}$ angular momentum in units $\hbar$. The factor $\frac{2}{3}$ in the term $-\frac{2}{3}\gamma_5\mathbf{S}\cdot\boldsymbol{\pi}$ in the Lagrangian (2) for the Fierz-Pauli theory is comparable to the factor 2 of the Dirac electron theory in its term with $-\boldsymbol{\alpha}\cdot\boldsymbol{\pi}=-2\gamma_5\mathbf{s}\cdot\boldsymbol{\pi}$, where $\mathbf{s}=\frac{1}{2}\boldsymbol{\sigma}$ is the spin-$\frac{1}{2}$ angular momentum in units $\hbar$.

4. COMMUTATION RELATIONS FOR THE "SPIN" MATRICES

One easily verifies the following relations between the matrices $\mathbf{K}$, $\mathbf{K}^\dagger$, $\mathbf{S}$, and $\boldsymbol{\sigma}$, and further relations obtained from the ones listed explicitly by cyclic permutation of x, y, and z:

$$2S_xK_x=K_x\sigma_x, \tag{7a}$$

$$2K_x^\dagger S_x=\sigma_xK_x^\dagger, \tag{7a*}$$

$$2S_xK_y-K_x\sigma_y=-(2S_yK_x-K_y\sigma_x)=3iK_z, \tag{7b}$$

$$2K_x^\dagger S_y-\sigma_xK_y^\dagger=-(2K_y^\dagger S_x-\sigma_yK_x^\dagger)=3iK_z^\dagger, \tag{7b*}$$

$$K_x^\dagger K_x=2, \tag{8a}$$

$$K_x^\dagger K_y=-K_y^\dagger K_x=-i\sigma_z, \tag{8b}$$

$$K_xK_x^\dagger=(9/4)-S_x^2, \tag{9a}$$

$$K_xK_y^\dagger+K_yK_x^\dagger=-(S_xS_y+S_yS_x), \tag{9b}$$

$$K_xK_y^\dagger-K_yK_x^\dagger=2iS_z, \tag{9c}$$

$$S_xS_y-S_yS_x=iS_z. \tag{9d}$$

For vector operators $\mathbf{A}$ and $\mathbf{B}$ we find from the above relations and the properties of the Pauli matrices $\boldsymbol{\sigma}$:

$$\mathbf{A}\cdot(\mathbf{K}\boldsymbol{\sigma}-2\mathbf{SK})\cdot\mathbf{B}=3i\mathbf{A}\cdot\mathbf{K}\times\mathbf{B}, \tag{10}$$

$$\mathbf{A}\cdot(\boldsymbol{\sigma}\mathbf{K}^\dagger-2\mathbf{K}^\dagger\mathbf{S})\cdot\mathbf{B}=3i\mathbf{A}\cdot\mathbf{K}^\dagger\times\mathbf{B}, \tag{10*}$$

$$\mathbf{A}\cdot\mathbf{K}^\dagger\mathbf{K}\cdot\mathbf{B}=2\mathbf{A}\cdot\mathbf{B}+i\mathbf{A}\cdot\boldsymbol{\sigma}\times\mathbf{B}, \tag{11}$$

$$\mathbf{A}\cdot(\mathbf{K}\mathbf{K}^\dagger+\mathbf{SS})\cdot\mathbf{B}=(9/4)\mathbf{A}\cdot\mathbf{B}-\tfrac{3}{2}i\mathbf{A}\cdot\mathbf{S}\times\mathbf{B}, \tag{12}$$

$$\mathbf{A}\cdot\boldsymbol{\sigma}\boldsymbol{\sigma}\cdot\mathbf{B}=\mathbf{A}\cdot\mathbf{B}-i\mathbf{A}\cdot\boldsymbol{\sigma}\times\mathbf{B}. \tag{13}$$

Here we used diadic notation in the left-hand members. Substituting $\mathbf{A}=\mathbf{B}=\boldsymbol{\pi}$, and using the first of the relations

$$\boldsymbol{\pi}\times\boldsymbol{\pi}=i\mathfrak{e}\mathfrak{B}, \quad \pi\pi_0-\pi_0\boldsymbol{\pi}=i\mathfrak{e}\mathfrak{E} \tag{14a-b}$$

following from (3) in an electromagnetic field $\mathfrak{E}$, $\mathfrak{B}$, we find

$$\boldsymbol{\pi}\cdot(\mathbf{K}\boldsymbol{\sigma}-2\mathbf{SK})\cdot\boldsymbol{\pi}=3\mathfrak{e}\mathfrak{B}\cdot\mathbf{K}, \tag{15}$$

$$\boldsymbol{\pi}\cdot(\boldsymbol{\sigma}\mathbf{K}^\dagger-2\mathbf{K}^\dagger\mathbf{S})\cdot\boldsymbol{\pi}=3\mathfrak{e}\mathfrak{B}\cdot\mathbf{K}^\dagger, \tag{15*}$$

$$\boldsymbol{\pi}\cdot\mathbf{K}^\dagger\mathbf{K}\cdot\boldsymbol{\pi}=2\boldsymbol{\pi}^2+\mathfrak{e}\mathfrak{B}\cdot\boldsymbol{\sigma}, \tag{16}$$

$$\boldsymbol{\pi}\cdot(\mathbf{K}\mathbf{K}^\dagger+\mathbf{SS})\cdot\boldsymbol{\pi}=(9/4)\boldsymbol{\pi}^2-\tfrac{3}{2}\mathfrak{e}\mathfrak{B}\cdot\mathbf{S}, \tag{17}$$

$$\boldsymbol{\pi}\cdot\boldsymbol{\sigma}\boldsymbol{\sigma}\cdot\boldsymbol{\pi}=\boldsymbol{\pi}^2-\mathfrak{e}\mathfrak{B}\cdot\boldsymbol{\sigma}. \tag{18}$$

Obviously the matrices $\mathbf{S}$, $\mathbf{K}$, $\mathbf{K}^\dagger$, and $\boldsymbol{\sigma}$ all commute with β and with γ_5.

5. FIELD EQUATIONS, SUBSIDIARY EQUATIONS, AND SOLUTION FOR THE INDEPENDENT VARIABLES

Independent variation of $Z^\dagger$, $\chi^\dagger$, and $\eta^\dagger$ in $\delta\int dt\int d^3\mathbf{x}\ L=0$ yields

$$\{\kappa\beta+\pi_0-\tfrac{2}{3}\gamma_5\mathbf{S}\cdot\boldsymbol{\pi}\}Z+\mathbf{K}\cdot\boldsymbol{\pi}\chi+\mathbf{K}\cdot\boldsymbol{\pi}\eta=0, \tag{19}$$

$$\mathbf{K}^\dagger\cdot\boldsymbol{\pi}Z+\{3\boldsymbol{\alpha}\cdot\boldsymbol{\pi}-(9/2)\kappa\beta\}\eta=0, \tag{20}$$

$$\mathbf{K}^\dagger\cdot\boldsymbol{\pi}Z+\{3\boldsymbol{\alpha}\cdot\boldsymbol{\pi}-(9/2)\kappa\beta\}\chi+\{(15/2)\boldsymbol{\alpha}\cdot\boldsymbol{\pi}-(9/2)\pi_0-9\kappa\beta\}\eta=0. \tag{21}$$

Equation (20) forms the first four subsidiary equations, corresponding to Fierz-Pauli's Eqs. (28)–(29). In principle, (20) (with suitable boundary conditions of vanishing of fields at infinity) enables us to express the four-component $\eta(x, y, z, t)$ in terms of the field $Z(x', y', z', t)$ and the electromagnetic field, all at the same time t. Therefore, the components of η may be called "dependent variables," as contrasted to independent canonical variables. Also the "derived variables" well known from other field theories of elementary particles[10] are dependent variables, although of a more special kind, as those can be expressed as polynomials in the canonical variables, and spatial derivatives of finite order of them, all taken at the same point. On the other hand, $\eta(x, y, z, t)$ depends on $Z(x', y', z', t)$ in a spatial neighborhood of the point $\{x, y, z\}$.

Solution of Eq. (20) for η by successive approximations in powers of the charge q becomes easy after multiplication of (20) by $\{\frac{1}{3}\boldsymbol{\alpha}\cdot\boldsymbol{\pi}-\frac{1}{2}\kappa\beta\}$, which gives

$$\{\tfrac{1}{3}\boldsymbol{\pi}\cdot\boldsymbol{\alpha}-\tfrac{1}{2}\kappa\beta\}\mathbf{K}^\dagger\cdot\boldsymbol{\pi}Z+\{\boldsymbol{\pi}\cdot\boldsymbol{\sigma}\boldsymbol{\sigma}\cdot\boldsymbol{\pi}+(9/4)\kappa^2\}\eta=0$$

or

$$\{\boldsymbol{\pi}^2-\mathfrak{e}\mathfrak{B}\cdot\boldsymbol{\sigma}+(9/4)\kappa^2\}\eta=4\pi f^{(0)}[Z], \tag{22}$$

where

$$f^{(0)}[Z(x,y,z,t)]=\{\tfrac{3}{2}\kappa\beta-\boldsymbol{\pi}\cdot\boldsymbol{\alpha}\}\mathbf{K}^\dagger\cdot\boldsymbol{\pi}Z(x,y,z,t)/12\pi. \tag{23}$$

Equation (22) with (3) can be rewritten as

$$\{\boldsymbol{\nabla}^2-(3\kappa/2)^2\}\eta=-4\pi f \tag{24}$$

with

$$f=f^{(0)}[Z]+\{\mathfrak{e}\mathfrak{B}\cdot\boldsymbol{\sigma}+\mathbf{p}^2-\boldsymbol{\pi}^2\}\eta/4\pi. \tag{25}$$

The solution of Eq. (24) satisfies

$$\eta(x, y, z, t)=\int d^3\mathbf{x}' \exp(-\tfrac{3}{2}\kappa r) f(x', y', z', t)/r, \quad (26)$$

with $r=|\mathbf{x}-\mathbf{x}'|$.

By (25)–(26) we solve (24) for η in successive approximations. By $e\to 0$ in Eq. (25), we first find $f^{(0)}$ as zero-order approximation to f. Inserting $f^{(0)}$ into (26) then yields the first approximation $\eta^{(1)}$ to η. Similarly, (26) expresses $\eta^{(n+1)}$ in terms of $f^{(n)}$, which in turn is given by (25) in terms of $f^{(0)}$ and $\eta^{(n)}$. By (26), $\eta(x, y, z, t)$ —or at least the first few terms in its expansion—is thus found to depend mainly on the fields in a small region with a radius of the order of magnitude $(1/\kappa)$ around the point (x, y, z) in three-dimensional space. From Eq. (20) it is seen that η vanishes for a particle of zero kinetic momentum ($\boldsymbol{\pi}Z=0$), and therefore η will be much smaller than Z for slow particles. (Compare Eqs. (26) and (23).)

In order to find the other four subsidiary equations, we multiply Eqs. (19), (20), and (21) by $\{-\boldsymbol{\pi}\cdot\mathbf{K}^\dagger\}$, $\{2\kappa\beta-\boldsymbol{\pi}\cdot\boldsymbol{\alpha}+\pi_0\}$, and $\{\frac{2}{3}\boldsymbol{\pi}\cdot\boldsymbol{\alpha}-\kappa\beta\}$, respectively, and we add the results. Using Eqs. (4), (14b), (15*), (16), (18) we thus find

$$-\mathfrak{e}\mathfrak{B}\cdot\mathbf{K}^\dagger\gamma_5 Z-i\mathfrak{e}(\mathfrak{E}\cdot\mathbf{K}^\dagger Z-3\mathfrak{e}\mathfrak{B}\cdot\boldsymbol{\sigma}\chi + (9/2)\kappa^2\chi-3\mathfrak{e}\mathfrak{B}\cdot\boldsymbol{\sigma}\eta-3i\mathfrak{e}(\mathfrak{E}\cdot\boldsymbol{\alpha}\eta=0,$$

or, with $\lambda=2\mathfrak{e}/3\kappa^2=2qh/3m^2c^3$,

$$\{1-\lambda\mathfrak{B}\cdot\boldsymbol{\sigma}\}\chi=\lambda(\gamma_5\mathfrak{B}+i(\mathfrak{E})\cdot(\boldsymbol{\alpha}\eta+\tfrac{1}{3}\mathbf{K}^\dagger Z). \quad (27)$$

We solve this equation for χ by multiplying it from the left by [20]

$$\{1-\lambda\mathfrak{B}\cdot\boldsymbol{\sigma}\}^{-1}\equiv\{1-\lambda^2\mathfrak{B}^2\}^{-1}\{1+\lambda\mathfrak{B}\cdot\boldsymbol{\sigma}\}. \quad (28)$$

We thus have solved for all dependent variables χ and η in terms of the independent canonical variables Z and the electromagnetic field. The equations of motion for the field Z are then given by Eq. (19) with the solutions for χ and η substituted.

6. THE MAGNETIC MOMENT OF SPIN-$\frac{3}{2}$ PARTICLES

Multiplying Eqs. (19), (20), and (21) by $\{\kappa\beta-\pi_0-\frac{2}{3}\gamma_5\boldsymbol{\pi}\cdot\mathbf{S}\}$, by $\{\frac{2}{3}\boldsymbol{\pi}\cdot\mathbf{K}\}$, and by $\{-(2/9)\boldsymbol{\pi}\cdot\mathbf{K}\}$, respectively, and adding the three products to $\pi_0^2 Z$, we find by Eqs. (4), (14b), (15), and (17):

$$\pi_0^2 Z=\{\kappa^2+\boldsymbol{\pi}\cdot\boldsymbol{\pi}-\tfrac{2}{3}\mathfrak{e}\mathfrak{B}\cdot\mathbf{S}-\tfrac{2}{3}i\mathfrak{e}(\mathfrak{E}\cdot\mathbf{S}\gamma_5\}Z + \mathfrak{e}(\gamma_5\mathfrak{B}+i(\mathfrak{E})\cdot\mathbf{K}\eta+\{\mathbf{K}\cdot\boldsymbol{\pi}(2\kappa\beta-\pi_0-\boldsymbol{\alpha}\cdot\boldsymbol{\pi}) + \mathfrak{e}(\gamma_5\mathfrak{B}+i(\mathfrak{E})\cdot\mathbf{K}\}\chi. \quad (29)$$

Similarly we derive, by adding $(2/9)(\pi_0+\boldsymbol{\pi}\cdot\boldsymbol{\alpha}-\kappa\beta)$ times the difference {Eq. (21)—Eq. (20)} to $\pi_0^2\eta$, and by using Eqs. (4), (14b), and (18):

$$\pi_0^2\eta=\{\kappa^2+\boldsymbol{\pi}\cdot\boldsymbol{\pi}-\mathfrak{e}\mathfrak{B}\cdot\boldsymbol{\sigma}\}\eta+\{\kappa^2-\kappa\beta\pi_0 + \tfrac{2}{3}\pi_0\boldsymbol{\pi}\cdot\boldsymbol{\alpha}+\tfrac{1}{3}\kappa\beta\boldsymbol{\alpha}\cdot\boldsymbol{\pi}+\tfrac{2}{3}\boldsymbol{\pi}\cdot\boldsymbol{\pi}-\tfrac{2}{3}\mathfrak{e}\mathfrak{B}\cdot\boldsymbol{\sigma}\}\chi. \quad (30)$$

According to Eq. (20), for slow particles η is smaller than Z by a factor v/c, while by Eq. (27) χ vanishes in absence of electromagnetic fields. If we neglect terms quadratic in the electromagnetic field as well as terms bilinear in the electromagnetic field and in (v/c), Eqs. (29)–(30) reduce to

$$\pi_0^2 Z\approx\{\kappa^2+\boldsymbol{\pi}^2-\tfrac{2}{3}\mathfrak{e}(\mathfrak{B}+i\gamma_5(\mathfrak{E})\cdot\mathbf{S}\}Z, \quad (31)$$

$$\pi_0^2\eta\approx\{\kappa^2+\mathfrak{p}^2\}\eta. \quad (32)$$

In the following we shall further neglect the imaginary term with $\gamma_5(\mathfrak{E}$ in Eq. (31).

Since $\mathcal{E}=-hc\pi_0$ was the kinetic energy, $m=\kappa h/c$ is apparently the rest mass of our spin-$\frac{3}{2}$ particles. We solve for the nonrelativistic energy $\mathfrak{W}$ by squaring the expression

$$-\pi_0=\kappa+(\mathfrak{W}-q\mathfrak{P})/hc, \quad (33)$$

which defines $\mathfrak{W}$, and by equating the result to $\pi_0^2\approx\kappa^2+\boldsymbol{\pi}^2-\frac{2}{3}\mathfrak{e}\mathfrak{B}\cdot\mathbf{S}$ from Eq. (31). Neglecting the square of the nonrelativistic energy $\mathfrak{W}$, and putting $\mathfrak{p}=\hbar\boldsymbol{\pi}$ for the kinetic momentum in cgs-units, we thus find

$$\{\mathfrak{W}-q\mathfrak{P}\}Z\approx(hc/2\kappa)\{\boldsymbol{\pi}^2-\tfrac{2}{3}\mathfrak{e}\mathfrak{B}\cdot\mathbf{S}\}Z \approx[\mathfrak{p}^2/2m-(qh/3mc)\mathfrak{B}\cdot\mathbf{S}]Z, \quad (34)$$

so that our spin-$\frac{3}{2}$ particles apparently have a magnetic moment

$$\boldsymbol{\mu}=(qh/3mc)\mathbf{S}. \quad (35)$$

Remembering that $\hbar\mathbf{S}$ was the spin angular momentum of the spin-$\frac{3}{2}$ part of the field, with z-component $\frac{3}{2}\hbar$, $\frac{1}{2}\hbar$, $-\frac{1}{2}\hbar$, or $-\frac{3}{2}\hbar$ according to (6), we find the gyromagnetic ratio for our particles to be $(q/3mc)$ and we find $(qh/2mc)$ for the maximum value of μ_z.

The η components of the field, which become important for fast particles only, behave like a spin-$\frac{1}{2}$ field with spin angular momentum $\frac{1}{2}\hbar\boldsymbol{\sigma}$ and magnetic moment $q\hbar\boldsymbol{\sigma}/2mc$ as seen by treating (30) similar to (29) by Eq. (33) going one approximation beyond Eq. (32). The gyromagnetic ratio of this part of the field is q/mc; but the maximum possible value for the corresponding μ_z value is again $qh/2mc$.

Our results, together with those found for Dirac electrons and for vector mesons,[21] suggest a spin magnetic moment $qh/2mc$ for *all* elementary particles of charge q, rest mass m, and low kinetic energy, for any spin different from zero. Thus a larger spin would always be compensated by a correspondingly smaller gyromagnetic ratio.

[20] Our χ corresponds to Fierz-Pauli's spinor field $d_{\dot\alpha}$, $-c^\alpha$; see Eq. (1). Their Eqs. (23)–(24), translated into our notation, express χ in terms of the components Z and $(\chi+2\eta)$ of the $a_\alpha^{\beta\nu}$, $b^{\alpha}_{\beta\dot\nu}$ field. We prefer to express χ in terms of Z and η as in (27) with (28), although this destroys the relativistic appearance of the formula. The reason for our preference is, of course, the fact that the other identities (20), by (23)–(26), express η and not $(\chi+2\eta)$ in terms of Z.

[21] Yukawa, Sakata, and Taketani, Proc. Phys.-Math. Soc. Japan **20**, 319 (1938); F. J. Belinfante, Physica **6**, 870 (1939).

The Hyperfine Structure of Hydrogen*

R. ARNOWITT†
Harvard University, Cambridge, Massachusetts
(Received July 8, 1953)

The two-body formalism of Schwinger is modified to consider the case of the hydrogen atom. The proton's anomalous moment is treated by adding a Pauli-type term to the Lagrangian. A perturbation theory based upon the Green's function is developed and the first-order correction to the Fermi hyperfine splitting of the ground state is calculated. The method of calculation used is that of Karplus and Klein in their positronium work. Aside from the usual renormalizations encountered, an extra infinity appears in the calculation associated with the assumption of a point anomalous magnetic moment for the proton. On the hypothesis that the proton's moment is actually distributed, cutoffs are inserted. The modified hyperfine formula leads to a new value of $\alpha: 1/\alpha = 137.0378$ for a cutoff at the meson length and $1/\alpha = 137.0374$ for a cutoff at the proton length.

I. INTRODUCTION

DURING the past two years, several derivations of relativistic two-body Green's function and wave-function equations have appeared in the literature.[1] The derivation of Bethe and Salpeter followed the methods of Feynman while that of Gell-Mann and Low followed those of Dyson. The approach that we shall use here is the one given by Schwinger, where use is made of the technique of variational derivatives with respect to external sources and the formalism developed in Schwinger's "Theory of Quantized Fields. I."[2]

The specific problem in which we shall be interested is the reduced mass corrections to the Fermi hyperfine splitting of the ground state of hydrogen. To obtain an adequate two-body equation for hydrogen, certain modifications must be made in Schwinger's derivation. First, we are here dealing with two distinguishable particles rather than with two particles of the same field. Second, account must be taken of the proton's meson anomalous moment. The latter is accomplished phenomenologically by adding a Pauli type term, $\frac{1}{2}\mu'\sigma_{\mu\nu}F_{\mu\nu}$ (where μ' is the anomalous magnetic moment), to the Lagrangian. The net effect is to allow the proton to interact with the electromagnetic field via its normal current and its spin current.

Aside from the usual infinities of quantum electrodynamics, two others appear in these calculations. The first is an ultraviolet divergence in certain of the Pauli moment terms. This is due to the fact that the Pauli moment introduces a point dipole. On the assumption that the anomalous moment is due to a meson-nucleon interaction, one may postulate that the moment actually has the extension of the order of the meson Compton wavelength and cut off all divergent integrals accordingly. Fortunately, the results depend upon the cutoff only logarithmically and hence the calculation is not sensitive to its precise value. The second difficulty involves an infrared divergence and is due to the fact that we have assumed free particle intermediate state Green's functions in the perturbation theory. The appropriate method of treating this difficulty for a hyperfine splitting has been shown by Karplus and Klein.[3] Since the spin-spin interactions are all high frequency, the infrared divergences will cancel if one makes the free particle approximation consistently throughout the entire calculation. As the actual calculations are similar to the ones done by Karplus and Klein, they will only be sketched here.

II. THE ELECTRON-PROTON TWO-BODY GREEN'S FUNCTION

For the system of coupled electron, proton, and photon fields, the Lagrange function may be taken as[4]

$$\begin{aligned}L=&-\tfrac{1}{4}[\bar{\psi},\gamma_{1\mu}(-i\partial_\mu-e_1A_\mu)\psi+m_1\psi]+\tfrac{1}{2}[\bar{\psi},\eta]\\&-\tfrac{1}{4}[\bar{\phi},\gamma_{2\mu}(-i\partial_\mu-e_2A_\mu)\phi\\&-\tfrac{1}{2}\mu'\sigma_{2\mu\nu}(\partial_\mu A_\nu-\partial_\nu A_\mu)\phi+m_2\phi]\\&+\tfrac{1}{2}[\bar{\phi},\zeta]+\text{Herm. conj.}+\tfrac{1}{4}F_{\mu\nu}F_{\mu\nu}\\&-\tfrac{1}{4}\{F_{\mu\nu},\partial_\mu A_\nu-\partial_\nu A_\mu\}+J_\mu A_\mu,\end{aligned}\quad(2.1)$$

where ψ and ϕ are the electron and proton field variables respectively. Subscripts "1" and "2" refer to electron and proton quantities. η and ζ are the prescribed external source for the electron and proton fields and J_μ for the photon fields. η and ζ (and their variations) anti-commute with all fermion field variables. The equations of motion obtained from (2.1) are

$$\begin{aligned}&[\gamma_{1\mu}(-i\partial_\mu-e_1A_\mu)+m_1]\psi=\eta,\\&[\gamma_{2\mu}(-i\partial_\mu-e_2A_\mu)\\&\qquad-\tfrac{1}{2}\mu'\sigma_{2\mu\nu}(\partial_\mu A_\nu-\partial_\nu A_\mu)+m_2]\phi=\zeta,\\&\partial_\nu F_{\mu\nu}=J_\mu+j_{1\mu}+j_{2\mu},\quad F_{\mu\nu}=\partial_\mu A_\nu-\partial_\nu A_\mu,\end{aligned}\quad(2.2)$$

* Part of a thesis submitted in partial fulfillment of the requirements for the degree of Doctor of Philosophy at Harvard University.
† Now at Radiation Laboratory, University of California, Berkeley, California.
[1] J. Schwinger, Proc. Nat. Acad. Sci. U. S. **37**, 452, 455 (1951); E. E. Salpeter and H. A. Bethe, Phys. Rev. **84**, 1232 (1951); M. Gell-Mann and F. Low, Phys. Rev. **84**, 350 (1951); M. Neuman, Phys. Rev. **85**, 129 (1952); H. Kita, Prog. Theor. Phys. (Japan) **7**, 217 (1952).
[2] J. Schwinger, Phys. Rev. **82**, 914 (1951).
[3] R. Karplus and A. Klein, Phys. Rev. **87**, 848 (1952).
[4] Natural units are employed throughout: $\hbar=c=1$.

where

$$j_{1\mu}=\tfrac{1}{2}e_1[\bar{\psi},\gamma_{1\mu}\psi],$$
$$j_{2\mu}=\tfrac{1}{2}e_2[\bar{\phi},\gamma_{2\mu}\phi]-\tfrac{1}{2}\mu'\partial_\lambda[\bar{\phi},\sigma_{2\lambda\mu}\phi]. \tag{2.3}$$

For any operator $F(x)$, one may define the quantity

$$\langle F(x)\rangle=(0\sigma_1|F(x)|0\sigma_2)/(0\sigma_1|0\sigma_2), \tag{2.4}$$

where σ_1 and σ_2 are two space-like surfaces and 0 signifies the vacuum state. The one-particle electron and proton Green's functions are defined by the equations[5]

$$G_1(x_1,x_1')=(\delta/\delta\eta(x_1'))\langle\psi(x_1)\rangle]_{\eta,\zeta\to0},$$
$$G_2(x_2,x_2')=(\delta/\delta\zeta(x_2'))\langle\phi(x_2)\rangle]_{\zeta,\eta\to0}. \tag{2.5}$$

By use of the fundamental dynamical principle,[2] the one-particle Green's functions may be expressed by

$$G_1(x_1,x_1')=i\langle(\psi(x_1)\bar{\psi}(x_1'))_+\rangle\epsilon(x_1,x_1'),$$
$$G_2(x_2,x_2')=i\langle(\phi(x_2)\bar{\phi}(x_2'))_+\rangle\epsilon(x_2,x_2'). \tag{2.6}$$

From the equations of motion (2.2) and the defining equations (2.5), it can be seen that

$$[\gamma_{1\mu}(-i\partial_{1\mu}-e_1\langle A_\mu(x_1)\rangle)+\mathfrak{M}_1]G_1(x_1,x_1')=\delta(x_1-x_1'),$$
$$[\gamma_{1\mu}(-i\partial_{2\mu}-e_2\langle A_\mu(x_2)\rangle)-\mu'\sigma_{2\mu\nu}\partial_{2\mu}\langle A_\nu(x_2)\rangle+\mathfrak{M}_2]\times G_2(x_2,x_2')=\delta(x_2-x_2'), \tag{2.7}$$

where

$$\mathfrak{M}_1=m_1+ie_1\gamma_1\frac{\delta}{\delta J(x_1)},$$
$$\mathfrak{M}_2=m_2+ie_2\gamma_2\frac{\delta}{\delta J(x_2)}+i\mu'\sigma_{2\mu\nu}\partial_\mu'\frac{\delta}{\delta J_\nu(x')}\Big]_{x'\to x}. \tag{2.8}$$

For the photon field, the equations of motion yield

$$-\partial_\nu^2\langle A_\mu(x)\rangle+\partial_\mu\partial_\nu\langle A_\nu(x)\rangle=J_\mu(x)+\langle j_{1\mu}(x)\rangle+\langle j_{2\mu}(x)\rangle, \tag{2.9}$$

where

$$\langle j_{1\mu}(x)\rangle=ie_1\,\mathrm{tr}\gamma_{1\mu}G_1(x,x),$$
$$\langle j_{2\mu}(x)\rangle=ie_2\,\mathrm{tr}\gamma_{2\mu}G_2(x,x)-i\mu'\partial_\lambda\,\mathrm{tr}\sigma_{2\lambda\mu}G_2(x,x), \tag{2.10}$$

the symmetric limit being understood on the right of (2.10). In analogous fashion, the one-particle Maxwell Green's function may be defined by

$$\mathcal{G}_{\mu\nu}(x,x')=(\delta/\delta J_\nu(x'))\langle A_\mu(x)\rangle=i[\langle(A_\mu(x)A_\nu(x'))_+\rangle-\langle A_\mu(x)\rangle\langle A_\nu(x')\rangle]. \tag{2.11}$$

[5] The variational derivatives with respect to η and ζ here (and elsewhere) are right variational derivatives, i.e., if $\delta_\eta F=\int F(x)\delta\eta(x)dx$, then $\delta F/\delta\eta=F(x)$. A convention is necessary as $F(x)$ and $\delta\eta(x)$ need not commute.

In the Lorentz gauge, this obeys the equation

$$-\partial^2\mathcal{G}_{\mu\nu}(x,x')=\delta_{\mu\nu}\delta(x-x')+ie_1\,\mathrm{tr}\gamma_{1\mu}(\delta/\delta J_\nu(x'))G_1(x,x)+ie_2\,\mathrm{tr}\gamma_{2\mu}(\delta/\delta J_\nu(x'))G_2(x,x)-i\mu'\partial_\lambda\,\mathrm{tr}\sigma_{2\lambda\mu}(\delta/\delta J_\nu(x'))G_2(x,x). \tag{2.12}$$

The two-particle electron-proton Green's function is given by

$$G_{12}(x_1x_2,x_1'x_2')=(\delta/\delta\eta(x_1'))(\delta/\delta\zeta(x_2'))(\langle(\psi(x_1)\phi(x_2))_+\rangle]_{\eta,\zeta\to0}\epsilon(x_1,x_2)$$
$$=-\langle(\psi(x_1)\phi(x_2)\bar{\psi}(x_1')\bar{\phi}(x_2'))_+\rangle\epsilon(x_1,x_1')\epsilon(x_2,x_2')\times\epsilon(x_1,x_2)\epsilon(x_2',x_1')\epsilon(x_1,x_2')\epsilon(x_2,x_1'), \tag{2.13}$$

and obeys the equations

$$\mathfrak{F}_1G_{12}=\delta(x_1-x_1')G(x_2,x_2'),$$
$$\mathfrak{F}_1\mathfrak{F}_2G_{12}=\delta(x_1-x_1')\delta(x_2-x_2'). \tag{2.14}$$

The $\mathfrak{F}$'s are the functional operators on the left of (2.7).

Due to the fact that we have been considering vacuum states on σ_1 and σ_2, the Green's functions defined above have all been outgoing wave Green's functions. It is convenient, then, to set the surfaces σ_1 and σ_2 at $+\infty$ and $-\infty$ and introduce the "matrix" notation of Schwinger,[1] x and p being used for particle operators, ξ and k for photon operators. We also introduce two quantities which are photon vectors and particle matrices, $\gamma_\mu(\xi)$ and $\sigma_{\mu\nu}(\xi)$, such that

$$(x|\gamma_\mu(\xi)|x')=\gamma_\mu\delta(x-x')\delta(\xi-x),$$
$$(x|\sigma_{\mu\nu}(\xi)|x')=\sigma_{\mu\nu}\delta(x-x')\delta(\xi-x). \tag{2.15}$$

By use of the vertex operators,

$$\Gamma_{1,2}(\xi)=-[\delta/\delta(e_{1,2}A(\xi))]G_{1,2}^{-1}, \tag{2.16}$$

the variational derivatives in $\mathfrak{M}$ may be re-expressed as an integral operator M:

$$\mathfrak{M}_1G_1=(m_1+ie_1^2\,\mathrm{T}\rho\gamma_1G_1\Gamma_1\mathcal{G})G_1=M_1G_1,$$
$$\mathfrak{M}_2G_2=(m_2+ie_2^2\,\mathrm{T}\rho\bar{\gamma}_2G_2\Gamma_2\mathcal{G})G_2=M_2G_2, \tag{2.17}$$
$$\bar{\gamma}_2(\xi)=\gamma_2(\xi)-i(\mu'/e_2)(k\cdot\sigma_2)(\xi).$$

In general, the one-particle proton operators are identical to the electron in form with γ replaced by $\bar{\gamma}$. The variational derivatives in the Maxwell Green's function may also be eliminated in favor of the integral operator P:

$$(k^2+P_1+P_2)\mathcal{G}=1,$$
$$P_{1\mu\nu}(\xi,\xi')=-ie_1^2\,\mathrm{Tr}\gamma_{1\mu}(\xi)G_1\Gamma_{1\nu}(\xi')G_1. \tag{2.18}$$

Turning to the two-body equation, one wishes to recast it into the form

$$\{[\gamma_2(p_2-e_2\langle A_2\rangle)-\mu'\sigma_{2\mu\nu}\partial_{2\mu}\langle A_{2\nu}\rangle+M_2]$$
$$\times[\gamma_1(p_1-e_1\langle A_1\rangle)+M_1]-I_{12}\}G_{12}=1_1 1_2. \quad (2.19)$$

On comparison with (2.14), one sees that the interaction operator I_{12} is given by

$$I_{12}G_{12}=G_2^{-1}(M_1-\mathfrak{M}_1)G_{12}, \quad (2.20)$$

which may be rearranged to

$$I_{12}G_{12}=-ie_1e_2\,\mathrm{T}\rho\gamma_1\Gamma_2\mathfrak{G}G_{12}$$
$$-ie_1\,\mathrm{T}\rho\gamma_1 G_1(\delta/\delta J)(I_{12}G_{12}). \quad (2.21)$$

The integral operators discussed in this section may all be expanded in a power series in e^2. The lowest-order interaction is

$$I^{(1)}=ie^2\,\mathrm{T}\rho\gamma_1\bar{\gamma}_2\mathfrak{G}^{(1)}$$
$$=ie^2\int d\xi d\xi'\gamma_{1\mu}(\xi)\bar{\gamma}_{2\mu}(\xi')D_+(\xi',\xi). \quad (2.22)$$

In general, the interaction operator is symmetric in the proton and electron indices. Thus, to second order it may be shown that

$$I_{12}=(ie^2\,\mathrm{T}\rho\Gamma_1\Gamma_2\mathfrak{G})_{\text{second order}}$$
$$+(ie^2)^2\,\mathrm{T}\rho\gamma_1 G_1{}^0(\mathrm{T}\rho'\gamma_1'\bar{\gamma}_2'\mathfrak{G}^{0\prime})G_2{}^0\bar{\gamma}_2\mathfrak{G}^0. \quad (2.23)$$

The superscript 0 means zeroth-order function. In these perturbation expansions for I_{12}, etc., the free particle intermediate state assumption has been made.

III. PERTURBATION THEORY

Salpeter[6] has presented a perturbation theory based on the two-body wave equation. We present here an alternate form based upon the Green's function. From Eq. (2.13), for the case $t_1, t_2>t_1', t_2'$, the Green's function may be written as

$$G_{12}=-\sum_\zeta \frac{(0\sigma_1|(\psi(x_1)\phi(x_2))_+|\zeta\sigma)}{(0\sigma_1|0\sigma)}$$
$$\times\frac{(\zeta\sigma|(\bar{\psi}(x_1')\bar{\phi}(x_2'))_+|0\sigma_2)}{(0\sigma|0\sigma_2)}$$
$$=-\sum_\zeta\psi_\zeta(x_1,x_2)\bar{\psi}_\zeta(x_1',x_2'), \quad (3.1)$$

where ζ is some complete set on surface σ including the total field energy. Introducing the center-of-mass and relative coordinates

$$X=(m_1x_1)/(m_1+m_2)+(m_2x_2)/(m_1+m_2)$$
$$=\mu_1x_1+\mu_2x_2, \quad (3.2)$$
$$x=x_1-x_2,$$

the factor $\exp(iP_{\mu\zeta}X_\mu)$ may be separated from ψ_ζ, where $P_{\mu\zeta}$ is the field energy-momentum eigenvalue. In general, we may set the momentum part to zero. For the equal-times situation, $t_1=t_2=t>t_1'=t_2'=t'$, the Green's function becomes

$$G_{12}(\mathbf{r}_1\mathbf{r}_2t,\ \mathbf{r}_1'\mathbf{r}_2't')$$
$$=-\sum_\zeta\psi_\zeta(\mathbf{r}_1\mathbf{r}_2)\exp(-iP_{0\zeta}T_0)\bar{\psi}_\zeta(\mathbf{r}_1'\mathbf{r}_2'), \quad (3.3)$$

where $T_0=t-t'$.

The eigenvalues, $P_{0\zeta}$, are infinitely degenerate. Such a set of eigenvalues (and eigenfunctions) may be replaced by a discrete set (for the bound states), P_{0n}. The P_{0n} are complex, the real part representing the energy of the two-body system, the complex part representing the possibility of decay (via the emission of photons and pairs). Thus, Eq. (3.3) may be replaced by

$$G_{12}(\mathbf{r}_1\mathbf{r}_2t,\ \mathbf{r}_1'\mathbf{r}_2't')$$
$$=-\sum_n\psi_n(\mathbf{r}_1\mathbf{r}_2)\exp(-iP_{0n}T_0)\bar{\psi}_n(\mathbf{r}_1'\mathbf{r}_2'), \quad (3.4)$$

where $\psi_n(x_1,x_2)$ presumably obeys the two-body wave equation. The situation is very similar to that of radioactive α decay. There, the continuum of positive energy eigenstates is replaced by a discrete set with complex eigenvalues, the complex part of the energy representing the possibility of decay of the α particle out of the nuclear well (in analogy to the decay of the two-body system via emission processes).

Equation (3.4) may be used as the basis of a perturbation theory for the eigenvalue P_0. Before doing this, however, it is best to extract out the various infinite constants implicit in electrodynamics. The Green's function equation, in the absence of an external field is

$$[(\gamma_1p_1+M_1)(\gamma_2p_2+M_2)-I_{12}]G_{12}=1_1 1_2. \quad (3.5)$$

It may be shown, to order α, that

$$\gamma_1p_1+M_1=(1+A_1)(\gamma_1p_1+m_1'+M_1{}^{(r)}), \quad (3.6)$$

where m_1' is the renormalized mass, A_1 is an infinite constant and $M_1{}^{(r)}$ is a finite residue. Similarly, Γ_1 may be shown to equal

$$\Gamma_1=(1+A_1)(\gamma_1+\Gamma_1{}^{(r)}), \quad (3.7)$$

where $\Gamma_1{}^{(r)}$ is finite. Referring to Eq. (2.23), one sees that to order α, the factor $1+A_1$ may be extracted from all terms of the bracket in (3.5) and be absorbed into the amplitude of G_{12}. A similar result holds for the proton quantities,[7] completing the mass and Green's function renormalizations. The remaining renormalization is that of the charge appearing in the interaction

[6] E. E. Salpeter, Phys. Rev. **87**, 328 (1952).

[7] The actual calculations of the proton's mass and vertex operators appears to run into difficulties due to the extra dipole divergences mentioned earlier. However, one may show from general invariance considerations that equations analogous to (3.6) and (3.7) hold for proton quantities. $M_2{}^{(r)}$ and $\Gamma_2{}^{(r)}$ are infinite but we may assume such integrals have cutoffs. These difficulties produce no net effects on the finite parts of the calculations.

function. It may be shown that the Maxwell Green's function, to first order, can be written as

$$\mathcal{G}=(1+B)(\mathcal{G}^0+\mathcal{G}^{(r)}), \tag{3.8}$$

where B is infinite and of order α, and $\mathcal{G}^{(r)}$ is finite (to within the dipole infinities). From (2.23), one may then write

$$I_{12}=e^2(1+B)[i\,\mathrm{Tr}\rho\Gamma_1\Gamma_2(\mathcal{G}^0+\mathcal{G}^{(r)})-e^2I^{(2)}], \tag{3.9}$$

where $I^{(2)}$ is the second order interaction of (2.23). Defining the renormalized charge as

$$e'^2=e^2(1+B), \tag{3.10}$$

all the charges appearing in I_{12} may be written in terms of e', to the desired order. Having completed the renormalizations, we will drop the prime notation and assume that in all future equations, the quantities appearing are the renormalized ones. As will be shown in the Appendix, $M^{(r)}$ and $\mathcal{G}^{(r)}$ produce no energy shifts to the order desired and hence may be neglected. $\Gamma_1{}^{(r)}$ produces the correction to the hyperfine formula corresponding to the first order anomalous magnetic moment of the electron. $\Gamma_2{}^{(r)}$ would produce a similar effect for the proton. As the first case has been included in previous calculations,[8] and the second effect may be assumed to have been included in the experimental value to be inserted for the protons's magnetic moment, these terms also need not be considered further.

Having completed the renormalization, one may proceed with the perturbation theory. Separating out from the interaction function a static, non-spin dependent part I_0,

$$I_{12}=I_0+I', \tag{3.11}$$

one may define the Green's function, G_0, by the equation

$$[(\gamma_1p_1+m_1)(\gamma_2p_2+m_2)-I_0]G_0=1_11_2. \tag{3.12}$$

In the electrodynamical case, I_0 is proportional to the Coulomb energy. A first-order expression for G_{12} may be obtained by an iteration procedure:

$$G_{12}=G_0+G_0I'G_0. \tag{3.13}$$

Considering the equal times situation where the separation T_0 of (3.4) is a large positive number, an expansion such as (3.4) may always be made for G_0, yielding

$$\begin{aligned}G_{12}&(\mathbf{r}_1\mathbf{r}_2t,\ \mathbf{r}_1'\mathbf{r}_2't')\\&=-\sum_n\psi_n{}^0(\mathbf{r}_1\mathbf{r}_2)\exp(-iP_{0n}{}^0T_0)\bar{\psi}_n{}^0(\mathbf{r}_1'\mathbf{r}_2')\\&\quad+\sum_{n,n'}\psi_n{}^0(\mathbf{r}_1\mathbf{r}_2)\exp(-iP_{0n}{}^0t)\int\bar{\psi}_n{}^0(x_1'',x_2'')\\&\quad\times I'\psi_{n'}{}^0(x_1''',x_2''')\exp(iP_{0n'}{}^0t')\bar{\psi}_{n'}{}^0(\mathbf{r}_1'\mathbf{r}_2'),\end{aligned} \tag{3.14}$$

where the superscript "0" means quantities related to G_0. We wish to rearrange (3.14) into a form resembling (3.4). The phases then will be the energy eigenvalues, the coefficients of each phase the wave functions. To obtain the phases, one need only consider terms in the second sum where $n=n'$.[9] These terms are

$$\begin{aligned}\sum_n\psi_n{}^0(\mathbf{r}_1\mathbf{r}_2)\Big[&\exp(-iP_{0n}{}^0T_0)\int\psi_n{}^0(x_1'',x_2'')\\&\times I'\bar{\psi}_n{}^0(x_1''',x_2''')\Big]\bar{\psi}_n{}^0(\mathbf{r}_1'\mathbf{r}_2').\end{aligned} \tag{3.15}$$

In combination with the first sum of (3.14), the bracket may be viewed as the first order expansion of an exponential, and hence to the required accuracy, the right side of (3.14) can be written as

$$\begin{aligned}-\sum_n\psi_n{}^0(\mathbf{r}_1\mathbf{r}_2)\exp(-iT_0)\\\times\Big[P_{0n}{}^0-i/T_0\int\bar{\psi}_n{}^0I'\psi_n{}^0\Big]\bar{\psi}_n{}^0(\mathbf{r}_1'\mathbf{r}_2').\end{aligned} \tag{3.16}$$

Thus the first order energy shift becomes

$$\begin{aligned}\Delta E^{(1)}=-(i/T_0)\int\bar{\psi}^0(x_1,x_2)\\\times I'(x_1x_2,x_1'x_2')\psi^0(x_1',x_2').\end{aligned} \tag{3.17}$$

To obtain the second-order shift, one iterates twice, giving, for the diagonal terms,

$$\begin{aligned}-\sum_n\psi_n{}^0\exp(-iP_{0n}{}^0T_0)\bar{\psi}_n{}^0+\sum_n\psi_n{}^0\exp(-iP_{0n}{}^0T_0)\\\times\Big[\int\bar{\psi}_n{}^0I'\psi_n{}^0+\int\bar{\psi}_n{}^0I'G_0I'\psi_n{}^0\Big]\bar{\psi}_n{}^0.\end{aligned} \tag{3.18}$$

Thus the second-order energy shift becomes

$$\Delta E^{(2)}=-(i/T_0)\int\bar{\psi}^0I'G_1G_2I'\psi^0, \tag{3.19}$$

where, in concordance with our plan of treating the infrared difficulty, we have replaced the intermediate state Green's function G_0 by the free particle approximation, G_1G_2.[10]

The energy shifts may be expressed in terms of momentum integrals. In view of the center-of-mass dependence, one may write (using a "box normalization"):

$$\psi^0(x_1,x_2)=\exp(iP_\mu X_\mu)V^{-\frac{1}{2}}(2\pi)^{-2}\int e^{ipx}\psi^0(p)dp. \tag{3.20}$$

[8] R. Karplus and A. Klein, Phys. Rev. **85**, 972 (1952).

[9] The off-diagonal elements will give the first-order perturbed wave functions.

[10] In turning the expansion of (3.18) into an exponential one really requires the presence of the term $\frac{1}{2}(i\Delta E^{(1)}T)^2$ as the expansion must be adequate to second order. This term is actually present in the second term of the bracket of (3.18), as may be seen by breaking the G_0 there into its bilinear sum. Since n is a bound state, this term corresponds to a low-frequency intermediate state and hence, for the hyperfine problem, may be neglected. In general, it would seem essential that the rigorous G_0 be used in (3.19).

Defining

$$I'(p,p')=(2\pi)^{-4}\int e^{-iP(X-X')}e^{-ipx}e^{ip'x'}\times I'(x_1x_2,x_1'x_2')dxdx'd(X'-X), \quad (3.21)$$

one obtains

$$\Delta E^{(1)}=-i\int\bar{\psi}^0(p)I'(p,p')\psi^0(p')dpdp', \quad (3.22)$$

$$\Delta E^{(2)}=-i\int\bar{\psi}^0(p)I'(p,p')G_1(\mu_1P+p')\times G_2(\mu_2P-p')I'(p',p'')\psi^0(p'')dpdp'dp''. \quad (3.23)$$

The bound-state zeroth-order wave functions obey the homogeneous equation,

$$[(\gamma_1p_1+m_1)(\gamma_2p_2+m_2)-I_0]\psi^0=0. \quad (3.24)$$

IV. CALCULATIONS

As shown in the preceding section, the energy shifts may be obtained in terms of matrix elements of the interaction between the lowest-order wave functions. Due to the fact that I_0 is a static interaction, it is possible to obtain an adequate solution for the wave function based upon an iteration scheme stemming from the nonrelativistic Coulomb wave function.

In momentum space, the lowest-order interaction (2.22) becomes

$$I(p,p')=\frac{ie^2}{(2\pi)^4}\frac{\gamma_1\gamma_2}{(p-p')^2}+\frac{\lambda e^2}{(2\pi)^4}\frac{\gamma_{1\mu}\sigma_{2\alpha\mu}(p_\alpha-p_\alpha')}{(p-p')^2},\qquad \lambda=\mu'/e. \quad (4.1)$$

Selecting out the non-spin-dependent static part for I_0, (3.24) becomes in momentum space,

$$[\mu_1P_0+p_0-(\boldsymbol{\alpha}_1\cdot\mathbf{p}+\beta_1m_1)]\times[\mu_2P_0-p_0-(-\boldsymbol{\alpha}_2\cdot\mathbf{p}+\beta_2m_2)]\psi(p)=-\frac{ie^2}{(2\pi)^4}\int\frac{dp'}{(\mathbf{p}-\mathbf{p}')^2}\psi(p'). \quad (4.2)$$

$\boldsymbol{\alpha}$ and β are the usual Dirac matrices. Defining an equal relative times wave function,

$$\phi(\mathbf{p})=(2\pi)^{-\frac{1}{2}}\int dp_0\psi(p), \quad (4.3)$$

Salpeter[6] has shown that an equation for ϕ may be derived, and that to a first approximation, ϕ is the Schrödinger Coulomb wave function. Putting this approximate function in on the right of (4.2), one obtains the wave function

$$\psi(p)=-\frac{i}{2\mu(2\pi)^{\frac{1}{2}}}\frac{(\mathbf{p}^2+\alpha^2\mu^2)\phi(\mathbf{p})}{[\mu_1P_s+p_0-(\boldsymbol{\alpha}_1\cdot\mathbf{p}+\beta_1m_1)]\times[\mu_2P_s-p_0-(-\boldsymbol{\alpha}_2\cdot\mathbf{p}+\beta_2m_2)]}, \quad (4.4)$$

where μ is the reduced mass of the electron and $P_s=m_1+m_2-\frac{1}{2}\alpha^2\mu$ is the energy of the ground state of hydrogen. It is convenient in treating the first order perturbation shift to return to coordinate space for the relative time variable via the equation

$$\psi(\mathbf{p},t)=(2\pi)^{-\frac{1}{2}}\int e^{-ip_0t}\psi(p)dp_0. \quad (4.5)$$

The calculation of $\psi(\mathbf{p},t)$ is very similar to that done by Karplus and Klein.[3] We will only state the result:

$$\psi(\mathbf{p},t)=(2\pi)^{-\frac{1}{2}}(m_1+m_2)^{-1}\alpha\phi(0)(\mathbf{p}^2+\alpha^2\mu^2)^{-2}K(\mathbf{p},t), \quad (4.6)$$

where

$$\begin{aligned}K(\mathbf{p},t)=(4E_1E_2)^{-1}&[\exp^+\{(m_1E_2+m_2E_1)\\&\times(2m_1+\boldsymbol{\alpha}_1\cdot\mathbf{p})(2m_2-\boldsymbol{\alpha}_2\cdot\mathbf{p})-\mathbf{p}^2[(E_2-E_1)\\&\times(2m_1+\boldsymbol{\alpha}_1\cdot\mathbf{p}-2m_2+\boldsymbol{\alpha}_2\cdot\mathbf{p})-(m_1E_2+m_2E_1)]\}\\&+\exp^-\{(2E_1E_2\epsilon(t)+m_1E_2-m_2E_1)\\&\times(2m_1+\boldsymbol{\alpha}_1\cdot\mathbf{p})(2m_2-\boldsymbol{\alpha}_2\cdot\mathbf{p})\\&-\mathbf{p}^2[(E_1+E_2)(2m_1+\boldsymbol{\alpha}_1\cdot\mathbf{p}-2m_2+\boldsymbol{\alpha}_2\cdot\mathbf{p})\\&+(2E_1E_2\epsilon(t)+m_2E_1-m_1E_2)]\}], \quad (4.7)\end{aligned}$$

and

$$\exp^{\pm}=e^{-i[E_1\epsilon(t)-m_1]t}\pm e^{-i[E_2\epsilon(t)+m_2]t},\qquad E=(\mathbf{p}^2+m^2)^{\frac{1}{2}},\quad \epsilon(t)=\begin{cases}+1 & t>0\\ -1 & t<0.\end{cases} \quad (4.8)$$

$\phi(0)$ is the value of the ground-state wave function at the origin in coordinate space.

We consider now the first-order energy shift with the first-order interaction. After subtracting out I_0, (4.1) may be divided into a "charge" and "dipole" part:

$$I^{(1)c}(p,p')=\frac{ie^2}{(2\pi)^4}\frac{\beta_1\beta_2}{(p-p')^2}\left[\boldsymbol{\alpha}_1\cdot\boldsymbol{\alpha}_2-\frac{(p_0-p_0')^2}{(\mathbf{p}-\mathbf{p}')^2}\right],\qquad I^{(1)d}(p,p')=\frac{\lambda e^2}{(2\pi)^4}\frac{\gamma_{1\mu}\sigma_{2\alpha\mu}(p_\alpha-p_\alpha')}{(p-p')^2}. \quad (4.9)$$

Substituting $I^{(1)c}$ into (3.22) yields

$$\Delta E^{(1)c}=-\frac{i}{2\pi}\frac{ie^2}{(2\pi)^4}\int\psi^*(\mathbf{p},t)e^{-ip_0t}\cdot\times\frac{\boldsymbol{\alpha}_1\cdot\boldsymbol{\alpha}_2-(p_0-p_0')^2/(\mathbf{p}-\mathbf{p}')^2}{(\mathbf{p}-\mathbf{p}')^2-(p_0-p_0')^2}e^{ip_0't'}\psi(\mathbf{p}',t'). \quad (4.10)$$

The p_0 and p_0' integrations may be performed upon using the usual outgoing wave perscription:

$$\Delta E^{(1)c}=\frac{\pi ie^2}{(2\pi)^4}\int\psi^*(\mathbf{p},t)\exp\{-i[(\mathbf{p}-\mathbf{p}')^2]^{\frac{1}{2}}|t|\}\times\frac{\boldsymbol{\alpha}_1\cdot\boldsymbol{\alpha}_2-1}{[(\mathbf{p}-\mathbf{p}')^2]^{\frac{1}{2}}}\psi(\mathbf{p}',t). \quad (4.11)$$

Inserting the wave function (4.6) into (4.11) gives[11]

$$\Delta E^{(1)e}=\frac{ie^2}{2(2\pi)^4}\frac{\alpha^2|\phi(0)|^2}{(m_1+m_2)^2}\times\int\frac{K(\mathbf{p},-t)}{(\mathbf{p}^2+\alpha^2\mu^2)^2}\frac{\exp\{-i[(\mathbf{p}-\mathbf{p}')^2]^{\frac{1}{2}}|t|\}}{[(\mathbf{p}-\mathbf{p}')^2]^{\frac{1}{2}}}\times[\boldsymbol{\alpha}_1\cdot\boldsymbol{\alpha}_2-1]\frac{K(\mathbf{p}',t)}{(\mathbf{p}'^2+\alpha^2\mu^2)^2}. \quad (4.12)$$

The calculation now proceeds exactly as the corresponding one done by Karplus and Klein. We desire the α^{-2} and α^{-1} parts of the integral which can be obtained from the part of the integrand which is large when at most one of the momentum variable is large. We also desire the spin-spin interactions as we are interested only in the hyperfine shift. These two conditions restrict the portions of the integrand which are relevant. Further, where one momentum variable is large, we will neglect the $\alpha^2\mu^2$ in the corresponding denominator. This corresponds to the neglecting of binding effects in the intermediate states and will produce its quota of infrared divergences. Upon carrying through these simplifications, the integrations may be performed yielding

$$\Delta E^{(1)e}=\frac{2\pi}{3}\frac{\alpha}{m_1m_2}\boldsymbol{\sigma}_1\cdot\boldsymbol{\sigma}_2|\phi(0)|^2\left[1-\frac{4\alpha}{\pi}-\frac{2\alpha}{\pi(m_1+m_2)}\times\left\{m_1\ln\frac{m_2}{2p}+m_2\ln\frac{m_1}{2p}\right\}\right], \quad (4.13)$$

where p is the infrared cutoff.

A similar calculation may be done for the dipole part of the interaction. The result here is[12]

$$\Delta E^{(1)D}=\frac{4\pi}{3}\frac{\alpha\lambda}{m_1}\boldsymbol{\sigma}_1\cdot\boldsymbol{\sigma}_2|\phi(0)|^2\left[1-\frac{4\alpha}{\pi}-\frac{2\alpha}{\pi(m_1+m_2)}\times\left\{m_1\ln\frac{m_2}{2p}+m_2\ln\frac{m_1}{2p}\right\}\right]. \quad (4.14)$$

We turn now to the effects of the second-order interaction [the second term of (2.23)] in the first order perturbation formula. This interaction contains the double photon processes and consists of three types of terms according to whether the proton interacts zero, once, or twice with the electromagnetic field via its spin current. In momentum space, the interaction is

$$I^{pp}=-\frac{e^4}{(2\pi)^8}\int dk\frac{N_1+N_2+N_3}{[(\mu_1P_s+p+k)^2+m_1^2][k-p'+p]^2\times[(\mu_2P_s+k-p')^2+m_2^2]k^2}, \quad (4.15)$$

where

$$N_1=\gamma_{1\mu}[m_1-\gamma_1(\mu_1P_s+p+k)]\times\gamma_1\gamma_2[m_2-\gamma_2(\mu_2P_s-p'+k)]\gamma_{2\mu},$$

$$N_2=i\lambda\gamma_{1\mu}[m_1-\gamma_1(\mu_1P_s+p+k)]\gamma_{1\lambda}\sigma_{2\alpha\lambda}\times(p'-p-k)_\alpha[m_2-\gamma_2(\mu_2P_s-p'+k)]\gamma_{2\mu}, \quad (4.16)$$

$$N_3=-\lambda^2\gamma_{1\mu}[m_1-\gamma_1(\mu_1P_s+p+k)]\gamma_{1\lambda}\sigma_{2\lambda\alpha}(p'-p-k)_\alpha\times[m_2-\gamma_2(\mu_2P_s-p'+k)]\sigma_{2\mu\beta}(k-p'+p)_\beta.$$

Since the interaction is already second order, we need not treat the integrals in the perturbation formula as accurately as before.

First, one requires only the low-momentum parts of the wave function and hence may set $\mathbf{p}$ and $\mathbf{p}'$ to zero in I^{pp}. Also, the p_0 poles, unlike the situation in the first order interaction, will occur at high-frequency values and give higher order contributions to the energy shift. Thus it is possible in general to set p and p' to zero in $I^{pp}(p,p')$. Under these conditions, (3.22) becomes:

$$\Delta E^{(1)pp}=-i(2\pi)^4|\phi(0)|^2I^{pp}(0,0). \quad (4.17)$$

This result is in direct agreement with the idea that for the hyperfine effects, only small distances are involved requiring only the wave function at the origin.

The calculation proceeds as follows: first, the spin-spin parts of the numerator are picked out. The three poles in the denominator may then be integrated. Following this, the remaining real variable integrations may be performed. The final answer is:

$$\Delta E^{(1)pp}=\frac{2\pi}{3}\frac{\alpha}{m_1m_2}\boldsymbol{\sigma}_1\cdot\boldsymbol{\sigma}_2|\phi(0)|^2\left[\frac{4\alpha}{\pi}+\frac{3\alpha}{2\pi(m_2-m_1)}\times\left\{m_2\ln\frac{m_1}{2p}-m_1\ln\frac{m_2}{2p}\right\}\right]+\frac{4\pi}{3}\frac{\alpha\lambda}{m_1}\boldsymbol{\sigma}_1\cdot\boldsymbol{\sigma}_2|\phi(0)|^2\times\left[\frac{4\alpha}{\pi}+\frac{3\alpha}{\pi}\ln\frac{m_1}{2p}\right]+\lambda^2\alpha^2\boldsymbol{\sigma}_1\cdot\boldsymbol{\sigma}_2|\phi(0)|^2\left[\frac{1}{6}-\frac{1}{m_2-m_1}\times\left\{4m_2\ln\frac{2\bar{p}}{m_2}-(3m_1+m_2)\ln\frac{2\bar{p}}{m_1}\right\}\right], \quad (4.18)$$

where $\bar{p}$ is a dipole ultraviolet cutoff. We have also assumed that the infrared cutoff is the same as in the previous calculations.

The final contribution to the energy shift that need be considered comes from the second-order perturbation formula. Here we consider only the lowest-order interaction:

$$\Delta E^{(2)}=-i\int\bar{\psi}(p)[I^{(1)e}(p,k)+I^{(1)d}(p,k)]\times G_1(\mu_1P_s+k)G_2(\mu_2P_s-k)[I^{(1)e}(k,p')+I^{(1)d}(k,p')]\psi(p'). \quad (4.19)$$

[11] $\psi^*(\mathbf{p},t)$ is not actually the complex conjugate of ψ. An analysis of its definition, (3.1), will show that for our function, (4.6), it is actually the time reversed function.

[12] I should like to thank Dr. W. A. Newcomb for finding an error in the calculation of this term.

As in the previous calculation, one may set $\not{p}$ and $\not{p}'$ to zero in the interaction terms, yielding

$$\Delta E^{(2)}=-i(2\pi)^4|\phi(0)|^2\int dk[I^{(1)e}(0,k)+I^{(1)d}(0,k)]G_1(\mu_1\not{P}_s+k)G_2(\mu_2\not{P}_s-k)\times[I^{(1)e}(k,0)+I^{(1)d}(k,0)]. \quad (4.20)$$

Again there are three types of terms corresponding to the three possible ways the proton may interact with the electromagnetic field. The calculation proceeds in an analogous fashion, giving for the energy shift:

$$\Delta E^{(2)}=\frac{2\pi}{3}\frac{\alpha}{m_1m_2}\boldsymbol{\sigma}_1\cdot\boldsymbol{\sigma}_2|\phi(0)|^2\left[\frac{\alpha}{2\pi(m_1+m_2)}\times\left(m_2\ln\frac{m_1}{2p}+m_1\ln\frac{m_2}{2p}\right)\right]-\frac{4\pi}{3}\frac{\alpha\lambda}{m_1}\boldsymbol{\sigma}_1\cdot\boldsymbol{\sigma}_2|\phi(0)|^2\times\left\{\frac{\alpha}{\pi(m_1+m_2)}\left[(3m_1+m_2)\ln\frac{m_1}{2p}-2m_1\ln\frac{m_2}{2p}\right]\right\}+\lambda^2\alpha^2\boldsymbol{\sigma}_1\cdot\boldsymbol{\sigma}_2|\phi(0)|^2\left\{\frac{1}{6}\frac{1}{m_1+m_2}\times\left[(3m_1-m_2)\ln\frac{2\tilde{p}}{m_1}+4m_2\ln\frac{2\tilde{p}}{m_2}\right]\right\}. \quad (4.21)$$

V. RESULTS

Adding up the results of the preceding section, the infrared divergences cancel. Keeping terms only to order m_1/m_2, the total shift due to reduced mass corrections may be written as[13]

$$\Delta E=\frac{4\pi}{3}\frac{\alpha\lambda_p}{m_1}\boldsymbol{\sigma}_1\cdot\boldsymbol{\sigma}_2|\phi(0)|^2\times\left[1-\frac{\alpha}{\pi}\frac{m_1}{m_2\mu_p}\left\{\left[3-\tfrac{3}{4}(\mu_p-1)^2\right]\ln\frac{m_2}{m_1}+\frac{9}{4}(\mu_p-1)^2\ln\frac{2\tilde{p}}{m_2}-\frac{1}{8}(\mu_p-1)^2\right\}\right], \quad (5.1)$$

where $\lambda_p=1/(2m_2)+\lambda$ and μ_p is the protons total magnetic moment expressed in units of the nuclear magneton. The coefficients in front of the bracket is the Fermi formula, modified by the usual reduced mass correction.

Neglecting the shift calculated here, Dumond and Cohen[14] have made a least-squares fitting of atomic constants and obtained a value for the fine structure constant of

$$1/\alpha=137.0377\pm0.0016. \quad (5.2)$$

Including the above corrections, one obtains

$$1/\alpha=\begin{cases}137.0378 & \text{for } \tilde{p}=\text{meson mass},\\ 137.0374 & \text{for } \tilde{p}=\text{proton mass},\end{cases} \quad (5.3)$$

the contributions from the Dirac and Pauli moments almost cancelling. The results are fairly insensitive to the cut-off value.

In evaluating the validity of the results, two points should be noted. Though the final formula is independent of the infrared cutoff we have assumed that all the cutoffs were equal. Since the divergences come from intrinsically different momentum integrations, this assumption need not be true. Recently, however, the two-body Green's function equation has been rearranged so that the infrared divergences can be eliminated from the beginning. It appears that the prescriptions used here are correct.[15] Difficulties also appear in dealing with the ultraviolet cutoff. In the dipole terms which are finite, we have assumed that the upper limits on the momentum are rigorously at infinity and have introduced cutoffs only in the divergent terms. Since the meson mass is not a particularly high frequency this procedure might disturb the values of the finite terms. The issue could be settled by inserting a form factor into the Pauli term rather than using cutoffs, but this would greatly complicate the calculations.

VI. ACKNOWLEDGMENTS

It is with great pleasure that I record my indebtedness to Professor J. Schwinger for suggesting this problem and for aid received throughout the course of my work. I also wish to thank Professor R. Karplus and Dr. A. Klein for suggesting that their method of calculation was applicable to this problem and for many helpful conversations explaining their technique.

APPENDIX

It will be shown here that both $M^{(r)}$ and $\mathcal{G}^{(r)}$ produce no contribution to the hyperfine splitting to the desired order. The interaction proportional to $M_1^{(r)}$ is

$$I(p,p')=M_1^{(r)}(\mu_1\not{P}_s+\not{p})[\gamma_2(\mu_2\not{P}_s-\not{p})+M_2^{(r)}(\mu_2\not{P}_s-\not{p})]\delta(p-p'). \quad (A.1)$$

First-order perturbation theory leads to an energy shift of

$$\Delta E=-i\int\bar{\psi}(p)M_1^{(r)}(\mu_1\not{P}_s+\not{p})[\gamma_2(\mu_2\not{P}_s-\not{p})+M_2^{(r)}(\mu_2\not{P}_s-\not{p})]\psi(p)dp. \quad (A.2)$$

Due to the $\delta(p-p')$ appearing in (A.1) only one

[13] This result is in agreement with that obtained by W. A. Newcomb (private communication).

[14] J. W. M. Dumond and E. R. Cohen, Special Technical Report No. 1, U. S. Atomic Energy Commission, Nov. 1952 (unpublished).

[15] Conversations with J. Schwinger and R. Karplus.

momentum integration remains in (A.2) and thus no spin-spin combinations can be formed. A similar phenomenon occurs in the second-order perturbation shift.

Upon evaluation of the first-order polarization operators, $\mathfrak{S}^{(r)}$ may be written as

$$\mathfrak{S}_{\mu\nu}{}^{(r)}(p)=-\delta_{\mu\nu}\frac{\alpha}{4\pi}\Big[4\Lambda^2\int_0^\infty\frac{ds}{s}\exp(-sm^2)+\int_0^1 du\frac{f_1(u)}{m_1{}^2+u(1-u)p^2}+\int_0^1 du\frac{f_2(u)}{m_2{}^2+u(1-u)p^2}\Big],\quad(A.3)$$

the first term having an extra dipole infinity. These terms lead to a second-order interaction. Considering the constant term first, one obtains an interaction of

$$I(p,p')=\text{const}\times 4\alpha^2\Lambda^2\gamma_1\gamma_2,\quad(A.4)$$

which leads to an energy shift of

$$\Delta E\sim\int\bar{\psi}(p)\gamma_1\gamma_2\psi(p')dpdp',\quad(A.5)$$

which has no spin-spin part. The evaluation of the energy shifts from the second and third terms would be analogous to the evaluation of $\Delta E^{(1)e}$ except that interaction is already second order and the low-frequency pole of D_+ has been replaced by a high-frequency pole. Thus these terms give no contribution to the desired order.

PHYSICAL REVIEW VOLUME 92, NUMBER 4 NOVEMBER 15, 1953

A New Modification of Classical Electromagnetic Theory*

A. SCHILD
Carnegie Institute of Technology, Pittsburgh, Pennsylvania
(Received June 19, 1953)

A fundamental particle is treated as a unit charge whose rest mass and space time coordinates are variables of its motion. Classical electrodynamics, in its action at a distance formulation, is obtained from an action principle which is simpler than the usual one. In this new action principle the rest mass of a particle is varied as well as the coordinates. The rest masses of interacting particles, although not assumed constant *a priori*, become constants as a consequence of the equations of motion. Modifications of the old action principle can yield purely electromagnetic rest masses which are, however, the same for all particles. Similar modifications of the new action principle give purely electromagnetic rest masses to all charged fundamental particles. In this new modification of electrodynamics, particles interacting at small distances no longer have constant rest masses.

1. INTRODUCTION

OF the many fields which play an important role in quantum physics, the one whose classical counterpart is most familiar is the electromagnetic field. It has been known for a long time that classical electrodynamics can be formulated in two equivalent forms, as a field theory (Faraday-Maxwell-Lorentz) or as a theory of action at a distance between charged particles.[1] In the case of electrodynamics the two formulations are of the same order of simplicity. Other fields (such as meson fields) could also be described classically in an equivalent action at a distance formulation but, in general, the two descriptions would not be equally simple.

In modern physics it is the field-theoretic point of view which has been stressed. Ignoring quantum mechanical considerations such as statistics, each type of free fundamental particle (photon, electron, meson, nucleon, etc.) is described by a set of field variables whose behavior is characterized by a different Lagrangian function. Interaction is characterized by additional Lagrangians which are functions of the field variables of two or more different fundamental particles. Even if this kind of description gave good results, it can hardly be regarded as satisfactory at a time when the number of fundamental particles is of order 20 and still increasing.

It may be claimed, with only some measure of truth perhaps, that all simple field theories modeled on electrodynamics have been examined exhaustively, and that not one of them shows any indications of explaining all processes involving fundamental particles. It therefore seems worthwhile to investigate systematically all simple modifications of electrodynamics in its action at a distance formulation. The present field theories may well turn out to be asymptotic approximations of an even more complicated and nonlocal field theory which corresponds to a simple equivalent action at a

* Supported in part by the Office of Scientific Research; U. S. Air Force.

[1] K. Schwarzschild, Nach. Akad. Wiss. Göttingen Math. physik. Kl. IIa **1903**, 128, 132, 245 (1903); H. Tetrode, Z. Physik **10**, 317 (1922); A. D. Fokker, Z. Physik **58**, 386 (1929); Physica **9**, 33 (1929); **12**, 145 (1932); J. A. Wheeler and R. P. Feynman, Revs. Modern Phys. **17**, 157 (1945); **21**, 425 (1949).

distance theory. Work in this direction has been done by Landé,[2] Groenewold,[3] Bopp,[4] Peierls, McManus,[5] and particularly by Feynman.[6]

In this paper we shall discuss a new and speculative kind of modification of classical electrodynamics in its action at a distance formulation. The principal idea is to give up the concept of a constant rest mass associated with a fundamental particle, and instead to treat the rest mass as a variable of the motion (like the coordinates). Some of the reasons for considering this possibility are given in the remainder of this section.

We know that the rest mass of fundamental particles is not, in fact, conserved. When electron-positron pairs annihilate, when neutrons or mesons decay, the total rest mass of the system changes. Usually such phenomena enter the theoretical description only with the process of quantization and the introduction of creation and annihilation operators. There seems to be no good reason why such changes of rest mass should not be incorporated in the classical theory before quantization.

From the mathematical point of view the requirement that the rest mass of a particle be constant is somewhat artificial and is quite independent of the requirement of relativistic invariance. The relativistic equation of motion of a particle is

$$dp_\mu/ds = F_\mu, \tag{1}$$

where

$$p_\mu = m dx_\mu/ds \tag{2}$$

is the momentum 4-vector of the particle, and F_μ is the 4-force which, in an action at a distance theory, is determined by the motion of the other particles. The requirement that the rest mass m be constant is equivalent to demanding that the 4-force be always perpendicular to the world line of the particle:

$$F_\mu p^\mu = 0. \tag{3}$$

In electrodynamics the condition (3) is satisfied in a natural manner. But this is not always so. For example, in the theory of a scalar potential V, giving rise to an inverse square law of attraction, the condition (3) can be satisfied only by subtracting out the tangential component from the simplest definition $\partial V/\partial x^\mu$ of the 4-force.

In Sec. 3 it will be shown that classical electrodynamics can be obtained from an action principle which is simpler than the usual one. In this new action principle the rest mass of a particle is varied as well as the coordinates. The constancy of the rest mass then follows as a consequence of the equations of motion. Simple modifications of this action principle yield theories in which the rest mass is no longer a constant of the motion.

Modifications of the usual action principle are possible which yield a purely electromagnetic rest mass for a fundamental particle. But this electromagnetic rest mass is unique, being determined by the particular modification used. The new action principle permits a new class of simple modifications in which the rest masses of all charged fundamental particles are of purely electromagnetic origin.

The ultimate object of the point of view adopted here is to explain nature in terms of a single law of interaction between fundamental particles of one kind only. Such a particle is characterized mainly by its charge e, a fundamental constant. At distances large compared to 10^{-13} cm, particles interact electromagnetically and their rest masses are automatically conserved. At small distances particles interchange not only momentum (mutual accelaration) but also rest mass. In the classical theory the rest mass is treated as a continuous variable, but it is hoped that quantization will introduce discreteness. In a quantized theory it is also expected that exchange of rest mass will be accompanied by exchange of spin. Neutral particles have little room in this type of theory; they are the agents of rest-mass exchange between charged particles and play a role analogous to electromagnetic interaction.

2. UNITS AND NOTATION

We choose units such that the velocity of light $c=1$ and the magnitude of the electronic charge $|e|=1$. The charge of a fundamental particle is then dimensionless and always

$$e = \pm 1. \tag{4}$$

Length and time are measured in cm, and mass in cm^{-1}, the electronic mass being

$$m_0 = 3.6\times 10^{12}\ \text{cm}^{-1}. \tag{5}$$

Greek suffixes range over 0, 1, 2, 3 and the coordinates $x^\mu \equiv (t, \mathbf{r})$ are real. Proper time is denoted by s and the Minkowskian metric given by

$$ds^2 = (dx^0)^2 - (dx^1)^2 - (dx^2)^2 - (dx^3)^2. \tag{6}$$

The usual conventions apply to summation dummies and to the raising and lowering of suffixes.

The rest mass of a particle is denoted by m. The electromagnetic potentials are $A_\mu \equiv (\phi, -\mathbf{A})$, and the electromagnetic field tensor is

$$F_{\mu\nu} = \partial A_\mu/\partial x^\nu - \partial A_\nu/\partial x^\mu. \tag{7}$$

When systems of particles are considered, the different particles are labeled by bracketed latin suffixes. Thus $x_{(a)^\mu}$, $e_{(a)}$, $m_{(a)}$, $\cdots$, are the coordinates, charge, rest mass, $\cdots$, of particle a, $A_{(a)\mu}$, $F_{(a)\mu\nu}$ describe the electromagnetic field at particle a due to the other

[2] A. Landé, Phys. Rev. **56**, 482 (1939); **76**, 1176 (1949); **77**, 814 (1950); J. Franklin Inst. **231**, 63 (1941).
[3] H. J. Groenewold, Physica **6**, 115 (1939).
[4] F. Bopp, Ann. Physik **42**, 573 (1943).
[5] H. McManus, Proc. Roy. Soc. (London) **A195**, 323 (1948); see also J. Irving, Proc. Phys. Soc. (London) **A62**, 780 (1949).
[6] R. P. Feynman, Phys. Rev. **74**, 939 (1948); a review article on the work of Bopp, Feynman, and others has recently been written by H. Hönl, Ergeb. exakt. Naturwiss. **26**, 291 (1952).

charges. The summation convention does not apply to these bracketed Latin suffixes.

3. MOTION OF A SINGLE PARTICLE

Before going on to the general problem of several particles interacting at a distance, we shall discuss the simpler case of a single charged particle in a known electromagnetic field. The field is given by electromagnetic potentials A_μ which are functions of the coordinates x^μ only.

The equations of motion of the particle can be obtained from the well-known action principle

$$\delta\int_{P_1}^{P_2}[m(dx_\mu dx^\mu)^{\frac{1}{2}}+eA_\mu dx^\mu]=0, \tag{8}$$

where the variations are assumed to vanish at the end points:

$$\delta x^\mu=0 \quad \text{at} \quad P_1, P_2. \tag{9}$$

This leads to the Lorentz equations

$$m\frac{d^2x_\mu}{ds^2}=e\frac{dx^\nu}{ds}F_{\nu\mu}. \tag{10}$$

Along the world line of the particle we now introduce a preferred (i.e., nongeneral) parameter u defined by

$$du=ds/m. \tag{11}$$

Then the momentum (2) of the particle is

$$p^\mu=dx^\mu/du, \tag{12}$$

and the rest mass m is given by

$$m^2=p^\mu p_\mu=\frac{dx^\mu}{du}\frac{dx_\mu}{du}. \tag{13}$$

In terms of the parameter u, the action principle (8) may be written in the form

$$\delta\int_{P_1}^{P_2}[p^\mu p_\mu+ep^\mu A_\mu]du=0, \tag{14}$$

where the variation is not only subject to the end conditions (9), but also to the auxiliary condition

$$\delta(p^\mu p_\mu)=0, \tag{15}$$

which expresses the fact that the constant rest mass m is not to be varied. Because of the auxiliary condition, the reformulation of the variational principle (8) in Eq. (14) is clumsy; it is given here only for comparison with the new action principle below.

For particles with constant rest mass m the parameters s and u are only trivially different. This is no longer the case when we consider a particle with variable rest mass. The motion of such a particle can be described by assigning any time-like world line parametrized arbitrarily by the monotonic parameter u. Analytically, this is equivalent to assigning the four functions

$$x^\mu=x^\mu(u). \tag{16}$$

The momentum of the particle and the variable rest mass can be obtained by differentiation, as in Eqs. (12) and (13). The only restriction on (16) is that the momenta be always time-like:

$$\frac{dx^\mu}{du}\frac{dx_\mu}{du}>0. \tag{17}$$

We now consider a new action principle for the motion of a particle with variable rest mass:

$$\delta\int_{u_1}^{u_2}L(x,\,p)du=0, \tag{18}$$

$$L\equiv p^\mu p_\mu+2ep^\mu A_\mu. \tag{19}$$

Here p^μ is not an independent variable but an abbreviation for dx^μ/du. In this variational principle the rest mass of the particle is varied as well as the coordinates x^μ; thus no auxiliary condition such as (15) is prescribed. On the other hand we add to the end conditions (9) the new restriction that the parameter u for the varied motion take on the same initial and final values u_1, u_2, as for the original motion.[7] We shall express this by writing

$$\delta x^\mu=0, \quad \delta u=0, \quad \text{for } u=u_1,\, u_2. \tag{20}$$

The Euler-Lagrange equations of the new variational principle (18) are

$$\frac{d}{du}\frac{\partial L}{\partial p^\mu}-\frac{\partial L}{\partial x^\mu}=0, \tag{21}$$

or, by (19),

$$dp_\mu/du=ep^\nu F_{\nu\mu}. \tag{22}$$

From these equations of motion and the skew-symmetry of $F_{\mu\nu}$ it follows that

$$p^\mu\frac{dp_\mu}{du}=\frac{1}{2}\frac{d}{du}(p^\mu p_\mu)=0,$$

and, by integration, that

$$m^2=p^\mu p_\mu=\text{constant}. \tag{23}$$

Using this result, it is now easily seen that Eqs. (22) are identical with the Lorentz equations of motion (10).

Thus we regain the equations of motion of classical electrodynamics. Although the constancy of the rest mass is not assumed *a priori*, it now follows as a consequence of the equations of motion. The Lagrangian (19) is rational in the derivatives $p^\mu=dx^\mu/du$, and

[7] The new end condition suggests the possibility of a 5-dimendional representation with u as a fifth coordinate. For a 5-dimensional theory with some similarity to the present one, see H. C. Corben, Nuovo cimento **9**, 235 (1952).

therefore the new action principle (18) is simpler than the old action principle (8).

The Euler-Lagrange equations (21) have, quite generally, the Jacobian integral

$$p^\mu \partial L/\partial p^\mu - L = \text{constant}. \tag{24}$$

If the Lagrangian L has the special form (19), this equation reduces to (23). Classical electrodynamics may be modified by retaining the action principle (18), (20), but with more general Lagrangians. For example, in Eq. (19) the potentials A_μ may be given as functions of the coordinates x^μ and of the momenta p^μ of the particle. Generalizations of this type are considered in Sec. 5. In these cases, Eq. (24) remains as an integral of the motion, but it no longer reduces to (23), so that the rest mass of a particle changes during its motion.

4. SYSTEMS OF PARTICLES

The physical laws governing the motion of several charged particles in electromagnetic interaction can be summarized in the Fokker[1] action principle:

$$\delta\Big[\sum_a m_{(a)} \int (dx_{(a)}{}^\mu dx_{(a)\mu})^{\frac{1}{2}} + \sum\sum_{a<b} e_{(a)} e_{(b)} \int\int \delta(\xi_{(ab)}{}^\nu \xi_{(ab)\nu}) dx_{(a)}{}^\mu dx_{(b)\mu}\Big] = 0. \tag{25}$$

The δ in the double integral is the Dirac delta function, and $\xi_{(ab)}{}^\mu$ is a vector joining two points on the world lines of the particles a and b:

$$\xi_{(ab)}{}^\mu = x_{(a)}{}^\mu - x_{(b)}{}^\mu. \tag{26}$$

If the motion of particle a is varied, the action principle (25) reduces to (8):

$$\delta \int [m_{(a)} (dx_{(a)}{}^\mu dx_{(a)\mu})^{\frac{1}{2}} + e_{(a)} A_\mu dx_{(a)}{}^\mu] = 0, \tag{27}$$

where

$$A_{(a)\mu} = \sum_{\substack{b \\ (b \neq a)}} e_{(b)} \int \delta(\xi_{(ab)}{}^\nu \xi_{(ab)\nu}) dx_{(b)\mu} \tag{28}$$

are electromagnetic potentials at particle a generated by the remaining particles of the system. The electromagnetic field tensor, derived from these potentials, satisfies Maxwell's equations.

Thus the action at a distance theory characterized by the Fokker action principle is essentially equivalent to classical electromagnetic field theory. There is, however, one important difference. The potentials (28) are not the usual retarded Lienard-Wiechert potentials, but are half the retarded plus half the advanced potentials. In their absorber theory of radiation,[1] Wheeler and Feynman have shown that in a universe with large numbers of charges such a theory not only reproduces the usual interaction by only retarded potentials, but that it also gives the correct relativistic radiation-reaction forces on a charged particle. We shall accept this general scheme and give no further discussion of possible difficulties associated with the advanced potentials.

We now replace the Fokker action principle (25) by a new action principle for charged particles with variable rest masses:

$$\delta\Big[\sum_a \int p_{(a)}{}^\mu p_{(a)\mu} du_{(a)} + \sum_a \sum_{\substack{b \\ (b \neq a)}} e_{(a)} e_{(b)} \times \int\int \delta(\xi_{(ab)}{}^\nu \xi_{(ab)\nu}) p_{(a)}{}^\mu p_{(b)\mu} du_{(a)} du_{(b)}\Big] = 0, \tag{29}$$

$$p_{(a)}{}^\mu \equiv dx_{(a)}{}^\mu / du_{(a)}.$$

Note that the double sum in (29) contains two identical interaction terms for each pair of distinct particles, whereas the double sum in (25) contains only one interaction term for each such pair. For the variation of the motion of particle a, this action principle reduces to

$$\delta \int_{u_{(a)1}}^{u_{(a)2}} [p_{(a)}{}^\mu p_{(a)\mu} + 2e_{(a)} p_{(a)}{}^\mu A_{(a)\mu}] du_{(a)} = 0, \tag{30}$$

$$A_{(a)\mu} = \sum_{\substack{b \\ (b \neq a)}} e_{(b)} \int \delta(\xi_{(ab)}{}^\nu \xi_{(ab)\nu}) p_{(b)\mu} du_{(b)}. \tag{31}$$

The action principle (30) is identical with (18), (19). It is again assumed that the u length,

$$\int_{u_{(a)1}}^{u_{(a)2}} du_{(a)},$$

of particle a is the same for the original and the varied motion. The electromagnetic potentials in (31) are identical with those of (28). The contribution $A_{(ab)\mu}$ of particle b to the potentials $A_{(a)\mu}$ at $x_{(a)}{}^\mu$ is easily obtained explicitly:

$$A_{(ab)\mu} = \tfrac{1}{2} e_{(b)} \frac{p_{(b-)\mu}}{\xi_{(ab-)\nu} p_{(b-)}{}^\nu} + \tfrac{1}{2} e_{(b)} \frac{p_{(b+)\mu}}{-\xi_{(ab+)\nu} p_{(b+)}{}^\nu}. \tag{32}$$

Here the $-$ and $+$ signs in the suffixes refer to the two points on the world line b which are respectively retarded and advanced relative to $x_{(a)}{}^\mu$ so that

$$\xi_{(ab-)\nu} \xi_{(ab-)}{}^\nu = \xi_{(ab+)\nu} \xi_{(ab+)}{}^\nu = 0. \tag{33}$$

This is illustrated in Fig. 1. The first term in (32) is one-half the usual retarded Lienard-Wiechert potential and the second term is the corresponding advanced potential. $A_{(ab)\mu}$ is homogeneous of degree zero in $p_{(b)\mu}$ so that only the direction of the world line b enters into this expression and not, for example, the rest mass $m_{(b)}$.

It follows from our previous discussion that the new action principle (29) gives the same physical results as

the Fokker action principle and thus reproduces classical electromagnetism. In particular, the rest mass of each particle is a constant of the motion.

5. ELECTROMAGNETIC SELF-ENERGY

The only null vector $\xi_{(aa)}{}^{\mu}$ from a point $x_{(a)}{}^{\mu}$ to a time like world line passing through the point is the zero vector,

$$\xi_{(aa\pm)}{}^{\mu}=0. \tag{34}$$

Thus, the self-field of a particle, given by (32) with $b=a$, is infinite. This is the usual Coulomb infinity of a point charge. It can be avoided if the δ-function in the Fokker action principle is replaced by some other approximating function f. As Feynman has shown,[6] the interaction term of a particle with itself is then finite and for a particle with moderate acceleration, reduces to the inertial term $\int mds$. Thus the mass of a particle can be ascribed to an electromagnetic origin. However, the electromagnetic rest mass m is uniquely determined by the *structure* function f. If this function is chosen to fit the mass of electrons, then the masses of other fundamental particles, such as protons, will not be purely electromagnetic. This difficulty can be overcome by replacing the δ function in the new action principle (29) by a function not only of $\xi_{(ab)}{}^{\mu}$ but also of the momenta $p_{(a)}{}^{\mu}$, $p_{(b)}{}^{\mu}$.

In order to be specific we shall discuss a simple structure function of the type proposed by Landé[2] and Groenewold.[3] The δ-function in (29) is replaced by

$$\delta(\xi_{(ab)}{}^{\nu}\xi_{(ab)\nu}-\lambda^2), \tag{35}$$

where λ is small and may, for the moment, be considered constant. The potentials, obtained with this structure function, are still given by (32). However, the retarded or advanced events are no longer connected by null

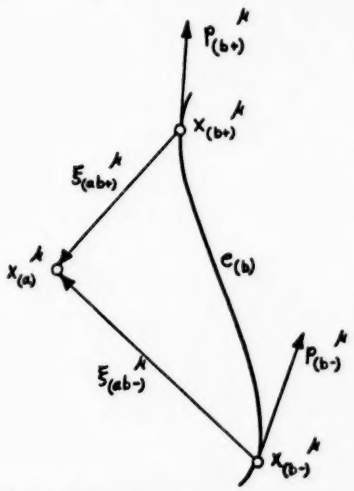

FIG. 1. Retarded and advanced potentials.

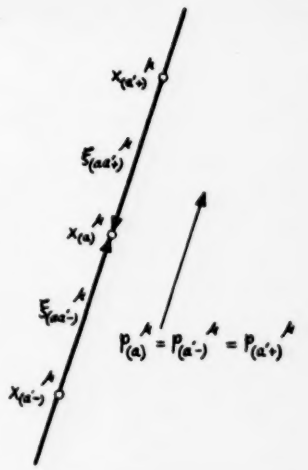

FIG. 2. Self-action for moderate acceleration.

vectors satisfying (33), but by time-like vectors of the small magnitude λ:

$$\xi_{(ab-)\nu}\xi_{(ab-)}{}^{\nu}=\xi_{(ab+)\nu}\xi_{(ab+)}{}^{\nu}=\lambda^2. \tag{36}$$

The potentials of a particle at a point on its own world line are now finite. They can easily be computed approximately if we neglect changes of the momentum of the particle during short time intervals of the order of λ. Then, as seen from Fig. 2,

$$\xi_{(aa'-)}{}^{\mu}=-\xi_{(aa'+)}{}^{\mu}=\lambda\frac{p_{(a)}{}^{\mu}}{(p_{(a)}{}^{\nu}p_{(a)\nu})^{\frac{1}{2}}}, \tag{37}$$

and

$$p_{(a'+)}{}^{\mu}=p_{(a'-)}{}^{\mu}=p_{(a)}{}^{\mu}. \tag{38}$$

The self-field of a particle, Eq. (32), is now given by

$$A_{(aa)\mu}=e_{(a)}\frac{p_{(a)\mu}}{\lambda(p_{(a)}{}^{\nu}p_{(a)\nu})^{\frac{1}{2}}}. \tag{39}$$

The self-action term of a particle is defined by

$$e_{(a)}\int A_{(aa)\mu}p_{(a)}{}^{\mu}du_{(a)}$$

$$=\int\int\delta(\xi_{(aa')}{}^{\nu}\xi_{(aa')\nu}-\lambda^2)p_{(a)}{}^{\mu}p_{(a')\mu}du_{(a)}du_{(a')}. \tag{40}$$

This becomes identical with the inertial term

$$\int p_{(a)}{}^{\mu}p_{(a)\mu}du_{(a)}, \tag{41}$$

if we put

$$\lambda^2=1/p_{(a)}{}^{\nu}p_{(a)\nu} \tag{42}$$

in the self-action term or, more generally,

$$\lambda^2=1/p_{(a)}{}^{\nu}p_{(b)\nu} \tag{43}$$

in the interaction term of two particles. In the deriva-

tion, the form (32), (36) of the modified electromagnetic potentials was used. This form is no longer rigorous when λ is not a constant, but it remains valid in the approximation of moderate accelerations made above.

This discussion suggests the action principle

$$\delta \sum_a \sum_b e_{(a)}e_{(b)} \int\int \delta\left(\xi_{(ab)^\nu}\xi_{(ab)\nu} - \frac{1}{p_{(a)^\nu}p_{(b)\nu}}\right) \times p_{(a)^\mu}p_{(b)\mu}du_{(a)}du_{(b)} = 0. \quad (44)$$

A diagonal term $b=a$ in the double sum is to be interpreted as

$$\int\int \delta\left(\xi_{(aa')^\nu}\xi_{(aa')\nu} - \frac{1}{p_{(a)^\nu}p_{(a')\nu}}\right) \times p_{(a)^\mu}p_{(a')\mu}du_{(a)}du_{(a')}, \quad (45)$$

where $u_{(a)}$ and $u_{(a')}$ are two points on the world line of particle a. Also $e_{(a)}e_{(a)}=1$, by (4).

We wish to show now that the modifying term λ, Eq. (43), is small. This cannot be done completely within the framework of the classical theory presented here. We shall use the fact that there exists no charged particle in nature with a rest mass smaller than that of the electron:

$$m \geqslant m_0. \quad (46)$$

Whether this can be derived from a quantized theory of the type considered here is a matter of speculation. We shall accept (46) as an empirical fact. In contrast to Euclidean geometry, the absolute value of the scalar product of two time-like vectors in Minkowski space is greater than or equal to the product of their magnitudes. Thus

$$|p_{(a)^\nu}p_{(b)\nu}| \geqslant m_{(a)}m_{(b)} \geqslant m_0^2. \quad (47)$$

It follows that λ, given by (43), satisfies the inequality

$$\lambda \leqslant 1/m_0 = 2.8\times 10^{-13} \text{ cm}. \quad (48)$$

The physical consequences of the modification (44) of classical electrodynamics can be summarized as follows:

For moderate accelerations, where we can neglect the changes in the momenta of particles during time intervals of the order of 10^{-13} cm or 10^{-23} sec, the self action terms ($a=b$) in (44) reduce to the corresponding inertial terms (41). Thus all rest masses are of electromagnetic origin.

When particles are at distances from each other which are large compared to 10^{-13} cm, the difference between (36) and (33) is negligible for $a\neq b$. The particles interact electromagnetically and each rest mass is a constant, being an integral of the motion.

When particles are close together their interaction is of a new type and is accompanied by changes in the rest masses.

The action principle (44) is not unique. Different action principles can be obtained by starting from structure functions other than (35). This lack of uniqueness is a drawback which the present theory shares with those of Bopp and Feynman.

There is one simple modification of (44) which will be mentioned here. Wheeler and Feynman[6] have suggested that, instead of distinguishing between positive and negative charges, one can, equivalently, consider particles moving forwards or backwards in time. Thus a particle whose momentum vector points into the future null cone ($p^4>0$) can be interpreted as carrying a positive charge, a particle whose momentum vector points into the past null cone ($p^4<0$) as carrying a negative charge. With this convention the most natural action principle of the general form of (44) can be written:

$$\delta \sum_a \sum_b \int\int \delta\left(\xi_{(ab)^\nu}\xi_{(ab)\nu} - \frac{1}{p_{(a)^\nu}p_{(b)\nu}}\right) \times p_{(a)^\mu}p_{(b)\mu}du_{(a)}du_{(b)} = 0. \quad (49)$$

In the old notation this means that λ^2 is given by

$$\lambda^2 = e_{(a)}e_{(b)}/p_{(a)^\nu}p_{(b)\nu}, \quad (50)$$

rather than by (43). This change has no effect on the self action terms since $(e_{(a)})^2=+1$. However, the interaction of unlike charges ($e_{(a)}e_{(b)}=-1$) is now propagated along space-like directions $\xi_{(ab\pm)^\mu}$. Thus the velocity of propagation exceeds the velocity of light, if only by very small amounts for particles that are not too close.

Electromagnetic Mass and a Particle Model in Darling's Theory of Elementary Particles*

HANS FREISTADT
Newark College of Engineering,† Newark, New Jersey
(Received July 10, 1953)

A description of a particle in Darling's theory of elementary particles by wave functions of the form $H_1^{(1)}(\kappa s)/\kappa s$ and $H_1^{(2)}(\kappa s)/\kappa s$[$H_1^{(1)}(x)$ is the Hankel function of the first kind of order 1, $s^2=c^2t^2-r^2$, $\kappa=m_0c/\hbar$] is discussed. It is shown that no current-charge density described by a conventional interpretation of these wave functions can exist. Hence, the classical interaction $j^\alpha A_\alpha$ associated with these wave functions cannot account for the empirical correction for electromagnetic mass previously used by the author.

IN nonlocal field theory, the usual partial differential equations of physics are replaced by difference equations involving a finite difference step (related to the "dimensions" of elementary particles), or equivalently, by differential equations of infinite order. One can interpret this as merely denoting a more intimate connection between field points or, alternatively, as giving a physical picture of an elementary particle. In the present paper, an attempt is made to apply the latter interpretation to Darling's theory of the elementary particles,[1] a nonlocal field theory, and to explore a consequence of such an interpretation.

As coordinates in the Minkowski world, we use $x^1=x, \cdots, x^4=ct$; $ds^2=g_{\alpha\beta}dx^\alpha dx^\beta=c^2dt^2-dr^2$, with $g_{\mu\nu}=\text{diag}\ (-1,-1,-1,1)$. We will also have occasion to use pseudo-spherical coordinates s, λ, θ, ϕ related to Cartesian coordinates by

$$x^1=s\sinh\lambda\sin\theta\cos\phi,$$
$$x^2=s\sinh\lambda\sin\theta\sin\phi,$$
$$x^3=s\sinh\lambda\cos\theta,$$
$$x^4=s\cosh\lambda.$$

Let $k_1=p_x/\hbar, \cdots, k_4=E/(\hbar c)$; $\kappa^2=k_\alpha k^\alpha$; $\kappa=m_0c/\hbar$. Then in the x representation of quantum mechanics, $k_\mu\rightarrow i\partial_\mu\equiv u_\mu$, a differential operator. Let $\delta^\mu=\partial/\partial u_\mu$, wherever the operation can be formally performed.

In Darling's theory, the fundamental difference operator is[2] a world symmetrical solution of the reciprocal[3] Klein-Gordon equation,

$$(\delta_\alpha\delta^\alpha+4\omega^2)M=0, \tag{1}$$

where ω is a universal constant of the dimension of length. Then

$$M=2J_1(2\omega u)/2\omega u, \tag{2}$$

where $J_1(x)$ is the Bessel function of order 1.

Darling,[1] Zilsel,[4] and the author[2] have discussed mass spectra resulting from the use of a difference calculus based on the operator M. Zilsel first suggested that the masses obtained in this manner are intrinsic masses, to which must be added a correction for electromagnetic mass. With the aid of a purely empirical curve (Fig. 1) for the electromagnetic mass correction, the author succeeded in including the masses of all particles known to date, except the neutron, into such a mass spectrum.

If nonlocal field theory is to give a picture of an elementary particle, one would expect that the correction for electromagnetic mass can be obtained from it. One might conceive of a particle in nonlocal field theory as a complex of finite extension, not only in space, but, in compliance with relativistic requirements, in time as well, thus constituting a material process which relates all world points within a certain time-like interval (presumably ω or 2ω) (the region between S and the light cone in Fig. 2.) The particle whose path is observed would be a sequence of such processes, the mechanism of reproduction being as yet unknown.[5]

It would seem in line with ideas of reciprocity to try a description of such a material process by means of a wave function of which M [Eq. (2)] is the reciprocal, i.e., world symmetrical solutions of the Klein-Gordon

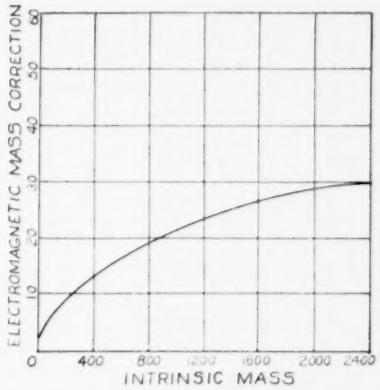

FIG. 1. Correction for electromagnetic mass as a function of intrinsic mass (in units of electron mass).

* Originally reported at the 1953 Washington meeting of the American Physical Society.

† This work was begun while at the Dublin Institute for Advanced Studies.

[1] B. T. Darling, Phys. Rev. **80**, 460 (1950).

[2] H. Freistadt, Phys. Rev. **87**, 198 (1952); Compt. rend. **235**, 23 (1952).

[3] M. Born, Revs. Modern Phys. **21**, 463 (1949).

[4] P. R. Zilsel, Phys. Rev. **82**, 557 (1951).

[5] See also E. Schrödinger, Endeavour **9**, No. 35 (1950).

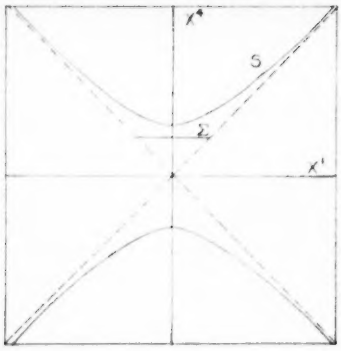

FIG. 2. Geometry for the discussion of a particle model in nonlocal field theory.

equation $(\partial_\alpha\partial^\alpha+\kappa^2)\Psi=0$. The real solution[6] $2J_1(\kappa s)/(\kappa s)$ [Minkowski world analog $\sin(kr)/(kr)$ as a solution of $(\nabla^2+k^2)\Psi=0$] cannot describe a charged particle, so we use the Minkowski world analog of $\exp(ikr)/(kr)$ and $\exp(-ikr)/(kr)$, which are the Hankel functions

$$\Psi=H_1^{(1)}(\kappa s)/(\kappa s), \quad \Psi^*=H_1^{(2)}(\kappa s)/(\kappa s). \tag{3}$$

Associated with such a wave function, there will be a current-charge density distribution,

$$j^\mu=\frac{\rho}{2i\kappa}(\Psi^*\partial^\mu\Psi-\Psi\partial^\mu\Psi^*), \tag{4}$$

which, in pseudo-spherical coordinates, has only an s component, $j^s=2\rho/(\pi\kappa^3 s^3)$, in the computation of which a well-known relation for Hankel functions[7] was used. The quantity ρ is a constant, having the dimensions of a charge density, to be determined from the normalization requirement that $\int_\Sigma j^\alpha d\Sigma_\alpha=e$, where Σ [Fig. (2)] is a constant-time space-like surface. The electromagnetic field A^μ associated with this current charge density would be obtained by solving

$$\partial_\alpha\partial^\alpha A^s=4\pi j^s. \tag{5}$$

The classical interaction of this electromagnetic field with the current-charge density would be observed as a proper density of mass $j^\alpha A_\alpha/c^2$ contributing the electromagnetic correction $\Delta m_0=(1/c^2)\int_\Sigma j^s A_s v^\alpha d\Sigma_\alpha$ to the rest-mass of the particle. ($v^\mu=dx^\mu/ds$ is the relativistic velocity.)

However, it is readily seen that Eq. (5) with current-charge density as given by Eqs. (3) and (4), does not have a regular solution. One concludes from this that a charge distribution described by a conventional interpretation of the wave functions (3) cannot exist. Indications are that the situation would not be improved by using solutions of the Dirac equation instead of solutions of the Klein-Gordon equation.

It remains to be seen whether a less naive picture of a particle in nonlocal field theory can be constructed successfully, or whether nonlocal field theory, to the extent to which it has physical significance, merely denotes a connection between field points different from that implicit in local field theory, where each field point interacts only with its immediate neighborhood.

It is a pleasure to thank Professor Schrödinger and other members of the Dublin Institute for Advanced Studies, in particular F. C. Roesler, N. Balasz, and A. M. Bork, for many stimulating discussions.

[6] These solutions were investigated by E. Schrödinger, Princeton Lectures, 1935 (unpublished).

[7] E. Jahnke and F. Emde, *Funktionentafeln* (Dover Publications, New York, 1945), p. 144.

Convergence of the Adiabatic Nuclear Potential. II

ABRAHAM KLEIN*
Physics Department, University of Rochester, Rochester, New York
(Received August 11, 1953)

A conjecture made in a previous paper concerning the non-convergence of the series of adiabatic nuclear potentials for meson pair theory obtained by means of perturbation methods is shown to be incorrect. The correct series is derived and summed and is in agreement with a result given previously by Wentzel. The same methods suffice for the derivation and summation of two additional series of potentials of the pseudoscalar theory with pseudoscalar coupling. One of these has as its leading term the one-pair potential of fourth order, and the other begins with the leading term of sixth order. Each series has the same radius of convergence which is determined by the condition $xe^x > 2\alpha$, where x is the separation of the nucleons in units of the meson Compton wavelength and $\alpha = (g^2/4\pi)(\mu/2M)$. With $(g^2/4\pi) = 15$, perturbation theory converges for $x > 0.85$; with $(g^2/4\pi) = 10$, for $x > 0.57$. The convergence for $x \lesssim 1$ is in any case very slow for these values of the coupling constant. The possibility remains that for substantially smaller values of the coupling constant, as are suggested by the inclusion of radiative corrections, perturbation calculations of adiabatic potentials may yield a meaningful first approximation when used in conjunction with a suitable cut-off.

I. INTRODUCTION

IN a previous paper,[1] a qualitative discussion of the behavior of the series of adiabatic potentials of the *ps-ps* theory was presented on the basis of the calculation of the leading terms through eighth order in the coupling constant. There appeared to be a definite indication of non-convergence of the series for $x \lesssim 1$, where $x = \mu r$ is the nucleon separation measured in units of the meson Compton wavelength, μ^{-1}. The attempt was then made to infer a general result for the leading pair term of the potential of order $4n$. The result put forward, without full proof, was that the perturbation series is catastrophically divergent. This result is, in fact, incorrect. The purpose of the present work is to demonstrate that it is possible to obtain, in the adiabatic limit, the general term in a few well-defined series of potentials, to investigate the convergence of these series, and to sum them.

The potentials to be investigated are the leading pair terms of order $4n$, considered in I; the potential of order $4n$ with one pair fewer, prototypes of which (one pair term of fourth order and three pair term of eighth order) were given in I; the leading terms of order $4n+2$. The latter can be characterized diagrammatically by open meson-line perimeters with end points at each of the nucleon positions. Thus the leading term is a sixth-order potential in which each nucleon undergoes one pair and one gradient interaction. The contribution of the sixth-order term has been previously computed[2] by means other than are contemplated here. The calculations are carried out in Secs. IIA, B, and C, respectively.

For the purposes of this presentation it is simplest to use the form of the theory which results from the Dyson[3] or Foldy[4] transformations,

$$\mathcal{H}'(x) = g\bar{\psi}(x)\gamma_5\tau_i\psi(x)\phi_i(x) \rightarrow (g^2/2M)\bar{\psi}\psi\phi^2 + (g/2M)\bar{\psi}\boldsymbol{\sigma}\tau_i\psi\cdot\boldsymbol{\nabla}\phi_i + \text{higher order terms.} \quad (1)$$

By computing the irreducible interactions that Eq. (1) contributes to the kernel of the relativistic two-body equation,[5-7] it is a straightforward matter to verify that the method proposed in I for the computation of the leading pair terms in the adiabatic limit is indeed applicable. The argument given there was that the restriction, in obtaining the leading contributions, to matrix elements with at most one nucleon pair at a time, as suggested by the original pseudoscalar coupling,[2,8] could be lifted; it was sufficient merely to demand that the requisite number of nucleon pairs be associated with the motion of each nucleon. This argument is indeed tantamount to carrying out the transformation of Eq. (1) term by term in the interaction function.

The potentials will be computed from an expression which is a trivial modification of Eq. (10) of I:

$$V(\mathbf{r}, \mathbf{r}') = -it^{-1}\int dt_1 dt_2 dt_1' dt_2' d\mathbf{R}' \times \exp[iM(t_1+t_2-t_1'-t_2')]I(x_1, x_2; x_1' x_2'). \quad (2)$$

Aside from the use of individual time coordinates, we have added, for reasons of symmetry, an additional time integration and correspondingly divided by a "large" time interval t.

* On leave for the summer of 1953 from the Society of Fellows, Harvard University, Cambridge, Massachusetts.

[1] A. Klein, Phys. Rev. **91**, 740 (1953), henceforth referred to as I.

[2] A. Klein, Phys. Rev. **90**, 1101 (1953).

[3] F. J. Dyson, Phys. Rev. **73**, 929 (1948).

[4] Berger, Foldy, and Osborn, Phys. Rev. **87**, 1061 (1952).

[5] J. Schwinger, Proc. Nat. Acad. Sci. U. S. **37**, 452, 455 (1951).

[6] E. E. Salpeter and H. A. Bethe, Phys. Rev. **84**, 1232 (1951).

[7] M. Gell-Mann and F. Low, Phys. Rev. **84**, 350 (1951).

[8] M. M. Levy, Phys. Rev. **88**, 725 (1952).

II. COMPUTATION OF POTENTIALS

A. Pair Potential of Order $4n$

For the case under consideration, the interaction function which enters Eq. (2) has the form[9]

$$I(x_1, x_2; x_{2n-1}, x_{2n}) = \sum 3(2)^{2n}(-i\lambda)^{2n}\int dx_3\cdots dx_{2n-2} \times[G(x_1-x_3)\cdots G(x_{2n-3}-x_{2n-1})]^{(1)} \times[G(x_2-x_4)\cdots G(x_{2n-2}-x_{2n})]^{(2)} \times\Delta(x_1-x_{i_1})\Delta(x_1-x_{i_2})\cdots \times\Delta(x_{2n-1}-x_{i_{n-1}})\Delta(x_{2n-1}-x_{i_n}). \quad (3)$$

Here $i_1, i_2, \cdots, i_n$ is one of the permutations of 2, 4, $\cdots 2n$, the coordinates of the second nucleon, which yields a closed meson-line perimeter; the summation is over the $n!(n-1)!/2$ such terms; $\lambda = g^2/2M$. Equation (3) can be determined either directly from the interaction Hamiltonian of Eq. (1) or can be inferred term by term from the form of the theory used in I. The same statement can be made for the other interactions to be used in this paper.

We insert Eq. (3) into Eq. (2) and immediately carry out the reduction to the adiabatic limit by means of the equation

$$\begin{aligned} G(x) &\cong i\delta(\mathbf{r})e^{-iMt}, \quad t>0 \\ &\cong 0, \qquad\qquad t<0. \end{aligned} \quad (4)$$

As in I, there results immediately a local interaction which is given by

$$V_{4n}(r) = it^{-1}3(2\lambda)^{2n}\sum\int_{-\infty}^{\infty}dt_1\int_{-\infty}^{t_1}dt_3\cdots \times\int_{-\infty}^{t_{2n-3}}dt_{2n-1}\int_{-\infty}^{\infty}dt_2\int_{-\infty}^{t_2}dt_4\cdots \times\int_{-\infty}^{t_{2n-2}}dt_{2n}\Delta(\mathbf{r}, t_1-t_{i_1})\Delta(\mathbf{r}, t_1-t_{i_2})\cdots \times\Delta(\mathbf{r}, t_{2n-1}-t_{i_{n-1}})\Delta(\mathbf{r}, t_{2n-1}-t_{i_n}). \quad (5)$$

Equation (5) was also obtained by the methods of I. The essential symmetry property required for its evaluation was overlooked, however.

Suppose we permute the time coordinates of one of the nucleons,

$$t_1 \to t_{\alpha_1}\cdots t_{2n-1}\to t_{\alpha_{2n-1}}. \quad (6)$$

Then in virtue of the definition of the set of perimeters, the integrand of each term of the sum in Eq. (5) is transformed into the integrand of another term of the sum. In short the integrand as a whole is invariant. On the other hand, the time integrations, previously subject to the condition $t_1>t_3>\cdots>t_{2n-1}$ are now subject to the condition $t_{\alpha_1}>t_{\alpha_3}>\cdots>t_{\alpha_{2n-1}}$. If we carry out all possible permutations of the time coordinates of the two particles independently and then average over the resulting $(n!)^2$ expressions, we obtain the following form for the potential:

$$V_{4n}(r) = it^{-1}3(2\lambda)^{2n}(n!)^{-2}\sum\int dt_1\cdots \times dt_{2n}\Delta(\mathbf{r}, t_1-t_{i_1})\Delta(\mathbf{r}, t_1-t_{i_2})\cdots \times\Delta(\mathbf{r}, t_{2n-1}-t_{i_{n-1}})\Delta(\mathbf{r}, t_{2n-1}-t_{i_n}), \quad (6)$$

in which the integrations are now carried out over the *entire* $2n$ dimensional space $t_1, t_2, \cdots t_{2n}$.

The remainder of the calculation is straightforward. We Fourier-analyze the meson propagation functions,

$$\Delta(\mathbf{r},t) = (2\pi)^{-4}\int d^4k\exp[i\mathbf{k}\cdot\mathbf{r}-ik_0t][\omega^2-k_0^2+i\eta]^{-1}, \quad (7)$$

interchange the order of momentum and temporal integrations, and perform the latter. For each term of the sum in Eq. (6) we then obtain $2n-1$ delta functions of linear combinations of the meson energies $k_{0,1}\cdots k_{0,2n}$ and one remaining time integral which cancels the factor t^{-1}. It is then possible to perform trivially $2n-1$ integrals with respect to the meson energies, leaving one such integral which we label with the variable k_0. At this stage it is seen that all $n!(n-1)!/2$ terms of Eq. (6) contribute equally to the sum, so that the latter is most simply rewritten as[10]

$$V_{4n}(r) = 3i(2\lambda)^{2n}(8\pi^3)^{-2n}(4\pi n)^{-1} \times\int d\mathbf{k}_1\cdots d\mathbf{k}_{2n}\exp[i(\mathbf{k}_1+\cdots+\mathbf{k}_n)\cdot\mathbf{r}] \times\int dk_0[(k_0^2-\omega_1^2)\cdots(k_0^2-\omega_{2n}^2)]^{-1} = -3\mu\alpha^{2n}(2^{2(n-1)}/n)(2/\pi)K_1(2nx)/x^{2n}, \quad (8)$$

where $\alpha = (g^2/4\pi)(\mu/2M)$. Equation (8) can also be inferred by expanding the exact solution given by Wentzel[11,12] for meson pair theory with stationary sources. From the results of the latter author, one can

[9] It is perhaps worthwhile to emphasize that the propagation functions employed are those defined, for example, in reference 5. We have been unconventional here and in references 1 and 2 in omitting identifying subscripts on these functions.

[10] See the appendix of reference 1 for the evaluation of the integral.

[11] G. Wentzel, Helv. Phys. Acta **15**, 111 (1942).

[12] The agreement of the result with that of reference 11 demonstrates the correctness of the assumption made in reference 1 that higher-order pair diagrams which do not consist of single closed meson perimeters are cancelled in the adiabatic limit by the iterates of lower-order diagrams.

obtain a closed expression for the sum

$$V(x)=\sum_{n=1}^{\infty} V_{4n}(x)$$
$$=-\frac{3\mu}{4\pi i}\int_0^\infty \frac{kdk}{(1+k^2)^{\frac{1}{2}}}\log\left\{\frac{1-(2\alpha e^{ikx}/x)^2}{1-(2\alpha e^{-ikx}/x)^2}\right\}$$
$$=-\frac{3\mu}{2\pi}\int_0^\infty \frac{kdk}{(1+k^2)^{\frac{1}{2}}}\tan^{-1}\left\{\frac{4\alpha^2\sin 2kx/x^2}{1-4\alpha^2\cos 2kx/x^2}\right\}. \quad (9)$$

The integral of Eq. (9) is well-defined for values of x which are larger than x_c, defined by

$$x_c=2\alpha. \quad (10)$$

It is, however, possible to investigate the convergence of the series *per se*, most simply by introducing the asymptotic form of the function

$$(2/\pi)K_1(2nx)\sim e^{-2nx}/(\pi nx)^{\frac{1}{2}}. \quad (11)$$

A straightforward application of the ratio test then informs us that the series converges provided that $x>x_c$, with x_c here defined by

$$x_c\exp(x_c)=2\alpha, \quad (12)$$

a less stringent condition than Eq. (10). We shall prefer for purposes of discussion the less accurate Eq. (12), since it will be seen that the same condition of convergence will obtain rigorously for the other series of potentials to be derived below. We therefore defer numerical discussion of Eq. (12) until this has been done.

B. Potential of Order $4n$ with One Pair Fewer

A typical diagram is shown in Fig. 3(a) of I. The number of distinct diagrams in the general order can be computed as the product of the number of ways of choosing two vertices of one of the nucleons for the gradient interaction by the number of ways of drawing continuous meson perimeters beginning with these points. The result is $n!(n+1)!/2$. There is actually twice this number of interactions, since either nucleon could have been selected to bear the gradient coupling. This will be taken account of in the final result. By arguments previously mentioned, the interaction can be shown to have the form

$$I(x_1x_2;x_{2n+1},x_{2n})=-\sum 3(2)^{2n}(-i\lambda)^{2n}(2M)^{-1}$$
$$\times\int dx_3\cdots dx_{2n-1}[G(x_1-x_3)\cdots G(x_{2n-1}-x_{2n+1})]^{(1)}$$
$$\times[G(x_2-x_4)\cdots G(x_{2n-2}-x_{2n})]^{(2)}(\boldsymbol{\sigma}_1\cdot\boldsymbol{\nabla}_{2j+1})$$
$$\times(\boldsymbol{\sigma}_1\cdot\boldsymbol{\nabla}_{2l+1})\Delta(x_1-x_{i1})\cdots\Delta(x_{2j+1}-x_{i,2j+1})\cdots$$
$$\times\Delta(x_{2l+1}-x_{i,2l})\cdots\Delta(x_{2n+1}-x_{in}), \quad (13)$$

where $\boldsymbol{\nabla}_{2j+1}$ operates on the variable $\mathbf{r}_{2j+1}$ for the first nucleon, etc., and the summation is over $n!(n+1)!/2$ terms.

The argument now proceeds precisely as in Sec. A. The adiabatic limit is first taken. The resulting static potential has an integrand which is invariant as a whole under independent permutations of the time coordinates of either particle. Averaging over all possible permutations which is, in this case, $n!(n+1)!$, we obtain the potential

$$V_{4n}'(r)=\mathrm{Lim}(\mathbf{r}_i\to\mathbf{r})\Big\{3(2\lambda)^{2n}[n!(n+1)!]^{-1}t^{-1}$$
$$\times\sum\int dt_1\cdots dt_{2n+1}(\boldsymbol{\sigma}_1\cdot\boldsymbol{\nabla}_j)(\boldsymbol{\sigma}_1\cdot\boldsymbol{\nabla}_l)$$
$$\times\Delta(r_1,t_1-t_{i1})\cdots\Delta(r_{2n},t_{2n+1}-t_{in})\Big\}. \quad (14)$$

The integrals over the time variables now require that $2n$ linear homogeneous equations be satisfied by the $2n$ meson energy variables. Summing over the $n!(n+1)!/2$ terms, we are left with

$$V_{4n}'(r)=-3(2)^{2n-1}\lambda^{2n}(8\pi^3)^{-2n}\int d\mathbf{k}_1\cdots$$
$$\times d\mathbf{k}_{2n}\exp[i(\mathbf{k}_1+\cdots+\mathbf{k}_n)\cdot\mathbf{r}]$$
$$\times\mathbf{k}_j\cdot\mathbf{k}_l[\omega_1^2\cdots\omega_j^2\cdots\omega_l^2\cdots\omega_{2n}^2]^{-1}$$
$$=3\mu\alpha^{2n}(\mu/2M)2^{2n-1}(1+x^{-1})^2e^{-2nx}/x^{2n}. \quad (15)$$

The sum of the series with Eq. (15) as general term is obtained trivially:

$$V'(x)=\sum_{n=1}^{\infty}V_{4n}'(x)=6\mu\alpha^2(\mu/2M)(1+x^{-1})^2e^{-2x}/x^2$$
$$\times[1-4\alpha^2e^{-2x}/x^2]^{-1}$$
$$=V_4'(x)[1-4\alpha^2e^{-2x}/x^2]^{-1}. \quad (16)$$

It is thus seen that Eq. (12) determines the radius of convergence of Eq. (16).

C. Potential of Order $4n+2$

Here one chooses a single gradient interaction for each particle. The total number of diagrams in the general order is easily found to be $[(n+1)!]^2$, and the interaction is given by

$$I(x_1,x_2;x_{2n+1},x_{2n+2})$$
$$=2^{2n}\boldsymbol{\tau}_1\cdot\boldsymbol{\tau}_2(-i\lambda)^{2n+1}(2M)^{-1}\sum\int dx_3\cdots dx_{2n}$$
$$\times[G(x_1-x_3)\cdots G(x_{2n-1}-x_{2n+1})]^{(1)}$$
$$\times[G(x_2-x_4)\cdots G(x_{2n}-x_{2n+2})]^{(2)}$$
$$\times(\boldsymbol{\sigma}_1\cdot\boldsymbol{\nabla}_{2j+1})(\boldsymbol{\sigma}_2\cdot\boldsymbol{\nabla}_{il})\Delta(x_1-x_{i1})\cdots$$
$$\times\Delta(x_{2n+1}-x_{in+1}), \quad (17)$$

where the summation is over $[(n+1)!]^2$ terms and the subscripts on the gradient operators are meant to imply that they operate on appropriate members of the set of coordinates for the first and second nucleon respectively. The remainder of the calculation differs in no wise from that described in Sec. B. It suffices therefore to state the result,

$$V_{4n+2}(r)=\mu\tfrac{1}{3}\tau_1\cdot\tau_2 2^{2n}\alpha^{2n+1}(\mu/2M)\times[\sigma_1\cdot\sigma_2+S_{12}]e^{-(2n+1)x}/x^{2n+1}. \quad (18)$$

The series of which Eq. (18) is the general term has the sum

$$\begin{aligned}V''(x)&=\sum_{n=1}^{\infty}V_{4n+2}(x)\\&=-\frac{4}{3}\mu\tau_1\cdot\tau_2\alpha^3(\mu/2M)(1+x^{-1})^2e^{-3x}/x^3\\&\qquad\times[\sigma_1\cdot\sigma_2+S_{12}][1-4\alpha^2e^{-2x}/x^2]^{-1}\\&=V_6(x)[1-4\alpha^2e^{-2x}/x^2]^{-1}. \quad (19)\end{aligned}$$

The same remarks about convergence as in Sec. B are therefore applicable.

III. DISCUSSION OF RESULTS

Conclusions concerning the validity of perturbation theory can be drawn immediately from the application of Eq. (12). Thus for $(g^2/4\pi)(\mu/2M)=1$, corresponding to $g^2/4\pi=15$, Eq. (12) requires $x>0.85$ for convergence, for $(g^2/4\pi)=10$, $x>0.57$. For such values of the coupling constant, it is clear that no plausible account of nuclear jorces can be based on the leading terms of the series. Moreover, as already indicated in I, the repulsive potential $V'(x)$ of Eq. (17) predominates numerically over the other pair terms to such extent that were the coupling constant as large as the above values, the possibility of obtaining agreement with the low-energy two-nucleon data from the *ps-ps* theory would effectively be ruled out.

However, all treatments of the potential problem which have taken into account radiative corrections[8,11,13] have indicated that as a consequence of self-interactions the pair coupling is strongly damped. If we take $(g^2/4\pi)_{\text{eff}}(\mu/2M)\sim 0.1$, which is probably as much of a reduction as self-energy effects are likely to produce, then our series converge for $x>0.17$. Under these circumstances, perturbation theory is applicable for distances as small as $x=0.5$. Assuming that the gradient interaction of Eq. (1) is undamped compared to the pair coupling, one has from this result a good indication of the domain of applicability of perturbation theory to the former interaction for which the effective expansion parameter is $(g^2/4\pi)(\mu/2M)^2\sim 0.1$.

A more direct attack on the applicability of perturbation theory to the gradient interaction will be presented in a subsequent publication. The author also hopes to discuss in later publications the relationship of the potentials computed in this paper to a possible consistent model for nuclear forces.

[13] M. Ruderman, Phys. Rev. **90**, 183 (1953); Brueckner, Gell-Mann, and Goldberger, Phys. Rev. **90**, 476 (1953).

The Green's Function Method for Strongly Interacting Particles*

MAURICE NEUMAN
Radiation Laboratory, University of California, Berkeley, California
(Received July 20, 1953)

The Green's function method is adapted to the description of strongly interacting particles which become more loosely bound as their number increases.

FORMALLY closed expressions for propagation functions, vertex, mass, and polarization operators have recently been constructed by Schwinger.[1] An expansion of these in terms of free particle propagators reproduces the covariant Feynman-Dyson perturbation theory. The attempted improvements on the latter have centered around efforts to obtain solutions to equations in which the propagation functions are left intact and only the lowest powers in the expansion of the remaining operators are retained. This procedure is partially justified on the grounds of the presumed weakness of certain interactions.

It is the purpose of this note to put the theory in a form appropriate to the description of a somewhat different physical situation. No interactions between particles are assumed to be weak. A complex of particles, will, however, be taken to be the more tightly bound the fewer the particles in it. As their number increases a looser structure results, which tends to break up into smaller, more tightly bound units. Thus, the propagation function associated with a large number of particles may be expanded in terms of those of smaller numbers, whereas the latter must be treated rigorously

The result of this procedure is a finite set of equations involving propagation functions up to a certain order. Only in the equation for the highest order propagation function is a generalized vertex operator introduced explicitly; in the others it is effectively replaced by Green's functions of a higher order than the one in which the vertex operator would ordinarily appear. Since this quantity is associated with transiton amplitudes involving creation and annihilation of particles and its expansion is equivalent to conventional perturbation theory, the modified procedure is suitable for a non-perturbation treatment of nonstationary processes like the production of mesons in nucleon-nucleon collisions.

The equations for the propagation function of one nucleon, S, and one meson, Δ, are

$$[\gamma p+m-g\,\mathrm{T}\rho\Gamma_0\phi+ig\,\mathrm{T}\rho\Gamma_0(\delta/\delta J)]S=1, \quad (1a)$$

$$(p^2+\mu^2)\Delta-ig\,\mathrm{Tr}\Gamma_0(\delta S/\delta J)=1, \quad (1b)$$

where Γ_0 is the zero'th order vertex operator explicitly defined for a given meson-nucleon coupling. If the system $1N+1M$ is assumed to be loosely bound, the vertex operator

$$\Gamma(\xi)=-\delta S^{-1}/\delta g\phi(\xi)$$

is introduced at this point. The equations then assume the form

$$(\gamma p+m-g\,\mathrm{T}\rho\Gamma_0\phi+\Sigma)S=1, \quad (1'a)$$

$$(p^2+\mu^2+\Pi)\Delta=1, \quad (1'b)$$

with

$$\Sigma=ig^2\,\mathrm{T}\rho\Gamma_0 S\Delta\Gamma, \quad (3a)$$

$$\Pi=-ig^2\,\mathrm{Tr}\Gamma_0 S\Gamma S. \quad (3b)$$

The operator $\Gamma(\xi)$ may be expanded in terms of Δ and S:

$$\Gamma(\xi)=\Gamma_0(\xi)-\delta\Sigma/\delta g\phi(\xi). \quad (4)$$

This procedure is inappropriate if not only $1N$ and $1M$ but also $1N+1M$ are regarded as being tightly bound. The Green's function corresponding to $1N+1M$ will be denoted by ${}^{1M}S$. Taking the variational derivative of (1a) with respect to $J(\xi)$ and observing that

$$\delta^2 S/\delta J(\xi)\delta J(\xi')=i[{}^{1M}S(\xi\xi')-\Delta(\xi\xi')S], \quad (5)$$

we obtain

$$\delta S/\delta J(\xi)=gS_0\Gamma_0(\xi'){}^{1M}S(\xi'\xi), \quad (6)$$

where the notation

$$S_0=(\gamma p+m-g\,\mathrm{T}\rho\Gamma_0\phi)^{-1} \quad (7a)$$

$$\Delta_0=(p^2+\mu^2)^{-1} \quad (7b)$$

was introduced. Equations (1) now become

$$S=S_0-ig^2\,\mathrm{T}\rho S_0\Gamma_0 S_0\Gamma_0\,{}^{1M}S, \quad (1''a)$$

$$\Delta=\Delta_0+ig^2\,\mathrm{Tr}\Delta_0\Gamma_0 S_0\Gamma_0\,{}^{1M}S, \quad (1''b)$$

explicit expression of S and Δ in terms of ${}^{1M}S$. Differentiating (1a) twice with respect to J and making use of (5) and (6) we obtain an equation for ${}^{1M}S$:[2]

$$\begin{aligned}&{}^{1M}S(\xi\bar{\xi})+igS_0\Gamma_0(\xi')(\delta\,{}^{1M}S(\xi\bar{\xi})/\delta J(\xi'))\\&+ig^2S_0\Gamma_0(\xi')\Delta(\xi'\bar{\xi})S_0\Gamma_0(\xi'')\,{}^{1M}S(\xi''\bar{\xi})\\&+ig^2S_0\Gamma_0(\xi')\Delta(\xi'\bar{\xi})S_0\Gamma_0(\xi'')\,{}^{1M}S(\xi''\xi)=S_0\Delta(\xi\bar{\xi}). \quad (8)\end{aligned}$$

* This work was performed under the auspices of the U. S. Atomic Energy Commission.

[1] J. Schwinger, Proc. Nat. Acad. Sci. U. S. **37**, 452 (1951). We employ the notation of this reference.

[2] This equation, in a somewhat different form, was previously given by S. Deser and P. C. Martin, Phys. Rev. **90**, 1075 (1953).

With the aid of (1″) we then have

$$
\begin{aligned}
&{}^{1M}S(\xi\bar{\xi})+igS_0\Gamma_0(\xi')\big(\delta\,{}^{1M}S(\xi\bar{\xi})/\delta J(\xi')\big)=\Delta_0(\xi\bar{\xi})S_0\\
&\quad+ig^2S_0\,\mathrm{Tr}\Delta_0(\xi\xi')\Gamma_0(\xi')S_0\Gamma_0(\xi'')\,{}^{1M}S(\xi''\bar{\xi})\\
&\quad-ig^2S_0\Delta_0(\xi\xi')\Gamma_0(\xi')S_0\Gamma_0(\xi'')\,{}^{1M}S(\xi''\bar{\xi})\\
&\quad+g^4S_0\Gamma_0(\xi')\Delta_0(\xi'\xi''')\,\mathrm{Tr}[\Gamma_0(\xi''')S_0\Gamma_0(\xi^{IV})\\
&\quad\times{}^{1M}S(\xi^{IV}\xi)]S_0\Gamma_0(\xi'')\,{}^{1M}S(\xi''\bar{\xi})\\
&\qquad\qquad+[\text{last two terms with }\xi\leftrightarrow\bar{\xi}].\qquad(9)
\end{aligned}
$$

At this point we may decide that a system more complex than $1N+1M$ is loosely bound and express the variational derivative occurring in (9) by means of a generalized vertex operator,

$$
\begin{aligned}
{}^{1M}\Gamma(\xi|\xi'|\bar{\xi})&=-\delta\,{}^{1M}S^{-1}(\xi\bar{\xi})/\delta g\phi(\xi')\\
&\cong\Gamma_0(\xi')\Delta^{-1}(\xi\bar{\xi}),\qquad(10)
\end{aligned}
$$

more explicitly defined by an expansion in terms of Δ, S and ${}^{1M}S$. The variational derivative term then gives rise to an interaction with the character of a self mass for the nucleon meson system:

$$
\begin{aligned}
&F\,{}^{1M}S(\xi\bar{\xi})+ig^2\Gamma_0(\xi')\Delta(\xi'\xi^{IV})[{}^{1M}S(\xi\xi'')\\
&\quad\times{}^{1M}\Gamma(\xi''|\xi^{IV}|\xi''')-\delta(\xi\xi''')S\Gamma(\xi^{IV})]\,{}^{1M}S(\xi'''\bar{\xi})\\
&\quad+ig^2\Gamma_0(\xi')\Delta(\xi'\xi)S_0\Gamma_0(\xi'')\,{}^{1M}S(\xi''\bar{\xi})\\
&\qquad+ig^2\Gamma_0(\xi')\Delta(\xi'\bar{\xi})S_0\Gamma_0(\xi'')\,{}^{1M}S(\xi''\xi)=\Delta(\xi\bar{\xi}).\qquad(8')
\end{aligned}
$$

Equation (1″) and (8′) with (10) treat complexes of particles $1N$, $1M$, $1N+1M$ rigorously and those with $1N+nM(n\geq 2)$ only approximately. An extension of this procedure would be to derive an expression for $\delta\,{}^{1M}S/\delta J(\xi)$ in terms of ${}^{2M}S$ and to augment (1″) and (9) with an equation for the latter quantity. The introduction of a vertex operator ${}^{2M}\Gamma$ in it would imply that systems $1N+nM(n\geq 3)$ are regarded as loosely bound.

We now re-examine the $2N$ equation,

$$
\tfrac{1}{2}[F^{(1)}\mathfrak{F}^{(2)}+F^{(2)}\mathfrak{F}^{(1)}]S^{(12)}=1^{(12)},\qquad(11)
$$

from this point of view. With the variational derivatives written out explicitly (11) becomes

$$
\tfrac{1}{2}F_0{}^{(12)}S^{(12)}+\tfrac{1}{2}ig^2\gamma^{(12)}(\xi)\big(\delta S^{(12)}/\delta gJ(\xi)\big)=1^{(12)},\qquad(12)
$$

where

$$
\begin{aligned}
F_0{}^{(12)}&=F^{(1)}F_0{}^{(2)}+F^{(2)}F_0{}^{(1)},\\
\gamma^{(12)}&=F^{(1)}\Gamma_0{}^{(2)}+F^{(2)}\Gamma_0{}^{(1)},\\
F_0&=S_0{}^{-1}.
\end{aligned}
$$

Assuming at first that $2N$ is tightly bound and $2N+nM(n\geq 1)$ is a loose structure, we introduce, in analogy to the previous work, a vertex operator:

$$
\begin{aligned}
\Gamma^{(12)}(\xi)&=-\delta S^{(12)-1}/\delta g\phi(\xi)\\
&\cong\Gamma^{(1)}(\xi)F^{(2)}+\Gamma^{(2)}(\xi)F^{(1)}=\Gamma_0{}^{(12)}(\xi),\qquad(13)
\end{aligned}
$$

and rewrite (12) in the form

$$
F^{(1)}F^{(2)}S^{(12)}+\tfrac{1}{2}(\Sigma^{(12)}-\Sigma_0{}^{(12)})S^{(12)}=1^{(12)},\qquad(14)
$$

with

$$
\Sigma^{(12)}=ig^2\,\mathrm{T}\rho\gamma^{(12)}S^{(12)}\Delta\Gamma^{(12)},\qquad(15)
$$

$$
\Sigma_0{}^{(12)}=F^{(1)}\Sigma^{(2)}+F^{(2)}\Sigma^{(1)}.\qquad(16)
$$

Thus, the interaction appears as the difference of two operators, each having the character of a self-mass. In the approximation $\Gamma_0{}^{(12)}$ of the right member of (13), we obtain after a short calculation:

$$
\tfrac{1}{2}(\Sigma^{(12)}-\Sigma_0{}^{(12)})=L^{(12)}F^{(1)}F^{(2)},\qquad(17)
$$

where

$$
\begin{aligned}
L^{(12)}&=\tfrac{1}{2}ig^2\,\mathrm{T}\rho\{\Gamma_0{}^{(1)}F^{(2)}S^{(12)}F^{(2)}S_0{}^{(2)}\Gamma_0{}^{(2)}\,{}^{1M}S^{(2)}\\
&\quad+\Gamma_0{}^{(2)}F^{(1)}S^{(12)}F^{(1)}S_0{}^{(1)}\Gamma_0{}^{(1)}\,{}^{1M}S^{(1)}\\
&\quad+\Gamma_0{}^{(1)}(F^{(2)}S^{(12)}F^{(1)}-1)S_0{}^{(1)}\Gamma_0{}^{(1)}\,{}^{1M}S^{(1)}\\
&\qquad+\Gamma_0{}^{(2)}(F^{(1)}S^{(12)}F^{(2)}-1)S_0{}^{(2)}\Gamma_0{}^{(2)}\,{}^{1M}S^{(2)}\},\qquad(18)
\end{aligned}
$$

and (12) with all systems $1N+nM$, $2N$ treated rigorously has the form

$$
(1+L^{(12)})F^{(1)}F^{(2)}S^{(12)}=1^{(12)}.\qquad(19)
$$

In order to include $2N+1M$ systems in this scheme, it is necessary to express the variational derivative in (12) in terms of ${}^{1M}S^{(12)}$. A procedure analogous to the one that yielded (6), and the identity

$$
\delta^2S^{(12)}/\delta J(\xi)\delta J(\xi')=i[{}^{1M}S^{(12)}(\xi\xi')-\Delta(\xi\xi')S^{(12)}],\qquad(20)
$$

lead in this case to the relation

$$
\begin{aligned}
F_0{}^{(12)}\big(\delta S^{(12)}/\delta gJ(\xi)\big)&=\gamma^{(12)}(\xi')\,{}^{1M}S^{(12)}(\xi'\xi)\\
&\quad+F^{(1)}S_0{}^{(1)}\Gamma_0(\xi')\,{}^{1M}S^{(1)}(\xi'\xi)\\
&\qquad+F^{(2)}S_0{}^{(2)}\Gamma_0{}^{(2)}(\xi')\,{}^{1M}S^{(2)}(\xi'\xi).\qquad(21)
\end{aligned}
$$

The quantity $\delta S^{(12)}/\delta J(\xi)$ is of considerable physical interest. It is directly related to the transition amplitude for the production of one meson in a nucleon-nucleon collision. If the various propagation functions occurring in (21) could be constructed, the equation would lead to a non-perturbation treatment of this nonstationary process. The extension of this method to the treatment of other nonstationary processes is obvious.

It is probably superfluous to add that the equations here obtained are exceedingly complicated. The general scheme, however, seems to be appropriate to the description of loosely bound large complexes of particles and tightly bound small ones, a notion quite alien to conventional perturbation theory.

Nuclear Forces in Pseudoscalar Meson Theory*

K. A. Brueckner and K. M. Watson†
Indiana University, Bloomington, Indiana
(Received June 18, 1953)

The nuclear forces in pseudoscalar meson theory are evaluated using a nonrelativistic approximation to the relativistic interaction. The potential is obtained in a form which allows explicit evaluation of the contribution due to the multiple scattering of the virtual mesons between the two nucleons. An approximate expression for the potential, including the multiple scattering of a single meson, is obtained in closed form. For $r<0.5\hbar/\mu c$, the multiple-scattering terms predominate and a power series expansion of the potential is non-convergent. On the other hand, for $r>0.5\hbar/\mu c$ the potential obtained can be approximated by the second- and fourth-order terms as obtained from perturbation theory. With these latter two terms and a phenomenological "repulsive core," quite satisfactory results are obtained for the low-energy properties of the two-nucleon system.

I. INTRODUCTION

RECENT experimental results[1] on the scattering of pions by nucleons have led to a considerable improvement of the understanding of the nature of the pion-nucleon interaction. At the same time the approximate techniques of computation in field theory have been greatly improved over the weak- or strong-coupling approximations previously used almost universally. These developments are particularly apparent in the study of meson-nucleon scattering where the experimental results have been given a qualitatively correct interpretation by Chew[2] and Bethe and Dyson,[3] who considered pseudoscalar meson theory. In the theory of of the scattering, it was found that only a slight improvement over the weak-coupling perturbation theoretic methods of calculation was necessary to give a very considerable improvement in the results. Considerations of the photomesonic processes[4] also seem to indicate that a fairly good agreement between theory and experiment exists.

As a result of this clarification in the experimental and theoretical aspects of some of the problems of meson physics, it has seemed worthwhile to re-examine the meson theory of nuclear forces to see to what extent previous results need to be amended or extended. Although we shall consider the pseudoscalar form of the coupling in pseudoscalar theory, it will become apparent that in this problem the pseudovector form of the coupling can be used to give approximately the same results.

The potential which we shall evaluate has been constructed by methods recently considered by the authors.[5] It differs from that obtained by the S-matrix method or by the usual techniques of perturbation theory in that it does not result from a power series expansion in the coupling constant. The successive terms in the potential are modified from the usual expansion in that for a given term in the potential series, the energies of the virtual mesons are modified by the interaction with the nucleons which results from the terms in the potential of lower order. The effect is to take into account at all times, in evaluating a given contribution to the potential, the interaction of the meson which is already given by previously evaluated terms in the potential series. This form of the potential expansion shows that in the S-matrix expression almost all of the terms of high order in the coupling constant are associated with the multiple scattering of the virtual mesons between the two nucleons. For example, in the potential term which if expanded in a power series in g has as leading term the usual g^4 contribution, the virtual mesons are not emitted into and absorbed from plane wave states but rather from the multiple-scattering state which results from the g^2 interaction of the mesons with the nucleons. This contribution to the potential also is more general than the usual g^4 result in that it includes an important subset of the g^6 contributions together with a subset of all contributions of still higher order. Evaluation of the two leading terms in the potential therefore includes not only all g^2, g^4, and the important g^6 contributions but also indicates the effects of a variety of additional terms of higher order.

In Sec. II we shall summarize the results of the calculation of the potential and of the low-energy scattering parameters; in Sec. III we shall obtain the formal expression for the first two terms in the potential; in Sec. IV the single and multiple scattering problem for the virtual mesons will be evaluated; in Sec. V the explicit form of the potential will be obtained, and finally in Sec. VI we shall consider the non-adiabatic corrections to the potential. Some concluding remarks will be made in Sec. VII.

II. SUMMARY OF RESULTS

The considerations of Secs. III, IV, and V indicate that the potential given by pseudoscalar theory is represented to a fairly good approximation by the

* Supported by a grant of the National Science Foundation.
† Now at the University of Wisconsin, Madison, Wisconsin.
[1] Anderson, Fermi, Nagle, and Yodh, Phys. Rev. **86**, 793 (1952).
[2] G. F. Chew, Phys. Rev. **89**, 591 (1953).
[3] H. Bethe and F. J. Dyson, Phys. Rev. **90**, 372 (1953).
[4] K. A. Brueckner and K. M. Watson, Phys. Rev. **86**, 923 (1952); B. T. Feld, Phys. Rev. **89**, 330 (1953).
[5] K. A. Brueckner and K. M. Watson, Phys. Rev. **90**, 699 (1953). This paper will hereafter be referred to as I.

second- and fourth-order potentials calculated throughout in the adiabatic limit using the nonrelativistic limit to the pseudoscalar coupling. In obtaining this result, the following procedure has been used: first, the relativistic coupling has been reduced to the well-known nonrelativistic form[6] in which the leading term in g is the usual pseudovector coupling and the next term is a pair coupling of the meson field. Previous estimates of radiative effects[7-9] on the pair formation of nucleons which is associated with the meson-pair term indicate that the term is probably considerably overestimated in the perturbation calculation; this effect is indicated by multiplying the pair term by a parameter which is estimated to have a value roughly $(1+g^2/4\pi)^{-1}$ but is left arbitrary in the potential evaluation. The calculation is then made treating the nucleons adiabatically. The qualitative features of the potential are the following: the contributions to the potential which arise from the meson pair term acting once or twice nearly cancel for $r>0.8\hbar/\mu c$ and give a repulsive core to the potential for $r<0.8\hbar/\mu c$, the exact strength and range depending on the extent to which the radiative effects are taken into account. Higher-order contributions from the pair term alone are also small if the pair damping is taken into account, in agreement with the exact nonrelativistic evaluation of the pair term by Wentzel.[8] The remaining contributions to the potential, which do not involve the pair term (or nucleon pair formation), then include all g^2, g^4, and g^6 contributions together with a subset of all higher-order terms. The evaluation of this potential in the adiabatic limit and the estimate of the terms of higher order than g^4 center about the calculation of the matrices for the scattering of the virtual mesons off the energy shell and the solution of the multiple scattering equations for the propagation of the meson between the two nucleons between emission and absorption. This calculation shows that the scattering by the nucleons individually is very weak off the energy shell and is fairly well described by the Born approximation, this result contrasting markedly with the scattering on the energy shell where the well-known resonance effects occur.[2,3] Using this result, an approximate evaluation of the multiple-scattering equation shows that the effect of higher orders so taken into account is attractive and sets in strongly only near the repulsive core radius ($r=0.3\hbar/\mu c$) and is less than a 30-percent correction outside $r=0.6\hbar/\mu c$, decreasing very rapidly for increasing r. It seems fairly clear from this result that the potential is rather uncertain near the core since the higher-order terms set in so strongly; it is also this region where radiative effects can be expected to start to modify the gradient-coupling terms appreciably. These uncertainties are reflected in the partially phenomenological insertion of a repulsive core of radius only roughly given by the theory; an increase in the potential strength near the core can of course be compensated by a small increase in the repulsive radius. The conclusion of this investigation into the higher-order multiple-scattering effects is that the potential is given to a fairly good approximation outside $r=0.6\hbar/\mu c$ by the g^2+g^4 contributions from the gradient coupling and inside this radius the strength is somewhat arbitrary and must be obtained phenomenologically by adjustments of the core radius.

A further estimate of the validity of the potential can be made by determining the errors of the adiabatic treatment. This has been done by evaluating the expectation value of the non-adiabatic corrections to the g^2 potential using the wave function obtained from the solution to the potential problem, as discussed in Sec. VI. This is a valid procedure if the nonadiabatic potential is a small perturbation. The result confirms this assumption since the expectation value of this correction is only about $\frac{1}{10}$ Mev compared to 20 Mev for the static potential itself.

The final evaluation of the problem has been made using the g^2+g^4 potentials which, as discussed above, are a good approximation to the more general potential considered in Secs. III and IV outside $r=0.6\hbar/\mu c$. Inside this region the arbitrariness in the potential strength is represented by an adjustable core radius which is expected to lie in the range 0.3–$0.5\hbar/\mu c$. The remaining arbitrary parameters of the theory are the coupling constant and the strength of the pair term in the meson-nucleon coupling. These two parameters cannot, however, be regarded as completely unspecified since the analysis of meson-nucleon scattering indicates that $g^2/4\pi\simeq 14$–15 and the estimate of radiative effects on the pair term suggests the pair coupling is quite weak. The results of the evaluation are given in Table I for the deuteron ground state and for the singlet low-energy scattering. The evaluation in the triplet state was done for us by Professor J. M. Blatt and Dr. M. H. Kalos at the University of Illinois using the Illiac (Illinois Automatic Computer); the results for the singlet state are those of Taketani *et al.*,[10] who used a potential very nearly identical with ours for the singlet states. The results are given for two choices of the strength of the pair-coupling term, first unmodified from the perturbation value, and second with the pair terms negligible corresponding to the full strength of the damping. The agreement with the experimental values is considerably better in the latter case which, however, cannot be regarded as significant since the principal effect of the pair terms comes in the very uncertain region between $r=0.3\hbar/\mu c$ (the core radius) and $r=0.6\hbar/\mu c$ where the multiple scattering terms appear strongly.

[6] F. J. Dyson, Phys. Rev. **73**, 929 (1948); L. L. Foldy, Phys. Rev. **84**, 168 (1951).
[7] S. Drell and E. M. Henley, Phys. Rev. **88**, 1053 (1952).
[8] G. Wentzel, Phys. Rev. **86**, 802 (1953).
[9] Brueckner, Gell-Mann, and Goldberger, Phys. Rev. **90**, 476 (1953).
[10] Taketani, Machida, and Onuma, Prog. Theoret. Phys. (Japan) **7**, 45 (1952).

TABLE I. Low energy parameters of the nucleon-nucleon system. The data for the triplet-even (deuteron) state is given for two values of the parameter λ which determines the strength of the pair coupling. $\lambda=1$ corresponds to undamped pair formation; $\lambda=0$ corresponds to negligible contributions from pair formation. The singlet data (reference 10) is given for $\lambda=0$; the results are quite insensitive to the pair terms which give a net repulsive effect quite weak compared with the very strong central attraction. The parameters are adjusted to give correctly the deuteron binding energy and the singlet scattering length. For comparison, the experimental values are $Q=2.73\times10^{-26}$ cm^2, r_e(triplet) $=1.71\times10^{-13}$ cm, and r_e(singlet) $=2.7\pm0.5\times10^{-13}$ cm.

	Triplet-even		Singlet-even	
	$\lambda=1$	$\lambda=0$		
$g^2/4\pi$	19.5	15.4	13.3	16.0
Q[a]	3.43×10^{-26} cm^2	2.83×10^{-26} cm^2		
$P_D(\%)$	7.54	6.12		
Effective range	1.93×10^{-13} cm	1.73×10^{-13} cm	2.10×10^{-13} cm	2.585×10^{-13} cm
Core radius	0.300×10^{-13} cm	0.300×10^{-13} cm	0.328×10^{-13} cm	0.384×10^{-13} cm

[a] Due to the method of integration used, these values for the quadrupole moment are not accurate to better than 5 or 10 percent.

It is interesting to note that the coupling constant which gives the correct fit to the nuclear force data agrees very well with the value of 15 deduced from the meson-nucleon scattering. The excellent overall agreement results in part from our treatment of the nonadiabatic terms as discussed in Sec. VI; other treatments[10,11a] have estimated these using the wave function given by the g^2 potential (therefore corresponding to an infinite expectation value of the kinetic energy) and found an effective fourth-order static potential which was very strong and repulsive, changing the sign of the central triplet even state interaction. The treatment of the nonadiabatic terms is not unambiguous; it is felt, however, that a correct estimate must be based at least on a reasonable wave function which reflects approximately the known properties of the deuteron ground state.

III. CONSTRUCTION OF THE POTENTIAL

A. An Approximate Nonrelativistic Reduction of the Pseudoscalar Coupling

The pseudoscalar coupling term which we shall consider is

$$H_{ps}=ig\bar{\psi}\gamma_5\tau_a\psi\phi_a. \tag{1}$$

This interaction is dominated in the weak-coupling approximation by nucleon-pair formation for which the matrix elements of the relativistic operator γ_5 are of the order of unity. This feature of the coupling can be made more explicit by a variety of transformations[6] which exhibit more clearly the nonrelativistic features of the theory; the leading terms in powers of g which result are, in nonrelativistic approximation,

$$H_{ps}=h+h_p, \tag{2}$$

where

$$h=(g/2M)\boldsymbol{\sigma}\cdot\boldsymbol{\nabla}(\boldsymbol{\tau}\cdot\boldsymbol{\phi})\rho(r), \quad h_p=(g^2/2M)\phi^2\rho(r). \tag{3}$$

Here $\rho(r)$ is the nucleon source density. The first term is the usual nonrelativistic approximation to the pseudovector coupling; the meson-pair term arises from the creation and annihilation of a nucleon pair and appears to dominate the interaction since $g\simeq15$.

It is evident from the observed interaction of pions with nucleons and scattering and production, which is predominantly in P states, that the strong S-state interaction which would appear to arise from the pair coupling term of Eq. (3) is rather unimportant. This suggests that for these phenomena at least the nucleon pair formation which gives rise to the pair-coupling term is suppressed. The explanation of this result has been given in a variety of ways:

1. In the scattering of mesons the potential which arises from the pair term is strongly repulsive and of rather short range,[3] with the result that it gives rise to quite weak scattering.

2. Drell and Henley[7] have shown that in a nonrelativistic treatment of the pseudoscalar coupling, a canonical transformation leads to a form of the theory in which the meson-pair term is very strongly damped so that the effective coupling is quite weak.

3. Wentzel[8] has obtained exact solutions considering only the meson-pair term and has found that its contribution to both nuclear forces and meson scattering is strongly damped, the coupling constant g^2 of the pair term being reduced approximately by a factor $[1+g^2/4\pi]^{-1}$.

4. Brueckner, Gell-Mann, and Goldberger[9] have considered the relativistic pseudoscalar theory and shown that the nucleon-pair formation is strongly damped by reactive effects associated with the strongly bound meson field. This differs somewhat from the results of the nonrelativistic theories in that the correct renormalization of the radiative effects shows that terms which do not involve nucleon pair formation are damped only weakly. The consequence of these considerations is that the coupling terms of Eq. (2) are better approximated by

$$H_{ps}\simeq h+[1+3g^2/16\pi^2]^{-1}h_p. \tag{2'}$$

These results suggest very strongly that the effects of nucleon pair formation are overestimated in the weak coupling treatment of pseudoscalar theory and that they may in fact play a rather unimportant role in the nuclear force problem, at least in the nonrelativistic region. It is felt that the various considerations (1 to 4 above) which give the strong pair damping can be used

[11a] A. Klein, Phys. Rev. **90**, 1101 (1953).

to estimate the effective pair coupling. We shall for the present leave the effect unspecified by writing the pair term as

$$h_p=\lambda(g^2/2M)\phi^2, \tag{4}$$

where λ expresses the effect of the damping and is accordingly probably rather small.

B. Formal Derivation

The two-nucleon potential is obtained by using the methods recently proposed by the authors.[5] The effects of nucleon recoil on the potential will be neglected in the first approximation. The corrections due to this effect (i.e., nonadiabatic corrections) will be considered at a later state (Sec. VI).

Using the methods of I, the potential is given as an infinite series of terms. The successive terms may each be classified according to the maximum number of virtual mesons present at once. We shall restrict ourselves to only those terms for which at most two mesons are simultaneously present in an intermediate state. This is a well-defined approximation and receives some justification when it is recalled that the "energy denominators" are larger when more mesons are present.

In terms of the interaction of Eq. (2), the first term in the potential series is

$$V_0=\text{D.P.}\Delta_0, \tag{5}$$

where

$$\Delta_0=h_p+h[E-H_0-h_p]^{-1}h. \tag{6}$$

The first term of Δ_0 contributes only to meson scattering; the second term gives both a nuclear force and a meson scattering contribution in which the virtual mesons emitted or absorbed by the linear coupling term h can be scattered by h_p. The notation "D.P." means taking just that part of the operator which is diagonal in meson occupation numbers; h and h_p are defined by Eq. (3). Following again the notation of I, we define $U_0(e)$ and $U_0(o)$ to be the nondiagonal parts (in terms of occupation numbers) of Δ_0 which produce or absorb an even and an odd number of meson pairs, respectively.

The second term in the potential series is

$$V_1=\text{D.P.}[U_0(o)(E-H_0-V_0-U_0(e))^{-1}U_0(o)]. \tag{7}$$

To make the evaluation of Eqs. (5) and (7) manageable we shall now adopt one further approximation; that is, we shall consider h_p to be a small perturbation and develop the potential

$$V=V_0+V_1 \tag{8}$$

in powers of h_p. In particular, we shall keep only terms linear and quadratic in h_p. The validity of this procedure depends on the assumption of strong damping of the pair term; i.e., on the parameter λ of Eq. (4) having a small value.

To facilitate a symbolic description of the terms in the potential we shall denote the creation of a single meson by an operator with a superscript "(+)" and the annihilation of a single meson by a superscript "(−)." Thus $h^{(+)}$ and $h^{(-)}$ represent the respective matrix elements of h for creation and absorption of a meson, respectively. h_p is bilinear in the meson-field variables, so we employ

$$h_p^{(++)},\quad h_p^{(+-)},\quad h_p^{(--)},$$

to denote the creation of two mesons, etc.

Then we may write Eq. (8) as

$$V=v(1p)+v(2p)+v_g. \tag{9}$$

These terms are classified according to the degree to which h_p occurs. Expanding Eqs. (5) and (7) in powers of h_p and retaining only g^2 and g^4 contributions in the small terms depending linearly and bilinearly on h_p, we easily obtain:

$$v_{2p}=h_p^{(--)}\frac{1}{a}h_p^{(++)}, \tag{10}$$

$$v(1p)=h^{(-)}\frac{1}{a}h_p^{(+-)}\frac{1}{a}h^{(+)}+h^{(-)}\frac{1}{a}h^{(-)}\frac{1}{a}h_p^{(++)}+h_p^{(--)}\frac{1}{a}h^{(+)}\frac{1}{a}h^{(+)}, \tag{11}$$

and

$$v_g=h^{(-)}\left[a-h^{(-)}\frac{1}{a}h^{(+)}\right]^{-1}h^{(+)}, \tag{12}$$

where

$$a\equiv E-H_0. \tag{13}$$

The symbol a will be frequently used for brevity in what follows. The terms $v(1p)$ and $v(2p)$ of Eqs. (10) and (11) can be easily interpreted since they have the usual form given by perturbation theory; v_g[11b] has a more complex structure and will be discussed in more detail in the next section. It is seen to depend only upon the gradient coupling term in the original interaction of Eq. (3).

If we were to expand the operator $[a-h^{(-)}(1/a)h^{(+)}]^{-1}$ and keep only the first two terms, then

$$v_g\simeq h^{(-)}\frac{1}{a}h^{(+)}+h^{(-)}\frac{1}{a}h^{(-)}\frac{1}{a}h^{(+)}\frac{1}{a}h^{(+)}. \tag{14}$$

These represent the so-called second- and fourth-order contributions to the nuclear potential, as obtained from the gradient coupling. The terms given by Eqs. (10), (11) and (14) are evaluated and discussed in detail in Sec. IV. In the rest of the present section we shall consider corrections to Eq. (14) which result from a

[11b] This modified fourth-order potential is identical with that derived in the Tamm-Dancoff method, restricting the maximum number of mesons present to two. (Added in proof.)

more careful analysis of Eq. (12). The reader who is not interested in the rather involved mathematical details of these corrections (which have been qualitatively discussed in Sec. II) may turn immediately to Sec. V.

C. Derivation of the Multiple Scattering Equations

Returning to Eq. (12), we observe that

$$u \equiv h^{(-)}(1/a)h^{(+)}. \tag{15}$$

may be interpreted as a "potential" for the scattering of the meson which is produced by the first $h^{(+)}$ in Eq. (12) and absorbed by the last $h^{(-)}$. Indeed, v_g may be rewritten as

$$v_g = h^{(-)}w(1/a)h^{(+)}, \tag{16}$$

where w satisfies the equation

$$w = 1 + (1/a)uw, \tag{17}$$

which describes the multiple scattering of the virtual mesons by the two nucleons. The form of the "potential" u can be made more explicit if we make use of the form of h, which is

$$h_1 + h_2, \tag{18}$$

where h_i contains the field variables ϕ evaluated at the position $\mathbf{z}_i$ of nucleon "i." We then have

$$u = h_1^{(-)}\underset{a}{1}h_1^{(+)} + h_2^{(-)}\underset{a}{1}h_2^{(+)} + h_1^{(-)}\underset{a}{1}h_2^{(+)} + h_2^{(-)}\underset{a}{1}h_1^{(+)}. \tag{15'}$$

The last two terms contribute negligibly to the scattering if the two nucleons are not close together, since they correspond to the absorption of the meson at one nucleon and the emission at the other. The first two terms of Eq. (18) we shall call u_1 and u_2, respectively; they are the potentials for scattering the meson at nucleons (1) and (2). Dropping the last two terms, which will be discussed later in Sec. IV, we have

$$w = 1 + (1/a)(u_1 + u_2)w, \tag{17'}$$

which has the solution[12]

$$\begin{aligned} w &= 1 + (1/a)(t_1 w_1 + t_2 w_2), \\ w_1 &= 1 + (1/a)t_2 w_2, \\ w_2 &= 1 + (1/a)t_1 w_1. \end{aligned} \tag{19}$$

Equations (19) represent a system of simultaneous integral equations to be evaluated in terms of the scattering matrices t_1 and t_2 for mesons from nucleons "1" and "2," respectively. We can obtain t_1 and t_2 by solving the auxiliary equations

$$W_1 = 1 + (1/a)u_1 W_1, \quad W_2 = 1 + (1/a)u_2 W_2, \tag{20}$$

which allow us to evaluate t_1 and t_2 in terms of u_1 and u_2, since we have from the definition of the scattering matrices

$$W_1 = 1 + (1/a)t_1, \quad W_2 = 1 + (1/a)t_2. \tag{21}$$

Equations (20) and (21) describe the scattering of a meson by either nucleon and so represent a two-body problem (i.e., one meson and one nucleon). The solution to Eq. (17) is reduced to a solution of Eqs. (19) and (20). Having found t_1 and t_2, the treatment of Eqs. (19) is made by the methods previously used by one of us.[13]

IV. SOLUTION OF THE MULTIPLE SCATTERING EQUATIONS

A. Determination of the Matrices t_1 and t_2

We need consider only one of the two sets of equations in Eqs. (20) and (21) since these differ only by an interchange of the nucleon indices "1" and "2." We shall therefore attempt to solve the equation referring to nucleon "1." In a momentum representation,

$$(\mathbf{q}'|u_1|\mathbf{q}) = -\frac{g^2}{8M^2}(2\pi)^{-3}\exp[i(\mathbf{q}-\mathbf{q}')\cdot\mathbf{z}_1][w_q w_{q'}]^{-\frac{1}{2}} \times [w_q + w_{q'}]^{-1}[\boldsymbol{\sigma}_1\cdot\mathbf{q}\boldsymbol{\sigma}_1\cdot\mathbf{q}']\boldsymbol{\tau}_1\cdot\mathbf{U}_q\boldsymbol{\tau}_1\cdot\mathbf{U}_{q'}{}^{+}. \tag{22}$$

Here $w_q = (q^2+\mu^2)^{\frac{1}{2}}$, etc., and $\boldsymbol{\sigma}_1$ and $\boldsymbol{\tau}_1$ are the spin and isotopic spin matrices, respectively, for nucleon "1." $\mathbf{U}_q$ is the absorption operator for the meson with momentum $\mathbf{q}$ and $\mathbf{U}_{q'}{}^{+}$, the creation operator for the meson with momentum $\mathbf{q}'$ (these quantities are vectors in charge-space). We have neglected the energy of the nucleons in Eq. (22). We shall also neglect it in solving Eqs. (19) and (20).

u_1 is diagonalized with respect to states of total spin and isotopic spin by means of projection operators.

$$\begin{aligned} E_{\frac{3}{2}} &= \tfrac{1}{3}[i\boldsymbol{\tau}_1\cdot\mathbf{U}_q\times\mathbf{U}_{q'}{}^{+}+2] \\ \text{and} \\ E_{\frac{1}{2}} &= -\tfrac{1}{3}[i\boldsymbol{\tau}_1\cdot\mathbf{U}_q\times\mathbf{U}_{q'}{}^{+}-1] \end{aligned} \tag{23}$$

represent the projection operators on to states of isotopic spin $\frac{3}{2}$ and $\frac{1}{2}$, respectively, for the single-meson single-nucleon system. When the meson is in an orbital P state with respect to the nucleon,

$$\begin{aligned} F_{\frac{3}{2}} &= \frac{1}{qq'}\frac{1}{4\pi}[i\boldsymbol{\sigma}_1\cdot\mathbf{q}\times\mathbf{q}'+2\mathbf{q}\cdot\mathbf{q}'], \\ F_{\frac{1}{2}} &= -\frac{1}{qq'}\frac{1}{4\pi}[i\boldsymbol{\sigma}_1\cdot\mathbf{q}\times\mathbf{q}'-\mathbf{q}'\cdot\mathbf{q}] \end{aligned} \tag{24}$$

represent the respective projection operators on to states of total angular momentum $\frac{3}{2}$ and $\frac{1}{2}$.

Introducing

$$\alpha = \frac{g^2}{4\pi}\left[\frac{1}{3\pi M^2}\right], \tag{25}$$

[12] K. M. Watson, Phys. Rev. **89**, 575 (1953).

[13] K. A. Brueckner, Phys. Rev. **89**, 834 (1953).

and using Eqs. (23) and (24), we can write Eq. (22) as

$$(\mathbf{q}'|u_1|\mathbf{q})=-\frac{\alpha}{4}\frac{qq'}{[w_q w_{q'}]^{\frac{1}{2}}}\frac{\exp[i(\mathbf{q}-\mathbf{q}')\cdot\mathbf{z}_1]}{w_q+w_{q'}}$$
$$\times[4E_{\frac{1}{2}}F_{\frac{1}{2}}+E_{\frac{1}{2}}F_{\frac{1}{2}}-2E_{\frac{1}{2}}F_{\frac{1}{2}}-2E_{\frac{1}{2}}F_{\frac{1}{2}}]. \quad (26)$$

This permits us to decompose the Eq. (20) for W_1 into four separate equations for the four eigenstates of spin and isotopic spin. The coefficient of $E_{\frac{1}{2}}F_{\frac{1}{2}}$, which we may call $u_1(\frac{3}{2},\frac{3}{2})$, in Eq. (26) is the strongest of the four potentials. We shall consider this state explicitly. The equation (20) for the $(\frac{3}{2},\frac{3}{2})$ state is

$$(\mathbf{k}|W_1(\tfrac{3}{2},\tfrac{3}{2})|\mathbf{k}_0)=\frac{1}{k_0^2}\delta(k-k_0)+\frac{\alpha}{w_k}\int q^2dq$$
$$\times\frac{\exp[i(\mathbf{q}-\mathbf{k})\cdot\mathbf{z}_1]}{[w_k w_q]^{\frac{1}{2}}}\frac{kq}{w_k+w_q}(q|W_1(\tfrac{3}{2},\tfrac{3}{2})|\mathbf{k}_0). \quad (27)$$

To solve this integral equation, we shall make the reasonable approximation of replacing w_q+w_k by the larger of the two variables w_q and w_k.[14] The resulting equation for $W_1(\frac{3}{2},\frac{3}{2})$ is

$$(k|W_1(\tfrac{3}{2},\tfrac{3}{2})|k_0)=k_0^{-2}\delta(k-k_0)$$
$$+\frac{\alpha k}{w_k}\left[\frac{\lambda_1(k)}{w_k}+\frac{\lambda_2(k)}{\mu}\right]\exp(-i\mathbf{k}\cdot\mathbf{z}_1), \quad (30)$$

where

$$\lambda_1(k)=\int_0^k\frac{q^3dq}{w_k^{\frac{1}{2}}}(q|W_1(\tfrac{3}{2},\tfrac{3}{2})|k_0)\exp(i\mathbf{q}\cdot\mathbf{z}_1),$$
$$\lambda_2(k)=\mu\int_k^\infty\frac{q^3dq}{w_k^{\frac{1}{2}}}(q|W_1(\tfrac{3}{2},\tfrac{3}{2})|k_0)\exp(i\mathbf{q}\cdot\mathbf{z}_1), \quad (31)$$

and α is defined by Eq. (25). Differentiating these expressions for λ_1 and λ_2 with respect to k and making use of Eq. (30) for $W_1(\frac{3}{2},\frac{3}{2})$, we finally obtain the coupled differential equations:

$$\frac{d\lambda_1}{dk}=\frac{\alpha k^4}{w_k^2}\left[\frac{\lambda_1}{w_k}+\frac{\lambda_2}{\mu}\right]+\frac{k_0}{w_0^{\frac{1}{2}}}\delta(k-k_0),$$
$$\frac{d\lambda_2}{dk}=-\frac{\alpha k^4\mu}{w_k^3}\left[\frac{\lambda_1}{w_k}+\frac{\lambda_2}{\mu}\right]-\frac{k_0\mu}{w_0^{\frac{1}{2}}}\delta(k-k_0), \quad (32)$$

with the boundary conditions that λ_1 vanishes at $k=0$ and that λ_2 vanishes at the cut-off momentum $k_{\max}$ which is introduced to approximate the recoil effects of the relativistic theory and which is necessary to give a finite result. These equations can readily be solved numerically; the following approximate method which gives a closed expression for the scattering matrix is also useful. A detailed comparison of the numerical results with the approximate solutions shows agreement to within the accuracy of the numerical calculations. In the nonrelativistic limit, it is easily shown that general solutions to Eq. (32) are

$$\lambda_1=C_2+C_1\alpha k^5/5\mu^3, \quad \lambda_2=C_1-\lambda_1, \quad (33)$$

where C_1 and C_2 are arbitrary constants. In the relativistic limit, the solutions are:

$$\lambda_2=\mu\alpha^{\frac{1}{2}}[C_3\cos\alpha^{\frac{1}{2}}k-C_4\sin\alpha^{\frac{1}{2}}k],$$
$$\lambda_1=C_3[\sin\alpha^{\frac{1}{2}}k-k\alpha^{\frac{1}{2}}\cos\alpha^{\frac{1}{2}}k]$$
$$+C_4[\cos\alpha^{\frac{1}{2}}k+k\alpha^{\frac{1}{2}}\sin\alpha^{\frac{1}{2}}k], \quad (34)$$

where C_3 and C_4 are arbitrary constants. The solutions which take proper account of the boundary conditions and of the delta function discontinuity at k_0 can be constructed from these. The two solutions for small and large k are then joined at $k=\mu$ where both limiting forms have approximate validity. The resulting expressions are very lengthy but they take on a simple form in two limiting cases. If $\alpha^{\frac{1}{2}}\tan(\alpha^{\frac{1}{2}}k_{\max})$ is less than one, or equivalently, if $0<g^2/4\pi<20$, for $k_{\max}=M$, then the scattering matrix

$$(k|t_1|k_0)=-\alpha k\left[\frac{\lambda_1}{w_k}+\frac{\lambda_2}{\mu}\right]\exp(-i\mathbf{k}\cdot\mathbf{z}_1) \quad (35)$$

is fairly well given (to within a factor of two) by the Born approximation result,

$$-\alpha\frac{kk_0}{[w_k w_0]^{\frac{1}{2}}}\exp[i(\mathbf{k}_0-\mathbf{k})\cdot\mathbf{z}_1]\times\begin{cases}1/w_k, & w_k>w_0\\ 1/w_0, & w_k<w_0.\end{cases} \quad (36)$$

This dependence on w_k and w_0 results from our approximation to the energy denominator w_k+w_0.

If $\alpha^{\frac{1}{2}}\tan(\alpha^{\frac{1}{2}}k_{\max})$ is larger than one, then the largest term in the scattering matrix is approximately

$$-\alpha\frac{kk_0}{[w_k w_0]^{\frac{1}{2}}}\alpha^{\frac{1}{2}}\tan(\alpha^{\frac{1}{2}}k_{\max}), \quad (37)$$

which can be very large if $\alpha^{\frac{1}{2}}k_{\max}\simeq\pi/2$ or, taking $k_{\max}=M$, if $g^2/4\pi=3\pi^2/4=23.3$. This value of the coupling constant is considerably larger than is compatible with the observed pion scattering; in this case, Bethe and Dyson have found that $g^2/4\pi\simeq15$. To verify this result for our approximate methods of solution, we have calculated the scattering of mesons on the energy shell and found that for $g^2/4\pi=15$, the resonance in the scattering occurs at somewhat less than 140 Mev, showing that this value of the coupling constant is consistent with our method of cutoff for high momenta. Accordingly, we can conclude that the Born approximation result [Eq. (26)] is not qualitatively a bad approximation for the scattering. It is noteworthy that for somewhat larger values of the coupling constant than appear to be indicated by the scattering experi-

[14] A similar approximation is discussed by H. Bethe in *Proceedings of the Third Annual Rochester Conference on High Energy Physics.*

ments, the nuclear forces would show a remarkable deviation from the perturbation theory results since the scattering of the virtual mesons would then be very strong.

B. Evaluation of the Multiple Scattering

We have found that to a fair approximation we can take

$$(\mathbf{k}|t_1|\mathbf{k}_0)=(\mathbf{k}|u_1|\mathbf{k}_0), \tag{38}$$

as given by Eq. (26). With this result, we shall return to the multiple-scattering equations (19). These equations are difficult to solve in general. Consequently, we shall make a number of approximations by which, it is felt, that we can obtain a qualitatively correct result. The first approximation involves our choice of the scattering matrices t_1 and t_2. We have remarked that Eq. (38) seems to be correct to within a factor of no more than two over the momentum range, k, $k_0<M$. Actually, we shall not use Eq. (38), but another form [see Eq. (49)] for the t's. This latter form seems to be at least *no worse* an approximation than is Eq. (38).

Our next approximation is connected with the fact that the integrals occurring in Eqs. (19) must be cutoff at high momenta if an unambiguous result is to be obtained. Since we started with an approximate interaction [Eq. (2)] which treats the nucleons as infinitely heavy, we cannot entirely remove these divergences by renormalization. On the other hand, we can identify and first remove the renormalization terms before introducing a cutoff into the theory. This seems quite reasonable and can easily be done.

We first note that if the power series solution for w,

$$w=1+\frac{1}{a}(t_1+t_2)+\frac{1}{a}\left(\frac{1}{a}t_1t_2+\frac{1}{a}t_2t_1\right)+\cdots, \tag{39}$$

is substituted into Eq. (16), characteristic terms such as

$$\frac{1}{a}\frac{1}{a}h_1^{(-)}t_1h_1^{(+)} \tag{40}$$

appear. These evidently describe a self-energy. On the other hand, such a combination as

$$\cdots\frac{1}{a}\frac{1}{a}\frac{1}{a}t_2t_1h_1^{(+)} \tag{41}$$

includes a renormalization of the coupling constant, as is evident from Fig. 1.

FIG. 1. Coupling-constant renormalization. The emission and re-absorption of the meson with momentum $\mathbf{k}'$ leads to renormalization of the coupling constant for the emission of the meson $\mathbf{k}$ which is subsequently scattered.

To remove the renormalization terms which can occur only in association with the first or last scattering, since the iteration $t_1a^{-1}t_2a^{-1}t_1\cdots$ itself contains no such effects, it is only necessary to isolate the first and last scattering from the remainder of the multiple-scattering problem. For this purpose, we express w_1 and w_2 of Eq. (19) as

$$\begin{aligned} w_1&=1+G_{11}(1/a)t_1+G_{12}(1/a)t_2,\\ w_2&=1+G_{21}(1/a)t_1+G_{22}(1/a)t_2. \end{aligned} \tag{42}$$

Substitution into Eq. (19) shows that

$$G_{22}=(1/a)t_1G_{12} \quad \text{and} \quad G_{11}=(1/a)t_2G_{21}, \tag{43}$$

where G_{12} and G_{21} satisfy the uncoupled integral equations

$$\begin{aligned} G_{12}&=1+\frac{1}{a}\frac{1}{a}t_2t_1G_{12}\\ &\text{and}\\ G_{21}&=1+\frac{1}{a}\frac{1}{a}t_1t_2G_{21}. \end{aligned} \tag{44}$$

The solution of those equations of course involves no renormalization difficulties.

When Eqs. (42) are substituted into Eq. (19) for w, there results

$$\begin{aligned} w=1+\frac{1}{a}t+\frac{1}{a}\frac{1}{a}t_2+\frac{1}{a}\frac{1}{a}t_1G_{11}t_2+\frac{1}{a}\frac{1}{a}t_1G_{12}t_2\\ +\frac{1}{a}\frac{1}{a}t_1G_{21}t_1+\frac{1}{a}\frac{1}{a}t_2G_{22}t_2. \end{aligned} \tag{45}$$

This form is particularly useful since, as required above, the first and last scatterings which are the only points at which renormalization effect can occur, are isolated from the rest of the multiple scattering.

On substituting this equation for w into Eq. (16) for v_θ, we see that the self-energies are of the form of Eq. (40) and result from the second and third terms only on the right side of Eq. (45). The only renormalizations of g^2 are of the form of Eq. (41) and can be removed if we express t_1 in terms of u_1 by using the identity

$$\frac{1}{a}t_1h_1^{(+)}=\frac{1}{a}u_1h_1^{(+)}+\frac{1}{a}\frac{1}{a}t_1u_1h_1^{(+)} \tag{46}$$

and carry out standard renormalization procedures on the divergent term

$$u_1(1/a)h_1^{(+)}. \tag{47}$$

We return now to the general multiple scattering problem. The potential

$$v_\theta=h^{(-)}w(1/a)h^{(+)}$$

can be described as due to the emission of a meson by $h^{(+)}$, its multiple scattering between the two nucleons,

and finally its reabsorption by $h^{(-)}$. After effecting the coupling constant renormalization, it is evident that we will obtain a similar expression, but one in which $h^{(+)}$ and $h^{(-)}$ are modified by radiative corrections. Also in this modified expression, a meson created, for instance, at nucleon "1" must be first scattered by nucleon "2," etc.

For simplicity in obtaining numerical results we shall not include the radiative corrections to $h^{(+)}$ and $h^{(-)}$, as mentioned above (although this would present no particular difficulties). These give somewhat shorter range corrections and do not seem to be qualitatively important.

We may next [see Eq. (45)] divide v_g into two types of terms: those for which the meson is re-absorbed by the same nucleon which originally emitted it and those for which it is reabsorbed by the other nucleon. The calculation of both types of terms is essentially the same, since in any case the solution to Eqs. (44) is involved. We shall first calculate the terms of the latter type and later return to those omitted. Then we must evaluate

$$v^{(1)} \equiv h_2{}^{(-)}(1/a)t_1G_{12}(1/a)t_2(1/a)h_1{}^{(+)} \equiv h_2{}^{(-)}G_{21}(1/a)h_1{}^{(+)}. \quad (48)$$

(to which we must add the same expression with "1" and "2" interchanged).

To determine G_{21} we must solve Eq. (44). Rather than to treat the states of spin and isotopic spin in detail, which is straightforward but exceedingly laborious, we shall set the t matrices for all the spin and isotopic spin states equal to the *largest* one [i.e., that for the $(\frac{3}{2}, \frac{3}{2})$ state]. This will presumably give us a reasonable upper limit on the magnitude of the multiple scattering effects. (We note that our final results would not have been qualitatively affected had we set all the submatrices t equal to the *smallest* one.)

On the basis of the conclusions of Part B of this section, we shall then set

$$(k|t_1|k_0) = -\frac{\Phi}{\mu^3}\frac{\mathbf{k}\cdot\mathbf{k}_0}{[w_k w_0]^{\frac{1}{2}}}\exp[i(\mathbf{k}_0-\mathbf{k})\cdot\mathbf{z}_1]. \quad (49)$$

The spin and isotopic spin matrices do not appear as a result of our setting the t's equal for the spin and isotopic spin substates, as mentioned above. The functional form in Eq. (49) is chosen as a compromise between Eqs. (36) and (37), Φ is taken to be independent of $\mathbf{k}$ and $\mathbf{k}_0$ and will later be assigned a magnitude to correspond as closely as possible to the strength of the t matrix for the $(\frac{3}{2}, \frac{3}{2})$ state.

With the choice (59) for the t's, we can easily solve Eq. (44) exactly. We first obtain from Eq. (49):

$$\left(\mathbf{k}\left|\frac{1}{a}\frac{t_1-t_2}{}\right|\mathbf{k}_0\right) = -\frac{2\pi^2\Phi^2}{\mu^6}\frac{\exp[i(\mathbf{k}_0\cdot\mathbf{z}_2-\mathbf{k}\cdot\mathbf{z}_1)]}{[w_k w_0]^{\frac{1}{2}}} \times[\mathbf{k}\cdot\mathbf{k}_0 L+\mathbf{k}_0\cdot\mathbf{R}\mathbf{k}\cdot\mathbf{R}R^{-2}N]. \quad (50)$$

In this equation, $\mathbf{R}=\mathbf{z}_1-\mathbf{z}_2$ and

$$L=\frac{1}{R}\frac{d}{dR}\left[\frac{e^{-\mu R}}{R}\right], \quad N=R\frac{dL}{dR}. \quad (51)$$

Substituting Eq. (50) into Eq. (43), we obtain

$$(\mathbf{k}|G_{21}|\mathbf{k}_0) = \delta(\mathbf{k}-\mathbf{k}_0) - \frac{2\pi^2\Phi^2}{w_k{}^{\frac{1}{2}}\mu^6}\exp(i\mathbf{k}\cdot\mathbf{z}_1) \times\int\frac{d^3q}{w_q{}^{\frac{1}{2}}}\exp(i\mathbf{q}\cdot\mathbf{z}_2)[\mathbf{k}L+\mathbf{k}\cdot\mathbf{R}\mathbf{R}R^{-2}N) \cdot\mathbf{q}(\mathbf{q}|G_{21}|\mathbf{k}_0). \quad (52)$$

Defining

$$\mathbf{\Lambda}=\int\mathbf{q}\frac{\exp(i\mathbf{q}\cdot\mathbf{z}_2)}{w_q{}^{\frac{1}{2}}}(\mathbf{q}|G_{21}|\mathbf{k}_0)d^3q \quad (53)$$

[$\mathbf{\Lambda}$ appears implicitly on the right hand side of Eq. (52)], multiplying both sides of Eq. (52) by $\mathbf{k}\exp(i\mathbf{k}\cdot\mathbf{z}_2)[w_k]^{-\frac{1}{2}}$, and integrating over $\mathbf{k}$, we obtain an algebraic equation for $\mathbf{\Lambda}$:

$$\mathbf{\Lambda}=\mathbf{k}_0\frac{\exp(i\mathbf{k}_0\cdot\mathbf{z}_2)}{w_0{}^{\frac{1}{2}}}+\frac{2\pi^2\Phi^2}{\mu^6}\mathbf{\Lambda}\cdot\int d^3k(\mathbf{k}L+\mathbf{R}\mathbf{k}\cdot\mathbf{R}R^{-2}) \times\mathbf{k}\frac{\exp(i\mathbf{k}\cdot\mathbf{R})}{w_k{}^2}. \quad (54)$$

Since L and N are functions only of R, the k integral is readily evaluated in terms of the derivatives of $e^{-\mu R}/R$. Solving Eq. (54) for $\mathbf{\Lambda}$ and substituting this into the right-hand side of Eq. (52), we obtain

$$(\mathbf{k}|G_{21}|\mathbf{k}_0) = \delta(\mathbf{k}-\mathbf{k}_0)+\eta\frac{\exp[i(\mathbf{k}_0\cdot\mathbf{z}_2-\mathbf{k}\cdot\mathbf{z}_1)]}{w_k{}^{\frac{1}{2}}w_0{}^{\frac{1}{2}}} \times\left\{\mathbf{k}\cdot\mathbf{k}_0 L+\mathbf{k}\cdot\mathbf{R}\mathbf{k}_0\cdot\mathbf{R}R^{-2}\left(\frac{\lambda L+N}{1-\lambda}\right)\right\}. \quad (55)$$

Here

$$\eta=\frac{2\pi^2\Phi^2}{\mu^6}\left[1-\left[\frac{2\pi^2\Phi}{\mu^3}\right]^2 L^2\right]^{-1} \quad (56)$$

and

$$\lambda=2\pi^2\eta R^2 N[2L+N]. \quad (57)$$

We obtain the nuclear potential $v^{(1)}$ on substituting Eq. (55) into the second of Eqs. (48). The integrals are easily done. For the central potential of the deuteron state (i.e., the spin triplet, isotopic-spin singlet state), we obtain Eq. (48) has to be multiplied by a factor of two, since we must add to that equation the one resulting from an interchange of the two nucleons:

$$v^{(1)} = -\frac{g^2}{4\pi}\left(\frac{\mu}{2M}\right)^2\mu\left\{\frac{e^{-\mu R}}{\mu R}+2\pi^2\eta \times\left[\frac{e^{-\mu R}}{\mu R}L^2+\frac{1}{\mu^3}\left(\frac{2NL+\lambda L^2+N^2}{1-\lambda}\right)(L+N)\right]\right\}. \quad (58)$$

To choose Φ to agree as well as possible with Eq. (26), we have taken

$$\Phi=(2\pi)^{-3}(\mu^2/4M^2)(\mu R)g^2. \tag{59}$$

The factor μR is inserted to correct for the factor $2\mu/(w_k+w_0)$ which was dropped from the (correct) form of Eq. (36) in Eq. (49). This is, of course, only a qualitative correction for the lost factor. On the other hand, were we to use the functional form (37) for the matrix t, we should have set $(\mu R)=1$ in Eq. (59). In any case, the presence of the factor (μR) does not greatly modify our conclusions concerning the strength of the multiple-scattering corrections. This results from the fact that the multiple-scattering corrections become important so rapidly at small distances that their importance seems to be qualitatively unaffected by the details of the calculations.

We observe from Eq. (58) that the multiple-scattering effects appear as an additive correction to the g^2 potential, $e^{-\mu R}/\mu R$ (starting with a term of g^6). Their importance is indicated in Fig. 2, where the g^2 potential is compared with Eq. (58). The multiple-scattering corrections become important at $\mu R=0.8$ for $g^2/4\pi=15$. The importance of the multiple-scattering correction seems to be due to the singularity of the gradient coupling. To show this, we have everywhere in Eq. (58) replaced $e^{-\mu R}$ by $(e^{-\mu R}-e^{-2\mu R})$. The importance of the multiple-scattering corrections is indeed reduced, as is indicated in the dotted curve of Fig. 2. For convenient comparison, the modified $v^{(1)}$ has been multiplied by a factor $e^{-\mu R}(e^{-\mu R}-e^{-2\mu R})^{-1}$. The result is the dotted curve in Fig. 2.

The actual importance of the multiple-scattering corrections in Eq. (58) have been considerably over-

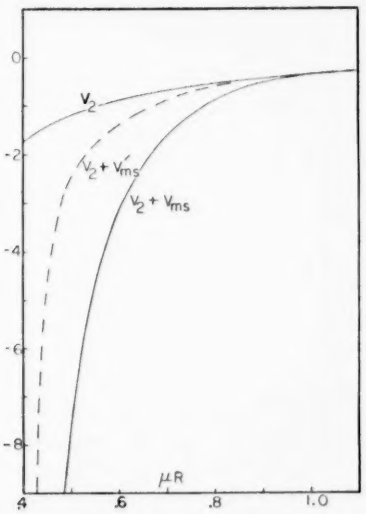

FIG. 2. Multiple-scattering corrections (starting as g^6) to the second-order potential. The dashed curve indicates the depression of the multiple scattering if radiative effects tend to decrease the singularity of the meson coupling. V_2 is taken to be $e^{-\mu R}/R$.

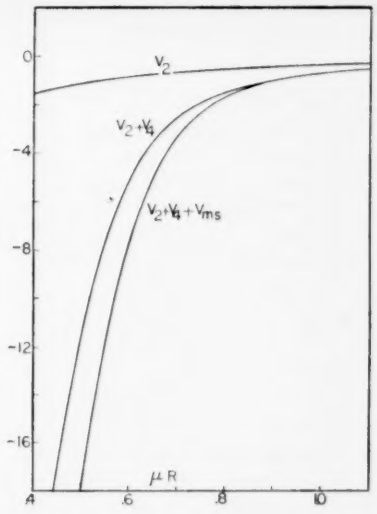

FIG. 3. Multiple-scattering corrections (starting as g^6) to the second- and fourth-order potentials. The notation is the same as in Fig. 2.

estimated in Fig. 2. This is due to our neglect of the fourth-order terms in the potential series, which is calculated in the next section. In Fig. 3 we present a comparison of the second order, the second plus fourth order, and the second plus fourth order plus the multiple-scattering terms (the latter, beginning with a sixth-order force term) for the central-force deuteron potential.

It is seen from Fig. 3 that for $\mu R\gg 1$ the second-order term predominates, while for $\mu R<1$ the higher-order terms are of more importance. However, the corrections to the fourth-order potential are not qualitatively important for $\mu R>0.5$. This is somewhat reassuring, especially when we recall that we have set the matrices t for the four states of spin and isotopic spin equal to the largest. On the other hand, had we set all the t's equal to the smallest, the multiple scattering would have become predominant for $\mu R=0.4$.

The results of Fig. 3 seem to be quite reasonable. The importance of higher-order corrections appear to set in at progressively smaller distances. However, for $\mu R<0.5$ we conclude that the power series expansion must break down completely. For $\mu R>0.5$ the sum of the second- and fourth-order potentials appears to be a valid approximation to the actual potential.

In this connection, the dotted curve of Fig. 2 suggests that if radiative corrections to the individual scattering processes should cut off the singular integrals which have been encountered, the expansion in terms of meson exchanges might be valid to somewhat shorter distances. Unless such a cutoff should occur, we conclude that a power series expansion of Eq. (58) is quite misleading (and divergent) for $\mu R<0.5$.

We must now say something about the terms which

have been omitted in our calculation of Eq. (58). Besides the terms (48) which we have calculated, there are also terms of the form

$$v^{(2)}=h_1^{(-)}G_{11}(1/a)h_1^{(+)}=h_1^{(-)}(1/a)t_2G_{21}(1/a)h_1^{(+)},$$

etc. The lowest-order correction to the curves of Fig. 3 which are obtained from this type are of $O(g^8)$. The multiple-scattering corrections are the same as before, since the same matrix G_{21} again appears. Because of the qualitative nature of our calculations of the multiple-scattering effects, there seems to be no point in explicitly calculating these latter terms.

We finally return to the two terms dropped in Eq. (15′) for the potential u. To estimate the importance of these, we have set

$$u=u_3\equiv h_1^{(-)}(1/a)h_2^{(+)}$$

and have calculated w [Eq. (17)]. Approximations similar to those already used were made. The resulting potential had a form very similar to that of Eq. (58). It was somewhat smaller in magnitude, but probably not significantly so.

It seems safe to conclude that in no sense have we obtained quantitative corrections to the fourth-order potential. On the other hand, we have seen the effects of higher-order meson exchanges set in at progressively small distances. It seems likely that in the region $\mu R<0.6$ the power series expansion breaks down completely. Outside this region it is not unlikely that the second plus fourth-order potentials may provide a reasonable approximation to the two-nucleon potential.

V. EVALUATION OF THE g^2 AND g^4 CONTRIBUTIONS TO THE POTENTIALS

Neglecting higher-order multiple-scattering contributions, as discussed in Sec. IV, we now evaluate the potential V of Eq. (9) using Eq. (14) for v_θ. The terms of order g^2 and g^4 in v_θ are denoted by v_2 and v_4, respectively. The diagrams representing these potentials are given in Fig. 4; the explicit potentials are

$$v_2=-(g/2M)^2\frac{\boldsymbol{\tau}_1\cdot\boldsymbol{\tau}_2}{(2\pi)^3}\int\boldsymbol{\sigma}_1\cdot\mathbf{k}\boldsymbol{\sigma}_2\cdot\mathbf{k}\frac{e^{i\mathbf{k}\cdot\mathbf{r}}}{w_k^2}d^3k,$$

$$v(1\text{-pair})=-\frac{6\lambda(g^2/2M)^2}{(2\pi)^6}\int\frac{d^3kd^3k'}{w^2w'^2}e^{i(\mathbf{k}+\mathbf{k}')\cdot\mathbf{r}},$$

$$v(2\text{-pair})=-\frac{3\lambda^2(g^2/2M)^2}{(2\pi)^6}\int\frac{d^3kd^3k'}{ww'[w+w']}e^{i(\mathbf{k}+\mathbf{k}')\cdot\mathbf{r}},$$

$$v_4=-\frac{(g/2M)^4}{(2\pi)^6}\int\frac{d^3kd^3k'}{w^2w'}e^{i(\mathbf{k}+\mathbf{k}')\cdot\mathbf{r}}\times\left\{\left(\frac{3}{w'}+\frac{2\boldsymbol{\tau}_1\cdot\boldsymbol{\tau}_2}{w+w'}\right)\times(\mathbf{k}\cdot\mathbf{k}')^2+\boldsymbol{\sigma}_1\cdot\mathbf{k}\times\mathbf{k}'\boldsymbol{\sigma}_2\cdot\mathbf{k}\times\mathbf{k}'\left(\frac{3}{w+w'}+\frac{2\boldsymbol{\tau}_1\cdot\boldsymbol{\tau}_2}{w'}\right)\right\}. \tag{60}$$

In these results we have not included the radiative corrections to the g^2 potential since explicit evaluation[15] shows that they are very small.

The evaluation of these integrals is straightforward; details are given in the appendix to reference 15. We find, with $\beta\equiv\mu[\mu/2M]^2g^2/4\pi$,

$$v_2=\tfrac{1}{3}\beta\boldsymbol{\tau}_1\cdot\boldsymbol{\tau}_2\left[\boldsymbol{\sigma}_1\cdot\boldsymbol{\sigma}_2+\frac{3+3x+x^2}{x^2}S_{12}\right]\frac{e^{-x}}{x},$$

$$v(1\text{-pair})=\beta\left[6\lambda\frac{g^2}{4\pi}\frac{\mu}{2M}\right]\left(\frac{1+x}{x^2}\right)^2e^{-2x},$$

$$v(2\text{-pair})=\beta\left[-3\lambda^2\frac{g^2}{4\pi}\right]\frac{1}{x^2}\frac{2}{\pi}K_1(2x),$$

$$v_4=\beta\left[-\frac{g^2}{4\pi}\frac{\mu^2}{4M^2}\right]\left(\frac{1}{x^3}\right)\frac{2}{\pi}\left\{\left[\frac{4+4x+x^2}{x}\times e^{-x}K_1(x)+(2+2x+x^2)K_0(x)e^{-x}\right]\times(3-2\boldsymbol{\tau}_1\cdot\boldsymbol{\tau}_2)+\left[(23+4x^2)K_0(2x)+\frac{23+12x^2}{x}K_1(2x)\right]\boldsymbol{\tau}_1\cdot\boldsymbol{\tau}_2-2\boldsymbol{\sigma}_1\cdot\boldsymbol{\sigma}_2\left[6K_0(2x)+\frac{6+4x^2}{x}K_1(2x)\right]+\tfrac{2}{3}\boldsymbol{\sigma}_1\cdot\boldsymbol{\sigma}_2(3-2\boldsymbol{\tau}_1\cdot\boldsymbol{\tau}_2)\left[K_0(x)e^{-x}(1+x)+\frac{2+2x+x^2}{x}K_1(x)e^{-x}\right]+\tfrac{1}{3}S_{12}\left[36K_0(2x)+\frac{45+12x^2}{x}K_1(2x)-(3-2\boldsymbol{\tau}_1\cdot\boldsymbol{\tau}_2)\left((1+x)K_0(x)e^{-x}+\frac{5+5x+x^2}{x}K_1(x)e^{-x}\right)\right]\right\},$$

where $S_{12}=3(\boldsymbol{\sigma}_1\cdot\mathbf{r}\boldsymbol{\sigma}_2\cdot\mathbf{r}/r^2)-\boldsymbol{\sigma}_1\cdot\boldsymbol{\sigma}_2$. The result for v_4 has been previously obtained by Taketani, Machida, and Onuma[10] who, however, used the S-matrix theory to obtain the potential and did not include the terms in $K_0(x)$ and $K_1(x)$. This result arises from a different treatment of the nonadiabatic correction to the g^2 potential; as discussed in detail in the next section.

[15] M. Lévy, Phys. Rev. **88**, 725 (1952).

The potential which results from the formation of one or two nucleon pairs in intermediate states is plotted in Fig. 5 for various values of λ. It is weak for $r>h/\mu c$ and becomes repulsive and strong for $r<0.8h/\mu c$. It is remarkable that the effect of changing λ from 1 to 0.2 is relatively small, having only the effect of slightly shifting the point at which the repulsion sets in strongly. This result differs markedly from previous results which did not take into account the effects of formation of one nucleon pair which give a strong spin independent repulsive potential, nearly cancelling the central attractive term resulting from the formation of two pairs.[16]

The contributions to the potential resulting from no pairs, i.e., those given by the linear nonrelativistic coupling $\boldsymbol{\sigma}\cdot\nabla\boldsymbol{\tau}\cdot\boldsymbol{\phi}$, give (Fig. 6) for even states a strong attractive singlet force, a weaker triplet force, and a strong tensor force of the correct sign which however changes sign at small distances. The central repulsion

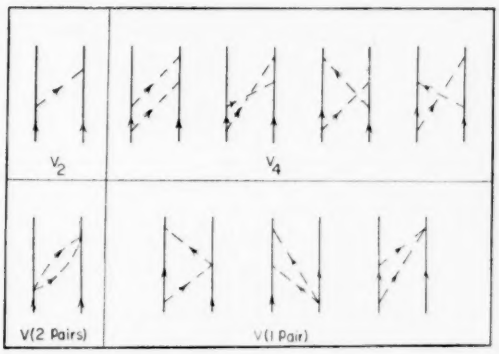

FIG. 4. Contributions to the various potentials. The time sequence of emissions and absorptions is indicated by the directions of the arrows.

associated with single-nucleon pair formation also gives a repulsive core which is dominant at small distances, $r\simeq\frac{1}{2}h/\mu c$. For the odd states (Fig. 7), the singlet force is repulsive and very strong; the triplet force is weak and attractive; and the tensor force has a sign opposite to that in even states at large distances but changes sign at $r\simeq 0.6h/\mu c$.

This very complicated result for the potential probably has an approximate validity in the non-relativistic region, for $r\geq 0.6h/\mu c$. It is very likely, as discussed in Sec. IV, that higher-order effects such as the strong multiple scattering of the virtual mesons which seems to set in at $r\simeq\frac{1}{2}h/\mu c$ will radically modify the potential in this region. It has become customary to approximate

[16] The large corrections to V (2 pairs) which have been found here seem to be in qualitative agreement with the S-matrix calculations of K. M. Watson and J. V. Lepore, Phys. Rev. **76**, 1157 (1949), using the pseudoscalar coupling. This can be seen from Fig. 3 of that paper, where V (2 pairs) was referred to as the "nonrelativistic" approximation.

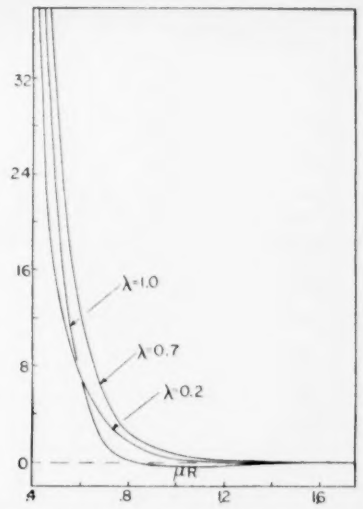

FIG. 5. The total-spin and isotopic-spin independent potential arising from the creation of one or two nucleon pairs in intermediate states. The parameter λ measures the extent of the damping of pair formation; $\lambda=1$ corresponds to no damping. $g^2/4\pi$ has been taken to be 15. The ordinate is in units of $(g^2/4\pi)[\mu/2M]^3\mu=11.8$ Mev.

these effects by a repulsive core at small distances; it seems however that although this may be the correct qualitative behavior, the effective radii of repulsion may be different for all six potentials. The matching of these results to experiment should also be attempted only at low energies where the nonstatic effects, such as the strong increase in the scattering of the virtual mesons, are small.

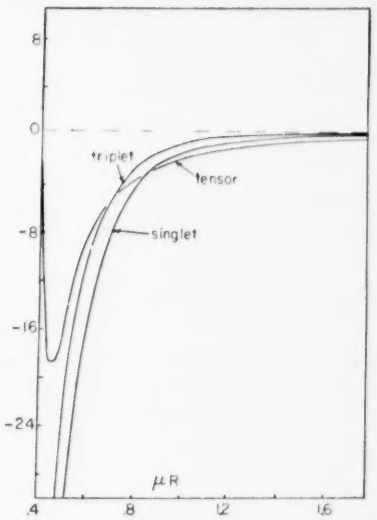

FIG. 6. The sum of potentials for even states which do not involve nucleon pair formation. The ordinate is in units of $(g^2/4\pi)[\mu/2M]^3\mu=11.8$ Mev.

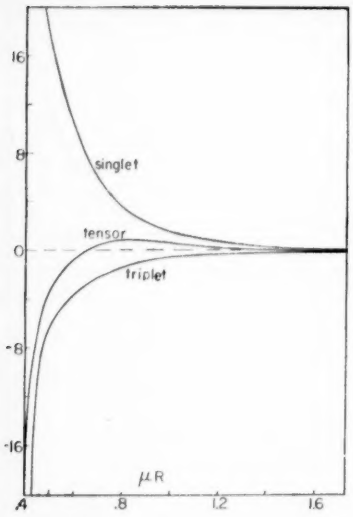

FIG. 7. The sum of potentials for odd states which do not involve nucleon pair formation. The ordinate is in units of $(g^2/4\pi)[\mu/2M]^2\mu = 11.8$ Mev.

VI. NONADIABATIC CORRECTIONS TO THE SECOND-ORDER POTENTIAL

It was originally pointed out by Levy[15] that a certain type of velocity-dependent corrections to the second order potential can be expressed as static corrections to the fourth-order potential. In the case of the pseudoscalar theory, if recoil is taken into account in evaluating the energies of the intermediate states, one obtains for the second-order potential in momentum space:

$$V^{(2)}(p,k) = -\boldsymbol{\tau}_1\cdot\boldsymbol{\tau}_2 \frac{g^2}{4M^2} \frac{\boldsymbol{\sigma}_1\cdot\mathbf{k}\boldsymbol{\sigma}_2\cdot\mathbf{k}}{w_k[w_k+E_p+E_{p-k}-E]}. \quad (62)$$

Here E is the energy eigenvalue (in this case the deuteron binding energy) and E_p and E_{p-k} are the nucleon kinetic energies for momenta $\mathbf{p}$ and $\mathbf{p}-\mathbf{k}$. The nonadiabatic terms in this potential, which appear through the explicit dependence on the nucleon momenta, can be separated if we write

$$V^{(2)}(p,k) = V_s^{(2)}(k) + \delta V(p,k), \quad (63)$$

where the static potential is

$$V_s^{(2)}(k) = -(g^2/2M)\boldsymbol{\tau}_1\cdot\boldsymbol{\tau}_2\boldsymbol{\sigma}_1\cdot\mathbf{k}\boldsymbol{\sigma}_2\cdot\mathbf{k}[1/w_k^2], \quad (64)$$

and the velocity dependent correction is

$$\delta V(p,k) = \frac{g^2}{4M^2}\boldsymbol{\tau}_1\cdot\boldsymbol{\tau}_2\left[\frac{\boldsymbol{\sigma}_1\cdot\mathbf{k}\boldsymbol{\sigma}_2\cdot\mathbf{k}}{w_k^2}\right]\frac{E_p+E_{p-k}-E}{w_k+E_p+E_{p-k}-E}. \quad (65)$$

To express this correction in terms of a static potential, using the method of Lévy, Klein[11] makes use of the nonrelativistic Schrödinger equation in momentum space:

$$\left(\frac{p^2}{M}-E\right)\phi(p) = \int[V_s^{(2)}(k)+\delta V(p,k)]\varphi(p-k)d^3k, \quad (66)$$

which determines the wave function $\varphi(p)$ correct to second order. If δV is treated as a perturbation, the relation

$$[E_p+E_{p-k}-E]\phi(p-k) \simeq \int V_s^{(2)}(k')\varphi(\mathbf{p}-\mathbf{k}-\mathbf{k}')d^3k' \quad (67)$$

can be used to eliminate the momentum dependence from δV. One then finds

$$\left[\frac{p^2}{M}-E\right]\phi(p) \simeq \int V_s^{(2)}(k)\phi^{(2)}(\mathbf{p}-\mathbf{k})d^3k - \int V_s^{(2)}(k')\left[\frac{1}{w_k}\right]V_s^{(2)}(k)\phi(\mathbf{p}-\mathbf{k}-\mathbf{k}')d^3kd^3k' \quad (68)$$

where the second term, arising from the velocity dependent δV, is now expressible as a static potential. Further investigation of this term shows that it gives rise to a very strong repulsive central force in the triplet even states, in fact changing the sign of the potential, and leads to rather unacceptable results for the deuteron ground state.

This method of approximating the nonadiabatic terms is, of course, valid only if they are in fact a small correction since only then is the above iterative procedure valid. The correction is, however, not small; its importance can be traced to the predominance of high-momentum components in the wave function $\phi(p)$ determined by Eq. (66). This is a consequence of the singularity of $V_s^{(2)}$ of Eq. (64) which in coordinate space has a singularity of $1/r^3$ with the result that $\phi(p)$ is a collapsed state with an infinite expectation value for the nucleon kinetic energies. An estimate of the velocity dependent corrections based on Eq. (66) is therefore probably erroneous.[17]

As an alternative procedure which does not make this possibly incorrect treatment of δV of Eq. (65), we have evaluated the velocity dependent terms making use of the entire static potential (second and fourth order and phenomenological repulsive core) to determine the wave function. This wave function is well behaved; the expectation value of the nucleon kinetic energies is quite low so that velocity dependent corrections should be small. The procedure we have followed therefore has been to neglect the velocity-dependent terms in v_2 and v_4, to evaluate the problem using the static potentials, and finally to determine the velocity-dependent corrections using the correct wave functions.

We have found empirically that an excellent fit to the tabulated wave function resulting from the numerical solution of the deuteron problem is (for the S-state

[17] A similar conclusion has been reached independently by Fukuda, Sawada, and Taketani (private communication).

alone)

$$\psi(r)=\frac{12}{7}[4\pi r_D]^{-1}[e^{-(r-r_0)/r_D}-e^{-3(r-r_0)/r_D}]\begin{pmatrix}1\\-\\r\end{pmatrix}$$

$$\text{for} \quad r>r_0$$

$$=0 \quad \text{for} \quad r<r_0, \tag{69}$$

where r_0 is the core radius and $r_D=h[ME]^{-\frac{1}{2}}$ is the deuteron radius. In evaluating the velocity dependent correction δV of Eq. (65), we have not considered the small D-state admixture. For the ground state of the deuteron, explicit evaluation then gives

$$\langle \delta V\rangle_{Av}\simeq -0.11 \text{ Mev}, \tag{70}$$

which is to be compared with a 20-Mev expectation value for the static potential. The velocity-dependent corrections therefore would modify the potential by less than 1 percent, and presumably have little effect on the solutions.

VII. CONCLUSIONS

We have seen that it is possible to derive a nucleon-nucleon potential, working entirely with a nonrelativistic approximation to the pseudoscalar meson theory, which gives a quantitative description of the low-energy properties of the two-nucleon system. The principal difficulties of the analysis concern the closely related questions of convergence of the potential expansions used (S matrix, non-covariant perturbation theory, or the method used in this paper) and the treatment of radiative corrections. We have depended rather strongly on the suppression of nucleon pair formation by radiative effects; the contributions to the potential from pair formation in high order calculated without taking into account such effects otherwise tend to be so large as to invalidate the power series expansions usually used.[11] Radiative effects associated with the low-momentum components of the meson coupling are, however, small so that they do not modify appreciably the potential (which arises from the low-momentum components) in the nonrelativistic region. In this region $[r>0.5h/\mu c]$ our investigations have also shown that the expansion in powers of the coupling constant converges fairly well in that multiple-scattering corrections which start as g^6 are not important corrections to the g^2+g^4 potential. We also have found that nonadiabatic effects are small, principally because the mean kinetic energies of the nucleons in the deuteron are low.

We have also concluded, however, that the potential expansion breaks down quite rapidly as r becomes less than $0.5h/\mu c$ as streng multiple scattering of the virtual mesons sets in, the precise value of r depending on the effect that radiative corrections, for example, have on the high-momentum components of the coupling. The treatment of this region is probably best left phenomenological; the uncertainties are most simply represented by the insertion of the adjustable core radius.

In most of these conclusions we are in qualitative agreement with the comments of Lévy[15] who also considered pseudoscalar theory, although the potential which he derived omitted several terms of importance at least equal to those which he retained. Our work is also closely related to that of Taketani *et al.*,[10] which differs principally in the treatment of the nonadiabatic corrections to the potential (which they found to be very important), but also in that they considered pseudovector coupling. Our conclusions are somewhat more optimistic than those of Klein[11] who also considered pseudoscalar coupling, principally because of the difference again of his treatment of the nonadiabatic terms and because of his estimate of the predominance of the contributions to the potential associated with nucleon-pair formation in high order. This estimate is very sensitive to the extent to which radiative corrections are taken into account; these were, however, not considered by Klein.

Finally, we would like to remark that it is at least possible to conclude that the nuclear potentials given by pseudoscalar meson theory, with the only freely adjustable parameter being the core radius (the coupling constant being fixed to within a small range by other experiments), give a remarkably adequate determination of the six parameters which characterize interactions of nucleons at low energy.

The authors are indebted to Drs. S. Drell, E. Henley, M. Ruderman, and A. Klein for very stimulating and useful discussions of this and related problems.

Nuclear Forces from *P*-Wave Mesons

E. M. HENLEY* AND M. A. RUDERMAN†
Columbia University, New York, New York
(Received August 7, 1953)

The nucleon-nucleon potential from meson exchange is related to a matrix describing the scattering of virtual and real mesons by nucleons. This meson-nucleon scattering matrix is calculated for p-wave mesons, using the model of Chew, which approximates experimental phase shifts for real mesons. The corrections to the g^3 and g^4 perturbation theory nuclear forces are evaluated. States involving the simultaneous existence of three or more mesons, none of which are absorbed by the same nucleon that emitted them, have been omitted in this treatment. Comparison of these and other results implies that this neglect is unjustified.

INTRODUCTION

An understanding of the nucleon-nucleon potential depends upon a correct description of the π-meson nucleon interaction. The analysis of recent meson-nucleon scattering experiments yields information on the behavior of free mesons and nucleons. The scattering of virtual mesons, which enters in an important way into nuclear force calculations, can be extrapolated from these experiments only for a specific model.

Perturbation theory fails to account for important features of the large p-wave real meson scattering. In particular the observed dominance of the scattering in the isotopic spin 3/2 state is absent. Chew[1] has suggested an approach which gives a scattering of free p-wave mesons in fair agreement with observation. In the spirit of this calculation we have investigated the nuclear force which results from the p-wave interaction of virtual mesons.

Section I is a demonstration of a relation between a nucleon-nucleon scattering matrix, which can be computed by the standard Feynman[2]-Dyson[3] prescriptions, and the nuclear force. In Sec. II we relate this nucleon-nucleon scattering matrix to the scattering of real and virtual mesons. Section III treats the scattering of real and virtual p-wave mesons by nucleons. Section IV gives the explicit results for the nuclear force calculation. The difference between these results and those of Watson and Brueckner[4] are discussed.

I. RELATION OF POTENTIAL TO NUCLEON-NUCLEON SCATTERING MATRIX

It is convenient to work with a scattering matrix for the two nucleon system which can, in principle, be calculated by the Feynman-Dyson techniques. In this section we derive a prescription for calculating the nuclear potential from this matrix.

We consider two free nucleons in the center-of-mass system, whose momentum energy vectors are $(\mathbf{p}_0, E_0)$ and $(-\mathbf{p}_0, E_0)$. The standard Feynman-Dyson rules give a power series expansion of the matrix element for the scattering of these nucleons into the states $(\mathbf{p}_1, E_0)$. Let this scattering matrix (whose leading term is proportional to g^2) be $\mathfrak{R}(\mathbf{p}_1, \mathbf{p}_0)$.

Since we shall be concerned only with nonrelativistic nucleons, we have $E_0 = M + p_0^2/2M$. The $\mathfrak{R}$ matrix is calculated for a scattering from $\mathbf{p}_0$ to any momentum $\mathbf{p}_1$, but the same fourth component $E_0 (p_1^2 \neq p_0^2)$.

Let $V(\mathbf{p}', \mathbf{p})$ be the solution of

$$V(\mathbf{p}', \mathbf{p}) = i\mathfrak{R}(\mathbf{p}', \mathbf{p}) - i\int d\mathbf{p}'' V(\mathbf{p}', \mathbf{p}'') \frac{M}{p''^2 - p^2 + i\delta} \mathfrak{R}(\mathbf{p}'', \mathbf{p}), \quad (6)$$

and $\phi(\mathbf{p}, E)$ a solution of

$$\left(\frac{p^2}{M} - E\right)\phi(\mathbf{p}, E) = \int d\mathbf{p}' V(\mathbf{p}, \mathbf{p}')\phi(\mathbf{p}', E). \quad (7)$$

A solution of (7) for $E = p_0^2/M$ is

$$\phi(\mathbf{p}) = \delta(\mathbf{p} - \mathbf{p}_0) + \frac{M}{p^2 - p_0^2 + i\delta} i\mathfrak{R}(\mathbf{p}, \mathbf{p}_0). \quad (8)$$

The spin indices have been suppressed for initial and final states, but introduce no complication. $\mathfrak{R}(\mathbf{p}, \mathbf{p}_0)$ has been constructed to give the correct amplitude for the scattering when $p^2 = p_0^2$. Therefore, for a given angular momentum state the solution (8) has the asymptotic form in coordinate space:

$$\psi(r \to \infty) \sim Y_{l,m}(\theta, \phi)(kr)^{-1}[\exp\{-i(kr - (l+1)\pi/2\} + S(k, l)\exp\{i(kr - (l+1)\pi/2\}]. \quad (9)$$

$S(k, l)$ is the Heisenberg S matrix[5] for the angular momentum l. [If the spin indices are included Eq. (9) holds for singlet states, and there is an analogous expression in terms of m, J, and $S(k, J)$ for triplet states.] If $S(k, l)$ can be analytically continued as a function of k to the negative imaginary axis, bound states correspond to zeros of S.[6] When $S = 0$,

$$\psi(r \to \infty) \sim (|k|r)^{-1} \exp(-|k|r). \quad (10)$$

---

* Frank B. Jewett Fellow.
† National Science Foundation Postdoctoral Fellow, on leave from the University of California, Berkeley, California.
[1] G. F. Chew, Phys. Rev. **89**, 591 (1953).
[2] R. P. Feynman, Phys. Rev. **76**, 749, 769 (1949).
[3] F. J. Dyson, Phys. Rev. **75**, 486, 1736 (1949).
[4] K. A. Brueckner and K. M. Watson, preceding paper [Phys. Rev. **92**, 1023 (1953)].
[5] W. Heisenberg, Z. Physik **120**, 513, 673 (1943); C. Møller, Kgl. Danske Videnskab. Selskab, Mat.-fys. Medd. **23**, No. 1 (1945).
[6] C. Møller, Kgl. Danske Videnskab. Selskab, Mat.-fys. Medd. **22**, No. 19 (1946).

Therefore, where a zero of $S(-ik', l)$, $k'>0$, corresponds to a bound state, solutions of Eq. (7), which are asymptotic to $r^{-1}\exp[-r(M|E|)^{\frac{1}{2}}]$, give the energy levels of the bound system.[7] The Schrödinger Eq. (7) then gives a correct description of scattering and bound states when $V(\mathbf{p}, \mathbf{p}')$ is a sufficiently short range potential. In the following the nucleon-nucleon potential is, therefore, taken to be $V(\mathbf{p}, \mathbf{p}')$ as defined by Eq. (6).

The Feynman-Dyson prescription gives $\mathfrak{R}(\mathbf{p}_1, \mathbf{p}_0)$ as a power series in g^2, where g is the meson-nucleon coupling parameter. In practice this series is approximated by including only a finite number of terms. If $\mathfrak{R}$ includes terms up to g^{2m} only, it is not sensible to solve for V in Eq. (6) to a higher power than $2m$.

II. NUCLEON-NUCLEON AND MESON-NUCLEON SCATTERING

The range of the nucleon-nucleon interaction depends upon the number of mesons exchanged between nucleons. We shall consider only those terms in the $\mathfrak{R}$ matrix where at most two mesons are exchanged although a meson may be scattered an arbitrary number of times by each nucleon. In general, these scatterings have only a slight effect upon the range of forces. The correction to the nuclear potential from these multiple scatterings can be expressed in terms of the matrix element for meson-nucleon scattering:

$$r(\boldsymbol{\sigma}_a; E_1, \mathbf{p}_1; E_0, \mathbf{p}_0; w_1, \mathbf{k}_1; w_0, \mathbf{k}_0), \tag{11}$$

see Fig. 1(a), where $(\mathbf{k}_0, w_0)$ and $(\mathbf{k}_1, w_1)$ are the 4-momenta of the incident and scattered meson, respectively. $(E_0, \mathbf{p}_0)$ and $(E_1, \mathbf{p}_1)$ are the 4-momenta of the incident and scattered nucleon, and $\boldsymbol{\sigma}_a$ is the Pauli spin operator which acts on the incident nucleon spin wave function. Four-momentum conservation gives

$$\begin{aligned} &E_1=E_0+w_0-w_1 \\ \text{and} \qquad &\\ &\mathbf{p}_1=\mathbf{p}_0+\mathbf{k}_0-\mathbf{k}_1, \end{aligned} \tag{12}$$

but none of the 4-momenta are assumed to be those of free particles.

In terms of Eq. (11) the $\mathfrak{R}^{(2)}$ matrix for the exchange of two mesons [see Fig. 1(b), (c)] is

$$\begin{aligned} \mathfrak{R}^{(2)}(\mathbf{p}_1, \mathbf{p}_0)=-\frac{1}{2}\left(\frac{1}{2\pi}\right)^4\int r(\boldsymbol{\sigma}_a; E_0, \mathbf{p}_1; E_0, \mathbf{p}_0; \\ w, \mathbf{k}; w, \mathbf{p}_1-\mathbf{p}_0+\mathbf{k})\{r(\boldsymbol{\sigma}_b; E_0, -\mathbf{p}_1; E_0, -\mathbf{p}_0; \\ -w, -\mathbf{k}; -w, -\mathbf{p}_1+\mathbf{p}_0-\mathbf{k})+r(\boldsymbol{\sigma}_b; E_0, -\mathbf{p}_1; \\ E_0, -\mathbf{p}_0; w, \mathbf{p}_1-\mathbf{p}_0+\mathbf{k}; w, \mathbf{k})\}(w^2-k^2-\mu^2+i\delta)^{-1} \\ \times[w^2-(\mathbf{p}_1-\mathbf{p}_0+\mathbf{k})^2-\mu^2+i\delta]^{-1}d\mathbf{k}dw. \end{aligned} \tag{13}$$

$\mathfrak{R}^{(1)}(\mathbf{p}_1, \mathbf{p}_0)$, the nucleon scattering amplitude when only one mesons is exchanged between different nucleons, can also be expressed in terms of Eq. (11). However, it is necessary to give an explicit form to the coupling between meson and nucleon fields. If, for example, this is taken to be $(g/\mu)\int\psi^*\boldsymbol{\sigma}\cdot\boldsymbol{\nabla}\sum_{i=1}^{3}\Phi_i\tau_i\psi d\mathbf{r}$ for symmetrical pseudoscalar mesons, then

$$\begin{aligned} \mathfrak{R}^{(1)}(\mathbf{p}_1, \mathbf{p}_0)=-i\Big[&(g/\mu)\boldsymbol{\sigma}_a\cdot\mathbf{k}_0\boldsymbol{\tau}_a\cdot\boldsymbol{\phi}_0 \\ &-(g/\mu)(2\pi)^{-4}\int dw'd\mathbf{k}'\boldsymbol{\sigma}_a\cdot\mathbf{k}'\boldsymbol{\tau}_a\cdot\boldsymbol{\phi}' \\ &\times r(\boldsymbol{\sigma}_a; \boldsymbol{\tau}_a; E_0, \mathbf{p}_1; E_0, \mathbf{p}_0; w', \mathbf{k}', \boldsymbol{\phi}'; 0, \mathbf{k}_0, \boldsymbol{\phi}_0) \\ &\times(w'^2-k'^2-\mu^2+i\delta)^{-1}(p_0{}^\nu\gamma^\nu+k_0{}^\nu\gamma^\nu-k'^\nu\gamma^\nu-M)^{-1}\Big] \\ &\times[\text{as above, with } a\rightarrow b,\ \mathbf{k}_0\rightarrow-\mathbf{k}_0,\ \mathbf{p}_0\rightarrow-\mathbf{p}_0,\ \mathbf{p}_1\rightarrow-\mathbf{p}_1] \\ &\times(k_0^2+\mu^2)^{-1}, \end{aligned} \tag{14}$$

where $\mathbf{k}_0=\mathbf{p}_1-\mathbf{p}_0$, and $\boldsymbol{\phi}$ is a unit vector in charge space, specifying the charge of the meson.

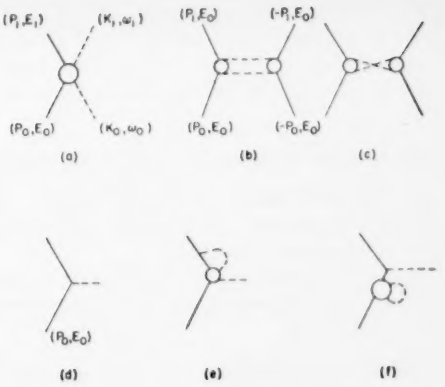

FIG. 1. (a) Representation of meson-nucleon scattering matrix; (b) and (c) contributions to the nucleon-nucleon scattering matrix in terms of (a); (d) lowest-order meson nucleon interaction; (e) and (f) all corrections to (d) expressed in terms of (a).

The simple meson-nucleon interaction Fig. 1(d) is corrected in Eq. (14) by terms represented by Fig. 1(e). Contributions from Fig. 1(f) have been omitted since they are the interactions of a free nucleon ($E_0=M+p_0^2/2M$) with its own meson field, which should be cancelled by a proper renormalization program for the free nucleon properties. Similar terms from Fig. 1(e), which are included in Eq. (14), will also be cancelled. (Appendix II.)

From Eq. (6), the potential is given in terms of Eq. (13) and Eq. (14) as

$$\begin{aligned} &V\approx V^{(1)}+V^{(2)}, \\ &V^{(1)}=i\mathfrak{R}^{(1)}(\mathbf{p}_1, \mathbf{p}_0), \\ &V^{(2)}=i\mathfrak{R}^{(2)}(\mathbf{p}_1, \mathbf{p}_0) \\ &\qquad+\int d\mathbf{p}\mathfrak{R}^{(1)}(\mathbf{p}_1, \mathbf{p})\frac{M}{p^2-p_0^2+i\delta}\mathfrak{R}^{(1)}(\mathbf{p}, \mathbf{p}_0). \end{aligned} \tag{15}$$

In general, for infinitely heavy nucleons, $V^{(2)}$ is real

[7] R. Jost and W. Kohn, Phys. Rev. 87, 977 (1952).

and finite although $\mathcal{R}^{(2)}$ is infinite, even for a renormalized meson theory. $V^{(1)}$ and $V^{(2)}$ are series containing all powers of g^2, but correspond, respectively, to the exchange of only one and two mesons between two nucleons.

III. SCATTERING OF REAL AND VIRTUAL MESONS

In this section we derive an approximation to the r matrix for the scattering of real and virtual mesons in the limit of infinite nucleon mass.

In perturbation theory, the r matrix for the scattering of p-state mesons symmetrically coupled to nonrelativistic nucleons is

$$r=-i\frac{g^2}{\mu^2}\frac{\boldsymbol{\sigma}\cdot\mathbf{k}_1\boldsymbol{\sigma}\cdot\mathbf{k}_0\boldsymbol{\tau}\cdot\boldsymbol{\phi}_1\boldsymbol{\tau}\cdot\boldsymbol{\phi}_0}{w_0}+i\frac{g^2}{\mu^2}\frac{\boldsymbol{\sigma}\cdot\mathbf{k}_0\boldsymbol{\sigma}\cdot\mathbf{k}_1\boldsymbol{\tau}\cdot\boldsymbol{\phi}_0\boldsymbol{\tau}\cdot\boldsymbol{\phi}_1}{w_1}, \quad (16)$$

where $\boldsymbol{\phi}_0$ and $\boldsymbol{\phi}_1$ are unit vectors in charge space specifying the charge of the incident and scattered meson. Equation (16) is valid for virtual mesons, where $w_1^2\neq k_1^2+\mu^2$ and $w_0^2\neq k_0^2+\mu^2$. Important higher-order effects can be computed by treating Eq. (16) as the Born approximation scattering from a meson-nucleon potential. The higher-order terms which are then included involve intermediate states which may have energies close to that of the incident meson and so can give large contributions. The sum r of all order scatterings from this potential satisfies the integral equation:

$$\begin{aligned}r(\boldsymbol{\sigma};\boldsymbol{\tau};\boldsymbol{\phi}_1,w_1,\mathbf{k}_1;\boldsymbol{\phi}_0,w_0,\mathbf{k}_0)&=-i\frac{g^2}{\mu^2}\frac{\boldsymbol{\sigma}\cdot\mathbf{k}_1\boldsymbol{\sigma}\cdot\mathbf{k}_0\boldsymbol{\tau}\cdot\boldsymbol{\phi}_1\boldsymbol{\tau}\cdot\boldsymbol{\phi}_0}{w_0}+i\frac{g^2}{\mu^2}\frac{\boldsymbol{\sigma}\cdot\mathbf{k}_0\boldsymbol{\sigma}\cdot\mathbf{k}_1\boldsymbol{\tau}\cdot\boldsymbol{\phi}_0\boldsymbol{\tau}\cdot\boldsymbol{\phi}_1}{w_1}\\&+\frac{g^2}{\mu^2}\left(\frac{1}{2\pi}\right)^3\int d\mathbf{k}\frac{\boldsymbol{\sigma}\cdot\mathbf{k}_1\boldsymbol{\sigma}\cdot\mathbf{k}\,\boldsymbol{\tau}\cdot\boldsymbol{\phi}_1\boldsymbol{\tau}\cdot\boldsymbol{\phi}}{2\omega w_0(w_0-\omega+i\delta)}\\&\times r(\boldsymbol{\sigma};\boldsymbol{\tau};\boldsymbol{\phi},\omega,\mathbf{k};\boldsymbol{\phi}_0,w_0,\mathbf{k}_0)+\frac{g^2}{\mu^2}\left(\frac{1}{2\pi}\right)^3\int d\mathbf{k}\\&+\frac{\boldsymbol{\sigma}\cdot\mathbf{k}\boldsymbol{\sigma}\cdot\mathbf{k}_1\boldsymbol{\tau}\cdot\boldsymbol{\phi}\boldsymbol{\tau}\cdot\boldsymbol{\phi}_1}{2\omega(w_0-\omega-w_1+i\delta)(w_0-\omega+i\delta)}\\&\times r(\boldsymbol{\sigma};\boldsymbol{\tau};\boldsymbol{\phi},\omega,\mathbf{k};\boldsymbol{\phi}_0,w_0,\mathbf{k}_0). \quad (17)\end{aligned}$$

Since the nucleon is fixed in space, the dependence of r on $\mathbf{p}$ and E is suppressed. The dependence of r on the charge of the mesons and nucleon, omitted from Eq. (11), is included in Eq. (16). w_1 and w_0 are fixed parameters unrelated to k_0 and k_1, but $\omega^2=k^2+\mu^2$.

The r matrix defined by Eq. (17) is the sum of the scattering represented by Feynman diagrams (a) and (b) of Fig. 2, and by arbitrary combinations of iterations of (a) and (b) such as (c), (d) and (e) of Fig. 2. Before a solution is attempted for all angular momentum and isotopic spin states certain mass and charge renormalizations will be performed, which alter parts of

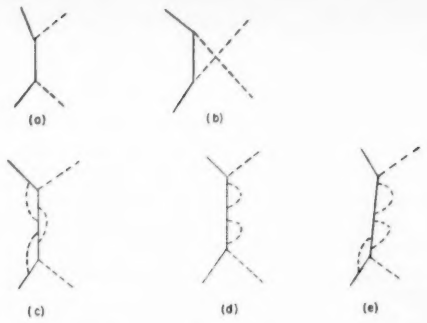

FIG. 2. (a), (b) Feynman diagrams for meson-nucleon scattering in lowest order perturbation theory; (c), (d), (e) higher order terms included in Eq. (17).

Eq. (17). For this purpose it is convenient to separate the matrix Eq. (17) into four integral equations for the scattering amplitudes $r_J{}^I$, with $J=1/2$, $3/2$ and $I=1/2$, $3/2$ giving, respectively, the total angular momentum and isotopic spin for the meson-nucleon system. Then

$$\begin{aligned}r=&(A\boldsymbol{\sigma}\cdot\mathbf{k}_1\boldsymbol{\sigma}\cdot\mathbf{k}_0+B\boldsymbol{\sigma}\cdot\mathbf{k}_0\boldsymbol{\sigma}\cdot\mathbf{k}_1)(\boldsymbol{\tau}_1\cdot\boldsymbol{\phi}_1\boldsymbol{\tau}_0\cdot\boldsymbol{\phi}_0)\\&+(C\boldsymbol{\sigma}\cdot\mathbf{k}_1\boldsymbol{\sigma}\cdot\mathbf{k}_0+D\boldsymbol{\sigma}\cdot\mathbf{k}_0\boldsymbol{\sigma}\cdot\mathbf{k}_1)(\boldsymbol{\tau}_0\cdot\boldsymbol{\phi}_0\boldsymbol{\tau}_1\cdot\boldsymbol{\phi}_1), \quad (18)\end{aligned}$$

where

$$\begin{aligned}A&=r_3{}^3/12+r_3{}^1/6+r_1{}^3/6+r_1{}^1/3,\\B&=r_3{}^3/4+r_1{}^3/2,\\C&=r_3{}^3/4+r_3{}^1/2,\\D&=3r_3{}^3/4.\end{aligned} \quad (19)$$

From Eqs. (17), (18) and (19)

$$\begin{aligned}r_3{}^3(w_1,w_0)=&i\frac{4g^2}{3w_1\mu^2}+\frac{4}{3}\frac{g^2}{\mu^2}\left(\frac{1}{2\pi}\right)^3\\&\times\int\frac{k^2d\mathbf{k}}{2\omega(w_0-\omega-w_1+i\delta)(w_0-\omega+i\delta)}r_3{}^3(\omega,w_0), \quad (20)\end{aligned}$$

$$\begin{aligned}r_1{}^3(w_1,w_0)=r_3{}^1(w_1,w_0)=&-i\frac{2}{3}\frac{g^2}{w_1\mu^2}\\&-\frac{2}{3}\frac{g^2}{\mu^2}\left(\frac{1}{2\pi}\right)^3\int\frac{k^2d\mathbf{k}r_3{}^1(\omega,w_0)}{2\omega(w_0-\omega-w_1+i\delta)(w_0-\omega+i\delta)}, \quad (21)\end{aligned}$$

$$\begin{aligned}r_1{}^1(w_1,w_0)=&-i\frac{3g^2}{w_0\mu^2}+3\frac{g^2}{\mu^2}\left(\frac{1}{2\pi}\right)^3\\&\times\int\frac{k^2d\mathbf{k}}{2\omega(w_0-\omega+i\delta)w_0}r_1{}^1(\omega,w_0)+i\frac{g^2}{3w_1\mu^2}\\&+\frac{1}{3}\frac{g^2}{\mu^2}\left(\frac{1}{2\pi}\right)^3\int\frac{k^2d\mathbf{k}}{2\omega(w_0-\omega+i\delta)(w_0-\omega-w_1+i\delta)}\\&\times r_1{}^1(\omega,w_0). \quad (22)\end{aligned}$$

The potential obtained from Eq. (16) is sufficiently singular that Eqs. (20)–(22) have no sensible solution.

If, however, Eq. (16) is assumed to vanish for $k>k_{\max}$, then solutions do exist.[8]

The quantities r_3^3, r_3^1, and r_1^3 contain contributions from Feynman diagrams of type (b) and (c) Fig. 1 only. On the other hand, r_1^1 arises from a variety of different kinds of Feynman diagrams [*viz*, Fig. 2 (a), (d), (e)], parts of which involve nucleon mass and charge renormalization.

To apply the renormalization prescriptions to r_1^1, Eq. (22) it is convenient to neglect the two terms with coefficient $\frac{1}{3}$ next to those with 3 and later to introduce them as a perturbation. The solution of the resulting integral equation represents the sum of diagrams of the type (a) and (d) of Fig. 2. [After renormalization this sum corresponds to the replacement of S_F by S_F' in Fig. 2(a).]

The self-energy of a free nucleon of infinite mass, Fig. 3(a), is

$$3\frac{g^2}{\mu^2}\left(\frac{1}{2\pi}\right)^3\int\frac{k^2d\mathbf{k}}{2\omega^2}. \tag{23}$$

Therefore, the nucleon mass M, in terms of the observed mass $M_{\exp}$, is given by

$$M=M_{\exp}-\frac{3g^2}{\mu^2}\left(\frac{1}{2\pi}\right)^3\int\frac{k^2d\mathbf{k}}{2\omega^2}. \tag{24}$$

If the Hamiltonian for the meson-nucleon system is written in terms of $M_{\exp}\to\infty$, then we also have a contribution represented by Fig. 3(d) from $M-M_{\exp}$. The matrix element represented by Fig. 3(c), when the incident nucleon is free, is

$$-3\frac{g^3}{\mu^3}\left(\frac{1}{2\pi}\right)^3\int\frac{k^2d\mathbf{k}}{2\omega(\omega-w_0-i\delta)}\frac{1}{w_0}\boldsymbol{\sigma}\cdot\mathbf{k}_0. \tag{25}$$

The sum of Figs. 3(b), (c), (d) thus gives

$$\frac{g}{\mu}\left[1-3\frac{g^2}{\mu^2}\left(\frac{1}{2\pi}\right)^3\int\frac{k^2d\mathbf{k}}{2\omega^3}-\frac{9}{2}\Delta'(w_0)\right]\boldsymbol{\sigma}\cdot\mathbf{k}_0, \tag{26}$$

with

$$\Delta'(w_0)=\frac{2}{3\pi}\frac{g^2}{4\pi}\frac{w_0}{\mu^2}\frac{1}{4\pi}\int_0^{k_{\max}}\frac{k^2d\mathbf{k}}{\omega^3(\omega-w_0-i\delta)}. \tag{27}$$

A further correction occurs when the self-energy part, Fig. 3(a), occurs for a free nucleon before the interaction $\boldsymbol{\sigma}\cdot\mathbf{k}_0$. When both nucleon legs are free ($w_0=0$), the total contribution of the self-energy part is included by putting $g\boldsymbol{\sigma}\cdot\mathbf{k}_0\to g_p\boldsymbol{\sigma}\cdot\mathbf{k}_0$ with

$$g_p=g\left(1-6\frac{g^2}{\mu^2}\left(\frac{1}{2\pi}\right)^3\int\frac{k^2d\mathbf{k}}{2\omega^3}\right). \tag{28}$$

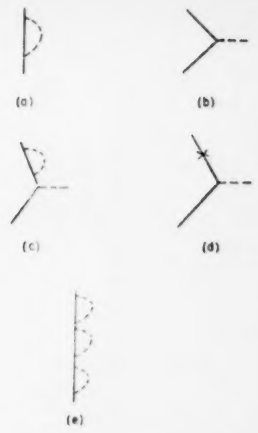

FIG. 3. Feynman diagrams relevant to the discussion of mass and charge renormalization.

Hence, if the experimental mass, $M_{\exp}$, and coupling constant, g_p, are used in the Hamiltonian, then the contribution of the self-energy part vanishes on free nucleon legs. Furthermore, for virtual nucleon propagation we obtain a correction from successive self-energy parts [Fig. 3(e)], which is given by the factor:

$$\sum_{n=0}^{\infty}\left[-\frac{9}{2}\Delta'(w_0)\right]^n=\left[1+\frac{9}{2}\Delta'(w_0)\right]^{-1}. \tag{29}$$

Insertion into Fig. 2(a) gives

$$-\frac{3ig_p^2}{w_0\mu^2}\frac{1}{1+(9/2)\Delta'(w_0)}. \tag{30}$$

Adding the two omitted terms of (22), we have

$$r_1^1\approx i\frac{g^2}{\mu^2}\left[-\frac{8[1-(9/4)\Delta'(w_0)]}{3w_0[1+(9/2)\Delta'(w_0)]}-\frac{g^2}{\mu^2w_0(2\pi)^3}\times\int\frac{k^2d\mathbf{k}}{2\omega(w_0-\omega)(w_0-\omega+w_1)[1+(9/2)\Delta'(w_0)]}+\frac{w_0-w_1}{3w_0w_1}\right]. \tag{31}$$

For a consistent treatment of the renormalization of the $r_J{}^I$ matrix it is also necessary to replace g by g_p and S_F by S_F' in Figs. 2(b) and 2(c). Otherwise self-energy corrections would arise even from the free nucleon legs.

After this substitution for g and S_f has been made $r_J{}^I$ can be written in terms of the two parameters g_p and $k_{\max}$ only. Insertion of the correction Eq. (29) into Eq. (20) for $r_3{}^3$ gives

$$r_3{}^3(w_1,w_0)=\frac{4ig_p{}^2}{3w_1\mu^2}\left[1+\frac{9}{2}\Delta'(-w_1)\right]^{-1}+\frac{4}{3}\frac{g_p{}^2}{\mu^2}\left(\frac{1}{2\pi}\right)^3\int\frac{k^2d\mathbf{k}[1+(9/2)\Delta'(w_0-\omega)]^{-1}[1+(9/2)\Delta'(w_0-\omega-w_1)]^{-1}}{2\omega(w_0-\omega-w_1+i\delta)(w_0-\omega+i\delta)}r_3{}^3(\omega,w_0); \tag{32}$$

[8] This is equivalent to the source considered by Chew (see reference 1).

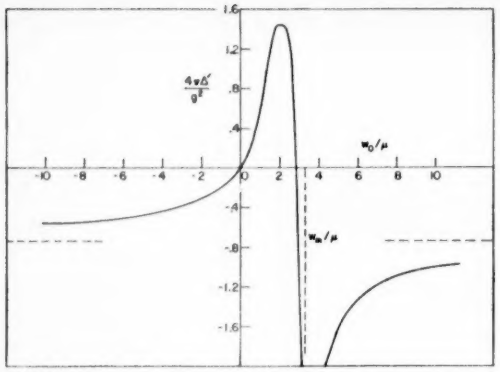

FIG. 4. Real part of $\Delta'(w_0)$ for $\omega_{\max}=3.2\mu$.

then, (appendix I)

$$r_3^3(w_1, w_0) \approx \frac{4ig_p^2}{3w_1\mu^2}\frac{[1-2\Delta'(w_0-w_1)]}{[1-2\Delta'(w_0)][1+(9/2)\Delta'(-w_0)]}. \quad (33)$$

Similarly

$$r_1^3(w_1, w_0) = r_3^1(w_1, w_0) \approx -\frac{2ig_p^2}{3w_1\mu^2}\frac{[1-\Delta'(w_1-w_0)]}{[1+\Delta'(w_0)][1+(9/2)\Delta'(-w_0)]}. \quad (34)$$

For the scattering of real p-wave mesons $w_1=w_0=(k_0^2+\mu^2)^{\frac{1}{2}}$ and $\Delta'(w_1-w_0)=0$. Equations (32) and (33) are then almost the same as those of Chew[1] for $\mu\leq w_0<w_{\max}$. However the factor $[1+(9/2)\Delta'(-w_0)]^{-1}$ was not included by him in obtaining a best fit to the experimental data, which occurred for

$$g_p^2/4\pi\approx 0.2 \quad \text{and} \quad w_{\max}\approx 3.2\mu. \quad (35)$$

(The neglected factor will increase r_3^3, r_1^3, and r_3^1 by about 25 percent for free meson scattering and thus necessitates a small change in $g_p^2/4\pi$ and $w_{\max}$.)

The function $\Delta'(w_0)$ is a measure of the departure of the matrix $r_J{}^I$ from that given in perturbation theory. The real part of $\Delta'(w_0)$, Eq. (27), is given by

$$\mathrm{Re}\Delta'(w_0)=\frac{g^2}{4\pi}\frac{2}{3\pi}\frac{1}{\mu^2}\left\{w_0^2\ln\left(\frac{k_{\max}+\omega_{\max}}{\mu}\right)+w_0k_{\max}-\frac{k_{\max}\mu^2}{\omega_{\max}}-\frac{\mu^3}{w_0}\cos^{-1}\frac{\mu}{\omega_{\max}}-R\right\}, \quad (36)$$

$$R=\frac{(w_0^2-\mu^2)^{\frac{1}{2}}}{w_0}\ln\left|\frac{(w_0^2-\mu^2)^{\frac{1}{2}}k_{\max}+w_0\omega_{\max}-\mu^2}{\mu(\omega_{\max}-w_0)}\right| \quad \text{for} \quad w_0^2\geq\mu^2,$$

$$R=\frac{(\mu^2-w_0^2)^{\frac{1}{2}}}{w_0}\cos^{-1}\left[\frac{\mu^2-w_0\omega_{\max}}{\mu(\omega_{\max}-w_0)}\right] \quad \text{for} \quad w_0^2\leq\mu^2,$$

and is plotted in Fig. 4. Asymptotically, for $|w_0|\to\infty$

$$\mathrm{Re}\Delta'(w_0)=-\frac{g^2}{4\pi}\frac{2}{3\pi}\frac{w_0}{\mu^2}\int_\mu^{\omega_{\max}}\frac{k^3d\omega}{\omega^2w_0}=-\frac{g^2}{4\pi}\frac{2}{3\pi}\frac{1}{\mu^2}\left\{k_{\max}\left(\frac{\omega_{\max}}{2}+\frac{\mu^2}{\omega_{\max}}\right)-\tfrac{3}{2}\mu^2\ln\left(\frac{\omega_{\max}+k_{\max}}{\mu}\right)\right\}. \quad (37)$$

For $-w_{\max}\leq w_0\leq\mu$, $(g_p^2/4\pi)\Delta'(w_0)$ is small and $r_J{}^I$ is close to the perturbation result.

IV. THE NUCLEAR FORCE

The potentials, $V^{(1)}$ and $V^{(2)}$ can be found by substitution of Eqs. (31), (33), and (34) into Eqs. (18) and (19) to yield r. From Eqs. (13) and (14), $\mathfrak{R}^{(1)}$ and $\mathfrak{R}^{(2)}$ can then be found, and Eq. (15) gives $V^{(1)}+V^{(2)}$. These calculations are performed in Appendix (II). The potential is approximately (see reference 14)

$$V=V^{(1)}+V^{(2)},$$

$$V^{(1)}\approx-\frac{g^2}{4\pi}\boldsymbol{\tau}_a\cdot\boldsymbol{\tau}_b\boldsymbol{\sigma}_a\cdot\boldsymbol{\nabla}\boldsymbol{\sigma}_b\cdot\boldsymbol{\nabla}\frac{e^{-\mu x}}{\mu^2 x}[1+0.07], \quad (38)$$

$$V^{(2)}\approx\left(\frac{g^2}{4\pi}\right)^2\mathrm{Lim}_{x_0\to x_1}\sum_{i,j=1}^{3}[\boldsymbol{\sigma}_a\cdot\boldsymbol{\nabla}_1\tau_a{}^i,\boldsymbol{\sigma}_a\cdot\boldsymbol{\nabla}_0\tau_a{}^j]\times[\boldsymbol{\sigma}_b\cdot\boldsymbol{\nabla}_1\tau_b{}^i,\boldsymbol{\sigma}_b\cdot\boldsymbol{\nabla}_0\tau_b{}^j]\frac{(x_0+x_1)K_0(\mu x_0+\mu x_1)}{2\pi x_0x_1\mu^4}$$

$$+\left(\frac{g^2}{4\pi}\right)^2\mathrm{Lim}_{x_0\to x_1}0.18\{\boldsymbol{\sigma}_a\cdot\boldsymbol{\nabla}_1,\boldsymbol{\sigma}_a\cdot\boldsymbol{\nabla}_0\}\{\boldsymbol{\sigma}_b\cdot\boldsymbol{\nabla}_1,\boldsymbol{\sigma}_b\cdot\boldsymbol{\Delta}_0\}\times\frac{e^{-\mu(x_0+x_1)}}{\mu^5x_0x_1}=\left(\frac{g^2}{4\pi}\right)^2\mu\frac{8}{\pi}\left\{\boldsymbol{\sigma}_a\cdot\boldsymbol{\sigma}_b\left[\frac{3}{\mu^3x^3}K_0(2\mu x)+\left(\frac{2}{\mu^2x^2}+\frac{3}{\mu^4x^4}\right)K_1(2\mu x)\right]-\boldsymbol{\tau}_a\cdot\boldsymbol{\tau}_b\left[\left(\frac{1}{\mu x}+\frac{23}{4\mu^3x^3}\right)\times K_0(2\mu x)+\left(\frac{3}{\mu^2x^2}+\frac{23}{4\mu^4x^4}\right)K_1(2\mu x)\right]-\left[\frac{3\boldsymbol{\sigma}_a\cdot\mathbf{x}\boldsymbol{\sigma}_b\cdot\mathbf{x}}{x^2}-\boldsymbol{\sigma}_a\cdot\boldsymbol{\sigma}_b\right]\left[\frac{3}{\mu^3x^3}K_0(2\mu x)+\left(\frac{1}{\mu^2x^2}+\frac{15}{4\mu^4x^4}\right)K_1(2\mu x)\right]\right\}+\left(\frac{g^2}{4\pi}\right)^2\mu 0.7\left\{\frac{1}{2\mu^2x^2}+\frac{4}{\mu^3x^3}+\frac{12}{\mu^4x^4}+\frac{12}{\mu^5x^5}+\frac{6}{\mu^6x^6}\right\}e^{-2\mu x}. \quad (39)$$

In Eq. (39), the subscripts 1 or 0 on the ∇-operator means that the differentiation is to be carried out only with respect to x_1 or x_0, respectively; $[\ ,\ ]$ is the commutator bracket, and $\{\ ,\ \}$ is the anticommutator bracket. These potentials are plotted in Fig. 5 for deuterium.

The first terms on the right-hand side of Eqs. (38) and (39) are the usual second- and fourth-order perturbation theory potentials. The correction to $V^{(1)}$ has the same shape and spin dependence as the perturbation result with approximately 7 percent of its magnitude. The dominant correction to $V^{(2)}$ is independent of spin and isotopic spin. It gives a short-range repulsion, about 20 percent of the perturbation theory central force in the ^3S state. The large departure from perturbation theory which is found for the scattering of real mesons is not reflected in the nuclear force because of the very different behavior of real and virtual mesons with the same momentum.[9]

The first term in Eq. (39) has also been obtained by Taketani, Machida, and Onuma,[10] Klein,[11] Feynman and Lopes,[12] and others, but differs in an important way from that of Brueckner and Watson,[4] who have analyzed this difference in detail. Its origin lies in the treatment of states with at most one meson at any time. The $\mathfrak{R}$ matrix, Eq. (13), has been calculated for the exchange of two meson with any time ordering. That part of it which is relevant to this discussion is represented in Fig. (6a), when $\min(t_1, t_2) > \max(t_3, t_4)$. Substitution of this $\mathfrak{R}$ into Eq. (6) gives a contribution to the potential of

$$\left(\frac{g^2}{4\pi}\right)^2 \frac{1}{4\pi^4}(3-2\boldsymbol{\tau}_a\cdot\boldsymbol{\tau}_b)\int d\mathbf{k}d\mathbf{k}' \times \frac{\boldsymbol{\sigma}_a\cdot\mathbf{k}\boldsymbol{\sigma}_a\cdot\mathbf{k}'\boldsymbol{\sigma}_b\cdot\mathbf{k}\boldsymbol{\sigma}_b\cdot\mathbf{k}' e^{i(\mathbf{k}+\mathbf{k}')\cdot\mathbf{x}}}{\omega^3\omega'^2\mu^4}. \quad (40)$$

This term is the difference between the potential $V^{(2)}$, Eq. (39), and that obtained by Brueckner and Watson. It is included in Eq. (39) and is big enough to change the ^3S attraction of Brueckner and Watson to a repulsion. [Addition of a repulsive core nullifies the effect of the very strong singular part of (40) at small x.] Brueckner and Watson point out that, in the Tamm-Dancoff formalism, this is one of a series of terms that comes from an expansion of the "velocity dependent" part of the one meson interaction. When the entire series of terms are included (no expansion), the contribution is much smaller than (40), and, indeed, quite negligible.[4] In this sense, the potential without (40) may be expected to be a better approximation than that including it. On the other hand, for neutral scalar mesons with fixed sources[13] a similar argument can be presented, but the required cancellation of the g^4 potential comes only when the term corresponding to Fig. (6a) is included.

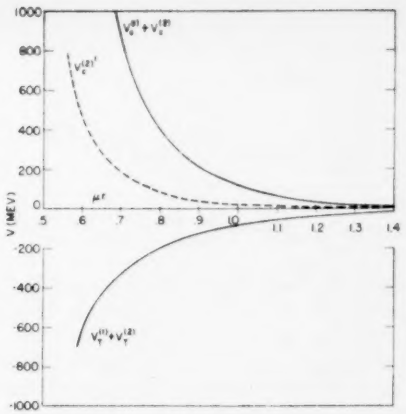

FIG. 5. $V^{(1)}+V^{(2)}$ for the deuteron $V_c^{(2)\prime}$ is the correction to the perturbation theory result. The central forces V_c are repulsive. V_t are the tensor forces.

The neutral scalar theory contains certain features similar to the case of interest, and we shall examine it following the method suggested by Brueckner and Watson. The Schrödinger equation, including the static approximation to those parts of the potential arising from two meson states, but treating the one meson contribution without approximation is

$$\left(\frac{p^2}{M}-\epsilon\right)\phi(\mathbf{p}) = \int \bar{V}(\mathbf{k})\phi(\mathbf{p}-\mathbf{k})d\mathbf{k} + \frac{g^2}{4\pi}\int \frac{T_p+T_{p-k}-\epsilon}{\omega^2(\omega+T_p+T_{p-k}-\epsilon)}\phi(\mathbf{p}-\mathbf{k})d\mathbf{k}, \quad (41)$$

where $T_p = p^2/2M$, and $\bar{V}(\mathbf{k})$ is the Fourier transform of

$$-\frac{g^2}{4\pi x}e^{-\mu x}\left[1+\frac{g^2}{4\pi}\frac{2K_0(2\mu x)}{\pi}\right] - \text{repulsive core}. \quad (42)$$

In this case, the correct potential is obtained by omitting the second term in (42). For sufficiently small repulsive core, or for large g^2, the second term of (42) contributes the major part of the attractive potential [as is the case with the g^4 potential, Eq. (39), with the parameters (35)]. If the second term on the right-hand side of Eq. (41) is expanded in powers of $(T_p+T_{p-k}-\epsilon)$, then the leading term of this expansion exactly cancels the second term of (42). Since the leading term is large, the expansion is, of course, suspect. On the other hand,

[9] The perturbation result for $V^{(2)}$ was valid because the important values of w_0 do not lie between μ and $w_{\max}$ where $\Delta'(w_0)$ contributed significantly. However, the production of a real meson in a nucleon-nucleon collision can be altered in an important way. The simplest Feynman diagram for this process is the production of the meson by one nucleon and the scattering of this meson (with energy as well as momentum transfer) by the other. This scattering can be expressed in terms of Eqs. (31), (33) and (34). The w_0 is that of the final free meson in the c.m. system of the meson and the nucleon from which it scattered. Since $w_{\max} > w_0 > \mu$, the correction from $\Delta'(w_0)$ are not negligible. Scattering is increased in the $I=J=\frac{3}{2}$ state, otherwise decreased. Therefore π^+ production from p-p collisions will be increased relative to π^- production from p-n collisions as observed.

[10] Taketani, Machida, and Onuma, Progr. Theor. Phys. **7**, 45 (1952).

[11] A. Klein, Phys. Rev. **90**, 1101 (1953).

[12] J. L. Lopes and R. P. Feynman, Notas de Fisica, No. 2 Centro Brasileiro de Pesquisas Fisicas Rio de Janeiro (unpublished).

[13] This problem can be solved exactly and gives $V=(g^2/4\pi)e^{-\mu x}/x$.

if Eq. (41) is solved without this second term of (42) for a bound state ($\epsilon<0$), then the contribution to the binding of the neglected term is

$$\frac{g^2}{4\pi}\int\frac{dk}{\omega^2}\phi^*(\mathbf{k})\left[1-\frac{\omega}{\omega+T_p+T_{p-k}-\epsilon}\right]\phi(\mathbf{p}-\mathbf{k})$$
$$\leq\frac{g^2}{4\pi}\int\psi^*(\mathbf{x})\frac{e^{-\mu x}}{x}\psi(\mathbf{x})d\mathbf{x}. \quad (43)$$

This is less than the contribution to the binding of the first term of (42). Therefore, for appropriate g^2 and core radius, (43) may be negligible next to the second term of (42), even though the first term in the expansion of (43) is large. But, if the term giving (43) is neglected, then the potential is given by (42), with the inclusion of the second term, which, in this example, should be omitted.

The entire term (43) includes contributions to V from the exchange of more than 2 mesons, but only one at a time [Fig. 6(b)]. Since the inclusion of all such terms almost cancels the $e^{-\mu x}K_0(2\mu x)$ contribution from [Fig. 6(a)], these higher order terms are not

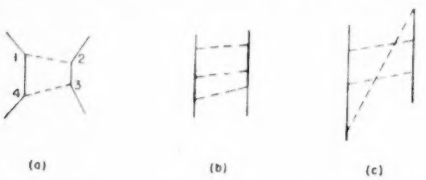

FIG. 6. (a) Feynman diagram for two meson exchange between space-time points 1, 2, 3, 4. (b) (c) Two types of meson exchange giving a g^6 term in $\mathfrak{R}$.

negligible. But for the neutral scalar theory, the $\mathfrak{R}$ from all diagrams representing the exchange of 3 mesons in any time sequence gives a zero contribution to the potential. Therefore, when Fig. 6(b) contributes significantly, then states with 3 mesons Fig. 6(c) will be of comparable magnitude.

The treatment of the neutral scalar theory thus suggests that states with three mesons which have been omitted by both Brueckner and Watson and by ourselves, are important enough to qualitatively change both potentials.

CONCLUSIONS

Corrections to the usual second and fourth order perturbation theory results of the nuclear force arise in two ways: (a) a virtual meson may be scattered an arbitrary number of times by one of the nucleons before being absorbed by it or by the other nucleon; (b) three or more mesons may exist at one time, no one of which are emitted and absorbed by the same nucleon.

The correction (a) is found to be small, but the neglect of (6) is unjustified and probably changes even the qualitative features of the usual[10–12] g^2+g^4 perturbation theory potential. With $(g^2/4\pi)$ adjusted to give a satisfactory description of real meson-nucleon scattering phase shifts, the calculated potential gives unsatisfactory deuteron properties.

It is a pleasure to thank Professors K. M. Watson and K. A. Brueckner for sending us a copy of their manuscript prior to publication, and for helpful discussion concerning it. We also gratefully acknowledge stimulating discussions with Professors R. Serber, N. Kroll, S. D. Drell, and Dr. C. Levinson.

This work was completed at Brookhaven National Laboratory. The authors are very grateful for the hospitality and courtesy extended to them.

APPENDIX I

Since we shall primarily be concerned with $r_J{}^I(w_0, w_0)$, it is convenient to first find the solution to Eq. (32) when $w_1=w_0$. This is

$$\bar{r}_3{}^3=i\frac{4}{3w_0}\frac{g_p{}^2}{\mu^2}\left[1+\frac{9}{2}\Delta'(-w_0)\right]^{-1}[1-2\Delta''(w_0)]^{-1},$$

where

$$\Delta''(w_0)=\frac{2}{3\pi}\frac{g_p{}^2}{4\pi}\frac{w_0}{\mu^2}\frac{1}{4\pi}\int_0^{k_{\max}}\frac{k^2d\mathbf{k}}{\omega^3(\omega-w_0-i\delta)}$$
$$\times\left[\frac{1+(9/2)\Delta'(-w_0)}{[1+(9/2)\Delta'(w_0-\omega)][1+(9/2)\Delta'(-\omega)]^2}\right].$$

$\Delta''(w_0)$ differs from $\Delta'(w_0)$ by the factor within the bracket. Now $\Delta''(w_0)$ is large for $w_0\sim 2\mu$. Furthermore, in the interval of integration for ω, $\Delta'(w_0-\omega)\ll 1$ for $g_p{}^2/4\pi\approx 0.2$ [see Fig. (3)]. Also $\Delta'(-\omega)$ is small in this interval [$\Delta'(-2\mu)\approx -0.06$]. Therefore near the maximum for Δ'' the bracket is close to 1 so we shall approximate $\Delta''\approx\Delta'$. This can be a bad approximation for $w_0\sim\omega_{\max}$ but these w_0 do not play an important role in the nuclear force for $x>\hbar/2\mu c$. However, the prime justification for putting $\Delta''\approx\Delta'$ is that an appreciable error in Δ' does not greatly change the nuclear potential. If we define $s_3{}^3$,

$$s_3{}^3\equiv r_3{}^3-\bar{r}_3{}^3,$$

then the solution for $s_3{}^3$ is

$$s_3{}^3(w_1, w_0)\approx 2\Delta'(w_0-w_1)\bar{r}_3{}^3(w_1, w_0)$$
$$-\frac{4}{3}\frac{g_p{}^2}{\mu^2}\left(\frac{1}{2\pi}\right)^3\int\frac{k^2d\mathbf{k}w_1s_3{}^3(\omega, w_0)}{2\omega^2(w_0-\omega+i\delta)(w_0-\omega-w_1+i\delta)}$$

and

$$s_3{}^3(w_0, w_0)$$
$$\approx+\frac{8}{3}\frac{g_p{}^2}{\mu^2}w_0\left(\frac{1}{2\pi}\right)^3\bar{r}_3{}^3(w_0, w_0)\int\frac{k^2d\mathbf{k}\Delta'(w_0-\omega)}{2\omega^3(w_0-\omega)}.$$

In the region $-2\mu<w_0<2\mu$, which is important for the virtual scattering contribution to the extra-core part of the nuclear force, $s_3{}^3(w_0, w_0)$ is less than $0.1r_3{}^3$.

It is therefore neglected in the text and only τ_3^3 is used in computing the nuclear force.

APPENDIX II

The potentials $V^{(1)}$ and $V^{(2)}$ will be found below by the method outlined in Sec. IV.

In Eq. (14) the correction to the perturbation result for $V^{(1)}$ contains $r(w_1, \mathbf{k}_1; 0, \mathbf{k})$. However, it is not appropriate to use expression (18) for r. When introduced into Eq. (14), the entire expression (18) includes terms from Feynman diagrams which give no contribution after renormalization. In particular, that part of r_1^1 which arises from the $1/w_0$ term of Eq. (22) (replacement of S_F by S_F') is to be neglected. When substituted into Eq. (14), the only part of r_1^1 which will be kept is $ig^2/3w_1\mu^2$. On the other hand, r_3^3, r_1^3, and r_3^1 are unaltered by these considerations.

When the integration over w' is performed in Eq. (14), the term $g_p^2\Delta'(w'-w_0)$ of Eqs. (24) and (25) is evaluated at $w_0=0$ and $w'=-(k^2+\mu^2)^{\frac{1}{2}}$, the relevant pole of the meson Green's function. Since $g_p^2\Delta'(-(k^2+\mu^2)^{\frac{1}{2}})\ll 1$ for all $\mathbf{k}$, this correction term can be neglected. Since furthermore, $\Delta'(0)=0$, r_3^3, r_3^1, and r_1^3 reduce to the perturbation theory result. Inclusion of r_1^1 then gives

$$V^{(1)}(\mathbf{k}_0)=\frac{g_p^2}{\mu^2}\boldsymbol{\tau}_a\cdot\boldsymbol{\tau}_b\frac{\boldsymbol{\sigma}_a\cdot\mathbf{k}_0\boldsymbol{\sigma}_b\cdot\mathbf{k}_0}{k_0^2+\mu^2}\times\left[1+\frac{1}{3}\frac{g_p^2}{\mu^2}\left(\frac{1}{2\pi}\right)^3\int\frac{k^2d\mathbf{k}}{2\omega^3}\right]. \quad \text{(a)}$$

In coordinate space, this is

$$V^{(1)}(x)=-[1+0.07]\boldsymbol{\tau}_a\cdot\boldsymbol{\tau}_b\frac{g^2}{4\pi}\boldsymbol{\sigma}\cdot\boldsymbol{\nabla}\boldsymbol{\sigma}\cdot\boldsymbol{\nabla}\frac{e^{-\mu x}}{\mu^2 x}, \quad \text{(b)}$$

which differs from the perturbation potential by the numerical factor $[1+0.07]$ in front of Eq. (b).

In evaluating $V^{(2)}$ it is useful to rewrite r of Eq. (18) as

$$r(\mathbf{k}_1, \mathbf{k}_0)=\sum_{i,j=1}^{3}(E\{\boldsymbol{\sigma}\cdot\mathbf{k}_1, \boldsymbol{\sigma}\cdot\mathbf{k}_0\}+F[\boldsymbol{\sigma}\cdot\mathbf{k}_1, \boldsymbol{\sigma}\cdot\mathbf{k}_0])\{\tau_i, \tau_j\}$$

$$+\sum_{i,j=1}^{3}(G\{\boldsymbol{\sigma}\cdot\mathbf{k}_1, \boldsymbol{\sigma}\cdot\mathbf{k}_0\}+H[\boldsymbol{\sigma}\cdot\mathbf{k}_1, \boldsymbol{\sigma}\cdot\mathbf{k}_0])[\tau_i, \tau_j], \quad \text{(c)}$$

where $\{\ ,\ \}$ is the anticommutator and $[\ ,\ ]$ the commutator of the quantities enclosed. Also, we have

$$E=r_3^3/3+r_1^3/3+r_1^1/12,$$
$$F=G=-r_3^3/6+r_1^3/12+r_1^1/12,$$
$$H=r_3^3/12-r_1^3/6+r_1^1/12.$$

Also, Eq. (13) may be rewritten as

$$\mathfrak{R}^{(2)}=-\left(\frac{1}{2\pi}\right)^4\frac{1}{4}\int(r^+(\mathbf{k}_1, \mathbf{k}_0)+r^-(\mathbf{k}_0, \mathbf{k}_1))_a(r^+(\mathbf{k}_0, \mathbf{k}_1)$$
$$+r^-(\mathbf{k}_1, \mathbf{k}_0))_b\frac{d\mathbf{k}_0d\mathbf{k}_1dw_0\delta(\mathbf{p}_1-\mathbf{p}_0+\mathbf{k}_1-\mathbf{k}_0)}{(w_0^2-k_0^2-\mu^2+i\delta)(w_0^2-k_1-\mu^2+i\delta)}, \quad \text{(d)}$$

where $r^+\equiv r(w_0, w_0)$ and $r^-\equiv r(-w_0, -w_0)$. In writing Eq. (d), use has been made of the fact that only terms symmetrical in w_0 contribute to $\mathfrak{R}^{(2)}$. Substitution of (c) into (d) gives for $\mathfrak{R}^{(2)}$

$$\mathfrak{R}^{(2)}=-\left(\frac{1}{2\pi}\right)^4\frac{1}{4}\int\{[3(E^++E^-)^2-2(G^+-G^-)^2\boldsymbol{\tau}_a\cdot\boldsymbol{\tau}_b]$$
$$\times\{\boldsymbol{\sigma}_a\cdot\mathbf{k}_1, \boldsymbol{\sigma}_a\cdot\mathbf{k}_0\}\{\boldsymbol{\sigma}_b\cdot\mathbf{k}_1, \boldsymbol{\sigma}_b\cdot\mathbf{k}_0\}-[3(F^+-F^-)^2$$
$$-2(H^++H^-)^2\boldsymbol{\tau}_a\cdot\boldsymbol{\tau}_b][\boldsymbol{\sigma}_a\cdot\mathbf{k}_1, \boldsymbol{\sigma}_a\cdot\mathbf{k}_0][\boldsymbol{\sigma}_b\cdot\mathbf{k}_1, \boldsymbol{\sigma}_b\cdot\mathbf{k}_0]\}$$
$$\times\frac{d\mathbf{k}_1d\mathbf{k}_0dw_0\delta(\mathbf{p}_1-\mathbf{p}_0+\mathbf{k}_1-\mathbf{k}_0)}{(w_0^2-k_0^2-\mu^2+i\delta)(w_0^2-k_1^2-\mu^2+i\delta)}, \quad \text{(e)}$$

where $E^+\equiv E(w_0, w_0)$ and $E^-\equiv E(-w_0, -w_0)$. $V^{(2)}$ is obtained by substituting $\mathfrak{R}^{(2)}$ into Eq. (15). $\mathfrak{R}^{(2)}$ is first calculated for a large but finite nucleon mass. On passing to the limit of infinite mass in Eq. (15), $V^{(2)}$ is a finite and well-defined integral of the form

$$\int\{\alpha_3^2(\chi_3^{3+}\pm\chi_3^{3-})^2+\alpha_0^2(\chi_1^{3+}\pm\chi_1^{3-})^2+\alpha_1^2(\chi_1^{1+}\pm\chi_1^{1-})^2$$
$$+2\alpha_3\alpha_0(\chi_3^{3+}\pm\chi_3^{3-})(\chi_1^{3+}\pm\chi_1^{3-})$$
$$+2\alpha_3\alpha_1(\chi_3^{3+}\pm\chi_3^{3-})(\chi_1^{1+}\pm\chi_1^{1-})$$
$$+2\alpha_1\alpha_0(\chi_1^{3+}\pm\chi_1^{3-})(\chi_1^{1+}\pm\chi_1^{1-})\}$$
$$\times\frac{d\mathbf{k}_1d\mathbf{k}_0dw_0\delta(\mathbf{p}_1-\mathbf{p}_0+\mathbf{k}_1-\mathbf{k}_0)}{(w_0^2-k_0^2-\mu^2+i\delta)(w_0^2-k_1^2-\mu^2+i\delta)}, \quad \text{(f)}$$

where $\alpha_i(i=0, 1, \text{or } 3)$ is a constant. In this form of writing $V^{(2)}$, the effect of the second term of Eq. (15) is to remove the infinities which occur from poles at $w_0=0$. The function χ_J^I is related to r_J^I by just the proper subtraction of these infinities.

As a typical term of (f) consider $\alpha_1^2[\chi_1^{1+}]^2$. The integration over w_0 can be performed exactly.[14] It is convenient to convert it to contour integration, choosing a contour that does not contain the branch points and poles of $1/[1+4\Delta'(w_0)]$.

It can be shown, that the poles and branch points of $F(w_0)\equiv 1/[1+a\Delta'(w_0)]$ always lie in the second and fourth quadrant of the complex plane, close to the real

[14] In the computation of contributions of r_1^1 to $V^{(2)}$, Eq. (31) was approximated by r_1^1:

$$r_1^1\approx -i\frac{8}{3}\frac{f^2}{\mu^2 w_0}\frac{1}{1+4\Delta'(w_0)}.$$

axis. Thus, if $w_0=x+iy$, then $F(w_0)$ is

$$F(w_0)\equiv\frac{1}{1+a\Delta'(w_0)}$$

$$=\frac{1}{1+a\dfrac{2}{3\pi}\dfrac{1}{4\pi}\left(\dfrac{g^2}{4\pi}\right)\dfrac{1}{\mu^2}\displaystyle\int\frac{k^2d\mathbf{k}}{\omega^3}\frac{(x+iy)(\omega-x+iy+i\delta)}{[(\omega-x)^2+(y+\delta)^2]}}. \quad (g)$$

Necessary, but not sufficient conditions for $F(w_0)$ to have poles is that the imaginary part of the denominator be zero and that the real part of the integral be one. Thus,

$$\int\frac{k^2d\mathbf{k}}{\omega^3}\frac{\delta x+y\omega}{[(\omega-x)^2+(y+\delta)^2]}=0,$$

$$a\frac{2}{3\pi}\frac{1}{4\pi}\left(\frac{g^2}{4\pi}\right)\frac{1}{\mu^2}\int\frac{x\omega-x^2-y^2-\delta y}{[(\omega-x)^2+(y+\delta)^2]}\frac{k^2d\mathbf{k}}{\omega^3}=-1. \quad (h)$$

For negative a the conditions (h) are possible only if x is positive and y is negative and small; for positive a, both conditions may be satisfied if x and y have opposite signs. In addition to poles, $F(w_0)$ has branch points at $w_0=\mu$ and $\omega_{\max}$. For Chew's value of $g_p^2/4\pi=0.2$ and $\omega_{\max}=3.2\mu$, the poles occur at $w_0\sim\omega_{\max}$ and only for r_1^3, r_3^1 and r_1^1.

For the term $\alpha_1^2[\chi_1^{1+}]^2$ of (f) all singularities of $F(w_0)$ occur in the fourth quadrant, and can be completely avoided by choosing a contour which encloses the upper half plane. Then

$$\frac{\alpha_1^2}{2\pi i}\int[\chi_1^{1+}]^2\frac{dw_0}{(w_0^2-\mu^2-k_0^2+i\delta)(w_0^2-k_1^2-\mu^2+i\delta)}$$

$$=-\frac{g^4}{\mu^4}\frac{32\alpha_1^2}{9(k_0^2+\mu^2)^{\frac{1}{2}}}\left[\frac{1}{k_0^2-k_1^2+i\delta}\right.$$

$$\left.\times\left(\frac{1}{1+4\Delta'(-(k_0^2+\mu^2)^{\frac{1}{2}})}\right)^2\right]+\text{a similar term}$$

$$\text{with } k_0\rightarrow k_1,\ k_1\rightarrow k_0. \quad (i)$$

For the term $\alpha_1^2[\chi_1^{1-}]^2$ of (f), the same result is obtained by integrating around the lower half plane. Most of the other terms in (f) cannot be integrated so simply. Thus, for $\chi_1^{1+}\chi_1^{1-}$, it is impossible to avoid including the branch points of $F(w_0)$, since they occur symmetrically above and below the real axis. These integrals were estimated by approximating $F(w_0)$ in the region $-\omega_{\max}\lesssim w_0\lesssim-\mu$, which contains all singularities of $F(-w_0)$. It can be shown that a good approximation to the integral obtains if the approximation is accurate in this region. A best fit to $F(w_0)$ of the form $A+Bw_0+Cw_0^2$ is used in this region. For $-\omega_{\max}\lesssim w_0\lesssim-\mu$, $\Delta'(w_0)$ is a slowly varying function (see Fig. 4), and this approximation should be sufficient. The best fits with the constants of Eq. (35) are

$$\frac{1}{1-2\Delta'(w_0)}\approx1.0165-0.0748w_0/\mu-0.0080w_0^2/\mu^2,$$

$$\frac{1}{1+\Delta'(w_0)}\approx0.9885+0.0289w_0/\mu+0.0034w_0^2/\mu^2,$$

$$\frac{1}{1+4\Delta'(w_0)}\approx\frac{1}{1+(9/2)\Delta'(w_0)}\approx0.9477+0.0928w_0/\mu+0.0118w_0^2/\mu^2. \quad (j)$$

With this approximation, the integrals over w_0, $\mathbf{k}_0$, and $\mathbf{k}_1$ can be evaluated directly. The integral over w_0 gives for the coordinate space representation of $V^{(2)}$:

$$V^{(2)}\approx\text{constant}\frac{g^4}{\mu^4}\operatorname*{Lim}_{r_0\rightarrow r_1}\int\left\{\frac{e^{i(\mathbf{k}_0\cdot r_0+\mathbf{k}_1\cdot r_1)}d\mathbf{k}_0d\mathbf{k}_1}{(k_0^2+\mu^2)^{\frac{1}{2}}(k_0^2-k_1^2+i\delta)}\right.$$

$$\times[(E_1-G_1\boldsymbol{\tau}_a\cdot\boldsymbol{\tau}_b)\{\boldsymbol{\sigma}_a\cdot\mathbf{k}_1,\boldsymbol{\sigma}_a\cdot\mathbf{k}_0\}\{\boldsymbol{\sigma}_b\cdot\mathbf{k}_1,\boldsymbol{\sigma}_b\cdot\mathbf{k}_0\}$$

$$-(F_1-H_1\boldsymbol{\tau}_a\cdot\boldsymbol{\tau}_b)[\boldsymbol{\sigma}_a\cdot\mathbf{k}_1,\boldsymbol{\sigma}_a\cdot\mathbf{k}_0][\boldsymbol{\sigma}_b\cdot\mathbf{k}_1,\boldsymbol{\sigma}_b\cdot\mathbf{k}_0]]$$

$$\left.+\text{terms symmetric to above with } \mathbf{k}_0\rightarrow\mathbf{k}_1,\ \mathbf{k}_1\rightarrow\mathbf{k}_0\right\}$$

$$+\text{constant}\frac{g^4}{\mu^4}\operatorname*{Lim}_{r_0\rightarrow r_1}\int\frac{e^{i(\mathbf{k}_0\cdot r_0+\mathbf{k}_1\cdot r_1)}dk_0dk_1}{(k_0^2+\mu^2)(k_1^2+\mu^2)}$$

$$\times[(10-1.4\boldsymbol{\tau}_a\cdot\boldsymbol{\tau}_b)\{\boldsymbol{\sigma}_a\cdot\mathbf{k}_1,\boldsymbol{\sigma}_a\cdot\mathbf{k}_0\}\{\boldsymbol{\sigma}_b\cdot\mathbf{k}_1,\boldsymbol{\sigma}_b\cdot\mathbf{k}_0\}$$

$$-(2.2-1.5\boldsymbol{\tau}_a\cdot\boldsymbol{\tau}_b)[\boldsymbol{\sigma}_a\cdot\mathbf{k}_1\boldsymbol{\sigma}_a\cdot\mathbf{k}_0][\boldsymbol{\sigma}_b\cdot\mathbf{k}_1,\boldsymbol{\sigma}_b\cdot\mathbf{k}_0]], \quad (k)$$

where

$$E_1=1.2\omega_0/\mu+0.68\omega_0^2/\mu^2,$$
$$F_1=40-0.45\omega_0/\mu+0.02\omega_0^2/\mu^2,$$
$$G_1=60-0.67\omega_0/\mu+0.03\omega_0^2/\mu^2,$$
$$H_1=0.67\omega_0/\mu+0.04\omega_0^2/\mu^2,$$

with $\omega_0=(k_0^2+\mu^2)^{\frac{1}{2}}$. Integration over $\mathbf{k}_0$ and $\mathbf{k}_1$ then gives Eq. (39) for $V^{(2)}$. Only the dominant correction to the perturbation result has been kept; ω_0^2/μ^2 terms are very small and have been neglected.

PHYSICAL REVIEW VOLUME 92, NUMBER 4 NOVEMBER 15, 1953

The Universal Fermi Interaction*

E. J. KONOPINSKI AND H. M. MAHMOUD
Physics Department, Indiana University, Bloomington, Indiana
(Received July 24, 1953)

On the basis of the hypothesis that the same form of interaction acts among any spin-½ particles, it is interesting to apply the interaction law found for β decay to the muon processes. The application is beset by two types of ambiguity. The first is due to the uncertainty in measured values of coupling constants, and particularly their signs. The second arises from the various ways in which the correspondence between the particles of μ and β decay may be taken. Arguments are presented that the unique correspondence established if two *like* neutrinos are ejected in μ decay is the correct one.

It is argued that previous interpretations of the Universal Fermi Interaction have been unjustifiably broad. Only processes in which two normal particles (*vs* antiparticles) are annihilated, and two created, should be expected. The positive muon must be treated as the normal-particle (if the neutron, proton and negatron are) in order to avoid the expectation that muon capture by a proton may yield electrons, contrary to experimental facts. The conclusion that two like neutrinos are ejected in μ decay follows immediately.

1. β AND μ DECAY

IN a recent paper,[1] a "phenomenological derivation" of the law of β decay led to the conclusion that it must be an "*STP* combination." This means that the interaction energy density is a linear combination of the well-known scalar (*S*), tensor (*T*) and pseudoscalar (*P*) forms. Experimental evidence was used to conclude that all three forms must be present and that the polar vector (*V*) and axial vector (*A*) forms should not be included.

The weakest point of the "derivation" was that only one piece of evidence, the singular spectrum of RaE, could be offered that the *TP* combination must be part of the correct law. A *VA*, *ST*, or *VAP* combination would otherwise do just as well as the *STP* combination. Since the publication of that result there has been experimental confirmation that the *T* component is an essential part of the law. This was shown by improved measurements[2] on the correlation between the nuclear recoil and the β emission of He^6. A similar measurement[3] on O^{14} is awaited with interest; it should provide an unambiguous check on the choice of the *S* or the *V* component in the coupling.

Meanwhile, the analysis[4] of RaE which led to the choice of the *TP* components receives further support. Konopinski and Langer[5] pointed out that the Petschek-Marshak analysis of the RaE spectrum yields the peculiar deviation from a statistical shape, (which is the shape to be expected normally) through the admission of an accidental, destructive interference between the *T* and *P* contributions. A corresponding slowing down of the RaE decay is then to be expected and this was found, in comparisons against the similar nuclei Hg^{205}, Tl^{206}, and Pb^{209}. Now Brysk reports[6] calculations, based on *jj*-coupled pairs of single-particle states, that the destructive interference in RaE is to be expected from a $T+P$ combination (in the conventional definition[5] of these forms). This contrasts in the expected way with the much shorter-lived Tl^{206}, where constructive interference is found instead. RaE has 83 protons and 127 neutrons, each being one more than enough to fill magic shells. Tl^{206} has 81 protons and 125 neutrons.

Some evidence for the inclusion of the *P* interaction, independent of the RaE case, has also been reported. Nordheim[7a] finds that once-forbidden transitions with $\Delta I=0$ (no spin change) are distinctly more rapid than $\Delta I=1$ transitions. Considering the lack of such a difference in allowed transitions, the extra contributions to the $\Delta I=0$, once-forbidden transitions are best ascribed to the *P* interaction, which makes its largest contribution to just such transitions.

The fact that the rates of muon decay and capture indicate the same interaction strength as does β decay and capture has led to the hypothesis of a Universal Fermi Interaction:[7b] the same coupling among *any* four fermions. It thus becomes interesting to examine the *STP* form of interaction in μ decay.

One available datum on muon processes which is sensitive to the form of interaction is the spectrum of the electrons from μ decay. Michel[8] has shown that, whatever specific form of Fermi coupling is assumed, the theoretical result for the spectrum can be written

* Supported by a grant from the National Science Foundation.
[1] H. M. Mahmoud and E. J. Konopinski, Phys. Rev. **88**, 1266 (1952).
[2] J. S. Allen and W. K. Jentschke, Phys. Rev. **89**, 902 (1953); B. M. Rustad and S. L. Ruby, Phys. Rev. **89**, 880 (1953).
[3] M. E. Rose, Phys. Rev. **90**, 1123 (1953).
[4] A. Petschek and R. Marshak, Phys. Rev. **85**, 698 (1952).
[5] E. J. Konopinski and L. M. Langer, Annual Reviews **2**, 261 (1952).
[6] H. Brysk, *Report of the Indiana Conference on Nuclear Spectroscopy and the Shell Model* (Indiana University, Bloomington, 1953); p. 27. Brysk also finds a larger *P* contribution than reported by Ahrens, Feenberg, and Primakoff, Phys. Rev. **87**, 663 (1952). M. Rudermann, Phys. Rev. **89**, 1227 (1953), presents other grounds for expecting a sufficiently large *P* contribution.
[7a] L. Nordheim, *Report of the Indiana Conference on Nuclear Spectroscopy and the Shell Model* (Indiana University, Bloomington, 1953), p. 21.
[7b] O. Klein, Nature **161**, 897 (1948). See also references 14 and 15. (Footnote added in proof.)
[8] L. Michel, Phys. Rev. **86**, 814 (1952).

(valid except for electron energies as low as $\frac{1}{2}$ Mev):

$$d\lambda/\lambda dW = 4(W^2/W_0^4)[3(W_0-W)+\tfrac{2}{3}\rho(4W-3W_0)], \quad (1)$$

where W is the electron energy and W_0 its end-point value. λ is the decay constant and ρ is a parameter which depends on the coupling used. The spectrum (1) has a vanishing intensity at the end-point for $\rho=0$, and larger finite intensities for larger ρ.

The experimental measurements of the μ-decay spectrum disagree with each other. Sagane, Gardner, and Hubbard[9] reported $\rho\approx 0$. Lagarrigue and Peyrou[10] give $\rho=0.19\pm0.12$ as the result of their own measurements and $\rho=0.075\pm0.20$ as the value deduced from Leighton, Anderson, and Seriff's data.[11] Finally, Bramson, Seifert, and Havens[12] find $\rho=0.41\pm0.13$.

An application of the *STP* coupling to the problem is handicapped by two sources of ambiguity. In the first place, the relative sizes of the S, T, and P components is known only roughly. According to Blatt,[13] G_S^2/G_T^2 may have any value from $\sim$0.3 to $\sim$1.0, where $G_{S,T}$ are the Fermi coupling constants for the S and T interactions. The pseudoscalar coupling constant, G_P, is known only to have about the same order of magnitude as the others. Moreover, the relative signs of the G's are important and unknown. One indication exists that $G_P=G_T$, in sign and magnitude; that is the work of Brysk mentioned above.

In the second place, the significance of the *STP* form for μ decay depends on the correspondence assumed between the particles participating in μ decay and those of β decay. Three different orderings are possible,[14] known as "simple charge exchange," "charge retention" and "antisymmetrical charge exchange." The last of these differs from the others in that the two neutral particles produced in the μ decay are presumed *like* neutrinos, i.e., one is not an antineutrino.

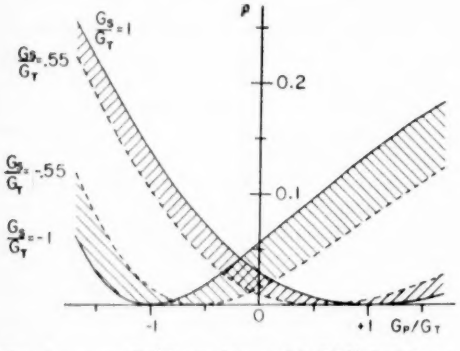

FIG. 1. ρ *versus* G_P/G_T consistent with $G_S^2/G_T^2=0.3$ to 1.

Without some reduction of the ambiguities, no useful predictions of the μ spectrum can be made from the *STP* law. Any value of ρ in the range obtained in the various experiments can be reproduced. The point of interest is that the values predicted for ρ are surprisingly restricted, even with the uncertainties about the G values, when one presumes that two like neutrinos are emitted in the μ decay. We confine our attention to this case, not only for the sake of making relatively unique predictions, but more important, because a proper interpretation of the universal interaction seems to indicate that the two neutrinos must be alike. The argument for this is presented in the next section; here we investigate its consequences for the μ spectrum.

When two like neutrinos are emitted, the *STP* interaction gives

$$\rho=\tfrac{3}{2}\frac{(G_S-G_P)^2}{2(G_S-G_P)^2+(G_S+6G_T+G_P)^2}. \quad (2)$$

We thus have, with $G_S^2/G_T^2=0.3$ to 1.0:

(a) $\rho=0$ for laws of the form $G_S(S+P)+G_TT$,

(b) $\rho=\frac{1}{2}$ for $G_sS+G_T(T-3P)$,

(c) $0.01<\rho<0.06$ if $G_P=0$,

(d) $\rho<0.14$ if $G_P/G_T=\pm1$.

These are the cases in which G_P is restricted to more plausible values. ρ is shown as a function of $G_P^2/G_T^2\lesssim 3$ in Fig. 1. To get as high a value as $\rho\approx0.4$, the largest reported by the experimenters, one would need $G_P^2/G_T^2\gtrsim 6$, which is highly implausible.

2. THE SIGNIFICANCE OF A UNIVERSAL INTERFERMIONIC COUPLING

The attractive hypothesis that a Fermi type of interaction exists among any four fermions may have a serious drawback. Besides accounting for the several known processes, it may lead to the expectation of processes which contradict experience—yet are consistent with conservation principles. Yang and Tiomno[15] tried to forbid the unwanted processes by defining intrinsic "generalized parity" contributions by pairs of fermions, in such a way that a "generalized parity" balance is violated in the unwanted processes. They were only partially successful in this. They could not forbid processes like $N+N\rightarrow\bar{N}+\bar{N}$ ($\bar{N}\equiv$antineutron) or $P+\mu\rightarrow P+e$, on their interpretation of the universal interaction, without postulating special, "*ad hoc*", rules against these.

Caianiello[16] reports that all unwanted processes can be successfully eliminated by adopting interactions in a special way. His procedure amounts to admitting coupling constants which are not just numbers, but quantities which transform in certain ways during

[9] Sagane, Gardner, and Hubbard, Phys. Rev. **82**, 557 (1951).
[10] A. Lagarrigue and C. Peyrou, J. phys. et radium **12**, 848 (1951).
[11] Leighton, Anderson, and Seriff, Phys. Rev. **75**, 1432 (1949).
[12] Bramson, Seifert, and Havens, Phys. Rev. **88**, 304 (1952).
[13] J. M. Blatt, Phys. Rev. **89**, 83 (1953).
[14] J. Tiomno and J. A. Wheeler, Revs. Modern Phys. **21**, 144 (1949).
[15] C. N. Yang and J. Tiomno, Phys. Rev. **79**, 495 (1950).
[16] E. R. Caianiello, Nuovo cimento **8**, 534 and 749 (1951); **9**, 336 (1952).

changes of coordinates. This seems to us undesirably artificial and also unnecessary.

A thesis of this paper is that former interpretations of the Universal interaction have been unnecessarily, and even unjustifiably, broad. We shall use what seems to us a better justified interpretation which makes the processes like $N+N\rightarrow\bar{N}+\bar{N}$ and $P+\mu\rightarrow P+e$ unformulable *ab initio*. A further concrete consequence will be the conclusion that the neutral particles ejected in μ decay are *like* neutrinos (i.e., one is not an antineutrino).

Consider the electron capture process:

$$P+e^-\rightarrow N+\nu. \tag{3}$$

When formulating this alone, it is clearly only a matter of nomenclature as to whether one considers all these to be normal particles, or whether one or more is treated as an antiparticle (hole). This follows from the well known "charge-conjugacy" of the Dirac equations. We shall adopt the convention of calling the particles symbolized in (3) normal particles, so that (3) entails the annihilation of two normal particles and the creation of two others.

When one next formulates a *second* process like the μ capture:

$$P+\mu^-\rightarrow N+\nu, \tag{4}$$

then it has physical consequences to treat the particles symbolized here as all normal. It implies that the neutrino of this process can be captured by a neutron to produce an electron, reversing (3), as well as the inverse of (4). It may be that the light neutral particle ejected in μ capture is an antineutrino ($\bar{\nu}$) instead, capable of being captured by neutrons to give muons, but not electrons; by protons to give positrons but not muons. It will be convenient to write all processes in terms of normal particles only, and since the creation of $\bar{\nu}$ is equivalent to the absorption of ν, we write the μ capture with antineutrino ejection as:

$$P+\mu^-+\nu\rightarrow N. \tag{5}$$

This is an *alternative* to (4), as a representation of the process.

Our way of writing (4) and (5) implies that the negative muon, μ^-, is the normal particle, while μ^+ is the antimuon. In relation to further processes, it may instead be more consistent to treat μ^+ as normal and μ^- as the antimuon. Hence, further alternatives to (4) and (5) are

$$\mu^+ \text{ normal}\begin{cases} P\rightarrow\mu^++N+\nu, & (6)\\ P+\nu\rightarrow N+\mu^+. & (7)\end{cases}$$

The corresponding alternatives, normal forms for μ decay are:

$$\mu^- \text{ normal}\begin{cases} \mu^-\rightarrow e^-+\nu+\nu & (8)\\ \mu^-+\nu\rightarrow e^-+\nu & (9)\\ \mu^-+\nu+\nu\rightarrow e^-, & (10)\end{cases}$$

$$\mu^+ \text{ normal}\begin{cases} \mu^++e^-\rightarrow\nu+\nu & (11)\\ \mu^++e^-+\nu\rightarrow\nu & (12)\\ \mu^++e^-+\nu+\nu\rightarrow 0. & (13)\end{cases}$$

It is now apparent that the chief distinction between the various alternatives is that the corresponding formulations must variously provide for annihilations of one, two, three, or four normal fermions.

The reaction (3) must first be provided for; an interaction energy operator must be introduced which annihilates two normal fermions and creates two others. Then (3) is to serve as a prototype of the universal interaction among fermions; the same form of operator is assumed to act on *any* fermions. All resulting processes consistent with conservation principles are expected to occur. In each case, the operator destroys just two fermions in occupied states (i.e., normal fermions) of the fields. With such a "universalization," μ capture and μ decay are predicted to occur, and moreover in the forms (4), (9) or (7), (11). The *two*-particle annihilation processes follow unavoidably from (3), unless arbitrary changes of the interaction form are introduced at each application.

Now it seems conspicuously unnecessary, and would require new justification, to introduce *additional* terms, which would repeat provisions for the μ-capture and μ-decay processes in the other ways, as represented by (5), (6), (8), (10), (12), and (13). New interaction operators would indeed be needed, capable of annihilating one, three or four normal particles instead of just two. It can be construed as inconsistent with a "universality" of the interaction, thus to fail to retain the prototype annihilation-creation properties, as one does the magnitude, and the covariant properties, of the interaction. Yet, one, three, and four normal particle annihilations have been included in previous interpretations: the process written $N+N\rightarrow\bar{N}+\bar{N}$, above, is an annihilation of four *normal* particles, $4N\rightarrow 0$; the process $P+\mu\rightarrow P+e$ may be the one-particle annihilation, $P\rightarrow P+\mu^++e$, if μ^+ should be regarded as normal.

As a physical argument, our objection to the broadening of "universality" by previous interpreters seems clear. When, for example, $a+b\rightarrow c+d$ occurs, we object to the implication that $b\rightarrow c+d+a$ also occurs. The last process may be $\bar{a}+b\rightarrow c+d$ and thus it is implied that that a particle b can annihilate either against a, or its antiparticle $\bar{a}$, to produce $c+d$. We object to this non-unique behavior of a which is to accompany the same behavior of b, c, d in the cases compared.

On the formal side, the situation is more complex. The contact interaction which gives $a+b\rightarrow c+d$ must

be proportional to the annihilation operators ψ_a, ψ_b and also the creation operators ψ_c^*, ψ_d^*. The interaction energy density will be the sum of invariant contractions of like covariant operations, Ω;

$$G\psi_c^*\Omega\psi_a\cdot\psi_d^*\Omega\psi_b. \tag{14}$$

When each participating fermion is in a positive energy state, $\psi\sim\exp(-iEt/\hbar)$ and (14) is proportional to

$$\exp[i(E_c-E_a+E_d-E_b)t/\hbar].$$

One thus can get a permanent transition, rather than virtual oscillations, only if $E_c-E_a+E_d-E_b=0$; hence the interpretation $a+b\rightarrow c+d$. If, for example, a is in a negative-energy state, $E_a=-\bar{E}_a$ then $E_b=E_c+\bar{E}_a+E_d$ as expected for $b\rightarrow c+d+\bar{a}$. Now, to formulate $b\rightarrow c+d+a$ one must substitute the creation of a for its annihilation in (14):

$$G\psi_c^*\Omega W\psi_a^*\cdot\psi_d^*\Omega\psi_b. \tag{15}$$

Here W is whatever operator is needed to preserve invariance. As is plausible, it can be shown that[17] $WK=C$, where K is the operation of complex conjugation and C is the well-known charge-conjugation operator; W is a symmetric, unitary matrix which is $W=c\beta\alpha_2$ in a Dirac representation and merely a phase factor $W=c$ in a Majorana representation. Thus, it is shown that, indeed a new interaction operator $(G\Omega C\cdot\Omega)$ has to be added to the prototype $(G\Omega\cdot\Omega)$ in order to have $b\rightarrow c+d+a$ as well as $a+b\rightarrow c+d$. The interaction (15) owes its interpretation as giving $b\rightarrow c+d+a$ to its being viewed as an operation $(G\Omega C\cdot\Omega)$, acting on a *positive* energy state ψ_a (and interpreted as *creating* it, because of the complex conjugation due to operator C). Now, it is well known that the *negative* energy state, as used in (14) to give $b\rightarrow c+d+\bar{a}$, is just[18] $C\psi_a$ when ψ_a is a positive energy state. Hence, the expression (15) with ψ_a a positive energy state is formally identical with (14) when ψ_a is a negative energy state. Thus it is only a forced reinterpretation which allows (15) to describe $b\rightarrow c+d+a$ instead of $b\rightarrow c+d+\bar{a}$. It seems that one cannot[19] formulate $b\rightarrow c+d+a$ at all, together with $b\rightarrow c+d+\bar{a}$, without this forced reinterpretation of a formally identical expression. This adds support to our view that one should not include 1, 3, and 4 normal particle annihilations when "universalizing" the Fermi interaction.

Our restriction to two normal-particle annihilations of course simplifies the task of eliminating unwanted processes. First, it is clear that it would always be difficult to eliminate the nonexistent[20] process, $P+\mu^-\rightarrow P+e^-$, if it is the negative muon that is a normal particle; certainly no procedure of the Yang-Tiomno type could do so. For the existence of $P+\mu^-\rightarrow N+\nu\leftarrow P+e^-$ implies the unwanted process immediately. On the other hand, if μ^+ is the normal muon, then $P+\mu^-\leftrightarrow N+\bar{\nu}$ [(7), rewritten in an appropriate non-normal form]. Now, the unwanted process cannot even be formulated, on our interpretation of the universal interaction; it would have to be the rejected one normal-particle annihilation, $P\rightarrow P+\mu^++e^-$ instead.

The conclusion that μ^- is the antimuon has concrete physical consequences. It would imply that energetic antineutrinos could not produce muons when captured by protons, in an experiment of the Reines-Cowan[21] type. Of course, pile antineutrinos are not sufficiently energetic to test this. There is a chance, however, that the large cosmic background contains sufficiently energetic ones. Antineutrinos would have to be distinguished from neutrinos by comparisons of electron productions in hydrogen and deuterium. There is also the problem of distinguishing muon and electron production to be solved.

For the μ decay, the conclusion that μ^+ is the normal muon implies that the two neutral particles ejected are *like* neutrinos, as in (9). Hence, the chief ambiguity of the μ-decay theory is removed. The "simple charge exchange" and "charge retention" theories are eliminated in favor of the "antisymmetrical charge exchange." This conclusion was already employed in the previous section.

Another unwanted process, $\mu\rightarrow e+e^++e^-$ is immediately eliminated. If μ^+ is normal, this cannot be expressed as a two normal particle annihilation. If μ^+ were the antimuon, the process could not be forbidden by a procedure of the Yang-Tiomno type.

A further attractive feature of the proposed theory is that *all* unwanted processes can be forbidden and by a less explicit procedure than Yang and Tiomno's. In addition to the hypothesis that μ^+ is the normal muon, only the "conservation of heaviness" is needed to forbid all unwanted processes. The latter principle expresses the observation that the disappearance of a normal nucleon must result in the appearance of a neutron or a proton. Whatever deeper principle is the cause of this, aside from the Yang-Tiomno theory, its acceptance forbids all the types of unwanted processes which remain to be considered. All that can be formulated (consistently with charge conservation, two

[17] As an alternative, a factor γ_5 may need to be included, depending on the properties of the spinor ψ_a under space inversion. This would yield the "odd" type of interaction introduced by Yang and Tiomno as an alternative to the conventional "even" type, (14). This point has no bearing on our conclusions.

[18] This is strictly true only for free particles. However, the number of particles is well-defined (diagonal) only in the field-free case.

[19] This conclusion is unchanged when the charge-conjugate description of antiparticles is used in place of the hole theory. Proper use of the charge-conjugate formalism needs care to make it consistent; the unavoidable existence of negative energy solutions, or their equivalents, forces consistency with the hole theory. We make the exposition briefer, and avoid discussion of what constitutes a proper interpretation of the charge-conjugate formalism, by adhering to the hole theory. We make explicit here only the point that in the charge-conjugate formalism, the energy operator is $-i\hbar\partial/\partial t$ and the momentum operator $-(\hbar/i)\nabla$, i.e., the complex conjugates of the usual operators.

[20] A. Lagarrigue and C. Peyrou, Compt. rend. **234**, 1873 (1952).

[21] F. Reines and C. L. Cowan, Phys. Rev. **90**, 492 (1953).

normal-particle annihilation, μ^+-normal, etc) violate the conservation principle for nucleons.

The Yang-Tiomno theory assigns definite (relative) phases to the transformations undergone by each spinor field in space inversions. The transformation is $\psi'=c\beta\psi$ with c an undetermined phase factor, $|c|^2=1$, in general. The indeterminacy cannot be removed[22] as for proper transformations, in which continuity with the identity transformation can be demanded. Nor is it necessary that on repetition, $c\beta\psi'=\psi$, because of the well-known two-valuedness of spinors: in rotations by 2π, $\psi\rightarrow\psi'=-\psi$! If one limits oneself to $c\beta\psi'=\pm\psi$, then $c=\pm 1$ or $c=\pm i$. These four are the possibilities to which Yang and Tiomno restricted themselves in defining their four "types" of spinor fields; it is sufficient for most purposes to consider only relations among the c's characterizing each spinor field, without specifying their values. The idea is to assign such values to c_N, c_P, c_e, c_μ, and c_ν that the interaction (14) exhibits invariance under inversion when applied to the wanted processes (3), (7), and (11), but not for any unwanted two-normal-particle annihilations (the *parity* conservation is contained in the requirement here).

The invariance of the interaction (14) in space inversions is easily seen to require

$$c_a c_b = c_c c_d. \tag{16}$$

Applied to (3), (7) and (11) this gives $c_P c_e = c_N c_\nu$ and $c_\mu c_e = c_\nu^2$. Following Yang and Tiomno, we can derive the condition $c_P = c_N$ from the pion-nucleon interaction. The result is that $c_P = c_N = c_H$ and $c_e = c_\mu = c_\nu = c_L$ are required by the wanted processes (the subscripts H, L stand for "heavy" and "light").

An elementary but tedious review of all the possible unwanted processes shows that, for most of them, (14) loses the required invariance if $c_H \neq c_L$. The prevention of processes of the type $N+N\rightarrow\nu+\nu$ seems to require the stronger conditions: $c_H^2 \neq c_L^2$. In the Yang and Tiomno scheme, $c^2=\pm 1$ only, hence c_H and c_L are required to differ by 90° of phase. This is the Yang-Tiomno expression of the principle of nucleon conservation.

3. CONCLUDING REMARKS

It should be pointed out that the above discussion did not include the possibility that the neutrino and antineutrino are indistinguishable, i.e., a Majorana rather than Dirac particle. We believe that this possibility is remote. The repeated failures to find the comparatively short-lived double β decay expected with Majorana neutrinos indicate this; moreover, the one case in which the existence of double β decay may have been proved conforms to expectations for a Dirac neutrino.[23]

It is interesting that the sum of interactions (14) and (15) is proportional to $(1+C)\psi_a$, if equal magnitudes and phases are given to the two interactions. Now $(1+C)\psi$ is just the Majorana wave function. Hence, the inclusion of (15) together with (14) implies at least partial behavior by particle a as a Majorana particle. Since the Majorana formalism is certainly incorrect for charged particles and neutrons, and highly questionable also for neutrinos, this adds to the doubt that anything but the double-annihilation interaction (14) should be part of the Universal coupling.

The failure of the Majorana formalism to conform to anything in nature adds interest to Caianiello's[22] argument that a Majorana field is non-covariant in inversions. To show this, Caianiello had to make a partial determination of the phase factor, c, of the spinor inversion transformation. He concluded that $c^2=+1$, hence $c=\pm 1$ only, by requiring that the inversion be continuous with the identity transformation when the space inversion is defined as a continuous rotation through an arbitrary fifth dimension.

The conclusion that the inversion phase is $c=\pm 1$, only, throws doubt on the conclusion of the last section: that c_H and c_L should differ by a factor i. This depends on whether the strong requirement $c_H^2 \neq c_L^2$ is actually needed to forbid processes like $N+N\rightarrow\nu+\nu$ or whether $c_H \neq c_L$ is sufficient. The latter is adequate if one requires that a factor like $\psi_c^* \Omega \psi_a$ of (14) preserve the proper covariance under inversion or whether only the invariance of the product (14) should be demanded. It should further be pointed out that the same condition (16) must be obeyed[24] for the phases generated by time reversal or charge conjugation. On these, there is no limitation to real c as, perhaps, for the space inversion. Further, for our essential conclusions we have only the requirement of the "conservation of heaviness" regardless of what specific basis this is given.

[22] See, however, the discussion of E. R. Caianiello's attempt [Phys. Rev. **86**, 564 (1952)] in the concluding section.

[23] H. Primakoff, Phys. Rev. **85**, 888 (1952).

[24] A. Gamba, Nuovo cimento **7**, 919 (1950).

Theory of Polarized Particles and Gamma Rays in Nuclear Reactions*

ALBERT SIMON
Oak Ridge National Laboratory, Oak Ridge, Tennessee
(Received August 6, 1953)

The complete specification of the spin states of a particle of spin i resulting from a nuclear reaction requires a knowledge of all irreducible spin tensor moments $T_\kappa^q(|\kappa| \leq q \leq 2i)$. A general calculation is made of the spin tensor moments arising from a nuclear reaction initiated by an arbitrarily polarized initial beam. All sums over magnetic quantum numbers are performed by the use of the S matrix and Racah formalisms. The results are expressed in terms of the G function which is related to the Fano X function. All selection rules follow from the properties of the G function. In particular, a generalization of the Eisner-Sachs selection rules are given. The problem of the detection of polarized particles is considered.

The S-matrix formalism is extended to include the possibility of gamma-rays in nuclear reactions. Analogous formulas to those of Blatt and Biedenharn are given for the angular distribution of gamma-rays. A simple recipe yields a general result for the polarization and angular distribution of radiation from aligned nuclei. Finally, the theory is extended to include the possibility of an arbitrarily polarized target nucleus as well.

I. INTRODUCTION

THE spin state of a beam of particles of spin i may be specified by giving the elements of its density matrix. The density matrix, however, can always be written as a linear sum of the irreducible spin tensor moments T_κ^q, where q is the rank of the tensor and κ is its component ($|\kappa| \leq q \leq 2i$). In a previous paper[1] an expression was given for the spin tensor moments arising from a nuclear reaction initiated by an unpolarized beam; i.e., one in which all initial tensor moments other than $q=\kappa=0$ vanish. It is the purpose of this paper to generalize the result to the case of an arbitrarily polarized initial beam.

In Sec. II an expression is obtained for the expectation value of a spin tensor operator resulting from a nuclear reaction. The complete dependence of the expression on the magnetic quantum numbers of the initial and final states is contained in Clebsch-Gordan coefficients. All sums over these magnetic quantum numbers are performed in Sec. III, and the final result is expressed in terms of the S matrix and a geometrical function for the initial and final states. Several general selection rules, including the generalization of the Eisner-Sachs selection rules, are listed in Sec. IV. Applications of the general result to the problems of the angular distribution and polarization of particles in nuclear reactions, detection of polarized particles, and radiations from polarized nuclei are made in Sec. V. Section VI discusses the extension of the formalism to include gamma rays in nuclear reactions. Section VII indicates the modifications which must be made if the target nuclei, as well as the incident particles, are polarized.

This paper can properly be regarded as the generalization of the results of Blatt and Biedenharn[2] to include the observation of the spin polarizations of the initial and final states of a nuclear reaction. It should be pointed out to the reader that there is a complete correspondence between this theory and the theory of angular correlation.[3] In this regard it should be noted that, although the X coefficient of Fano is the natural function to use in angular correlation problems, the geometrical G function introduced below seems to be more convenient for the problem of nuclear reactions in which the initial state is a plane wave. This same effect is apparent in the results of BB where the Z coefficient is a more natural function for the angular distribution than the Racah coefficient. The G function is the generalization of the Z coefficient and bears the same relation to the Fano X function as the Z coefficient does to the Racah function.

II. NOTATION AND GENERAL EXPRESSION FOR THE POLARIZATION

As in Sec. I, we consider the reaction

$$a+X \rightarrow Y+b, \tag{2.1}$$

in which particle a collides with nucleus X. Particle b emerges at an angle θ to the direction of the incident beam, and Y is the residual nucleus. All quantities are measured in the center-of-gravity system. It is assumed that the spin polarization measurements in the final state are made upon particle b.

The system before collision is described by the channel spin s, the relative orbital angular momentum l, and the channel index α which defines the type of incoming particle (neutron, proton, etc.) as well as its energy and the state of the target nucleus. The channel spin s is the total spin angular momentum in the entrance channel and is formed by the vector addition of the intrinsic spin i of the incoming particle and the

* This paper is based on work performed for the U. S. Atomic Energy Commission at the Oak Ridge National Laboratory.

[1] A. Simon and T. A. Welton, Phys. Rev. **90**, 1036 (1953); references to this paper will be designated by I.

[2] J. M. Blatt and L. C. Biedenharn, Revs. Modern Phys. **24**, 258 (1952); references to this paper will be designated by BB.

[3] U. Fano, National Bureau of Standards Report 1214 (unpublished). The author wishes to take this opportunity to thank Dr. Fano for permission to see a manuscript by Fano and Racah in advance of publication.

spin I of the target nucleus. The state of the system after the reaction will be described by primed quantities.

A convenient expression for the asymptotic form of the outgoing wave is provided by the use of the S-matrix formalism. If the colliding system, which is taken to be a plane wave along the z axis, has the initial quantum numbers α, s, and m_s, the corresponding final wave function in the state $\alpha' s' m_s'$ has the form [see BB (3.12)]

$$\psi(\alpha s m_s, \alpha' s' m_s', \theta\phi) \sim i\lambda_\alpha \left(\frac{v_\alpha}{v_{\alpha'}}\right)^{\frac{1}{2}} \frac{\exp(ik_{\alpha'} r_{\alpha'})}{r_{\alpha'}} \times \phi_{\alpha'} q(\alpha s m_s, \alpha' s' m_s'; \theta\phi)\chi(s' m_s'),$$

where v_α and k_α are the relative velocity and wave number, respectively, in channel α: $\phi_{\alpha'}$ is the product of internal wave functions of nucleus Y, and particle b corresponding to the specification α'; $\chi(s' m_s')$ is the final channel spin wave function and

$$q(\alpha s m_s, \alpha' s' m_s'; \theta\phi) = \pi^{\frac{1}{2}} \sum_{J=0}^{\infty} \sum_{l=|J-s|}^{J+s} \sum_{l'=|J-s'|}^{J+s'} \sum_{\pi=\pm 1} i^{l-l'}(2l+1)^{\frac{1}{2}} \times (l\, s\, 0\, m_s | l\, s\, J\, m_s)(l'\, s'\, \mu'\, m_s' | l'\, s'\, J\, m_s) \times R(\alpha s l, \alpha' s' l'; J\pi) Y_{l'\mu'}(\theta\phi). \quad (2.3)$$

The quantity $(l\, s\, 0\, m_s | l\, s\, J\, m_s)$ is the Clebsch-Gordan coefficient defined as in Condon and Shortley.[4] The R matrix, which is related to the scattering matrix S by $R \equiv 1 - S$, is evaluated in the representation specified by the quantum numbers $\alpha s l J m_j$ and π. Here J is the total angular momentum of the colliding system, m_j is its orientation, and π is the parity. It has been assumed that no external forces are acting on the system. As a result, then, S must be diagonal in J and π and must be independent of m_j as has been made clear in the notation. In this representation the S matrix is symmetric and unitary. The summations over l and l' in Eq. (2.3) are to be extended only over those values which satisfy the parity condition. For pure elastic scattering S is related to the phase shift δ by $S = \exp(2i\delta)$.

The initial spin state of the colliding system in channel α is most conveniently specified by the use of the density matrix. For our purposes this may be defined as follows. The initial system may be described as a statistical mixture of channel spin states χ^γ, and the results of any *physical* measurement are obtained by performing a suitable average over the elements γ of the statistical ensemble. If we now expand the statistical spin states in terms of the basic channel spin functions $\chi(s m_s)$, we have

$$\chi^\gamma = \sum_{s, m_s} a^\gamma(s m_s)\chi(s m_s).$$

An element of the density matrix is then defined as

$$\rho(s_1 m_1; s_2 m_2) = \langle a^\gamma(s_1 m_1)^* a^\gamma(s_2 m_2)\rangle_\gamma, \quad (2.4)$$

where the brackets denote an average over γ and where for simplicity m_{s1} is replaced by m_1, etc. It is clear that the measured value of any operator O in the final channel α' is now given by the average over the elements γ of the initial ensemble of the expression

$$\sum a^\gamma(s_1 m_1)^* a^\gamma(s_2 m_2)(\psi^*(\alpha s_1 m_1, \alpha' s_1' m_1'; \theta\phi) \times |O|\psi(\alpha s_2 m_2, \alpha' s_2' m_2'; \theta\phi)),$$

where the sum is over $s_1 m_1 s_2 m_2 s_1' m_1' s_2'$ and m_2'. Hence, by Eq. (2.4) the resultant expression, after averaging, becomes

$$\sum \rho(s_1 m_1; s_2 m_2)(\psi^*(\alpha s_1 m_1, \alpha' s_1' m_1'; \theta\phi) \times |O|\psi(\alpha s_2 m_2, \alpha' s_2' m_2'; \theta\phi)).$$

If it is assumed that the operator O corresponds to a measurement upon the spin $\mathbf{i}'$ of particle b at an angle θ, we have

$$O \equiv O(\mathbf{i}') r_{\alpha'}^2 d\Omega$$

where $d\Omega$ is the solid angle. This expression, combined with Eq. (2.2), yields the following result for the measured intensity (note that normalization is to unit incident flux)

$$\langle O(\mathbf{i}')\rangle = \lambda_\alpha^2 \sum \rho(s_1 m_1; s_2 m_2) q^*(\alpha s_1 m_1, \alpha' s_1' m_1'; \theta\phi) \times q(\alpha s_2 m_2, \alpha' s_2' m_2'; \theta\phi) \times (\chi(s_1' m_1') | O(\mathbf{i}') | \chi(s_2' m_2')). \quad (2.5)$$

Complete statistical information on the spin states of a particle of spin i may be obtained by specifying the elements of the density matrix or alternatively by specifying the values of the irreducible spin tensor moments T_κ^q ($|\kappa| \leq q \leq 2i$). Note that there are $(2i+1)^2$ independent elements in each description. It is especially convenient to use the tensor moments since the low-ranking tensors correspond naturally to such physical quantities as the differential cross section and polarization and since these elements transform covariantly under rotation. As in I, all tensor operators are defined so as to agree with the definitions given by Racah[5] and are so normalized that

$$T_0^q = P_q(i_z'/[i'(i'+1)]^{\frac{1}{2}}). \quad (2.6)$$

A partial listing of these operators is given in Sec. V. Since the tensor operators and the elements of the density matrix form complete sets, it should be possible to expand the density matrix in terms of the initial tensor moments. This expansion is performed in Appendix A. For the case of an unpolarized target nucleus the result is

$$\rho(s_1 m_1; s_2 m_2) = \frac{[(2s_1+1)(2s_2+1)]^{\frac{1}{2}}}{(2I+1)}(-1)^{m_2 - i + I} \times \sum_q \frac{(2i)!(2q+1)^{\frac{1}{2}}}{[(2i-q)!(2i+q+1)!]^{\frac{1}{2}}}(s_1 s_2 - m_1 m_2 | s_1 s_2 q - \kappa) \times \frac{W(i s_1 i s_2; I q)}{P_q([i/(i+1)]^{\frac{1}{2}})} T_\kappa^q, \quad (2.7)$$

[4] E. U. Condon and G. H. Shortley, *The Theory of Atomic Spectra* (Cambridge University Press, Cambridge, 1951).

[5] G. Racah, Phys. Rev. **62**, 442 (1942); references to this paper will be denoted by R.

where the tensor moments T_{κ}^{q} are with respect to the incoming particle of spin i. Note that $\kappa=m_1-m_2$. Hence, for a definite input tensor moment, all dependence on the magnetic quantum numbers is contained in a Clebsch-Gordan coefficient.

The operator $O(\mathbf{i}')$ will now be chosen to be any spin tensor operator $T_{\kappa'}^{q'}$. The reduction of the resultant spin matrix element $(\chi(s_1'm_1')|T_{\kappa'}^{q'}|\chi(s_2'm_2'))$ has been performed previously in Appendix A of I. It was shown in I (A.2) that

$$\begin{aligned}(\chi(s_1'm_1')|T_{\kappa'}^{q'}|\chi(s_2'm_2'))&=(-1)^{i'-\kappa'-i'+m_1'}(2q'+1)^{-\frac{1}{2}}[(2i')!]^{-1}\\&\times[(2s_1'+1)(2s_2'+1)(2i'-q')!(2i'+q'+1)!]^{\frac{1}{2}}\\&\times W(i's_1'i's_2';I'q')(s_1's_2'-m_1'm_2'|s_1's_2'q'-\kappa')\\&\times P_{q'}([i'/(i'+1)]^{\frac{1}{2}}).\end{aligned}\tag{2.8}$$

If we combine Eqs. (2.3), (2.5), (2.7), and (2.8), as well as Eq. I (2.8) for the product of two spherical harmonics, the following result is obtained:

$$\begin{aligned}\langle T_{\kappa'}^{q'}\rangle=&\frac{(\pi)^{\frac{1}{2}}\lambda_a^2(2i)!(2q+1)^{\frac{1}{2}}[(2i'-q')!(2i'+q'+1)!]^{\frac{1}{2}}}{2(2I+1)(2i')!(2q'+1)^{\frac{1}{2}}[(2i-q)!(2i+q+1)!]^{\frac{1}{2}}}\\&\times\frac{P_{q'}([i'/(i'+1)]^{\frac{1}{2}})}{P_q([i/(i+1)]^{\frac{1}{2}})}\sum(-1)^{\kappa-\kappa'+i-i'-I+I'+l_2-l_1-l_2'+l_1'}\\&\times(2l_1+1)(2l_2+1)(2l_1'+1)(2l_2'+1)(2s_1+1)\\&\times(2s_2+1)(2s_1'+1)(2s_2'+1)/(2r'+1)]^{\frac{1}{2}}\\&\times R(\alpha l_1s_1,\alpha'l_1's_1';J_1\pi_1)^*R(\alpha l_2s_2,\alpha'l_2's_2';J_2\pi_2)\\&\times W(is_1is_2;Iq)W(i's_1'i's_2';I'q')(l_1'l_2'00|l_1'l_2'r'0)\\&\times Y_{r',\kappa'-\kappa}(\theta\phi)T_{\kappa}^{q}\sum_{m_1}\sum_{m_1'}[(s_1s_2-m_1m_2|s_1s_2q-\kappa)\\&\times(s_1's_2'-m_1'm_2'|s_1's_2'q'-\kappa')\\&\times(l_1'l_2'-\mu_1'\mu_2'|l_1'l_2'r'\kappa'-\kappa)(l_1s_10m_1|l_1s_1J_1m_1)\\&\times(l_2s_20m_2|l_2s_2J_2m_2)(l_1's_1'\mu_1'm_1'|l_1's_1'J_1m_1)\\&\times(l_2's_2'\mu_2'm_2'|l_2's_2'J_2m_2)],\end{aligned}\tag{2.9}$$

where the first sum is over $l_1l_2l_1'l_2's_1s_2s_1's_2'J_1J_2\pi_1\pi_2$ and the auxiliary variable r'.

It has been assumed in this expression that there is only a single input tensor moment T_{κ}^{q}. (The effects of several input moments are additive.) Note that only two magnetic quantum numbers are still independent, since $\kappa=m_1-m_2$ and $\kappa'=m_1'-m_2'$. The remaining geometrical sums are eliminated in the next section.

III. ELIMINATION OF MAGNETIC SUMS AND GENERAL EXPRESSION FOR TENSOR MOMENTS

The sums over m_1 and m_1' may be eliminated by the repeated use of some Racah identities which have been summarized in a review paper by Biedenharn *et al.*[6] In particular, the identities BBR (1), (14), (18), (19), and the properties of the Fano X coefficient [reference 3 and also I, Appendix B] are needed. The details of this procedure, which is laborious but not illuminating, will not be given here, since the specific steps for a similar reduction were given in I.

The magnetic sum can be shown to reduce to the following expression

$$\begin{aligned}\sum_{r,L}&(-1)^{s_2'-s_2+l_2'+l_2}(2J_1+1)(2J_2+1)[(2q+1)(2q'+1)\\&\times(2r'+1)(2r+1)]^{\frac{1}{2}}(l_1l_200|l_1l_2r0)\\&\times(rq0\kappa|rqL\kappa)(r'q'\kappa-\kappa'\kappa'|r'q'L\kappa)\\&\times X(J_1l_1s_1;Lrq;J_2l_2s_2)X(J_1l_1's_1';Lr'q';J_2l_2's_2'),\end{aligned}\tag{3.1}$$

where X is the coefficient defined by Fano,[3] and L and r are auxiliary variables. This expression is the generalization of I (3.1).

If Eq. (3.1) is substituted in Eq. (2.9), there results an expression for the final tensor moment $T_{\kappa'}^{q'}$. The tensor moment $T_{\kappa'}^{q'}$, however, is measured with respect to the coordinate system with z axis along the direction of the incident particle. A more convenient and symmetrical form results if the final tensor moment is measured with respect to a coordinate system along the direction of the final particle. If the incident beam direction is denoted by $\mathbf{k}$ and the scattered direction by $\mathbf{k}'$, let us choose a new coordinate system with z' axis along $\mathbf{k}'$ and with the y' axis along $\mathbf{k}\times\mathbf{k}'$. The Euler angles of this rotation are then $(\phi,\theta,0)$ relative to the original coordinate system.

The spin tensor operator $T_{u'}^{q'}$ in the new system is then related to the spin tensor operators $T_{\kappa'}^{q'}$ in the original coordinate system by the relation[7]

$$T_{\mu'}^{q'}=\sum_{\kappa'}D_{\kappa',\mu'}^{(q')}(\phi,\theta,0)T_{\kappa'}^{q'},$$

where $D_{\kappa',\mu'}^{(q')}$ is an element of the three-dimensional rotation group. The complete dependence on κ' of the expression for $T_{\kappa'}^{q'}$ is now contained in the factors

$$(-1)^{-\kappa'}(r'q'\kappa-\kappa'\kappa'|r'q'L\kappa)Y_{r',\kappa'-\kappa}(\theta,\phi).$$

Hence, the new tensor moment contains the transformed factors

$$\sum_{\kappa'}(-1)^{-\kappa'}D_{\kappa',\mu'}^{(q')}(\phi,\theta,0)(r'q'\kappa-\kappa'\kappa'|r'q'L\kappa)\times Y_{r',\kappa'-\kappa}(\theta,\phi).$$

The sum over κ' may be performed by expressing $Y_{r',\kappa'-\kappa}$ as a D function and using a relation for the product of two D functions [see the paragraph in I

[6] Biedenharn, Blatt, and Rose, Revs. Modern Phys. **24**, 249 (1952); references to this paper will be designated by BBR.

[7] E. Wigner, *Gruppentheorie* (F. Vieweg, Braunschweig, 1931), p. 165.

following I (6.5)]. The transformed factors become

$$(-1)^{\kappa}(r'q'0\mu'|r'q'L\mu')D_{\kappa,\mu'}{}^{(L)}(\phi,\theta,0)[(2r'+1)/4\pi]^{\frac{1}{2}}.$$

The complete expression for the final spin tensor moment $T_{\kappa'}{}^{q'}$ (measured with respect to the scattered axis) resulting from an initial spin tensor moment $T_{\kappa}{}^{q}$ (measured with respect to the incident axis) is obtained by substituting Eq. (3.1) in Eq. (2.9) and making the transformation described in the previous paragraph. The result is

$$\langle T_{\kappa'}{}^{q'}\rangle=\frac{\lambda_a{}^2(2i)![(2i'-q')!(2i'+q'+1)!]^{\frac{1}{2}}(2q+1)^{\frac{1}{2}}P_{q'}([i'/(i'+1)]^{\frac{1}{2}})}{4(2I+1)(2i')![(2i-q)!(2i+q+1)!]^{\frac{1}{2}}(2q'+1)^{\frac{1}{2}}P_q([i/(i+1)]^{\frac{1}{2}})}\sum R^*(\alpha l_1 s_1,\alpha' l_1' s_1';J_1\pi_1)$$
$$\times R(\alpha l_2 s_2,\alpha' l_2' s_2',J_2\pi_2)W(is_1\,is_2;Iq)W(i's_1'i's_2';I'q')(-1)^{s_2+s_2'+i-I+\nu'-I'+\kappa'}D_{\kappa,\kappa'}{}^{(L)}(\phi,\theta,0)T_{\kappa}{}^{q}$$
$$\times G_{\kappa}{}^*(J_1l_1s_1,L\quad q,J_2l_2s_2)G_{\kappa'}(J_1l_1's_1',L\quad q',J_2l_2's_2'),\quad(3.2)$$

where the sum is over $l_1l_2l_1'l_2's_1s_2s_1's_2'J_1J_2\pi_1\pi_2L$, and where the G function is defined in terms of the X function as (note that this definition has been changed somewhat from that given in a previous communication[8]):

$$G_{\kappa}(J_1l_1s_1,L\quad q,J_2l_2s_2)$$
$$=[(2l_1+1)(2l_2+1)(2s_1+1)(2s_2+1)]^{\frac{1}{2}}$$
$$\times[(2J_1+1)(2J_2+1)(2q+1)(2L+1)]^{\frac{1}{2}}$$
$$\times i^{l_1+l_2}\sum_r(l_1l_200|l_1l_2r0)(qL\kappa-\kappa|qLr0)$$
$$\times X(J_1l_1s_1,Lrq,J_2l_2s_2).\quad(3.3)$$

Equation (3.2) is the most general result derived in this paper. All selection rules are contained in the G coefficient. These selection rules are discussed in the next section. A short summary of the properties of the G function is contained in Appendix B. In addition, two alternative expressions for G are given in Eqs. (B.7) and (B.8). Although these expressions are less symmetric than Eq. (3.3), they are much simpler for computational purposes and for many algebraic reductions, such as occur in changes of representation.

IV. SELECTION RULES AND DEGREE OF ANGULAR COMPLEXITY

The selection rules for any nuclear problem, corresponding to specific choices of q, q', κ, and κ', can easily be read off from the properties of the G coefficient. Some of these are mentioned in the next section. A few general statements may also be made.

(a) If the subscripts 1 and 2 are interchanged in Eq. (3.2), the resulting expression may be restored to its original form by the use of the symmetry properties of the G function and BBR (14). The only new factor appearing after this process is the phase factor $(-1)^{q+q'}$. Hence, if $q+q'$ is even, the elements of the R matrix in a calculation can always be written in the form $R^*(1)R(2)+R(1)R^*(2)$. If $q+q'$ is odd, an interference term $R^*(1)R(2)-R(1)R^*(2)$ always results.

It was pointed out in I (footnote 13) that the elements of the S matrix resulting from the use of perturbation theory or the Born approximation are all real. Hence, in these approximations, there will be no contribution to a process in which $q+q'$ is odd.

(b) If both κ and κ' are zero, Eq. (B.4) along with conservation of parity requires that $q+q'$ be even. Thus, for example, there can be no transitions from $q=0$, $\kappa=0$ to $q=1$, $\kappa=0$. This is the reason why the polarization produced in a nuclear reaction lies along the tangent plane.

(c) The maximum complexity of the angular dependence is given by the largest permissible value of L. If there is a largest incident orbital angular momentum $l_{\max}$, total angular momentum $J_{\max}$ or final orbital momentum $l'_{\max}$, the largest value of L is given by the simultaneous conditions

$$L\leq\begin{cases}2l_{\max}+q\\ 2l_{\max}+q-1 & (\kappa'=0,\kappa\neq0,\ q+q'\text{ odd})\\ 2J_{\max}\\ 2l'_{\max}+q'\\ 2l'_{\max}+q'-1 & (\kappa=0,\kappa'\neq0,\ q+q'\text{ odd}).\end{cases}$$

These rules are easily seen to follow from Eqs. (B.2), (B.3), and (B.4).

V. APPLICATIONS TO SPECIFIC PROCESSES

An expression for a given reaction measurement is obtained by a particular choice of q, q', κ, and κ' in Eq. (3.2). For example, an initially unpolarized beam is specified by $T_{\kappa}{}^{q}=1$ for $q=\kappa=0$ and zero for all other values. It is convenient to list the values of some of the simpler tensor moments in terms of spin operators $\mathbf{s}$:

$$T_0{}^0=1,\quad T_0{}^1=\mathbf{s}_z/[s(s+1)]^{\frac{1}{2}},$$
$$T_{\pm1}{}^1=\mp(\mathbf{s}_x\pm i\mathbf{s}_y)/[2s(s+1)]^{\frac{1}{2}},$$
$$T_0{}^2=[3\mathbf{s}_z{}^2-s(s+1)]/[2s(s+1)],$$
$$T_{\pm1}{}^2=\mp(\sqrt{6}/4)[(\mathbf{s}_z\pm i\mathbf{s}_y)\mathbf{s}_z+\mathbf{s}_z(\mathbf{s}_z\pm i\mathbf{s}_y)]/[s(s+1)],$$
$$T_{\pm2}{}^2=(\sqrt{6}/4)(\mathbf{s}_z\pm i\mathbf{s}_y)(\mathbf{s}_z\pm i\mathbf{s}_y)/[s(s+1)].$$

Angular Distribution of Nuclear Reactions

The angular distribution resulting from an unpolarized initial beam corresponds to $q'=q=\kappa'=\kappa=0$. The result given in BB (3.16), (4.5), and (4.6) is obtained

[8] A. Simon, Phys. Rev. **90**, 991 (1953). Equation (1) of this letter has a misprint in it. The phase factor should be $(-1)^{\kappa}$ rather than $(-1)^{\kappa'}$.

from Eq. (3.2) by use of Eq. (B.9) and BBR (30).

$$\frac{d\sigma}{d\Omega}=\frac{\lambda_\alpha^2}{4(2i+1)(2I+1)}\sum(-1)^{s'-s}R^*(\alpha sl_1,\alpha' s'l_1';J_1\pi_1)$$
$$\times R(\alpha sl_2,\alpha' s'l_2';J_2\pi_2)Z(l_1J_1l_2J_2,sL)$$
$$\times Z(l_1'J_1l_2'J_2;s'L)P_L(\cos\theta),\quad(5.1)$$

where the sum is over $ss'l_1l_2l_1'l_2'J_1J_2\pi_1\pi_2$ and L.

Polarized Particles From Nuclear Reactions

The result given in I(3.2) for the polarization resulting from a reaction initiated by unpolarized particles is easily obtained by setting $q'=1$, $\kappa'=\pm1$ and $q=\kappa=0$. Note that I(3.2) is the expectation value of the operator $\mathbf{i}'/[i'(i'+1)]^{\frac{1}{2}}$. This is related to f, the percentage polarization in the final state, by

$$d|\mathbf{P}|=[i'/(i'+1)]^{\frac{1}{2}}fd\sigma,\quad(5.2)$$

where $d\sigma$ is the differential cross section for the reaction.

Detection of Polarized Particles of Spin 1/2

The most convenient way to detect the polarization of a spin-$\frac{1}{2}$ particle is to observe the angular distribution of a subsequent reaction initiated by this particle. A general expression for this cross section can be derived.

Let $\mathbf{k}_1$ be the direction of an initially unpolarized beam, which produces a polarized particle of spin i ($i=\frac{1}{2}$). The intermediate particle i is taken off in the direction $\mathbf{k}_2$, which is specified by the angles θ, ϕ with respect to $\mathbf{k}_1$, and allowed to bombard an unpolarized nucleus of spin I. The final reaction product which is of spin i' is observed in the direction $\mathbf{k}_3$, which has the angles $\theta'\phi'$ relative to $\mathbf{k}_2$. The spin of the final residual nucleus is I'. (Note that *only* the intermediate particle i need be of spin $\frac{1}{2}$.)

The initial system in state 1, being unpolarized, will contain only the tensor moment $q=0$, $\kappa=0$. The intermediate system then contains the three tensor moments T_0^0, T_1^1, and T_{-1}^1. (Note that T_0^1 is excluded by selection rule (b) of Sec. IV; all tensor moments are measured with respect to the beam axis.) These tensors contribute additively to the final angular distribution, which is the expectation value of T_0^0 in the final state.

One component of the final measurement can be written symbolically as $T_0^0(1)\rightarrow T_0^0(2)\rightarrow T_0^0(3)$, which is clearly equivalent to $d\sigma(\theta)d\sigma(\theta')$. Here $d\sigma(\theta)$ is the differential cross section for the first reaction, and $d\sigma(\theta')$ is what the cross section would be for the second reaction *if the intermediate beam were unpolarized*. The remaining components are simplified if one verifies that by the symmetry properties of the R matrix, the properties of the D function,[7] and Eq. (3.2)

$$T_{\pm1}^1(2)\rightarrow T_0^0(3)=3(2i'+1)(2I'+1)/[(2i+1)(2I+1)]$$
$$\times[T_0^0(3)\rightarrow T_{\mp1}^1(2)].\quad(5.3)$$

Now by Eq. (5.2) the last bracket in the above expression can be written essentially as

$$[i/(i+1)]^{\frac{1}{2}}f(3\rightarrow2)d\sigma(3\rightarrow2),\quad(5.4)$$

where $f(3\rightarrow2)$ is the percentage polarization which would result if the second reaction were reversed in time, with the system in state 3 being unpolarized. But clearly

$$(2i'+1)(2I'+1)d\sigma(3\rightarrow2)=(2i+1)(2I+1)d\sigma(2\rightarrow3)$$
$$\equiv(2i+1)(2I+1)d\sigma(\theta').\quad(5.5)$$

If we combine Eqs. (5.2), (5.3), (5.4), and (5.5), the second component of the final angular distribution can be written as

$$T_0^0(1)\rightarrow T_{\pm1}^1(2)\rightarrow T_0^0(3)$$
$$=\mathbf{n}_1\cdot\mathbf{n}_2f(1\rightarrow2)f(3\rightarrow2)d\sigma(\theta)d\sigma(\theta'),$$

where $\mathbf{n}_1\sim\mathbf{k}_1\times\mathbf{k}_2$ and $\mathbf{n}_2\sim\mathbf{k}_2\times\mathbf{k}_3$ are unit vectors along the indicated normals to the scattering planes.

The observed angular distribution has the complete form

$$d\sigma(\theta)d\sigma(\theta')[1+\mathbf{n}_1\cdot\mathbf{n}_2f(1\rightarrow2)f(3\rightarrow2)].\quad(5.6)$$

Hence, the polarization is directly related to the azimuthal asymmetry of the second reaction. A similar result was given by Lepore[9] for the special case of the double elastic scattering of spin $\frac{1}{2}$ particles by spin zero nuclei. With these restrictions $f(3\rightarrow2)=f(2\rightarrow3)$, and Lepore's result follows.

Radiations from Polarized Nuclei

The problem of the decay of an arbitrarily polarized initial nucleus can be regarded as a special case of the general result given in Eq. (3.2). If the radiating nucleus is taken to be in the state designated by $\alpha J\pi$, the specialization is made by the following recipe:

(a) Replace $S(\alpha l_1s_1,\alpha'l_1's_1',J_1\pi_1)$ with

$$S(\alpha0J,\alpha'l_1's_1';J\pi)\delta(l_1,0)\delta(s_1,J).$$

(b) Set $i=J$ and $I=0$.

(c) Divide Eq. (3.2) by $\pi\lambda_\alpha^2$.

This recipe assures that there will be only a single initial state of the entire system of angular momentum J. In addition, the amplitude of this state is chosen to be unity.

The application of this recipe to Eq. (3.2) results in the following expression

$$T_{\kappa'}^{q'}=\frac{(2J)![(2i'-q')!(2i'+q'+1)!(2q+1)]^{\frac{1}{2}}P_{q'}([i'/(i'+1)]^{\frac{1}{2}})}{4\pi(2i')![(2J-q)!(2J+q+1)!(2q'+1)]^{\frac{1}{2}}P_q([J/(J+1)]^{\frac{1}{2}})}R^*(\alpha0J,\alpha'l_1's_1';J\pi)R(\alpha0J,\alpha'l_2's_2';J\pi)$$
$$\times W(i's_1'i's_2';I'q')(-1)^{s_2'+i'-I'+\kappa'+\kappa}D_{\kappa,\kappa'}^{(q)}(\phi,\theta,0)G_{\kappa'}(Jl_1's_1',q\quad q',Jl_2's_2')T_\kappa^q,\quad(5.7)$$

[9] J. V. Lepore, Phys. Rev. **79**, 139 (1950).

where the sum is only over $l_1'l_2's_1'$ and s_2'. Here T_κ^q is a spin tensor moment of the arbitrarily polarized initial nucleus. The final tensor moment $T_{\kappa'}^{q'}$ of the particle i' is measured with respect to its direction of motion $\mathbf{k}'$. The angles θ, ϕ relate $\mathbf{k}'$ to the initial axis of quantization of J.

Expressions for the angular distribution ($q'=\kappa'=0$) and polarization ($q'=1$, $\kappa'=\pm1$) of the emitted particles are easily obtained from Eq. (5.7). Up to the present time, chief interest has been centered on gamma radiation by polarized nuclei. In this case, the channel spin representation is not convenient; and, instead, one must use a representation involving the multipole expansions of the gamma-ray field. This point is treated in the next section. It is worth noting that, when the nuclear polarization has been accomplished by magnetic or electric fields, the resultant cylindrical symmetry requires that only initial tensor moments with $\kappa=0$ appear. The angular dependence then simplifies since

$$D_{0,\kappa}^{(q)}(\phi,\theta,0)=(-1)^{(\kappa-\kappa)/2}\times[(q-|\kappa|)!/(q+|\kappa|)!]^{\frac{1}{2}}P_q^\kappa(\theta),$$

where P_q^κ is the usual associated Legendre function.

VI. GAMMA RAYS IN NUCLEAR REACTIONS

The S-matrix formalism may be extended to include the possibility of gamma rays in nuclear reactions. In this case, the vector potential $\mathbf{A}$ plays the role of the "wave function" for the particle. A formal proof of this equivalence which will not be given here requires the procedure of second quantization.[10]

The vector potential field is customarily expanded in terms of electric and magnetic multipoles, $\mathbf{A}(L,M,p)$. The total angular momentum of the multipole and the z component are denoted by L and M. The "parity" symbol p, which is defined to have the value 0 for magnetic radiation and 1 for electric radiation, is related to the actual parities in the vector field by

$$\text{parity}=(-1)^L \quad \text{for } p=0, \text{ magnetic}$$
$$=(-1)^{L+1} \qquad p=1, \text{ electric}.$$

The specific definition of the multipoles which will be used in this section is as follows:

$$\mathbf{A}(L,M,p)=-\sqrt{2}\sum_{\kappa,l}{}'(l\,1\,M-\kappa\,\kappa|l\,1\,L\,M)\times(L\,1\,-1\,1|L\,1\,l\,0)i^{l-L}\mathbf{u}_\kappa Y_{l,M-\kappa}(\theta,\phi)\times\exp[i(kr-l\pi/2)], \quad (6.1)$$

where the prime on the summation symbol indicates that only the term $l=L$ is to be included in the sum if $p=0$ and only the terms $l=L\pm1$ if $p=1$. The symbol $\mathbf{u}_\kappa$ denotes an irreducible component of the vector part of $\mathbf{A}$ and is defined in terms of the unit vectors $\mathbf{e}_1\mathbf{e}_2\mathbf{e}_3$ along the coordinate axis as

$$\mathbf{u}_{\pm1}=\mp(\mathbf{e}_1\pm i\mathbf{e}_2)/\sqrt{2}, \quad \mathbf{u}_0=\mathbf{e}_3.$$

Note that $\mathbf{A}(L,M,p)$ as written above consists of outgoing spherical waves only. The incoming spherical waves have the same definitions, but with a reversed sign in the exponential.

The normalization of $\mathbf{A}(L,M,p)$ has been chosen so that its absolute square integrates to unity over the solid angle. The first Clebsch-Gordan factor has the algebraic values:

$$(L\,1\,-1\,1|L\,1\,L\,0)=-1/\sqrt{2};$$
$$(L\,1\,-1\,1|L\,1\,L+1\,0)=[L/2(2L+1)]^{\frac{1}{2}};$$
$$(L\,1\,-1\,1|L\,1\,L-1\,0)=[(L+1)/2(2L+1)]^{\frac{1}{2}};$$

and in this form the multipoles may be recognized as essentially those given by Goertzel.[11] We prefer to keep this factor in the form of a Clebsch-Gordan coefficient, since a single algebraic expression will then suffice for all multipoles. The multipoles as defined above are everywhere transverse to the radial direction, as may be easily verified. The remaining longitudinal multipoles, which are excluded in the case of the electromagnetic field, are obtained immediately by replacing

$$(L\,1\,-1\,1|L\,1\,l\,1) \quad \text{by} \quad (L\,1\,0\,0|L\,1\,l\,0)$$

in Eq. (6.1).

The composite system consisting of a gamma-ray and a residual (or target) nucleus of spin I is now specified by the quantum numbers αJm_JLp, where J and m_J are the total angular momentum and z component of the entire system. This representation is very similar to the representation in which the angular momentum and spin of a bombarding "particle" (in this case a gamma ray of spin 1) are combined to form a definite j (which is the L of the multipole), which then combines with the nuclear spin I to form a total state specified by J and m_J. Our previous formulas for the particle reactions may now be extended to include gamma rays by simply changing from the channel spin to the multipole representation. Let us consider first the case of a reaction in which a particle comes in and a gamma ray comes out.

Particle In and Gamma Ray Out

For this reaction we wish to use a mixed representation for the R matrix in which the initial states are still in the channel spin representation, and the final states are in the multipole representation. By the usual transformation theory,

$$R(\alpha ls,\alpha'l's',J\pi)\rightarrow\sum_{L'p'}R(\alpha ls,\alpha'L'p';J\pi)\times(L'p'J\pi\|l's'J\pi). \quad (6.2)$$

Racah[12] has shown that the transformation matrix,

[10] See, e.g., J. A. Spiers, *Directional Effects in Radioactivity* (National Research Council of Canada, Ontario, 1949), Appendix II.

[11] G. Goertzel, Phys. Rev. **70**, 905 (1946).

[12] G. Racah, Phys. Rev. **63**, 367 (1943).

which represents the recoupling of three angular moments (l, 1, and I) must have the form of a Racah function. It is easy to show that the exact relation is

$$(L'p'J\pi\|l's'J\pi)$$
$$=-\sqrt{2}[(2L'+1)(2s'+1)]^{\frac{1}{2}}W(l'\,1\,J\,I';\,L's')$$
$$\times(L'\,1\,-1\,1|\,L'\,1\,l'\,0)i^{L'-l'}\delta(l',\,p'), \quad (6.3)$$

where the δ symbol vanishes if l' does not have the proper parity corresponding to p' and has the value unity otherwise. If Eqs. (6.2) and (6.3) are now substituted in the general expression of Eq. (3.2), the sums over s_1', s_2', l_1', and l_2' may then be performed without any detailed knowledge of the R matrix. (Note that $i'=1$.) The sum over s_2' is performed first by the use of BBR (17). Then this identity is used again to obtain the sum over s_1'.

We prefer not to do the sum on l_1' and l_2' explicitly in order that a single expression be valid for all choices of the multipole "parity." The final result is

$$T_{\kappa'}^{q'}=\frac{\lambda_a^2(2i)![(2-q')!(3+q')!]^{\frac{1}{2}}(2q+1)^{\frac{1}{2}}P_{q'}(\sqrt{\frac{1}{2}})}{12(2I+1)[(2i-q)!(2i+q+1)!(2q'+1)]^{\frac{1}{2}}P_q([i/i+1]^{\frac{1}{2}})}\sum R^*(\alpha l_1s_1,\,\alpha'L_1'p_1';\,J_1\pi_1)$$
$$\times R(\alpha'_2s_2,\,\alpha'L_2'p_2';\,J_{2\pi_2})(L_1'\,1\,-1\,1|\,L_1'\,1\,l_1'\,0)(L_2\;1\,-1\,1|\,L_2'\,1\,l_2'\,0)\delta(l_1',\,p_1')\delta(l_2',\,p_2')$$
$$\times[(2J_1+1)(2J_2+1)]^{\frac{1}{2}}(-1)^{L_2-L_1'+l_1'-l_2'}(-1)^{J_2+s_2+L_1'+q'-L+i-I-I'+\kappa'}W(is_1is_2;\,Iq)W(J_1L_1'J_2L_2';\,I'L)$$
$$\times D_{\kappa,\kappa'}^{(L)}(\phi\theta0)\,T_\kappa^q\,G_\kappa^*(J_1l_1s_1;\,L\quad q;\,J_2l_2s_2)G_{\kappa'}(L_1'l_1'1;\,L\quad q';\,L_2'l_2'1), \quad (6.4)$$

where the sum is over $l_1l_2s_1s_2J_1J_2\pi_1\pi_2L_1'L_2'p_1'p_2'l_1'$ and l_2'. It is worth reminding the reader that the δ symbols signify that for magnetic multipole radiation, $p=0$, we have $l=L$. For electric multipole radiation $p=1$, we have $l=L\pm1$.

The meaning of the final spin tensor moments $T_{\kappa'}^{q'}$ for the gamma-ray case requires some clarification. It is clear that a pure gamma-ray state requires only two states U_1 and U_{-1}, corresponding to right and left circular polarization respectively for its description. Hence the statistical density matrix will have only four independent components, rather than nine as would be the case for the usual particle of spin one. Since our selection rules appear to allow all tensor moments up to $q'=2$, it is also clear that only four of these moments may be independent in the gamma-ray case.

A comparison with the listing of spin operators at the beginning of Sec. V resolves the ambiguity. First of all, it is easy to recognize that the tensor moments T_1^1, T_{-1}^1, T_1^2, and T_{-1}^2 must be identically zero. To see this, note that these four operators are proportional to the spin operators s_+ or s_- which have nonzero matrix elements only between states whose magnetic components differ by unity. The only available states for the gamma ray are U_1 and U_{-1} which differ by 0 or 2. In addition, the operator T_0^2 is equivalent to T_0^0 since both these states have $s_z^2=1$. Hence, the four independent operators are T_0^0, T_0^1, T_2^2, and T_{-2}^2. These have simple relations to the physical measurements which are listed below:

T_0^0	intensity
$\sqrt{2}\,T_0^1$	circular polarization intensity
$4\sqrt{\frac{2}{3}}\,T_2^2$	$Ae^{-i2\phi}$ where A is the intensity of the linear polarization, and ϕ is its azimuthal angle relative to the normal to the scattering plane.
$4\sqrt{\frac{2}{3}}\,T_{-2}^2$	$Ae^{i2\phi}$

These parameters are essentially the Stoke's parameter description of the polarization of a beam of light as has been clearly pointed out by Fano.[3] A more complete discussion may be found in Appendix A of this reference.

The relations given above between the polarization of a gamma-ray and its tensor moments allows several selection rules to be read off from Eq. (6.4). These are:

(a) Circularly polarized light cannot result from a nuclear reaction initiated by unpolarized particles (i.e., no $T_0^0\rightarrow T_0^1$). This is a special case of the selection rule given in Sec. IV (b).

(b) Linearly polarized light cannot be the product of a nuclear reaction initiated by s-wave particles of spin $\frac{1}{2}$.[13] To see this, note that the "tetrad" condition on the first G function $(l_1\,l_2\,L\,q)$ requires that L be either 1 or 0. However, $\kappa'=\pm2$ for linear polarization. Hence, the second G function must vanish by Eq. (B.5).

Gamma Ray In and Particle Out

The derivation of this result follows in a manner similar to the previous case. The only added difficulty is that one must recall that incident gamma-rays of right and left circular polarizations, upon expansion into multipoles, have opposite phases for the amplitudes of the electric components. In particular, if one expands a plane wave along the z axis of circular polarization P $(P=\pm1)$ into multipoles, the probability amplitude of the state of multipolarity L and parity p $(=0$ or $1)$ is $(P)^p i^{L+1}[(2L+1)\pi/2]^{\frac{1}{2}}\lambda$, which differs from the particle case by the extra factor $(P)^p$.

[13] This result was also obtained by Biedenharn, Rose, and Arfken, Phys. Rev. **83**, 683 (1951), by invoking Lloyd's theorem. The use of Lloyd's theorem, which is only an approximate relation [see F. Coester, Phys. Rev. **89**, 620 (1953)], is unnecessary in this problem since the result is an exact selection rule. To see this, note that the sums over m and M in Eq. (3) of Biedenharn *et al.* can be performed and reduce the anisotropic term to zero identically. The alternative proof of Lloyd's theorem given in footnote 5 of this reference is then invalid.

Now if the initial density matrix is expressed in terms of the averaged amplitudes of the states of circular polarization $a(+1)$ and $a(-1)$, we have:

$$D_{1,1}=|a(+1)|^2,$$
$$D_{-1,-1}=|a(-1)|^2,$$
$$D_{1,-1}=a^*(+1)a(-1),$$
$$D_{-1,1}=a(+1)a^*(-1).$$

As we have just seen, however, the terms $a(-1)$ will have the factors $(-1)^p$ in the multipole expansion. In addition, it is clear from the spin operator definition of the tensor moments that

$$T_0^0=D_{1,1}+D_{-1,-1},$$
$$T_0^1\sim D_{1,1}-D_{-1,-1},$$
$$T_2^2\sim D_{1,-1},$$
$$T_{-2}^2\sim D_{-1,1}.$$

Hence, the proper initial tensor moments for the gamma-ray case are:

$$T_0^0[1+(-1)^{p_1+p_2}]/2,$$
$$T_0^1[1-(-1)^{p_1+p_2}]/2,$$
$$T_2^2(-1)^{p_2},$$
$$T_{-2}^2(-1)^{p_1}.$$

In addition, the new expression must be multiplied by $\frac{3}{2}$ to correct for the statistical factor. The final expression for the case of a gamma-ray incident and a particle emerging is then:

$$T_{\kappa\kappa'}^{qq'}=\frac{\lambda_\gamma^2[(2i'-q')!(2i'+q'+1)!(2q+1)]^{\frac{1}{2}}P_{q'}([i'/i'+1]^{\frac{1}{2}})}{2(2I+1)(2i')![(2-q)!(3+q)!(2q'+1)]^{\frac{1}{2}}P_q(1/\sqrt{2})}\sum R^*(\alpha L_1 p_1,\alpha' l_1' s_1';J_1\pi_1)R(\alpha L_2 p_2,\alpha' l_2' s_2';J_2\pi_2)$$
$$\times(L_1\,1\,-1\,1|L_1\,1\,l_1\,0)(L_2\,1\,-1\,1|L_2\,1\,l_2\,0)\delta(l_1,p_1)\delta(l_2,p_2)[(2J_1+1)(2J_2+1)]^{\frac{1}{2}}\,i^{L_1-L_2-l_1+l_2}$$
$$\times(-1)^{J_2+s_2'+L_1+q-L+i'-I'-I+\kappa'}W(J_1L_1J_2L_2;IL)W(i's_1'i's_2';I'q')D_{\kappa,\kappa'}^{(L)}(\phi,\theta,0)$$
$$\times G_\kappa^*(L_1\,l_1\,1;L\quad q;L_2\,l_2\,1)G_{\kappa'}(J_1l_1's_1';L\quad q';J_2l_2's_2')f(p_1p_2q\kappa)T_\kappa^q,\quad(6.5)$$

where

$$f(p_1p_2q\kappa)=[1+(-1)^{p_1+p_2}]/2\quad\text{for } q=\kappa=0,$$
$$=[1-(-1)^{p_1+p_2}]/2\qquad q=1,\ \kappa=0,$$
$$=(-1)^{p_2}\qquad q=2,\ \kappa=2,$$
$$=(-1)^{p_1}\qquad q=2,\ \kappa=-2.$$

Gamma Ray In and Gamma Ray Out

This expression follows immediately from the previous results.

$$T_{\kappa\kappa'}^{qq'}=\frac{\lambda_\gamma^2[(2-q')!(3+q')!(2q+1)]^{\frac{1}{2}}P_{q'}(1/\sqrt{2})}{6(2I+1)[(2-q)!(3+q)!(2q'+1)]^{\frac{1}{2}}P_q(1/\sqrt{2})}$$
$$\times R^*(\alpha L_1p_1,\alpha' L_1'p_1';J_1\pi_1)R(\alpha L_2p_2,\alpha' L_2'p_2';J_2\pi_2)$$
$$\times(L_1\,1\,-1\,1|L_1\,1\,l_1\,0)(L_2\,1\,-1\,1|L_2\,1\,l_2\,0)$$
$$\times(L_1'\,1\,-1\,1|L_1'\,1\,l_1'\,0)(L_2'\,1\,-1\,1|L_2'\,1\,l_2'\,0)$$
$$\times\delta(l_1p_1)\delta(l_2p_2)\delta(l_1'p_1')\delta(l_2'p_2')(2J_1+1)(2J_2+1)$$
$$\times i^{L_1-L_2-l_1+l_2-L_1'+L_2'+l_1'-l_2'}(-1)^{I-I'+L_1'+L_1+q+q'+\kappa'}$$
$$\times W(J_1L_1J_2L_2;IL)W(J_1L_1'J_2L_2';I'L)$$
$$\times D_{\kappa,\kappa'}^{(L)}(\phi,\theta,0)T_\kappa^qG_\kappa^*(L_1l_1\,1;L\quad q;L_2l_2\,1)$$
$$\times G_{\kappa'}(L_1'l_1'\,1;L\quad q';L_2'l_2'\,1)f(p_1p_2q\kappa),\quad(6.6)$$

where f has the same definition as in Eq. (6.5).

Angular Distribution of Nuclear Reactions Involving Gamma Rays

The most frequent use of the previous general results are in the analysis of angular distributions of nuclear reactions. For this reason, it is convenient to list the results for the special case of the angular distribution ($q'=\kappa'=0$) resulting from a reaction initiated by unpolarized beams ($q=\kappa=0$). The results are expressed in terms of the Z coefficient defined in BB (4.3).

Particle In and Gamma Ray Out

$$d\sigma=(\lambda^2/2)(2i+1)^{-1}(2I+1)^{-1}$$
$$\times\sum R^*(\alpha l_1s,\alpha' L_1'p_1';J_1\pi_1)$$
$$\times R(\alpha l_2s,\alpha' L_2'p_2';J_2\pi_2)(L_1'\,1\,-1\,1|L_1'\,1\,l_1'\,0)$$
$$\times(L_2'\,1\,-1\,1|L_2'\,1\,l_2'\,0)\delta(l_1',p_1')\delta(l_2',p_2')$$
$$i^{L_2'-L_1'+l_1'-l_2'}(-1)^{s-I'-L+L_1'-L_2'+1}$$
$$\times W(J_1L_1'J_2L_2';I'L)Z(l_1J_1l_2J_2;sL)P_L(\theta)$$
$$\times Z(l_1'L_1'l_2'L_2';1\,L)$$
$$\times[(2J_1+1)(2J_2+1)]^{\frac{1}{2}}d\Omega,\quad(6.7)$$

where the sum is over $l_1l_2L_1'L_2'l_1'l_2'p_1'p_2'sJ_1J_2\pi_1\pi_2$ and L.

Gamma Ray In and Particle Out

$$d\sigma=(\lambda^2/4)(2I+1)^{-1}\sum R^*(\alpha L_1p,\alpha' l_1's';J_1\pi_1)$$
$$\times R(\alpha L_2p,\alpha' l_2's';J_2\pi_2)(L_1\,1\,-1\,1|L_1\,1\,l_1\,0)$$
$$\times(L_2\,1\,-1\,1|L_2\,1\,l_2\,0)\delta(l_1p)\delta(l_2p)$$
$$\times[(2J_1+1)(2J_2+1)]^{\frac{1}{2}}i^{L_2-L_1+l_1-l_2}$$
$$\times(-1)^{s'-I-L+L_1-L_2+1}W(J_1L_1J_2L_2;IL)$$
$$\times Z(l_1L_1l_2L_2;1\,L)Z(l_1'J_1l_2'J_2;s'L)$$
$$\times P_L(\theta)d\Omega,\quad(6.8)$$

where the sum is over $L_1L_2l_1l_2J_1J_2\pi_1\pi_2l_1'l_2's'p$ and L.

Gamma Ray In and Gamma Ray Out

$$d\sigma=(\lambda^2/2)(2I+1)^{-1}\sum R^*(\alpha L_1 p,\alpha' L_1' p_1';J_1\pi_1)R(\alpha L_2 p,\alpha' L_2' p_2';J_2\pi_2)(L_1\,1\,-1\,1\,|\,L_1\,1\,l_1\,0)$$
$$\times(L_2\,1\,-1\,1\,|\,L_2\,1\,l_2\,0)(L_1'\,1\,-1\,1\,|\,L_1'\,1\,l_1'\,0)(L_2'\,1\,-1\,1\,|\,L_2'\,1\,l_2'\,0)\delta(l_1 p)\delta(l_2 p)$$
$$\times\delta(l_1',p_1')\delta(l_2',p_2')(2J_1+1)(2J_2+1)i^{L_1-L_2-l_1+l_2-L_1'+L_2'+l_1'-l_2'}(-1)^{I-I'+L_1'+L_1-L_2'-L_2}W(J_1L_1J_2L_2;IL)$$
$$\times W(J_1L_1'J_2L_2';I'L)Z(l_1L_1l_2L_2;1L)Z(l_1'L_1'l_2'L_2';1L)P_L(\theta)d\Omega, \quad (6.9)$$

where the sum is over $L_1L_2L_1'L_2'l_1l_2l_1'l_2'J_1J_2\pi_1\pi_2pp_1'p_2'$ and L.

Gamma Radiation from Polarized Nuclei

The general result for gamma radiation is obtained by applying the recipe given under the last subheading of Sec. V to Eq. (6.4) .The result is

$$T_{\kappa'}^{q'}=\frac{(2J+1)![(2-q')!(3+q')!(2q+1)]^{\frac{1}{2}}P_{q'}(\sqrt{\frac{1}{2}})}{12\pi[(2J-q)!(2J+q+1)!(2q'+1)]^{\frac{1}{2}}P_q([J/J+1]^{\frac{1}{2}})}\sum R^*(\alpha 0J,\alpha' L_1' p_1';J\pi)R(\alpha 0J,\alpha' L_2' p_2';J\pi)$$
$$\times(L_1'\,1\,-1\,1\,|\,L_1'\,1\,l_1'\,0)(L_2'\,1\,-1\,1\,|\,L_2'\,1\,l_2'\,0)\delta(l_1',p_1')\delta(l_2',p_2')i^{L_2'-L_1'+l_1'-l_2'}$$
$$\times(-1)^{L_1'+J-I'+q'+q+\kappa+\kappa'}D_{\kappa,\kappa'}^{(q)}(\phi,\theta,0)T_\kappa^q W(JL_1'JL_2';I'q)G_{\kappa'}(L_1'l_1'1;q\quad q';L_2'l_2'1), \quad (6.10)$$

where the sum is over $L_1'L_2'l_1'l_2'p_1'$ and p_2'. Note that the polarized nucleus has spin J and parity π. Its initial tensor moments are T_κ^q. If polarization is achieved by electric or magnetic fields, only the terms with $\kappa=0$ are present.

If we specialize the above expression, we obtain several results already given in the literature.[14]

VII. POLARIZED TARGET NUCLEI

The previous results in this paper have all been specialized to the case of a polarized beam of particles of spin i incident upon an unpolarized target nucleus of spin I. The more general problem is one in which the target nucleus is polarized as well. (We assume, however, that the incident particle and nucleus are incoherent.) The expansion of the density matrix in terms of tensor operators is no longer that given in Eq. (2.7) but rather has the form:

$$\rho(s_1m_1;s_2m_2)$$
$$=\sum_q(-1)^{s_1-s_2-q+m_2}(s_1s_2-m_1m_2\,|\,s_1s_2q-\kappa)\mathfrak{T}_\kappa^q, \quad (7.1)$$

where

$$\mathfrak{T}_\kappa^q=\sum_{a,b,\lambda}\frac{(2i)!(2I)!(2a+1)(2b+1)[(2s_1+1)(2s_2+1)]^{\frac{1}{2}}}{[(2i-a)!(2i+a+1)!(2I-b)!(2I+b+1)!]^{\frac{1}{2}}}$$
$$\times\frac{(-1)^{s_2}(ab\lambda\kappa-\lambda\,|\,ab q\kappa)}{P_a([i/i+1]^{\frac{1}{2}})P_b([I/I+1]^{\frac{1}{2}})}$$
$$\times X(iai;s_1qs_2;IbI)T_\lambda^a(i)T_{\kappa-\lambda}^b(I). \quad (7.2)$$

This result is derived in Appendix A. Equation (7.2) expresses the generalized tensor moment for the initial system in terms of the individual tensor moments $T_\lambda^a(i)$ and $T_{\kappa-\lambda}^b(I)$, defined in the usual manner, of the incident particle and target nucleus respectively.

All previous results in this paper are generalized to the case of polarized target nuclei by replacing T_κ^q with $\mathfrak{T}_\kappa^q$ along with a change of normalization which is obvious from a comparison of Eqs. (7.1) and (2.7).

The author wishes to express his thanks to Dr. Theodore A. Welton for many valuable discussions and suggestions.

APPENDIX A. EXPANSION OF THE DENSITY MATRIX IN TERMS OF TENSOR OPERATORS

An element of the density matrix in the channel spin representation may be written as an average of the expectation value of an operator over the statistical ensemble. If $\chi(sm)$ is a channel spin wave function of channel spin s and z component m, an element of the density matrix is

$$\rho(s_1m_1;s_2m_2)=\langle\chi(s_1m_1)\chi^*(s_2m_2)\rangle_{Av}. \quad (A.1)$$

The channel spin wave function is defined in terms of the spin wave functions for the incident particle i and target nucleus I as

$$\chi(sm)=\sum_{m_i}(i\,I\,m_i\,m-m_i\,|\,i\,I\,s\,m)\chi(im_i)\chi(I\,m-m_i). \quad (A.2)$$

If Eq. (A.2) is substituted in Eq. (A.1) and if it is assumed that wave functions of the target nucleus and incident particle are incoherent, one immediately obtains

$$\rho(s_1m_1;s_2m_2)=\sum_{m_i,m_i'}(i\,I\,m_i\,m_1-m_i\,|\,i\,I\,s_1\,m_1)$$
$$\times(i\,I\,m_i'\,m_2-m_i'\,|\,i\,I\,s_2\,m_2)$$
$$\times\rho_i(m_i,m_i')\rho_I(m_1-m_i,m_2-m_i'), \quad (A.3)$$

[14] N. R. Steenberg, Proc. Phys. Soc. (London) **65**, 791 (1952) and **66**, 391 (1953); H. A. Tolhoek and J. A. M. Cox, Physica **29**, 101 (1953). These authors treat the angular distribution and polarization of gamma rays from aligned nuclei for the case of pure multipoles only. The correspondence to the notation of Tolhoek and Cox is as follows:

$$T_0^0=1;\quad T_0'=P\xi_3/\sqrt{2};\quad T_1^2+T_{-1}^2=-\sqrt{6}P\xi_1/4;$$
$$i(T_1^2-T_{-1}^2)=\sqrt{6}P\xi_2/4.$$

where ρ_i and ρ_I are the density matrices for the individual particles.

The general covariance properties of ρ may be obtained directly from Eq. (A.1), however. If P_r denotes the operation of a rotation r of the coordinate system, there follows immediately:

$$P_r\rho(s_1m_1;\,s_2m_2)=\sum_{\lambda,\lambda'}D_{\lambda,\,m_1}^{(s_1)}(r)D_{\lambda',\,m_2}^{*(s_2)}(r)\times\langle\chi(s_1\lambda)\chi^*(s_2\lambda')\rangle_{Av}, \quad \text{(A.4)}$$

where D is an element of the rotation group. By Eq. (16a) of reference 7, the product of two D coefficients may be expressed as a single D coefficient. If we use this, Eq. (A.4) may be written

$$=\sum_{\lambda-\lambda',q}(-1)^{-m_2}(s_1\,s_2\,m_1-m_2|\,s_1\,s_2\,q\,m_1-m_2)\times D_{\lambda-\lambda',\,m_1-m_2}^{(q)}(r)\mathfrak{T}_{\lambda-\lambda'}{}^q, \quad \text{(A.5)}$$

where the sum on λ and λ' has been replaced by a sum on $\lambda-\lambda'$ and λ', and where

$$\mathfrak{T}_{\lambda-\lambda'}{}^q=\sum_{\lambda'}(-1)^{\lambda'}(s_1\,s_2\,\lambda-\lambda'|\,s_1\,s_2\,q\,\lambda-\lambda')\times\langle\chi(s_1\lambda)\chi^*(s_2\lambda')\rangle_{Av}. \quad \text{(A.6)}$$

It is clear from Eq. (A.5) that $\mathfrak{T}_{\lambda-\lambda'}{}^q$ transforms under rotation as a tensor of rank q. Hence in the limit of zero rotation, Eq. (A.5) goes into the desired expansion.

$$\rho(s_1m_1;\,s_2m_2)=\sum_q(-1)^{-m_2}\times(s_1\,s_2\,m_1-m_2|\,s_1\,s_2\,q\,m_1-m_2)\mathfrak{T}_{m_1-m_2}{}^q. \quad \text{(A.7)}$$

By the unitary property of the Clebsch-Gordon coefficient, this may be written

$$\mathfrak{T}_{m_1-m_2}{}^q=\sum_{m_2}(-1)^{m_2}(s_1\,s_2\,m_1-m_2|\,s_1\,s_2\,q\,m_1-m_2)\times\rho(s_1m_1;\,s_2m_2). \quad \text{(A.8)}$$

If we substitute Eq. (A.3) in the above, there results

$$\mathfrak{T}_{m_1-m_2}{}^q=\sum(-1)^{m_2}(s_1\,s_2\,m_1-m_2|\,s_1\,s_2\,q\,m_1-m_2)\times(i\,I\,m_i\,m_1-m_i|\,i\,I\,s_1\,m_1)(i\,I\,m_i'\,m_2-m_i'|\,i\,I\,s_2\,m_2)\times\rho_i(m_i,\,m_i')\rho_I(m_1-m_i,\,m_2-m_i'), \quad \text{(A.9)}$$

where the sum is over m_2, m_i, and m_i'.

It is now necessary to express the particle density matrices in terms of their tensor moments. Once again this follows from the operation P_r upon the density matrix for the particle i, say. The analogous result to (A.7) is

$$\rho_i(m_i,\,m_i')=\sum_a(-1)^{-m_i'}\times(i\,i\,m_i-m_i'|\,i\,i\,a\,m_i-m_i')\mathfrak{T}_{m_i-m_i'}{}^a, \quad \text{(A.10)}$$

where

$$\mathfrak{T}_\kappa{}^a=\sum_\lambda(-1)^{\lambda'}(i\,i\,\lambda-\lambda'|\,i\,i\,a\,\kappa)\langle\chi(i\lambda)\chi^*(i\lambda')\rangle_{Av}.$$

Since $\mathfrak{T}_\kappa{}^a$ transforms as an irreducible tensor of rank a under rotation it must differ from the usual spin tensor operator $T_\kappa{}^a$, defined in Eq. (2.6), by a normalization factor only. In order to determine this factor, let us evaluate $\mathfrak{T}_\kappa{}^a$ and $T_\kappa{}^a$ for the special case of an ensemble having only the single state $\chi(i,\,i)$ and for $\kappa=0$. Then

$$\mathfrak{T}_0{}^a=(-1)^i(i\,i\,i\,-i|\,i\,i\,a\,0).$$

From the definition of $T_0{}^a$ given in Eq. (2.6),

$$T_0{}^a=P_a([i/i+1]^{\frac{1}{2}}).$$

Hence, in general,

$$\mathfrak{T}_\kappa{}^a=\frac{(-1)^i(i\,i\,i\,-i|\,i\,i\,a\,0)}{P_a([i/i+1]^{\frac{1}{2}})}T_\kappa{}^a. \quad \text{(A.11)}$$

If we combine Eq. (A.11) with a relation obtained from BBR(1) and R(16),

$$(i\,i\,i\,-i|\,i\,i\,a\,0)=(2i)\,!(2a+1)^{\frac{1}{2}}[(2i-a)\,!(2i+a+1)\,!]^{-\frac{1}{2}}, \quad \text{(A.12)}$$

and substitute in (A.10), we have

$$\rho_i(m_i,\,m_i')=\sum_a(-1)^{i-m_i'}\frac{(2i)\,!(2a+1)^{\frac{1}{2}}}{[(2i-a)\,!(2i+a+1)\,!]^{\frac{1}{2}}}\times\frac{(i\,i\,m_i-m_i'|\,i\,i\,a\,m_i-m_i')}{P_a([i/i+1]^{\frac{1}{2}})}T_{m_i-m_i'}{}^a. \quad \text{(A.13)}$$

An analogous formula holds for ρ_I. If Eq. (A.13) is substituted in (A.9), we have an expression for the generalized tensor moment of the system in terms of the individual particle tensor moments.

$$\mathfrak{T}_{m_1-m_2}{}^q=\sum(-1)^{i+I}\frac{(2i)\,!(2a+1)^{\frac{1}{2}}(2I)\,!(2b+1)^{\frac{1}{2}}}{[(2i-a)\,!(2i+a+1)\,!(2I-b)\,!(2I+b+1)\,!]^{\frac{1}{2}}}\frac{T_{m_1-m_i'}{}^a(i)T_{m_1-m_2-m_i+m_i'}{}^b(I)}{P_a([i/i+1]^{\frac{1}{2}})P_b([I/I+1]^{\frac{1}{2}})}\times\sum[(i\,i\,m_i-m_i'|\,i\,i\,a\,m_i-m_i')(i\,I\,m_i\,m_1-m_i|\,i\,I\,s_1\,m_1)\times(i\,I\,m_i'\,m_2-m_i'|\,i\,I\,s_2\,m_2)(s_1\,s_2\,m_1-m_2|\,s_1\,s_2\,q\,m_1-m_2)\times(I\,I\,m_1-m_i\,m_i'-m_2|\,I\,I\,b\,m_1-m_2+m_i'-m_i)], \quad \text{(A.14)}$$

where the first sum is over a, b, and m_i-m_i'. The second sum is over m_2 and m_i.

The details of the elimination of the second sum will not be given here since several similar reductions have been illustrated before. The final result is in the form of an X function, as might have been anticipated. The

entire second sum becomes

$$=(-1)^{a+i+I}[(2a+1)(2b+1)(2s_1+1)(2s_2+1)]^{\frac{1}{2}}$$
$$\times(a\ b\ m_i-m_i'\ m_1-m_2+m_i'-m_i|a\ b\ q\ m_1-m_2)$$
$$\times X(i\ a\ i;\ s_1\ q\ s_2;\ I\ b\ I). \quad \text{(A.15)}$$

If we substitute Eqs. (A.15) and (A.14) in Eq. (A.7) we obtain the result given in Eq. (7.2).

The special case of an unpolarized initial nucleus corresponds to $b=0$. Equation (2.7) of the text then follows immediately from Eq. (7.2) by the use of I(B.1).

APPENDIX B. SOME PROPERTIES OF THE G FUNCTION

The G function may be defined in terms of the Fano X function[15] as

$$G_\kappa\begin{pmatrix}a & b & c\\ d & & f\\ g & h & i\end{pmatrix}=[(2a+1)(2b+1)(2c+1)(2d+1)$$
$$\times(2f+1)(2g+1)(2h+1)(2i+1)]^{\frac{1}{2}}i^{b+h}$$
$$\times\sum_e\left[(b\ h\ 0\ 0|b\ h\ e\ 0)\right.$$
$$\left.\times(f\ d\ \kappa-\kappa|f\ d\ e\ 0)X\begin{pmatrix}a & b & c\\ d & e & f\\ g & h & i\end{pmatrix}\right]. \quad \text{(B.1)}$$

By the use of BBR (1), (5), and the symmetry properties of the X function, it is clear that the interchange of the two outer rows of the G function or of the two outer columns simply multiplies the G function by the phase factor $(-1)^{a+d+g+c+f+i}$.

The "triad" conditions for the nonvanishing of the X function also immediately yield the condition that the elements of each of the outer rows and columns of the G function must form possible vector triads in order that G shall not vanish:

$$(abc),\ (adg),\ (ghi),\ (cfi)\ \text{"triads."} \quad \text{(B.2)}$$

In addition, the two "triad" conditions involving e yield a less restrictive condition on the G function which is that the four central elements $(d\ b\ f\ h)$ must form a possible vector "tetrad:"

$$(d\ b\ f\ h)\ \text{"tetrad."} \quad \text{(B.3)}$$

In the special case of $\kappa=0$, this last condition becomes more restrictive. By BBR (5) we must have $b+h+e$ = even integer and $f+d+e$ = even integer. Hence,

$$b+h+f+d=\text{even integer for } \kappa=0. \quad \text{(B.4)}$$

From the properties of the Clebsch-Gordon coefficients, it is also clear that d and f must satisfy the conditions:

$$d\geq\kappa,\quad f\geq\kappa. \quad \text{(B.5)}$$

Two alternative expressions for the G functions are often useful. These are obtained by first substituting in Eq. (B.1) the expression for X in terms of Racah functions.[15] The resultant expression is

$$G_\kappa(abc;d\quad f;ghi)$$
$$=i^{b+h}[(2a+1)(2b+1)(2c+1)(2d+1)$$
$$\times(2f+1)(2g+1)(2h+1)(2i+1)]^{\frac{1}{2}}$$
$$\times\sum_{e,z}[(-1)^{a+b+c+d+e+f+g+h+i}(2z+1)^{\frac{1}{2}}$$
$$\times W(bdcg;za)W(dbfh;ze)W(gchf;zi)$$
$$\times(b\ h\ 0\ 0|b\ h\ e\ 0)(f\ d\ \kappa-\kappa|f\ d\ e\ 0)]. \quad \text{(B.6)}$$

For simplicity in printing, we have written the arguments of G on a single line. The two expressions for G are now obtained by performing the sum on e by the use of BBR (18) in either of two possible orderings of b, h and f, d. The two expressions are

$$G_\kappa(abc;d\quad f;ghi)$$
$$=i^{b+h}[(2a+1)(2b+1)(2c+1)(2d+1)(2f+1)$$
$$\times(2g+1)(2h+1)(2i+1)]^{\frac{1}{2}}(-1)^{a+g+c+i+\kappa}$$
$$\times\sum_z[(-1)^z(f\ h\ \kappa\ 0|f\ h\ z\ \kappa)(d\ b\ \kappa\ 0|d\ b\ z\ \kappa)$$
$$\times W(bdcg;za)W(gchf;zi)], \quad \text{(B.7)}$$

and

$$G_\kappa(abc;d\quad f;ghi)$$
$$=i^{b+h}[(2a+1)(2b+1)(2c+1)(2d+1)(2f+1)$$
$$\times(2g+1)(2h+1)(2i+1)]^{\frac{1}{2}}(-1)^{d+f+\kappa}$$
$$\times\sum_z[(-1)^z(f\ b\ \kappa\ 0|f\ b\ z\ \kappa)(d\ h\ \kappa\ 0|d\ h\ z\ \kappa)$$
$$\times W(hdia;zg)W(aibf;zc)]. \quad \text{(B.8)}$$

The G function reduces to a simpler form when one of the elements is zero. The following forms are obtained from Eqs. (B.1), (B.4), and (B.5) by the use of BBR (30) and I(B.1):

$$G_0(abc;d\quad 0;ghi)$$
$$=\delta_{ci}(-1)^{c-g}(2c+1)^{\frac{1}{2}}i^dZ(bahg;cd); \quad \text{(B.9)}$$

$$G_\kappa(a0c;d\quad f;ghi)$$
$$=\delta_{ac}i^h[(2i+1)(2a+1)(2g+1)(2d+1)(2f+1)]^{\frac{1}{2}}$$
$$\times(f\ d\ \kappa-\kappa|f\ d\ h\ 0)W(dahi;gf); \quad \text{(B.10)}$$

$$G_\kappa(0bc;d\quad f;ghi)$$
$$=\delta_{bc}\delta_{dg}i^{b+h}[(2h+1)(2d+1)(2f+1)]^{\frac{1}{2}}(-1)^{d+i}$$
$$\times(f\ i\ \kappa-\kappa|f\ i\ b\ 0)(d\ h\ \kappa\ 0|d\ h\ i\ \kappa), \quad \text{(B.11)}$$

where the Z coefficient is defined in BB (4.3). The remaining forms follow by the use of the symmetry conditions.

[15] For the properties of the X function see reference 3 and also Appendix B of I.

Letters to the Editor

PUBLICATION of brief reports of important discoveries in physics may be secured by addressing them to this department. The closing date for this department is five weeks prior to the date of issue. No proof will be sent to the authors. The Board of Editors does not hold itself responsible for the opinions expressed by the correspondents. Communications should not exceed 600 words in length and should be submitted in duplicate.

Solutions of the Meson-Nucleon Equation in the Adiabatic Limit

R. ARNOWITT,
Radiation Laboratory, Department of Physics, University of California, Berkeley, California
AND
S. DESER,*
Harvard University, Cambridge, Massachusetts
(Received July 7, 1953)

THE relativistic meson-nucleon equation,[1] $[(\gamma p+m)(k^2+\mu^2)-I]\psi=0$, upon reduction to three-dimensional form, may be used to examine the stability of meson-nucleon systems (bound and virtual states) as well as scattering. Such an investigation has been made for the isotopic spin 3/2 state, with lowest order interaction (crossed meson graph) in the adiabatic limit, but keeping both "large" and "small" components in the resulting equation. In momentum space, the three-dimensional equation becomes

$$(K-\omega_p-H)\phi_i(\mathbf{p})=\frac{g^2}{(2\pi)^3}\left[\frac{1}{2\omega_p}-\frac{\Lambda_-}{K+\omega_p+E_p}\right]\tau_j\tau_i \int\frac{\beta m+\boldsymbol{\alpha}\cdot(\mathbf{p}+\mathbf{p}')-(\mu_1-\mu_2)K}{m^2+(\mathbf{p}+\mathbf{p}')^2-(\mu_1-\mu_2)^2K^2}\phi_j(\mathbf{p}')d\mathbf{p}', \quad (1)$$

where $K=m+\mu+E$ is the total energy of the system, $\mu_1=\mu/(m+\mu)$, $\mu_2=m/(m+\mu)$, $H=\boldsymbol{\alpha}\cdot\mathbf{p}+\beta m$, and Λ_- is the negative energy free particle projection operator. Multiplying by $K-H+\omega_p$ (to rationalize the kinetic energy term) and returning to coordinate space, one obtains an equivalent Dirac equation of the form

$$(W-H)\phi_i(\mathbf{r})=\int V_{ij}(\mathbf{r},\mathbf{r}')\phi_j(\mathbf{r}')d\mathbf{r}'; \quad W=m+\frac{E(E+2\mu)}{2(m+\mu+E)}, \quad (2)$$

where

$$V_{ij}(\mathbf{r},\mathbf{r}')=\frac{g^2}{4\pi}\frac{\tau_j\tau_i}{4K}[KQ_m(\mathbf{r}+\mathbf{r}')+(K-\beta m-\boldsymbol{\alpha}\cdot\mathbf{p}) \{Q_\mu(\mathbf{r}+\mathbf{r}')-Q_m(\mathbf{r}+\mathbf{r}')\}]\times[\beta m-(\mu_1-\mu_2)K-\boldsymbol{\alpha}\cdot\mathbf{p}']Y(r');$$
$$Y(r)=(1/r)\exp(-r/\rho); \quad Q_\mu(\mathbf{r})=-\frac{1}{2\pi^2}\frac{1}{r}\frac{\partial}{\partial r}K_0(\mu r). \quad (3)$$

The range of the Yukawa well, $\rho^{-1}=[m^2-(\mu_1-\mu_2)^2K^2]^{\frac{1}{2}}$, is energy dependent. The integral operator, $V(\mathbf{r},\mathbf{r}')$, was approximated by a multiplicative exchange potential. In so doing, $mQ_m(\mathbf{r}+\mathbf{r}')$ was replaced by $\delta(\mathbf{r}+\mathbf{r}')$ and the terms proportional to $Q_\mu-Q_m$ were neglected as $Q_\mu-Q_m$ is logarithmic at the origin (and hence not highly singular). The potential for the 3/2 state then becomes

$$V=(g^2/8\pi m)[H-(\mu_1-\mu_2)K]Y(r)P, \quad (4)$$

where P is the exchange operator. The angular parts of the wave function may be separated out in the usual fashion, via the constants of motion J, $K=\beta(\boldsymbol{\sigma}\cdot\mathbf{L}+1)$. The resulting coupled radial equations for the two components u/r, v/r are

$$\left[\frac{d}{dr}-\frac{k}{r}+(-1)^l\frac{g^2}{8\pi m}\frac{\partial}{\partial r}Y\right]u(r) =-\left[W+m-(-1)^l\frac{g^2}{8\pi m}\{2m-\mu-(\mu_1-\mu_2)E\}Y\right]v(r), \quad (5)$$

$$\left[\frac{d}{dr}+\frac{k}{r}-(-1)^l\frac{g^2}{8\pi m}\frac{\partial}{\partial r}Y\right]v(r) =\left[W-m-(-1)^l\frac{g^2}{8\pi m}\{\mu-(\mu_1-\mu_2)E\}Y\right]u(r). \quad (6)$$

In order to examine the structure of the solutions, the Yukawa potentials were replaced by "equivalent" square wells, $\bar{V}$, defined by $\int_0^\infty Vr^2dr=\bar{V}\int_0^\rho r^2dr$.[2] Eliminating $v(r)$ from the equations, one obtains a Schrödinger equation for u of the form

$$\left[\frac{d^2}{dr^2}-\frac{k(k-1)}{r^2}-\frac{2k}{r}a\frac{g^2}{4\pi}+b\left(\frac{g^2}{4\pi}\right) +c\left(\frac{g^2}{4\pi}\right)^2+W^2-m^2\right]u(r)=0, \quad r<\rho \quad (7)$$

$$\left[\frac{d^2}{dr^2}-\frac{k(k-1)}{r^2}+W^2-m^2\right]u(r)=0, \quad r>\rho \quad (8)$$

The coefficients a, b, c are energy dependent. The appearance of a g^4 term in Eq. (7) reflects the elimination of v from Eqs. (5) and (6). Replacing the $1/r$ term in (7) by a square well, one obtains a total well which is repulsive for $j=1/2, 5/2, \cdots$ and attractive for certain ranges of $g^2/4\pi$ for $j=3/2, 7/2 \cdots$.

Assuming the V_i^0 particle to be a virtual state of the p, π^- system at an energy $E\sim 40$ Mev, with isotopic spin 3/2 and an angular momentum of $l=5$, a lifetime of 2×10^{-10} second was obtained. The allowed values of the coupling constant that give this result are $g^2/4\pi=9.0, 13.5$. For the latter case no other virtual or bound states can form in the low-energy region.

The above equations were also applied to calculate the total π^+-p cross section at 37 Mev. The result (for $g^2/4\pi=13.5$) is 19.3 mb.[3]

First-order nonadiabatic corrections to the potential have been examined and appear not to change the results qualitatively. More detailed calculations are now in progress.

* Now at The Institute for Advanced Study, Princeton, New Jersey.
[1] S. Deser and P. Martin, Phys. Rev. **90**, 1075 (1953).
[2] The $1/r$ and $1/r^3$ singularities were smoothed to a $\ln r$ and $1/r$ respectively near the origin, as suggested by the integral operator Q_m.
[3] This result may be compared with the experimental values of 10.9 ± 3 mb and 11.8 ± 1.0 mb at that energy obtained by C. E. Angell and J. P. Perry [Phys. Rev. **91**, 1289 (1953); **92**, 835 (1953)], and the value 7.9 ± 2.2 mg obtained at 33 Mev by S. L. Leonard and D. H. Stork [Bull. Am. Phys. Soc. **28**, No. 4, 19 (1953)].

Production of Acceptor Centers in Germanium and Silicon by Plastic Deformation

W. C. ELLIS AND E. S. GREINER
Bell Telephone Laboratories, Murray Hill, New Jersey
(Received September 16, 1953)

PLASTIC deformation of germanium and silicon by bending and in tension has been reported by Gallagher[1] and by Treuting.[2] In recent experiments compression has been used to deform N-type germanium crystals of 5 and 26 ohm-cm resistivity about 5 percent at 500° and 650°C, respectively. X-ray studies showed that the deformation produced a range of orientations grouped about the principal one for the crystal. In both specimens the conductivity was changed to P-type, and the resistivity values for the deformed germanium were 1.5 and 3 ohm-cm, respectively. These changes correspond to the introduction of about 10^{15} acceptor centers/cm^3.

Control germanium specimens that were only heated, and not compressed, were included simultaneously in the furnace. No, or insignificantly small, changes in resistivity were obtained for the controls. This is considered conclusive evidence that the acceptor centers have an origin in the deformation. They may be at dislocations, introduced into the small regions, or on the small angle boundaries between regions, in the deformed structure. Dislocation models in deformed germanium have been discussed by Seitz[3] and by Shockley.[4]

A similar introduction of acceptor centers has been obtained with silicon of N-type and 6 ohm-cm resistivity. When this silicon was compressed 2.5 percent at 725°C, it remained N-type but the resistivity increased to 150 ohm-cm. When the same silicon was compressed 18 percent at 850°C, the resistivity increased to 50 ohm-cm and both N and P regions were found in the sample. These resistivity changes correspond to an introduction of about 10^{15} acceptor centers/cm³. As in the case of germanium, controls that were heated only were included simultaneously in the furnace. No significant changes in resistivity were obtained in the controls.

Values of mobilities used in calculation were for undeformed material.[5,6] The number of acceptor centers may be different to the extent that mobilities are different in deformed structures.[7]

[1] C. J. Gallagher, Phys. Rev. **88**, 721 (1952); Bull. Am. Phys. Soc. **28**, No. 4, 10 (1953).
[2] R. G. Treuting, J. Metals **4**, 1944 (1952).
[3] F. Seitz, Phys. Rev. **88**, 722 (1952).
[4] W. Shockley, Phys. Rev. **91**, 228 (1953).
[5] J. R. Haynes and W. Shockley, Phys. Rev. **81**, 835 (1951).
[6] J. R. Haynes and W. C. Westphal, Phys. Rev. **85**, 680 (1952).
[7] D. L. Dexter and F. Seitz, Phys. Rev. **86**, 964 (1952).

Thermal Conductivity of Copper between 0.25°K and 4.2°K*

JAMES NICOL† AND T. P. TSENG
Department of Physics and Astronomy, Ohio State University, Columbus, Ohio
(Received September 18, 1953)

SOME years ago, Heer and Daunt initiated measurements on the thermal conductivity of metals below 1°K, their first observations being on Sn and Ta.[1] This work led immediately to the practical realization of superconducting thermal "valves"[2] and to an understanding of the significance of lattice conduction at extremely low temperatures. Subsequently, similar measurements by us have been made on Pb[3] and Cu. Whereas many other observations below 1°K on the thermal conductivity of superconducting metals, such as Pb, have since been reported,[4] data below 1°K on normal metals, such as Cu, are unavailable. It is considered that the results, given below, for Cu are of twofold interest, first in relation to the theory of electrons in metals, and second, as a guide in technical problems arising in cryogeny below 1°K.

The experimental arrangements for the observations below 1°K were similar to those used previously,[1] consisting of two approximately equal chromium potassium alum cylinders of about 15 cc each, separated from one another by a distance of approximately 30 cm and connected thermally to each end of the specimen of interest by copper mountings of large cross section. The thermal contact between the salts and their copper mountings was made by high-pressure molding. The two salt cylinders were simultaneously cooled to low, but different, temperatures by the magnetic method, and the thermal conductivity of the metallic specimen linking the two was calculated from observations of the rate at which the cylinders equalized temperature. The dimensions of the specimens were so chosen that the time for equalization was long enough (about 1 hour) to enable observations to be made to at least 0.001°K. The stray influx of heat from the surroundings was kept low in order to minimize errors of computation. The temperatures of the salts were obtained from susceptibility measurements, using an ac bridge method.[5] The ac bridge, using a decade mutual inductance constructed by Hayes,[6] has a sensitivity such that, with a primary field of 0.1 gauss rms at 28 c/s, temperature differences of less than 0.1 milli-degrees can be readily observed at, for example, 0.5°K.

For the temperature range 1°K to 4.2°K, customary steady heat flow techniques were used for the conductivity measurements, employing carbon thermometers and direct ohmic heating.

The thermal resistance between the salts was found to be composed of two terms; (a) the resistivity of the Cu sample and (b) the thermal contact resistances between the salts and their copper mountings. This term (b) was found to be proportional to T^{-2}, as has been discussed previously by Mendoza[7] and by Goodman,[4] and the factor of proportionality was obtained from our observations made at 0.5°K. As will be seen from the table of results given below, this term (b) represented only a small correction to the results down to 0.5°K.

In order to calculate the heat flow between the samples, it was necessary to estimate the heat leak from external sources into each salt individually. On the assumption that these heat leaks were proportional to (*a*) the difference in temperature between each salt and the surrounding chamber, and (*b*) the area of each salt, the constant of proportionality could be obtained by calculation from the observed total heat leak at any one instant. It was found that a unique value of this constant allowed computations to be made, regarding the heat leak, which were in good agreement with the experimental data over periods of time exceeding one hour and corresponding intervals of temperature.

The copper sample was a polycrystalline wire of 27.2-cm length and 0.025-cm diameter, and was of commercial grade high-purity magnet wire, supplied by General Electric Company. The observed thermal conductivity, K as a function of temperature is shown in Fig. 1 and Table I. It will be observed that within the limits of experimental error K is a linear function of T down to 0.25°K. If one puts $K=\alpha T$, then our observed value of α is 1.76 watts/cm deg². Previous results in the temperature range 1.2°K to 4°K give $\alpha=0.6$;[8] $\alpha=0.58$;[9] $\alpha=4.7$;[10] and $\alpha=2.0$.[11] The fact that our value of α is somewhat less than that observed by the two latter groups of workers is due probably to small differences in purity of the samples.

At temperatures below those reported herewith, the thermal resistance between the salts appeared to include more highly tem-

TABLE I. Observed thermal conductivity as a function of temperature.

Obs. mean temp. °K	Obs. temp. diff. °K	Barrier temp. drop at salt A °K	Barrier temp. drop at salt B °K	Temp. diff. along Cu °K	Corrected mean temp. °K	Thermal cond. of Cu watt units
0.810	0.011	0.001	0.001	0.009	0.810	1.30
0.787	0.059	0.005	0.004	0.050	0.787	1.17
0.672	0.036	0.004	0.003	0.029	0.673	1.09
0.657	0.114	0.014	0.009	0.091	0.660	0.87
0.608	0.108	0.014	0.001	0.093	0.615	0.92
0.416	0.242	0.076	0.023	0.143	0.443	0.91
0.400	0.180	0.047	0.019	0.114	0.414	0.79
0.346	0.046	0.008	0.008	0.030	0.346	0.55
0.259	0.242	0.077	0.010	0.155	0.293	0.53

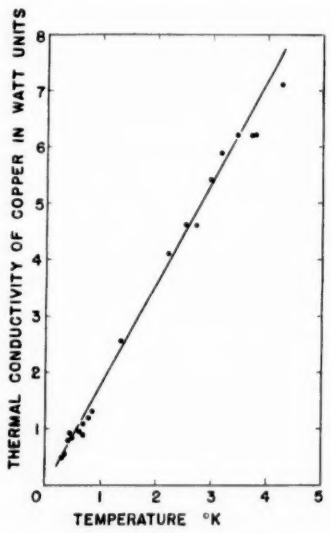

FIG. 1. Thermal conductivity (in watt units) of pure copper as a function of absolute temperature.

perature dependent terms than those given by terms (*a*) and (*b*) above. This additional temperature dependency was not considered to be due to any primary processes occurring in the copper specimen, since similar dependencies were separately observed in experiments on the thermal conductivity of superconducting Pb in the same temperature region. It is possible that these effects were due to diffusional or relaxational processes in the salts themselves.

The observed linear dependence of K on temperature indicates that the thermal conductivity is electronic in character and is limited only by impurity scattering. Moreover, the linear temperature function is a direct reflection of the linear dependence of the electronic specific heat on the absolute temperature. It is of interest to note, therefore, that this linear function appears experimentally to be valid down to as low a temperature as 0.25°K, especially in view of the possible deviations from linearity which have been considered to occur due to exchange and correlation forces.[12]

We wish to thank Dr. J. G. Daunt for his aid and discussions in the work and Messrs. W. L. Pillinger and R. C. Sapp for their generous assistance in the experiments and computations. We thank also the Research Corporation for their continued support.

[*] Assisted by a contract between the U. S. Atomic Energy Commission and the Ohio State University Research Foundation.
[†] Now at Amherst College, Amherst, Massachusetts.
[1] C. V. Heer and J. G. Daunt, Phys. Rev. **76**, 854 (1949). See also C. V. Heer, Ph.D. Dissertation, Ohio State University, 1949 (unpublished).
[2] See reference 1 and Heer, Barnes, and Daunt, Phys. Rev. **91**, 412 (1953).
[3] J. Nicol, Ph.D. Dissertation, Ohio State University, 1952 (unpublished). Also J. Nicol and J. G. Daunt, Proc. Cryogenics Conf. Schenectady, 1952 (unpublished), p. 68.
[4] For example, on Sn: B. B. Goodman, Proc. Phys. Soc. (London) **66**, 217 (1953); on Pb: J. L. Olsen and C. A. Renton, Phil. Mag. **43**, 946 (1952); on Sn, In, Ta, Cb, and Al: K. Mendelssohn and C. A. Renton, Phil. Mag. **44**, 776 (1953).
[5] Casimir, de Haas, and de Klerk, Physica **6**, 241 (1939).
[6] W. B. Hayes, M. Sc. Thesis, Ohio State University, 1950 (unpublished).
[7] E. Mendoza, Ceremonies Langevin-Perrin, Paris, 1948 (unpublished), p. 53.
[8] J. F. Allen and E. Mendoza, Proc. Cambridge Phil. Soc. **44**, 280 (1947).
[9] Andrews, Spohr, and Webber, Phys. Rev. **78**, 342 (1950).
[10] R. Berman and D. K. C. MacDonald, Proc. Roy. Soc. (London) **A211**, 122 (1952).
[11] K. Mendelssohn and H. M. Rosenberg, Proc. Phys. Soc. (London) **A65**, 385 (1952).
[12] See for example: E. P. Wohlfarth, Phil. Mag. **41**, 534 (1950) and **44**, 281 (1953).

Paramagnetic Resonance Absorption in Graphite*

J. G. CASTLE, JR.
Department of Physics, University of Buffalo, Buffalo, New York
(Received September 22, 1953)

THE two-dimensional freedom of the carriers in graphite is very suitable for the study of graphite's electronic structure by magnetic resonance techniques. Recently the author has observed, with Yale University's spectrometer,[1] magnetic resonance absorption in several samples of graphitized materials at 9242 Mc/sec and room temperature. Each sample showed only a single absorption line. The preliminary data are presented now in order to report the first observation of magnetic resonance absorption in systems that are approximately two-dimensional.

The graphite samples were prepared from powdered materials so as to have all of the graphitic planes throughout each sample aligned normal to a selected direction. The samples, in the form of thin films, were mounted on thin dielectric strips. Sample A contained well-purified Ceylon graphite which was powdered, mixed with liquid polystyrene, and oriented with almost all the planes parallel to the supporting film. Visual inspection indicated a high degree of alignment. Samples B, C, and D contained powder made of coke which was milled to a mean particle size of 1–2 microns and graphitized to 3000°C. The graphitic planes in sample B were oriented parallel to the supporting film and in C, perpendicular. For D, the powder was not imbedded in a dielectric medium. Sample E contained machining dust from well-purified aritificial graphite, oriented parallel.

The magnetic field was measured by observing the proton resonance absorption in pure mineral oil. The positional error in the proton frequency was less than three kc/sec. The modulation amplitude of the magnetic field was less than the observed half-widths.

The g-value for sample A is 1.003 times that of a system of free electron spins, each with the moment μ_0 (1.00115). The absorption, described in Table I, can be attributed to the spin resonance of the

TABLE I. Spin resonance absorption in graphite at 3 cm.

Sample	Crossover proton frequency Mc/sec	Half-width at half-power gauss
A—Ceylon ∥	14.016 ±0.005	5 ±1 +
B—1μ ∥	14.000 ±0.008[a]	9 ±2
C—1μ ⊥	14.00[a]	~20
D—1μ loose	14.000 ±0.008	9 ±2
E	14.00[a]	~10

[a] Slightly asymmetric.

carriers in graphite. The lines are quite sharp and the frequency of collisions with the edges of micron-size crystallites (assuming the small estimated effective mass for motion parallel to the graphitic planes) is of the order of the observing frequency. Therefore, the mechanism of carrier spin absorption requires that the collisions of the carriers with the edges of the planes do not frequently disturb the carriers' spin orientation.

Measurements of the static susceptibility[2] of the same powder as in B, C, and D gave the density of ferromagnetic impurities. On the basis of this density, the amount of ferromagnetic impurity in each of these samples was estimated to be less than fifty micrograms. Even in larger amounts, ferromagnetic impurities would not have seriously interfered with the observed line shapes for the modulation used.

With the graphitic planes arranged parallel to the static magnetic field, as for sample A, B, D, and probably E, the cyclotron resonance[3] was undoubtedly quenched. Since the intensity of the line in sample C was approximately the intensity in B, it is unlikely that the cyclotron resonance predominated in sample C. Furthermore, the small effective mass for motion parallel to the graphitic plane, requiring as it does a rather different g-value, dictates against the observed lines being associated with the cyclotron resonance of the carriers.

There is apparently very little artificial broadening of the magnetic resonance lines in graphite as has been observed in metals.[4] The two-dimensional freedom and the sample orientation employed lead one to expect no broadening from the diffusion mechanism and no shift of the g-value due to eddy currents. Several interesting details of the absorption in graphite are under further experimental study.

The author is grateful to Professor Robert Beringer for the use of his equipment and to Mark A. Heald for considerable assistance in taking the data.

[*] This work was supported by the U. S. Office of Naval Research.
[1] R. Beringer and J. G. Castle, Jr., Phys. Rev. **78**, 581 (1950).
[2] H. T. Pinnick, (to be published).
[3] W. Shockley, Phys. Rev. **90**, 491 (1953).
[4] Griswold, Kip, and Kittel, Phys. Rev. **88**, 951 (1952).

Some Consequences of Possible Degeneracy of Energy Bands in Ge†

EDWARD N. ADAMS, II
Institute for Nuclear Studies and Chicago Midway Laboratories, University of Chicago, Chicago, Illinois
(Received August 19, 1953)

CALCULATIONS of Herman[1] and Herman and Callaway[2] indicate that for diamond and germanium a triple degeneracy occurs at the band edge for both the conduction and valence bands, and that the degeneracy in the conduction band is probably six-

fold. Such degeneracies, if they exist, will require a modification of the interpretation of certain experimental results to a significant extent.

It is easily shown that if there are g_c degenerate conduction bands and g_v degenerate valence bands, the usual formula relating the carrier densities becomes

$$n_e n_h = 4(2\pi mkT/\alpha h)^3 g_c g_v \exp(-E_g/kT), \quad (1)$$

in which $\alpha \equiv m/m_{eff}$ is the geometric mean of α_e and α_h, the effective mass ratios for the electrons and holes, respectively, and the other symbols have familiar meanings. Equation (1) with $g_c = g_v = 1$ has been used to interpret experiments designed to determine the change of E_g with temperature.[2,4] Writing E_g as $E_0 - \beta T$, it is seen that the factor $\exp(\beta/k)$ occurs in Eq. (1) in just the same way as the factor $g_c g_v$. Accordingly, if $g_c g_v$ is different from unity the value of β deduced from the experiments must be corrected.

On the basis of Herman's results we would choose $g_v = 3$ and $g_c = 3$, 6. The uncertainty in g_c arises from the circumstance that there are two points of lowest energy in each conduction band with a low maximum in between. The expected behavior depends strongly on the height of the maximum, so we have considered two values of g_c to indicate the range of uncertainty. Thus the combined effect of the degeneracies is a factor 9, 18 in Eq. (1). Expressing this factor as a correction to β we get values $\Delta\beta = -1.9$, -2.5×10^{-4} ev/°K. The presently accepted value[5] is $\beta = 1\times10^{-4}$ ev/°K corresponding to a "pre-exponential" factor of 3.5.

Since β has been determined in several ways with substantial agreement among the various experimental values, it seems reasonable to absorb the degeneracy factor by a changed interpretation of another quantity in Eq. (1). The most natural assumption is that the effective mass factor is actually much smaller than unity. In order to leave β unchanged one must postulate values $\alpha = 2.1$, 2.6.

It is not clear how the change in α should be divided between α_e and α_h. There exists some evidence[6] that most of the change is due to the difference of α_e from unity. If we adopt this assumption and take $\alpha_h = 1$ we find $\alpha_e = 4.4$, 6 which values are probably consistent with the data on impurity scattering.[6] It should be noted that although a value of $\alpha_e \sim 3$ has been suggested by Fan,[4] the present considerations should not be considered as improving agreement between the optical data and the electrical data. On the contrary, the value of α we deduce is one which leaves the disagreement exactly as it was before. A mass still smaller than we suggest would be required if Fan's results are to be in agreement with the interpretation of the electrical data.

According to the deformation potential theory the electron mobility is proportional to $\alpha_e^{5/2}/\beta_c^2$ if β_c denotes that part of β which arises from the conduction band. The smaller values of the effective mass which were deduced above would imply considerably larger theoretical mobilities. With the most optimistic adjustment of values the theoretical mobilities would be too large by a factor 5. Thus, our smaller effective mass values would force the conclusion that some other mechanism of energy loss, e.g., band-to-band scattering, is more important than the scattering due to the deformation potential.

The discussion above may be summarized as follows: the additional density of states resulting from the degeneracy of bands predicted by Herman would require a changed interpretation of existing data on carrier densities. Effective masses would have to be smaller than unity, the range of values being such that $\alpha_e \alpha_h \sim 4$–6. The deformation potential as the dominant source of lattice scattering would have to be abandoned.

Since silicon probably has the same band structure as germanium and diamond to the approximation of Herman's calculation, the above considerations and conclusions apply to silicon *mutatis mutandis*. Since the present situation as regards relation of theory to experiment is satisfactory, the existing harmony would disappear when account is taken of the degeneracy.

While the current theoretical situation in germanium and silicon undoubtedly needs to be improved upon, it seems to be rather more satisfactory without the additional degeneracy predicted by Herman. We think it worth while to point out, therefore, that even if the predicted band structure should eventuate, a relatively weak mechanism may be acting to at least partly remove this degeneracy. The spin-orbit coupling,[7] for example, might provide the requisite splitting of the degenerate P bands, since the overall splitting of the corresponding P levels in Ge is of the order[8] of 0.2 ev. A band structure split by spin-orbit coupling would permit a number of interesting possibilities for special properties in the infrared. However, putting aside the question of mechanism, we believe that the considerations discussed above provide weak but definite evidence that the predicted degeneracy in the band structure of Ge and Si does not in fact occur.[9]

† This work supported in part by the U. S. Air Force.

[1] Frank Herman, Phys. Rev. **88**, 1210 (1952).
[2] F. Herman and J. Callaway, Phys. Rev. **89**, 518 (1953).
[3] J. Bardeen, and W. Shockley, Phys. Rev. **80**, 72 (1950).
[4] H. Y. Fan, Phys. Rev. **82**, 900 (1951).
[5] W. Shockley, *Electrons and Holes in Semiconductors* (D. Van Nostrand Company, Inc., New York, 1950), p. 336.
[6] P. P. Debye, and E. Conwell, Phys. Rev. **87**, 1131 (1952).
[7] I am indebted to Dr. R. J. Elliot of Harwell for pointing out to me this possibility. I believe that he plans to give a detailed discussion of the spin-orbit coupling in Ge in a forthcoming paper.
[8] C. Moore, *Ultraviolet Multiplet Tables*, National Bureau of Standards Circular No. 488 (1952), Sec. II, p. 89.
[9] It has been called to my attention that in some as yet unpublished work Debye and Conwell consider using $|E_{1v}| - |E_{1c}| = |E_{1g}|$ rather than $|E_{1v}| + |E_{1c}| = |E_{1g}|$ as Bardeen and Shockley did. Nothing in the present study should be understood to assert that the deformation potential theory in its present form would not permit such an analysis. However, if one believes that existing agreement between theory and experiment is fortuitous (or unconvincing), there is not any difficulty in finding a theoretical model to account for the small mobilities in any case, since scattering between degenerate bands would normally be expected to occur and can always be invoked to reduce the mobilities. The point of this note is just to remark that if satisfactory agreement between theory and experiment *already exists* on the assumption of nondegenerate bands and the deformation potential theory, and if the assumption of degeneracy destroys the existing agreement, then there is some reason to suspect that the degeneracy is not actually present.

Radiation Damage in Insulators

W. PRIMAK, L. H. FUCHS, AND P. DAY
Chemistry Division, Argonne National Laboratory, Lemont, Illinois
(Received September 18, 1953)

THE behavior of the properties of a number of insulators exposed within a nuclear reactor is currently under investigation.[1] Among other effects which take place, changes in properties have been observed which are attributed to phenomena such as those discussed by Seitz,[2] resulting from processes initiated by the passage of energetic neutrons through the material. Some of the changes thus far determined have been—in diamond: increases in energy content, increases in lattice constant, decreases in density; in silicon carbide: a decrease in density, an increase in lattice constant, an increase in energy content; in quartz: a decrease in density, an increase in lattice constant and a marked diffuseness in the back-reflection region of the x-ray diffraction patterns (not present in diamond and silicon carbide), a marked change in rotatory power and a decrease in refractive index, a change in heat capacity;[3] in vitreous silica: increases in density, and increases in the refractive index. The energy content increases produced in diamond and silicon carbide were of the order of magnitude 100 cal/g; the density changes in all these substances were of the order of magnitude of one percent. These changes were found to be progressive. They cannot be described in terms of the product of slow-neutron flux and time. A complete description requires specifying the neutron flux as a function of energy which is not available; but as well as it is known, it gives in conjunction with Seitz's theory the correct order of magnitude for the number of displaced atoms one estimates from some of the property changes.

The changes in properties which take place on heating the irradiated substances are termed annealing phenomena. It has been found that the different properties of a substance may not all anneal simultaneously and different substances may behave

quite differently. As examples of this complexity, the increases in energy content of diamond and silicon carbide were found to begin to anneal at 150°C and were progressive (though not uniform) over some hundreds of degrees while the changes in lattice constant (and density) seemed to anneal less readily, requiring somewhat higher temperatures. On annealing irradiated quartz, two of the properties, the density and refractive index, were found to exhibit further decreases below temperatures of about 600°C, and it was not until higher temperatures were reached that a change in the direction of the properties of unirradiated quartz began to take place. Annealing of the major properties in quartz was sluggish below the quartz-Tridymite transition, and it is therefore presumed that restoration of the original state of the substance by annealing may not be possible after extensive irradiation. All of the observed effects are similar to those described for the metamict minerals.[4] Magnesium oxide, spinel, and sapphire have been irradiated and show effects which are an order of magnitude smaller than for the above substances, as might be expected from conclusions reached in studies of metamict minerals.[5] The damaging which is here described may therefore be termed, in the older nomenclature, an artificial metamictization.

Radiation damage in quartz has been reported by Berman[6] who measured its thermal conductivity. Wittels' recent announcement of the marked alteration in its x-ray diffraction pattern[7] has made it desirable to make our results on this subject more widely known even though the work is still in progress. Wittels' work and ours seem to be in substantial agreement although we have found that small changes in the x-ray diffraction patterns are easily observed between 500 and 600°C, somewhat lower than reported by him, and small changes in the density occur by 450°C, the region in which Berman observed substantial annealing of the thermal conductivity changes.

The results announced here were obtained by a number of people. The irradiations were prepared by L. H. Fuchs and W. Primak, who with P. Day measured some of the properties. W. H. Zachariasen and later S. Siegel and J. Taylor made the x-ray diffraction studies. The energy contents were determined by E. J. Prosen, W. H. Johnson, W. A. Fraser, and L. B. Eddy at the National Bureau of Standards. The results will be reported in detail in several papers.

[1] An oral paper on this subject was delivered by W. Primak at a Ceramic Conference, Battelle Memorial Institute, October 28, 1952 (unpublished).
[2] F. Seitz, Discussions Faraday Soc. **5**, 280 (1949).
[3] It has been brought to our attention that M. H. Wittels has recently also observed such a change in heat capacity.
[4] A. Pabst, Am. Mineralogist **37**, 137 (1952).
[5] P. Pellas, Compt. rend. **233**, 369 (1951).
[6] R. Berman, Proc. Roy. Soc. (London) **A208**, 90 (1951).
[7] M. H. Wittels, Phys. Rev. **89**, 656 (1953).

The Magnetic Susceptibility of Germanium*

D. K. Stevens† and J. H. Crawford, Jr.
Oak Ridge National Laboratory, Oak Ridge, Tennessee
(Received September 24, 1953)

In preparation for a study of the effect of fast neutron bombardment on the magnetic properties of Ge, the specific magnetic susceptibility χ of both p- and n-type Ge with various impurity concentrations has been measured as a function of temperature in the range from 65°K to 300°K. The Faraday method was used throughout and the specimens were single crystals cut in the form of cubes 0.5 cm on edge.[1] The susceptibility balance was a refinement of the type used by Hutchison and Reekie[2] as modified by McGuire and Lane,[3] special features of which will be described elsewhere. The balance is sufficiently sensitive to detect differential weight changes of 0.2 μg. An Arthur D. Little Bitter-type electromagnet furnished the inhomogeneous magnetic field, (HdH/dz $\sim 10^8$ gauss^2 cm^{-1}). The field was controlled to better than 0.05 percent by means of the Hall voltage developed across a germanium crystal.[4] The value of HdH/dz was determined for each specimen by the magnetic buoyancy effect of oxygen, whose volume susceptibility κ at 760 mm Hg and 20°C is $1.434\pm0.004 \times 10^{-7}$ cgs unit.[5] The absolute precision of the calibration is ± 0.6 percent. The relative precision of χ *vs* T data on any one sample, however is better than ± 0.1 percent. Measurements of χ as a function of field strength indicated the absence of ferromagnetic impurity.

Curves of the diamagnetic susceptibility *vs* temperature for representative specimens are shown in Fig. 1. Curves 1, 2, and 5

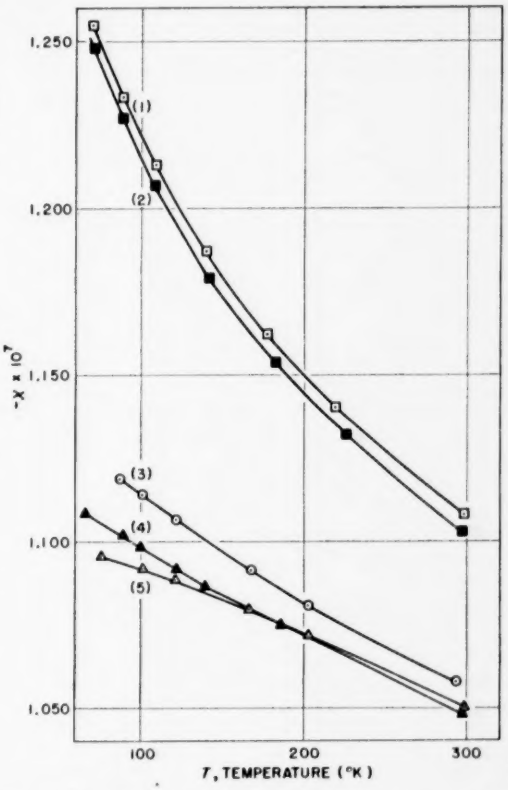

Fig. 1. Diamagnetic susceptibility *vs* temperature curves for single crystal cubes of germanium. Curves 1 and 2 are for low-resistivity n-type material, while 3 and 4 are for low-resistivity p-type material. Curve 5 is for high-resistivity n-type germanium.

are those of n-type samples whose room temperature electron concentrations were 7×10^{17}, 1×10^{18} and 1.3×10^{14} cm^{-3}-respectively, while curves 3 and 4 were obtained for p-type Ge in which the hole concentrations were 5.4×10^{17} and 2.1×10^{17} cm^{-3}-respectively. The carrier concentrations were inferred from Hall coefficient measurements made on plates cut adjacent to one of the cube faces.[6]

In their treatment of the magnetic behavior of gray tin, Busch and Mooser[7] divide the magnetic susceptibility into three parts: (1) the diamagnetic contribution χ_a due to the tin atoms alone which they assume to be temperature-independent, (2) the paramagnetic contribution χ_I due to those impurity atoms or ions which possess an unpaired electron, and (3) the free carrier contribution χ_c which has both a paramagnetic spin component and a diamagnetic Landau orbital component, the latter being greater the smaller the effective mass of the carrier. In the case of Ge it appears from Fig. 1 that in contrast to the assumptions concerning $\alpha-$Sn the term χ_a is temperature-dependent, the slope of all of

the χ *vs* T curves being $\sim 2.5 \times 10^{-11}$ cgs units/deg in the high-temperature range. The curve of the high-resistivity material (curve 5) shows concave downward curvature which is characteristic of both *n*- and *p*-type high-resistivity germanium. The curves for low-resistivity material are markedly concave upward, this being more pronounced for the *n*-type specimens. This difference in curvature is presumably due to the sum of the impurity and carrier contributions (χ_I and χ_c) which would be negligible in the case of curve 5. Thus, it appears that the Landau orbital dimagnetism of the free carriers exceeds the paramagnetism of the free carriers and impurities with unpaired electrons in both electron and hold conductors. From considerations similar to those of Busch and Mooser for the case of $\alpha-$Sn it can be shown that for germanium the ratio of the free electronic mass to the carrier effective mass is ~ 4 for holes and ~ 6 for electrons.

A more detailed report of this work based on more extensive data will be submitted for publication in the near future.

One of the authors (D. K. Stevens) is indebted to Professor H. D. Crockford for his aid in the capacity as advisor from the University of North Carolina.

* Part of a dissertation submitted by D. K. Stevens to the University of North Carolina in partial fulfillment of the requirements for the Ph.D. degree.
† Formerly a predoctoral fellow of the Oak Ridge Institute of Nuclear Studies from the University of North Carolina. Present address: Oak Ridge National Laboratory, Oak Ridge, Tennessee.
[1] The authors are indebted to Miss Louise Roth of Purdue University for preparing samples.
[2] T. S. Hutchison and J. Reekie, J. Sci. Instr. **23**, 209 (1946).
[3] T. R. McGuire and C. T. Lane, Rev. Sci. Instr. **20**, 489 (1949).
[4] Thanks are due to J. C. Pigg of this laboratory for the design of the field control equipment, details of which are being submitted for publication.
[5] P. W. Selwood, *Magnetochemistry* (Interscience Publishers, Inc., New York, 1943), p. 29.
[6] We are indebted to J. W. Cleland of this laboratory for the Hall coefficient measurements.
[7] G. Busch and E. Mooser, Z. Physik. Chem. **198**, 23 (1951).

The Contribution of Solar x-Rays to *E*-Layer Ionization

E. T. Byram, T. A. Chubb, and H. Friedman
United States Naval Research Laboratory, Washington, D. C.
(Received September 24, 1953)

ATTEMPTS to attribute *E*-layer ionization to absorption of solar ultraviolet radiation lead to serious difficulties. The most recent rocket measurements[1] of the intensity of the solar continuum in the neighborhood of 1200A indicated an upper limit of about 0.01 ergs cm^{-2} sec^{-1} per 100A corresponding to a black body temperature of 4500°K. The extrapolated intensity at 1000A would be less than 0.0004 ergs cm^{-2} sec^{-1} per 100A, and the intensity of radiation capable of ionizing the atmospheric constituents ($800 < \lambda < 1000$A) would be entirely inadequate to account for *E*-layer ionization. On the other hand, it has been known for some time that the soft x-ray spectrum between 10A and 100A furnishes a source of ionizing radiation with absorption coefficients appropriate for layer formation between 100 km and 120 km. The x-ray possibility was first indicated by Hulburt[2] and by Vegard[3] in 1938. Since Edlén,[4] in 1940, identified the lines of the visible coronal spectrum with highly ionized atoms such as Fe XV and Ca XIII, it has been recognized that the solar corona may be a source of x-rays of sufficient intensity to make an important contribution to *E*-layer ionization. More recently, Hoyle and Bates[5] treated the x-ray absorption process in detail and concluded that conditions for *E*-layer formation were satisfied by an x-ray spectrum with a maximum either near 38A or near 9.5A.

Rocket experiments performed since 1948 have provided positive evidence for soft x-rays in the ionosphere. Detection was accomplished with photographic films,[6] thermoluminescent materials,[7] and photon counters.[8] In the latter type of experiment, intensity data were telemetered to a ground station continuously throughout the flight. The first photon-counter experiment[8] was performed in V-2 No. 49, September 1949, using counters with beryllium windows capable of transmitting an appreciable percentage of the x-ray flux up to a wavelength of about 10A. X-rays were detected only above 87 kilometers, from which it was concluded that the spectrum had a short-wavelength limit at about 7A. Between this limit and the spectral cutoff of the photon counters at 10A, the x-ray flux incident on the earth's atmosphere amounted to between 10^{-4} and 10^{-3} ergs cm^{-2} sec^{-1}.

In May 1952, counters flown in two Aerobee rockets again gave indication of x-rays above 90 km. These tubes also used beryllium windows, but the apertures were larger than those of V-2 No. 49 and the sensitivity at 7A was about ten times greater. The results emphasized again the fact that the x-ray spectrum of a quiet sun had a well defined short-wavelength limit at about 7A. No information however was obtained regarding the x-ray flux beyond 10A.

An experiment to determine the x-ray intensity out to 100A was attempted in a Viking rocket (No. IX) in December, 1952. A number of tubes were prepared with windows of graded x-ray spectral transmission characteristics, utilizing thin films of beryllium, aluminum, soft glass, and nitrocellulose. Tube dimensions and gas fillings were selected in combination with the above window materials to produce bands of spectral response peaking in different parts of the spectrum. Although the rocket attained an altitude of 218 km, it developed an excessively high roll rate and faulty telemetering, which left only a small portion of the experimental data suitable for interpretation. Sufficient information was obtained from three tubes, however, to indicate a large flux of x-rays above 10A within the *E*-region. A photon counter with an aluminum window, 0.00025 inch thick, sensitive to radiation between 8 and 20A, measured a flux of about 0.6 erg cm^{-2} sec^{-1}. The variation with altitude is shown in Fig. 1. Two tubes with nitrocellulose windows, sensitive to wavelengths as long as 60A, detected about 1.0 erg cm^{-2} sec^{-1} at the top of the atmosphere.

Although none of the attempts to measure the full x-ray spec-

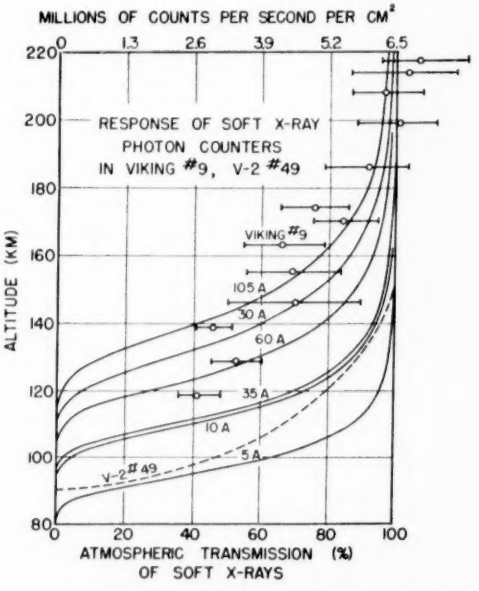

FIG. 1. Variation with altitude of the atmospheric transmission of soft x-rays. The solid lines are computed from absorption coefficients published by A. H. Compton and S. K. Allison [*X-Rays in Theory and Experiment* (MacMillan and Company, New York, 1935)]. The dashed curve is the averaged experimental data of two beryllium window photon counters in V-2, 49. Each open circle is the average of approximately 15 exposures of an aluminum window photon counter flown in Viking IX. The length of the bar through the circle represents the rms deviation of the data. The rocket was stable to 118 km with the photon counter looking away from the sun. Above 118 km the rocket rolled very rapidly and the tube received about 200 exposures to the sun.

trum have thus far been entirely successful, the partial results described above do show that the solar x-ray spectrum supplies of the order of one or two ergs cm^{-2} sec^{-1}, which is adequate to account for all of E-layer ionization. If the effective rate of electron production q is computed from the simple recombination law

$$q=\alpha N_e^2,$$

where α, the effective recombination coefficient,[9-13] is taken as 2×10^{-8} cm^3 sec^{-1}, and N_e, the electron density, is about 10^5 cm^{-3}, then q must be about 400 electrons cm^{-3} sec^{-1}. The production of this rate of ionization would require only about 10^{-1} erg cm^{-2} sec^{-1}. The excess energy observed in the Viking IX experiment may therefore be indicative of a relatively high ratio of negative ions to electrons[13-15] in the E-layer, or a higher value for the effective recombination coefficient than has been deduced from radio reflection measurements.

[1] Byram, Chubb, Friedman, and Gailar, Phys. Rev. **91**, 1278 (1953).
[2] E. O. Hulburt, Phys. Rev. **53**, 344 (1938).
[3] L. Vegard, Geofys. Publikasjoner **12**, No. 5 (1938).
[4] B. Edlén, Z. Astrophys. **22**, 30 (1942) and Monthly Notices Roy. Astron. Soc. **105**, 323 (1945).
[5] D. R. Bates and F. Hoyle, Terr. Mag. Atmos. Elec. **53**, 51 (1948).
[6] T. R. Burnight, Phys. Rev. **76**, 165 (1949).
[7] Tousey, Watanabe, and Purcell, Phys. Rev. **83**, 792 (1951).
[8] Friedman, Lichtman, and Byram, Phys. Rev. **83**, 1025 (1951).
[9] E. O. Hulburt, Phys. Rev. **55**, 639 (1939).
[10] J. N. Bhar, Indian J. Phys. **13**, 253 (1939).
[11] A. J. Higgs, Monthly Notices Roy. Astron. Soc. **102**, 24 (1942).
[12] T. R. Gilliland, Nat. Geograph. Soc., Solar Eclipse Series No. 2, 88 (1942).
[13] C. W. McLeish, Can. J. Research **A26**, 137 (1948).
[14] E. O. Hulburt, Phys. Rev. **46**, 822 (1934).
[15] Bates, Buckingham, Massey, and Unwin, Proc. Roy. Soc. (London) **A170**, 322 (1939).
[16] H. S. W. Massey, Proc. Roy. Soc. (London) **A163**, 542 (1937).

Nonsymmetric Unified Field Theories

W. B. Bonnor
University of Liverpool, Liverpool, England

(Received April 6, 1953; revised manuscript received October 5, 1953)

Kurşunoğlu[1] has recently proposed an interesting modification of Einstein's nonsymmetric unified field theory. In the modified form the doubts about the compatibility of the field equations do not arise because the latter can be derived from a variational principle; and it is claimed that the new field equations imply the Lorentz equations of motion for an electric charge. To derive the equations of motion, Kurşunoğlu uses the assumption that mass is entirely electromagnetic in origin. It appears, however, from a study of the static, spherically symmetric solutions of the field equations, that this assumption is not justified by the theory. I have not succeeded in obtaining the exact solutions of Kurşunoğlu's equations, but it is not difficult to obtain an approximation which gives an insight into their probable nature.

The proposed field equations are

$$R_{\underset{\sim}{\alpha\beta}}=-p^2(a_{\alpha\beta}-b_{\alpha\beta}), \tag{1}$$

$$R_{\underset{\sim}{\alpha\beta},\gamma}+R_{\underset{\sim}{\beta\gamma},\alpha}+R_{\underset{\sim}{\gamma\alpha},\beta}=-p^2I_{\alpha\beta\gamma}, \tag{2}$$

$$\mathfrak{g}^{\underset{\sim}{\alpha\beta}}{}_{,\beta}=0, \tag{3}$$

in which p^2 is a fundamental constant and all the other quantities have the same meanings as in Einstein's theory except

$$a_{\alpha\beta}=g_{\underset{\sim}{\alpha\beta}},$$
$$b^{\alpha\beta}=\mathfrak{g}^{\underset{\sim}{\alpha\beta}}/(-\det\mathfrak{g}^{\underset{\sim}{\alpha\beta}})^{\frac{1}{4}}.$$

The approach to the problem is similar to that in the case of the static, spherically symmetric solutions in Einstein's theory.[2,3] Using spherical polar coordinates and considering the purely electric case (magnetic field zero), we may take as the only nonzero $g_{\alpha\beta}$:

$$g_{11}=-\alpha,\quad g_{22}=-\beta,\quad g_{33}=-\beta\sin^2\theta,\quad g_{44}=\gamma,\quad g_{23}=-g_{32}=f\sin\theta,$$

where α, β, γ, and f are functions of r only. Equations (1) and (2) reduce to

$$\begin{aligned}R_{11}&=p^2\alpha[1-(1+f^2/\beta^2)^{-\frac{1}{2}}],\\ R_{22}&=p^2\beta[1-(1+f^2/\beta^2)^{\frac{1}{2}}],\\ R_{44}&=-p^2\gamma[1-(1+f^2/\beta^2)^{-\frac{1}{2}}],\\ R_{\underset{\sim}{23}}&=-p^2f+c,\end{aligned} \tag{4}$$

where c is a constant of integration, and the $R_{\alpha\beta}$ have the values calculated previously[3] (with $w=0$). Equation (3) is empty in the purely electric case. We assume that the tensor $a_{\alpha\beta}$ determines the metric of the space (though the same conclusions follow if $b_{\alpha\beta}$ is taken for this purpose), and that for large values of the radial coordinate r, this metric shall tend to that of the Schwarzschild solution for a point mass m. We suppose also that the electric field for large r shall be that of a point charge e, so that, as we are using spherical polar coordinates, g_{23} must have at large r the form $ie\sin\theta$. These suppositions are met if we assume a solution of the form

$$\alpha=1+2m/r+\sum_{n=2}^{\infty}h_n/r^n,\quad \beta=r^2,$$
$$\gamma=1-2m/r+\sum_{n=2}^{\infty}k_n/r^n,\quad f=ie+i\sum_{n=1}^{\infty}e_n/r^n, \tag{5}$$

h_n, k_n, e_n being constants. These expansions in powers of $1/r$ will give no information about the fields in the neighborhood of the origin, but will be of interest for distant regions.

Substituting (5) into (4), and supposing that $p^2\neq0$, it is found, after a long but straightforward calculation, that the solutions are

$$\begin{aligned}\alpha&=[1-2m/r+\tfrac{1}{2}e^2p^2/r^2+O(r^{-4})]^{-1},\\ \gamma&=1-2m/r+\tfrac{1}{2}e^2p^2/r^2+O(r^{-4}),\\ f&=i[e-4me/p^2r^2+O(r^{-4})].\end{aligned} \tag{6}$$

The constants m and e are arbitrary, and it becomes clear during the course of the calculation that no further arbitrary constants will arise.

It thus appears that the static, spherically symmetric solution has two distinct arbitrary constants, corresponding to mass and charge. If this solution is taken as referring to the electron and if mass is electromagnetic in origin, a relation between the constants would be expected. If m is taken as zero so that the solution contains only the arbitrary constant e, the terms in $1/r$ in the metric tensor vanish and the form of the gravitational field for large r does not allow any concentration of mass near the origin. It is noteworthy that since for large r the gravitational field is determined by the terms in $1/r$ in α and γ, and the electric field by the numerical term in f, the constant p does not affect the fields at large distances.

The electromagnetic origin of mass would be attractive in a nonsymmetric unified field theory because the charge density, which is defined, would presumably determine the mass density, which is not explicitly defined. If, as appears from the above, the hypothesis cannot be sustained, one has to consider how masses are to be represented. In Kurşunoğlu's theory it seems at first sight possible that part of the component $\mathfrak{T}_4{}^4$ of the pseudo stress-energy-momentum tensor density might represent mass density. However, if, as is suggested by the above solution, the masses and charges of particles may be assigned separately, the theory ought to give an account of the gravitational fields of uncharged masses; but if one abolishes the electromagnetic field by putting $g_{\underset{\sim}{\mu\nu}}=0$ the field equations reduce to those of general relativity for empty space, and $\mathfrak{T}_4{}^4$ reduces simply to the term $\mathfrak{t}_4{}^4$ of the pseudo tensor density $\mathfrak{t}_\nu{}^\mu$, which certainly does not represent mass density. Thus $\mathfrak{T}_4{}^4$ cannot in general contain a term representing mass density, and matter must presumably be represented by singularities in the field quantities. It is then necessary to suppose, since the charge is spread out over space (the charge density in (6) is proportional to df/dr), that charge can exist not associated

with matter; this is the case in all the static, spherically symmetric solutions in Einstein's form of the theory.[2,3]

[1] B. Kurşunoğlu, Phys. Rev. **88**, 1369 (1951).
[2] W. B. Bonnor, Proc. Roy. Soc. (London) **209**, 353 (1951).
[3] W. B. Bonnor, Proc. Roy. Soc. (London) **210**, 427 (1951).

The de Haas-van Alphen Effect in Arsenic

TED G. BERLINCOURT
United States Naval Research Laboratory, Washington, D. C.
(Received September 30, 1953)

THE de Haas-van Alphen effect (periodic dependence of magnetic susceptibility upon magnetic field) has been observed in a single crystal of arsenic. The torsion balance method[1] was used, the crystal being suspended in a horizontal magnetic field with a binary axis vertical and its trigonal axis horizontal. The measurements were carried out at liquid helium temperatures in magnetic fields between 22 and 25 kilogauss. The specimen, which exhibited good crystal development, was cleaved perpendicular to its trigonal axis from a large crystalline mass of Fisher A892 "Purified Arsenic." Earlier failure to observe any effect in arsenic[2] can probably be ascribed to poorer crystal quality and the unavailability of sufficiently high fields.

The nature of the de Haas-van Alphen effect in arsenic is illustrated in Fig. 1, where CH^{-2}, the couple per unit mass (in

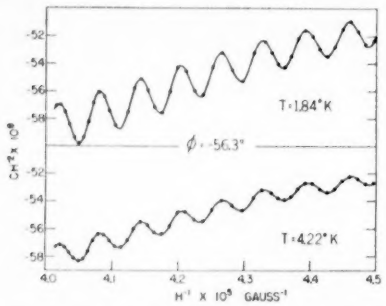

FIG. 1. Arsenic: CH^{-2}, the couple per unit mass in dyne-cm per gram acting on the crystal divided by the square of the magnetic field, *versus* the reciprocal of the magnetic field.

dyne-cm per gram) acting on the crystal divided by the square of the magnetic field (a quantity proportional to the difference in magnetic susceptibility along and at right angles to the trigonal axis) is plotted against the reciprocal of the magnetic field for an angle of $\phi=-56.3°$ between the trigonal axis and the magnetic field. (The sign of ϕ was determined according to the convention adopted by Shoenberg[1] in his study of antimony.) The data presented in Table I for the angular dependence of the period β/E_0 of the oscillations suggest that the constant energy surfaces for the de Haas-van Alphen electrons in arsenic probably fit the general scheme proposed by Shoenberg for bismuth and antimony. The amplitude a of the oscillations in CH^{-2} at 24 390 gauss is also listed in Table I. The degeneracy parameter E_0 for the de Haas-van Alphen electrons was calculated from the temperature dependence of the amplitude and was found to be $E_0=26\times10^{-14}$ erg. From the field dependence of the amplitude, the value for the temperature damping parameter x was found to be approximately 6°K at $\phi=-56.3°$ indicating high impurity content in the crystal. A spectrochemical analysis of fragments from the same batch of arsenic revealed impurities of approximately 1 percent Sb, 0.1 percent Bi, 0.1 percent Pb, and traces of Cu, Mg, Si. However, since addition of comparable amounts of impurities to tin,[1,3] which has parameters β and E_0 comparable with those of arsenic, had the effect only of increasing x (and consequently decreasing a), while leaving β and E_0 unaltered; the values quoted

TABLE I. Angular dependence of the period β/E_0 and the amplitude a of the oscillations in C/H^2 at 24 390 gauss.

ϕ	$(\beta/E_0)\times10^7$ (gauss^{-1})	$a\times10^8$ 4.22°K	1.84°K
−71.7°	5.34	0.21	0.59
−56.3	6.27	0.72	1.59
−41.0	6.81	0.37	
−26.4	6.73	0.56	
−11.9	6.27	0.57	
−0.7	5.44	0.38	
16.2	5.79		0.46
30.7	5.85		0.74
45.6	5.28		1.00
60.7	4.52		0.34
76.2	~3.9		~0.05

here for the latter parameters are probably also characteristic of pure arsenic.

It should be pointed out that the slow shift of the mean of the oscillations (See Fig. 1) cannot as yet be explained. It seems unlikely that ferromagnetic impurity could account for the shift, since it should presumably be saturated at fields well below 25 kilogauss, and since a broad maximum in this shift was observed for two different orientations. It would be tempting to attribute the shift to a very long period de Haas-van Alphen term, but the presence of such a term was not at all obvious in a graph of CH^{-2} *versus* ϕ. Since such a long period term would likely be more dependent upon purity,[4] investigation of this feature is being reserved for experiments on high purity arsenic.

[1] D. Shoenberg, Trans. Roy. Soc. (London) **245**, 1 (1952).
[2] Ted G. Berlincourt, Phys. Rev. **88**, 242 (1952).
[3] T. Croft, Annual Project Report, University of Pennsylvania, 1953 (unpublished).
[4] D. Shoenberg and M. Z. Uddin, Proc. Roy. Soc. (London) **A156**, 701 (1936).

Paramagnetic Resonances in Irradiated Glasses

E. L. YASAITIS AND B. SMALLER
Chemistry Division, Argonne National Laboratory, Lemont, Illinois
(Received October 2, 1953)

PARAMAGNETIC resonances have been detected in glasses which had been exposed to gamma radiation. The experimental data were taken over a frequency range of 18 to 375 Mc/sec. The equipment used was $\frac{1}{4}$-λ coaxial line regenerative detector developed for the 100- to 375-Mc/sec frequency range while the 18- to 100-Mc/sec range was covered by a cathode-above-ground regenerative detector with conventional tank coil wound around the sample. Both circuits were used in conjunction with a dual field modulation technique[1] designed for previous experiments. The detection limit was 2×10^{14} spins, requiring a 10^5 r exposure. The free radical diphenyl picryl hydrazyl was used both for intensity and field calibration.

The glass samples used fell into two groups: those containing borosilicate, and the boron-free glasses. The non-boron glasses, lead, lime, vitreous silica, and boron-free Pyrex (Corning No. 728) showed a prominent resonance at a gyromagnetic ratio of $g=2.0$, with minor differences in their subsidiary spectra. While the boron-free Pyrex spectra consisted of a singlet line, the lime and lead glasses at 375 Mc/sec showed doublet structure centered at $g=2.00$. A detailed study of the vitreous silica resonance yielded a precise value of g of 2.004 ± 0.004, independent of frequency. Subsidiary resonances were noted at lower g values.

The borosilicate glasses, Pyrex, Kovar, Vycor, Nonex, and uranium glass, when irradiated and investigated at 375 Mc/sec, displayed four distinct resonances having line widths of 1 to 2 gauss separated by 10 to 15 gauss. The complex structure may be presumed to be due to the presence of B^{11}, with $I=3/2$. However, although the strong field spectra correspond to a splitting constant of 80 Mc/sec, at weak fields anomalous effects remain to be explained.

All glasses except the vitreous silica showed a strong irradiation-independent resonance at $g=4.00\pm0.20$ and this is presumably due to some paramagnetic impurity.

Measurement of the optical densities of a series of gamma-irradiated samples of lime glass revealed that the paramagnetic resonance amplitude varied linearly with optical density. Likewise, with annealing at 200°C, the signal amplitude decreased proportionately with bleaching. For the gamma-ray excitation, the dependence of spin concentration on total radiation showed a saturation characteristic with an initial efficiency of, roughly, 20 ev per spin created.

Further studies on the processes involved will be published more completely in the near future.

[1] B. Smaller and E. Yasaitis, Rev. Sci. Instr. **24**, 991 (1953).

Visible Light from Localized Surface Charges Moving across a Grating

S. J. Smith* and E. M. Purcell
Lyman Laboratory, Harvard University, Cambridge, Massachusetts
(Received September 25, 1953)

It occurred to one of the authors (EMP) that if an electron passes close to the surface of a metal diffraction grating, moving at right angles to the rulings, the periodic motion of the charge induced on the surface of the grating should give rise to radiation. A simple Huygens construction shows the fundamental wavelength to be $d(\beta^{-1}-\cos\theta)$, in which d is the distance between rulings, β stands for v/c as usual, and θ is the angle between the direction of motion of the electron and the light ray. If $d=1.67$ microns, as in a typical optical grating, and if electrons of energy around 300 kev are used, the light emitted forward should lie in the visible spectrum. As for intensity, if we assume that the surface charge traversing the hills and dales is equivalent to a point charge e oscillating with an amplitude $d/10$, we find that in the forward direction the radiation (in laboratory coordinates) should amount to 40×10^{-12} erg (about ten photons) per sterad per millimeter of electron path. Only if the electron path lies within perhaps $d/2$ of the grating will the surface charge be so well localized. Nevertheless, with a reasonable electron current density over the surface an easily detectable amount of light should be produced. In fact, under the assumed conditions, the total radiation per cm² of grating surface, in milliwatts, should be about four times the electron current density parallel to the surface in amp/cm².

We have tried the experiment, using a small pressure-insulated Van de Graaff generator and electron accelerator tube. A 5-microampere beam, focused electrostatically and magnetically to a diameter of 0.15 mm and diverging less than 0.004 radian, is adjusted by deflection coils to pass over a flat grating,[1] just grazing its surface. The 48-mm long path across the grating, viewed from a forward position 10 or 20 degrees off the beam, appears as a sharp, luminous, colored line on the surface of the grating. The color of the light changes with angle of observation and beam voltage in the manner expected. The light is strongly polarized with the electric vector perpendicular to the grating. The effect of varying d can be investigated by rotating the grating in its own plane (a test suggested by E. H. Land) and here, too, the color changes as predicted.

The spectrum of the light has been recorded at low dispersion by photographing the source through a transmission grating. Light from the electron track is collected by a collimating lens, where an arc-shaped aperture restricts the range of angles θ, passed through the analyzing grating and received by a 35-mm camera ($f=90$ mm) focused for infinity. With this arrangement only one point on the line source is in good focus. Figure 1 shows a sequence of such photographs in which only the electron velocity was varied. Within the accuracy of our still rather crude measurements of wavelength and voltage, the predicted dependence of wavelength on v, d, and θ is quantitatively confirmed by the spectrograms. On spectrograms taken at $\theta=30°$, radiation of half the fundamental wavelength is detectable. Higher harmonics appear in considerable intensity at 90°, where we find radiation of one-third, one-fourth, and one-fifth the fundamental wavelength.

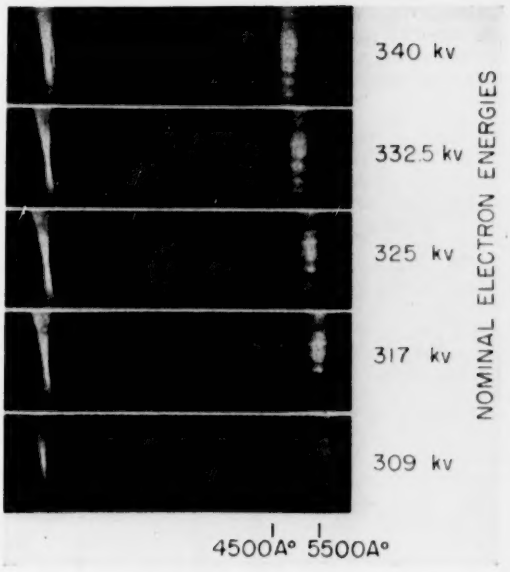

Fig. 1. Spectrogram of the light emitted from the grating surface at $\theta=20°$. Central images are vertically aligned on the left. First-order spectra appear on the right. Light was accepted over an interval of 3.5° in θ; this corresponds to a spread in wavelength of about 350° and accounts for the width of the first-order line. Striations in the first-order line are presumably due to vertical irregularities on the surface of the grating. The exposure time for each spectrum was about 60 seconds, on Linagraph Pan.

Although many details remain to be studied, we believe these observations establish the reality of the effect and suggest that it may have interesting applications.

* Recipient of a General Electric Fellowship in Applied Physics for 1952–53.
[1] Obtained from Baird Associates, Cambridge, Massachusetts.

Derivation and Renormalization of the Tamm-Dancoff Equations*,†

Behram Kurşunoğlu
Laboratory of Nuclear Studies, Cornell University, Ithaca, New York
(Received August 10, 1953)

In this note we show that (1) the derivation of Tamm-Dancoff (T.D.) equations for two nucleons (as well as for meson-nucleon scattering) from the covariant Bethe-Salpeter[1] (B.S.) equation can be simplified to a remarkable degree, and (2) the renormalizations in the T.D. method can be achieved in a covariant manner without having the difficulties presented by the original T.D. method.

We introduce the spinor function $\psi(12)$ by the relation

$$\chi(12)=\int S_{F'a}(11')\beta_a\psi(1'2)d1'+\int S_{F'b}(22')\beta_b\psi(12')d2', \quad (1)$$

where $\chi(12)$ is the B.S. wave function for two nucleons. By using (1) in the B.S. equation we obtain

$$[(\beta\gamma_\mu\partial_\mu+\beta M)_a+(\beta\gamma_\mu\partial_\mu+\beta M)_b]\psi(12)$$
$$=-\int g(121'2')\psi(1'2')d1'd2', \quad (2)$$

where $\mathcal{I}(121'2')$ is the interaction operator and M is Schwinger's[2] mass operator.

In momentum space, neglecting radiative corrections to the nucleon propagators, the wave functions $\chi(12)$ and $\psi(12)$ are related by

$$\chi(p_\mu)=\left[\frac{1}{H_a(\mathbf{p})-\frac{1}{2}E-p_0}+\frac{1}{H_b(-\mathbf{p})-\frac{1}{2}E+p_0}\right]\psi(p_\mu). \quad (3)$$

One of the ways of deriving a 3-dimensional equation from the covariant B.S. equation consists in (i) defining an equal-time wave function by $\chi(\mathbf{p})=\int\chi(\mathbf{p},p_0)dp_0$, and (ii) using the approximation of replacing $\psi(p_\mu)$ in (3) by a 3-dimensional "wave function" $\psi(\mathbf{p})$. The procedure (ii) differs from that of Klein[3] only by way reducing the B.S. equation by one degree with the use of the transformation (1) which includes also radiative corrections to the nucleon propagators. The use of (i) and (ii) in the B.S. equation leads to the T.D. equation. The use of the approximation (ii) is, of course, the only drawback of the theory. A step forward of not using (i) and (ii) has recently been taken by Dyson,[4] and it may well avoid some of the difficulties about the physical meaning of a 4-dimensional two-body wave function. Despite that, one is inclined to believe that a 4-dimensional wave function must have some deep-seated implications. In any case, Dyson's equation for positive energy projection of his wave function is equivalent to the above approximation.

With the radiative corrections, the relative energy p_0-dependence of the B.S. wave function will assume the form

$$\chi(p_\mu)=[S_{F'a}(\tfrac{1}{2}K_\mu+p_\mu)\beta_a+S_{F'b}(\tfrac{1}{2}K_\mu-p_\mu)\beta_b]\psi(\mathbf{p}). \quad (4)$$

From (3) one obtains

$$\chi(\mathbf{p})=2\pi i[\Lambda_+{}^a(\mathbf{p})\Lambda_+{}^b(-\mathbf{p})-\Lambda_-{}^a(\mathbf{p})]\psi(\mathbf{p})=2\pi i\Lambda_-{}^{ab}(\mathbf{p})\psi(\mathbf{p}).$$

For meson-nucleon scattering the p_0-dependence of the wave function can be defined by

$$\chi(p_\mu)=[S_{F'}(aK_\mu+p_\mu)\beta+\Delta_{F'}(bK_\mu-p_\mu)]\psi(\mathbf{p}), \quad (5)$$

where c is a constant and $a+b=1$. The B.S. equation for meson-nucleon scattering can be written down without much difficulty and such an equation has already been used.[5,6]

Now the B.S. equation for two nucleons, in the c.m. system, in momentum space reads

$$\chi(p_\mu)=-S_{F'a}(\tfrac{1}{2}K_\mu+p_\mu)S_{F'b}(\tfrac{1}{2}K_\mu-p_\mu)\int I_{F'}(p_\mu,p_\mu',K_\mu)\chi(p_\mu')d^4p'. \quad (6)$$

The complete T.D. equation is obtained by two steps in the following order: (a) we integrate both sides of (6) with respect to p_0; (b) we use (4) and then integrate the interaction operator with respect to the remaining relative energy variables. The resulting equation is

$$\int[S_{F'a}(\tfrac{1}{2}K_\mu+p_\mu)\beta_a+S_{F'b}(\tfrac{1}{2}K_\mu-p_\mu)\beta_b]dp_0\psi(\mathbf{p})=-\int dp_0d^4p'S_{F'a}(\tfrac{1}{2}K_\mu+p_\mu)S_{F'b}(\tfrac{1}{2}K_\mu-p_\mu)I_{F'}(p_\mu,p_\mu',K_\mu)\times[S_{F'a}(\tfrac{1}{2}K_\mu+p_\mu')\beta_a+S_{F'b}(\tfrac{1}{2}K_\mu-p_\mu')\beta_b]\psi(\mathbf{p}'). \quad (7)$$

When the radiative corrections are neglected, (7) reduces to

$$\Lambda_-{}^{ab}\psi(\mathbf{p})=-\frac{1}{2\pi i}\int dp_0d^4p'S_{Fa}(\tfrac{1}{2}K_\mu+p_\mu)S_{Fb}(\tfrac{1}{2}K_\mu-p_\mu)\times I_F(p_\mu,p_\mu',K_\mu)S_{Fa}(\tfrac{1}{2}K_\mu+p_\mu')\beta_aS_{Fb}(\tfrac{1}{2}K_\mu-p_\mu')\beta_b\times[H_a(\mathbf{p}')+H_b(-\mathbf{p}')-E]\psi(\mathbf{p}'), \quad (8)$$

which for the positive energy projection of the wave function leads to the same results as that of Lévy[7] and Klein.[3] We note that Eq. (7) is in a form for carrying out the mass and charge renormalizations first in a covariant fashion and then by integration of the resulting expression with respect to the relative energy variables, leading to the renormalized T.D. equation. The integration of the renormalized parts of the kernel over the relative energy variables will not be very easy, but the procedure is unambiguous.

The integrals over the p_0's in (8) can be simplified considerably by noting that, e.g., an expression like $(A-p_0)^{-1}$ or $(A-p_0-p_0')^{-1}$ under the integral sign can be written as $i\int_0^\infty\exp[-i\alpha(A-p_0)]d\alpha$, in which A has a small negative imaginary part. In the G^4 term of the B.S. kernel, for example, one has 4 terms with 10 factors of the above form in each of the 4 terms, and when all the p_0 integrals are performed, the resulting δ-functions under the integral sign provide 3 linear algebraic equations for 10 positive parameters α, β, γ, etc. Because of the positive character of the parameters α, β, γ, etc. there are only 6 possibilities of eliminating 3 of the 10 parameters α, β, γ, etc., and these lead to 6 matrix elements for each of the 4 terms of the G^4-order B.S. kernel. The actual performance of the above method of calculation and writing down all of the 24 matrix elements corresponding to a B.S. diagram (meson lines crossed or the iterated ladder) takes very little time, and the parameters α, β, γ, etc. can be correlated with the T.D. diagrams. The extension of the above method, with the use of (5), to meson-nucleon scattering is straightforward.

A thorough examination of the non-adiabatic terms and the radiative corrections for the two-nucleon problem is in progress and will be reported in the near future.

The author is grateful to Professor H. A. Bethe for interesting discussions.

* Research supported by the Turkish Government and the U. S. Office of Naval Research.
† Part of this work was reported at the Washington Meeting of the American Physical Society, April 29, 1953.

[1] E. E. Salpeter and H. A. Bethe, Phys. Rev. **84**, 1232 (1951).
[2] J. Schwinger, Proc. Nat. Acad. Sci. U. S. **37**, 452 (1951).
[3] A. Klein, Phys. Rev. **90**, 1101 (1953).
[4] F. J. Dyson (unpublished manuscript).
[5] S. Deser and P. C. Martin, Phys. Rev. **90**, 1075 (1953).
[6] W. M. Visscher, Cornell Thesis, 1953 (unpublished).
[7] M. M. Lévy, Phys. Rev. **88**, 72 and 725 (1952).

Velocity Distribution of the Pair Components in π^0 Decay

O. Halpern and K. Baumann
American Express Company, Zürich, Switzerland
(Received September 8, 1953)

THE alternate modes of decay of the neutral meson ($\pi^0\to2\gamma$, $\pi^0\to\gamma+e^-+e^+$) have recently been the subject of various theoretical[1] and experimental[2] studies.

A closer theoretical investigation has shown to us that characteristic differences may be expected to occur if comparison is made, e.g., with the process of nuclear conversion[3] of a γ ray. While in this last-mentioned process the energy of the pair created equals that of the otherwise directly emitted photon with the total momentum of the pair remaining indefinite, we encounter a very different situation in the process $\pi^0\to\gamma+e^-+e^+$ which can most easily be visualized in the rest system of the decaying meson.

The process in question can be thought of as consisting of two steps; the first is the emission of two equal photons with opposite directions of propagation, the second the creation of a pair by one of these photons. The conservation theorems allow a range of photon energy between 0 and $\mu_0c^2/2-2m^2c^2/\mu_0$ (m = electron mass, μ_0 = mass of the neutral meson). The pair created must therefore have an energy lying between $\mu_0c^2/2+2m^2c^2/\mu_0$ and μ_0c^2, while its total momentum must equal that of the virtual photon by which it is created and will therefore range from $\mu_0c/2-2m^2c/\mu_0$ to 0.

This difference in the conservation rules valid for the creation of the pair accounts for certain deviations from the customarily observed law of distribution of energy between the two components of the pair. One finds that about $\frac{2}{3}$ of all processes lead to a real photon, the energy of which differs from the maximum energy possible by not more than one percent. Although energy is almost conserved in the creation of a large fraction of all the pairs, in about 40 percent of all processes the energy limit of the slower pair component is larger than $5mc^2$. This behavior is most pronounced for those processes in which the photon energy lies either very near its maximum value or deviates from it by at least $5mc^2$.

It should be pointed out that the magnitude of the kinetic energy of the decaying meson can be calculated from the conservation laws, if one is able to measure the energies of the pair components as well as the angles between the direction of propagation of the decaying meson and the pair components. This assumes that one can, at least approximately, draw a line from the star in which the π^0 meson is created to the intersection of the paths of the pair components. No recourse needs to be had in this case to the previously observed energy distribution of charged π mesons; one can measure directly the primary energy of the individual neutral meson.

A detailed report on the calculations leading to the results quoted and to their extension to the decay of moving mesons will soon be submitted to *The Physical Review*.

One of the authors (O.H.) wants to express his gratitude to Professor C. F. Powell and his collaborators Dr. Perkins and Dr. Anand for much interesting information on the experimental status of these questions.

[1] R. H. Dalitz, Proc. Phys. Soc. (London) **A64**, 667 (1951).
[2] Daniel, Davies, Hulvey, and Perkins, Phil. Mag. **43**, 753 (1952); Lindenfeld, Sachs, and Steinberger, Phys. Rev. **89**, 531 (1953); other papers by the Bristol group on the present subject are in the process of publication.
[3] J. R. Oppenheimer and L. Nedelski, Phys. Rev. **44**, 948 (1939).

Total Cross Sections for 169-Mev Neutrons

A. E. Taylor*
Gustaf Werner Institute for Nuclear Chemistry, University of Uppsala, Uppsala, Sweden
(Received September 21, 1953)

THE present work has been the first of a series of experiments with high-energy neutrons produced by the 230-cm synchrocyclotron at the University of Uppsala. Neutrons were produced by proton bombardment of an internal Be target, and the experiment consisted of good-geometry transmission measurements in a well collimated neutron beam. A coincidence counter telescope was used to detect recoil protons from a thin polyethylene disk placed in the beam. This counter telescope consisted of three scintillation counters feeding a diode bridge type coincidence circuit.[1] Aluminum absorbers were placed between the second and the third counters in order to set a lower-energy limit to the recoil protons detected, and the effective neutron energy was calculated[2] to be 169 Mev with a possible error of 4 Mev.

The hydrogen cross section was determined by measuring the attenuation of the neutron beam in samples of polyethylene and graphite containing the same amounts of carbon. Similarly the difference between the deuterium and hydrogen cross sections was found from samples of ordinary and heavy water containing the same amounts of oxygen. The cross sections determined are as follows:

Hydrogen	49.2 ± 1.6 mb
Deuterium $-$hydrogen	23.1 ± 2.0 mb
Carbon	323 ± 3 mb
Oxygen	430 ± 5 mb

The quoted errors are standard deviations based on the total number of counts. A more detailed account of the work will be published later.

The author wishes to thank Professor The Svedberg for extending the facilities of his laboratory; Professor Niels Bohr and Sir John Cockcroft for the opportunity of working under CERN auspices; and many members of the Gustaf Werner Institute, in particular Dr. H. Tyrén for active encouragement, U. Tallgren, R. Alphonce, A. Johansson, and members of the cyclotron operating crew for help and assistance.

* Now at the Atomic Energy Research Establishment, Harwell, Berkshire, England.
[1] Dickson, Salter, Gunnill, Dolley, and Cassels, Harwell Atomic Energy Research Establishment Report G/R 1038, 1952 (unpublished).
[2] A. E. Taylor and E. Wood, Phil. Mag. **44**, 95 (1953).

The Interpretation of Bhabha's Theory of Particles of Maximum Spin 3/2

W. A. Hepner and D. R. Workman
Department of Mathematics, Imperial College of Science, London, England
(Received September 8, 1953)

BHABHA'S theory[1] of particles of maximum spin $\frac{3}{2}$, characterized by the representation scheme R_3 $(\frac{3}{2}, \frac{3}{2})$, has the peculiar feature that the normalization is negative for all states with the higher of the two possible values $(\mu, 3\mu)$ of the rest mass, and the application of the customary probability interpretation leads to the difficulty of negative probabilities. For this reason, and doubtless also because of the greater complexity of the noncommutative algebra involved, very little has been published on the results of this equation, apart from Le Couteur's work[2] on the scattering of mesons by these particles. In order to get some clue about a possible interpretation, it may be helpful if some of the peculiar consequences are brought out in high relief in a very simple, illustrative case. We have therefore studied the magnitudes and behavior of the reflection and transmission coefficients of Bhabha's particles at a discontinuity V (>0) of the electric potential, the well-known problem treated by Klein for the Dirac electron.[3] Similar considerations will apply to other cases with static potential, e.g. Coulomb scattering.

The analysis of this problem[4] shows that, with incident particles of the lower mass μ and of energy ω, the states of higher mass and negative normalization can occur only in conjunction with states of lower mass such that the total current is conserved in accordance with the equation $1 = R_1 - R_3 + T_1 - T_3$, where R_1, R_3, (T_1, T_3) are the magnitudes of the reflected (transmitted) currents of particles of lower and higher mass, divided by the incident current. For example, with $\omega = 5\mu$ and $eV = 3\mu$, one obtains $R_1 = 52$, $R_3 = 59$, $T_1 = 8$, $T_3 = 0$. This would mean that, apart from ordinary reflection and transmission of the original incident current, the barrier also gives rise to a concomitant creation of pairs of particles of different mass and opposite charge, which are also reflected and transmitted, the energy of each particle being the same as the incident energy. Now it is clear that the energy of these pairs cannot be obtained from the static field, and they cannot, therefore, be considered as real. This indicates that physically interpretable results may be derived from this theory by subtracting the contributions arising from the unreal created pairs and applying the ordinary probability interpretation to the rest. The calculation shows that the ratio of the created to the incident current increases from zero, at $\omega = 3\mu$, to a maximum, which may be of the order of several thousands, and then decreases to the finite limit $eV/2\mu$ for very high incident energies. On the other hand, the proportion of the created particles of lower mass in the reflected and transmitted currents follows no simple pattern. While under conditions of total reflection of the incident current the created particles, too, are totally reflected, in the other extreme case of total transmission (that is, in the limit of very high incident energies) all the created particles go into the reflected current $(R_1 \to R_3 \to eV/2\mu,\ T_1 \to 1,\ T_3 \to 0)$, as though they were totally transmitted *from* the barrier region into free space.

Whatever the interpretation of the higher mass states, it is of some interest to note that, in the energy regions where no states of higher mass can be involved (that is, with incident energies less than 3μ and potential energies less than 2μ), the ordinary probability interpretation can be applied without modification. This leads, first of all, to the significant result that in the nonrelativistic limit of incident particles of the lower mass, and with small potentials (so that the transmitted kinetic energy is small and positive), the particles actually behave like Dirac electrons. Moreover, as long as no states of higher mass are involved, this unmodified interpretation can consistently be continued even in the relativistic region where significant deviations from the behavior of Dirac electrons occur. In the present illustrative case one finds that, with the values of eV/μ of 0.5 and 1, the reflection coefficient R is always much greater than for the Dirac electron;

for example, with $eV=0.5\mu$ and $\omega=1.6\mu$, one obtains 0.33, as compared with 0.14 for the Dirac electron, while with $\omega=1.85\mu$ the values are 0.16 and 0.03, respectively. Apart from this difference in magnitude, there is also a typical minimum of R with increasing incident energy below $\omega=3\mu$, which is impossible with the Dirac electron, where R drops montonically to zero for such high values of ω. Similar marked effects in the region of validity of the ordinary interpretation can be found in other more realistic problems (e.g., Coulomb and Compton scattering, details of which will be given elsewhere), and they may thus lead to tests of the theory regardless of questions of interpretation in other regions.

[1] H. J. Bhabha, Revs. Modern Phys. **17**, 200 (1945); Proc. Indian Acad. Sci. **A21**, 241 (1945).
[2] K. J. Le Couteur, Proc. Cambridge Phil. Soc. **44**, 63 (1947).
[3] O. Klein, Z. Physik **53**, 157 (1929). Without discussing intensities, the energy regions of total reflection of a particle with two mass states have been considered by G. Pétiau, Rev. Sci. Instr. **85**, 135 (1947).
[4] For the calculation of the required expansion coefficients it is convenient to use a basic orthonormal set of (16-component) solutions that are also eigensolutions of the spin in the direction of motion. This is most readily obtained by transformation from the rest system, and by use of a certain canonical transformation. See W. A. Hepner, Phys. Rev. **81**, 290 (1951); **84**, 744 (1951).

The Single-Time Bethe-Salpeter Equation

WILHELM MACKE
Instituto de Fisica Teórica, Sao Paulo, Brazil
(Received September 8, 1953)

IN a recent issue of this journal, Dyson[1] published a note about the Tamm-Dancoff method for treating the interaction of two particles in bound states. In this note he proposes to replace the usual wave function

$$a(N)=(\phi_0, A(N)\Psi), \tag{1}$$

by another one,

$$a(N', N)=(\Psi_0, C(N')A(N)\Psi), \tag{2}$$

and get

$$(W-E_N+E_{N'})a(N', N)=(\Psi_0, [C(N')A(N), H']\Psi) \tag{3}$$

as an equation of motion for $a(N', N)$. The notation here is the same as in Dyson's letter. By comparison of (2) with the paper of Gell-Mann and Low[2] it can be easily seen that $a(0, 2)$ is the single-time form of the Bethe-Salpeter wave function for two particles in positive free-energy states.

To find an equation for $a(0, 2)$ only, there are two possibilities. First, it can be developed by solving Eq. (3) and eliminating afterwards all components $a(N', N)$ with the exception of $a(0, 2)$. The other way consists in the transformation of the Bethe-Salpeter equation, given in its most general form, into a single-time four-component equation, as was proposed by the author[3] and outlined in three papers,[4,5] the first of them (I) giving the general derivation of the single-time equation. The second paper (II) is concerned with possible transformations of that equation into other forms, and in the third paper (III) the process of renormalization for this single-time equation is described.

The results show that the wave equation for $a(0, 2)$ can be given by

$$a(0, 2)=fa(0, 2), \tag{4}$$

just as in the Tamm-Dancoff case, where f is an integral operator which can be represented by a totality of "time-ordered graphs" given by Lévy. This totality does not contain vacuum graphs, as Dyson shows. But further on, the analytical meaning of f is rather different from the Tamm-Dancoff case, as is shown explicitly in (II), where the two methods are compared. Here, as well, the totality of graphs is different, and also the energy denominators are different in some cases.

The derivation of (4) from Dyson's equation of motion can be found directly by, first, writing out the interaction operator H' of (3) and eliminating all the $a(N', N)$ with the exception of $a(0, 2)$. Then the graphic representation for all virtual states and transitions can be constructed in the same way as Lévy did, but here it will contain also the "absent particles" N' with negative energies. These particles N' now can be represented by lines running backward, and by application of the rules of partial fraction decomposition, as given in (I), Eq. (4) is obtained, with an operator f which is identical with the operator $'f_F'+'f_G'$ in Eq. (14) of (II).

As was discussed in (II), something can also be said about the relations between the different wave function definitions given in (1) and (2). As there is a connection between the two vacuum states,

$$\Psi_0=P\exp\left(-i\int_{-\infty}^{0}H'dt\right)\phi_0, \tag{5}$$

there follows from (1) and (2) a relation of the form

$$a(0, 2)=ga(2). \tag{6}$$

The quantity g is calculated in (II). Here it can be found also as an integral operator, representable by Lévy graphs, if one substitutes (5) into (2). The exponential function needs to be expanded, the time integrations to be performed, and H' to be represented by the related creation and annihilation operators. All $a(N)$ for $N\neq 2$ can then be eliminated by the Tamm-Dancoff method and so finally an explicit form for g can be found.

[1] F. J. Dyson, Phys. Rev. **90**, 994 (1953).
[2] M. Gell-Mann and F. Low, Phys. Rev. **84**, 350 (1951).
[3] W. Macke, Phys. Rev. **91**, 195 (1953).
[4] W. Macke, I and II, Z. Naturforsch. (to be published).
[5] W. Macke, III, Nuovo cimento (to be published).

The Fission Yields of Ru^{103} and Ru^{106}

W. H. HARDWICK
Atomic Energy Research Establishment, Harwell, Berkshire, England
(Received September 14, 1953)

THE generally accepted values for the fission yields of Ru^{103} and Ru^{106} for natural uranium using pile neutrons were obtained by Glendenin and Steinberg.[1] These fission yields have been redetermined for natural uranium irradiated in the Harwell pile. Under the experimental conditions the contribution from fast fission was considered to be negligible. Ru^{106} (as Rh^{106}) and the reference standards Ba^{140} and Cs^{137} were determined by β counting. The disintegration rate of Ru^{103} was found by γ counting, assuming the decay scheme proposed by Kondaiah[2] and Mei,[3] and with allowance for the γ's arising from the Ru^{106} present. This allowance was determined by β and γ counting pure Ru^{106} separated from old fission products.

An end-window geiger tube was used for β counting. It was calibrated against a "4π" counter of Isotopes Division, Atomic Energy Research Establishment, and checked using a Ra D–E–F source whose disintegration rate was known from α counting. The Ru^{106} aliquots for counting were evaporated on thin plastic film and always contained less than 0.1 mg of carrier. Under these conditions scattering and self-absorption corrections are less than 1 percent.

The γ scintillation counter employed a sodium iodide crystal 1.75 inches in diameter, and 0.75 inch thick. It was calibrated using sources of Au^{198} and Cs^{137}. These two isotopes were chosen because γ emission from Au^{198} is almost wholly 0.41 Mev, and γ emission from Cs^{137} almost wholly 0.66 Mev. The Ru^{103} γ energy of 0.49 Mev is intermediate, and it was assumed that the efficiency of the γ counter for the Ru^{103} γ would thus lie between the values found for the Au^{198} and Cs^{137} γ's. Story[4] has reviewed the published data and, allowing for conversion, has estimated that 93 percent of β emissions from Au^{198} are accompanied by 0.41 Mev γ's, and 82 percent of the β emissions from Cs^{137} are accompanied by 0.66 Mev γ's. Using these data, the efficiency of the γ counter was found to be 2.88 percent for Au^{198}, and 2.73 percent for Cs^{137}. The efficiency for Ru^{103} was taken to be 2.8 percent.

Four samples of uranium metal were irradiated, one for seven

days, one for a month, and two for six months. The samples were dissolved in warm nitric acid. Aliquots were evaporated with ruthenium metal carrier, and fused with a $KOH-KNO_3$ mixture to ensure exchange between fission product and carrier. The ruthenium was then converted to RuO_4 by periodate oxidation and purified by distillation and solvent extraction.

The Ba^{140} activities in the 7-day and one-month irradiations were determined by the method of Glendenin and Steinberg,[5] modified by Cook.[6] The Cs^{137} activities in the six-month irradiations were determined by J. G. Cuninghame and M. Sizeland, using a perchlorate separation followed by β counting.

From the saturation activities, the fission yields of Ru^{103} and Ru^{106} were calculated relative to Ba^{140} for the seven-day and one-month irradiations. The fission yield of Ba^{140} was taken to be 6.2 percent. The saturation activities for Ru^{106} and Cs^{137} were calculated for the 6-month irradiation, and assuming a fission yield of 6.15 percent[7] for Cs^{137}, the fission yield of Ru^{106} was found. The values obtained are given in Table I.

TABLE I. Fission yields of Ru^{103} and Ru^{106}. Summary of experimental results.

Irradiation period	7 days	1 month	6 months	
Standard	Ba^{140}	Ba^{140}	Cs^{137}	Cs^{137}
Fission yield Ru^{103}	2.8	2.9	—	—
Fission yield Ru^{106}	0.37	0.38	0.38	0.39

The probable error in the determination of the value for Ru^{103} is ± 5.7 percent and for $Ru^{106} \pm 7.6$ percent. These errors are largely due to the uncertainties in the fission yields of Ba^{140} and Cs^{137} and the half-lives of Ru^{106} and Cs^{137}.

Thus the values for the percentage fission yields were found to be 2.85 ± 0.16 for Ru^{103} and 0.38 ± 0.03 for Ru^{106}. They are lower than Glendenin and Steinberg's values which were 3.7 and 0.52 for Ru^{103} and Ru^{106}. In both determinations the ratio of the Ru^{103} and Ru^{106} yields is nearly the same, being approximately seven.

I am grateful to Dr. J. M. Fletcher for suggesting this work and to him and Dr. G. B. Cook for most helpful discussions; also to the Director of the Atomic Energy Research Establishment, Harwell, for permission to publish this letter. Full details are being given in Atomic Energy Research Establishment Report C/R 1180.

[1] L. E. Glendenin and E. P. Steinberg, *Radiochemical Studies: The Fission Products* (McGraw-Hill Book Company, Inc., New York, 1951), Paper No. 103, National Nuclear Energy Series, Plutonium Project Record, Vol. 9, Div. IV.
[2] E. Kondaiah, Phys. Rev. **79**, 891 (1950).
[3] J. G. Mei, Phys. Rev. **79**, 429 (1950).
[4] J. M. Fletcher and J. Story, Harwell Atomic Energy Research Establishment Report C/R 1078 (unpublished).
[5] L. E. Glendenin and E. P. Steinberg, reference 1, Paper No. 288.
[6] G. B. Cook and H. Willis (unpublished).
[7] H. G. Thode, Can. J. Phys. **31**, 517 (1953).

The Total $\pi^- - p$ Cross Section at 840 and 470 Mev*

A. M. SHAPIRO, C. P. LEAVITT, AND F. F. CHEN
Brookhaven National Laboratory, Upton, New York
(Received September 10, 1953)

THE total $\pi^- - p$ cross section has been measured at 840 Mev. Since this value appeared considerably higher than that measured at 450 Mev,[1] the measurement was repeated at the lower energy to confirm the difference with the same experimental arrangement and apparatus.

The experimental arrangement is shown in Fig. 1. A Be target, 6 in.$\times$2 in.$\times$2 in., was placed in a straight section of the Brookhaven cosmotron and bombarded by 2.2-Bev protons. Particles emitted from the target at an angle of 32° to the proton direction passed through a 3-in. diameter collimator in the concrete shielding wall.

This beam was then magnetically analyzed, and particles of the proper sign and momentum entered a threefold defining telescope.

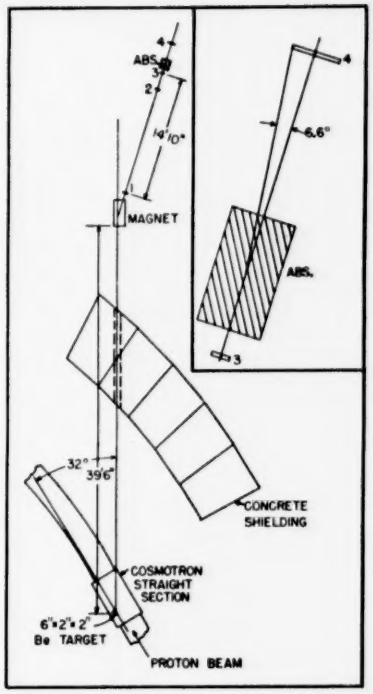

FIG. 1. Experimental arrangement.

The resolution of the analyzing magnet was measured using a current-carrying wire. The half-angle which the third defining counter subtended at the magnet was 0.32°, corresponding to a meson energy resolution of ± 20 Mev. Carbon and polyethylene absorbers were placed after the third counter, and at a variable distance behind them a large fourth counter measured the transmitted beam.

Fast plastic scintillators were used, the first three being $2\frac{1}{2}$ in. and the fourth $6\frac{1}{4}$ in. in diameter. Three- and four-fold coincidences were made in a Garwin-type[2] circuit, modified[3] in a manner permitting fast multifold coincidences. The resolving time of the circuit was about 4×10^{-9} sec.

The composition of the analyzed beam of negative particles entering the telescope was determined by careful analysis of the absorption of the beam in Cu and Pb. The only contamination observed was that of μ mesons, which amounted to (2 ± 2) percent and (5 ± 3) percent for the 870- and 500-Mev beams, respectively. (These energies correspond to 840 and 470 Mev mean energy in the absorbers.)

Runs made with two different sets of absorbers and taken over a period of several months have given statistically consistent results. The carbon absorber was spaced out to fill the same physical volume as the polyethylene, and the two contained nearly equal numbers of carbon atoms. Most of the data were taken with 28.18 g/cm² of C and 32.65 g/cm² of CH_2, which gave a hydrogen attenuation of approximately 7 percent. The C and CH_2 absorbers were frequently interchanged to eliminate the effects of any slight drifts in the equipment.

The 840-Mev measurements were made with two geometries. In the "poor" geometry, the fourth counter subtended at the center of the absorber a half-angle of 6.6°; in the "good" geometry, a half-angle of 2.1°. The $\pi^- - p$ cross sections measured with these two geometries, and corrected for the μ contamination, were 44 ± 4 mb and 57 ± 5 mb, respectively. (All errors are standard deviations.) These values of σ must be corrected for two secondary

effects which are different for the two geometries. The value of σ (poor) is low because some products of the $\pi^- - p$ interaction will pass through the last counter. On the other hand, σ (good) is high because a few more mesons are multiply scattered out of the last counter by the CH_2 than by the C attenuator, when the "good" geometry is used. We have assumed that 3 percent of the $\pi^- - p$ interactions give a charged secondary traveling within 6.6° of the beam direction, and 0.3 percent within 2.1°. This corresponds to the condition that all the interactions are elastic scatterings with an isotropic distribution in the center-of-mass system, or to the condition that $\frac{1}{3}$ of the interactions are elastic scatterings with a $\cos^2\theta$ distribution and that the rest send no charged products into the last counter. From a detailed multiple Coulomb scattering calculation it was found that about 9 and 7 percent of the mesons were scattered out of the last counter by the CH_2 and C absorbers, respectively, in the "good" geometry position, while no mesons were so lost in the "poor" geometry position. With these corrections the value of σ for both geometries becomes 47 mb. Thus the total $\pi^- - p$ cross section is 47 ± 5 mb, for a mean energy in the absorber of 840 Mev. The stated error includes an estimate of the uncertainties in the corrections.

We have repeated the above measurements with 500-Mev incident mesons using mainly the 6.6° geometry. With similar corrections, the total $\pi^- - p$ cross section was found to be 27 ± 5 mb for a mean pion energy of 470 Mev. This agrees well with the value of 25 ± 3 mb at 450 Mev found previously at this laboratory.[1]

We find therefore a rise of approximately 20 mb in the total $\pi^- - p$ cross section from 470 to 840 Mev. Since the cross section has been found to be 34 ± 3 mb at 1.5 Bev,[4] and, very recently, 47 ± 4 mb at 1.0 Bev,[4] a second peak in the neighborhood of 900 Mev is indicated. Further study of this energy region has been undertaken by Lindenbaum and Yuan, and Piccioni and Cool.

We should like to thank Dr. George B. Collins and Professor J. Steinberger for their important roles in the initial stages of this experiment, and the many members of the cosmotron group who made it possible.

* This work was performed under the auspices of the U. S. Atomic Energy Commission.

[1] S. J. Lindenbaum and L. C. L. Yuan, Phys. Rev. (to be published).
[2] R. L. Garwin, Rev. Sci. Instr. 21, 569 (1950).
[3] Leon Madansky (private communication).
[4] Cool, Madansky, and Piccioni (private communication).

Evidence for Subshell at $Z=96$

GLENN T. SEABORG
Radiation Laboratory and Department of Chemistry, University of California, Berkeley, California
(Received September 18, 1953)

THE evidence is decisive that major nuclear shells are completed at 82 protons and 126 neutrons (both represented by the nuclide Pb^{208}) and these, along with major shells at 82 neutrons and certain lower nucleon numbers (N or $Z=20$, 28, 50), are well explained by the strong spin-orbit coupling model of Mayer[1] and Haxel, Jensen, and Suess.[2] This model suggests the filling of quantun states at certain intermediate points, and there is an accumulating amount of evidence that such "subshells" are also discernible, for example, at $Z=58$[3-5] and $Z=64$.[6,7]

The evidence from alpha radioactivity, both (1) the effect of the nuclear radius shrinkage on the relationship between energy and half-life and (2) the discontinuities in the plots of energy *vs* mass number at constant Z, gives a striking indication[8] of the closing of major shells at $Z=82$ and $N=126$. Application of these sensitive criteria as tests for the much smaller "subshell" effects in the regions $Z>82$ and $N>126$ leads to some evidence for such a subshell at $Z=96$ (curium).

Since it has been shown that the Gamow-Gurney-Condon type of formula for alpha decay applies very well to the ground state to ground state transition for even-even alpha emitters,[8] the known[9] alpha energies and partial half-lives were used in the Preston[10] form of the formula to calculate the nuclear radii of a number of even-even nuclides in the range $Z=84$ to 98. Using these radii, a value of r_0 was calculated for each nuclide from the relationship radius$=r_0A^{\frac{1}{3}}$ and the plot in Fig. 1 of the average value of r_0 (r_0 generally decreasing with increasing Z) for each element indicates a just discernible minimum or plateau at $Z=96$. The average value of r_0 for each element was plotted because there is no discernible regular variation of r_0 with A at constant Z.

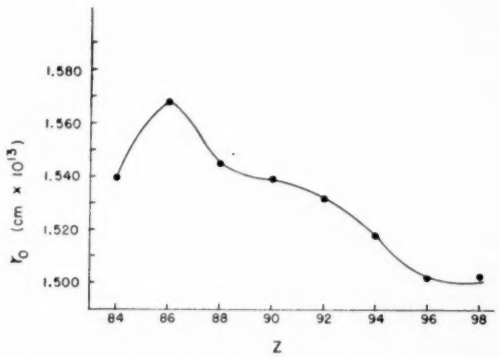

FIG. 1. Plot of average values of r_0 *vs* Z. The following isotopes are included: Po^{212}, Po^{214}, Po^{216}, Po^{218} for Po; Em^{220}, Em^{222} for Em; Ra^{222}, Ra^{224}, Ra^{226} for Ra; Th^{226}, Th^{228}, Th^{230}, Th^{232} for Th; U^{230}, U^{232}, U^{234}, U^{236}, U^{238} for U; Pu^{236}, Pu^{238}, Pu^{240}, Pu^{242} for Pu; Cm^{242}, Cm^{244} for Cm; Cf^{246}, Cf^{248} for Cf.

The stable shell of 82 protons is attained upon completion of the $h_{11/2}$ level and the spin of Bi^{209} (9/2) indicates that the 83rd proton begins the filling of the $h_{9/2}$ level as might be expected. However, if the $h_{9/2}$ level is raised in energy as more protons are added, so that the $f_{7/2}$ and $f_{5/2}$ are filled before the $h_{9/2}$ levels, one might expect subshell effects at $Z=90$ and 96. If the quantum states are filled in this order, the variation of r_0 with Z should perhaps also indicate an effect $Z=90$. A careful consideration of the values of r_0 in the region on both sides of $Z=90$ points to a barely discernible plateau in the variation of r_0 with Z at this atomic number.

In the case of $Z=96$ there is an additional argument which points to the completion of a subshell here. The known odd-even isotopes of berkelium, Bk^{243} and Bk^{245}, are highly "hindered"[8] in their most prominent modes of alpha decay, i.e., they decay much slower than the simple formula would indicate. This exceptional degree of hindrance is not observed for similar (odd-even) isotopes of any other odd Z alpha-particle emitter with the exception of bismuth ($Z=83$) where the slowed rates of decay are presumably to be associated with the closed proton shell (and consequent shrunken radius) at $Z=82$.

There are other lines of evidence which may also point to the filling of the $f_{7/2}$ and $f_{5/2}$ before the $h_{9/2}$ proton states. The spins of Np^{237} [11] and Am^{241} [12] are both 5/2 as expected on this basis. On the other hand, the spins of Ac^{227} [13] and Pa^{231} [14] have both been reported as 3/2, indicating perhaps that the odd proton occupies the $p_{3/2}$ state, whereas spins of 7/2 and 5/2 corresponding to $f_{7/2}$ and $f_{5/2}$ states, respectively, would be expected. Whether or not this indicates a breakdown of the single-particle model, it does seem to indicate that arguments based on spin values cannot be conclusive here. It is interesting to add that a consideration of the systematics of beta radioactivity in this region also leads to the assignment of spectroscopic states in agreement with the suggested higher position of the $h_{9/2}$ level energetically.

It is interesting to note that arguments based on spin values[15] indicate that in the case of neutrons the $f_{7/2}$ level fills before the $h_{9/2}$ level just after the completion of the major shell at 82 neutrons. Thus, the situation is analogous to that postulated for protons although the evidence is not clear on the relative position of the $f_{5/2}$ and $h_{9/2}$ neutron levels.

It seems likely that in the region following the major closed shell at 126 neutrons, which is completed with the filling of the $i_{13/2}$ states, the $i_{11/2}$ level is not occupied until the $g_{9/2}$ and possibly also the $g_{7/2}$ and $d_{5/2}$, etc., states are filled. Attempts to apply the aforementioned criteria of alpha-decay data do not lead to any discernible evidence for subshells up to $N=148$. Successful application of these criteria here probably awaits both a larger quantity of and more accurate alpha-decay data in this region. There is only one spin value known in this region, that of U^{235}, which has been reported as 5/2 or 7/2 with the former value the more probable.[16] Since U^{235} has 143 neutrons, either spin value would fit nicely with the view that the $i_{11/2}$ level lies above the $g_{9/2}$, $g_{7/2}$, and $d_{5/2}$ levels.

The generous help of F. Asaro and D. C. Dunlavey in making numerous calculations is gratefully acknowledged.

[1] M. G. Mayer, Phys. Rev. **75**, 1969 (1949); **78**, 16, 22 (1950).
[2] Haxel, Jensen, and Suess, Phys. Rev. **75**, 1766 (1949), Z. Physik **128**, 295 (1950).
[3] H. E. Duckworth and R. S. Preston, Phys. Rev. **82**, 468 (1951).
[4] Duckworth, Kegley, Olson, and Stanford, Phys. Rev. **83**, 1114 (1941).
[5] G. P. Dube and S. Jha, Phys. Rev. **85**, 1042 (1952).
[6] Coryell, Brightsen, and Pappas, Phys. Rev. **85**, 732 (1952); C. D. Coryell, Ann. Rev. Nuc. Sci. **2**, 305 (1953).
[7] Rasmussen, Thompson, and Ghiorso, Phys. Rev. **89**, 33 (1953).
[8] Perlman, Ghiorso, and Seaborg, Phys. Rev. **77**, 26 (1950).
[9] Hollander, Perlman, and Seaborg, Revs. Modern Phys. **25**, 469 (1953); additional data: Cf^{248}—partial half-life 260 days, energy 6.26 Mev [E. K. Hulet, Ph.D. thesis, University of California Report UCRL-2283, August, 1953 (unpublished)]; U^{230}—energy 5.886 Mev, Th^{226}—energy 6.342 Mev, Ra^{222}—energy 6.567 Mev, U^{232}—energy 5.318 Mev [F. Asaro (private communication)]; U^{228}—energy 4.187 Mev, Th^{224}—energy 3.998 Mev [B. G. Harvey (private communication)]; Cf^{246}—partial half-life 40.6 hr [D. C. Dunlavey (private communication)].
[10] M. Preston, Phys. Rev. **71**, 865 (1947).
[11] F. S. Tompkins and M. Fred, J. Opt. Soc. Am. **39**, 357 (1949).
[12] M. Fred and F. S. Tompkins, Phys. Rev. **89**, 318 (1953).
[13] Tompkins, Fred, and Meggers, Phys. Rev. **84**, 168 (1951).
[14] J. E. Mack, Revs. Modern Phys. **22**, 64 (1950).
[15] P. F. A. Klinkenberg, Revs. Modern Phys. **24**, 63 (1952).
[16] G. L. Stukenbroeker and J. R. McNally, J. Opt. Soc. Am. **40**, 336 (1950).

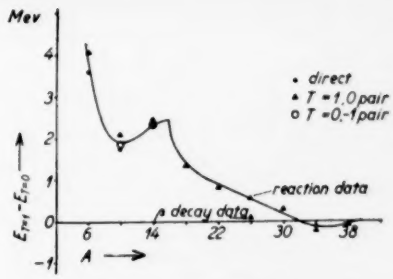

FIG. 1. The $E_{T=1}-E_{T=0}$ value as a function of A for $A=4n+2$ nuclei.

Possible 0→0 (no) β Transitions in $4n+2$ Nuclei

O. KOFOED-HANSEN
Institute for Theoretical Physics, University of Copenhagen, Copenhagen, Denmark
(Received October 1, 1953)

THE 0→0 (no) β transitions so far identified take place between the $T=1$ states of nuclei of mass number $4n+2$, n being an integer. The cases are $C^{10}\rightarrow B^{10*}$,[1] $O^{14}\rightarrow N^{14*}$, and $Cl^{34}\rightarrow S^{34}$.[2] These transitions occur because the β^+ energy is large and because the energy difference between the $T=1$ and $T=0$ states is relatively small for these nuclei. The value of $E_{T=1}-E_{T=0}$ can be estimated by comparing Q values or $E_\beta{}^{\max}$ data for the $T_z=1$, $T_z=0$ partners or similar data for the $T_z=0$, $T_z=-1$ partners with correction for the neutron-proton mass difference and the Coulomb energy difference $(0.62/A^{\frac{1}{3}})\cdot(Z-1)Z$, or directly when the $T=1$ state is observed in a $T_z=0$ nucleus (Li^6, B^{10}, N^{14}, and Cl^{34}). Such an analysis leads to the curve shown in Fig. 1. The trend of the curve agrees with the observation made by Arber and Stähelin[3] that in Cl^{34} the $T=1$ state lies below the $T=0$ state. The closed shell 2×8 shows up as a peak in the curve.

The nuclear matrix element for the 0→0 ($\Delta T=0$, no) transition is independent of nuclear models. It just depends on the assumption of charge independence of nuclear forces,[3] and one finds

$$\left|\int 1\right|^2=T(T+1)-T_{z_1}T_{z_2}=2$$

for $T=1$ transitions.

So long as T is a "good quantum number" one would therefore expect ft to be constant for these transitions, and an experimental investigation of this constancy of ft would be a very valuable method for checking the validity of the charge independence of nuclear forces. High precision in the ft values is of course needed.

Moreover, this ft value would help in the determination of the amount of Fermi interaction present in β decay. For $g_F=g_{GT}$,[4] the expected ft value would be 2650, in general agreement with the uncertain values for C^{10}: $ft=6000\pm3000$ and O^{14}: $ft=3300\pm900$ and in close agreement with the more accurate value for Cl^{34}: $ft=2700\pm200$.

For $A>18$, the entire series of $4n+2$ nuclei should exhibit two 0→0 transitions per mass number. It happens, however, in cases where $E_{T=1}-E_{T=0}>0$ and the odd-odd isobar has a low-spin ground state or excited state below the $T=1$ state, that the latter state may decay preferably by a γ transition. In Table I a list is given of the states in question of mass number $18\leqslant A\leqslant 58$. The $T_z=0$ state can be obtained by (p,n) reactions and the $T_z=-1$ state by $(He^3,3n)$ reactions although many other reactions are also available. A systematic search for these transitions seems very promising. It is of interest to note that the value[5] $E_\beta{}^{\max}=3.1$ Mev for the Al^{26} decay disagrees with the mass determination from the reactions $Mg^{25}(d,n)Al^{26}$: $Q=5.58$,[6] and $Mg^{25}(d,p)Mg^{26}$: $Q=8.88$,[7] which give $\Delta Mc^2=2.52$ Mev. The latter point fits into the curve in Fig. 1, whereas the $E_\beta{}^{\max}$ value suggests that the transition actually observed is the 0→0 ($\Delta T=0$, no) transition. In agreement with this suggestion the observed values $E_\beta{}^{\max}=3.1$ and $t=6.6$ sec leads to $ft=2700$.

Further observed cases of short-lived states in the $4n+2$ family are 0.40-sec V^{46}, 0.28-sec Mn^{50} and 0.18-sec Co^{54}.[8] If the Coulomb energy difference minus the proton-neutron mass difference is used for a calculation of $E_\beta{}^{\max}$ under the assumption of a 0→0 ($\Delta T=0$, no) transition, ft values of ~2700 result for these decays.

The A^{34} decay would be extremely interesting in connection with β-recoil experiments, since it is a monatomic gas and decays by pure Fermi interaction.

The present considerations are results of discussions with Mr.

TABLE I. Expected values of $E_\beta{}^{\max}$ and half-life t for possible 0→0 (no) β transition of mass number $A=4n+2$, $18\leq A\leq 58$.[a] In those cases where experimental data already exist these data are given in brackets.

A	Element	Expected $E_\beta{}^{\max}$ (Mev)	Expected t (sec)[b]	Element	Expected $E_\beta{}^{\max}$ (Mev)	Expected t (sec)[b]
18	Ne	2.46	17	F	γ unstable	
22	Mg	3.06	7	Na	γ unstable	
26	Si	3.64	3.4	Al	3.22(3.1)	6(6.7)
30	S	4.19	1.8	P	γ unstable	
34	A	4.71	1	Cl	4.33(4.45)	1.5(1.45)
38	Ca	5.21	0.7	K	4.84	0.9
42	Ti	5.69	0.4	Sc	5.34	0.6
46	Co	6.16	0.3	V	5.81	0.39(0.40)
50	Fe	6.61	0.2	Mn	6.28	0.27(0.28)
54	Ni	7.06	0.16	Co	6.73	0.20(0.18)
58	Zn	7.50	0.12	Ca	7.17	0.15

[a] The uncertainty in the expected $E_\beta{}^{\max}$ arises from the uncertainty in the Coulomb correction, and the uncertainty in the expected half lives t arises from the uncertainties in $E_\beta{}^{\max}$ and in $ft=2650$. The Fermi integral has been calculated by the method of Moszkowski. (See reference 5.)
[b] The expected half-lives are the partial half-lives only; β-decay branching may reduce these values. This will occur especially in Ne^{18} and S^{30}.

Aage Bohr, Professor T. Lauritsen, Dr. B. Mottelson, and Mr. Aage Winther to whom I want to express my sincere gratitude.

[1] Sherr, Muether, and White, Phys. Rev. **75**, 282 (1949); R. Sherr and J. B. Gerhart, Phys. Rev. **91**, 909 (1953).
[2] W. Arber and P. Stähelin, Helv. Phys. Acta. **26**, 433 (1953).
[3] E. Wigner and E. Feenberg, Repts. Progr. Phys. **8**, 274 (1941).
[4] A. Winther and O. Kofoed-Hansen, Kgl. Danske Videnskab. Selskab, Mat.-fys. Medd. **27**, No. 14 (1953); O. Kofoed-Hansen and A. Winther, Phys. Rev. **86**, 428 (1952).
[5] Hollander, Perlman, and Seaborg, Revs. Modern Phys. **25**, 469 (1953).
[6] Swann, Mandeville, and Whitehead, Phys. Rev. **79**, 598 (1950).
[7] Van Patter, Speiduto, Endt, Buechner, and Enge, Phys. Rev. **85**, 142 (1952).
[8] W. M. Martin and S. W. Breckon, Can. J. Phys. **30**, 643 (1952).

The β Spectrum of RaD†

E. Huster
Physikalisches Institut, University of Marburg/Lahn, Marburg, Germany
(Received June 8, 1953; revised manuscript received September 28, 1953)

In negative β decay the binding energy of the orbital electrons of the daughter atom exceeds that of the parent atom. The question of how this energy excess, $\Delta E_e = E(Z+1) - E(Z)$, is disposed of has been discussed theoretically since 1937. Goldstein[1] and Hebb[2] came to the conclusion that ΔE_e is carried away by the β particle, the result being a cutoff at the low-energy end of the β spectrum at 16 kev for $Z=82$, according to the Fermi-Thomas model of the atom. This looked plausible because there is no appreciable coupling of the neutrino with the atomic electrons.

Some β emitters having an upper energy limit E_0 of the same order of magnitude as E_e should thus have a spectrum with a line shape about the endpoint. Among these elements, RaD seemed best suited for examination because it can be introduced into a proportional counter in the form of gaseous lead tetramethyl, the measurement thus avoiding difficulties by self-absorption and backscattering. β decay of RaD is followed by a strongly converted γ ray of 46.5 kev. In most disintegrations the proportional counter will therefore measure the sum of the energies of the β particle and the secondary radiations caused by the conversion, i.e., the sum of the energies of the β particle and the γ ray. Thus the measured distribution should give immediately the shape of the β spectrum shifted towards higher energies by 46.5 kev. But the counter gives finite line-width for a monoenergetic line and thus flattens the steep beginning of the spectrum. The correction for this is the only important one. In the case of solid sources corrections are more complicated.[3]

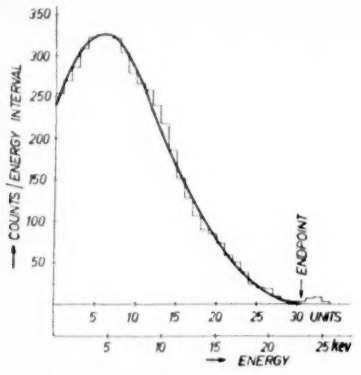

FIG. 1. β spectrum of RaD, uncorrected. (Corrections are needed from 0 to 4 kev).

The pulse output of the counter was analyzed by the method of Curran *et al.*[4] Figure 1 shows the result. The smooth curve corresponds to a straight Kurie-plot from the endpoint down to 7.5 kev, below which it is fitted to the measured distribution (without corrections).

There is no cutoff at 16 kev; i.e., ΔE_e is shared between electron and neutrino. This agrees with recent theoretical considerations.[5]

After the experiments described here had been finished, Jaffe and Cohen[6] published their results on the disintegration of RaD. They used almost the same experimental methods, and arrived at the same result as to the disposal of ΔE_e. However, they found $E_0 = 15.2 \pm 1$ kev, while the Kurie-plot corresponding to Fig. 1 gives $E_0 = 23.0$ kev with an estimated accuracy of ± 2.5 kev. An error of more than -3.0 kev seems not to be compatible with the experimental results. Energy calibrations were made by superimposing the K rays of Ag and the γ ray of RaD from external sources. Jaffe and Cohen calibrated in a similar manner, taking the widths of the calibration lines as a check of the proportionality of the counter. Proportionality of the whole apparatus near the endpoint ($E_0 + 46.5$ kev) could not be directly measured. Perhaps this may cause the discrepancy in the values of E_0.

Figure 1 shows a maximum in the energy distribution at about 4.5 ± 2.5 kev (Jaffe and Cohen: 2.7 kev). (The uncertainty in its position is caused by deficiencies in the calibration: neither Jaffe and Cohen nor the present author disposed of γ sources strong enough in comparison with the gaseous source.) At the moment it cannot be said whether the maximum is real or not. The correction for finite line-width is somewhat difficult, and that made by Jaffe and Cohen leads to a rather broad uncertainty in the shape of the spectrum below 3 kev. It can, however, be shown that the real shape below 4 kev can be calculated with an accuracy of 5 percent. Calculation shows that a maximum below 2.5 kev may be caused by finite line-width; if it lies at higher energies it must be real.

In all cases the calculation exhibits a marked deficit of β particles at low energies compared with the Fermi theory neglecting screening of the nucleus by the orbital electrons. (This is confirmed by the quite simple calculation of the shape the counter gives to a theoretically allowed spectrum with $E_0 = 23$ or 15 kev, shifted by 46.5 kev towards higher energies.) Screening diminishes the probability of emission at low energies. Computations are not yet available in the case of RaD, but are now in progress at the University of Marburg. However, there are doubts that the effect of screening is sufficiently high to explain a pronounced maximum, if it should exist.

A full account of the experimental work and the necessary corrections will soon be published elsewhere.

† Communicated at the Deutscher Physikertag, Berlin, September 1952. Physik. Verhandl. 3, 187 (1952).
[1] L. Goldstein, J. phys. et radium **8**, 235, 316 (1937).
[2] M. H. Hebb, Physica **5**, 701 (1938).
[3] Insch, Balfour, and Curran, Phys. Rev. **85**, 805 (1952).
[4] Curran, Angus, and Cockroft, Phil. Mag. **11**, 36 (1949).
[5] R. Serber and H. S. Snyder, Phys. Rev. **87**, 152 (1952); H. M. Schwartz, Phys. Rev. **86**, 195 (1952).
[6] A. A. Jaffe and S. G. Cohen, Phys. Rev. **89**, 454 (1953).

The 0^+ States of the Light Odd-Odd Nuclei

P. Stähelin
Swiss Federal Institute of Technology, Zürich, Switzerland
(Received September 23, 1953)

Nuclear states with zero spin and even parity have been found in $_{19}K^{38}$, $_{17}Cl^{34}$, and $_{13}Al^{26}$.[1] Their half-lives are (0.95 ± 0.03) sec, (1.58 ± 0.05) sec, and 6.3 sec, respectively. They decay by positron emission directly into the ground state of the neighboring even-even isobars A^{38}, S^{34}, and Mg^{26}. The disintegration energies correspond closely to the decrease of Coulomb energy.

Assuming a uniform distribution of the nuclear charge in a spherical volume and using the empirical mass differences, we can calculate a nuclear radius R.[2] In Fig. 1 the resulting values of $r_0 = RA^{-\frac{1}{3}}$ are plotted against the number of protons. The black points refer to the well-known mirror transitions. They show that at least for $A > 20$ a useful approximation of the Coulomb energy results from the value $r_0 = 1.43 \times 10^{-13}$ cm. The open circles, representing K^{38}, Cl^{34}, and Al^{26}, fit well to this value of r_0. That means

that the Coulomb energy (together with the neutron-proton mass difference) accounts for the whole energy difference between the 0^+ states of the neighboring isobars with $A=38$, with $A=34$, and with $A=26$.[3]

This result confirms not only the assumption of charge symmetry but even of charge-independence of the nuclear forces. Furthermore it allows us to assign isotopic spin $T=1$ to the 0^+ states of Al^{26}, Cl^{34}, and K^{38}. This assignment is confirmed by the constancy of the $\log ft$ values: K^{38} (3.35 ± 0.07), Cl^{34} (3.47 ± 0.06), and Al^{26} (3.52 ± 0.10). These values also may be compared with the corresponding values of O^{14} (3.52 ± 0.10) and C^{14} (3.31 ± 0.15).[4] From the mean value (3.44 ± 0.05) we deduce a Fermi coupling constant $(1.51\pm0.08)\times10^{-49}$ erg cm^3. This result agrees with the value $(1.55\pm0.10)\times10^{-49}$ erg cm^3 which Kofoed-Hansen and Winther[5] derived from the ft values of odd-A nuclei.

The assignment of isotopic spin one to the 0^+ states does not imply that the isotopic spin is a good quantum number. The high purity of isotopic spin in these particular cases probably arises from the fact that the next admissible states with the same spin and the same parity, but with different isotopic spin, occur only at much higher excitation energies.

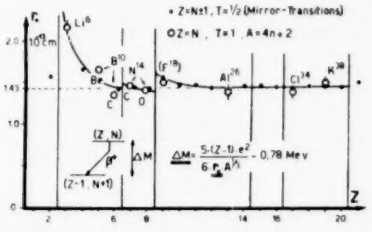

FIG. 1. Reduced nuclear radii $r_0=RA^{-1/3}$, calculated from the empirical disintegration energies.

The smooth dependence of r_0 on the atomic number (Fig. 1) enables us to predict the position of the 0^+ levels in P^{30}, Na^{22} and F^{18}. The analogous states of N^{14}, B^{10}, and Li^6 have been found empirically.[4] In every odd-odd nucleus with an equal number of protons and neutrons we therefore know the relative positions of the lowest $(T=1)$ and $(T=0)$ levels. Figure 2 shows the corresponding level schemes. The spin assignments are taken from reference 1.[6]

From the new spin assignments there also follow some small modifications of the diagram given by King and Peaslee[7] for the ground-state spins of odd-odd nuclei with neutrons and protons filling equivalent shells. In the new diagram, Fig. 3, the low-lying isomers of the $f_{7/2}$ shell have been plotted as additional points. The most puzzling feature of this diagram, the steady

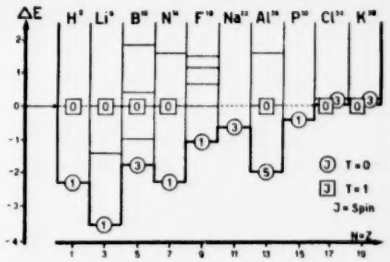

FIG. 2. Level schemes of the odd-odd nuclei containing an equal number of protons and neutrons. As a basis of reference the 0^+ states $(T=1)$ are arbitrarily put to the same level.

growth of the spin with every added pair of nucleons in the lower half of the $1p$ shell and in the lower half of the $1d$ shell, is still unchanged, and the prediction of spin five for Al^{26} by King and Peaslee[7] is verified. It looks as if all the orbits were paired, while all the spins are aligned. In the $1d_{3/2}$ shell and in the $1f_{7/2}$ shell, however, holes and particles seem to be nearly equivalent, which indicates prevalence of $j-j$ coupling.

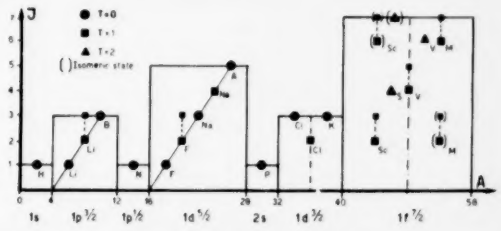

FIG. 3. Spins of the light odd-odd nuclei.

A detailed report will appear in *Helvetica Physica Acta*. I am grateful to Dr. P. Preiswerk for many helpful discussions.

[1] W. Arber and P. Stähelin, Helv. Phys. Acta **26**, 433 (1953) and Helv. Phys. Acta (to be published); P. Stähelin and P. Preiswerk, Nuovo cimento **10**, 1219 (1953) and Helv. Phys. Acta (to be published).

[2] H. A. Bethe, Phys. Rev. **54**, 436 (1938).

[3] It seems very likely that this statement also holds for $A=14$, for $A=10$, and for $A=6$. The deviations from a smooth curve in Fig. 1 are probably due to the insufficient approximation of the Coulomb term (compare reference 4).

[4] F. Ajzenberg and T. Lauritsen, Revs. Modern Phys. **24**, 321 (1952).

[5] O. Kofoed-Hansen and A. Winther, Phys. Rev. **86**, 428 (1952).

[6] The isomerism of Al^{26} proposed in reference 1 has found a recent confirmation in the fact that $\sigma[Al^{27}(\gamma,n)]$ seems to be three times as high if the neutrons are counted instead of the electrons which are emitted from the 6.3-sec isomeric state [Montalbetti, Katz, and Goldemberg, Phys. Rev. **91**, 659 (1953)].

[7] R. W. King and D. C. Peaslee, Phys. Rev. **90**, 1001 (1953)

Proceedings of the American Physical Society

Minutes of the New Mexico Meeting Held at Albuquerque, September 2, 3, 4, and 5, 1953

THE 1953 September meeting of the American Physical Society—the Summer Meeting in the West—was held at Albuquerque, New Mexico on the Campus of the University of New Mexico, on Wednesday, Thursday, Friday, and Saturday, September 2, 3, 4, and 5, 1953. The choices of place and time were fortunate, since the meeting was one of the best attended meetings of the Society ever held in the West. There were 436 paid registrations, and about 600 people attended the excellent popular lecture by E. Fermi. The weather was perfect and local arrangements were outstanding. The Secretary wishes to thank Professor V. H. Regener for his work not only during the meeting, but also in connection with the preparation of the program. There were an unusually large number of invited papers, and a very fine session arranged by F. N. Frenkiel for our Division of Fluid Dynamics. In the absence of Dr. Frenkiel, R. J. Seeger presided. Post-deadline papers were given by D. L. Hill, L. Wilets, and K. W. Ford; Alexander Goetz; John E. Evans; Richard E. Stroup and Robert A. Oetjen; and L. Trilling.

The banquet of the Society was very well attended and we were honored by the presence of Governor Edwin Mechem of New Mexico. Alan T. Waterman, Director of the National Science Foundation, was the after dinner speaker.

J. Kaplan, *Local Secretary for the Pacific Coast*
University of California,
Los Angeles 24, California

Errata Pertaining to Papers I1, I2, I3, I4, and P4

I1, I2, and I3, by R. L. Walker, J. G. Teasdale, and V. Z. Peterson; A. V. Tollestrup, J. C. Keck, and R. M. Worlock; and R. F. Bacher, J. C. Keck, V. Z. Peterson, J. G. Teasdale, A. V. Tollestrup, R. L. Walker, and R. M. Worlock, respectively. To the title of each of these abstracts, add a footnote, "This work was supported by the U. S. Atomic Energy Commission."

I4, by James Terrell, W. E. Scott, J. S. Gilmore, and C. O. Minkkinen. Instead of 5.45 ± 0.16 (percent yield in U^{235} at 4.85 Mev), read 5.39 ± 0.16.

P4, by C. D. Jeffries. In line 13, instead of $I(Ti^{49})=7.2$, read $I(Ti^{49})=7/2$. In line 17, instead of $\mu(Ti^{47})=-0.7866$, read $\mu(Ti^{47})=-0.7871$.

PROGRAMME

WEDNESDAY MORNING AT 10:00

Student Union Ballroom

(DAROL FROMAN, presiding)

Invited Papers

A1. Fission with Moderate Energy Neutrons. R. W. SPENCE, *Los Alamos Scientific Laboratory.* (30 min.)

A2. The Energy Released in Fission. R. B. LEACHMAN, *Los Alamos Scientific Laboratory.* (30 min.)

A3. Fission and Nuclear Models. JOHN A. WHEELER, *Princeton University.* (45 min.)

WEDNESDAY AFTERNOON AT 2:00

Room 101, Mitchell Hall

(E. J. WORKMAN, presiding)

Invited Paper

B1. The Size-Determination of Submicroscopic Particles by Long Wavelength X-Ray Diffraction. BURTON HENKE, *California Institute of Technology.* (30 min.)

Contributed Papers

B2. Acoustic Approximation to Weak Shock Diffraction. CRAIG C. HUDSON, *Sandia Corporation.*—Using Friedlander's[1] application of the Sommerfeld diffraction formula, the pressure fields for the diffraction of a weak shock by right-angle wedges has been approximated. The total field is separated into a diffraction region and a turbulence region by the free boundary formed by the contact of the vortex with the surface. The Friedlander formulas are applied in the diffraction region with good agreement to experimentally obtained fields. An anomaly is pointed out in the case of a back corner where the acoustic approximation cannot work. Calculations are made for both square and peaked waves.

[1] Friedlander, Proc. Roy. Soc. (London) **186**, 322–67 (1946).

B3. Properties of the Hugoniot Function.* R. D. COWAN, *Los Alamos Scientific Laboratory.*—The Hugoniot relation $E(p, v) = E_0 + (p+p_0)(v_0-v)/2$ (where $E(p, v)$ and E_0 are, respectively, the internal energies of the material behind and in front of the shock) together with the equation of state of the material behind the shock defines a Hugoniot curve in the (p, v) plane. In terms of the Hugoniot function $H(p, v) \equiv E(p, v) - E(p_0, v_0) + (p+p_0)(v-v_0)/2$, the Hugoniot relation becomes $H(p, v) = E_0 - E(p_0, v_0) = \text{constant} \geqq \text{zero}$. (The equality sign holds if the material is not altered chemically by the shock; the inequality holds otherwise, as for example in the detonation of high explosive.) The differential of the Hugoniot function may be written $dH = TdS + \{(v-v_0)dp - (p-p_0)dv\}/2 = TdS + r^2 d\theta/2$, where r and θ are the polar coordinates of (p, v) referred to (p_0, v_0) as the origin. Given a family of adiabats $dS = 0$, this expression provides a simple means of mapping qualitatively the family of curves $dH = 0$ (one of which is the actual shock curve) and of deriving properties such as the variation of entropy along the curves.

* An extension of a paper by H. Weyl, AMG-NYU No. 46 (AMP Note No. 12).

B4. New Studies of Nitrogen Afterglows.* MARX BROOK, *University of California, Los Angeles.*—A flow system was used to mix the nitrogen afterglow with a rare gas downstream from the discharge. The intensity distribution in the first positive afterglow bands was compared with the intensity modifications produced by mixing nitrogen with a rare gas prior to the discharge. The same intensity shifts to the red are produced in both cases. An analysis of the current theories of active nitrogen will be given in the light of the results. It will be shown that the Cario-Kaplan hypothesis as well as the molecular ion theory of Mitra cannot account for the nitrogen afterglow. The most probable mechanism is an atomic recombination process in a three-body collision. The transition from the $^5\Sigma$ to the $B^3\Pi$ state is forced by the collision,

$$[N + N \rightleftarrows N_2(^5\Sigma)] + N_2 \rightarrow N_2(B^3\Pi) + N_2, \quad N_2(B^3\Pi) \rightarrow N_2 A^3\Sigma + h\nu.$$

* This work has been sponsored by the Geophysics Research Directorate of the Air Force Cambridge Research Center, Air Research and Development Command.

B5. Quantitative Analysis of the Lower Ionosphere.* H. K. KALLMANN, *University of California, Los Angeles.*—A quantitative analysis has been made of the physical properties of the atmosphere between 80 km and 130 km altitude. Average pressure density and temperature, as well as individual particle concentration and electron densities, have been calculated. In accordance with theory and observation, one can now be certain that molecular oxygen is dissociated under the influence of solar radiation, and that molecular and atomic oxygen is ionized by solar radiation of $\lambda < 1000$A and $\lambda < 910$A, respectively. Taking this into account, it has been found that the calculated density and pressure data are in good agreement with the observed data as presented in the Rocket Panel Report.[1] The temperatures obtained between 80 km and 220 km are between the maximum and minimum values proposed by the Panel. When the calculated values for neutral particle

densities are used to determine the radiation effect of the sun upon the lower ionosphere, the variation of electron density with altitude is found, corresponding to the so-called *E* layer. Contrary to present-day investigations, a continuous and not a parabolic electron layer formation is obtained.

* This work has been sponsored by the Geophysics Research Directorate of the Air Force Cambridge Research Center, Air Research and Development Command.
[1] The Rocket Panel, Phys. Rev. **88**, 1027 (1952).

B6. Pulsed Searchlight System for Upper Atmosphere Density Studies.* S. S. FRIEDLAND, H. S. KATZENSTEIN, J. KATZENSTEIN, D. P. LINDORFF, G. S. TIMOSHENKO, AND L. E. WILLIAMS, *The University of Connecticut.*—A pulsed searchlight system has been developed to measure the light scattered at various altitudes of the upper atmosphere A Westinghouse FGL-1 krypton-filled flash lamp is placed at the focus of a 60-in. searchlight. The lamp is loaded at 100 watt-sec and discharged with a 20μsec pulse width by a manual trigger. An RCA 5819 photomultiplier is placed at the focus of a similar searchlight located at the same site; both searchlights being directed vertically upward. The photomultiplier is "gated on" for a period of 20μsec as follows: (1) the "reference gate" is opened at a time after the flash sufficient for the light to travel up to and back from a reference altitude. (2) The "measurement gate" is opened at a time after the flash sufficient for the light to travel up to and back from any desired altitude. (3) The "noise gate" is opened at a time sufficiently long after the flash so that light detected by the photomultiplier consists only of background light. The pulse from the noise gate is subtracted from the pulse from the measurement gate pulse. The resulting signal is compared to the reference gate pulse. It is assumed that the ratio in light scattering between the signal and reference altitude is the same as the ratio of molecular densities of the atmospheres at these altitudes.

* The research reported in this paper has been sponsored by the Geophysics Research Directorate of the Air Force Cambridge Research Center, Air Research and Development Command.

B7. Stratospheric Temperature Profiles Obtained from Searchlight Measurements. L. ELTERMAN, *Air Force Cambridge Research Center.*—Measurements of atmospheric densities have been made with the "searchlight technique," using improved instrumentation.[1] The density distributions are sufficiently accurate so that corresponding temperature profiles are readily obtained. The density-temperature equation requires the evaluation of an integration constant, which is accomplished by using radiosonde information and, in addition, considering physically acceptable temperature lapse rates. Five temperature profiles are derived up to 60 km which represent stratospheric conditions over New Mexico during October 1952.

[1] L. Elterman, Geophysics Research Paper No. 10, 1951.

B8. Seasonal Trend of Atmospheric Ozone as Revealed by the Solar-Telluric Band at 9.6 Microns.* ARTHUR ADEL, *Arizona State College.*—An extensive record has been obtained of the absorption of solar radiation by atmospheric ozone in the interval 9.2 to 10.1 microns. Seventy-two independent observations made on seventy days are scattered over the various months of the year. The data are suitable for a first examination of the seasonal trend of stratospheric ozone as revealed by an infrared band. The absorptions are reduced to a quantity proportional to the amount of ozone, and the curve of seasonal change in this quantity is strikingly similar to the seasonal trend in ozone as revealed by the long-accepted method of ultraviolet absorption. This further usefulness of the 9.6-micron band of ozone as an atmospheric parameter is thus established.

* Supported in part by the Geophysics Research Division, Air Force Cambridge Research Center, Air Research and Development Command.

B9. Atmospheric Ozone Fluctuations at Albuquerque.* I. GERALD BOWEN, *University of New Mexico.*—The concentration of surface ozone measured at Albuquerque shows morning peaks which occur under certain meteorological conditions. The peaks are observed near the time when the stable night-time lapse rate becomes adiabatic in the lower layers. The value of the ozone concentration reached during such a morning peak often is the highest for the day; occasionally it is exceeded by later rises. The rate of surface heating is sometimes reduced at the time of the ozone peaks, simultaneously with the destruction of the stable lapse rate. This phenomenon does not occur if surface winds during the night have mixed the lower air to a considerable height, or if for any reason the nocturnal lapse rate has remained fairly steep.

* Supported by Air Force Cambridge Research Center, Air Research and Development Command.

B10. Variation of Natural Radioactivity in the Atmosphere with Altitude. MARVIN H. WILKENING, *New Mexico Institute of Mining and Technology.*—A study of the vertical distribution of radon and its decay products in the lower atmosphere has been made utilizing data taken during plane flights and at ground stations having different altitudes. The vertical span ranged from ground level (4000 feet) to 16 000 feet for the plane flights and from 4600 to 10 300 feet for the ground-level measurements. An alpha scintillation detector was used to count samples collected both by electrostatic precipitator and "negative wire" techniques. The limited precipitator data obtained suggest that on typical fair-weather days, the decrease of activity with altitude in the lower atmosphere is approximately linear and drops to one-half its ground-level value in about 2500 feet. The negative wire samples show a smaller decrease in activity with altitude. A monitor using an electrostatic precipitator for sample collection was operated at four ground-level stations each at a different altitude. The average activity decreased with altitude in much the same way as did the precipitator samples collected in the plane flights. Under ideal conditions the general decrease in activity with altitude can be explained in terms of the decrease in density, radioactive decay, and vertical transport by eddy diffusion in the atmosphere.

B11. Critical Conditions For Ice Formation on Silver Iodine Nuclei.* ROBERT J. MCCARTY,† *New Mexico Institute of Mining and Technology.*—The time interval between exposure of dry silver-iodide nuclei to water vapor and the appearance of a microscopic ice crystal is measured as a function of the nuclei temperature and the water-vapor pressure. The time interval becomes very long as certain critical combinations of nuclei temperature and water-vapor pressure are approached, the approach being made conveniently along either a path of constant nuclei temperature or along a path of constant water-vapor pressure. Values for the critical conditions are approximated by extrapolating to infinite time an empirically derived function relating the observed time intervals to the variable condition. Two sets of critical conditions have been determined for ice formation on silver iodide nuclei, one corresponding to the set of dew points, the other lying between the set of dew points and the set of frost points.

* Supported by the U. S. Office of Naval Research.
† Now at the Alamogordo Air Base.

B12. Electron Traps in Ice. E. AVERY, L. GROSSWEINER, AND M. MATHESON, *Argonne National Laboratory.*—Measurement of thermoluminescence in ice irradiated with hard x-rays at $-196°C$ has shown that the nature of the glow curve varies with the purity and irradiation history of the sample. The thermoluminescence associated with pure well-annealed ice of low-oxygen content showed distinct glow peaks at $-165°C$, $-117°C$, and $-97°C$ for heating rates of several degrees per

minute. The most prominent peak, at −117°C, obeyed first-order kinetics with a trap depth of 0.26 ev and frequency factor of 1.9×10^{6} sec^{-1}. Ice which contained oxygen, either by direct addition or diffusion in from the atmosphere, exhibited decay over a broad temperature range. The presence of hydrogen peroxide, whether added or formed *in situ* by heavy irradiation, suppressed all glow peaks markedly. The interpendence of the glow peaks and the nature of the electron traps and luminescent centers will be discussed.

B13. New Method for the Approximate Calculation of Effective Ionic Radii. N. EFREMOV, *1061 Intervale Avenue, New York 59, New York.*—A new form of the periodic system of ions (consisting of three segments: ions with negative valence from 4 to 1, left; ions with positive valence from 1 to 4, middle; and ions with positive valence from 4 to 7, right segment) has been proposed. Its generalized scheme is a matrix consisting of several series of total numbers (1, 2, 3, 4, 5, 6, 7, etc.). These matrix numbers characterizing ions are coefficients used for the calculation of all the effective ionic radii for the crystalline lattices of the NaCl type. Other coefficients used for the calculation of ionic radii are: the principal quantum number n and a certain constant (P or P') which can be derived from the Rydberg constant (calculation of the ionic radii of the positive elements with high valence) or the constant P or P' and the matrix number characterizing the tetravalent positive ions of the given period (calculation of the radii with positive and negative valence from 1 to 4). Values calculated by this method are in substantial agreement with the values determined by Goldschmidt and Pauling.

WEDNESDAY AFTERNOON AT 2:00

Room 102, Mitchell Hall

(R. E. HOLZER, presiding)

Contributed Papers

C1. Spectral Distributions of Filtered X-Ray Beams. W. J. RAMM and M. N. STEIN, *Signal Corps Engineering Laboratory.*—The energy distribution of the radiation from a commercial x-ray tube was analyzed with a pulse-height spectrometer for several tube potentials and various amounts of filtration. The results are compared with empirically calculated distributions obtained by using Kramer's well-known formula for the distribution of continuous x-ray spectra. The selection of absorbers to obtain a desired spectral distribution and certain aspects of the calculations will be discussed.

C2. The Long-Lived Phosphorescent Components of Thallium-Activated Sodium Iodide. L. R. MEGILL AND C. R. EMIGH, *Los Alamos Scientific Laboratory.*—Using a Co^{60} source as a means of primary irradiation, the long-lived phosphorescent decay of thallium-activated sodium iodide crystal has been studied at a crystal temperature of 29.9±0.1°C. A set of decay curves has been obtained by using different primary radiation exposure times varying from 5 seconds to 120 hours. These curves have been arbitrarily analyzed in terms of exponential decay components. The following set of mean lives for the different trap depths are consistent with all these complex decay curves: 0.23±0.04, 0.92±0.11, 3.1±0.3, 8.8±0.8, 28±3, 90±3, and 510±100 minutes. The initial intensities of the exponential components approach constant values with an increase in exposure time and to a first-order approximation follow a very simple monomolecular trap theory. The effect on the mean lives which is due to a change in the crystal temperature will be discussed. The data have been obtained using a 5819 photomultiplier as the detector and a vibrating reed electrometer to measure the current output of the photomultiplier.

C3. Magnetoelectrostatics. E. T. BENEDIKT, *Convair (Consolidated Vultee Aircraft Corp.).*—The possibility of producing electrostatic fields by means of unhomogeneous magnetic fields has been considered in the past by the author.[1] This effect is due to the mechanical force to which a system of magnetically polarized particles is subjected when under the action of an unhomogeneous magnetic field. If these particles are, in addition, electrically charged, their (necessarily non-uniform) equilibrium distribution will be characterized by an electrostatic field. The results of new theoretical studies regarding classical and quantum-mechanical as well as thermodynamical aspects of these phenomena will be presented.

[1] Paper given at the June 1948 meeting of the American Physical Society in Pasadena, California. Abstract appeared in Phys. Rev. **74**, 1563 (1948).

C4. Topology of Magnetic Fields. W. M. ELSASSER AND K. MCDONALD, *University of Utah.*—Textbooks state that the condition $\nabla\cdot H=0$ implies that the magnetic lines of force are closed. Following Slepian,[1] who points out that this is not generally true, we have tried to put his arguments into quantitative form. If the electric current-density is assumed continuous everywhere, the family of field lines has singularities only at points or curves where $H=0$, but the condition $\nabla\cdot H=0$ prevents the lines from terminating there. The fields whose lines close upon themselves are characterized by certain symmetry or other restrictive conditions, for instance, that each line be confined to a plane. In the general case a line approaches arbitrarily close to any point of at least a region of space ("ergodic" behavior). Studies of this behavior may be used to advantage to clarify the conditions under which amplificatory processes in magnetohydrodynamics can or cannot[2] occur.

[1] J. Slepian, Am. J. Phys. **19**, 87 (1951).
[2] T. G. Cowling, Monthly Notices Roy. Astron. Soc. **94**, 39 (1934).

C5. Magnetic Shielding Produced by a Rotating Conducting Tube. ALFREDO BAÑOS, JR., *University of California, Los Angeles.*—The problem of deflecting the beam in high-energy accelerators employing an intense magnetic field or the problem of obtaining a field free region over a limited volume between the pole pieces or in the fringing field may possibly be solved by using a conducting tube rotating at right angles to the magnetic field. Because of eddy currents, the field inside the tube, which turns out to be uniform, is materially reduced and can be oriented in any direction (on a plane perpendicular to the axis of the tube) by adjusting the available parameters: ratio of outer to inner radius, conductivity of the material, permeability of the material (assumed constant for magnetic materials), and angular frequency of rotation. The power requirements are determined in terms of these parameters, and it is shown that for copper and iron

tubes the required power per unit of length may not be prohibitive at 60 cycles if the magnetic field to be shielded does not exceed 10 000 gauss. Power requirements for solid shafts are also considered in this investigation, and the results obtained are found in complete agreement with those of Frank.[1]

[1] N. H. Frank, "Eddy current losses in a conducting shaft rotating in a magnetic field," M. I. T. Research Laboratory of Electronics, Report No. 23 (November 20, 1946).

C6. Distribution of Sizes of Spheres in a Solid from a Study of Slices of the Solid. WALTER P. REID, *U. S. Naval Ordnance Test Station.*—It is assumed that spheres are distributed throughout an otherwise uniform solid and that one wishes to determine the distribution of sizes among these spheres from the distribution of sizes among circles observed when the solid is cut by a plane. Integral equations have been determined connecting functions used to represent various size distributions of circles and of spheres so that any of the functions may be calculated if one of them is known. Another possibility is to draw random lines on the planes and determine the distribution of sizes of the intercepted chords. To determine information concerning the number of spheres of a given size, it is only necessary to have information about the chords in the neighborhood of that size or the circles of that size and larger. Corresponding frequency distribution curves for spheres, circles, and chords have been calculated.

C7. Cleavage Surfaces of Germanium Crystals. I. H. CHRISTENSEN, C. J. CALBICK, AND E. E. THOMAS, *Bell Telephone Laboratories, Inc.*—Single crystals of germanium were cleaved on (111) planes and the resulting surfaces examined optically, electron-optically, and by x-rays. Two particular samples, I and II, are discussed in this and the following paper. Both crystals showed the exceedingly low fracture strength characteristic of germanium.[1] The cleavage was cataclysmic in nature since fracture striae attributable to clearly defined and complex shock wave systems[2] were seen. Sample I, drawn from the melt in the standard way, showed about 25 percent of the cleavage surface to be imperfect. Sample II, drawn from the melt of previously zone-refined material,[3] showed imperfections in 5–10 percent of its surface. Sample I was n type with $\rho = 50$ ohm-cm and hole lifetime of 260 μsec, while sample II possessed intrinsic conduction at room temperature with a donor-minus-acceptor concentration of about 3×10^{13}/cm^3. Cracking phenomena observed optically on these and other germanium surfaces are believed to stem from defects in the original crystal structure.

[1] E. E. Schumacher, Am. Inst. Mining Met. Engrs. Trans. **88**, 1097 (1950).
[2] Nadai, *Theory of Flow and Fracture of Solids* (1950), Vol. I, p. 204.
[3] W. G. Pfann and K. M. Olsen, Phys. Rev. **89**, 322 (1953).

C8. Cleavage Surfaces in Germanium Crystals. II. C. J. CALBICK, H. CHRISTENSEN, AND E. E. THOMAS, *Bell Telephone Laboratories, Inc.*—The cracking phenomena described in germanium samples I and II of the previous paper are more strikingly shown by electron than by optical micrography. In addition to enhanced detail in rough and fissured areas, smooth areas traversed by cleavage steps only were observed. It was noted also that the relatively more imperfect sample I showed correspondingly more numerous cracks and greater extent of rough areas than sample II. The complex surface structure must have its basic cause in imperfections existing in the crystal before cleavage. Seitz' theory[1] of coalescence of vacancies into sheets, followed by collapse of the sheets with formation of dislocation rings, has recently received experimental confirmation by Hoffman, Anders, and Crittenden,[2] who measured the stresses during annealing of nickel films deposited by evaporation. The sheets of vacancies are reminiscent of the microcracks of the Griffith theory of fracture strength. It is suggested that during the cataclysmic process of cleavage, such microcracks may enlarge and widen to form the observed cracks, which are of the order of 200A wide.

[1] F. Seitz, *Advances in Physics* **1**, 43 (1952).
[2] Hoffman, Anders, and Crittenden, J. Appl. Phys. **24**, 231 (1953).

C9. A Single Crystal Neutron Diffraction Study of Heavy Ice. S. W. PETERSON AND H. A. LEVY, *Oak Ridge National Laboratory.*—The structure of heavy ice at -50°C has been investigated by means of the single-crystal neutron diffraction method. Complete (01·0) zone data was obtained out to $\sin\theta/\lambda = 0.77$. Fourier and least-squares procedures were used in structure refinement. The deuterium atoms were found to be in disordered positions corresponding to a double minimum potential barrier in full agreement with the Pauling model of ice and with the powder diffraction data of Wollan, Davidson, and Shull.[1] The short deuterium oxygen distance was found to be 1.01A and the D$-$O$-$D angle closely tetrahedral. A few measurements made at -130°C indicated no significant structural difference at the lower temperature. The resulting centrosymmetrical structure is not compatible with the piezoelectricity[2] sometimes claimed for ordinary ice. In addition it does not support, but is not definitely incompatible with, Bjerrum's considerations[3] on the nature of the disorder in ice.

[1] Wollan, Davidson, and Shull, Phys. Rev. **75**, 1348 (1949).
[2] Rossmann, Experientia **6**, 182 (1950).
[3] Niels Bjerrum, Science **115**, 385 (1951).

C10. Behavior of Metals at Elevated Temperatures. EDWARD W. LAROCCA, *U. S. Naval Ordnance Test Station.*—Measurements of rupture times of a chromium-nickel-iron alloy were made in various atmospheres and at varied temperatures and stresses. The activation energy of the rupture process is shown to be stress-dependent and not constant over the temperature range studied, 900° to 1200°C.

C11. Reformulation of Solid-State Electronic Boltzmann Equation. J. S. LOMONT, *U. S. Naval Ordnance Test Station.*—The customary derivation of the Boltzmann transport equation for conduction electrons in crystals assumes that $\partial_t f$ is the sum of two terms due to external fields and collision processes. The collision term is expressed in terms of a transition probability, and explicitly takes account of the exclusion principle; whereas the field term is derived on classical grounds and ignores both the exclusion principle and the binding of the electrons. The derivation is therefore a hybrid one, half classical and half quantum mechanical. If one re-examines the derivation of the collision term, one sees that this term will give the entire $\partial_t f$ if the transition probability due to collisions is replaced by the transition probability due to both the external fields and collisions. The resulting new form of the Boltzmann equation is thus given a unified quantum-mechanical derivation. To compare the two forms of the equation, one can (and must), without recourse to perturbation theory, calculate the transition probability of free electrons due to an external electric field. Using this to calculate the field term one gets the old $(\mathbf{F}\cdot\nabla_k f)$ term plus a term nonlinear in the distribution function. The corresponding general calculation for the tight-binding approximation cannot be made.

C12. Elastic Description of a High-Amplitude Spherical Pulse in Steel. WILLIAM A. ALLEN, *U. S. Naval Ordnance Test Station.*—Extensive calculations have been performed with the IBM card programmed electronic calculator to evaluate a problem in elasticity that simulates the effect of a cylindrical charge of high explosive detonated in intimate contact with a steel plate. Although elastic theory has been extrapolated into a regime where it is known not to apply, insight can be obtained on the origin of the negative component of the pulse which produces tensile fracture in the specimen.

Agreement between experiment and elastic theory improves as the stresses decay to sonic proportions.

C13. Suppression of AlO in the Wake of Ultra-Speed Pellets. WILLIAM C. WHITE, *U. S. Naval Ordnance Test Station.*—Time-resolved spectrograms of aluminum ultra-speed pellets have been obtained along trajectories where the velocity is decreasing rapidly. The AlO bands were observed to be suppressed for a length of time depending upon the position of the pellet along its trajectory. The time of suppression is a few μsec at the beginning of the trajectory, a maximum of over 100μsec at five feet, and goes to 0μsec at approximately 12 feet. It is felt that after the pellet reaches the five-foot point where its velocity is about 4.5 km/sec, the suppression of AlO becomes velocity-dependent and hence may be controlled by the temperature behind the shock wave.

C14. Electrical Conductance and Structure Studies of Thin Bi Films Evaporated on Glass* P. J. BRYANT, H. U. RHOADS, AND A. H. WEBER, *Saint Louis University.*—The electrical conductance[1] of thin Bi films (thickness 2–310A) evaporated in vacuum onto glass substrates was measured and correlated with an electron microscope and electron diffraction examination of the films. Film thickness was determined by a radioactive tracer method.[2] Preparation of the standard deposits, construction of the conductance apparatus, and the technique of sample preparation are described. The electrical conductance for films about 0.5×0.15 cm in surface dimensions was sensibly constant at 1.30×10^{-14} ohm^{-1} for thin deposits (2–75A). A transition region was found between 90–130A in which the conductance increases by a factor of 10^{12}. Electron micrographs show film structures for which the observed conductance changes are the expected ones. For the region 2–20A the structure consists of flower-like deposits of Bi along with large areas void of metallic deposit; at about 20A small dispersed particles appear, these particles form separate aggregates for thicknesses up to about 90A. The aggregates then form into a structure of continuous paths. At 310A electrical resistivity is 1.60×10^{-4} ohm-cm (bulk metal value, 1.19×10^{-4} ohm-cm), and the structure is virtually continuous.

* Assisted by a National Science Foundation grant.

[1] L. W. Friedrich and A. H. Weber, Phys. Rev. **66**, 248 (1944); D. F. O'Brien and A. H. Weber, Phys. Rev. **60**, 574 (1941).

[2] J. J. Antal and A. H. Weber, Rev. Sci. Instr. **23**, 424–26 (1952).

C15. The Effects of High Sputtering Rates on the Resistivities of Sputtered Gold Films.* RICHARD B. BELSER, *Georgia Institute of Technology.*—Measurement of the temperature of a glass substrate subjected to sputtering from a 2-inch disk gold cathode at 100-ma sputtering rate indicated that temperatures as high as 250–300°C were experienced. These temperatures are sufficient to cause artificial aging of sputtered gold films. Initial resistivity measurements of gold films sputtered at successively higher currents in 20-ma steps showed a decrease in initial resistivity from 5.3ρ_b at 20 ma to 3.7ρ_b at 100 ma. These films, however, upon artificial aging in an infrared vacuum oven dropped in resistivity to values under 2ρ_b. These tests have indicated that sputtered gold films are very resistant to artificial aging in comparison with evaporated gold films or sputtered silver films. Resistance stability is also displayed at room temperature. The apparent stability of these films is of importance in their use for coatings of quartz piezoelectric crystals.

* Supported by the U. S. Army Signal Corps.

WEDNESDAY AFTERNOON AT 2:00

Geology Auditorium

(W. A. FOWLER, presiding)

Contributed Papers

D1. Effects of Chemical Structure on Stopping Powers for High-Energy Protons.* T. J. THOMPSON,† *University of California Radiation Laboratory, Berkeley.*—A study has been made of the stopping power of various elements and compounds for a high-energy proton beam. The stopping powers of four elements hydrogen, carbon, nitrogen, and oxygen and twenty-nine compounds of these elements have been measured with a high degree of accuracy. The stopping power of a fifth element, chlorine, has been inferred from its compounds. An effort has been made to determine whether or not the relative stopping power of a compound is strictly an additive function of the elements which form the compound. The results indicate that the relative stopping power of a compound as a whole is an additive function of the elements in the compound to within about one percent. The largest percentage deviations occur with the hydrogen atoms in the compound and are of the order of two percent. The percentage deviations decrease rapidly with increasing atomic number. There appears to be a measureable chemical effect. For example, the stopping power of carbon and hydrogen is higher in unsaturated compounds than in saturated compounds.

* This paper is a complete report of work done at the University of California Radiation Laboratory and first reported in part at the Berkeley meeting of the American Physical Society, December 28, 1951.

† Now at University of California, Los Alamos Scientific Laboratory, Los Alamos, New Mexico.

D2. The Disintegration of C^{12}, B^{11}, and B^{10} by Fast Neutrons.* GLENN M. FRYE AND LOUIS ROSEN, *University of California, Los Alamos Scientific Laboratory.*—Detailed measurements on the stars produced in C^{12} unloaded, B^{11} loaded, and B^{10} loaded Ilford *C2* emulsions by 12- to 20-Mev neutrons have been used to identify approximately 2000 $C^{12}(n, n')3\alpha$ reactions[1] and a small number of $B^{10}(n, 2\alpha)H^3$ and $B^{11}(n, \alpha)Li^{8*}\rightarrow Be^{8*}\rightarrow 2\alpha$ reactions.[2,3] The neutrons were generated by the large Los Alamos electrostatic accelerator, using the $T(d, n)He^4$ reaction. The emulsions were positioned around the circumference of a circle with the tritium target at the center. The geometry was such that the variation of the incident neutron energy at each plate was $\leq$0.8 Mev. Results will be given for the variation of cross section with energy for C^{12} disintegrations. An attempt is presently being made to determine whether this reaction proceeds through intermediate stages involving excited states of C^{12} and Be^8, and if so, which excited states are involved.

* Work performed under the auspices of the U. S. Atomic Energy Commission.

[1] L. L. Green and W. M. Gibson, Proc. Phys. Soc. (London) **A62**, 296 (1949).

[2] J. L. Perkin, Phys. Rev. **81**, 892 (1951).

[3] E. Pickup, Phys. Rev. **74**, 495 (1948).

D3. The Angular Distributions of the Long-Range α Particles from $N^{15}(p,\alpha)C^{12}$. G. C. NEILSON, D. B. JAMES, AND C. A. BARNES, *University of British Columbia.*—The angular distributions of the long-range alpha particles have been studied with a helium-filled proportional counter for proton energies between 0.5 and 1 Mev. The proton beam from the electrostatic accelerator bombarded evaporated KNO_3(60 percent N^{15}) targets about 20 kev thick. The angular distributions, normalized such that $I(90°)=1$, were multiplied by the yield at 90°[1] and analyzed into the form $A+B\cos\theta+C\cos^2\theta$.

Ep in Mev	A	B	C
0.500	1.13±0.03	−0.37±0.01	−0.11±0.04
0.750	1.40±0.09	−0.90±0.06	−0.11±0.13
0.850	3.00±0.13	−2.46±0.09	−0.45±0.19
0.900	4.10±0.18	−3.57±0.11	−0.53±0.24
0.950	6.50±0.17	−3.86±0.12	−2.64±0.24
0.975	7.60±0.26	−3.87±0.08	−3.76±0.38

Preliminary analysis indicates that the 0.338-Mev resonance corresponds to an O^{16} state of $J=0+$ formed with p-wave protons and the 1.05-Mev resonance to an O^{16} state of $J=1-$ formed with s and d-wave protons.

[1]Schart, Fowler, and Lauritsen, Phys. Rev. **86**, 525 (1952).

D4. The Gamma Rays from the $T(p,\gamma)He^4$ Reaction. J. B. WARREN AND G. M. GRIFFITHS, *University of British Columbia.*—Using scintillation counter technique the gamma-ray energy, measured relative to the $Li^7(p,\gamma)Be^8$ reaction, is 20.3±0.4 Mev at 90° to incident protons of 800-kev energy. This corresponds to a Q value of 19.7±0.4 Mev in accord with the mass values. The yield appeared to be lower than expected from previous work.[1] Preliminary data on the angular distribution show it to be nearly pure $\sin^2\theta$ and to be represented by $\sin^2\theta+0.13\pm0.03$ at $Ep=800$ kev. Neutrons are in evidence well below the (p,n) threshold.

[1] Argo, Gittings, Hemmendinger, Jarvis, Taschek, Phys. Rev. **78**, 691 (1950).

D5. The Gamma Rays from the $D(p,\gamma)He^3$ Reaction. G. M. GRIFFITHS AND J. B. WARREN, *University of British Columbia.*—Using scintillation counting technique the gamma-ray energy has been measured and fits the relation $E_{\gamma(90°)}=[5.50\pm0.03+\frac{3}{4}Ep]$ Mev. The Doppler shift of the gamma-ray frequency as a function of angle has been determined and has the full value expected assuming the gamma radiation is emitted in a time short compared to the slowing down time. The excitation function has been measured from 250-kev to 1.8-Mev bombarding proton energy and the cross section at 1 Mev is about 6×10^{-30} cm². Careful measurements of the angular distribution show, after allowing for the neutrons produced by knock-on deuterons, that there is a small yield at 0°. The distribution has the form $\sin^2\theta+b$ where $b=0.046\pm0.005$ for $Ep=1$ Mev and $b=0.025\pm0.006$ for $Ep=1.75$ Mev.

D6. A High-Pressure Cloud-Chamber Investigation of Protons Scattered by 300-Mev Neutrons.* JOHN DEPANGHER,† *University of California, Berkeley.*—An investigation of the protons scattered by 300-Mev neutrons has been conducted in a magnetic field with a Wilson cloud chamber filled with hydrogen at a pressure of ten atmospheres. The energy spectrum will be presented for the neutrons which are produced in a 1¾-in. thick LiD target by 340-Mev protons from the Berkeley cyclotron. The angular distribution data, consisting of 2057 tracks whose neutron energies exceed 200 Mev, cover the range of angles 10°–180° for the neutrons in the center-of-mass system. When the data are normalized to a total cross section of 35 mb, they agree well with the work of Kelly *et al.*,[1] but the yield of neutrons with small scatter angles is considerably below that which is predicted by phenomenological theories. Evidence for the reactions $n+p\rightarrow\pi^0+d$, $n+p\rightarrow\pi^++2n$, and $n+p\rightarrow\gamma+d$ will be presented.

* Work performed under the auspices of the U. S. Atomic Energy Commission.
† Now with the Hanford Atomic Products Operation, General Electric Company, Richland, Washington.
[1] Kelly, Leith, Segrè, and Wiegand, Phys. Rev. **83**, 923 (1951).

D7. Gamma Rays and Internal Pairs from Be^9+H^1.* ROBERT J. MACKIN, JR., *Kellogg Radiation Laboratory, California Institute of Technology.*—Gamma radiation following $Be^9(p,\alpha)Li^{6*}$, resonant at $Ep=2.565$ Mev,[1] has been studied with a magnetic lens spectrometer using 1.9 percent resolution. The gamma-ray energy, determined from Compton and photoelectron spectra, is 3572±12 kev. It may be necessary to subtract a 26-kev Doppler shift from this figure. The internal-pair (positron) spectrum agrees most closely (to 4.5 percent) with the assignment of the radiation as magnetic dipole. The theoretical electric-quadrupole spectrum falls 13 percent above the experimental points, about 1.5 times the probable error. Theoretical spectra for all other assignments differ from experiment by more than twice the probable error. The magnetic-dipole character is consistent with other data pertaining to the states involved. Capture radiation from the same resonance is 10^{-3} times as intense and has energy 8.1±0.2 Mev. It thus appears to lead to the 0.72-Mev state of B^{10}. The soft cascade radiation was not detectable above the background from the 3.57-Mev gamma rays.

* Assisted by the joint program of the U. S. Office of Naval Research and the U. S. Atomic Energy Commission.
[1] R. B. Day and R. L. Walker, Phys. Rev. **85**, 582 (1952).

D8. Gamma Rays from $N^{14}(p,\gamma)O^{15}$.* C. W. LI, *Kellogg Radiation Laboratory, California Institute of Technology.*—Capture gamma radiations from $N^{14}(p,\gamma)O^{15}$ have been investigated with the primary object to get information on the levels of O^{15} corresponding to low-energy resonances in $N^{14}+p$, which are of importance in the production of stellar energy through the carbon-nitrogen cycle. Nitrogen gas targets, 10 to 20 kev thick, were used and the gamma rays were detected with a NaI(Tl) scintillation counter and registered by oscilloscope pictures and a ten-channel differential discriminator.[1] The excitation curve of gamma rays for the bombarding energy 0.6 to 2.5 Mev agreed with the main part of the excitation curve for the induced O^{15} positron activity.[2] A number of cascade transitions were revealed. For the 1.06-Mev resonance, the following gamma rays have been established: (1) 8.34 Mev, strong; (2) 3.04±0.03 Mev and 5.27±0.03 Mev, strong; (3) 1.46±0.03 Mev and 6.82±0.08 Mev, weak. Direct transitions to the ground state from all the resonances studied are relatively strong, probably indicating that the spins are not larger than 5/2 for the corresponding levels.

* Assisted by the joint program of the U. S. Office of Naval Research and the U. S. Atomic Energy Commission.
[1] Woodbury, Day, and Tollestrup, Phys. Rev. (to be published).
[2] D. B. Duncan and J. E. Perry, Phys. Rev. **82**, 809 (1951).

D9. Elastic Scattering of Protons by N^{14}.* T. S. WEBB, C. W. LI, AND W. A. FOWLER, *Kellogg Radiation Laboratory, California Institute of Technology.*—Measurements have recently been made of the absolute differential cross section for the elastic scattering of protons by N^{14}, using a magnetic spectrometer with protons accelerated in the 2-Mev electrostatic generator. An arrangement has been made for condensing NH_3 on a copper backing by using liquid nitrogen, and the solid NH_3 targets so obtained have been used. Preliminary measurements for bombarding energies in the range 0.5 to 1.7 Mev have been made at $\cos\theta=-0.9$; $-1/\sqrt{2}$; $-1/\sqrt{3}$ and 0, where θ is the scattering angle in the center-of-mass system. Two prominent scattering anomalies were observed with

maxima at 1.07 and 1.60 Mev corresponding to the levels of O^{16} at 1.06 and 1.55 Mev as observed in the $N^{14}(p, \gamma)O^{15}$ reaction. These anomalies are superposed on a background which decreases less rapidly than the calculated Rutherford cross section, the experimental value being approximately equal to Rutherford at 0.7 Mev and rising to over twice Rutherford at 1.7 Mev. Further experimental work and analysis are now in progress.

* Assisted by the joint program of the U. S Office of Naval Research and the U. S. Atomic Energy Commission.

D10. Energy Levels in N^{14} from the Scattering of Protons by C^{13}.* EDMUND A. MILNE, *Kellogg Radiation Laboratory, California Institute of Technology.*—The differential cross section for the elastic scattering of protons by C^{13} has been determined in the energy range from 0.45 to 1.60 Mev at angles of 50, 90, 120, and 160 degrees in the center-of-mass system. Marked anomalies were found in the scattering at 0.556, 1.16, 1.47, and 1.55 Mev corresponding to the 8.06-, and 8.62-Mev levels in N^{14} reported by Seagrave[1] and two new levels at 8.90 and 8.98 Mev. The spins and parities of these states have been determined from a preliminary analysis of the data which also indicates an effect due to the broad resonance at 1.25 Mev in $C^{13}(p, \gamma)N^{14}$ reported by Seagrave. The assignment for the 8.06-Mev level is $J=1^-$, for the 8.62-Mev level $J=0^+$, and for the broad 8.70-Mev level $J=0^-$. For the 8.90-Mev level $J=2^-$ or 3^-, and for the 8.98-Mev level $J=1^+$, 2^+, or 3^+.

* Assisted by the joint program of the U. S. Office of Naval Research and the U. S. Atomic Energy Commission.
[1] John Seagrave, Phys. Rev. **85**, 197 (1952).

D11. Gamma-Rays from $Li^7(p, \gamma)Be^8$.* ALFRED A. KRAUS, JR.,† *Kellogg Radiation Laboratory, California Institute of Technology.*—The excitation functions of the γ rays from the reactions $Li^7(p, \gamma)Be^8$ and $Li^7(p, p'\gamma)Li^{7*}$ have been measured in the energy range of 400 kev to 1400 kev. The detector was a 1½-in. diameter by 2 in. long NaI(Th) crystal scintillation counter. The soft γ rays from the first excited state of Li^7 follow the excitation curve of Brown, Snyder, Fowler, and Lauritsen.[1] The hard γ rays from Be^8 exhibit the well-known resonance at the 441-kev proton energy. In addition they are also resonant at the 1050-kev resonance of the soft γ rays. Possible assignments of the spin and parity of the 18.14-Mev level of Be^8 will be discussed in the light of angular distribution measurements of the hard γ rays.

* Supported by the joint program of the U. S. Office of Naval Research and the U. S. Atomic Energy Commission.
† G. E. Fellow in Physics, 1952–1953.
[1] Brown, Snyder, Fowler, and Lauritsen, Phys. Rev. **82**, 159 (1951).

D12. Reactions and Scattering of Protons on Li^7.* D. A. LIBERMAN AND R. F. CHRISTY, *Kellogg Radiation Laboratory, California Institute of Technology.*—An analysis in terms of s- and p-wave phase shifts has been made of the recent data[1] on the elastic scattering of protons on Li^7 between energies of 360 and 1400 kev. The principal features of the elastic scattering in the neighborhood of the 440-kev resonance and also the spherical symmetry of the resonant γ rays are explained by a $J=1$ even compound state formed by p-wave protons with channel spins 1 and 2 in a ratio of 1 to 5. This particular channel spin ratio corresponds to a particular state in either an LS or jj coupling scheme. An analysis is also being made of the region about the 1030-kev resonance, including both the elastic scattering data and recent experiments in this laboratory on the angular distribution of the inelastically scattered protons.

* Assisted by the joint program of the U. S. Office of Naval Research and the U. S. Atomic Energy Commission.
[1] W. D. Warters, thesis, California Institute of Technology (1953) and a paper to be published in the Physical Review.

D13. Angular Distributions of the $F^{19}(p, \alpha)O^{16}$ Reaction.* R. W. PETERSON, W. A. FOWLER, AND C. C. LAURITSEN, *Kellogg Radiation Laboratory, California Institute of Technology.*—A study of the angular distributions of the three short-range alpha groups from the $F^{19}(p, \alpha\gamma)O^{16}$ reaction at proton capture resonances from 874 kev to 1.69 Mev has been undertaken. Preliminary measurements at the 874- and 935-kev resonances are in agreement with the level assignments of Seed and French.[1] The α_2 and α_3 groups were observed at several angles at the 874 resonance with high resolution, using photographic plates as the detector in order to determine if either was a doublet containing the 2^- state as predicted on the basis of the alpha-particle model. No evidence of such a doublet was found, and an upper limit on the maximum separation of such a doublet was set at 3 kev. In addition, a search for shorter-range alpha groups was made. The excitation energy ranges of 7.1 to 7.94 Mev and 8.11 to 9.12 Mev in O^{16} were investigated with a negative result.

* Assisted by the joint program of the U. S. Office of Naval Research and the U. S. Atomic Energy Commission.
[1] A. P. Seed and J. French, Phys. Rev. **88**, 1007 (1952).

D14. Proton Stopping Cross Section of Lithium.* M. BADER, W. A. WENZEL, AND W. WHALING, *Kellogg Radiation Laboratory, California Institute of Technology.*—The energy loss of 450-kev protons passing through a thin film of Li metal has been measured with an electrostatic analyzer and a double-focusing magnetic spectrometer. The film of Li(~250 kev thick) was deposited by vacuum evaporation on a thin Al foil. The thickness of the Li was determined by a quantitative chemical analysis of the Li deposited simultaneously on a tantalum surface of known area. The purity of the deposited Li was determined by a momentum analysis of protons scattered from a thick Li target deposited with the test layer. A negligible surface contamination of O was the principal impurity present. At $E_p=440$ kev the proton stopping cross section is $4.69\pm0.15\ 10^{-15}$ ev-cm². Measurements of relative values determine the stopping cross section at other proton energies. Preliminary results for a similar measurement of Na will be presented.

* Assisted by the joint program of the U. S. Office of Naval Research and the U. S. Atomic Energy Commission.

THURSDAY MORNING AT 9:00

Student Union Ballroom

(E. FERMI, presiding)

Invited Papers

E1. Origin and Propagation of Air Showers. KURT SITTE, *Syracuse University.* (30 min.)
E2. Transition Phenomena. R. B. BRODE, *University of California, Berkeley.* (20 min.)
E3. Recent Work on Penetrating Showers. W. D. WALKER, *University of Rochester.* (30 min.)
E4. Some Recent Results on *V* Particles. C. D. ANDERSON, *California Institute of Technology.* (30 min.)
E5. Evidence for the General Magnetic Field of the Sun from Cosmic Rays. M. S. VALLARTA, *University of Mexico.* (30 min.)

Contributed Papers

E6. Emulsion Study of a Large Shower. I. The Hard Component. P. S. FREIER AND J. E. NAUGLE, *University of Minnesota.*—A high-energy interaction between a heavy primary and a nucleus of the glass backing of the emulsion has been studied. The core of the shower, a fragment of charge 5, travels 4.72 cm in a single 400-micron G-5 emulsion. The 36 ± 5 shower particles travel a total of 3.9 geometric mean free paths in the emulsion. In this distance 2 nuclear interactions are observed. A third nuclear interaction is observed in a facing emulsion; however, the total path length has not been measured in this plate. All of the shower particles have a grain density corresponding to the plateau value for this emulsion, and relative scattering measurements show that their energies are >40 bev. Two of the secondary interactions have $\lesssim 4$ evaporation particles and show a definite dense and diffuse cone. The third shower has 7 evaporation particles and does not show a separation into a dense and diffuse cone. Analysis of the angular distributions of these showers gives energies from 40–400 bev for these three secondaries. Analysis of the angular distribution of the shower particles gives an energy of about 5×10^4 bev/nucleon for the incident heavy.

E7. Emulsion Study of a Large Shower. II. The Soft Component. J. E. NAUGLE AND P. S. FREIER, *University of Minnesota.*—In the shower described in paper I, 9 pairs of particles have been observed to begin in the emulsion or to enter the emulsion from the glass in the first cm of emulsion and within an angle of 0.1 radian from the shower core. If one assumes that all of the hard particles observed in this same cone are pi mesons and that the pairs originate from the materialization of γ rays from the decay of neutral mesons with zero lifetime, then the ratio of the number of observed pairs to shower particles will give a lower limit for the ratio of neutral meson to charged mesons produced in this event. This ratio is 0.44 ± 0.13. The electrons of these pairs were followed a total of 23.5 cm of emulsion. In this distance 11 tridents (direct pair production by electrons) were observed, giving a mean free path of 2.1 ± 0.7 cm. The theory of Bhabba[1] predicts a value of 12.5 cm for a 50-bev electron and 7.4 cm for a 500-bev electron. Thus, the experimental cross section is larger than that predicted by theory by at least a factor of two.

[1] H. J. Bhabba, Proc. Roy. Soc. (London) **152**, 559 (1935).

E8. Multiple Cores in Air Showers.* OSMAN EL-MOFTY, *University of California, Berkeley* (*introduced by* ROBERT B. BRODE).—Multiple cores in cosmic-ray air showers are difficult to observe because of the overlapping of the cores. After transition to equilibrium with water, the cores are much smaller and readily identified. Decoherence measurements of the coincidences between pulses in ionization chambers have been made for depths in water from 0 to 3 meters and with separation of the chambers up to 6 meters. The decoherence measurements are consistent with an average air shower at 9000 feet which has about 20 cores within a distance of about 5 meters from the shower's center.

* Assisted by the joint program of the U. S. Office of Naval Research and the U. S. Atomic Energy Commission.

E9. North-South Observations of the Ratio of Positive to Negative Cosmic-Ray Mesons.* ROBERT B. BRODE, *University of California, Berkeley.*—Observations of the east-west asymmetry in the ratio of positive to negative μ mesons are normally made with the axis of the equipment horizontal and pointing to the magnetic north. Since the magnetic dip is 60° at Berkeley, inclining the axis of the equipment at $\pm30°$ to the horizontal places the plane of measurement approximately parallel or perpendicular to the earth's magnetic field. The east-west asymmetry of the ratio of positive to negative μ mesons observed at an inclination of $\pm30°$ to the horizontal is not essentially different from that observed in the vertical plane. The theory of this asymmetry based on the different path length of positive and negative particles caused by their deflection in the earth's magnetic field indicates that there should be little difference in the ratio of positive to negative μ mesons for inclination of the axis from the horizontal.

* Assisted by the joint program of the U. S. Office of Naval Research and the U. S. Atomic Energy Commission.

E10. Time Variations in Cosmic-Ray Intensity Underground. MERCEDES M. AGOGINO, *University of New Mexico.*—An experiment to investigate the time variation of cosmic-ray intensity during the solar and sidereal day is being performed at Albuquerque, New Mexico. Two countertube telescopes are located fifty feet underground, one facing east and the other west, both at 45° zenith angles, thus giving them a separation of approximately 7 hours in hour angle. The equipment is rotated through 180° about a vertical axis at the beginning of each hour so that the eastern and western telescopes are interchanged. Analysis of three months' data has given the counting rate for the two directions for each two hours during the sidereal and solar day with a standard deviation of 0.2 percent. Harmonic analysis of the four curves thus obtained does not indicate a clearcut sidereal or solar variation of cosmic-ray intensity greater than may be expected from the quoted statistical error. In each of the four curves a maximum fluctuation of 0.6 percent was found among the 2-hour values. The experiment is being continued.

THURSDAY MORNING AT 9:00

Geology Auditorium

(F. N. FRENKIEL, presiding)

Invited Papers

Division of Fluid Dynamics

F1. Examples of Flow Patterns at and near Mach One. GOTTFRIED GUDERLEY, *Wright Air Development Center.* (40 min.)

F2. Slender Bodies of Revolution at Transonic Speeds. JULIAN D. COLE, *California Institute of Technology.* (40 min.)

F3. Steady and Unsteady Phenomena at Transonic Speeds. ADOLF BUSEMANN, *Langley Aeronautical Laboratory.* (40 min.)

Contributed Papers

F4. Interference of Underwater Sound Caused by Surface Reflection and Upward Refraction. F. H. SANDERS, *Pacific Naval Laboratory.*—Experiments have been carried out at Nodales Channel, British Columbia, on the interference patterns resulting from surface reflection of high audio-frequency sound. Differences in intensity as great as forty decibels have been observed, and some extrema are identifiable at ranges in excess of 2000 yards. Oceanographic conditions in the channel were such as to produce very slight upward refraction. Under such conditions Young[1] has predicted that the time difference between the surface-reflected and the direct-sound paths will pass through a minimum at a certain value of the range. In consequence, interference extrema should exist only if the time difference between the two paths exceeds a certain integral number of half-periods, and two ranges should exist at which an extremum of given order can occur. Experimental observations confirm these predictions. The relation between the observed ranges of the extrema and the other parameters concerned is discussed and compared with Young's theory and with expressions developed by R. W. Stewart.

[1] R. W. Young, J. Acoust. Soc. Am. **19**, 1 (1947).

F5. "Lloyd Mirror" Interference in the Presence of Slight Uniform Refraction. R. W. STEWART, *Pacific Naval Laboratory.*—A ray theory is developed to describe the location of positions of reinforcement and annulment of reflected and direct radiation in the presence of a small velocity gradient. Angles are assumed small enough that two terms of the Maclaurin's series expansion are sufficient to describe the trigonometric functions. Account is taken of the difference in velocity, the curvature of the rays, and the displacement of the point of reflection caused by the refraction. The result is expressed as a series, the first term of which gives the ordinary Lloyd Mirror result for grazing incidence. The second term gives the modification resulting from the nonuniformity of the velocity, and the higher terms give the effects of the curvature of the rays. The first two terms above are shown to yield very similar results to the theory of Young.[1] The theory is applied to the behavior of sound in calm isothermal water.

[1] R. W. Young, J. Acoust. Soc. Am. **19**, 1 (1947).

F6. Thermal Microstructure in the Ocean. W. N. ENGLISH, *Pacific Naval Laboratory.*—A dual-channel ac thermistor bridge and a dc thermistor thermometer have been developed for the study of thermal microstructure in the ocean. Fluctuations as small as 0.01 F° can be recorded. The time constant is about one second. Temperature fluctuations varying from a few hundredths to a few tenths of a degree have been found in all water examined, even in so-called "isothermal" water. Fluctuations were greatest when tidal velocity was least. Transit of temperature structure from one horizontal pair to another can be followed and time to give average velocity of water movement. A high correlation has been observed between rate of change of temperature on a single thermistor and mean gradient measured by a horizontal pair.

F7. Some Correlation Studies of Sound Fluctuations in the Ocean. H. L. GRANT AND R. W. STEWART, *Pacific Naval Laboratory.*—Observations have been made of the fluctuation of sound intensity in the ocean in thoroughly mixed water and in the presence of positive and negative temperature gradients. At a frequency of 18 kc and ranges of about one-half mile, fluctuations of all periods from a fraction of a second to many hours have been detected. The cross correlation between intensities measured at different points in a sound field is found to average nearly zero for vertical separations even as small as two feet. For horizontal separations the cross correlation is quite high at a few feet, but drops to about 0.5 at separations of twenty feet. Not only does the sound fluctuate, but the short-term mean amplitude of the fluctuation varies over wide limits in an apparently random manner.

THURSDAY AFTERNOON AT 2:00

Student Union Ballroom

(H. A. BETHE, presiding)

Invited Papers

G1. Neutron Diffraction by Ferromagnetic and Antiferromagnetic Substances. M. K. WILKINSON, *Oak Ridge National Laboratory.* (30 min.)

G2. Neutron Diffraction by Paramagnetic Substances. W. C. KOEHLER, *Oak Ridge National Laboratory.* (30 min.)

G3. An Experiment to Detect the Free Neutrino. Part I. FREDERICK REINES, *Los Alamos Scientific Laboratory.* (30 min.)

G4. An Experiment to Detect the Free Neutrino. Part II. C. L. COWAN, JR., *Los Alamos Scientific Laboratory.* (30 min.)

Contributed Papers

G5. Background in a Neutrino Experiment.* F. B. HARRISON, C. L. COWAN, JR., AND F. REINES, *Los Alamos Scientific Laboratory, University of California.*—We shall discuss the different types of background encountered in the neutrino experiment[1] described in the two invited papers of this session. Since we require a pair of pulses associated in time, the contribution of random coincidences from single counts (gamma-ray background) can be computed from the counting rate of single pulses and the resolving time. Associated pairs of pulses may, for example, be due to the following causes: μ-meson decay in the scintillator tank; μ-meson capture in the tank and surroundings, giving fast neutrons which give one pulse from proton recoil and another from neutron capture; the N component of cosmic rays, giving fast neutrons from stars in the tank and surroundings; and fast neutrons from the pile. Estimates will be made of how much each of these types of background contribute to the counting rate.

* Work performed under the auspices of the U. S. Atomic Energy Commission.
[1] F. Reines and C. L. Cowan, Jr., Phys. Rev. **90**, 492 (1953).

G6. Liquid Scintillators for Large Volume Detectors.* F. N. HAYES, LLOYD WILLIAMS, C. L. COWAN, JR., AND F. REINES, *Los Alamos Scientific Laboratory, University of California.*—The physical properties required of a solution which is to be used in large volume detectors employing liquid scintillators are: (1) good efficiency as scintillators *per se*, (2) light emission in the frequency range most suitable for detection by the photomultiplier tubes, (3) mean free path for absorption of this light which is large compared to the detector dimensions, and (4), in the event neutrons are to be detected, a high cross section for neutron capture which is associated with good scintillator response. A number of solutions were developed which satisfied the above criteria.[1] These scintillators will be discussed together with the chemistry of their preparation.

* Performed under the auspices of the U. S. Atomic Energy Commission.
[1] Cowan, Reines, Harrison, Anderson, and Hayes, Phys. Rev. **90**, 493 (1953).

G7. Device for Testing Large Numbers of Photomultipliers.* A. BROUSSEAU, C. L. COWAN, JR., AND F. REINES, *Los Alamos Scientific Laboratory, University of California.*—One of the problems met in constructing a detector which utilizes many photomultiplier tubes working in parallel is that of selecting suitable tubes and balancing them to uniform gain. The criteria applied include absence of after pulses, satisfactory gain, stability over a period of time, a fair energy resolution, and low dark current. Selection and balancing is accomplished using a multiple-chamber dark box in which each of ten tubes may be placed under test independently along with their sockets and voltage divider netowrks. A variable low-intensity light source and a NaI crystal and radioactive source are provided for both static and dynamic testing. Currents from the cathodes and anodes may be measured and pulses may be observed with associated amplifier and oscilloscope. A description of applications and results obtained will be given.

* Performed under the auspices of the U. S. Atomic Energy Commission.

G8. Liquid Scintillation Detectors to Accommodate Human Subjects.* [1] R. L. SCHUCH, E. C. ANDERSON, C. L. COWAN, JR., F. B. HARRISON, F. N. HAYES, AND F. REINES, *Los Alamos Scientific Laboratory, University of California.*—A steel insert 20 inches in diameter, 30 inches high with a 0.015-inch wall was placed in a detector in the shape of a circular cylinder measuring 28 inches in diameter and 30 inches high. The 4-inch thick annular region was filled with a scintillator solution of toluene-terphenyl-alpha naphthylphenyloxazole. Forty-five RCA 5819 photomultipliers, connected in parallel were placed around the cylinder walls. Energy gates were 0.3 to 2.0 Mev. The detector was shielded by 4 inches of lead except for the top of the insert which was left open. K^{40} in a test phantom gave a counting efficiency of 14 percent, corresponding to a counting rate of 78 per second from the K^{40} in a 70-kg man. Measured values using human subjects ranged from 30 to 80 counts per second above a background of 837 ± 6 per second. 0.2μC of Ra shielded by a human subject gave 1133 counts per second or about 15 percent efficiency, indicating the possibility of detection of Ra well below presently established tolerance levels.

* Performed under the auspices of the U. S. Atomic Energy Commission.
[1] To be published in Nature.

G9. Some Properties of Large Liquid Scintillation Detectors.* E. C. ANDERSON, C. L. COWAN, JR., AND F. REINES, *Los Alamos Scientific Laboratory, University of California.*—Preliminary to the experiment to detect the free neutrino, an investigation of the general properties of large liquid scintillation detectors was carried out.[1] A pilot model of 50 liters volume (40 cm diameter by 40 cm deep) using 32 photomultipliers was first operated in October, 1952. The signal output from gamma rays was estimated to be about 85 equivalent electrons per Mev from the photocathodes with all tubes in parallel and a scintillator of terphenyl plus alpha-naphthyl phenyl oxazole in toluene. The energy resolution was about 25 percent (half-width at half-height) at one Mev. The full-scale detector, a cylinder of 300 liters volume, using 90 photomultipliers had an energy resolution of about 10 percent at one Mev. The broadening in the smaller detector is due to end effects since in that case the gammas are not completely degraded by multiple Compton scattering before escaping. By adding cadmium propionate to the solution and observing delayed coincident pulses, a very sensitive detector was obtained for events involving a neutron, produced in prompt or delayed coincidence with a charged particle.

* Performed under the auspices of the U. S. Atomic Energy Commission.
[1] Cowan, Reines, Harrison, Anderson, and Hayes, Phys. Rev. **90**, 493 (1953).

THURSDAY AFTERNOON AT 4:15

Room 101, Mitchell Hall

(J. KAPLAN, presiding)

Contributed Papers

H1. Ionization Loss in Nuclear Emulsions.* JOHN R. FLEMING AND J. J. LORD, *University of Washington.*—A 400-micron Ilford G5 plate was exposed successively to 227, 122, 77, and 33-Mev negative pions and also to slow negative muons from the Chicago cyclotron. The plate kindly furnished by Professor Schein and Professor Anderson was rotated 45° after each exposure so that the tracks of different energy could be distinguished and in addition so that track grain and blob densities could be made over a restricted portion of a single plate. Correcting for the average track length in the emulsion, the grain densities for pions of 31, 81, 120, 224 Mev and the decay electrons from muons were, respectively, 75.28, 51.61, 47.11, 36.91, 42.06, per 100μ, where each average value is based on more than 11 000 grains. The corresponding blob densities over the same tracks were, respectively, 44.49, 35.94, 34.44, 27.08, 30.72 per 100μ. Assuming the grain densities to be proportional to the energy loss for exchanges less than 5 kv, the above measured values agree well with the calculation of Sternheimer based on the Fermi, Halpern-Hall type considerations. Theory gives a 14 percent difference between plateau and minimum ionization in excellent agreement with the measured 12.0±percent between 224-Mev pions and muon decay electrons.

* Supported in part by the U. S. Office of Naval Research and the U. S. Atomic Energy Commission.

H2. Ionization of Relstivistic Cosmic-Ray μ Mesons.* H. R. SNODGRASS, *University of California, Berkeley.*—Proportional counters filled with argon and range-interval defining Geiger counters were employed to study the variation of ionization with momentum for μ mesons. The ionization values were analyzed to yield the most probable ionization and the average ionization for four momentum intervals: 0.25 to 0.63 to 1.17 to 2.38 to >2.38 Bev/cy. The distribution of the ionizations was also examined for the four momentum intervals. The equipment was calibrated by normalization to the minimum ionizing momentum group. The values of the most probable ionization and the average ionization showed a consistent rise with increasing momentum, indicating that the theoretical logarithmic rise is valid for μ-meson momenta of up to 5 Bev/cy. The distribution of the ionization values was compared with the Landau[1] and the Blunck-Leisegang[2] theories. The observed frequency of small ionization values was much larger than predicted by Landau and more nearly in agreement with the theory of Blunck-Leisegang.

* Assisted by the joint program of the U. S. Office of Naval Research and the U. S. Atomic Energy Commission.
[1] L. Landau, J. Phys. U.S.S.R. **8**, 201 (1944).
[2] O. Blunck and S. Leisegang, Z. Physik **128**, 500 (1950).

H3. Cascade Decay of *V* Particles. I.* C. D. ANDERSON, E. W. COWAN, R. B. LEIGHTON, AND V. A. J. VAN LINT, *California Institute of Technology.*—Three cloud-chamber exposures of a charged V particle apparently decaying into a V^0 particle in a magnetic field have been taken at Pasadena. In a similar previous case,[1] the V^0 particle could not be classified as to type. The new data provide strong evidence for the reality of cascade decays, and identify the V^0 particle as a V_1^0 (decaying into $p+\pi^-$). In all three cases the parent charged V particle is negative (as in the case of reference 1), and emits a negative π or μ meson. The above conclusions are based on measurements of (1) relative positions of decay points in the cloud chamber, (2) "coplanarity," (3) momenta and ionizations of secondary particles, and (4) position and number of nuclear events in which V particles might originate. In all three cases the line of flight of the V^0 particle makes a much smaller angle with the positive decay product than with the negative, $\theta_+/\theta_-=0.16, 0.22$, and 0.41, thus indicating the decay products of the V^0 particle to have unequal masses.

* Supported in part by the joint program of the U. S. Office of Naval Research and the U. S. Atomic Energy Commission.
[1] Armenteros, Barker, Butler, Cachon and York, Phil. Mag. **43**, 597 (1952).

H4. Cascade Decay of *V* Particles. II.* E. W. COWAN, C. D. ANDERSON, R. B. LEIGHTON, AND V. A. J. VAN LINT, *California Institute of Technology.*—In one of the three cases of the preceding abstract, the positive particle in the V^0 decay has a momentum of 880±100 Mev/cy, and ionization 1.7 times minimum, determining by counting droplets. This is consistent with a proton but not with a π meson, indicating the V^0 particle is not of the type that decays into two π mesons. The Q value is 39±10 Mev assuming $\pi-p$ decay, and 36±10 Mev assuming $\pi-\pi$ decay. The latter value is much lower than the usual range of values for $\pi-\pi$ decay. It can further be shown, on the assumption of a two-body decay, using only the momenta and included angle of the two decay particles that the observed angular asymmetry about the line of flight of the neutral particle is too great to correspond to a decay into two π mesons. The charged secondary of the V^- decay has a momentum of 64±10 Mev/cy, an estimated ionization of 2–4 times minimum, and is therefore either a π or μ meson. On the assumption that the V^- particle decays into a V_1^0 and a π or μ meson, the best Q value, obtained from 2 of the 3 cases, is 60±15 Mev for a π meson and 62±15 Mev for a μ meson secondary. The calculated mass-values of the charged V particle on these two assumptions are 2570±30 and 2510 ±30m_e, respectively.

* Supported in part by the joint program of the U. S. Office of Naval Research and the Atomic Energy Commission.

H5. Charged and Neutral *V* Particles.* W. B. FRETTER AND E. W. FRIESEN, *University of California, Berkeley.*—Charged and neutral V particles observed in a 40-cm ×50-cm cloud chamber at sea level will be described. The chamber is filled with helium which allows ionization measurements to be made by drop counting. Curvature measurements in the average field of 8000 gauss appear to be reliable to 0.01 m^{-1}. The precision measurements of curvatures and angles are corrected for the effects of magnification, magnetic field variation, and gas displacement. Some of the observed V^0 particles are consistent with the V_1^0 ($p+\pi$, $Q=37$ Mev) and the V_2^0 ($\pi+\pi$, $Q=214$ Mev). Several of the particles, however, appear to be inconsistent with these interpretations. Most of the charged V particles can be interpreted as kappa particles.

* Assisted by the joint program of the U. S. Office of Naval Research and the U. S. Atomic Energy Commission.

H6. Cloud-Chamber Observation of the Decay of a τ Meson.* V. A. J. VAN LINT AND G. H. TRILLING, *California Institute of Technology.*—In a new apparatus at Pasadena consisting of a vertical array of four cloud chambers in a field of 8000 gauss, the decay in flight of a τ meson has been observed. The event is of interest because the tracks of the

decay products are long (35, 18, 18 cm) and lend themselves to accurate momentum measurement (188 ± 6; 127 ± 10; 103 ± 8 Mev/cy). The track of the τ meson is short and its momentum not directly measurable. Within experimental error the direction of the τ meson coincides with the vector sum of the momenta of the charged decay products, thus indicating the absence of neutral secondaries, in agreement with previous results. The τ meson is negative; in the only other case in which the sign of charge of a τ meson could be determined, it was found to be positive.[1] The specific ionization and curvature of the tracks are consistent with the assumption of π meson secondaries. On this assumption the energy release of the τ meson is 70 ± 3 Mev corresponding to a mass of $964\pm6m_e$. The τ meson was not observed to originate in a nuclear event, thus there is no evidence here as to its mode of production.

* Supported in part by the joint program of the U. S. Office of Naval Research and the Atomic Energy Commission.
[1] R. B. Leighton and S. D. Wanlass, Phys. Rev. **86**, 426 (1952).

H7. Cross Section for the Production of Penetrating Cosmic-Ray Showers in Oxygen.* JAMES F. KENNEY AND VICTOR H. REGENER, *University of New Mexico.*—An experiment is being performed at Capillo Peak, New Mexico at an altitude of 2800 m to determine the cross section for penetrating shower production by neutral N rays in oxygen. The collision length for this event is measured in ethyl alcohol and in oxalic acid, and the oxygen cross section is obtained by the method of differences. The value of this cross section seems to fall fairly close to that predicted by the geometric nuclear model. With further improvement of the statistical accuracy, the data from this experiment will be combined with those obtained from previous experiments with similar equipment using light and heavy water.[1] This will lead to an evaluation of the nuclear cross section for the production of penetrating showers in carbon, hydrogen, and deuterium.

* Supported in part by the National Science Foundation.
[1] G. W. Rollosson, Phys. Rev. **87**, 71 (1952); Froman, Kenney, and Regener, Phys. Rev. (to be published).

H8. Cross Section for Production of Penetrating Cosmic-Ray Showers. ROY THOMAS, *University of New Mexico.*—Highly energetic neutrons interacting with nuclei create showers of energetic protons, neutrons, π-mesons, etc. The usual theoretical approach is to assume that at very high energies the nucleons in a nucleus may be considered as free. One then calculates the cross section as a function of the nuclear radius and a collision mean-free path for an incident neutron in nuclear matter. The suggestion made in this paper is to consider the opposite view. We define an interaction volume directly proportional to the nuclear binding energy. Any incident neutron of sufficient energy which penetrates this interaction volume will initiate a penetrating shower. The cross section is proportional to the two-thirds power of the nuclear binding energy. Transparency of light nuclei to penetrating shower production thus follows with the introduction of only one parameter to be fitted to the experimental data. With any other theory one needs at least two parameters to explain the transparency of light nuclei.

THURSDAY AFTERNOON AT 4:15

Room 102, Mitchell Hall

(C. D. ANDERSON, presiding)

Contributed Papers

I1. Photoproduction of Positive Mesons from Hydrogen: Magnetic Spectrometer Method. R. L. WALKER, J. G. TEASDALE, AND V. Z. PETERSON, *California Institute of Technology.*—The differential cross section for photoproduction of positive pions in hydrogen has been measured at angles from 40° to 150° in the center-of-mass system, for photon energies from 220 to 475 Mev. An attempt will be made to extend this range of angles. Mesons produced by 500-Mev bremsstrahlung in a high-pressure gas target are analyzed by a large magnet with wedge-shaped pole pieces and counted by two large liquid scintillation counters in coincidence, placed at the focal point of the magnet. A typical arrangement of counters and magnet accepts mesons emitted in a solid angle of 0.01 steradians with a momentum resolution of nine percent. This corresponds to a spread in incident photon energies of 10 Mev in the low-energy region and 50 Mev at the high-energy end. Range measurements of the analyzed particles show that most of them are π mesons but that some μ mesons are counted as expected. The flight path of the mesons is long, and corrections for $\pi-\mu$ decay amount to a factor 1.2 to 1.8, depending on the meson energy. Results obtained so far are reported in the third abstract of this series.

I2. Angular Distribution of Positive Photomesons from Hydrogen: Counter Telescope Method. A. V. TOLLESTRUP, J. C. KECK, AND R. M. WORLOCK, *California Institute of Technology.*—The angular distribution and excitation curve for the process $\gamma+p\rightarrow\pi^++n$ have been obtained for gamma-ray energies between 225 and 475 Mev. This experiment was done simultaneously with the accompanying magnetic spectrometer experiment, but it is independent of that experiment except for the common beam monitoring equipment. The mesons from the high-pressure, low-temperature hydrogen target were identified by measuring their ionization for a fixed residual range with a scintillation counter telescope consisting of 3 counters in coincidence and a fourth in anticoincidence. The meson energy, as deduced from its range in copper, and its angle determine the photon energy. The energy resolution of the counter telescope was determined by the amount of absorber between the last two counters. This was chosen so that the spread of meson energies accepted was 10 Mev which corresponded typically to a 20-Mev spread in photon energy. The background corrections due to mesons from the walls of the hydrogen target and to accidental coincidences in the telescope are about 10 percent, and the statistical errors are in general about 5 percent. Excitation curves were run at angles corresponding to angles of 50°, 70°, 90°, 110°, 130°, and 150° in the c.m. system, and from smoothed curves the angular distribution was obtained. The results are discussed in the last paper of this series.

I3. Photoproduction of Positive Mesons from Hydrogen: Results. R. F. BACHER, J. C. KECK, V. Z. PETERSON, J. G. TEASDALE, A. V. TOLLESTRUP, R. L. WALKER, AND R. M. WORLOCK, *California Institute of Technology.*—The center-of-mass differential cross section for photoproduction of positive pions from hydrogen has been measured by the methods described in the two previous abstracts, in the angular range 40° to 150°,

for photons from 220 to 475 Mev. (Photon energies refer to the Laboratory System.) Results obtained by the two methods are in essential agreement. At 90°, $d\sigma/d\omega$ has a maximum of 2.7×10^{-29} cm²/sterad near 280 Mev and falls by a factor 5 at 450 Mev. The maximum in the excitation curve is even more pronounced at larger angles, but less pronounced at smaller ones. At 40° (c.m.) the peak occurs near 350 Mev, and at 450 Mev the cross section has decreased only to 0.7 the peak value. Angular distributions in the center-of-mass system show a marked assymetry about 90°, which changes character from low energy to high. Below 325 Mev, there is a backward maximum, whereas above 375 Mev, there is a forward maximum. The total cross section reaches a maximum near 290 Mev and decreases by about a factor 3 at 450 Mev. The results below 300 Mev agree with the data already reported from Berkeley and Cornell.

I4. Yield of Mo^{99} from Fission of U^{235} and U^{238}.† JAMES TERRELL, W. E. SCOTT,* J. S. GILMORE, AND C. O. MINKKINEN, *University of California, Los Alamos Scientific Laboratory.*—A double fission chamber was used to measure the fissions produced in one-inch diameter, 25-gram disks of U^{235} and normal uranium. Thin foils of the same material, mounted on either side of the disks, were fission counted during irradiation. Corrections were applied for counting losses and the effects of fission-produced and scattered neutrons from the disks. Fast neutrons were produced by P−T, D−D, and D−T reactions; the thermal neutron source was the Los Alamos Homogeneous Reactor. The yield of Mo^{99} was determined by chemical separation of molybdenum from the disks, followed by absolute beta counting. Absolute calibration was done with the aid of John P. Balagna of this laboratory. Results obtained so far (Mo^{99} atoms per fission) are tabulated here, with estimated standard deviations. The thermal value

	Thermal	0.95	1.55	4.85	14.2	(Mev)
U^{235}	6.14±0.16	6.10±0.16		5.45±0.16		(percent)
U			6.19±0.15	6.45±0.16	5.68±0.14	(percent)

and the decrease with increasing energy are consistent with other determinations.[1]

† Work done under the auspices of the U. S. Atomic Energy Commission.
* Major, United States Air Force, now at Kirtland Air Force Base, New Mexico.
[1] *Radiochemical Studies: The Fission Products* (McGraw-Hill Book Company, Inc., New York, 1951), National Nuclear Energy Series, Div. IV, Vol. 9.

I5. The Energy Distribution of Slowed Fission Fragments.* J. A. NORTHROP AND J. E. BROLLEY, JR., *University of California, Los Alamos Scientific Laboratory.*—A conventional gridded ion chamber has been used to measure the energy distribution of fission fragments slowed by a UO_2 absorber. A 20μ g/cm² layer of $U^{235}O_2$ 2 in. in diameter vacuum evaporated on a 0.030-in. tantalum backing and placed in a beam of thermal neutrons from the Los Alamos Homogeneous Reactor provided the source of fission fragments. These were slowed by a uniform layer of $U^{238}O_2$ evaporated directly over the first. A series of six such foils, each having a 20μ g/cm² $U^{235}O_2$ base layer, but $U^{238}O_2$ layers varying from 0 to 1 mg/cm², were mounted on a wheel inside the ion chamber in such a way that they could be successively rotated into the neutron beam. The high uniformity of these foils made it possible to obtain fission curves in which the ratio of the light peak to the valley between is 14:1, even after slowing the fragments in the UO_2. There is some evidence for complex structure on the high-energy side of the heavy particle peak of the unslowed fragments. Preliminary results for the initial energy loss of fission fragments in UO_2 is 0.020 Mev-cm²/μ g (light fragment), 0.017 Mev-cm²/μ g (heavy fragment).

* Work done under the auspices of the U. S. Atomic Energy Commission.

I6. Velocity Distributions of Slowed Fission Fragments. H. W. SCHMITT AND R. B. LEACHMAN, *University of California, Los Alamos Scientific Laboratory.*—The velocity distributions of slowed fission fragments have been measured by a method similar to that used by Leachman[1] in the determination of the velocity distributions of fission fragments from the thermal fission of U^{233}, U^{235}, and Pu^{239}. In our measurements, fragments from the thermal fission of U^{235} are slowed by perpendicular passage through thin nickel or aluminum absorbers as follows: 1.1 mg/cm² Ni, 1.1 mg/cm² Al, 1.4 mg/cm² Al. The slowed-fragment velocity distributions show a definite irregularity in the heavy peak but a less pronounced irregularity in the light peak. This difference in irregularities is at least partially explained by the better resolution in the measurements of the heavy fragment groups. These irregularities are in agreement with the fine structure in the mass yield of fission as found by Glendenin *et al.*[2] The fact that the irregularities are more prominent in the distributions obtained with more absorbing foils can be explained in terms of shell effects and processes of energy loss of fission fragments in matter.

[1] R. B. Leachman, Phys. Rev. **87**, 444 (1952).
[2] Glendenin, Steinberg, Inghram, and Hess, Phys. Rev. **84**, 860 (1951).

THURSDAY EVENING AT 8:00

Student Union Ballroom

(V. H. REGENER, presiding)

Public Lecture

J1. Developments in High-Energy Physics. E. FERMI, *University of Chicago.*

FRIDAY MORNING AT 9:00

Student Union Ballroom

(N. E. BRADBURY, presiding)

Invited Papers

K1. Beta Spectra. L. M. LANGER, *Indiana University.* (30 min.)

K2. Nuclear Isomers. M. GOLDHABER, *Brookhaven National Laboratory.* (30 min.)

K3. Excitation of Heavy Nuclei by the Electric Field of Low-Energy Protons. CLYDE MCCLELLAND, *Massachusetts Institute of Technology.* (20 min.)

K4. Light Particle Reactions. R. F. TASCHEK, *Los Alamos Scientific Laboratory.* (30 min.)

K5. Cross Sections of Proton Reactions. W. A. FOWLER, *California Institute of Technology.* (30 min.)

Contributed Papers

K6. Deuteron Disintegration by 9.7-Mev Protons.* JUANITA H. GAMMEL, *University of California, Los Alamos Scientific Laboratory.*—The angular distribution of protons emitted in inelastic $p-d$ scattering has been measured between 25° and 90° in the laboratory system. These results are a by-product of a $p-d$ elastic scattering experiment[1] performed with a multiplate camera and the 9.7-Mev proton beam from the Berkeley cyclotron. A total of 1085 inelastically scattered protons from five runs were observed. The cross section obtained for emission of protons of energy >1 Mev is 104±20 millibarns (the deuteron disintegration cross section is one-half of the total cross section for emission of protons). The angular distribution is as follows: 25°, 73±15 mb; 30°, 53±11 mb; 40°, 31±6 mb; 50°, 19±4 mb; 60°, 10±2 mb; 70°, 4±1 mb; 80°, 1±0.5 mb; 90°, 0±0.5 mb. Additional work is now in progress to determine the distribution in energy of the disintegration protons at 37.5°. A theoretical interpretation of available data on inelastic $p-d$ and $n-d$ scattering will be presented by R. M. Frank and J. L. Gammel.

* Work performed under the auspices of the U. S. Atomic Energy Commission.

[1] Allred, Armstrong, Bondelid, and Rosen, Phys. Rev. **88**, 433 (1952).

K7. Inelastic Scattering of Protons and Neutrons by Deuterons. R. M. FRANK AND J. L. GAMMEL, *University of California, Los Alamos Scientific Laboratory.*—By assuming that the range of nuclear forces is small compared to the size of the deuteron and the wavelength of the incoming particle ("zero range" approximation) and using something like the impulse approximation, a connection between the cross sections for elastic and inelastic $p-d$ or $n-d$ scattering is derived. The results of this simple theory are compared with available experimental data, and the agreement between the two is much better than the crude assumptions of the theory merit. An interesting consequence of the theory is that the connection between the elastic and inelastic scattering cross sections is independent of the properties of the two-body forces. The elastic scattering cross section depends hardly at all on the exchange properties of the two-body $n-p$ potential (provided it gives the binding energy of the deuteron correctly) and the $n-n$ potential,[1] and the connection suggests that the same is true of the inelastic scattering cross section. This is in disagreement with more elaborate calculations of Bransden and Burhop.[2] Another consequence is that the ratio of the cross section for absorption of neutrons from a partial wave of angular momentum l by inelastic scattering to the cross section for elastic scattering for the same partial wave is independent of l. This makes it possible to calculate the effect of the inelastic scattering on the elastic scattering in a simple way, as explained in the following paper.

[1] R. S. Christian and J. L. Gamnel, Phys. Rev. **91**, 100 (1953).
[2] B. H. Bransden and E. H. S. Burhop, Proc. Phys. Soc. (London) **A63**, 1337 (1950).

K8. Elastic Scattering of Protons and Neutrons by Deuterons at High Energy. J. L. GAMMEL, *University of California, Los Alamos Scientific Laboratory.*—The "phase shifts" which appear in an analysis of high-energy $n-d$ or $p-d$ elastic scattering must be complex numbers, since inelastic scattering also occurs. A modification of Born's approximation is presented which takes account of the effect of the inelastic scattering on the elastic scattering. From it complex phase shifts are derived which satisfy requirements imposed on them by the condition that particles be conserved. These are substituted into the exact scattering formula for $n-d$ inelastic scattering, so that the calculation is at least a valid phase shift analysis of the data, and in addition contains an effort to take account of the effect of the inelastic scattering. Even when the worst properties of the three-dimensional Born approximation are avoided by substituting phase shifts calculated in Born approximation into the exact scattering formula, calculations of the angular distribution for elastic scattering give a cross section for backward scattering which is much too large. A recent calculation suggests that this is due in part to the neglect of tensor forces. However, the present calculation with central forces only is in agreement with the experiments. It is not maintained that the effects of tensor forces are in fact negligible but only that they can be reproduced by the same "equivalent" central potential which reproduces their effects in high energy $n-p$ scattering. It is shown that at low energies (14 Mev) neglect of the effect of inelastic scattering on the elastic scattering is justified.

K9. Small Angle Cross Sections for the Scattering of Protons by Tritons. M. E. ENNIS AND A. HEMMENDINGER, *University of California, Los Alamos Scientific Laboratory.*—Measurements of the differential elastic scattering cross sections of tritons for protons have been made using a 14-inch inside diameter scattering chamber with a proportional counter movable from 140° on one side of the forward direction of the beam through the zero position to 90° on the other. These cross sections were determined as a function of laboratory angle from the scattered proton yields for angles from 15° to 60° and from the yields of the recoil tritons for angles from 62.8° to 136.8°. Measurements were made at eleven energies from 0.990 Mev to 2.548 Mev, with five of these clustered near the 1.019-Mev threshold of the $T(p, n)He^3$ reaction. Comparison with the cross sections reported by Hemmendinger *et al.*[1] shows the values obtained in the present work to be larger in the angular range near 150° in the center-of-mass system and smaller elsewhere. Agreement with the results of Claassen *et al.*[2] is good for the two energies for which comparable data are available.

[1] Hemmendinger, Jarvis, and Taschek, Phys. Rev. **76**, 1137 (1949).
[2] Claassen, Brown, Freier, and Stratton, Phys. Rev. **82**, 589 (1951).

K10. Scattering of Fast Neutrons by He^4.* JOHN D. SEAGRAVE, *University of California, Los Alamos Scientific Laboratory.*—Angular distributions of neutrons elastically scattered by He^4 have been measured for neutron energies of 2.61, 4.53, 5.54, 6.50, and 14.2 Mev. The technique used was similar to that of Adair.[1] The pulse-height distribution of the recoiling alphas was observed in a large proportional counter filled with a mixture of helium and krypton; however, a neutron collimator was employed and the neutron beam was transverse to the axis of the counter, thus minimizing the wall effect, for which a correction was applied. All five distributions are similar and are characterized by strong scattering of the neutrons in the forward direction, a minimum for neutrons scattered near 120° in the center-of-mass system, and a smaller peak for backscattering. The ratio of differential cross sections $\sigma_{back}/\sigma_{min}$ increases smoothly with energy over the range studied. These distributions are in agreement with the n-He^4 distributions predicted from the phase-shift analysis of p-He^4 scattering by Dodder and Gammel[2] but seem to be in disagreement with the results of Huber and Baldinger.[3]

* Work performed under the auspices of the U. S. Atomic Energy Commission.

[1] R. K. Adair, Phys. Rev. **86**, 155 (1952).

[2] D. C. Dodder and J. L. Gammel, Phys. Rev. **88**, 520 (1952), and private communication.

[3] P. Huber and E. Baldinger, Helv. Phys. Acta **25**, 435 (1952).

FRIDAY MORNING AT 9:00

Geology Auditorium

(J. KAPLAN, presiding)

Invited Papers

L1. Atmospheric Propagation of Sounds from Explosions. E. F. COX, *Sandia Corporation.* (30 min.)

L2. High-Altitude Winds by Meteor-Train Photography. WILLIAM LILLER AND F. L. WHIPPLE, *Harvard College Observatory.* (30 min.)

L3. Thunderstorm Electricity. E. J. WORKMAN, *New Mexico Institute of Mining and Technology.* (30 min.)

L4. Measurements of World-Wide Electrical Effects. R. E. HOLZER, *University of California, Los Angeles.* (30 min.)

Contributed Papers

L5. The Automatic Recording of the Zodiacal Light.* VICTOR H. REGENER, *University of New Mexico.*—Automatic recording equipment for the Zodiacal Light has been put into operation at the Capillo Peak Observatory. A parabolic mirror of diameter 60 inches is positioned by means of a servo system in such a manner as to scan the night sky in equatorial coordinates. The output of a photomultiplier tube mounted at the focus of the mirror governs, through an amplifier of special design, the pattern executed by the spot of an oscilloscope tube in 18 discrete steps. At the same time, a lens of short focal length is made to travel in a plane parallel to the surface of a film in synchronism with the 60-inch mirror and in such a way as to project an image of the oscilloscope screen onto the surface of the film. A map of the night sky in terms of light intensity is thus automatically obtained. Isophotes can be plotted directly into such a map by connecting points where the amplifier changes from one step to the next because of a passing of the light intensity through a certain value.

* Supported, in part, by Air Force Cambridge Research Center.

L6. Procedure for the Evaluation of Automatic Zodiacal Light Recordings. RICHARD J. RUNGE, *University of New Mexico.*—The automatic records of the intensity of the light of the night sky obtained at the Capillo Peak Observatory give uncorrected intensities in terms of right ascension and declination. This paper discusses the procedure used in applying corrections for background and for extinction. The maps which are automatically drawn by the instrument are evaluated first for background intensity not caused by the zodiacal light. Extinction corrections are then applied on the basis of star intensities observed with the same instrument during the same night. Thus, extraterrestrial intensity records are obtained for the zodiacal light in terms of stellar magnitudes per square degree.

L7. The Focusing of Short Electromagnetic Waves by Means of the Fresnel Half-Period Zone Plate. H. GEORGE OLTMAN, *University of New Mexico.*—The theory of the Fresnel Half-Period Zone Plate is applied to the construction of a highly directional focusing device, or "lens," for short electromagnetic waves. Two models have been constructed for a wavelength of 11 cm, one with two obstructed zones and a maximum diameter of 4.2 meters, the other with five obstructed zones and a maximum diameter of 4.8 meters. These zones were made of wire mesh. The characteristics of the two models are: Power gain 25 and 56, angular definition of the image of a point source (to the half-power point) 0.6°, and useful total angular width of the field approximately 50°. A device of this kind should find applications in radio-astronomical work.

L8. Ion Density in the *E*-Layer by the Use of a Sounding Rocket.* L. B. LINFORD, O. C. HAYCOCK, J. I. SWIGART, C. L. ALLEY, AND C. D. WESTLUND, *University of Utah,* AND J. R. LIEN, *Air Force Cambridge Research Center.*—A successful ionosphere experiment has been carried out with an Aerobee rocket. Transmission times for seven different frequencies from 0.4 to 1.4 megacycles above the critical frequency were compared with the transmission time for 470 megacycles. The zenith was 84 miles. Excellent dispersion curves were obtained. From the data, the index of refraction, the ion density, and the collision frequency can be calculated through the *E*-layer.

* This work was carried out under Contract No. AF 19(604)-384 with the Geophysics Research Division of the Air Force Cambridge Research Center.

FRIDAY AFTERNOON AT 2:00

Student Union Ballroom

M1. Panel Discussion on Artificial Mesons, led by E. FERMI. Some of the panel members are J. LEPORE, FRANK CRAWFORD, R. F. CHRISTY, R. L. WALKER, AND H. A. BETHE. (2 hours)

FRIDAY AFTERNOON AT 4:15

Room 101, Mitchell Hall

(M. GOLDHABER, presiding)

Contributed Papers

N1. Contribution of Collective Motion to the Magnetic Moments of Heavy Nuclei. KENNETH W. FORD, *Princeton University and Los Alamos Scientific Laboratory.*—The coupling of the motion of individual nucleons to the nuclear surface oscillations affects the nuclear magnetic moment in two ways: (1) The surface interaction provides a mechanism of configuration interaction and mixes different particle states. (2) The bulk motion of nuclear matter represented by the surface waves contributes directly to the moment. These two effects have been calculated in the limits of weak and strong coupling of nucleon to nuclear surface.[1] The predicted deviations from the Schmidt lines are qualitatively alike in the two limits, quantitatively greater for strong coupling, but not great enough to explain the largest observed deviations. From the $l+\frac{1}{2}$ Schmidt line, the direction of deviations and qualitative differences among nuclei in magnitude of deviation are explained. From the $l-\frac{1}{2}$ Schmidt line, the predicted deviations are small and largely opposite in direction to the observed deviations. The calculations afford additional indirect evidence for a diminished anomalous moment of the nucleon in the presence of nuclear matter.

[1] Second effect previously calculated by Foldy and Milford, Phys. Rev. **80**, 751 (1950), Bohr, Phys. Rev. **81**, 134 (1951), and Davidson and Feenberg, Phys. Rev. **89**, 856 (1953).

N2. A New First Excited State of an Even-Even Nucleus Kr^{80}.* GERTRUDE S. GOLDHABER AND MICHAEL MCKEOWN, *Brookhaven National Laboratory.*—The 18-min isomer Br^{80} is shown to emit γ rays of 620-kev energy which follow a low-intensity (3–5 percent) β-ray branch. Beta-gamma coincidences are observed, indicating that the gamma transition takes place in Kr^{80}. No γ transitions were found to follow the positron or K-capture branch. The intensity observed is compatible with a spin and parity assignment $1+$ for the ground state of Br^{80}, while the 620-kev state in Kr^{80} is probably $2+$. The energy observed fits well into the pattern for the energy of the first excited state of even-even nuclei.[1,2]

* Work carried out under the auspices of the U. S. Atomic Energy Commission.
[1] P. Preiswerk and P. Stähelin, Helv. Phys. Acta **24**, 623 (1952).
[2] G. Scharff-Goldhaber, Phys. Rev. **90**, 587 (1953).

N3. Energy Levels in Hafnium Isotopes.* D. J. HUGHES, W. Y. KATO, AND J. S. LEVIN, *Brookhaven National Laboratory.*—The nuclear energy levels in the hafnium isotopes at excitation energy just above neutron binding energy have been measured by observation of neutron resonances in normal hafnium and several of its separated isotopes. Total cross sections were measured with the Brookhaven fast chopper in the neutron energy region 0–100 ev; above 100 ev the resolution is insufficient to resolve the resonances. For most of the resonance measurements the samples of partially enriched isotopes used were of the order of 200 mg. Below 100 ev only one resonance occurs in Hf^{178} and one in Hf^{180}, the balance of the resonances found in normal hafnium (about 25 below 100 ev) being assigned to Hf^{177} or Hf^{179}. Thus, although Hf^{174} and Hf^{176} have not been measured as yet, none of the resonances observed in normal hafnium are in these isotopes. In several cases, apparently single resonances in normal hafnium have been shown to be superpositions of levels in Hf^{177} and Hf^{179} by their strength and slight energy shifts in the enriched isotope samples.

* Work carried out under contract with the U. S. Atomic Energy Commission.

N4. Bound State Corrections in the Two-Body System. THOMAS FULTON, *Harvard University,* AND ROBERT KARPLUS, *University of California Radiation Laboratory, Berkeley.*—Available expressions[1–3] for two-body equations contain an interaction kernel which treats particles in intermediate states as free. In situations where the binding is important, such as the calculation of low-energy electrodynamic corrections, a more accurate treatment is necessary. A satisfactory formalism has been developed for systems in which an instantaneous interaction is responsible for the binding. The procedure may then be used to evaluate the effects of small retarded perturbations. It consists of summing those binding interactions which occur during the retarded perturbations and which never should have been expanded as "small" effects. The result is expressed in terms of the two-body Green's function of the instantaneous interacting system. This function occurs to describe the propagation of the two particles in the intermediate state. Applications to electrodynamic systems, to which the method is particularly suitable, are in progress.

[1] J. Schwinger, Proc. Natl. Acad. Sci. U. S. **37**, 452, 455 (1951).
[2] H. A. Bethe and E. E. Salpeter, Phys. Rev. **84**, 350 (1951).
[3] R. Karplus and A. Klein, Phys. Rev. **87**, 848 (1952).

N5. An *R*-Matrix Formulation of the Statistical Theory of Nuclear Reactions.* R. G. THOMAS, *University of California, Los Alamos Scientific Laboratory.*—By means of the Wigner-Teichmann channel elimination procedure, an exact expression is obtained for $f_e(E)^{-1}$, the inverse logarithmic derivative for the entrance channel e, in terms of the E_λ, the γ_λ of all channels, the shift factors, and the penetration factors P_r of the reaction channels r. The cross section for compound nucleus formation is determined by the real and imaginary parts of this quantity. If the off-diagonal absorption widths $\Gamma_{\lambda\mu}=2\Sigma_r P_r\gamma_{\lambda r}\gamma_{\mu r}$, comprising individual terms which are as likely to be positive as negative, are negligible compared with the diagonal absorption widths $\Gamma_{\lambda\lambda}$, and if $\Gamma_{\lambda\lambda}\gg D$, D being the level spacing, then the expression for $f_e(E)^{-1}$ reduces

to the value of the *ee* component of the R matrix at the complex energy $E+\frac{1}{2}i\langle\Gamma_{\lambda\lambda}\rangle_{Av}$. The Feshbach-Weisskopf schematic theory assumption that $f_{ee}=-iK$ follows by neglecting the real part of this component and by using the $\langle\gamma_{\lambda e}{}^2\rangle_{Av}=D/\pi K$ relation for evaluation of the imaginary part. In their more recent theory, which involves the consideration of a complex square well potential, the real part of this component is important. It will also be shown that if the $\Gamma_{\lambda\mu}$ are negligible, the compound nucleus will decay in a manner which is independent of how it is formed.

* Work performed under the auspices of the U. S. Atomic Energy Commission.

N6. A State in C^{12} Predicted from Astrophysical Evidence.* F. HOYLE, *Cambridge University* AND D. N. F. DUNBAR, W. A. WENZEL, AND W. WHALING, *Kellogg Radiation Laboratory, California Institute of Technology.*—It is assumed that oxygen and carbon are produced in stars that have largely exhausted their central hydrogen by the reactions: $2He^4\rightarrow Be^8$; $Be^8+He^4\rightarrow C^{12}$; $C^{12}+He^4\rightarrow O^{16}$. The observed cosmic abundance ratio of He:C:O can be made to fit the yields calculated for these reactions if the reaction $Be^8(\alpha,\gamma)C^{12}$ has a resonance near 0.31 Mev, corresponding to a level at 7.68 Mev in C^{12}.[1] A level had previously been reported at 7.5 Mev.[2] The 16-in. double-focusing magnetic spectrometer has been used in an analysis of the α-spectrum from $N^{14}(d,\alpha)C^{12}$ covering the excitation energy range from 4.4 to 9.2 Mev in C^{12}. The level was found at 7.68 ± 0.03 Mev. No other levels were found, although a group 1 percent as strong as the transition to the 4.4-Mev state could have been detected. At $E_d=620$ kev, $\theta_{lab}=90°$, the transition to the 7.68-Mev state is 6 percent as strong as that to the state at 4.43 Mev.

* Assisted in part by the joint program of the U. S. Office of Nava Research and the U. S. Atomic Energy Commission.
[1] F. Hoyle, to appear in the Astrophys. J.
[2] See F. Ajzenberg and T. Lauritsen, Revs. Modern Phys. **24**, 321 (1952).

FRIDAY AFTERNOON AT 4:15

Room 102, Mitchell Hall

(R. F. TASCHEK, presiding)

Contributed Papers

O1. Gamma-ray Absorption Measurements. P. R. HOWLAND, W. E. KREGER, AND R. A. TAYLOR, *U. S. Naval Radiological Defense Laboratory.*—The absorption of gamma-rays in NaI(Tl), Cu, Ta, W, and Hg was measured using a narrow beam geometry and a NaI(Tl) scintillation counter as an energy selective detector. Measurements were made using the gamma rays from Zn^{65}, Cs^{137}, and Co^{60}. Corrections for coherent scattering and small angle Compton scattering were made. Absorption coefficients are compared with theory and results of other workers. Linearity of the scintillation detector system was checked up to counting rates of 300 000 counts per minute, and was found to be better than $\pm\frac{1}{2}$ percent over the range used. An accuracy of $\pm\frac{1}{2}$ percent was obtained for the absorption coefficients. The NaI(Tl) absorption coefficient uncorrected for small angle Compton scattering and coherent scattering was 0.2755 ± 0.0014 cm^{-1} at 0.661 Mev and 0.1991 ± 0.0010 cm^{-1} at 1.11 Mev. Other values will be presented. The work is being continued.

O2. Gamma Radiation from Neutron Excitation of Zirconium and Hafnium. C. W. MALICH AND C. E. FANEUFF, *Naval Research Laboratory.*—The energy spectra of the gamma radiation produced by 14-Mev neutron bombardment of zirconium and of hafnium has been investigated with a NaI(Tl) crystal and multichannel analyzer. The observed counting rates per unit energy interval have maxima near 200 kev and decrease approximately exponentially with increasing energy to 9 or 10 Mev, more rapidly for hafnium than for zirconium. The maxima are due primarily to the 206-kev level in NaI[1] and backscattered gamma rays. Reproducible indications of discrete lines are superposed on the general continua. At low energies these can be ascribed to NaI and to Pb shielding, at intermediate energies they may result from degraded neutrons or $d(d,n)$ contamination, and at high energies are attributed to levels in zirconium or hafnium. An analysis of secondary effects in the detector and scattering by the material investigated is being used to compute cross sections *vs* energy and to identify possible levels.

[1] R. B. Day (private communication).

O3. Long-Lived Activity in Highly Irradiated Niobium. D. L. DOUGLAS, A. C. MEWHERTER, AND R. P. SCHUMAN, *Knolls Atomic Power Laboratory.**—A long-lived activity has been found in two samples of spectrographically pure niobium metal irradiated one and two years, respectively, in the Chalk River reactor. The niobium was purified from tantalum by cellulose column chromatography[1] and by methyldioctylamine extractions.[2] The purified niobium initially contained mainly 35*d* Nb^{95}; after considerable decay it showed the presence of another activity which followed Nb^{95} when passed through an anion exchange column[3] and in the standard fission-product procedure. The long-lived activity has three gamma rays, 0.70 Mev (92 percent), 0.87 Mev (92 percent), and 1.57 Mev (8 percent), as shown by scintillation spectrometry; also a 0.50-Mev beta ray as shown by Feather analysis. The activity has shown no decay over a period of two months. If the activity is Nb^{94}, its half-life is 2.2×10^4 years, based on a capture cross section of 1.1 barns for Nb^{93}. Also, the Nb^{94} has a capture cross section of about 15 barns based on the specific activity of Nb^{93}.

* Operated by the General Electric Company for the U. S. Atomic Energy Commission.
[1] A. F. Williams, J. Chem. Soc. **1952**, 3155.
[2] G. W. Leddicotte and F. L. Moore, J. Am. Chem. Soc. **74**, 1618 (1952).
[3] K. A. Kraus, G. E. Moore, J. Am. Chem. Soc. **73**, 9 (1951).

O4. Determination of the Neutron Spectrum and Absolute Yield of a Plutonium-Beryllium Source.* LEONA STEWART, *University of California, Los Alamos Scientific Laboratory.*—A plutonium-beryllium neutron source has the advantages of high neutron yield, low gamma-ray intensity, and very long half-life. The neutron spectrum from such a source, composed of 13 grams of plutonium and 7 grams of beryllium as $PuBe_{13}$ (density 3.7 g/cc), was measured by means of proton recoils in nuclear research emulsions with approximately 15° angular resolution. The source and plates were isolated from scattering materials by a Nylon cord suspension. The data obtained from 2114 observations indicate the neutrons have a maximum energy of approximately 10.5 Mev, and the observed spectrum shows marked similarities with published data on

polonium-beryllium[1] and radium-beryllium.[2,3] The present results show intensity maxima at 3.0, 4.4, 7.2, and 9.6 Mev. A comparison is made between the present data and previously reported energy levels in the residual carbon nucleus. The absolute yield of neutrons above 0.5-Mev energy is $9.4\pm1.9\times10^5$ neutrons/sec.

* Work performed under the auspices of the U. S. Atomic Energy Commission. Submitted as a Master's thesis to the University of Texas, January, 1953.
[1] B. G. Whitmore and W. B. Baker, Phys. Rev. **78**, 799 (1950).
[2] H. T. Richards, MDDC-1504 (1944).
[3] D. L. Hill, AECD-1945 (1947).

O5. Cross Sections for Production of In^{115m} and Au^{197m} by Inelastic Scattering of Neutrons. H. C. MARTIN, B. C. DIVEN, AND R. F. TASCHEK, *University of California, Los Alamos Scientific Laboratory.*—Cross sections for the reactions $In^{115}(n, n')In^{115m}$ and $Au^{197}(n, n')Au^{197m}$ have been measured from the reaction thresholds to 5.5 Mev. The lowest mean energy for which the In^{115m} excitation was observed was 440 kev with an energy spread of ±100 kev; the cross section rises to a peak value of 0.36 barn at 2.5 Mev. The lowest mean energy for which the Au^{197m} excitation was observed was 420 kev with an energy spread of ±40 kev; the cross section rises to a peak value of 1.3 barns at 2.5 Mev. Since the $Au^{197}(n, n')Au^{197m}$ reaction threshold gives a maximum value for the excitation energy of the isomeric state, the value obtained is of interest in connection with the decay scheme of Au^{197}.[1] For each reaction, the peak value of the excitation cross section is roughly what might be expected in view of the total inelastic scattering cross section and the spins of the ground state and metastable state.[2] Both cross sections show irregularities which are evidence of energy levels in the target nuclei.

[1] J. W. Mihelich and A. de Shalit (to be published).
[2] B. Margolis (private communication).

O6. The Electron and Positron Spectrum of Zn^{65} above 5 Kev. J. F. PERKINS AND S. K. HAYNES, *Vanderbilt University.*—The electron and positron spectrum of Zn^{65} has been measured with a magnetic lens spectrometer, using very thin sources and counter windows. The positron Fermi plot is found to be linear to 50 kev, in contradiction to certain reports that the positron spectrum was complex. Because of a low-energy tail on the K Auger lines there is a 4 percent uncertainty in the integrated K Auger intensity. From the observed intensities of K Augers, positrons, and conversion electrons, and values of capture branching ratio, fluorescence yield, and L- to K-capture ratios taken from the literature, the intensity ratios of the various spectral components are obtained. The resulting conversion coefficient, $\alpha=(2.56\pm0.29)\times10^{-4}$, agrees with other experimental values and strongly suggests an $E2$ transition. The observed ratio of K capture to ground state to positrons $=28.0\pm3.2$ is in satisfactory agreement with the recently calculated[1] theoretical value of 29.0 for an allowed transition, which in view of the high ft value establishes the l forbidden character of the transition.

[1] P. Zweifel (private communication).

FRIDAY AFTERNOON AT 4:15

Room 122, Mitchell Hall

(L. M. LANGER, presiding)

Contributed Papers

P1. Excitation Functions for the $(n, 2n)$ Reactions in Ge, Sc, As, Tl, and Ni. S. J. BAME, JR.* *University of California, Los Alamos Scientific Laboratory.*—Relative yields as a function of energy for the $(n, 2n)$ reactions in Ge^{70}, Sc^{45}, As^{75}, Tl^{203}, and Ni^{58} have been obtained. The $T(d, n)He^4$ reaction was used as a source of neutrons with energies between 12 and 18 Mev by making use of the angular energy dependence of the reaction. The $(n, 2n)$ products were chemically separated from other activities and counted by the Radio Chemistry group at Los Alamos. Corrections were applied for the laboratory angular distribution of neutrons from the source. The reaction thresholds for As, Tl, and Ni are known from (γ, n) thresholds to be 10.2 ± 0.2, 8.9 ± 0.2, and 11.9 ± 0.2 Mev. The data agree well with these values. Threshold values for Ge and Sc are 11.8 ± 0.3 Mev and 11.3 ± 0.3 Mev, determined from the $(n, 2n)$ data. The yield curves have the same general shape, rising from the threshold to a maximum value, then falling smoothly to around 70 percent of the maximum at 18 Mev. The energies at which the maximum yields occur are approximately 14.8, 15.3, 15.9, 16.2, and 16.2 Mev for Tl, As, Sc, Ge, and Ni.

* Work done under the auspices of the U. S. Atomic Energy Commission.

P2. Isotopic Abundances of Palladium. JOHN R. SITES, GEORGE CONSOLAZIO,* AND RUSSELL BALDOCK, *Stable Isotope Research and Production Division, Oak Ridge National Laboratory.*†—In the course of investigating calutron separated isotopes of palladium, a difference from the published isotopic abundance values for natural palladium was observed. The new values to be reported in atom percent are Pd^{102}, 0.96; Pd^{104}, 10.97; Pd^{105}, 22.23; Pd^{106}, 27.33; Pd^{108}, 26.71; and Pd^{110}, 11.81.

* Watertown Arsenal, Watertown Massachusetts.
† This paper is based on work performed for the U. S. Atomic Energy Commission by Carbide and Carbon Chemicals Company, a Division of Union Carbide and Carbon Corporation, at the Oak Ridge National Laboratory.

P3. Electromagnetic Separation of Pd, Pt, and Ru Isotopes. W. A. BELL, JR., L. O. LOVE, C. E. NORMAND, AND W. K. PRATER, *Stable Isotope Research and Production Division, Oak Ridge National Laboratory.**—Appreciable quantities of the isotopes of Pd, Pt, and Ru have been electromagnetically separated in high-temperature source units. Ion beams up to 30 ma at the isotope collector were achieved. Bombardment of graphite charge containers by 35-kv electrons produced the temperature, in excess of 2000°C, required to vaporize sufficient metallic charge to support the ionization arc. The heat shielding problem and its solution are discussed.

* This paper is based on work performed for the U. S. Atomic Energy Commission by Carbide and Carbon Chemicals Company, a Division of Union Carbide and Carbon Corporation, at the Oak Ridge National Laboratory.

P4. The Spin and Magnetic Moment of Ti^{47} and Ti^{49}. C. D. JEFFRIES, *University of California, Berkeley.*—The complex nuclear induction signal from $TiCl_4$ previously reported[1] has been re-examined under higher resolution. It is found that the structure is actually a superposition of two resonance lines with a relative separation of about one part in 3800. By the

use of Oak Ridge separated isotopes the resonance lines have been identified as those of Ti^{47} and Ti^{49}. The ratio of the resonance frequency of these nuclei to that of Cl^{35} in $TiCl_4$ has been measured to be $\nu(Ti^{47})/\nu(Cl^{35})=0.57493\pm0.00006$, and $\nu(Ti^{49})/\nu(Cl^{35})=0.57508\pm0.00006$. By comparing the widths and amplitudes of the two Ti signals, their spins have observed to be $I(Ti^{47})=5/2$ and $I(Ti^{49})=7.2$. Both Ti resonance signals are negative with respect to that of Cl^{35}, indicating that the magnetic moments are negative. The magnetic moments are found to be, in units of the nuclear magneton, $\mu(Ti^{47})=-0.7866$, and $\mu(Ti^{49})=-1.102$. These values are in agreement with those predicted by the scheme of Schawlow and Townes.[2]

[1] Jeffries, Loeliger, and Staub, Phys. Rev. **85**, 478 (1952).
[2] A. L. Schawlow and C. H. Townes, Phys. Rev. **82**, 268 (1951). The calculated value for $\mu(Ti^{47})$ is in error and should be -0.80 (private communication).

P5. Angular Distribution of Neutrons from $O^{18}(p, n)F^{18}$.† HANS MARK AND CLARK GOODMAN, *M.I.T.*—The reaction $O^{18}(p, n)F^{18}$ was studied using monoenergetic protons from the Rockefeller electrostatic generator. The targets were made by oxidizing tantalum disks in enriched (20 percent O^{18}) oxygen which was obtained from Professor Alfred O. Nier. It was possible to obtain a surface layer of $Ta_2O_5^{18}$ which was roughly 20 kev thick for 3-Mev protons. The neutron yield in the forward direction was measured using a long counter.[1] Resonances were observed at proton energies $E_p=2.657$, 2.778, 3.050, 3.170, 3.268, 3.385, 3.494 Mev in agreement with Richards *et al.*[2] Additional resonances were observed at $E_p=2.732$, 3.665, 3.756 Mev. The angular distribution of neutrons at several energies was measured using a proton recoil counter.[3] The most probable spin and parity assignments for the various excited states have been made. The results seem to indicate that in the energy range $E_p=3.0$ to 3.5 the resonance structure is not simple but that there exists a broad state upon which the sharp resonances are superposed.

† Work jointly supported by the U. S. Office of Naval Research and the U. S. Bureau of Ships.
[1] Roseborough, McCue, Preston, and Goodman, Phys. Rev. **83**, 1133 (1951).
[2] Richards, Smith, and Browne, Phys. Rev. **80**, 524 (1950).
[3] Kay, Mark, and Goodman, Phys. Rev. (to be published).

P6. The Scattering of Fast Neutrons by Iron, Lead, and Chromium.* M. A. ROTHMAN, D. W. KENT, AND C. E. MANDEVILLE, *Bartol Research Foundation of the Franklin Institute.*—Fast neutrons of 3.7-Mev energy have been inelastically scattered in Fe, Pb, and Cr. Using a NaI—Tl crystal, a photomultiplier, and pulse-height selection, gamma rays are detected from iron at 0.88 Mev, from lead at 2.65 Mev, and from chromium at 1.43 Mev. The neutron energy spectrum obtained, using 4.2-Mev incident neutrons, a chromium scatterer, and photographic emulsion detection, shows two unresolved groups: the elastic group and another, inelastic, corresponding to a Q of about -1.4 Mev.

* Assisted by the joint program of the U. S. Office of Naval Research and the U. S. Atomic Energy Commission.

P7. Angular Distribution of Neutrons Scattered from Aluminum, Iron, and Lead.* W. D. WHITEHEAD AND S. C. SNOWDON, *Bartol Research Foundation of the Franklin Institute.*—The differential cross sections for the scattering of 3.7-Mev neutrons by Al, Fe, and Pb have been measured between 13° and 140° with an angular resolution of ±10 degrees. The measurements were performed in a ring geometry in which the angle variation was accomplished by an axial movement of the ring. Corrections for the higher-order scattering have been determined experimentally by varying the thickness of the scatterer and extrapolating to zero thickness. Since the energy response of the neutron detector (Zn—s Lucite button mounted on a photomultiplier) does not permit complete discrimination against the low-energy neutrons, the differential cross sections are not the elastic cross sections. However, a crude estimate indicates that the low-energy neutrons do not contribute more than 20 percent to the measured differential cross sections. The cross sections exhibit strong maxima in the forward direction. Iron and lead have secondary maxima at 110° and 90°, respectively. The total cross sections were also measured at 3.7 Mev by a standard transmission experiment giving 2.55, 3.51, and 7.60 barns for Al, Fe, and Pb, respectively, in good agreement with the values of Nereson and Darden.[1] The difference between the total cross section and integral of our differential cross section gives a measure of the total inelastic cross-section.

* Assisted by the joint program of the U. S. Office of Naval Research and the U. S. Atomic Energy Commission.
[1] N. Nereson and S. Darden, Phys. Rev. **89**, 775 (1953).

FRIDAY EVENING AT 7:00

Hilton Hotel

(J. KAPLAN, presiding)

Banquet of the American Physical Society

After-dinner speaker: A. T. WATERMAN

SATURDAY

Excursions (to be announced)

SUPPLEMENTARY PROGRAMME

SP1. Structure and Resistivities of Gold Films Deposited by Evaporation and Sputtering.*,† RICHARD B. BELSER, *Georgia Institute of Technology.*—Gold films of 1000 angstrom's thickness, deposited on glass microscope slides by normal evaporation procedures at about 10^{-5} mm of Hg pressure, have been found to have an initial resistivity of approximately $2\rho_b$. These films change in resistance slowly at room temperature and may drop 15 percent in two weeks. When heated to 250–300°C, they drop further in resistivity to a value approximately 65 percent of the initial value of $1.3\rho_b$. Heating to higher temperatures, about 450°C, may cause the film to aggregate resulting in a high or unmeasurable resistivity. Sputtered gold films, on the other hand, have an initial resistivity dependent on the sputtering rate. At a nominal high sputtering rate, 40–50 ma, the resistivity will be approximately $4.5\rho_b$. Such films do not change in resistance with room temperature. Heating to 300°—400°C causes a considerable reduction in resistivity to values in the range $1.5–2.0\rho_b$. In some instances, and at high sputtering rates, even higher temperatures appear necessary to produce a reduction to the minimum resistivity. The greater resistance of these films to aging at room or elevated temperatures appears to be related to occluded gas and lattice imperfections produced by bombardment during the severe sputtering action.

* To be given at the end of Session C if the chairman rules that time permits.

† Supported by U. S. Army Signal Corps.

SP2. Indium, a Versatile Solder to Metals and Nonmetals.*,† RICHARD B. BELSER, *Georgia Institute of Technology.*—Indium is a soft silvery metal of 155°C melting point. In the molten state it adheres to many metals and nonmetals and continues to adhere upon solidification. This dual ability makes it a valuable laboratory and industrial material. Some adherence has been obtained with indium to twenty-four metals and 18 nonmetals. The metals tested include most common industrial metals, and the nonmetals include glass, ceramics, quartz, mica, metallic oxides, and silicious minerals. A flux is useful in soldering to metals near or below indium in the electrochemical series, but fluxes are not useful for soldering to the active metals or to nonmetals. Fluxes appear to inhibit wetting of these materials. A number of indium-rich alloy solders were tested for strengths and melting points. Alloys with small percentages of silver and larger percentages of lead and tin appear useful. These solders have been found valuable for mechanical suspension, electrical connections, soldering to thin metal films, mounting piezoelectric crystals, and glass to metal vacuum seals.

* To be given at the end of Session C if the chairman rules that time permits.

† Supported by U. S. Army Signal Corps.

Author Index to Papers Presented at the Albuquerque Meeting

Adel, Arthur—B8
Agogino, Mercedes M.—E10
Allen, William A.—C12
Anderson, C. D.—E4
——, E. W. Cowan, R. B. Leighton, and V. A. J. van Lint—H3
Anderson, E. C., C. L. Cowan, Jr., and F. Reines—G9
Avery, E., L. Grossweiner, and M. Matheson—B12
Bacher, R. F., J. C. Keck, V. Z. Peterson, J. G. Teasdale, A. V. Tollestrup, R. L. Walker, and R. M. Worlock—I3
Bader, M., W. A. Wenzel, and W. Whaling—D14
Bame, S. J., Jr.—P1
Baños, Alfredo, Jr.—C5
Bell, W. A., Jr., L. O. Love, C. E. Normand, and W. K. Prater—P3
Belser, Richard B.—C15, SP1, SP2
Benedikt, E. T.—C3
Bowen, I. Gerald—B9
Brode, Robert B.—E2, E9
Brook, Marx—B4
Brousseau, A., C. L. Cowan, Jr., and F. Reines—G7
Bryant, P. J., H. U. Rhoads, and A. H. Weber—C14
Busemann, Adolf—F3
Calbick, C. J., H. Christensen, and E. E. Thomas—C8
Christensen, H., C. J. Calbick, and E. E. Thomas—C7
Cole, Julian D.—F2
Cowan, C. L., Jr.—G4
Cowan, E. W., C. D. Anderson, R. B. Leighton, and V. A. J. van Lint—H4
Cowan, R. D.—B3
Cox, E. F.—L1
DePangher, John—D6
Douglas, D. L., A. C. Mewherter, and R. P. Schuman—O3
Efremov, N.—B13
Elasasser, W. M. and K. McDonald—C4
El-Mofty, Osman—E8
Elterman, L.—B7
English, W. N.—F6
Ennis, M. E. and A. Hemmendinger—K9
Fermi, E.—J1
——, J. Lepore, Frank Crawford, R. F. Christy, R. L. Walker, and H. A. Bethe—M1
Fleming, John R. and J. J. Lord—H1
Ford, Kenneth W.—N1
Fowler, W. A.—K5
Frank, R. M. and J. L. Gammel—K7
Freier, P. S. and J. E. Naugle—E6
Fretter, W. B. and E. W. Friesen—H5
Friedland, S. S., H. S. Katzenstein, J. Katzenstein, D. P. Lindorff, G. S. Timoshenko, and L. E. Williams—B6
Frye, Glenn M. and Louis Rosen—D2
Fulton, Thomas and Robert Karplus—N4
Gammel, J. L.—K8
Gammel, Juanita—K6,
Goldhaber, Gertrude S. and Michael McKeown—N2
Goldhaber, M.—K2
Grant, H. L. and R. W. Stewart—F7
Griffiths, G. M. and J. B. Warren—D5
Guderley, Gottfried—F1
Harrison, F. B., C. L. Cowan, Jr., and F. Reines—G5
Hayes, F. N., Lloyd Williams, C. L. Cowan, Jr., and F. Reines—G6
Henke, Burton—B1
Holzer, R. E.—L4
Howland, P. R., W. E. Kreger, and R. A. Taylor—O1
Hoyle, F., D. N. F. Dunbar, W. A. Wenzel, and W. Whaling—N6
Hudson, Craig C.—B2
Hughes, D. J., W. Y. Kato, and J. S. Levin—N3
Jeffries, C. D.—P4
Kallmann, H. K.—B5
Kenney, James F. and Victor H. Regener—H7
Koehler, W. C.—G2
Kraus, Alfred A., Jr.—D11
Langer, L. M.—K1
LaRocca, Edward W.—C10
Leachman, R. B.—A2
Li, C. W.—D8
Liberman, D. A. and R. F. Christy—D12
Liller, William and F. L. Whipple—L2
Linford, Leon B., O. C. Haycock, J. I. Swigart, C. L. Alley, C. D. Westlund, and J. R. Lien—L8
Lomont, J. S.—C11
Mackin, Robert J., Jr.—D7
Malich, C. W. and C. E. Faneuff—O2
Mark, Hans and Clark Goodman—P5
Martin, H. C., B. C. Diven, and R. F. Taschek—O5
McCarty, Robert J.—B11
McClelland, Clyde—K3
Megill, L. R. and C. R. Emigh—C2
Milne, Edmund A.—D10
Naugle, J. E. and P. S. Freier—E7
Neilson, G. C., D. B. James, and C. A. Barnes—D3
Northrop, J. A. and J. E. Brolley, Jr.—I5
Oltman, George H.—L7
Perkins, J. F. and S. K. Haynes—O6
Peterson, R. W., W. A. Fowler, and C. C. Lauritsen—D13
Peterson, S. W. and H. A. Levy—C9
Ramm, W. J. and M. N. Stein—C1
Regener, Victor H.—L5
Reid, Walter P.—C6
Reines, Frederick—G3
Rothman, M. A., D. W. Kent, and C. E. Mandeville—P6
Runge, Richard J.—L6
Sanders, F. H.—F4
Schmitt, H. W. and R. B. Leachman—I6
Schuch, R. L., E. C. Anderson, C. L. Cowan, Jr., F. B. Harrison, F. N. Hayes, and F. Reines—G8
Seagrave, John D.—K10
Sites, John R., George Consolazio, and Russell Baldock—P2
Sitte, Kurt—E1
Snodgrass, H. R.—H2
Spence, R. W.—A1
Stewart, Leona—O4
Stewart, R. W.—F5
Taschek, R. F.—K4
Terrell, James, W. E. Scott, J. S. Gilmore, and C. O. Minkkinen—I4
Thomas, R. G.—N5
Thomas, Roy—H8
Thompson, T. J.—D1
Tollestrup, A. V., J. C. Keck, and R. M. Worlock—I2
Vallarta, M. S.—E5
van Lint, V. A. J. and G. H. Trilling—H6
Walker, R. L., J. G. Teasdale, and V. Z. Peterson—I1
Walker, W. D.—E3
Warren, J. B. and G. M. Griffiths—D4
Webb, T. S., C. W. Li, and W. A. Fowler—D9
Wheeler, John A.—A3
White, William C.—C13
Whitehead, W. D. and S. C. Snowdon—P7
Wilkening, Marvin H.—B10
Wilkinson, M. K.—G1
Workman, E. J.—L3

CONTENTS—*Continued*

Letters to the Editor:

Solutions of the Hesse-Nordsieck Equation in the Adiabatic Limit . R. Arnowitt and S. Deser 1061

Production of Acceptor Centers in Germanium and Silicon by Plastic Deformation . . . . . W. C. Ellis and E. S. Greiner 1061

Thermal Conductivity of Copper between 0.29°K and 4.2°K . James Nicol and T. P. Tsang 1062

Paramagnetic Resonance Absorption in Graphite . . . . . J. G. Castle, Jr. 1063

Some Consequences of Possible Degeneracy of Energy Bands in Ge . Edward N. Adams, II 1063

Radiation Damage in Semiconductors . . . . . W. Primak, L. H. Fuchs, and P. Day 1064

Magnetic Susceptibility of Germanium . . . . . D. K. Stevens and J. H. Crawford, Jr. 1065

Contribution of Solar X-Rays to *E*-Layer Ionization . . . . . E. T. Byram, T. A. Chubb, and H. Friedman 1066

Nonquantizable Unified Field Theories . . . . . W. B. Bonnor 1067

de Haas-van Alphen Effect in Arsenic . . . . . Ted G. Berlincourt 1068

Paramagnetic Resonances in Irradiated Glasses . . . . . E. L. Yasaitis and B. Smaller 1068

Visible Light from Localized Surface Charges Moving Across a Grating . . . . . S. J. Smith and E. M. Purcell 1069

Derivation and Renormalization of the Tomo-Dancoff Equations . . Bahram Kursunoğlu 1069

Velocity Distribution of the Pair Components in α^2 Decay . . . O. Halpern and K. Bauman 1070

Total Cross Sections for 140-Mev Neutrons . . . . . A. E. Taylor 1071

Interpretation of Bhabha's Theory of Particles of Maximum Spin 3/2 . . . . . W. A. Hepner and D. R. Workman 1071

Single-Time Bethe-Salpeter Equation . . . . . Wilhelm Macke 1072

Fission Yields of Ru^{103} and Ru^{105} . . . . . W. H. Hardwick 1072

Total $\pi^- - p$ Cross Section at 340 and 470 Mev . . . . . A. M. Shapiro, C. P. Leavitt, and F. F. Chen 1073

Evidence for Subshell at $Z=90$ . . . . . Glenn T. Seaborg 1074

Possible $0 \rightarrow 0$ (no) β Transitions in $4n+2$ Nuclei . . . . . O. Kofoed-Hansen 1075

β Spectrum of Ra D . . . . . E. Hunter 1076

0^+ States of the Light Odd-Odd Nuclei . . . . . P. Stähelin 1076

Proceedings of the American Physical Society:

Minutes of the New Mexico Meeting held at Albuquerque, September 2, 3, 4, and 5, 1953 (Corresponding to *Bulletin of the American Physical Society*, Volume 28, No. 5.) . . 1078

CONTENTS

THE PHYSICAL REVIEW SECOND SERIES, VOLUME 92, No. 4 NOVEMBER 15, 1953

Non-Maxwellian Distribution in a Shock Front and the Anomaly of the Clausius-Mosotti Temperature . . . Harl K. Sen 851

Condition on Uniform Field Breakdown in Electron-Attaching Gases . . . Ronald Gabelle and Morris L. Reeves 857

Saturation Effects in Paramagnetic Resonance . . . A. H. Eschenfelder and R. T. Weidner 869

Transition Temperatures of Superconductors . . . B. T. Matthias 874

Irreversible Thermodynamics of Thermoelectric Effects in Inhomogeneous Anisotropic Media . . . Charles A. Domenicali 877

Change of Electrical Conductivity of Sodium Chloride upon Bombardment with High-Energy Protons . . . Edgar A. Pourtoiois 881

Interaction of a Nonrelativistic Particle with a Scalar Field with Application to Slow Electrons in Polar Crystals . . . Tsung-Dao Lee and David Pines 883

Electronic Polarizabilities of Ions in Crystals . . . Jack R. Tessman, A. H. Kahn, and William Shockley 889

Influence of Irradiation on the Characteristics of a Glow Discharge in Pure Rare Gases . . . K. W. Meissner and W. F. Miller 896

Note on the Interchange of Rotational and Vibrational Energy in Collisions of Diatomic Molecules . . . Edward H. Kerner 899

Microwave Spectra of CsF, CsCl, and CaF₂ . . . A. Honig, M. L. Stitch, and M. Mandel 901

Decay of Rb^{100} . . . Bernd Kahn and W. S. Lyon 902

Angular Correlation of the Gamma Rays from Mn^{56} . . . F. R. Metzger and W. B. Todd 904

Spontaneous Fission Yields from Uranium and Thorium . . . George W. Wetherill 907

Alpha-Gamma Angular Correlation in Lanthanum (Tb^{157}) . . . G. M. Temmer and J. M. Wyckoff 913

Neutron-Deficient Isotopes of Thallium . . . I. Bergström, R. D. Hill, and G. de Pasquali 918

Large-Angle Scattering of Cs^{137} Gamma Rays . . . Thomas D. Stickler 923

Half-Life of Zr^{93} . . . Earl K. Hyde 927

Angular Correlation of the Cascade Gamma Rays from the Decay of Au^{198} . . . Carlton D. Schrader 928

Method for the Determination of the End-Point Energy of Beta Emitters . . . M. Ferro 931

Technetium of Mass Number 98 . . . John K. Lavdi, M. L. Pool, D. N. Kundu, and R. A. Howe 934

Gamma Rays from Proton Bombardment of B^{10} . . . R. W. Krone and L. W. Seagondollar 935

Scintillation Spectrometer Determination of L-Capture to K-Capture Ratio in Cd^{109} and I^{125} . . . E. der Mateosian 938

Excitation Function for the Photodisintegration of Beryllium . . . R. Nathans and J. Halpern 940

Resonant Effects and Spin Dependence in Potential Scattering of Slow Neutrons . . . W. Selove 941

Influence of Electric and Magnetic Fields on Angular Correlations . . . A. Abragam and R. V. Pound 943

Nuclear Spin Relaxation by Translational Diffusion . . . H. C. Torrey 962

Compton Scattering of 2.62-Mev Gamma Rays by Polarized Electrons . . . S. B. Gunst and L. A. Page 970

Positive Pi-Meson Interactions in Beryllium . . . F. H. Tenney and J. Tinlot 974

High-Energy Electron Scattering and Nuclear Structure Determinations . . . R. Hofstadter, H. R. Fechter, and J. A. McIntyre 978

Interpretation of Electron Scattering Experiments . . . L. I. Schiff 982

Magnetic Moments of Neutron and Proton . . . F. J. Belinfante 994

Intrinsic Magnetic Moment of Elementary Particles of Spin ½ . . . F. J. Belinfante 997

Hyperfine Structure of Hydrogen . . . R. Arnowitt 1002

New Modification of Classical Electromagnetic Theory . . . A. Schild 1009

Electromagnetic Mass and a Particle Model in Dirac's Theory of Elementary Particles . . . Hans Frielendt 1015

Convergence of the Adiabatic Nuclear Potential. II . . . Abraham Klein 1017

Green's Function Method for Strongly Interacting Particles . . . Maurice Neuman 1021

Nuclear Forces in Pseudoscalar Meson Theory . . . K. A. Brueckner and K. M. Watson 1023

Nuclear Forces from P-Wave Mesons . . . E. M. Henley and M. A. Ruderman 1036

Universal Fermi Interaction . . . E. J. Konopinski and H. M. Mahmoud 1045

Theory of Polarized Particles and Gamma Rays in Nuclear Reactions . . . Albert Simon 1050

(continued on cover three)

LANCASTER PRESS, INC., LANCASTER, PA.